MASARYK UNIVERSITY

Faculty of Science

Martin KLVAŇA

STRUCTURE-DYNAMICS-FUNCTION RELATIONSHIPS OF HALOALKANE DEHALOGENASES

Dissertation thesis

Supervisor: Assoc. Prof. RNDr. Miroslav Němec, CSc. Brno, 2009

Bibliografická identifikace / Bibliographic identification

Jméno a příjmení autora / Author name:	Martin Klvaňa
Název dizertační práce / Dissertation thesis title:	Vztahy mezi strukturou, dynamikou a funkcí halogenalkandehalogenáz / Structure-dynamics-function relationships of haloalkane dehalgoenases
Studijní program / Study programme:	Biologie / Biology
Studijní obor / Field of study:	Mikrobiologie / Microbiology
Školitel / Supervisor:	Assoc. Prof. RNDr. Miroslav Němec, Csc.
Rok obhajoby / Defence year:	2010
Klíčová slova / Keywords:	Protein, enzym, halogenalkandehalogenáza, vnořené aktivní místo, tunel, odchod produktů, výměna molekul vod, molekulově-dynamická simulace, návrh mutantů, CAVER / Protein, enzyme, haloalkane dehalogenase, buried active site, tunnel, product release, water exchange, molecular dynamics simulation, design of mutants, CAVER

Acknowledgements

My PhD research has been made possible by the following institutions:
Masaryk University, Supercomputing Center Brno, EML Research, Kobe University

. . . and with financial support from the Ministry of Education of the Czech Republic:
Grant MSM0021622412

Below follows my list of people to whom I would like to say *thank you*:

Study supervisor: **Assoc. Prof. RNDr. Miroslav Němec, Csc.**
Department of Microbiology
Faculty of Science, Masaryk University
Brno, Czech Republic

Research supervisor: **Assoc. Prof. Jiří Damborský, Ph.D.**
Loschmidt Laboratories
Department of Experimental Biology
Faculty of Science, Masaryk University
Brno, Czech Republic

Methodological advisor: **Dr. Rebecca C. Wade**
Molecular and Cellular Modeling Group
EML Research
Heidelberg, Germany

Technical advisor: **Mgr. Jan Brezovský**
Loschmidt Laboratories
Department of Experimental Biology
Faculty of Science, Masaryk University
Brno, Czech Republic

Publications co-authors: Pavel Banáš, Radka Chaloupková, Jiří Damborský, Jan Dohnálek, Pavel Dvořák, Táňa Koudeláková, Petr Kulhánek, Ivana Kutá-Smatanová, Michal Kutý, Yuji Nagata, Michal Otyepka, Martina Pavlová, Zbyněk Prokop, Alena Stsiapanava, Masataka Tsuda, Rebecca C. Wade.

Software co-authors: Filip Andres, Petr Beneš, Jan Brezovský, Eva Chovancová, Jiří Damborský, Petr Jaša, Barbora Kozlíková, Petr Medek, Antonín Pavelka, Jiří Sochor, Tibor Szabó, Matúš Zamborský.

Laboratory colleagues: Šárka Bidmanová, Jan Brezovský, Radka Chaloupková, Eva Chovancová, Pavel Dvořák, Andrea Fořtová, Khomaini Hasan, Petr Jeřábek, Táňa Koudeláková, Marta Monincová, Tomáš Mozga, Antonín Pavelka, Martina Pavlová, Zbyněk Prokop, Veronika Šťěpánková.

Other scientists: Takashi Nakamura, Alexander Shug, Shigenori Tanaka, Hirofumi Watanabe.

How can I put it? Life is like video footage: Hard to edit, directors, that never understood it.

— Robert F. Diggs

Abstrakt

Vždycky dělám to, co neumím, abych se případně naučil, jak to dělat.

— Pablo Picasso

Bílkoviny, geny a genetický kód jsou nejzákladnějšími funkcemi pro život. V živých organismech plní bílkoviny řadu funkcí z nichž katalytická funkce některých bílkovin, tzv. enzymů, je tou nejzásadnější, protože enzymy urychlují specifické chemické reakce, nezbytné k životním procesům. Pochopení základních principů života vyžaduje detailní pochopení funkce enzymů. Jelikož funkce enzymu je určena jeho strukturou a dynamikou, objasnění funkce vyžaduje pochopení vztahu mezi strukturou, dynamikou a funkcí pro každý jednotlivý enzym. Tyto tři vlastnosti musi být navíc vnímány z evolučního hlediska, protože nic v biologii nemá smysl, pokud to neni bráno z pohledu evoluce. Každý jednotlivý enzym si zaslouží být studován, protože každý enzym může poskytnout důležité informace o strukturně-dynamicko-funkčních vztazích, které mohou být případně zobecněny pro další enzymy, potažmo bílkoviny jako celek, a to z důvodu omezeného množství možného trojrozměrného uspořádání struktury bílkoviny.

α/β-hydrolázové trojrozměrné uspořádání je jedním z nejuniverzálnějších, protože podporuje řadu hydrolytických funkcí, včetně hydrolytické dehalogenace katalyzované enzymy halogenalkandehalogenázami. Tyto enzymy přitahují pozornost vědců přes dvacet let z mnoha důvodů, včetně toho, že náleží k univerzálnímu trojrozměrnému uspořádání, a že díky schopnosti podílet se na odstraňování jedovatých halogenovaných sloučenin vnesených do životního prostředí člověkem mají potenciálně nezanedbatelný ekologický význam. Halogenalkandehalogenázy katalyzují hydrolytickou dehalogenaci halogenovaných alifatických uhlovodíků na příslušný alkohol, halogenidový anion a proton. Hydrofóbní charakter substrátů halogenalkandehalogenáz vyžaduje, aby bylo aktivní místo těchto enzymů vnořené, a tím chráněno od vnějšího vodného prostředí. Na druhou stranu, výměna molekul vod, substrátu a produktů mezi vnořeným aktivním místem a vnějším prostředím musí být zajištěna tak, aby umožnila učinnou dehalogenační funkci. S cílem lépe pochopit procesy výměny reakčních molekul na atomární úrovni, molekulově-dynamické simulace byly provedeny s halogenalkandehalogenázou DhaA z bakterie *Rhodococcus rhodochrous* NCIMB 13064. Na základě těchto simulací byly navrženy mutace a místa vhodná k mutacím v cestách, které mohou potenciálně sloužit k výměně molekul. Tyto cesty a výměnné procesy byly dále podrobně prozkoumány a interpretovány ve světle experimentálních dat: mutageneze, dehalogenační aktivity, stability sekundární struktury a trojrozměrné rentgenové krystalové struktury.

Účinný mechanismus umožnující kontrolovanou výměnu molekul byl vytvořen v enzymu DhaA nahrazením některých alifatických aminokyselinových zbytků velkými aromatickými v hlavní výměnné cestě, tzv. hlavním tunelu. Tímto bylo dosaženo až 26ti násobného zvýšení účinnosti mutantů DhaA v dehalogenaci jedovaté sloučeniny 1,2,3-trichlorpropanu. Vnesené mutace způsobily, že se hlavní tunel změnil z trvale otevřeného na přechodně otevřený, který se otevírá a zavírá podle fáze reakčního cyklu. Přechodné otevření může být vyvoláno molekulami vody, které vstupují z vnějšího prostředí do aktivního místa, kde solvatují produkty reakce. Na druhou stranu, v nepřítomnosti halogenidového aniontu v aktivním místě, je toto dostatečně odstíněno od vnějšího prostředí a brání molekulám vod ve vstupu do aktivního místa, kde by mohly soupeřit s molekulou substrátu a bránit tak jeho vazbě do reaktivní pozice pro první chemický krok dehalogenační reakce. Cesty nalezené v halogenalkandehalogenáze DhaA a jejích mutantech, a mechanismy výměny substrátu, produktů a vod naznačují důležitost dynamiky pro funkci halogenalkandehalogenáz. Nalezené cesty také posloužily jako počáteční zkušební sada při vývoji algoritmu CAVER 2.0, sloužícího pro rychlý výpočet a charakterizaci cest, které vedou z vnořené dutiny v bílkovině na povrch. Tento přístup má, v kombinaci s molekulovou dynamikou, potenciál dále podněcovat výzkum s cílem pochopit vztahy mezi strukturou, dynamikou a funkcí bílkovin s vnořeným vazebným či aktivním místem.

Klíčová slova: Protein, enzym, halogenalkandehalogenáza, vnořené aktivní místo, tunel, odchod produktů, výměna molekul vod, molekulově-dynamická simulace, návrh mutantů, CAVER

Abstract

I am always doing that which I cannot do, in order that I may learn how to do it.

— Pablo Picasso

Proteins, genes and genetic code are the most fundamental functions required for life. Among the proteins, those with catalytic functions, the so-called enzymes, are fundamentally the most important because they speed up specific and otherwise too slow chemical reactions to sustain living processes. Understanding the underlying principles of life thus requires understanding enzyme function to the very deepest level. Since the function is determined by protein structure and dynamics, elucidation of the underlying principles of enzyme function requires detailed understanding of relationships between structure, dynamics and function for every particular enzyme. Moreover, these properties must be considered from evolutionary perspective because nothing in biology has sense unless in the view of evolution. Every single enzyme is worth of study because every enzyme can reveal important information on the structure-dynamics-function relationships, that might be possibly generalised to some other enzymes, and proteins in general, when considering limited space of three-dimensional protein folds.

α/β-hydrolase fold is one of the most versatile protein folds as it supports various hydrolytic functions including hydrolytic dehalogenation catalysed by haloalkane dehalogenases. These enzymes have attracted scientists since 80s for many reasons, including their belonging to the versatile fold and potentially high ecological importance in removal of toxic halogenated xenobiotics from polluted environment. Haloalkane dehalogenases perform hydrolytic dehalogenation of halogenated aliphatic hydrocarbons to corresponding alcohol, halide anion and proton. Hydrophobic nature of the substrate implies necessity for the active site to be buried in the protein core, shielded from the bulk solvent. Contrary, exchange of water, substrate and products between the buried active site and bulk solvent must be efficient for effective dehalogenating function. Aimed at gaining better understanding of the exchange processes at atomic level, molecular dynamics simulations of haloalkane dehalogenase DhaA from *Rhodococcus rhodochrous* NCIMB 13064 were employed/conducted: (i) to design mutations and hot spots for mutagenesis in exchange pathways; (ii) to identify product release and water exchange pathways, protein-product, protein-water and product-water interactions; and (iii) to interpret them in the light of experimental data: mutagenesis, dehalogenating activities, secondary structure stabilities and three-dimensional protein X-ray crystal structures.

An efficient gating mechanism allowing controlled exchange of molecules was established in the DhaA enzyme by introducing aromatic substitutions in the main exchange route, the so-called main tunnel, causing up to 26-fold improvement in catalytic performance of DhaA mutants towards non-natural xenobiotic, 1,2,3-trichloropropane. The mutations caused change of the main tunnel from permanent to transient that opens temporarily according to the phase of reaction cycle. Transient opening can be induced by water from bulk solvent that enters the active site to solvate products. On the other hand, in the absence of the halide anion in the active site, the shielding is efficient to hinder water from entering the active site where it would unfavourably compete with a substrate and disturb its binding into reactive position for initial chemical step of the dehalogenating reaction. Pathways identified in the DhaA haloalkane dehalogenase and its mutants and mechanisms of substrate, product and solvent exchange signify importance of dynamics for the function of haloalkane dehalogenases. The identified pathways also serve as an initial validation set for development of CAVER 2.0 tunnel calculation algorithm, an approach for rapid evaluation of possible pathways leading from a buried cavity to surface in proteins that has, together with molecular dynamics simulations, a potential to stimulate further research on proteins aimed at understanding structure-dynamics-function relationships of proteins with buried binding or active sites.

Keywords: Protein, enzyme, haloalkane dehalogenase, buried active site, tunnel, product release, water exchange, molecular dynamics simulation, design of mutants, CAVER

Contents

It's Yourz! The world in the palm of your hand.
— Robert F. Diggs

1 Introduction

A textbook is like a guide who tells you "there are thirty-six chambers in the castle" and shows you only compartment ceiling in the castle souvenir shop.

1.1 Life

1.1.1 Definition of life

Fundamental functions of life. Genes, genetic code and proteins are the most fundamental functions required for life **(Ruiz-Mirazo et al., 2004; Ikehara, 2005)**. Genes are segments on double-stranded deoxyribonucleic acid (dsDNA) coding for single-stranded ribonucleic acids (ssRNA) via nucleotide base-pairing complementarity, or functioning directly as regulatory elements.

RNA functions. RNA molecules function in translation (mRNA, tRNA and rRNA), ribosome maturation (snoRNA), RNA processing (snRNA and sno RNA), replication (telomerase RNA in eukaryotes), editing (eukaryotes), protein translocation (SRP RNA), cellular transport (vRNA in eukaryotes), translation quality control (tmRNA in eubacteria) and functions of many others has not yet been determined **(Jeffares et al., 1998; Meli et al., 2001)**. Of all the types of RNA, tRNA is principally the most important because it plays the central role in translation of nucleotide sequence of mRNA into amino acid sequence of a protein by using the language of a genetic code, i.e. specific assignment of amino acids to nucleotide triplets **(Nirenberg et al., 1965; Söll et al., 1965)**, while ribosome increases rate and fidelity of the process **(Woese, 2001; Rodnina et al., 2007)**.

Protein functions. Proteins have catalytic (enzymes) or non-catalytic function; the latter includes structural proteins, transport proteins, motor proteins, signaling proteins, storage proteins, receptors, some hormones, and antibodies **(Schmidt & Lamzin, 2007)**. Of all the protein functions, enzymes are principally the most important because they speed up specific and otherwise too slow chemical reactions **(Koshland Jr., 2002b)**. If a constant source of energy is available, the increased rate of enzyme-catalysed reactions allows highly organised, high-entropy living organism to maintain itself against unevitable thermodynamic losses via processes of metabolism **(Koshland Jr., 2002b; Ruiz-Mirazo et al., 2004; Mulkidjanian & Galperin, 2007)**.

Enzymes. Enzyme kinetics depends on concentration of both enzymes and their substrates. Therefore, to sustain life, living organisms are organised into compartments, cells, i.e. containers of a limited volume, surrounded by a semi-permeable active boundary, a membrane, and eventually by additional structures **(Koshland Jr., 2002b; Ruiz-Mirazo et al., 2004)**. Even in the limited volume of a cell, however, thousands of reactions are occurring at the same time. In order to prevent enzymes to be confused by other reactions, they are characterised by seclussion, i.e. by some degree of substrate specificity on hand **(Morowitz, 1999; O'brien & Herschlag, 1999; Ruiz-Mirazo et al., 2004)**, and by some degree of plasticity on the other hand **(O'brien & Herschlag, 1999; Ruiz-Mirazo et al., 2004)**.

Evolution. Regeneration and repair of structures of a living organism, as the fight against thermodynamic losses, is not perfect, thus leading to gradual decay, which can be especially harmful if the decay is associated with changes in DNA **(Koshland Jr., 2002b)**. Living organisms use a clever trick to prevent from the decay – starting over via DNA replication and cell division, eventually by the birth of an infant **(Koshland Jr., 2002b)**. Even the replication, however, is not perfect and therefore leads to changes in DNA and consequently in gene products. Depending on the change, and interaction with external environment, the change can be harmful, harmless or even beneficial for the living organism. The trade-off between perfection of regeneration and repair, and errors in the processes defines the ability of a living system to change, i.e. to evolve, to improvise **(Koshland Jr., 2002b; Mulkidjanian & Galperin, 2007)**. Evolution alone is, however, too slow process for an organism occurring in rapidly changing environment. Therefore, living organisms also possess feedback and feedforward adaptability mechanisms, implemented in the program defined by DNA **(Koshland Jr., 2002b)**.

PICERAS. In summary, life is based on seven fundamental principles – program, improvisation, compartmentalisation, energy, regeneration, adaptability and seclussion (PICERAS), as noted by Koshland Jr. **(2002b; Fig 1)**.

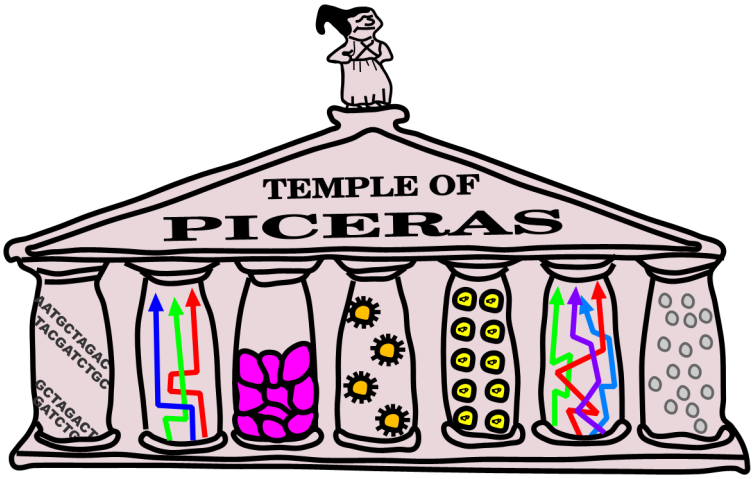

Fig 1 | PICERAS. There are seven pillars of life (from left to right): program (P), improvisation (I), compartmentalisation (C), energy (E), regeneration (R), adaptability (A) and seclussion (S). Redrawn according to Koshland Jr. **(2002b)**.

1.1.2 Origin of life

Key macromolecules in PICERAS. Two types of biological macromolecules, nucleic acids and proteins, play the two key roles in the PICERAS to sustain life of a living organism – informational (DNA and RNA) and catalytic (RNA and proteins). Evolutionary, it is not clear whichever of the three macromolecules came first.

Theories on the origin of life. It is generally accepted that: (i) biotic era, characteristic by existence and evolution of living organisms, was preceded by a pre-biotic era; and (ii) the first biotic, i.e. living, organism, being at the same time the Last Universal Common Ancestor (LUCA) and appearing presumably 3.8 billion years ago **(Maher & Stevenson, 1988)**, i.e. only 200 million years after the end of Earth's bombardment **(Davies, 2001)**, already possessed the PICERAS **(Koshland Jr., 2002b)**. It is also assumed that RNA molecules preceded DNA and that RNA molecules in contemporary organisms are relics of an ancient, pre-biotic era. Consequently, two alternative scenarios on the origin of life were proposed and described as RNA world hypothesis by Gilbert **(1986; Fig 2a)**, and [GADV]-protein world hypothesis by Ikehara **(2002; Fig 2b)**.

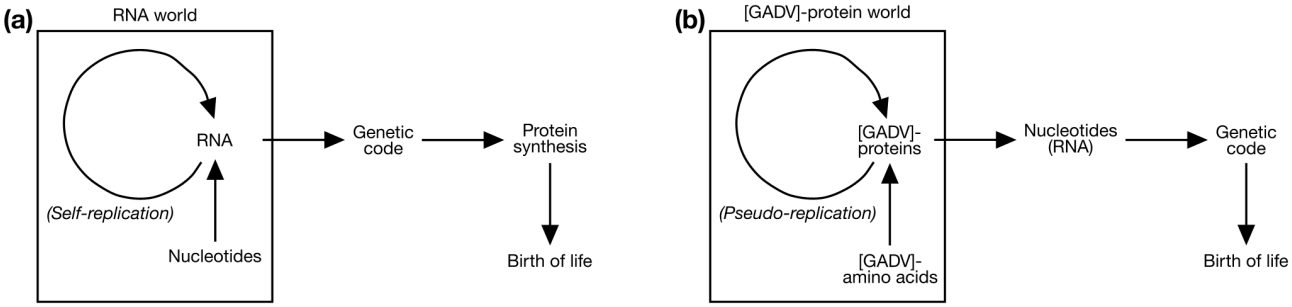

Fig 2 | Two hypotheses on the origin of life. **(a)** RNA-world hypothesis, **(b)** [GADV]-protein world hypothesis. Redrawn according to Ikehara **(2002)**.

RNA world hypothesis. According to RNA world hypothesis, chemical reactions involving inorganic and simple organic compounds yielded ribonucleotides which oligomerised and polymerised into RNA molecules possessing, at first, ultra-violet (UV) light-driven self-replication ability **(Mulkidjanian & Galperin, 2007)**, information storage and structural role **(Yarus, 1999; Woese, 2001; Brosius, 2003; Chen et al., 2007)**. Subsequently, RNA molecules acquired additional catalytic functions resulting in a primitive RNA-metabolising system **(Yarus, 1999; Woese, 2001; Brosius, 2003; Chen et al., 2007)** surrounded by a membrane composed of subunits synthesised by RNA **(Ma & Yu, 2006; Chen et al., 2007)**. Association of RNA molecules with amino acids **(Yarus, 1988; Yarus & Christian, 1989; Kuhn & Waser, 1994; Knight & Landweber, 1998; Yarus, 1998; Szathmáry, 1999; Yarus, 1999)** led to the origin

and evolution of genetic code governed by the order of appearance, i.e. biosynthesis, of amino acids **(Tables 1 and 2; Kuhn & Waser, 1994; Szathmáry, 1999)** and two physico-chemical constraints **(Table 3; Szathmáry, 1999; Lehmann, 2000)**: (i) hydrophobicity, involved in the process of attachment of amino acid to tRNA, and (ii) volume, involved in peptide bond formaton via stereopopulation control **(Milstien & Cohen, 1970; Szathmáry, 1999)**. Establishing of the genetic code determined the relationship between RNA and proteins and resulted in transition from the RNA world to RNA-protein (RNP) world. Most of RNA catalytic functions, especially those with limiting chemical steps, i.e. not diffusion **(Jeffares et al., 1998)**, were passed to more catalytically versatile and/or efficient proteins **(Cech, 1993; Müller, 2006; Chen et al., 2007)** ultimately leading to seperation of phenotype from genotype in both space and type of macromolecule **(Szathmáry, 1999; Dworkin et al., 2003; Ruiz-Mirazo et al., 2004)**. Although, the first proteins of RNP world are thought to be non-catalytic chaperone-like RNA binding proteins **(Poole et al., 1998)**.

Table 1 | Sequence of the amino acids in the order in which they were coded for.[a,b]

Group 1	Group 2	Group3
Gly	Lys	Phe
Ala	Arg	Tyr
Asp/Glu	Gln/Asn	His
Val	Pro	Cys
Leu/Ile		Met
Ser		Trp
Thr		

[a]Redrawn according to Kuhn & Waser **(1994)**.
[b]Groups and amino acids within each group are ordered by the order of appearance.

Table 2 | Origin of genetic code.[a,b]

Stage	Code
A	GGC and GCC
B	GNC
C	GNN
D	PuNN
E	NNN
F	Pu/Py[c]
G	AUN/UPuPu[d]

[a]According to Kuhn & Waser **(1994)**.
[b]N = G/C/A/T; Pu = G/C; Py = A/T.
[c]Distinguishing Pu/Py at 3rd position.
[d]Differentiating AUN and UPuPu.

Arguments in favour of the RNA world hypothesis. The RNA world hypothesis is based on discovery of self-splicing of *Tetrahymena* pre-rRNA in early 1980s **(Kruger et al., 1982; Guerrier-Takada et al., 1983)**. Since then, many catalytic RNA molecules have been identified. The RNA world hypothesis is further supported by the following findings: (i) dual, informational and catalytic, function of RNA **(Müller et al., 2006)**; (ii) experimentally demonstrated RNA-catalysed RNA synthesis **(Johnston et al., 2001)**; (iii) ability of RNA to catalyse amino acid activation, aminoacyl-tRNA synthesis and peptide bond formation **(Meli et al., 2001; Steitz & Moore, 2003; Vlassov et al., 2005; Rodnina et al., 2007)**; (iv) presence of conserved nucleotide cofactors in contemporary enzymes **(White, 1976; Benner et al., 1989)**; (v) RNA-primed DNA replication **(Itoh & Tomizawa, 1980)**; (vi) feasible synthesis of DNA from RNA precursors **(Lazcano et al., 1988)**; (vii) high catalytic rate compared to uncatalysed reaction, e.g. 350/min rate of RNA cleavage by *Tetrahymena* ribosyme corresponding to ~ 10^{11} acceleration **(Cech, 1993; Jeffares et al., 1998)**; (viii) versatility of RNA catalyst, e.g. transesterification and hydrolysis of phosphate diesters and monoesters, aminoacyl eseterase activity, general acid-base catalysis, and metal ion-assisted catalysis **(Cech, 1993; Doudna & Lorsch, 2005)**; and (ix) catalytic superiority of proteins over RNA **(Jeffares et al., 1998)**.

Arguments against the RNA world hypothesis. At the same time, however, RNA world hypothesis still suffers from several unresolved issues of which at least some might be unresolvable **(Ikehara, 2002)**: (i) pre-biotic synthesis of nucleotides under presumed pre-biotic conditions has not been demonstrated so far **(Orgel, 1998; Ma & Yu, 2006; Anastasi et al., 2007)**; (ii) polyphoshpates were not abundant in pre-biotic compounds **(Keefe & Miller, 1995)**; (iii) alternative possibility of RNA being result of a biotic invention **(Lazcano & Miller, 1996; Orgel, 1998; Anastasi et**

al., 2007), i.e. being preceded by a simpler informational macromolecule, denoted generally as XNA [e.g. TNA, threose nucleic acid **(Anastasi et al., 2007)**, GNA, glycol nucleic acid **(Anastasi et al., 2007)**, or PNA, backbone of ethylenediamine monoacetic acid **(Nielsen, 1993)**], seems also unlikely just for the same reasons of unfeasible synthesis of building blocks and/or their polymerisation, and transition from XNA to RNA **(Orgel, 1998; Anastasi et al., 2007)**; (iv) although our inability to synthesise RNA under presumed pre-biotic conditions cannot be taken to mean that the particular thing cannot be done **(Woese, 2001; Pross, 2004)**, if RNA could be formed in the pre-biotic era, then much simpler amino acids **(Di Giulio, 1997; Ikehara, 2005; Chen et al., 2007)** and their polymers, proteins, could be formed as well **(Di Giulio, 1997; Ikehara, 2005)**; therefore, pure RNA world could have never existed; instead, RNA were in actual fact tRNA-like molecules covalently linked to polypeptides **(Di Giulio, 1997)**; (v) it is impossible for RNA to self-replicate because RNA does not have stable tertiary structure required to exhibit genetic function on nucleotide sequence as a template, whereas RNA must be folded into stable tertiary structure to exhibit catalytic functions; and (vi) last, and most importantly, RNA world hypothesis treats origin of genes, genetic code, proteins and life independently **(Table 4; Ikehara, 2002; Ikehara, 2005)**, providing space for the question of 'how self-replicated RNA could acquire any genetic information for protein synthesis?' **(Szathmáry, 1999; Ikehara, 2005)**.

Table 3 | Symmetrical representation of universal genetic code.[a,b,c,d,e,f]

1st position	2nd position				3rd position
	U	**C**	**G**	**A**	
U	Phe	Ser	Cys	Tyr	**U**
	Phe	Ser	Cys	Tyr	**C**
	Leu	Ser	Trp	Stop	**G**
	Leu	Ser	Stop/Sec[g]	Stop	**A**
C	Leu	Pro	Arg	His	**U**
	Leu	Pro	Arg	His	**C**
	Leu	Pro	Arg	Gln	**G**
	Leu	Pro	Arg	Gln	**A**
G	Val	Ala	Gly	Asp	**U**
	Val	Ala	Gly	Asp	**C**
	Val	Ala	Gly	Glu	**G**
	Val	Ala	Gly	Glu	**A**
A	Ile	Thr	Ser	Asn	**U**
	Ile	Thr	Ser	Asn	**C**
	Met	Thr	Arg	Lys	**G**
	Ile	Thr	Arg	Lys	**A**

[a]According to Lehmann **(2000)**.
[b]Nucleotides are ordered by hydrophilicity from U (most hydrophilic) to A (most hydrophobic).
[c]Amino acids are ordered by hydrophobicity from left (most hydrophobic) to right (most hydrophilic).
[d]Small and large amino acids (except for Asn, Arg and Trp) are coded by codons with G/C and A/U at the second position, respectively.
[e]Degeneracy symmetry is highlighted with a thick line.
[f]Four-fold and two-fold degenerate codon families are indicated by light yellow and white boxes, respectively.
[g]Selenocysteine (Sec) is encoded by UGA codon only in presence of SECIS element in mRNA of selenoproteins.

[GADV]-protein world hypothesis. All the above mentioned deficiencies of the RNA world hypothesis have been addressed by the alternative [GADV]-protein world hypothesis **(Ikehara, 2002)** that states that there has never been RNA world and that proteins composed of four amino acids, Gly, Ala, Asp and Val, preceded RNA. According to the [GADV]-protein world hypothesis, the four amino acids, present in pre-biotic era, was the first and the simplest set of amino acids to form water-soluble globular [GADV]-proteins via pseudo-replication in absence of genes **(Ikehara, 2002; Ikehara, 2005)**. [GADV]-proteins satisfied first four out of six crucial indices of globular proteins at an extremely high probability: (i) hydrophobicity (Ala) and hydrophilicity (Asp); (ii) α-helix formabilities (Ala); (iii) β-sheet formabilities (Val); (iv) β-turn formabilities (Gly); (v) acidic amino acid content; and (vi) basic amino acid content **(Ikehara, 2002)**. Importance of the six indices is deduced from the fact that they are constant in proteins encoded by genes of different %GC content **(Ikehara, 2002; Ikehara, 2005)**. Additionally, Asp would be indispensable in the

construction of a catalytic centre on primeval proteins **(Ikehara, 2005)**. It is believed that some [GADV]-proteins could acquire peptide-bond formation catalytic function **(Ikehara, 2002)**. Due to limited variety of proteins that could be formed from the four amino acids, the catalytic [GADV]-proteins would become abundant. Expanding [GADV]-proteins discovered catalysis of nucleotide and oligonucleotide synthesis. In this step, tight relationship between [GADV]-proteins and nucleotides resulted in origin and evolution of a genetic code, because genetic code is too complex to be formed with one stroke **(Ikehara, 2005)**. [GADV]-amino acids became associated with various GNC primeval tRNA molecules (N = G, C, A, or T) by specific interaction between [GADV]-amino acids and oligonucleotides containing GNC, forming GNC primeval genetic code **(Ikehara, 2005)**. Lengthwise arrangement of [GADV]-amino acids and GNC primeval tRNA complexes accelerated [GADV]-protein synthesis through GNC primeval genetic code system and formation of (GNC)n primeval genes through phosphodiester bond formation among GNC codons **(Ikehara, 2005)**. Single-stranded (GNC)n primeval genes developed to produce double-stranded RNA (dsRNA) yielding primitive dsRNA genes and enabling inheritance and evolution of genetic information during propagation of RNA sequences from ancestors to descendants. (GNC)n primeval genes and GNC primeval genetic code evolved to genes and universal genetic code system of LUCA **(Table 3)** through $(SNS)_n$ primitive gene-SNS primitive genetic code system (S = G or C) by incorporating additional amino acids (Leu, Pro, His, Gln, Arg and Glu) into water-soluble globular proteins with high probability **(Ikehara et al., 2002)**, causing: (i) decreasing %GC content of genes; (ii) increasing variability of protein functions; and (iii) expanding the metabolism **(Ikehara, 2002; Ikehara, 2005)**.

Table 4 | Hypotheses related to the origin of life.[a]

Origin of	Ikehara's hypotheses [Ikehara, 2002]	Examples of hypotheses by other scientists
Life	[GADV]-protein world	RNA-world **(Gilbert, 1986)**
Gene	GC-NSF(a)	Gene duplication **(Ohno, 1970)**
	(SNS)n	Exon shuffling **(Gilbert et al., 1997)**
Genetic code	GNC primitive code	RNY code[b] **(Shepherd, 1981)**
	SNS primeval code	WWW code[c] **(Jimenéz-Sánchez, 1995)**
		Mitochondrial-type code **(Osawa,1995)**
Protein	GC-NSF(a) 0^{th}-order structure	Sequence theory **(Dill, 1990)**
	SNS 0^{th}-order structure	Structure theory **(Dill, 1990)**

[a]According to Ikehara **(2002)**.
[b]R = purine, N = any nucleotide base, Y = pyrimidine.
[c]W = A or U.

Arguments in favour of [GADV]-Protein world hypothesis. The [GADV]-protein world hypohesis, based on the essential co-evolution of genes, genetic code and proteins **(Table 4; Ikehara, 2002)**, is supported by the following arguments: (i) conserved regions among homologeous proteins indicate that the proteins were produced from one common ancestor, but not selected out independently from the sequence space with large diversity **(Ikehara, 2002)**; (ii) amino acids were undoubtedly present on the early Earth **(Miller, 1953; Weber & Miller, 1981; Chen et al., 2007)**; (iii) Gly, Ala, Asp and Val could easily be formed on primitive Earth **(Miller, 1974)**; (iv) order of appearance of amino acids, Gly, Ala, Asp, Val, Pro, Ser, Glu, Leu/Thr, Arg, Ile/Gln/Asn, His, Lys, Cys, Phe, Tyr, Met and Trp **(Table 1; Kuhn & Waser, 1994; Trifonov, 2004)** is coincident to a high degree with GNC-SNS primitive genetic code hypothesis **(Ikehara, 2005)**; (iv) genes can originate in overprinting antisense strands of GC-rich (> 60%) bacterial genes due to highly biased repeating $(GNC)_n$ sequence on sense strands with long non-stop frames (NSFs) on the corresponding antisense strands **(Ikehara & Okazawa, 1993; Ikehara et al., 1996; Ikehara, 2005)**; (v) feasibility of formation of enzymatically active [GADV]-peptides formation was proven experimentally by repeating dry-heating cycles and by solid phase peptide synthesis **(Rode et al., 1997)**, yielding [GADV]-peptides that possessed peptide bond hydrolysis activity with bovine serum albumin and β-galactoside bond hydrolysis activity **(Ikehara, 2005)**; the former activity is just opposite of peptide bond formation thus backward reaction is theoretically possible **(Ikehara, 2005)**.

Origin of life mystery. Thus, although RNA world hypothesis has been widely accepted and more and more evidences suggest the existence of RNA world during the origin of life, the scenario concerning the origin of the RNA world remains blurry **(Ma & Yu, 2006)**. The RNA world hypothesis can, as well as its alternative [GADV]-protein world hypothesis prove to be wrong, or we may simply never understand the origin of informational and catalytic macromolecules at the fullest **(Trevors & Abel, 2004)**.

Early evolution of genes. Genome of the LUCA was fragmented eukaryotic-like dsDNA **(Poole et al., 1998)**. Transition from RNA to DNA had to occurr with higher DNA stability **(Müller et al., 2006)** and high fidelity of DNA

replication and repair systems being the primary reasons **(Lupas et al., 2001)**. Early genes were only ~45 to 60 nucleotides in length **(Gilbert et al., 1997)**] and were fragmented due to low efficiency of transcription and translation processes **(Poole et al., 1998)**. Consequently, early genes encoded short peptides **(McLachlan, 1972; Lupas et al., 2001)** that self-assembled into small multi-peptide complexes to perform function **(Lupas et al., 2001)**. The advantageous higher protein stability, higher robustness of the protein function against structural changes and facilitating folding by removing processes of peptide diffusion, encounter and complex formation **(Demchenko, 2001)** led to evolution of longer genes via fusion of shorter ones **(Lupas et al., 2001)**, thus encoding larger proteins that might be of polyphyletic origin **(Lupas et al., 2001)** and in which the structural changes could more efficiently fine-tune protein function **(Koshland Jr., 1976; Koshland Jr., 1998)**. Even in the LUCA, however, genes were separated by introns which are believed to appear early in the evolution **(Doolittle, 1978; Gilbert et al., 1997)**.

Early evolution of genome organisation. Rapid reproduction **(Poole et al., 1998)** and thermophily **(Poole et al., 1998)** as a response on the surrounding environment were the driving forces for the loss of introns **(Gilbert et al., 1997)**, organisation of genome into single DNA molecule and its circularisation **(Poole et al., 1998)**, and for reduced dependence on ssRNA functionalities **(Poole et al., 1998)**, ultimately leading to origin of prokaryotes. Such a prokaryote-like model could conceivably have arisen more than once in evolution **(Poole et al., 1998)**. Hence, instead of being more ancient or more primitive than eukaryotes, prokaryotes are, in fact, more derived forms, adopted to harsh and rapidly changing environment **(Jeffares et al., 1998; Poole et al., 1998)**. Interestingly, genome organisation of modern eukaryotes and their metabolism, heavily dependent on RNA, resemble those of the LUCA **(Jeffares et al., 1998; Poole et al., 1998)**.

1.2 Protein structure

1.2.1 Primary structure

Amino acids. Proteins are linear, unbranched polymers of α-L-amino acids **(Sanger et al., 1955)**, defined by genetic code and nucleotide sequence of a gene. There are altogether 20 amino acids defined by the universal genetic code and thus definable by the gene, plus selenocysteine indirectly encoded by otherwise stop codon into the so-called selenoproteins **(Table 3)**. Hence, when omitting selenoproteins, for a protein composed of N amino acids, there are 20^N possible protein sequences, the so-called primary structures. The amino acids have common methenyl (-C_αH), carboxyl (-COOH), and, except for Pro, amino (-NH_2) group, and differ one to each other by a substituent attached to the C_α atom **(Table 5)**. The substituents can be classified into several overlapping groups according to: (i) size (tiny, small or large); (ii) type ofalkyl chain (aliphatic linear or cyclic, or aromatic); (iii) polarity (hydrophobic, hydrophilic or amphiphilic); (iv) net charge (neutral or charged); (v) pK_a of ionisable group (acidic or basic); and (vi) capacity for participating in standard hydrogen bonding interaction (donor or acceptors, or both, or none) **(Fig 3; Livingstone & Barton, 1993)**. There are two special amino acids – Gly with no substituent on C_α atom, and Pro with amino group participating with the substituent in a five-membered heterocycle.

Table 5 | Structure of amino acids. (pp. 20-21)

Amino acid[a]	Structure[b]	Amino acid[b]	Structure[b]
Glycine (Gly, G)	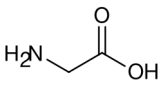	Tyrosine (Tyr, Y)	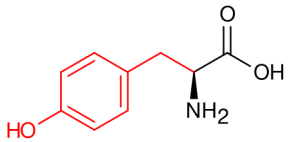
Alanine (Ala, A)	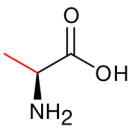	Tryptophan (Trp, W)	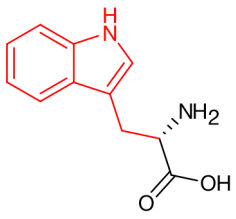

Amino acid[a]	Structure[b]	Amino acid[b]	Structure[b]
Valine (Val, V)	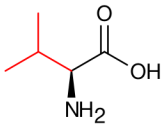	Methionine (Met, M)	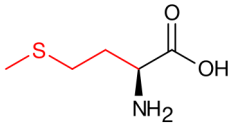
Leucine (Leu, L)	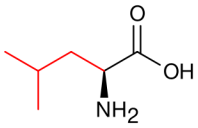	Cysteine (Cys, C)	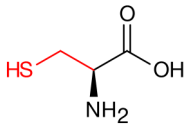
Isoleucine (Ile, I)	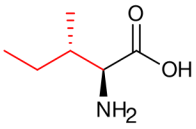	Selenocysteine (Sec, U)	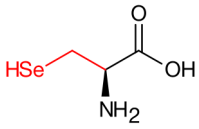
Proline (Pro, P)	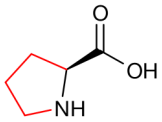	Serine (Ser, S)	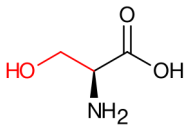
Phenylalanine (Phe, F)	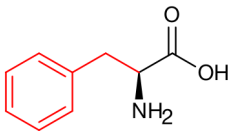	Threonine (Thr, T)	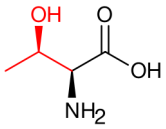
Asparagine (Asn, N)	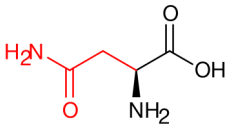	Histidine (His, H)	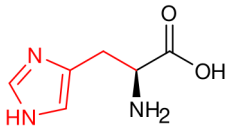
Glutamine (Gln, Q)	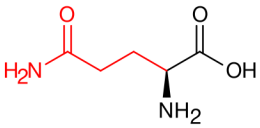	Lysine (Lys, K)	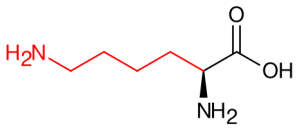
Aspartic acid (Asp, D)	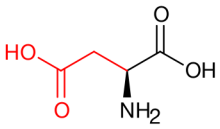	Arginine (Arg, R)	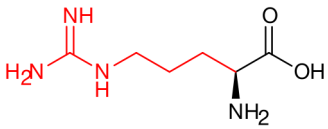
Glutamic acid (Glu, E)	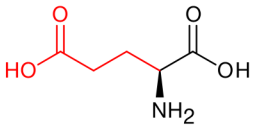		

[a]Three- and one-letter abbreviations are given in parentheses.
[b]Side-chains are highlighted in red.

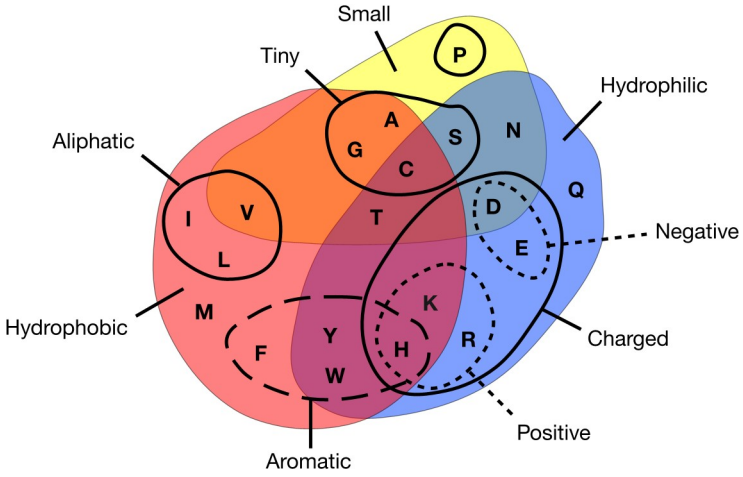

Fig 3 | Physico-chemical properties of amino acids. Redrawn according to Livingstone & Barton **(1993)**.

Amino acid residues. Incorporation of amino acids into the protein occurs via formation of the so-called peptide bond between carboxyl group of the last incorporated amino acid in the growing polypeptide chain attached to tRNA and the free amino group of the following amino acid attached to another tRNA molecule **(Woese, 2001; Rodnina et al., 2007)**. The residual part of the amino acid incorporated into the polypeptide chain, i.e. the amino acid residue, is constituted of two parts – main-chain (also known as "backbone") and side-chain. Main-chain is formed by -[NH-C_αH-CO]- group in all amino acid residues except for Pro (-[N-C_αH-CO]-), Gly (-[NH-$C_\alpha H_2$-CO]-), first amino acid residue with free main-chain amino group ([NH_2-C_αH-CO]-; N-terminus) and last amino acid residue with free main-chain carboxyl group (-[NH-C_αH-COOH]; C-terminus). Side-chain is formed by substituent on the C_α atom. The substituent is unchanged upon incorporation but may undergo function-specific chemical modification or chemical modification associated with protein aging. The main-chain distinguishes only Gly and Pro, whereas the rest of amino acids is left undistinguishable. Side-chains, on the other hand, distinguish all the 21 amino acid residues.

1.2.2 Secondary structure

Protein backbone ω dihedral angle. Peptide bond can exist in two resonance structures because of the resonance of electrons between the double bond of the carbonyl group and the amide N-C bond. Consequently, N-C bond is ~10% shorter than that found in usual C-N amine bonds, and has ~ 40% double-bond character **(Scheme 1; Pauling et al., 1951; Eisenberg, 2003)**. Due to electron delocalisation between atoms of the peptide bond, atoms of -[C_α(i)-CO-NH-C_α(i+1)]- group, where *i* is the rank of an amino acid residue in the protein sequence, lie in the same plane, and HN-CO ω dihedral angle should be ideally planar. Although, ω dihedral angle can deviate from planarity as much as by ~ 40° with tendency for lower (< 180°) values **(Pauling et al., 1951; Ramachandran, 1968; Head-Gordon et al., 1991; MacArthur & Thornton, 1996; Eisenberg, 2003)**.

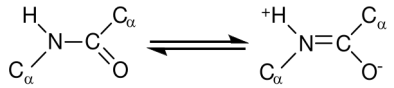

Scheme 1 | Resonance of peptide bond.

Protein backbone φ and ψ dihedral angles. Direction of the protein backbone is determined by two dihedral angles, φ and ψ, between two adjacent planes defined by -[C_α(i)-CO-NH-C_α(i+1)]- and -[C_α(i+1)-CO-NH-C_α(i+2)]- groups, respectively **(Fig 4; Pauling et al., 1951; Ramachandran et al., 1963)**. Values of φ and ψ dihedral angles are somewhat restricted due to (i) the constraints of ω dihedral angle, (ii) steric limitation from amino acid side-chains, and (iii) regular nature of the protein backbone **(Pauling et al., 1951; Ramachandran et al., 1963; Aurora et al., 1997)**. The three constraints imposed on the protein backbone, together with hydrogen bonding capacity of the backbone amide and carbonyl groups, cause that certain segments of the protein backbone exist as remarkably regular geometries, the so-called secondary structure elements – either helical **(Pauling et al., 1951)** or extended **(Pauling & Corey, 1951b; Pauling & Corey, 1951c; Pauling & Corey, 1951d; Pauling & Corey, 1951f)**.

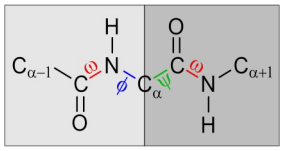

Fig 4 | Main-chain dihedral angles. Main-chain direction is defined by two dihedral angles, φ and ψ, between two planes (shaded by light and dark grey), determined by ω dihedral angle.

Amino acid residue propensities. Different amino acid residues show different propensities for being part of the secondary element, i.e. global propensities **(Penel et al., 1999)**. Additionally, in the case of a helical geometry, different amino acid residues show different propensities for being located at different positions within the helix, i.e. local propensities **(Penel et al., 1999)**, and also, except for Ala and Gly, adopting different side-chain conformations, (defined by χ_1 and χ_2 dihedral angles), depending on the position within the helix, i.e. rotamer propensities **(Doig et al., 1997; Penel et al., 1999)**. Although, the physical background for secondary structure propensities is not yet fully understood **(Avbelj & Fele, 1998)**.

Helical geometry. Helical geometry was first proposed for globular proteins, haemoglobin and myoglobin, and for fibrous proteins, α-myosin and keratin, by Pauling, Corey and Branson **(Pauling et al., 1951)** and its uniformly right-handed twist was identified by Kendrew and co-workers **(Kendrew et al., 1958; Kendrew et al., 1960; Kendrew, 1962)**. Helical geometry is the preferred state for the main-chain **(Pauling et al., 1951)** and thus the most abundant secondary structure geometry **(Ismer et al., 2008)**.

Three types of helices. There are three types of a helical geometry in proteins **(Ismer et al., 2008)** – α-helix, also known as "3.7-helix" **(Pauling & Corey, 1950; Pauling et al., 1951; Pauling & Corey, 1951a; Pauling & Corey, 1951d; Pauling & Corey, 1951e)**, 3_{10}-helix **(Richardson & Richardson, 1988)** and π-helix **(Low & Baybutt, 1952; Fodje & Karadaghi, 2002; Armen et al., 2003)**. They differ in (i) the number of residues per turn, (ii) the hydrogen bonding pattern they form, (iii) radius, and (iv) occurrence in proteins determined by stability of the particular helical geometry and by functional role **(Table 6 and Fig 5; Ismer et al., 2008)**. Of the three types of a helical geometry, α-helix is the most frequent, 3_{10}-helix is less frequent and π-helix is the least common **(Baker & Hubbard, 1984; Barlow & Thornton, 1988)**. 3_{10}-helix and π-helix can be present as transient defect structures in α-helices at low temperature (~ 0°) as a consequence of difference in relative thermodynamic stability, i.e. the difference in the free energy of formation between the three helical geometries **(Mikhonin & Asher, 2006)**.

Table 6 | Properties of helical conformations.

Property	**Helical conformation**		
	3_{10}	**α**	**π**
Occurrence in X-ray crystal structures of proteins (%)[a]	~ 20	~ 80	< 1
Number of amino acid residues per turn[a]	3.12	3.66	4.5
Hydrogen bonding pattern between NH and CO groups in the core of the helix[a]	i, i+3	i, i+4	i, i+5
Radius (Å)[a]	1.96	2.17	2.66
Unit rise (Å)[b]	2.0	1.5	1.2
Length (average number of amino acid residues)	3-5[c]	14[d]	7[b]
Special features	–	–	Cylindrical hole down the centre of the helix[e]

[a] According to Ismer et al. **(2008)**.
[b] According to Fodje & Karadaghi **(2002)**.
[c] According to Richardson & Richardson **(1988)**.
[d] According to Gunasekaran et al. **(1998)**.
[e] According to Low & Baybutt **(1952)**.

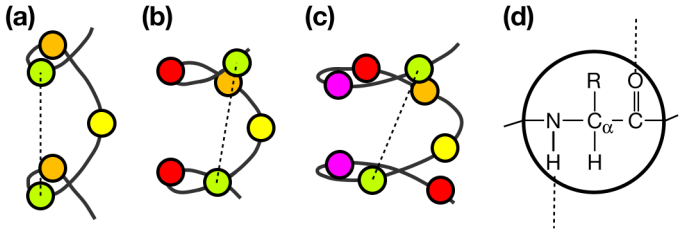

Fig 5 | Geometry of helical conformations. **(a)** 3_{10}-helix, **(b)** α-helix, **(c)** π-helix; amino acid residues are represented by spheres **(d)**. Main-chain hydrogen bonding is indicated by dashed lines. Redrawn according to Ismer **(2008)**.

Stabilising interactions in α-helix. α-helix is the most frequent secondary structure element in proteins **(Barlow & Thornton, 1988)**. With its mean length of 14 amino acid residues **(Gunasekaran et al., 1998)**, α-helix is by ten and seven amino acid residues longer than typical 3_{10}-helix and π-helix, respectively **(Richardson & Richardson, 1988; Fodje & Karadaghi, 2002)**, which is the consequence of easier elongation of α-helix compared to the other two types of helical conformation **(Rohl & Doig, 1996)**. α-helix-forming tendencies of amino acid residues are determined by loss of side-chain conformational entropy upon helix formation and possibility of compensation by stabilising interactions between side-chains or between side-chain and backbone **(Aurora et al., 1997)** because the first four amide hydrogens, amino acid residue positions denoted as N-cap **(Presta & Rose, 1988; Aurora & Rose, 1998)**, N1 **(Cochran et al., 2001)**, N2 **(Cochran & Doig, 2001)** and N3 **(Iqbalsyah & Doig, 2004)**, and last four carbonyl oxygens, amino acid residue positions denoted as C3, C2, C1 and C-cap **(Presta & Rose, 1988; Aurora & Rose, 1998)** of protein backbone in α-helix necessarily lack intra-helical hydrogen bonds **(Richardson & Richardson, 1988; Aurora & Rose, 1998)**. These unsatistifed atoms are capped by alternative hydrogen bond partners, hydrophobic interactions **(Aurora & Rose, 1998)**, and electrostatic interactions between side-chains of terminal amino acid residues and the partial charges on unsatisfied polar groups **(Shoemaker et al., 1987; Avbelj & Fele, 1998; Avbelj, 2000)**. The hydrogen bonds are donated by conventional OH and NH groups **(Aurora & Rose, 1998; Penel et al., 1999)** and remarkably also by non-conventional CH, CH_2 and CH_3 groups **(Pauling, 1960; Green, 1974; Jeffrey & Maluszynska, 1982; Derewenda et al., 1995; Vargas et al., 2000; Scheiner et al., 2001; Manikandan & Ramakumar, 2004)**. The non-conventional C-H...O hydrogen bonds are by no means insignificant, because for every three conventional hydrogen bonds in α-helix there are two C-H...O hydrogen bonds **(Manikandan & Ramakumar, 2004)**. The non-conventional C-H...O hydrogen bonds in α-helices account for ~ 58% of all C-H...O hydrogen bonds in a protein thus singifying their importance for stabilisation of α-helices **(Manikandan & Ramakumar, 2004)**.

Amino acid propensities in α-helix. The most prominent amino acid residue propensity features of α-helix are (i) strong energetic and structural "preferences" for N1, N2 and N3 differing greatly one to each other and from positions within α-helix interior **(Doig et al., 1997; Penel et al., 1999)**. Specifically, there are high propensities for negatively charged amino acid residues (ionic forms of Asp and Glu) at N-terminus **(Cochran et al., 2001; Cochran & Doig, 2001)** and positively charged amino acid residues (ionic form of His) at C-terminus of α-helix **(Shoemaker et al., 1985)**, giving rise to α-helix dipole moment **(Chou & Fasman, 1974; Wada, 1976; Hol et al., 1978; Sheridan et al., 1982; Shoemaker et al., 1985; Shoemaker et al., 1987)**, Note, the term "α-helix propensity" does not mean "α-helix preference" **(Creamer & Rose, 1992)** because α-helical conformation is the preferred state of the backbone **(Pauling & Corey, 1951f)**, whereas α-helix-disfavouring factors must arise in the side-chains **(Creamer & Rose, 1992; Aurora et al., 1997)**. Among all the amino acid residues, the side-chain of Ala is the least destabilising **(Merutka & Stellwagen, 1990b; Creamer & Rose, 1992)**.

3_{10}-helix. 3_{10}-helix can be formed at N- and C-termini of α-helices **(Baker & Hubbard, 1984; Barlow & Thornton, 1988)** as an intermediate in the (un)folding of α-helices **(Millhauser, 1995)**. Such a free interconversion between α- and 3_{10}-helical geometries is possible due to absence of a disallowed region of backbone conformational space, defined by φ and ψ dihedral angles, for L-amino acid residues **(Rohl & Doig, 1996; Armen et al., 2003)**. Initiation of 3_{10}-helix is easier than α-helix because one fewer amino acid residue needs to be fixed in a helical conformation before the first hydrogen bond is formed **(Rohl & Doig, 1996)**. On the other hand, 3_{10}-helix elongation is much less favourable compared to α-helix. Therefore, 3_{10}-helix is usually only three to five amino acid residues long **(Richardson & Richardson, 1988)**. Another factor, influencing whether 3_{10}-helix or α-helix is favoured or whether both are possible, is the amino acid residue at N-cap position **(Doig et al., 1997)**. 3_{10}-helix is characteristic by high

propensity for His at the N-cap position, whereas Ser and Thr at the N-cap position disfavours 3_{10}-helix and favours α-helix, and Asp/Asn/Pro may lead to either 3_{10}-helix and α-helix **(Doig et al., 1997)**.

π-helix. π-helix is the least common among the three types of helices because of its lowest stability due to strong temperature dependence **(Ismer et al., 2008)** caused by (i) energetically unfavourable φ and ψ dihedral angles, (ii) presence of 1 Å hole down the centre of the π-helix which is, however, too narrow for access by a water molecule **(Low & Baybutt, 1952)** thus causing loss of van der Waals interactions, and (iii) higher number of residues (five) that must be oriented correctly before the first (i, i+5) hydrogen bond can be formed. Hence, initiation of π-helix is more entropically unfavourable compared to α-helix and 3_{10}-helix **(Rohl & Doig, 1996)**. For all these reaosns, π-helix has been long considered as extremely rare and unstable in proteins. However, according to recent estimates, ~ 10% of proteins contain a π-helix as a conserved structural feature among functionally related proteins **(Weaver, 2000; Fodje & Karadaghi, 2002)**. The least ease of initiation of π-helix among helical conformations is compensated by its high length, seven to thirteen amino acid residues long with the most common length of seven amino acid residues **(Fodje & Karadaghi, 2002)**. Additionally, π-helix has characteristic amino acid composition **(Fodje & Karadaghi, 2002)**. Asn shows extremely high propensity for middle of π-helix **(Fodje & Karadaghi, 2002)**. Aromatic amino acid residues (Phe, Trp and Tyr) and large aliphatic (Ile, Leu and Met) show high propensities for being located at termini of π-helix, thus providing stability to π-helix via favourable interactions between the termini of π-helix **(Fodje & Karadaghi, 2002)**. Pro shows extremely high propensity for position right after π-helix, thus causing termination of π-helix **(Fodje & Karadaghi, 2002)**.

Extended geometry. Unlike helical geometry, extended geometry, the so-called β-strand, cannot exist on its own because the hydrogen bonding pattern must be established between two sequentially distal segments with extended geometry along the protein backbone. Therefore, β-strand, exists due to higher hierarchy geometry – a β-sheet, first observed in β-keratin **(Pauling & Corey, 1951b; Pauling & Corey, 1951c; Pauling & Corey, 1951d; Pauling & Corey, 1951f)**.

1.2.3 Tertiary structure

Secondary versus tertiary structure. Helices and β-sheets can both be considered as well to the secondary as to the tertiary structure elements **(Creamer & Rose, 1992; Yang & Honig, 1995a; Yang & Honig, 1995b; Pal & Chakrabarti, 2000)** because helix and strand formation are guiding events in protein folding **(Cohen et al., 1979; Aurora et al., 1997; Baldwin & Rose, 1999a; Baldwin & Rose, 1999b; Gong et al., 2005; Rose et al., 2006)** and their properties are influenced by interaction with rest of the protein **(Scholtz et al., 1991; Creamer & Rose, 1992; Otzen & Fersht, 1995; Yang & Honig, 1995b)** and surrounding solvent **(Tanford et al., 1960; Blundell et al., 1983; Nelson & Kallenbach, 1986; Buck et al., 1993; Jasanoff & Fersht, 1994; Waterhous & Johnson, 1994; Blanco et al., 1994; Schönbrunner et al., 1996; Luo & Baldwin, 1998; Avbelj & Fele, 1998)**.

Tertiary aspects of α-helices. α-helices in globular proteins have the following interdependent properties **(Kumar & Bansal, 1998)**: (i) position in the protein sequence; (ii) length; (iii) amino acid residue composition; (iv) geometry; and (v) position in the globular protein. The mean length of α-helix depends on its curvature and is 12 ± 3, 14 ± 5 and 20 ± 6 amino acid residues for linear, curved and kinked α-helices, respectively, with no correlation between the geometry and α-helix position in the globule. The amino acid residue composition depends on position in the globular protein, α-helix geometry and length. α-helices with large curvature show increased propensities for Leu, Gln, Lys and Cys; kinks are often associated with presence of amino acid residues with low α-helix propensities. Amino acid residues with larger side-chains or side-chains with larger number of functional groups more frequently occur in longer α-helices. Position of an α-helix in the globular protein can be classified into three categories: largely buried, partially buried or largely exposed; 66% of α-helices belong to the first category. Most importantly, as the result of arrangement of α-helix in the context of the rest of the protein sequence, it shows alternating pattern of hydrophobic and hydrophilic amino acid residues that gives rise to an amphipathic character of α-helix **(Schiffer & Edmundson, 1967; Xiong et al., 1995)** which is, for example, mainfested by increased propensity for hydrophobic amino acid residue and decreased propensity for polar and negatively charged amino acid residues at N1 position compared to N2 because of larger burial of N1 compared to more solvent exposed N2 position **(Penel et al., 1999)**.

α-helix stability in globular proteins. α-helical state would not be well populated without significant enhancement **(Creamer & Rose, 1992)**. The enhancement is realised by scaling, requiring, however, more than 100 amino acid residues long α-helix **(Creamer & Rose, 1992)**. α-helices in proteins have, however, only 14 amino acid residues on average, thus enhancement must be provided by a different mechanism – via interaction of the α-helix with other parts of the protein molecule **(Scholtz et al., 1991; Creamer & Rose, 1992)**, which additionally influences shape and amino acid residue propensities of α-helices.

Tertiary aspects of β-sheet. Due to absence of long-range dipole-dipole interactions in β-strands, the existence of β-strands is dependent on their mutual association via cross-strand main-chain–main-chain hydrogen bonding and side-chain–side-chain hydrophobic interactions into β-sheets, which requires bringing distal segments of the protein sequence close in space **(Yang & Honig, 1995b)**. Thus, β-sheets have elements of both secondary (β-strand) and tertiary (β-sheet) structure **(Pal & Chakrabarti, 2000)**. Therefore, although large hydrophobic amino acid residues show high propensities for β-sheet, the propensities of amino acid residues for β-sheet are context dependent, because β-sheet formation is not associated with individual amino acid residues but involves pairwise interactions between side-chains **(Otzen & Fersht, 1995; Yang & Honig, 1995b)**. Yet another characteristic feature of β-sheets is that they are invariably twisted in the right-handed direction **(Richardson, 1976; Yang & Honig, 1995b)**; the dominant determinant of the β-sheet twist are tertiary interactions with rest of the protein **(Yang & Honig, 1995b)**.

Architecture of β-sheet. There are three types of β-sheets – parallel, anti-parallel and mixed. Parallel β-sheet is composed of two or more β-strands running in the same direction; anti-parallel β-sheet is composed of two or more β-strands running in opposite directions; and mixed β-sheet is composed of both parallel and anti-parallel β-strands **(Fig 6)**. β-strands are topologically connected in β-sheet by a hairpin or a crossover. The former type of topological connection is also known as "plain" or "same end" connection; the latter is also known as "cross" or "opposite-end" connection and exists in two types, right- and left-handed **(Richardson, 1976)**.

Additional stabilising interactions in β-sheet. Besides the main-chain hydrogen bonding between adjacent β-strands and van der Waals interactions between hydrophobic side-chains of the β-strands, β-sheets are further considerably stabilised by electrostatic interactions **(Avbelj & Fele, 1998; Avbelj, 2000)** and non-conventional $C_\alpha H$...OC hydrogen bonds **(Derewenda et al., 1995; Fabiola et al., 1997)**. The strength of these hydrogen bonds can be as much as a half of the strength of conventional hydrogen bonds **(Vargas et al., 2000; Scheiner et al., 2001)**, which is -5 kcal mol^{-1} on average **(McDonald & Thornton, 1994)**. Additionally, the non-conventional hydrogen bonds involving side-chain CH groups are also extensively present in β-sheets **(Fabiola et al., 1997)**. Propensities for being involved in CH...OC hydrogen bonding interactions varies among amino acid residues with clear preference for Val and Thr **(Fabiola et al., 1997)**.

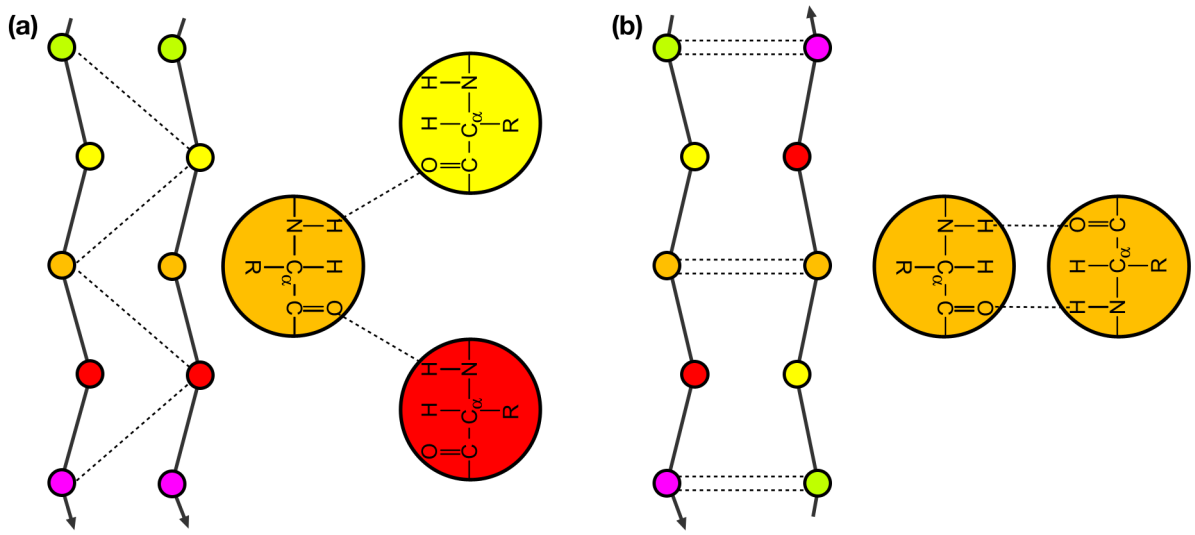

Fig 6 | Geometry of β-sheet. **(a)** Parallel β-sheet, **(b)** anti-parallel β-sheet; main-chain hydrogen-bonding is indicated by dashed lines; amino acid residues are represented by spheres; direction of protein backbone is indicated by arrows. Anti-parallel β-sheet is more stable due to parallel hydrogen bonds.

β-bulges. Regular arrangement of β-strands in β-sheet can be disturbed by one amino acid residue insertion or deletion, causing presence of a β-bulge, i.e. region between two consecutive β-type main-chain hydrogen bonds **(Richardson et al., 1978)**. β-bulge consists of two amino acid residues on one β-strand and one amino acid residue on the other β-strand, causing slight bend in the β-sheet **(Richardson et al., 1978)**. β-bulges mostly occur between anti-parallel β-strands whereas they are extremely rare in parallel β-strands **(Richardson et al., 1978)**. β-bulges are thought to be an evolutionary conserved feature because they function to (i) compensate for effects of single amino acid residue insertion or deletion within the β-sheet, (ii) provide strong local twist which is required to form closed β-barrel structures, (iii) influence direction in which β-strand leaves the β-sheet, and (iv) influence orientation of functionally critical side-chains **(Richardson et al., 1978)**.

Packing of α-helices and β-sheets in globular proteins. Taking together, secondary elements are not isolated one to each other but pack **(Crick, 1952; Pauling & Corey, 1953)** via strand-strand (to form β-sheet), helix-helix, helix-sheet and sheet-sheet interactions **(Chothia et al., 1977)**. The arrangement of secondary structure elements is such as to allow (i) the secondary structure elements to occupy conformations close to the free energy minimum, and (ii) buried amino acid residues to occupy the same volume as if they were free amino acids **(Chothia et al., 1977)**. α-helices associate via packing of ridges of one α-helix into grooves of another α-helix **(Chothia et al., 1977)**. Deviations from the idealised model depends on the twist and exact radius of α-helices and on the size of side-chains **(Chothia et al., 1977)**. If two adjacent α-helices are arranged in opposite direction they can interact more favourably due to interactions of macrodipoles of the α-helices **(Shoemaker et al., 1985)**. Thus, α-helix dipole may be an important factor in protein folding **(Shoemaker et al., 1985)**. α-helix can pack onto β-sheet with its axis being (i) equal to zero, i.e. α-helix is arranged in parallel to the β-strands of the β-sheet, providing continuous helix-sheet contact, (ii) < 0, i.e. helix-sheet contact occurs in the middle, and (iii) > 0, helix-sheet contacts occur at the ends, providing an internal cavity **(Chothia et al., 1977)**. Sheet-sheet packing can be established by packing of a single β-sheet folded over by means of a local right-handed supertwist or by two independent β-sheets with rotation between the β-sheets influencing regions of strongest contacts: the larger is the rotation, the stronger are the contacts in the middle compared to the rest of the β-sheets **(Chothia et al., 1977)**.

Globular protein structure. Secondary elements cannot, for steric reasons, follow one another directly **(Rose et al., 2006)**, and are therefore interspaced by turns, also known as "tight turns", or loops, also known as "loose turns" or "random coils" **(Chou, 2000)** which together account for about half of protein structure on average **(Fitzkee et al., 2005a)**. Although, turns are sometimes considered to belong among secondary structure elements **(Barlow & Thornton, 1988)**. The protein interior is comprised almost exclusively of residues from either helices or strands, because of their capacity to provide buried main-chain carboxamides with intramolecular hydrogen bonding partners **(Stickle et al., 1992)** whereas turns and loops are more frequently located at solvent-exposed regions of the globule. Turns and loops allow main-chain direction reversal and thus packing of the secondary elements into globular, tertiary structure **(Kendrew et al., 1958; Kendrew et al., 1960; Chou, 2000)**, with rugged surface with clefts, and with cavities in the interior of the globule **(Fig 7)**. Presence of clefts and cavities in globular proteins is a consequence of heterogenous packing because some highly ordered regions are being mixed with many regions not as highly ordered **(Socolich et al., 2005)** due to liquid-like rather than solid-like distribution of packing intensities **(Liang & Dill, 2001; Lindorff-Larsen et al., 2005)**.

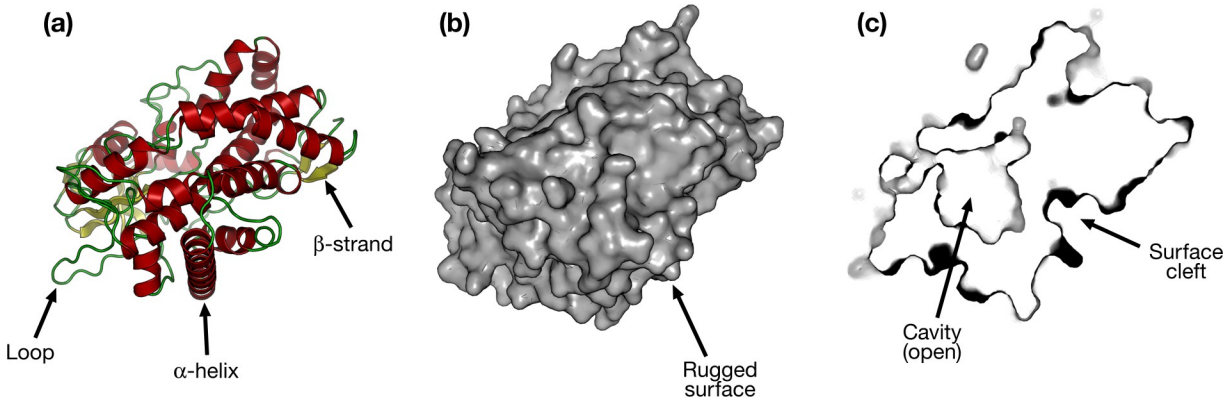

Fig 7 | An example of a globular protein (cytochrome P450eryF from *Saccharopolyspora erythraea*; PDB-ID 1Z8O). **(a)** Cartoon representation of a globular protein showing presence and arrangement of α-helices (red) and β-sheets (yellow), connected by loops and turns (green); **(b)** surface representation of protein showing overall globular shape and rugged surface; **(c)** slice through the surface representation showing surface clefts and an internal cavity open to the surface at two sites. Depending on the context, cavity can be also called "pocket" (in the context of a ligand binding/unbinding) or "tunnel/channel" (in the context of a ligand ingress/egress).

Turns. There are five classes of turns distinguished according to number of amino acid residues: α-turn composed of five amino acid residues **(Toniolo, 1980)**, β-turn composed of four amino acid residues of which i+1 or i+2 is Gly, **(Venkatachalam, 1968)**, γ-turn composed of three amino acid residues **(Némethy & Printz, 1972)**, δ-turn composed of two amino acid residues **(Toniolo, 1980)** and π-turn composed of six amino acid residues) **(Toniolo, 1980)**. β-and γ-turn can connect β-strands of anti-parallel β-sheet **(Venkatachalam, 1968; Némethy & Printz, 1972)**. Each type of turn has several different trajectories to reverse the main-chain direction which is reflected by different sub-types

of turns **(Chou, 2000)**. Turns share two common features: (i) distance between C_α of first and last amino acid residues is < 7 Å, and (ii) in most cases, intra-turn hydrogen bond is formed between CO group of the first and NH group of the last amino acid residue. Turns also have specific amino acid residue propensities, although amino acid residue sequences in turns are much more variable compared to secondary structure elements **(Yang et al., 1996)**.

Loops. Loops are formed by more than six amino acid residues that connect two adjacent secondary elements or form N-terminal or C-terminal tail of the protein **(Chou, 2000)**. Due to higher length of loops compared to turns, loops show higher structural variability and thus also significantly contribute to the arrangement of secondary elements in the globular proteins. The structural variability does not necessarily mean that loops are unstructured, but rather that there are larger number of possible architectures and interactions in loops that precludes classification **(Chou, 2000)**. Loops show the same types of interactions as made by secondary structure elements. Additionally, two loops can be kept in proximity to each other by a β-bridge interaction, i.e. a β-sheet-like main-chain–main-chain hydrogen bonding interaction between one amino acid residue provided by one loop and two amino acid residues from another loop **(Kabsch & Sander, 1983)**.

Protein backbone distorsions. Local constraints, e.g. requirement for sharp change in protein backbone direction and/or overcoming steric clashes, may impose strain to force φ and ψ protein backbone dihedral angles into unusual values. If present in the protein structure, the unusual φ and ψ dihedral angles are most frequently associated with Asn, Asp, His, Ser and Thr, whereas infrequently with bulky hydrophobic amino acid residues. Typically, the unusual φ and ψ dihedral angles more frequently occur in long irregular segments and less frequently in short segments up to five amino acid residues. Some such strained irregular segments are involved at N- and C-termini of α-helices and β-strands **(Gunasekaran et al., 1996)**. Importantly, unusual φ and ψ angles can be associated with biological role **(Petock et al., 2003)** and hence can be conserved in structurally and/or functionally related proteins **(Gunasekaran et al., 1996)**.

Protein folding. The process of attaining functional tertiary structure of a protein, the so-called folding, is the last step during conversion of genetic information into biological function **(Zeeb & Balbach, 2004)**. During the process of folding, polypeptide chain of specific sequence switches from unfolded to specific native structure, the so-called fold or domain that can be regarded as a specific structural, functional and evolutionary unit, although definition of a protein domain is fuzzy in literature **(Rose et al., 2006)**. Folding occurs: (i) spontaneously; (ii) with the aid of chaperones and chaperonines **(Demchenko, 2001)**; (iii) according to protein template, e.g. folding of IA3 protein with aspartic proteinase A serving as the template **(Li et al., 2000)** and formation of inclusion bodies as an extreme case of template (mis)folding **(Demchenko, 2001)**; (iv) on protein-protein fragments association, e.g. folding of ribonuclease A, staphylococcal nuclease, cytochrome c, thioredoxin and barnase **(Demchenko, 2001)**, or folding is preceded by self-assembly, e.g. folding of Trp receptor **(Demchenko, 2001)**. Chaperones and chaperonines function by minimising aggregation largely by binding to partially folded proteins in a nucleotide dependent reaction that sequesters the proteins from one another, thereby reducing their effective concentration while they are afforded the opportunity to fold **(Mu et al., 2008)**. Chaperones exhibit broad but well-determined substrate specificity with absence of highly specific protein recognition features **(Demchenko, 2001)**. Hence, a protein folds according to its primary protein structure, or in other words, every protein contains all the information needed to reach the final fold **(Anfinsen et al., 1961; Kendrew, 1962)** while the folding is eventually guided by interactions with other protein(s) that have co-evolved with the protein **(Jager et al., 2008)**.

Folding pathway hypothesis. In late 1960s, Levinthal proposed, that protein sequence includes also information on intermediate states of folding that define the folding pathway, i.e. a sequence of events which follow one another so as to carry the protein from the unfolded to a uniquely folded state **(Fig 8b; Levinthal, 1968; Levinthal, 1969)**. Levinthal argued, that without such a folding pathway, random exploration of the practically infinite number of potential states would otherwise have made the folding in biologically relevant time, ranging from microsecond **(Myers & Oas, 2002; Liu et al., 2008)** to millisecond time-scale **(Rose et al., 2006)**, impossible, known as the so-called Levinthal paradox **(Fig 8a; Levinthal, 1968; Levinthal, 1969)**.

Folding funnel hypothesis. The folding pathway hypothesis was replaced by folding funnel hypothesis, pioneered by Anfinsen **(Fig 8cd; Anfinsen, 1973; Bryngelson et al., 1995; Dill & Chan, 1997; Chan & Dill, 1998; Deechongkit et al., 2006)**. The folding funnel hypothesis states that (i) folding is the process of searching for global energy minimum structure **(Anfinsen, 1973)**, (ii) energy landscape of all possible conformations has the shape of a funnel **(Anfinsen, 1973)**, (iii) folding occurs essentially via directed search by gradient towards a lower energy state, i.e. towards the bottom of a folding funnel **(Frauenfelder et al., 1991; Bryngelson et al., 1995)**, and (iv) every unique sequence has its own funnel **(Rose et al., 2006)**.

Energy landscape of a folding funnel. Depending on the energy landscape, the folding funnel can be approximated as smooth **(Fig 8c)** or rugged **(Fig 8d)**. Smooth folding funnel, an approximation for folding of some small single-

domain proteins (e.g. artificial WW domain), results in a two-state (also known as "down-hill" or "class I" or "HP+") folding process in which: (i) protein occurs "only" as either unfolded or native structure at any time; (ii) unfolding is often a reverse process of folding **(Chan & Dill, 1998)**; (iii) folding speed aproaches the theoretical maximum of ~ 0.1 to ~ 1 μs **(Hagen et al., 1996; Chang et al., 2003; Liu et al., 2008)** and (iv) rate-limiting is the conformational searching because of entropic barriers. Rugged folding funnel (also known as "class II" or "HP"), an approximation for folding of large multi-domain proteins, on the other hand, provides kinetic traps that can result in misfolding or aggregation into inclusion bodies **(Kane & Hartley, 1988; Demchenko, 2001)** due to fast collapse into the kinetic traps and slower barrier climbing out of the traps at some regions of the funnel **(Chan & Dill, 1998)**, which is manifested by presence of folding intermediates **(Anfinsen, 1973; Jager et al., 2008)**. In the case of the rugged folding funnel, both folding and unfolding can occurr via multiple and different pathways **(Ma et al., 2000)**. Importantly, difference between class I and II folding reactions lies not in the mechanism of their folding but only in the stability of their intermediates **(Baldwin & Rose, 1999b)**.

Protein folding bases. Fold is necessarilly the result of interaction of close and distal amino acid residues of the protein sequence. So far, however, consensus has not yet been reached as to whether the interactions between amino acid side-chains (side-chain–based protein folding) or between main-chain atoms (backbone-based protein folding) are crucial in the folding process.

Side-chain–based protein folding. Widely accepted side-chain–based protein folding is supported by the following arguments: (i) side-chains of the 21 natural amino acid residues are responsible for discrimination of a funnel energy landscape because the main-chain (except for Gly and Pro) is chemically equivalent and thus lacks the discriminative power **(Aurora et al., 1997)**; (ii) different amino acid residues prefer different location in secondary structure elements that pack to hide hydrophobic side-chains in the protein core and to expose hydrophilic side-chains to the outside water environment **(Kendrew, 1962)**, the so-called hydrophobic collapse phenomenon; (iii) α-helix is the preferred state for main-chain **(Pauling & Corey, 1951f)**, but some side-chains lose sufficient conformational entropy in an α-helix that they push the protein backbone towards the only other allowed region, extended, i.e. β-strand **(Aurora et al., 1997; Baldwin & Rose, 1999a)**. Thus, side-chain conformational entropy must play a crucial role in selecting between α-helix and β-sheet **(Aurora et al., 1997)**. Indeed, conformational transition from β-strand to α-helical conformation requires overcoming unfavourable free energy barrier of ~ 1.5 kcal mol^{-1} due to side-chain modulation of the free energies of local main-chain electrostatic interactions, which is large enough to account for the distinct propensities of amino acid residues in α-helix and β-sheet **(Avbelj, 2000)**.

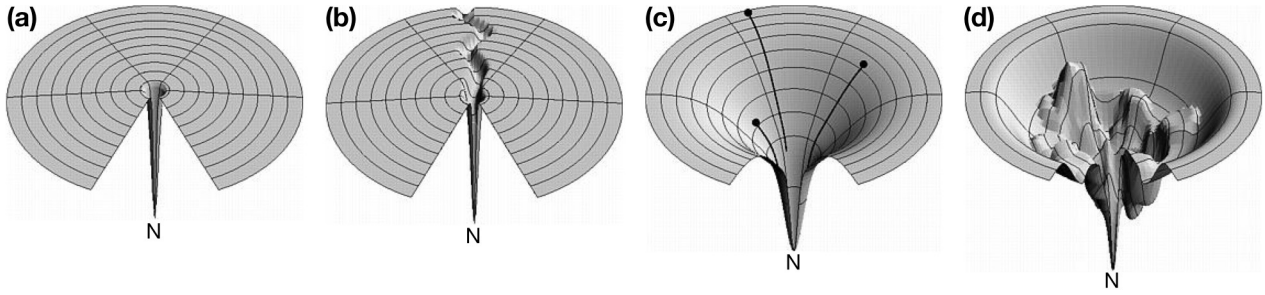

Fig 8 | Protein folding hypotheses. **(a)** Random search; **(b)** folding pathway; **(c)** smooth funnel; **(d)** rugged funnel. N – native fold. Adapted from Dill & Chan **(1997)**.

Side-chain–side-chain interactions. Side-chain–based protein folding signifies importance of interactions between side-chains for protein folding. Side-chains can interact by short range van der Waals and long range electrostatic interactions including conventional and non-conventional CH...O hydrogen bonds. Importantly, hydrophobic interactions are the primary stabilising factor of β-sheet **(Koehl & Levitt, 1999)**. Stabilisation of globular tertiary structure can be further enhanced by presence of a covalent disulphide bond between sulphydryl groups of two Cys amino acid residues in various structural patterns **(Mas et al., 1998; Mas et al., 2001; Gupta et al., 2004)**. The Cys amino acid residues for disulphide bridge interaction can be any of loops, β-strands or helical conformations **(Mas et al., 1998; Mas et al., 2001; Gupta et al., 2004)**. Salt bridges can significantly, by as much as -17 kcal mol^{-1}, contribute to stability of a folded protein **(Baldwin, 2007)**. Protein stability is thus dependent on pH due to differences between pK_a values of the amino acid residues in the native and unfolded state of the protein and inversely, protein structure affects the pK_a values of amino acid residues, thus influencing protonation state of ionisable side-chains **(Baldwin, 2007)**. While side-chain–side-chain interactions can be favourable in the folded protein and thus provide stability to protein **(Burley & Petsko, 1985; Matthews et al., 1987; Matsumura et al.,**

1989; Serrano & Fersht, 1989; Serrano et al., 1990; Serrano et al., 1991; Anderson et al., 1993; Clarke & Fersht, 1993; Britton et al., 1995; Waldburger et al., 1995; Thapar et al., 1996; Mansfeld et al., 1997; Strop & Mayo, 2000; Pace et al., 2000; Makhatadze et al., 2003; Schwem et al., 2003; Puchkaev et al., 2003; Eijsink et al., 2005), significance of these effects is not yet fully understood **(Gray et al., 2001; Eijsink et al., 2004)**. Moreover, presence of such interactions does not specify their role in the folding process **(Rose et al., 2006)**. Furthermore, folding is associated with, and thus opposed by, a loss of conformational entropy **(Pal & Chakrabarti, 1999; Chakrabarti & Pal, 2001; Penel & Doig, 2001; Jarymowycz & Stone, 2006)**, especially for closely packed buried amino acid residues that can be even locked into a single rotamer **(Penel & Doig, 2001)**. Hence, although widely accepted, side-chain–based protein folding may not be ultimately the correct view **(Rose et al., 2006)**.

Backbone-based protein folding. Alternative theory of protein folding mechanism, backbone-based protein folding, has been recently proposed by Rose et al. **(2006)**, who argue the following: (i) unfolded state is preorganised thus entropy loss upon folding is not so large; (ii) side-chains play only limited role in selecting between secondary structure elements and loops; (iii) hydrogen bonding predominates during protein folding over hydrophobic collapse **(Baldwin, 2007)**; (iv) folding reaction is all-or-none process with proteins either folded or unfolded, whereas there is only a negligible population of partially folded intermediates implying that conformation and stability are two separable features, which is manifested by the fact, that protein folding, in contrast to stability, is only marginally influenced by specific amino acid residue interactions of a protein **(Oliveberg, 2001)**; (v) osmolytes fold proteins by influencing the unfolded population; (vi) regardless of protein sequence, most proteins fold and unfold under similar conditions; (vii) there is only limited number of protein domains **(Chothia, 1992)**; (viii) hydrogen bonding is important determinant of secondary structures, thus even the unfolded protein may possess some regions of secondary structure elements; indeed, even in unfolded state, α-helices do not melt to random coil conformations, but rather exist in polyproline II conformation consisting of left-handed helices with three amino acid residues per turn, where the peptide bonds are hydrogen bonded to water **(Barron et al., 1997; Fleming et al., 2005; Mikhonin & Asher, 2006)**; individual amino acid residues in unfolded protein cluster in the α-helix, β-sheet and polyproline II regions of φ and ψ dihedral angle space and they flicker between these regions at rates ~ 10^{12} s^{-1} at room temperature **(Barron et al., 1997)**; (ix) not only sequence-dependent funnel landscape but also structure-dependent but sequence-indifferent landscape imposes major constraints on any sequence-dependent folding model; (x) local protein backbone steric restrictions cause that e.g. three or more amino acid residues in α-helical conformation cannot be immediately followed by amino acid residue from β-sheet without encountering a steric clash; (xi) top-down protein architecture is a consequence of bottom-up self-assembly process **(Rose, 1979)**.

Folding mystery. Despite the immense number of interactions between amino acid residues, the free energy difference between native and unfolded state is only ~ 5 to ~ 15 kcal mol^{-1} which corresponds to the energy of single to three conventional hydrogen bonds **(Jarymowycz & Stone, 2006; Rose et al., 2006)**. It remains a mystery how such a small difference can be sufficient to guide the folding towards the bottom of the funnel-shape free energy landscape and what kind of interactions are crucial during this process **(Socolich et al., 2005; Rose et al., 2006; Baldwin, 2007; Schmidt & Lamzin, 2007; Lupas, 2008)**, especially when considering that number of conceivable native to unfolded pathways for even a small protein of 100 amino acid residues is of the order at least 10^{30} and possibly much larger **(Fitzkee et al., 2005b)**.

Robustness of protein folds. Protein folds evolved from small, manifested by occurrence of structurally similar fragments in contemporary proteins **(Lupas et al., 2001)**, towards larger size **(Koshland Jr., 1976; Koshland Jr., 1998)** with typical contemporary protein having ~ 300 amino acid residues **(Kent, 2009)** which imposes robustness to the fold even in the protein core **(Matthews, 1993)**. The robustness means that: (i) many protein amino acid residues simply serve as scaffolding for the final orientation of a few critical amino acid residues in appropriate alignments **(Koshland Jr., 1976)**; (ii) some changes in the protein sequence, especially in surface-exposed loops, are tolerated without any significant effect on the specific native protein fold **(Pascarella & Argos, 1992)** whereas others, especially those involving amino acid residues located in buried parts of protein structure and those involved in α-helices and β-sheets are more constrained and thus less prone to fixation of such a mutation **(Koehl & Levitt, 1999)**; (iii) mutations often reduce stability but rarely alter overall fold **(Chothia & Lesk, 1986; Dalal et al., 1997; Baldwin & Rose, 1999b; Orengo et al., 2002)**.

Protein domain space. Considering the robustness of protein folds greatly reduces the protein folding problem because current estimates suggest that there are altogether only ~ 10^4 folds used in nature **(Chothia, 1992; Govindarajan et al., 1999; Vitkup et al., 2001)**. The folds are conventionally classified according to secondary structure composition and arrangement into mainly/all α-folds, mainly/all β-folds, mixed (α+β)-folds with β-sheet preceded or followed, but not interrupted, by α-helices, mixed α/β-folds with α-helices present in some connections between β-strands of a β-sheet, and unclassified folds **(Murzin et al., 1995; Orengo et al., 1997; Hubbard et al.,**

1998; Cuff et al., 2009). Other folds have been either not yet sampled by the evolutionary process as demonstrated recently by de novo design of a novel globular protein fold, Top7 **(Fig 9; Kuhlman et al., 2003)** or have been explored but have not found useful, or are not possible due to physical constraints **(Kuhlman et al., 2003)**. These considerations suggest that free energy landscape is presculpted **(Hoang et al., 2004)** into a few thousands of intrinsically stable domains unmasked upon switching from unfolding to folding conditions, thus specific sequences, selected during evolution, are needed to discriminate among the possibilities in this repertoire **(Rose et al., 2006)**. Hence, there must be rather a limited but specific number and distribution of amino acid residues and interactions **(Socolich et al., 2005)**, the so-called conformational gatekeepers **(Otzen & Oliveberg, 1999)** that determine the protein fold **(Kendrew, 1962; Koshland Jr., 1976; Otzen & Oliveberg, 1999; Oliveberg, 2001; Friedberg & Margalit, 2002; Socolich et al., 2005; Deechongkit et al., 2006; Jager et al., 2008)**. These amino acid residues are essentially conserved and co-evolved **(Socolich et al., 2005)**.

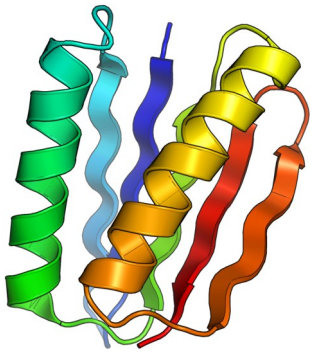

Fig 9 | Top7 de novo fold. Top7 fold (PDB-ID 1QYS) is a successfully computationally designed novel 93-amino acid residue α/β-fold with novel sequence and topology. The Top7 fold is composed of five-stranded anti-parallel β-sheet, packed on one side by two α-helices. The topology of the Top7 fold is: β2-β1-α1-β3-α2-β5-β4. N-terminus, blue; C-terminus, red.

Evolution of protein folds. From evolutionary point of view, limited number of protein folds is a consequence of either divergent and convergent evolution. Protein folds related via divergent evolution are homologues, i.e. they evolved from a common ancestor and mostly share similar tertiary structure due to the fact that tertiary protein structures are much more highly conserved during evolution than protein sequences **(Chothia & Lesk, 1986; Dalal et al., 1997; Baldwin & Rose, 1999b; Orengo et al., 2002)**. At low sequence identities, a significant proportion of homologues are likely to be paralogues, i.e. relatives tha have arisen through gene duplication within a genome and often acquired new functions **(Reeves et al., 2006)**. Protein folds related via convergent evolution evolved from disimilar protein sequences into similar, but not homologeous, tertiary protein structures due to limitation of possible number of arrangements of secondary structure elements in three-dimensional space by physical constraints **(Kendrew, 1962; Gibrat et al., 1996; Orengo et al., 1998)**.

Fold embellishments. Similarity of homologeous tertiary structures can be obscurred via permutations, rearrangements, and accretions, i.e. larger insertions and deletions **(Lupas et al., 2001)**. The accretions are thought to originate via gene duplication and/or fusion and shuffling, the processes that are considered to be the main mechanisms of origin of new genes within the frame of RNA world hypothesis **(Lupas et al., 2001; Orengo et al., 2002)**, and are often associated with different functions, e.g. changes in binding pocket, mediating domain-domain interactions and promoting oligomerisation states **(Teichmann et al., 1999; Reeves et al., 2006)**. The secondary structure embellishments often tend to be co-located in the globular protein and involve β-sheet or α-helices leading to up to more than two-fold difference in number of secondary structure elements between otherwise structurally similar proteins **(Reeves et al., 2006)**. α-helices are inserted as single elements, whereas β-sheet embellishments occur via peripheral additions, subtractions or extensions to existing β-sheets **(Reeves et al., 2006)** and they are responsible e.g. for variable number of β-strands (5 to 13) in the β-sheet of proteins possessing α/β-hydrolase fold **(Reeves et al., 2006)**. An extreme case of a fold embelishment is an acquisition of an entire domain leading to a multi-domain protein.

Fold change. Although typically, tertiary protein structure is more conserved than primary protein sequence

(Chothia & Lesk, 1986; Dalal et al., 1997; Baldwin & Rose, 1999b; Orengo et al., 2002), two homologeous proteins may possess different folds due to fold change via one or more of the following events **(Grishin, 2001)**: (i) insertions, deletions and substitutions; (ii) circular permutations on gene level **(Goldenberg, 1989)**, facilitated by gene duplication **(Russell & Ponting, 1998)**; (iii) circular permutations on protein level due to close proximity of N- and C-termini, e.g. cleavage and ligation of the two fragments in concanavalin A **(Cunningham et al., 1979)**; (iv) β-strand invasion or withdrawal; and (v) β-hairpin flip/swap rearrangements within β-sheet.

1.2.4 Quarternary Structure

Protein complexes. Some proteins fold on template of another protein **(Li et al., 2000; Demchenko, 2001)** or a pair of unfolded proteins form native folded structure only on the association **(Demchenko, 2001)**. Some proteins fold individually but exert biological function only in association with one or more other proteins (dimer to multimer), either same (homo-) or different (hetero-), or may form even higher hierarchical arrangement, macromolecular complex, e.g. ribosome **(Ramakrishnan & Moore, 2001)** and flagella **(Samatey et al., 2001)**. Because of limited number of protein folds, ~ 10^4 **(Chothia, 1992; Vitkup et al., 2001)**, there must be also limited number of protein-protein interaction types. Indeed, recent estimate suggests existence of ~ 10^4 protein-protein interaction types of which 2×10^3 is already known **(Aloy et al., 2005)**.

1.3 Protein function

1.3.1 Protein-ligand binding

Binding. Proteins essentially function by interaction with other proteins, nucleic acids or other macromolecules, or small molecules and ions, i.e. ligands, via the so-called binding **(Halperin et al., 2002; Manjasetty et al., 2008)**. In order for a protein to bind a ligand, it must be larger than ligand, provide three-dimensional binding site and show complementarity with ligand in both structure and interactions **(Koshland Jr., 1976)**. The interactions include hydrophobic interactions, van der Waals interactions, electrostatic interactions and hydrogen bonding interactions **(Copeland, 2000a)**. Proteins bind ligands into clefts or crevices on protein surface or into a pocket buried in the protein core, depending on ligand chemical nature. Hydrophilic ligands bind on rather exposed hydrophilic protein surface, whereas hydrophobic ligands prefer binding into a rather hydrophobic pocket and thus combat the major obstacle of a living system, which is not so much the need to "activate" water to react when needed as the need to prevent water from reacting in cases where it is not needed to do so **(Koshland Jr., 1976)**. Although almost all hydrophilic amino acid residues are located on protein surface, some of them can be buried and these rare exceptions have some special function within the protein **(Kendrew, 1962)**.

Determinants of protein-ligand binding. Protein-ligand complex formation depends on (i) concentration of both partners, the higher the concentration, the higher the chance of protein-ligand encounter, (ii) diffusion of the two binding partners, and (iii) affinity of a ligand to the binding site **(Gohlke & Klebe, 2002)**. In case of a buried binding site, there is an additional determinant of the protein-ligand association and dissociation: diffusion of a ligand into the buried binding pocket, which can occur via a tunnel or, for small ligands with zero net charge, through the protein matrix.

Protein-ligand binding affinity. Assuming a protein with a single binding site for a ligand, any molecule of protein is either free or ligand bound, and likewise, any ligand must be either free or bound to a protein **(Copeland, 2000b)**. Under any specific conditions, an equilibrium will be established between the free and bound forms of the protein, due to reversibility of protein-ligand complex formation **(Scheme 2) (Copeland, 2000b)**:

$$[P] + [L] \underset{k_{-1}}{\overset{k_1}{\rightleftharpoons}} [PL]$$

Scheme 2 | Protein-ligand binding.

The position of the equilibrium can be described quantitatively by the so-called dissociation constant, K_d **(Eq 1) (Copeland, 2000b)**:

$$K_d = \frac{[P][L]}{[PL]}$$

Eq 1 | Dissociation constant.

where [P], [L] and [PL] refer to concentration of protein, ligand and protein-ligand complex, respectively. Relative affinity, i.e. strength of binding, is inversely proportional to the dissociation constant: the tighter the ligand binds, the lower the value of the dissociation constant **(Copeland, 2000b)**. At equilibrium, the concentration of protein-ligand complex is constant. Assuming [P] << [L], the relationship between [P], [L], [PL] and K_d can be described by the so-called Langmuir isotherm equation **(Eq 2)**:

$$[PL] = \frac{[P]}{1 + \frac{K_d}{[L]}}$$

Eq 2 | Langmuir isotherm.

Formation of protein-ligand complex as a function of ligand concentration, the so-called binding isotherm, has typically hyperbolic shape **(Fig 10)**. However, if the assumption on [P] << [L] is not valid, which is the case of the ligand showing very strong affinity to the protein, then the relationship between [P], [L], [PL] and K_d cannot be described by the Langmuir isotherm, but instead using quadratic equation that is rigorously correct for any protein-ligand binding interaction **(Eq 3)**:

$$[PL] = \frac{[P] + [L] + K_d - \sqrt{([P] + [L] + K_d)^2 - 4[P][L]}}{2}$$

Eq 3 | Quadratic equation for protein-ligand binding.

The dissociation constant can be related to the Gibbs free energy of binding **(Eq 4)**:

$$\Delta G_{binding} = RT\ln(K_d)$$

Eq 4 | Gibbs free energy of binding.

where R is universal gas constant and T is temperature.

Biological response to protein-ligand binding. Binding of a ligand to the protein is a specific recognition process **(Koshland Jr., 1976; Gohlke & Klebe, 2002)** resulting in some kind of an action, i.e. biological response of the protein to the bound ligand. According to the response, two types of proteins can be distinguished – (i) non-catalytic, e.g. receptors and signaling proteins, and (ii) catalytic, the so-called enzymes. The latter respond, alone or with the aid of non-protein compounds, the so-called cofactors or coenzymes, to a specific bound ligand, a substrate, in an active site, by its chemical modification into another entity or entities, product(s) **(Schmidt & Lamzin, 2007)**, that finally leave the active site to free the space for another substrate to bind.

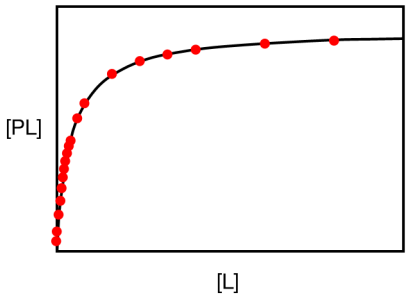

Fig 10 | Langmuir isotherm for protein-ligand complex, [PL], formation as a function of ligand concentration, [L]. Note, deviations from the hyperbolic shape occur for example when protein contains multiple non-equivalent binding sites. Redrawn according to Copeland **(Copeland, 2000b)**.

1.3.2 Protein fold, function and evolution

Protein fold and function. Protein folds differ by tendency to be associated with enzymatic or non-enzymatic functions **(Hegyi & Gerstein, 1999)**: α/β-folds are disproportionally associated with enzymes, especially transferases and hydrolases, whereas all-α-folds and small folds in general are associated with non-enzymes **(Hegyi & Gerstein, 1999)**. (α+β)-folds have an equal tendency either way **(Hegyi & Gerstein, 1999)**.

Functional variability and evolution. One function can be accomplished by more than one fold and vise versa **(Hegyi & Gerstein, 1999)**. It seems that nature tends to reinvent enzymatic function, i.e. convergent evolution, more often than modify already existing function, i.e. functional divergence **(Hegyi & Gerstein, 1999)**. The most versatile (promiscuous) enzymatic functions, hydrolases and O-glycosyl glucosidases, are associated with seven folds each **(Hegyi & Gerstein, 1999)**. The five most versatile folds are TIM-barrel **(Jones, 2003)**, Rosmann **(Hegyi & Gerstein, 1999)**, ferredoxin **(Hegyi & Gerstein, 1999)**, α/β-hydrolase (**Hegyi & Gerstein, 1999; Li et al., 2008)** and P-loop NTP hydrolase **(Hegyi & Gerstein, 1999)**. All these five folds are mixed α/β-folds which are thought to be generic scaffolds because they are capable of accommodating more than six functions **(Hegyi & Gerstein, 1999)**. For example, versatility of TIM-barrel fold, which is known to support over 60 different functions **(Watson et al., 2005)**, has been demonstrated by successful design of catalytic activity into enzymatically inert bacterial protein thioredoxin **(Bolon & Mayo, 2001)**, and versatility of α/β-hydrolase fold allows multiple possibilities of organisation of a functional amino acid residues via "migration" (also known as "hopping") within the protein primary sequence, without loss or change of function **(Todd et al., 2002)**. The functional group migration can occur towards stabilisation of protein structure and/or optimisation of less efficient proteins by loss of an "old" functional amino acid residue by mutation and recruitment of the new elsewhere in the protein **(Todd et al., 2002)**. The functional variability also depends on modular organisation of proteins. Multi-domain proteins show higher functional variability at a given sequence identity compared to single domain proteins with function similarity confidence level shifted from 40% for single-domain to 60% for multi-domain proteins **(Orengo et al., 2002)**.

Protein function in the context of a living organism. Even proteins with 100% identity, however, can have different functions depending on where they are expressed in a living organism **(Whisstock & Lesk, 2003)**. Thus, full understanding of protein function cannot be achieved by considering the protein function only in the context of the protein itself, but requires also considering the protein function in the context of entire metabolic network of the living organism **(Watson et al., 2005)**. Importantly, evolutionary selection acts on function, not on structure **(Russ et al., 2005)**. Therefore, whether particular change in the structure caused by mutation(s) **(Teichmann et al., 1999; Todd et al., 2001; Orengo et al., 2002)** becomes fixed depends on function of the mutant protein within the context of a complex ensemble of reactions in the living organism **(Gray et al., 2001)**. Since change in binding affinity does not necessarily lead to affected fitness of the living organism, whereas change or loss of function may have often adverse effect on the living organism, protein functions are more conserved than ligand specificities **(Teichmann et al., 2001)**.

1.3.3 Enzymes

Enzyme function. Enzymes are known to catalyse ~ 4000 different reactions **(Schomburg et al., 2004)**. According to catalytic function **(Caetano-Anollés et al., 2009)** but not guided by evolutionary considerations **(Valencia, 2005)**, enzymes are conventionally classified into six classes, defined by the first digit of the so-called Enzyme Commission (EC) number: oxidoreductases (EC 1), transferases (EC 2), hydrolases (EC 3), lyases (EC 4), isomerases (EC 5), and ligases (EC 6) **(Caetano-Anollés et al., 2009)**. Enzymes within each class are further distinguished by three subsequent digits, each providing increasingly detailed specification of enzyme function: the second digit (sub-class) specifies chemical compound or group involved in the reaction, the third digit (sub-subclass) specifies type of the reaction and the fourth digit (serial identifier) specifies metabolites and cofactors **(Caetano-Anollés et al., 2009)**.

Functional features of enzymes. Enzymes have two key inter-related functional features **(Copeland, 2000c; Copeland, 2000d; Copeland, 2000e; Copeland, 2000f; Copeland, 2000g, Copeland 2000h)**: (i) rate acceleration, described by enzyme kinetics (see 1.3.3.1) and by source of catalytic effect (see 1.3.3.2); and (ii) substrate specificity described by source of catalytic effect (see 1.3.3.2). These two features together define the enzyme reaction mechanism which is the key determinant of biological role of every enzyme.

1.3.3.1 Enzyme kinetics

Reaction progress curves. The enzyme-catalysed reaction usually comprises three steps: (i) substrate binding; (ii)

chemical modification; and (iii) product release **(Brown, 1902; Schmidt & Lamzin, 2007)**. Upon mixing enzyme with its substrate, enzyme-substrate encounter is followed by the loss of substrate and production of product **(Fig 11)**. At very early portion of the reaction, up to the time when about 10% of the initial substrate has been converted to product, the increase in product formation, and substrate depletion as well, is approximately linear with time **(Copeland, 2000c)**. For this limited time period, the so-called initial velocity (further "velocity"), v_0, can be approximated by the following equation **(Eq 5)**:

$$v_0 = \frac{-\Delta[\mathrm{S}]}{\Delta t} = \frac{\Delta[\mathrm{P}]}{\Delta t}$$

Eq 5 | Initial velocity.

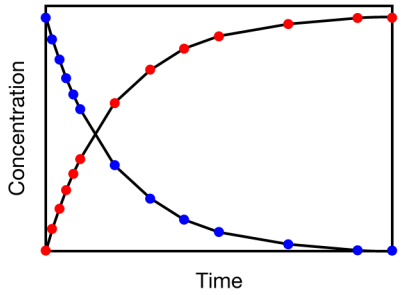

Fig 11 | Reaction progress curves for the loss of substrate (●) and production of product (●) during enzyme-catalysed reaction. Substrate depletion curve is the mirror image of the product appearance curve. Redrawn according to Copeland **(Copeland, 2000c)**.

Effects of substrate concentration on velocity. The velocity is apparently saturable at high substrate concentrations **(Fig 12; Copeland, 2000c)**. The qualitative description for the substrate dependence of enzyme-catalysed reaction was provided by Brown **(Scheme 3; Brown, 1902)**:

$$[\mathrm{E}] + [\mathrm{S}] \underset{k_{-1}}{\overset{k_1}{\rightleftharpoons}} [\mathrm{ES}] \xrightarrow{k_2} [\mathrm{E}] + [\mathrm{P}]$$

Scheme 3 | Brown scheme of enzymatic reaction.

where [E], [S], [ES] and [P] refer to concentration of enzyme, substrate, enzyme-substrate complex and product, respectively, k_1 is the rate constant for enzyme-substrate complex formation, k_{-1} is the rate constant for enzyme-substrate complex dissociation, and k_2 is the rate constant for chemical step of the reaction and product release. Depending on number of distinct chemical steps, k_2 is splitted into corresponding rate constants (i.e. k_2, k_3, k_4 etc.), which can be comprised into single k_{cat} rate constant **(Copeland, 2000c)**.

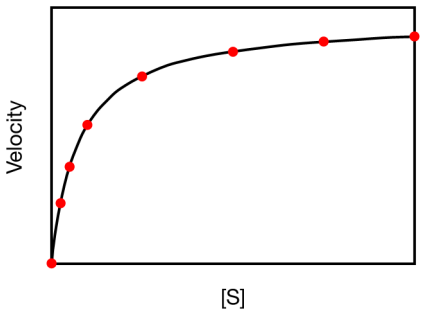

Fig 12 | Substrate dependence of enzyme-catalysed reaction velocities. Three distinct regions of the curve can be identified: (i) at low substrate concentration, [S], the velocity appears to display first-order behaviour, tracking linearly with substrate concentration; (ii) at very high [S], the velocity switches to zero-order behaviour, displaying no dependence on substrate concentration; (iii) in the intermediate region, the velocity displays curvilinear dependence on [S].

The rapid equilibrium model of enzyme kinetics. Assuming that a rapid equilibrium is established between the reactants, E and S, and the ES complex, followed by slower conversion of the ES complex back to free enzyme and product(s), i.e. assuming that $k_{cat} << k_{-1}$, and assuming [S] >> [E], Henri **(Henri, 1903)**, and Michaelis and Menten

(Michaelis & Menten, 1913) independently arrived to the following description of the reaction velocity as a hyperbolic function of [S], known as Henri-Michaelis-Menten equation **(Eq 6)**:

$$v = \frac{V_{max}[S]}{K_s + [S]} = \frac{V_{max}}{1 + \frac{K_s}{[S]}}$$

Eq 6 | Henri-Michaelis-Menten equation.

where K_s is equilibrium dissociation constant, k_{-1}/k_1, and V_{max} is maximum reaction velocity that is reached at infinite [S] **(Eq 7)**:

$$V_{max} = k_{cat}[E]$$

Eq 7 | Maximum velocity.

The steady-state model of enzyme kinetics. The rapid equilibrium model of enzyme kinetics is valid only if $k_{cat} << k_{-1}$. More general description of enzyme kinetics can be provided by steady-state model, that does not require $k_{cat} << k_{-1}$. The steady state refers to a time period of the enzymatic reaction after fast (millisecond time-scale) burst of ES formation. In the steady state, the rate of ES complex formation is exactly matched by its rate of decay to free enzyme and products, under the condition of [E] << [S] **(Copeland, 2000c)**. Since k_{cat} cannot be neglected, the steady-state expression for the reaction velocity **(Eq 8)** substitutes K_s by K_m **(Eq 9)**:

$$v = \frac{V_{max}[S]}{K_m + [S]} = \frac{V_{max}}{1 + \frac{K_m}{[S]}}$$

Eq 8 | Briggs-Haldane Equation.

$$K_m = \frac{k_{-1} + k_{cat}}{k_1}$$

Eq 9 | K_m constant.

Although **Eq 8** is different from **Eq 6**, it is commonly referred to as Henri-Michaelis-Menten equation **(Copeland, 2000c)**.

Significance of K_m. K_m, also known as "Michaelis constant", is the [S] that provides a reaction velocity that is half of the maximal velocity obtained under saturating substrate conditions **(Copeland, 2000c)**. In other words, K_m is the [S] at which half of enzyme active sites are filled with substrate in the steady state **(Copeland, 2000c)**. The lower the K_m, the lower [S] is needed to fill half of enzyme active sites with substrate, and thus the higher is the affinity of the substrate to the enzyme active site **(Copeland, 2000c)**. However, although K_m is considered as a good measure of binding affinity in most cases, since K_m depends also on k_{cat} **(Eq 9)**, it must be beared in mind that K_m can be less than, greater than, or equal to binding constant; hence K_m is referred to as "apparent binding constant" and should generally be considered as kinetic, not thermodynamic, constant **(Copeland, 2000c; Koshland Jr., 2002a)**. Only under the specific conditions that $k_{cat} << k_{-1}$ are K_m and K_s equivalent **(Copeland, 2000c)**.

Significance of k_{cat}. k_{cat} defines the maximal velocity at which an enzymatic reaction can proceed at a fixed concentration of enzyme and infinite availability of substrate **(Copeland, 2000c)**. In other words, k_{cat}, also known as "turnover number", defines number of catalytic turnover events that occur per unit time **(Copeland, 2000c)**. Since k_{cat} often reflects multiple chemical steps, it does not provide detailed information on the rates of any of the individual steps subsequent to the substrate binding **(Copeland, 2000c)**. Instead, k_{cat} provides a lower limit on the rate constant of the slowest, i.e. rate-limiting step following substrate binding **(Copeland, 2000c)**. Resolving individual chemical steps is possible at pre-steady state phase of enzyme-catalysed reaction (millisecond time-scale), i.e. before the equilibrium for [ES] is established **(Copeland, 2000c)**.

Enzyme performance. The best measure of enzyme performance is provided by k_{cat}/K_m ratio, which is sometimes referred to as "specificity constant". However, the term "specificity constant" can be deceptive, because conformational change, that might occur during enzymatic reaction, can be part of k_{cat} and/or K_m but k_{cat}/K_m does not evaluate either conformational change or the ability to discriminate between substrate structures **(Koshland Jr., 2002a)**. k_{cat}/K_m term summarises the net advantage or disadvantage of a mutation to the enzyme, and thus the term "performance

constant" seems to be a more accurate and descriptive designation for this concept **(Koshland Jr., 2002a)**. The higher is k_{cat}/K_m, the better is the enzymatic performance **(Koshland Jr., 2002a)**.

Enzyme perfection. The fact, that the enzyme has a maximum velocity for a given substrate under given conditions, that cannot be further enhanced by increased concentration of a substrate, is caused by limitation of enzyme activity caused by the slowest step along the reaction cycle, which can be any of rate of substrate binding, or any of the multiple steps contributing to k_{cat} **(Copeland, 2000c)**. Some enzymes, e.g. acetylcholinesterase or carbonic anhydrase, display k_{cat}/K_m values of 10^8 - 10^9 M^{-1} s^{-1}, which is at the diffusion limit **(Copeland, 2000c)**. Such enzymes are said to have achieved kinetic perfection, because they are limited by the rate of diffusion of molecules in solution **(Copeland, 2000c)**. The diffusion limit does not set an upper limit on the catalytic performance because it can be overcome by compartmentalisating themselves and their substrates within close proximity **(Copeland, 2000c)**. This can be accomplished by assembling enzymes and substrates into organised multienzyme complexes, e.g. at cellular membrane, in such a way that product of one enzymatic reaction, which is substrate for another enzyme, is channeled into the second enzyme without the need for diffusion through solution, hence the so-called substrate channeling mechanism **(Copeland, 2000c)**.

Deviation from Henri-Michaelis-Menten hyperbolic kinetics. Henri-Michaelis-Menten kinetics is valid only for catalytic reactions in homogeneous (water) phase. Lipase-catalysed lipolytic reactions which occur at the lipid-water interface cannot be described by Henri-Michaelis-Menten equations **(Jaeger & Reetz, 1998)**. Deviations from Henri-Michaelis-Menten kinetics can be also caused by inhibition and cooperativity **(Copeland, 2000c)**.

Enzyme inhibition. Inhibitors are substrates, products or other ions or molecules that decrease enzyme's activity by binding to the enzyme. Some inhibitors, the so-called reversible inhibitors, establish their binding equilibrium with the enzyme on a time-scale that is rapid with respect to the turnover rate of the enzyme-catalysed reaction **(Scheme 4; Copeland, 2000e)**:

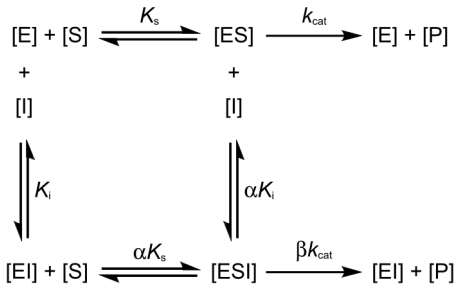

Scheme 4 | Equilibrium inhibition.

Depending on values of α and β factors, three types of inhibitor interaction with enzyme are distinguished: (i) competitive ($\alpha = \infty$, $\beta = 0$), (ii) non-competitive ($0 < \alpha < \infty$, $\beta = 0$) and (iii) uncompetitive ($\alpha << 1$, $\beta = 0$) **(Fig 13; Copeland, 2000e)**. Other inhibitors, the so-called tight-binding inhibitors bind to their target enzyme with such a high affinity that the population of free inhibitor molecules is significantly depleted by formation of enzyme-inhibitor complex **(Copeland, 2000f)**. Many tight-binding inhibitors establish equilibrium on the time-scale of enzymatic turnover, thus displaying a change in initial velocity with time **(Copeland, 2000g)**. Such inhibitors act as the so-called slow-binding or time-dependent inhibitors; three different modes of interaction between an inhibitor and enzyme can be distinguished to result in slow binding kinetics **(Fig 14; Copeland, 2000g)**. All these inhibitiory mechanisms are important for fine-tuning enzyme action in a complex metabolic network, but may also lead to an undesired defect in enzyme's biological role in the case of a non-natural inhibitor or non-natural concentration of an inhibitor supplied by external environment or by impaired (decoupled, imbalanced) elements of the metabolic network.

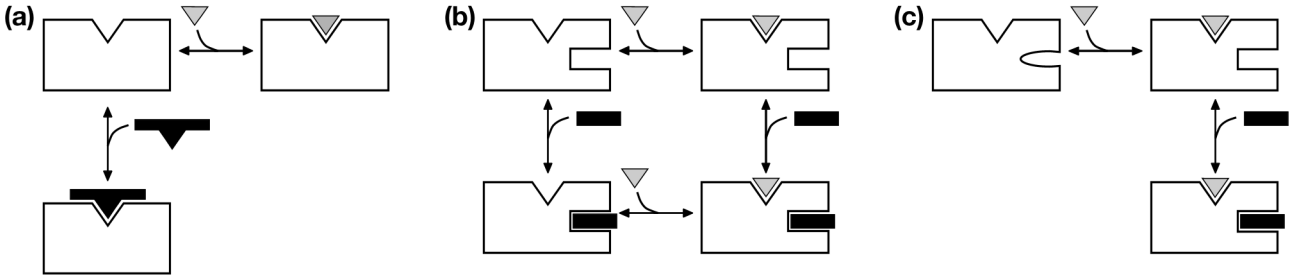

Fig 13 | Three types of inhibitor interactions with the enzyme. **(a)** Competitive inhibition, **(b)** non-competitive inhibition, **(c)** uncompetitive inhibition; enzyme, white; substrate, grey; inhibitor, black. Redrawn according to Copeland **(2000e)**.

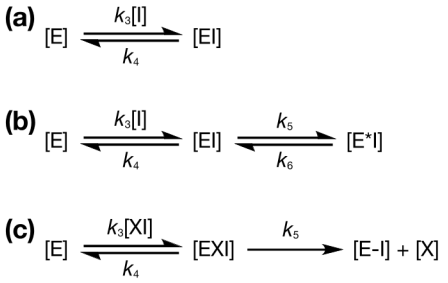

Fig 14 | Three types of time-dependent inhibition. **(a)** simple reversible slow binding, **(b)** enzyme isomerisation, **(c)** irreversible enzyme inactivation by affinity labeling/covalent modification or mechanism-based inhibition. The inhibition schemes describe competing reactions for enzyme-catalysed reaction in absence of inhibitor. Redrawn according to Copeland **(2000h)**.

Cooperativity. In some oligomeric enzymes, each subunit contains an active site centre for substrate binding and catalysis. The active sites can act independently on each other (no cooperativity) thus displaying classical Henri-Michaelis-Menten behaviour, or the binding of ligands at one active site of the enzyme can increase (positive cooperativity) or decrease (negative cooperativity) affinity to other active sites **(Copeland, 2000h)**. According to the so-called allostery concept, cooperativity is achieved via structural changes transmitted through protein; although, structural change does not necessarilly imply cooperativity **(Koshland Jr. & Hamadani, 2002)**. Allosteric effects can occur between separate binding sites for the same ligand, i.e. homotropic cooperativity, or by binding of a structurally unrelated ligand, the so-called allosteric effector, at a distant separate site, i.e. heterotropic cooperativity **(Copeland, 2000h)**. Ligands that cause positive and negative heterotropic cooperativity are referred to as allosteric activators and repressors, respectively **(Copeland, 2000h)**. Two major models were proposed to explain cooperativity in proteins **(Fig 15; Copeland, 2000h)**: (i) concerted transition or symmetry model, also known as "MWC model" **(Monod et al., 1965)** and (ii) sequential model, also known as "KNF model" **(Koshland Jr. et al., 1966)**. MWC model suggests that subunits change shape in concerted manner to preserve the symmetry of the entire molecule as it transforms from the conformation "T" to the conformation "R" under the influence of a ligand **(Monod et al., 1965)**. This model, however, does not explain negative cooperativity **(Koshland Jr. & Hamadani, 2002)**. KNF model is model of all three possible situations: positive cooperativity, negative cooperativity and no cooperativity **(Koshland Jr. et al., 1966; Koshland Jr., 1976; Koshland Jr., 1996)**. KNF model is based on (i) induced conformational changes transmitted through subunit interactions and (ii) capacity of the protein to be distorted which is the key programmed feature of the protein **(Koshland Jr. et al., 1966; Koshland Jr., 1976; Koshland Jr., 1996)**.

Role of cooperativity for protein function. Cooperativity is one of the well established phenomena that makes living possible **(Koshland Jr. & Hamadani, 2002)**. Positive cooperativity causes amplification of the sensitivity of signal. Negative cooperativity, on the other hand, decreases sensitivity to Henri-Michaelis-Menten behaviour but in the process of doing that, the negative cooperativity extends the range over which some response is generated **(Koshland Jr. & Hamadani, 2002)**.

Rate of enzymatic reaction. In summary, overall rate of enzyme action is dependent on (i) rate of diffusion, (ii) substrate binding affinity, (iv) chemical modification, i.e. type and complexity of the reaction and free energy

barrier(s), (v) product release, (v) presence/absence of cooperativity, (vi) presence/absence of inhibitors and mode of their action, and (vii) physicochemical parameters of the environment, e.g. temperature, pH, pressure, presence and concentration of inorganic and organic compounds.

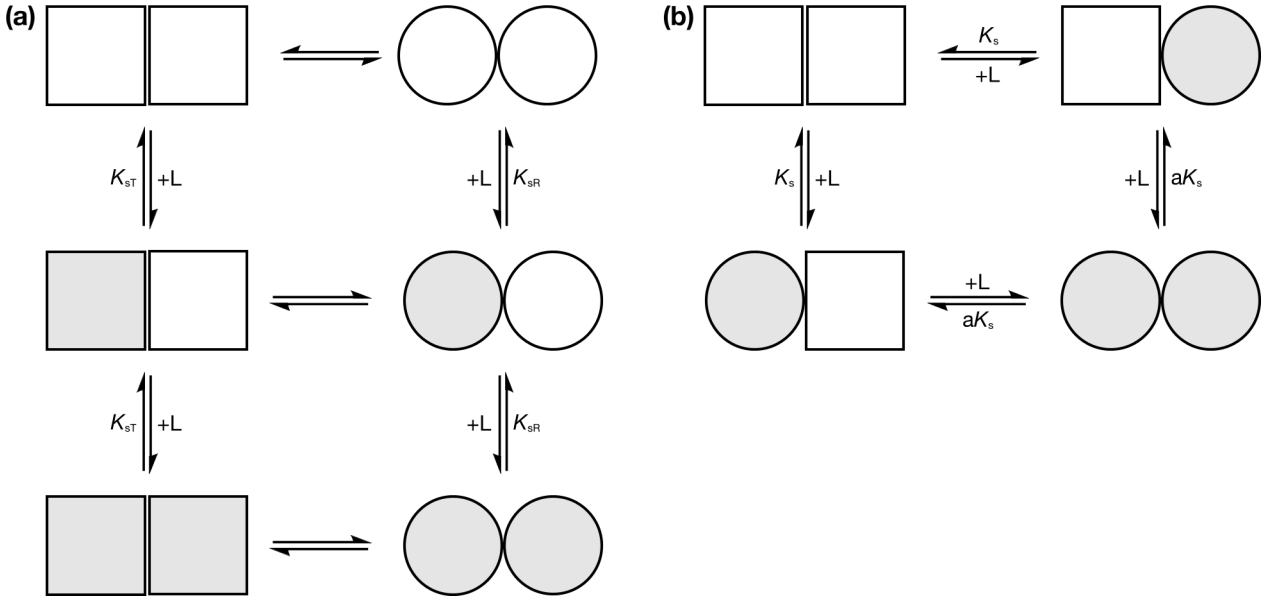

Fig 15 | Models of cooperativity. **(a)** MWC model of positive cooperativity, **(b)** KNF model of positive, negative and no cooperativity. In the KNF model, positive, negative and no cooperativity occurs when a < 1, a > 1 and a = 1, respectively. L, ligand; white shape, free protein; grey shape, protein-ligand complex. Redrawn according to Copeland **(2000h)**.

1.3.3.2 Catalytic effect

Key-lock model. Both substrate specificity and rate acceleration results from the precise three-dimensional structure of the active site **(Copeland, 2000d)**. In 1884, Fischer proposed the so-called key-lock model of substrate specificity based on observation that invertase from beer yeast hydrolyses α-glucoside but not β-glucosides while emulsin operates oppositely, i.e. enzyme and glucoside have to fit to each other like a lock and key in order to exert a chemical effect on each other **(Fig 16; Fischer, 1894)**. The key-lock theory was further supported by steric repulsions in organic reactions and by the fact that kinetics of enzyme action is compatible with an enzyme substrate complex. Major implication of the key-lock model is appreciation of the importance of well ordered, highly specific three-dimensional structure as a necessary prerequisite for protein function **(Mirsky & Pauling, 1936)**. The enzyme active site was thought by Fischer to be a rigid and sturdy lock which would have exact fit with only one substrate, the key **(Ma et al., 2000)**. Thus, the specificity of enzyme catalysis was thought to be the result of matching a lock with the correct key **(Ma et al., 2000)**.

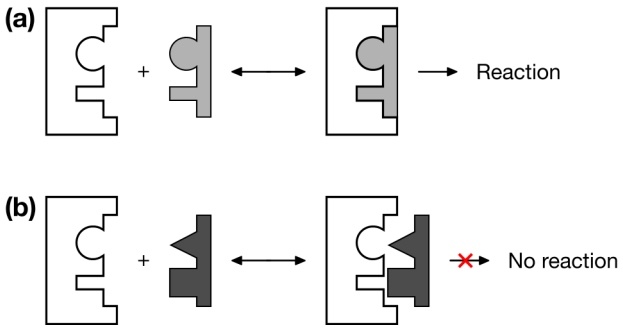

Fig 16 | Early view of substrate specificity through key-lock model. **(a)** A substrate (light grey) fits to the active site of an enzyme (white) like a key to the lock; **(b)** a non-substrate (dark grey) does not fit and thus cannot be converted by the enzyme to product(s).

Transition state stabilisation. The early key-lock hypothesis was formulated far before development of transition state theory **(Pauling, 1946)**, hence it viewed the ground state of enzyme-substrate complex as the relevant configuration **(Copeland, 2000d)**. However, the enzyme active sites have evolved to best complement the substrate transition state structure, rather than the ground state, because the catalytic power of enzymes is due to stabilisation of transition state of the reaction compared to uncatalysed reaction, hence lowering the activation energy barrier to product formation **(Fig 17; Pauling, 1946)**. The activation energy, E_a, is related to k_{cat} by the following equation **(Eq 10)**:

$$k_{cat} = \frac{k_b T}{h} \exp\left(\frac{-E_a}{RT}\right)$$

Eq 10 | The relationship between catalytic constant and activation energy.

where k_B is Boltzmann constant, T is temperature, h is Planck's constant and R is universal gas constant. Hence, a linear decrease in activation energy caused by transition state stabilisation of enzyme-catalysed reaction compared to uncatalysed reaction leads to an exponential increase in k_{cat} and thus an exponential increase in reaction rate **(Copeland, 2000d)**. Transition state stabilisation can cause rate acceleration up to 10^{11} or even more **(Wolfenden, 1969; Garcia-Viloca et al., 2004)**. Lowering the free energy barrier of the transition state of the reaction is necessary because a typical chemical reaction has an activation barrier of 30 to 80 kcal mol^{-1} **(Ma et al., 2000)**, whose overcoming by non-catalysed reaction would be to slow to sustain life **(Wolfenden & Snider, 2001)**. Impressive power of enzymes can be demonstrated by the fact that reduction of barrier height by ~ 8 kcal mol^{-1} in enzyme, which corresponds to a single strong hydrogen bond, can cause an increase of ~ 10^6 in the rate constant at room temperature **(Soriano et al., 2005)**.

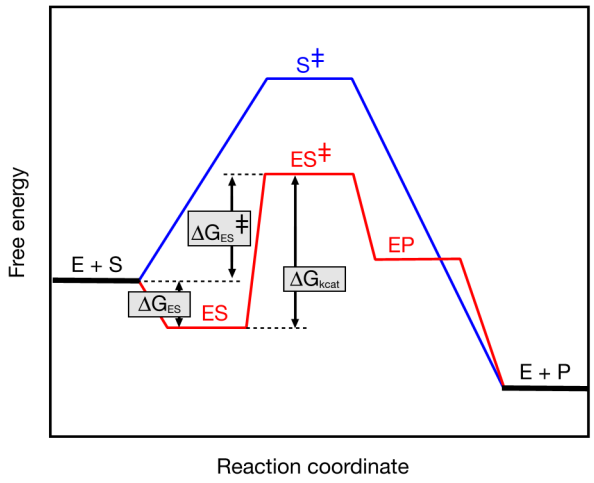

Fig 17 | Energy level diagram of enzyme-catalysed (–) and the corresponding uncatalysed (–) chemical reaction. Transition states, $S^‡$ and $ES^‡$, are the highest energy structures along the three-dimensional reaction coordinate. The initial states, E + S, and final states, E + P, are energetically identical in the catalysed and uncatalysed reactions (–). E, free enzyme; S, free substrate; ES, enzyme-substrate complex; $S^‡$, free transition state; $ES^‡$, enzyme-substrate transition state; EP, enzyme-product complex; P, free product; ΔG_{ES}, net energy gain that results from the realisation of enzyme-substrate binding energy; ΔG_{kcat}, amount of energy that must be expended to reach the transition state; $\Delta G_{ES}^‡$, free energy of activation. In multiple-step enzyme-catalysed reaction, the single $ES^‡$ transition state can be splitted into multiple intermediate and transition states. Redrawn according to Copeland **(Copeland, 2000d)**.

"Loose" versus "tight" transition state. The widely accepted view of enzymatic catalysis as tight binding of the substrate to the transition-state structure causing lowering the activation energy may be, however, oversimplified because the real meaning of a transition state is a surface, not a single saddle point on the potential energy surface **(Ma et al., 2000)**. Thus, transition state can be loose causing that the entire transition state region, rather than a single saddle point, contributes to reaction kinetics **(Ma et al., 2000)**. Therefore, instead of optimising binding to a well-defined transition-state structure, enzymes are optimised by evolution to bind efficiently with a transition-state ensemble **(Ma et al., 2000)**. In an extreme case, e.g. electron transfer reaction, there is no saddle point controlling reaction kinetics **(Ma et al., 2000)**.

Transmission coefficient. In some cases, an additional though minor contribution to the rate acceleration comes from the so-called transmission coefficient, which is composed of three components: (i) non-equilibrium effects, i.e. deviation of equilibrium distribution in phase space **(Garcia-Viloca et al., 2004)**; (ii) quantum-mechanical tunneling **(Garcia-Viloca et al., 2004)**; and (iii) dynamical recrossing of transition state **(Garcia-Viloca et al., 2004; Nam et al., 2004; Tousignant & Pelletier, 2004; Soriano et al., 2005)**. These minor effects can cause additional rate acceleration up to 10^3.

Total catalytic effect. Transition state stabilisation and transmission coefficient together define the enhancement of the reaction rate achieved by the enzyme compared to the non-catalysed reaction in water, and eventually gas phase

(Martí et al., 2001; Cui & Karplus, 2002; Devi-Kesavan & Gao, 2003), the so-called catalytic effect, also known as "enzymatic proficiency" **(Warshel, 1991; Radzicka & Wolfenden, 1995; Cannon & Benkovic, 1998)**. The catalytic effect is reported to be up to 10^{17}-fold **(Radzicka & Wolfenden, 1995; Benkovic & Hammes-Schiffer, 2003)** or up to 10^{19} **(Wolfenden & Snider, 2001)** whereas some uncatalysed reactions have half-times approaching the age of the Earth **(Wolfenden & Snider, 2001)**.

Chemical mechanisms for transition state stabilisation. There are five major categories of chemical mechanisms used by enzymes to achieve transition state stabilisation **(Copeland, 2000d)**: (i) approximation, i.e. greatly increased effective concentration of substrate in the active site with respect to its concentration in solution; (ii) covalent catalysis, i.e. breaking the reaction into multiple steps composed of formation and breakdown of covalent intermediates via nucleophilic, electrophilic or redox catalysis; (iii) general acid-base catalysis involving proton transfer; (iv) conformational distorsion involving enzyme and/or substrate conformational changes, induced-fit **(Koshland Jr., 1958; Koshland Jr., 1976; Koshland Jr., 1995)**, induced-strain **(Copeland, 2000d)** or conformational selection **(Karush, 1950; Lightstone & Bruice, 1996; Lightstone et al., 1997; Lightstone et al., 1998; Bruice & Lightstone, 1999; Bruice & Benkovic, 2000; Ma et al., 2000; Bruice, 2002; Sullivan & Holyoak, 2008)**, to drive the complex towards the transition state **(Fig 18)**; and (v) preorganisation of the active site for transition state complementarity, i.e. substituting solvent by protein and solvating the transition state more than water does **(Warshel & Levitt, 1976; Warshel, 1978; Warshel & Florián, 1998; Warshel & Papazyan, 1998; Ma et al., 2000; Shurki et al., 2002; Warshel, 2003; Olsson & Warshel, 2004; Warshel et al., 2006)**. Any enzyme exploits several or all of these often interdependent and to some extent undistinguishable mechanisms to achieve overall rate enhancement **(Copeland, 2000d)**.

Induced-fit model of substrate specificity. Even if the key-lock model will be considered as referring to transition-state configuration, it does not explain all cases **(Koshland Jr., 1958)**. For example, key-lock theory would predict equal rates for hydrolysis of ribose-5'-phosphate by 5'-nucleotidase as for adenylic acid at enzyme saturation, and molecule similar to substrate binds to the enzyme but is not converted, e.g. α-methyl glucoside smaller by two hydrogen atoms to maltose binds to amylomaltase and functions as competitive inhibitor of this enzyme, but is not hydrolysed. Such anomalous behaviours can be explained by Koshland Jr.'s induced-fit theory **(1958)**. Induced-fit theory states the following **(Koshland Jr., 1958)**: (i) precise orientation of catalytic groups is required for enzyme action; (ii) the substrate may cause an appreciable change in the three-dimensional relationships of the amino acids at the active site; (iii) the changes in the protein structure caused by a substrate bring the catalytic groups into proper orientation for reaction whereas a non-substrate does not. Thus the idea of a fit is retained from the key-lock theory; and the fit occurs only after the changes have been induced by the substrate itself **(Koshland Jr., 1958)**. Induced-fit model can be metaphorically described as "hand in glove" model **(Koshland Jr., 1958)**. When a "good" substrate binds to the active site, the binding forces between the enzyme and the substrate are used to drive the enzyme into an energetically less favourable but catalytically active conformation **(Fig 18a; Copeland, 2000d)**. Induced-fit model is supported by (i) flexible nature of portions, if not all, of the protein **(Koshland Jr., 1958)**, (ii) conformational changes caused by small molecules, e.g. reversible denaturation of enzymes by urea **(Koshland Jr., 1958)**, (iii) substrate-promoted isotopic exchange, i.e. substrate is necessary to promote the proper orientation of catalytic groups **(Koshland Jr., 1958)**, and (iv) protein X-ray crystallography **(Anderson et al., 1979)**.

Key-lock model versus induced-fit model. Induced-fit model is sometimes errorneously referred in literature as an alternative to key-lock model. In fact, the induced-fit model is an extension of the key-lock model to account for systems that cannot be accounted for by the key-lock model **(Koshland Jr., 1995)**. The induced-fit model keeps the necessity of enzyme-substrate complementarity and adds induced-fit mechanism, to account for protein flexibility, as the necessary step for achieving the complementarity for some systems **(Koshland Jr., 1958; Koshland Jr., 1976; Koshland Jr., 1995)**: The best explanation of the actual relationship between key-lock and induced-fit models could be provided and was provided by Koshland himself **(Quote 1; Koshland Jr., 1995)**:

> (...) *The induced fit theory is no more a refutation of Fischer's key-lock principle than the Heisenberg atom was of the Bohr atom or the modern DNA sequences are of the one gene-one enzyme hypothesis. A new theory must explain all the existing facts that pertain to it at the time of its enunciation. Gradually the new theory becomes accepted and then acquires anomalies due to the new facts uncovered after its enunciation. That in turn generates a newer theory which elicits new techniques to test it and its predictions. These new techniques then uncover facts which eventually require further new theories and so on. The new theories are built on components of the old principles. It is said that each scientist stands on the shoulders of the giants who have gone before him. There can be no more honored place than to stand on the shoulders of Emil Fischer. (...)*

Quote 1 | From Koshland **(1995)**.

Conformational selection. Even when enzyme does not seem to undergo ligand-induced conformational changes upon ligand binding, conformations sampled by free enzyme and substrate, and by enzyme and substrate upon enzyme-substrate association usually change **(Ma et al., 2000)**. Such situations cannot be on principle accounted for by rigid key-lock model but instead by conformational selection model, also known as "population shift model" **(Sullivan & Holyoak, 2008)** **(Fig 18b)**. Conformational selection model is generally applicable for all systems, in some, though, preceded by or accompanied by induced-fit step **(Sullivan & Holyoak, 2008)**. Conformational selection and induced-fit are complementary, rather than mutually exclusive models **(Sullivan & Holyoak, 2008)**. Anyway, key-lock model is obsolete and should not be used for description of substrate specificity although it might be still considered useful for providing basic, simplified understanding of the term "complementarity" **(Ma et al., 2000)**.

Induced-strain model. In some cases, the active conformation sampled by the enzyme can be the preferred enzyme configuration, whereas substrate binding requires distorsion from the active conformation **(Copeland, 2000d)**. The binding forces between enzyme and substrate are then directly used to induce strain in the substrate molecule, distorting it towards the transition state structure to facilitate reaction, hence the induced-strain model **(Fig 18c)** **(Copeland, 2000d)**.

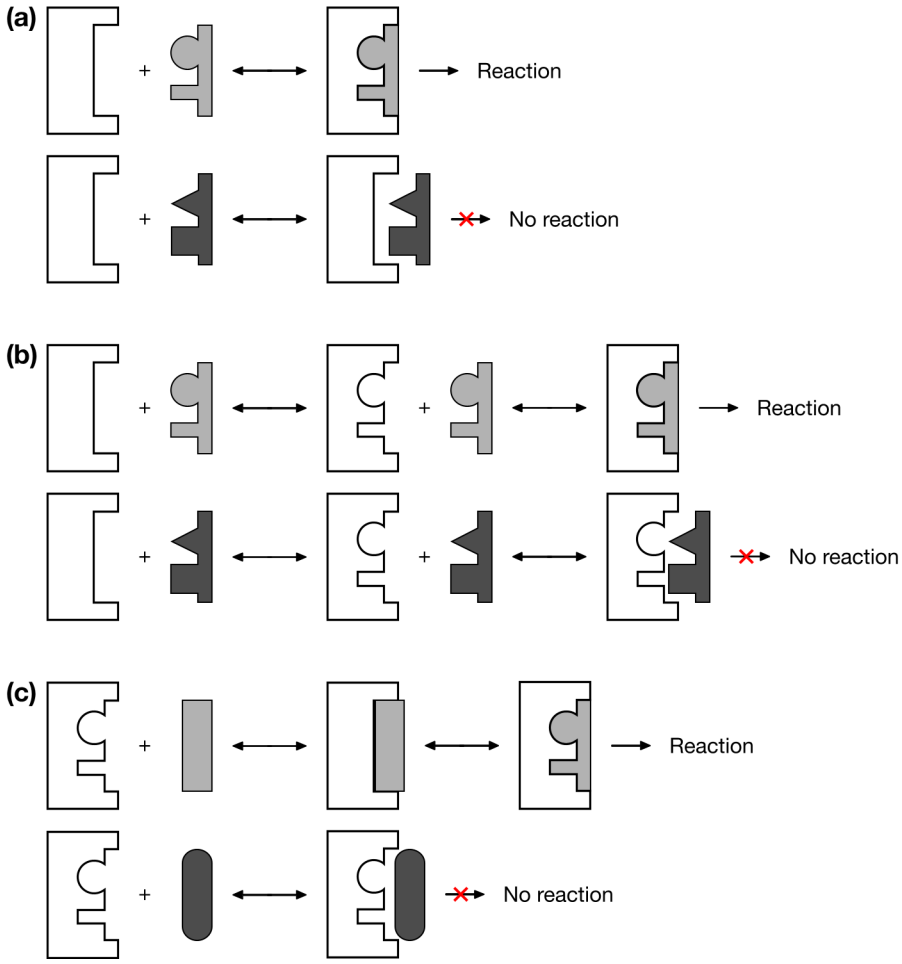

Fig 18 | Models of conformational distorsions for transition state stabilisation. **(a)** Induced-fit model, **(b)** conformational selection model, **(c)** induced-strain model. Enzyme, white; substrate, light grey; non-substrate, dark grey. Induced-fit and conformational selection models are demonstrated on enzyme conformational distorsions; substrate can be distorted, too.

1.4 Protein dynamics

1.4.1 Protein conformations

Protein as an engine. Proteins are engines and engines essentially work by action in time, which involves movements **(Koshland Jr., 1976; Koshland Jr., 1996; Parak, 2003; Karplus & Kuriyan, 2005; Igumenova et al., 2006; Rueda et al., 2007)**. Therefore, a static protein structure is an inadequate approximation in describing complex nature of protein function **(Karush, 1950; Wolfenden, 1974; Parak, 2003; Busenlehner & Armstrong, 2005; Igumenova et al., 2006; Jarymowycz & Stone, 2006)**.

Four dimensions of a protein. Protein is not a three- but rather a four-dimensional system because each atom has a specific position in three-dimensional space and the fourth dimension is being provided by time **(Lupas, 2008)**. In other words, a protein molecule is dynamic in time, i.e. atoms change positions with respect to each other with progress of time **(Supplementary file md.avi; Lakowicz & Weber, 1973; Austin et al., 1975; Frauenfelder et al., 1979; Janin & Wodak, 1983; Bennett & Huber, 1984; Chothia & Lesk, 1985; Baldwin & Rose, 1999a; Frauenfelder et al., 2001; Jarymowycz & Stone, 2006)**. At any particular time, a protein molecule has a specific three-dimensional structure, the so-called conformation, that corresponds to a region of a configurational space surrounding the local minimum on a free energy landscape **(Kurzyński, 1998)**. Protein dynamics is manifested by sampling of conformational space via overcoming energy barriers between different conformations, and thumbling around those conformations **(Fig 19; Cooper, 1976; Ma et al., 2000; Kurakin, 2009; Skjaerven et al., 2009)**.

Protein ensemble. Different molecules within protein ensemble may have different conformations at a particular moment and each fluctuates dynamically over time **(Lakowicz & Weber, 1973; Austin et al., 1975; Frauenfelder et al., 1979; Janin & Wodak, 1983; Bennett & Huber, 1984; Chothia & Lesk, 1985; Baldwin & Rose, 1999a; Frauenfelder et al., 2001; Jarymowycz & Stone, 2006)**. Hence, every protein ensemble must conceptually have some, often different, concentration of different conformations in equilibrium **(Fig 19; Yu & Koshland Jr., 2001; Carlson, 2002; Parak, 2003; Sousa et al., 2006; Kurakin, 2009)**. Heterogeneity of an ensemble of protein molecules is a consequence of protein molecules not having well defined energy minimum **(Parak, 2003; Sousa et al., 2006)**. Prevalence of any particular conformation depends on relevant energy barrier and population of the starting conformation **(Jarymowycz & Stone, 2006)**.

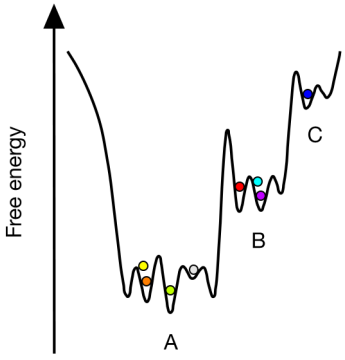

Fig 19 | Protein conformational landscape. Any protein molecule exists in solution as a population of interconverting conformations, shown here as minima on the free energy curve, which represents a one-dimensional cross-section through the high-dimensional energy surface of a protein. In the example given, a population of conformations is composed of three families (*A*, *B*, and *C*). Families are composed of groups of related conformations, while groups, in turn, are composed of yet smaller divisions (not shown), providing hierarchy of free energy barrier heights. Different protein molecules (circles) of an ensemble may have different conformations at a given time. Redrawn according to Kurakin **(2009)**.

Functional Conformations. Since only subset of conformational states is competent for any particular protein function **(Jarymowycz & Stone, 2006)**, protein conformations have to interconvert to perform a function **(Yonetani et al., 1998; Piana et al., 2002; Parak, 2003; Cascella et al., 2004; Bourgeois & Royant, 2005; Busenlehner & Armstrong, 2005; Karplus & Kuriyan, 2005; Igumenova et al., 2006; Carnevale et al., 2006; Jarymowycz & Stone, 2006; Mittermaier & Kay, 2006; Sousa et al., 2006; Rueda et al., 2007; Helms, 2007; Liu et al., 2007; Jager et al., 2008; Laberge & Yonetani, 2008; Yonetani & Laberge, 2008; Skjaerven et al., 2009)**. Functional properties of a protein is the manifestation of (i) functional properties of each competent state, (ii) population of these states, i.e. thermodynamics of the ensemble and (iii) rates of interconversion between different conformations, i.e. kinetics of the ensemble **(Jarymowycz & Stone, 2006; Kurakin, 2009)**.

1.4.2 Hierarchy of motions in time and space

Time-scales and amplitudes. Motions show hierarchy in both time and space **(Austin et al., 1975; Henzler-**

Wildman et al., 2007a). Protein motions occur on time-scales ranging from 10^{-14} to 10^{12} s and covering amplitudes ranging from 0.01 Å to more than 100 Å and with energy variation of 0.1 to 100 kcal mol^{-1} **(Fig 20; Brooks III et al., 1988; Kurzyński, 1998; Karplus, 2000)**. Several types of motions can be distinguished according to time-scale, amplitudes and impact on protein: vibrational motions and conformational motions; the latter includes local, spider-web, rigid-body and global motions.

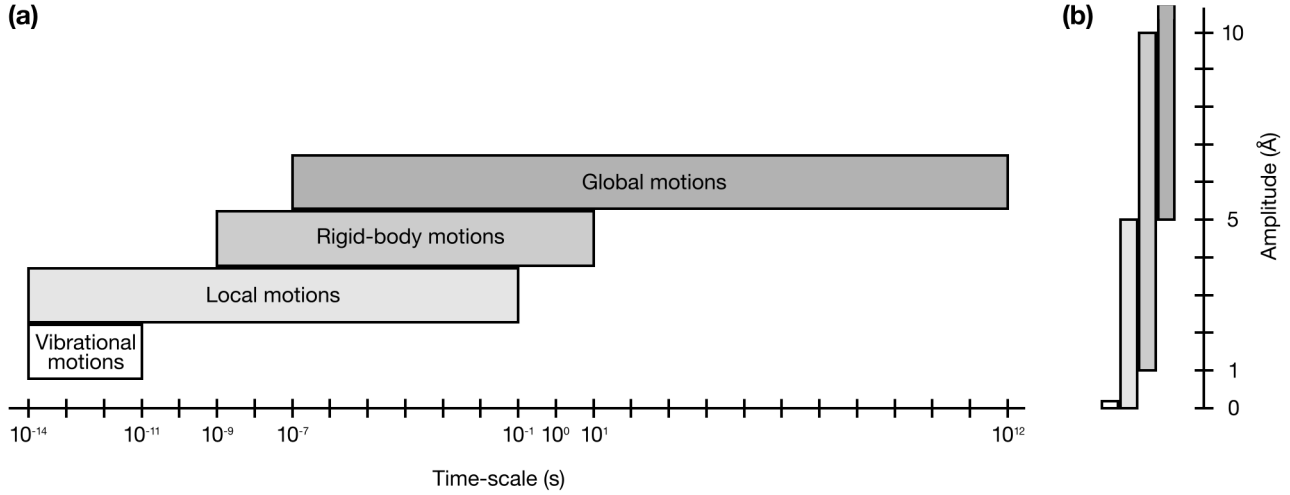

Fig 20 | Hierarchy of motions in time and space. **(a)** Time-scales of various protein motions, **(b)** amplitudes of the protein motions. The boundaries for local, rigid-body and global motions are context dependent to some extent and thus cannot be strictly defined.

Vibrational motions. Vibrational motions range from 10^{-14} s to 10^{-11} s, i.e. from weakly damped localised N-H and C-H stretching modes to overdamped collective modes involving the whole protein domains **(Kurzyński, 1998)**. This vibrational spectrum can be divided into two parts at 2×10^{-13} s whose energy corresponds to temperature 300 K **(Kurzyński, 1998)**. The high-frequency vibrational modes, from 10^{-14} s to 2×10^{-13} s, involve mainly the stretching and bending bonds **(Kurzyński, 1998)**. The low-frequency vibrational modes, from 2×10^{-13} s to 10^{-11} s, involve mainly the collective torsional motions in dihedral angles about the bonds **(Kurzyński, 1998)**. Only the low-frequency vibrational modes contribute to thermal properties, entropy and thermal heat, of proteins **(Kurzyński, 1998)**. Vibrational dynamics is approximated by damped harmonic oscillations subjected to weaker or stronger stochastic perturbations **(Kurzyński, 1998)**. This description is, however, oversimplified, because of anharmonicity of actual vibrations in the period range 10^{-12} to 10^{-11} s **(Kurzyński, 1998)**.

Local motions. Local motions have amplitude of 0.01 to 5 Å, occur on time-scale of 10^{-14} to 10^{-1} s **(McCammon & Karplus, 1980; Rueda et al., 2007; Skjaerven et al., 2009)**, and involve atomic fluctuations, side-chain motions **(Kendrew, 1962)**, and loop motions **(Brooks III et al., 1988)**. Unexpectedly, there is no correlation between amino acid side-chain rigidity and depth of burial, packing density and no inverse correlation between amino acid side-chain rigidity and solvent accessibility surface area **(Igumenova et al., 2006)**. Hence, solvent exposed amino acid residues are not necessarily the most mobile or flexible **(Igumenova et al., 2006)**. Additionally, there can be large difference between dynamics of main-chain and side-chain part of an amino acid residue in a protein **(Lee et al., 2000; Igumenova et al., 2006)**. A special case of local motions are the so-called spider-web motions, i.e. small interconnected local motions that occur over extensive distance (up to more than 100 Å) through smaller than 1 Å displacements of atoms **(Koshland Jr., 1976; Koshland Jr., 1995; Koshland Jr., 1996; Yu & Koshland Jr., 2001)**.

Rigid-body motions. Rigid-body motions are rooted in protein backbone of loops and involve displacement of helix, and shear and hinge movements of domain and subunit in relation to another **(Brooks III et al., 1988; Gerstein et al., 1994)**. These motions have larger amplitudes, on the order of 1 to 10 Å, and consequently occur on longer time-scales, 10^{-9} to 1 s **(Yu & Koshland Jr., 2001; Kay, 2005; Skjaerven et al., 2009)**.

Global motions. The largest changes are associated with global motions, e.g. helix-coil transition and folding/unfolding. These motions have amplitudes over 5 Å and occur on the longest time-scale from 10^{-7} to 10^{12} s **(Brooks III et al., 1988; Kurzyński, 1998; Karplus, 2000; Skjaerven et al., 2009)**. The upper limit of global motions, 10^{12} s, is an upper limit of waiting time for spontaneous unfolding of the protein in physiological conditions **(Kurzyński, 1998)**. Interestingly, rate of many enzymatic reactions occurs at the rate in the middle of the protein dynamics time-scale, i.e. 10^{-3} s **(Kurzyński, 1998)**.

Protein folding/unfolding dynamics. Although native protein must be stable enough to have a defined three-dimensional fold it must be dynamic enough not only to be capable of performing biological role **(Henzler-Wildman et al., 2007a; Henzler-Wildman et al., 2007b)** but also to be capable of reaching the native fold. Individual amino acid residues in unfolded protein cluster in the α-helix, β-sheet and polyproline II regions of φ and ψ dihedral angle space and they flicker between these regions at rates ~ 10^{12} s^{-1} at room temperature **(Barron et al., 1997)**. Hence, these fast motions occur on the same picosecond time-scale as rearrangements of the hydrogen bond network in bulk water **(Ohmine & Tanaka, 1993)** and are therefore coupled with them. Thus the rapid "flicker" motions are promoted by insertion of bulk water molecules via a repertoire of transient hydrated turn conformations **(Barron et al., 1997)**. Folding process, functionally important as the last step during conversion of genetic information into biological function **(Zeeb & Balbach, 2004)**, has the upper speed limit estimated to ~ 10^{-6} s based on the diffusion-controlled rate of collision of sequentially distant segments of an unfolded protein **(Hagen et al., 1996)** which is assumed to determine the shortest time for the initial collapse to a compact structure **(Barron et al., 1997; Deechongkit et al., 2006)**, or even 10^{-7} s **(Chang et al., 2003)**. Mean waiting time of spontaneous unfolding in physiological conditions is 10^{3} to 10^{12} s, depending on equilibrium populations of native and unfolded state; the higher the equilibrium population of native state over unfolded state, i.e. the more stable the native state is, the longer is the mean waiting time of spontaneous unfolding **(Kurzyński, 1998)**. Thus, 10^{12} s is the upper limit of the relaxation spectrum of protein conformational transitions **(Kurzyński, 1998)**. Protein folding is oppossed by a loss of conformational entropy that is further enhanced by correlated (also known as "coupled") motions **(Jarymowycz & Stone, 2006)**. It might be expected that evolutionary pressure selects for natural folded proteins with relatively few correlated motions **(Jarymowycz & Stone, 2006)**.

Effect of temperature on protein dynamics. Internal protein motion is temperature-dependent and increases with increasing tempertature **(Kurzyński, 1998; Jarymowycz & Stone, 2006)**. Protein specific motions, that allow the molecular engine to fulfill its function, occur only above the so-called dynamical transition temperature T_{dt}, also known as "T_c" **(Parak, 2003)**. Below T_{dt}, ~ 150 to ~ 200 K, certain protein motions essential to biological activity may cease completely **(Bourgeois & Royant, 2005)**, functional action of the protein is not activated, and the molecule is in "stand-by" state **(Parak, 2003)**. Dynamics below T_{dt} is characterised by density of phonon states, as in solids **(Parak, 2003)**. The phonons act as a "thermal bath" supplying the energy for all processes of protein dynamics **(Parak, 2003)**. Below T_{dt}, nearly all molecules are trapped in a rigid conformation; only phonon vibrations occur, and jump into the flexible conformation is very seldom **(Parak et al., 2006)**. Above T_{dt}, protein molecule in flexible conformation performs diffusive motions of its segments, side-chains, diffusive motions of larger segments, e.g. haem group in myoglobin and diffusion motions of helical elements **(Parak et al., 2006)**. These diffusive structural fluctuations are lubricant for structural changes that are essential for the biological role **(Parak et al., 2006)**. Thus, proteins show rather complex dynamic behaviour **(Parak et al., 2006; Rueda et al., 2007)**: (i) femtosecond to picosecond time-scale fast vibrations provided by thermal phonon bath; and (ii) above T_{dt}, characteristic temperature diffusive modes, the so-called Brownian motions of groups, e.g. side-chains at time-scale 1 to some 100 ps, and α-helices, and collective motions of larger segments at time-scale from 0.1 ns to 100 ns or longer **(Parak et al., 2006)**. As the temperature increases, an amino acid side-chain itself tends to explore a larger volume **(Igumenova et al., 2006)**. However, the "dynamic volume" occupied by its neighbours also tends to increase as their excursions increase, sterically constraining the side-chain **(Igumenova et al., 2006)**. Thus, neighbouring side-chain motions tend to be positively correlated by their steric interactions **(Igumenova et al., 2006)**.

Link between time-scale and function. It is assumed, that "functionally relevant motions" are those that involve conformational transitions and occur at a time-scale of a protein function **(Foster et al., 2007; Henzler-Wildman et al., 2007a; Henzler-Wildman et al., 2007b)**. Conformational transitions are purely stochastic activated processes, characterised by a spectrum of relaxation times of the number equal to the number of conformational states (~ 10^{10}) **(Kurzyński, 1998)**. In the physiological conditions, spectrum of relaxation times of conformational transitions begins at 10^{-11} s and involves local side-chain rotations and hydrogen bond rearrangements on the protein surface, related to overcoming the energy barriers on the order of 10 kJ mol^{-1} **(Kurzyński, 1998)**. Microsecond to millisecond motions are the fastest motions for which direct link to protein function, originally proposed by Austin et al. **(1975)**, has been established **(Wolf-Watz et al., 2004; Bourgeois & Royant, 2005; Kay, 2005; Boehr et al., 2006; Foster et al., 2007; Henzler-Wildman et al., 2007a; Henzler-Wildman et al., 2007b)**. Moreover, recent studies on Cdc42Hs signal transduction protein **(Loh et al., 2001)** and PDZ domain **(Fuentes et al., 2004)** suggest that allosterically relevant motions may occur on sub-nanosecond time-scale **(Igumenova et al., 2006)**.

Link between different time-scales. Very little is understood about the connection of such functionally relevant millisecond to microsecond movements with much faster (picosecond to nanosecond) local atomic fluctuations

(Tousignant & Pelletier, 2004; Foster et al., 2007; Henzler-Wildman et al., 2007b). Nonetheless, picosecond to nanosecond dynamics have been proposed to generally have functional importance for (i) kinetics of the conformational ensemble, i.e. rate of interconversion between different conformations, (ii) thermodynamics of the conformational ensemble, i.e. populations of the conformational states, (iii) conformational entropy, i.e. distribution of conformational states, and (iv) coupled (correlated) motions **(McCammon & Karplus, 1977; Karplus McCammon, 1981; Schotte et al., 2003; Schotte et al., 2004; Jarymowycz & Stone, 2006; Henzler-Wildman et al., 2007a; Henzler-Wildman et al., 2007b)**. Thus, the term "functionally relevant motion" may, in fact, cover entire time-scale of protein dynamics because fast motions with small amplitudes can function as a lubricant for motions that occur on longer time-scales and amplitudes including those directly linked to protein function **(McCammon & Karplus, 1977; Karplus McCammon, 1981; Bruice & Benkovic, 2000; Jarymowycz & Stone, 2006; Parak et al., 2006; Henzler-Wildman et al., 2007a; Henzler-Wildman et al., 2007b)**.

Protein dynamics complexity. The large time-scale range, overlapping time-scales for different types of motions, diversity of motions themselves, and dependence on protein structure hierarchy and temperature indicate immense complexity of protein dynamics which is still only poorly understood, as noted for myoglobin, the most popular model system to study protein dynamics **(Genberg et al., 1991; Jackson et al., 1994; Srajer et al., 2001; Parak, 2003; Parak et al., 2006)**.

1.4.3 Conformational changes upon ligand binding

Protein dynamics upon ligand binding. Proteins are dynamic themselves **(Koshland Jr., 1976; Koshland Jr., 1996)**, i.e. in the absence of a ligand, i.e. in the native folded state. Protein-ligand association then often results in change in distribution of conformational states of the protein **(Fig 21; Kurakin, 2009)**. Hence, proteins do not have a structure rigid enough to form a lock **(Ma et al., 2000; Jarymowycz & Stone, 2006)**. Discovery of the importance of protein dynamics upon ligand binding has led to modification of Fischer's key-lock model of rigid-body protein-ligand association to conformational selection **(Karush, 1950; Sullivan & Holyoak, 2008)** and induced-fit **(Koshland Jr., 1958; Koshland Jr., 1976)** models.

Conformational selection. Protein-ligand interactions may stabilise the best-fitting member from an ensemble of conformations in equilibrium **(Karush, 1950; Sullivan & Holyoak, 2008)**. Thus, protein samples active conformation on its own even in the unliganded state. Upon ligand binding, however, the population of the active conformation in the ensemble of conformations in equilibrium increases compared to unliganded state **(Fig 21; Kurakin, 2009)**. This mechanism is of general importance for almost every protein because the highest populated conformations of a free protein are not necessarily the most populated conformations in the protein-ligand complex; in fact, it is seldom the case **(Carlson, 2002; Teague, 2003; Sousa et al., 2006)**.

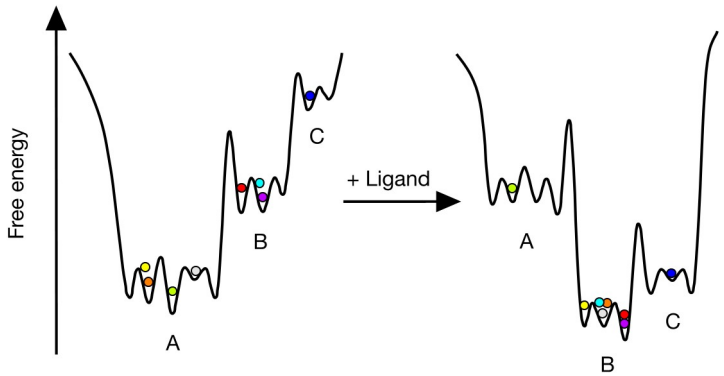

Fig 21 | Reshaping of protein conformational landscape upon ligand binding. Ligand binding to a protein often leads to redistribution of protein conformations and altered rates of their interconversions. In the example given, ligand binding causes change in the prevalent protein conformation in the ensemble from *A* to *B*. Such redistribution can be caused also by other changes in the internal state of the protein, e.g. by mutation or chemical modification, or by changes in external conditions, e.g. by pH, pressure, temperature and ionic strength. Redrawn according to Kurakin **(2009)**,

Induced-fit binding. Induced-fit theory of Koshland Jr. states that dynamic fit between protein and ligand is achieved only upon ligand binding whereas free protein is not able to reach the active conformation on its own **(Koshland Jr., 1976)**. Additionally, a protein that has occluded binding site and that shows the ability to form encounter complex with the ligands, e.g. lid-gated active site of some lipases, or secondary, tertiary etc. binding sites, also known as "docking sites", e.g. in myoglobin, must operate by an induced fit mechanism instead of conformational selection **(Sullivan & Holyoak, 2008)**. This means, that not only ligand-induced conformational changes of a protein for proper alignment of binding or, in the case of an enzyme, catalytic amino acid residues, but also ligand-induced conformational changes of a protein for making the binding site (in)accessible to the ligand, are consistent with the induced-fit mechanism **(Sullivan & Holyoak, 2008)**. An induced fit event must be essentially followed/accompanied by the conformational selection event thus the two mechanisms of ligand binding complement rather than contradict each other **(Sullivan & Holyoak, 2008)**.

Scenarios of induced-fit binding. The induced fit can be considered also inversely, i.e. that protein changes ligand dynamics or mutually, i.e. both protein and ligand change conformations upon association **(May & Zacharias, 2005)**. Therefore, generalised induced-fit model has three possible scenarios for protein-ligand binding **(Jarymowycz & Stone, 2006)**: (i) one component is template for structural rearrangement of the second component **(Jarymowycz & Stone, 2006)**; (ii) each binding partner becomes substantially rigid during association, i.e. mutual induced-fit **(Jarymowycz & Stone, 2006)**; (iii) ligand binding increases flexibility in the binding site, e.g. when an ordered water molecule is replaced by a hydrophobic ligand, or the increase in flexibility is widespread, or the increase in flexibility occurs in regions distant from the active site via long-range effects **(Jarymowycz & Stone, 2006)**.

Ligand-induced motion types. Ligand-induced changes in proteins involve (i) local motions **(Jarymowycz & Stone, 2006)**, (ii) hinge domain motions **(Gerstein et al., 1994)**, (iii) shear domain motions **(Gerstein et al., 1994)** and (iv) spider-web motions **(Koshland Jr., 1995; Yu & Koshland Jr., 2001)**. Different ligands can induce different protein motions **(Prasad & Mitra, 2002)**.

Long-range dynamic effects. Dynamic communication across protein upon ligand binding can be achieved by long-range dynamic effects via three mechanisms **(Jarymowycz & Stone, 2006)**: (i) perturbation induces conformational change of a protein including remote region **(Jarymowycz & Stone, 2006)**; (ii) perturbation induces conformational change of amino acid residues located at and/or near the site of perturbation thus leading to modification of the strength of their interactions with amino acid residues located between the perturbation site and remote amino acid residues **(Jarymowycz & Stone, 2006)**; there may be several alternative pathways connceting the binding site to the remote site via alternative intervening amino acid residues **(Jarymowycz & Stone, 2006)**; (iii) perturbation does not induce any change in the average structure of the protein but instead affects the dynamics of amino acid residues both at the perturbation site and at the remote site **(Jarymowycz & Stone, 2006)**. For many proteins, such functionally relevant transmission of information occurs in the absence of large structural rearrangement which suggests important role for fast (sub-nanosecond) side-chain motions **(Loh et al., 2001; Fuentes et al., 2004; Igumenova et al., 2006)**.

Role of correlated (coupled) motions in ligand binding. The negative pressure associated with entropy reduction upon induced-fit protein-ligand binding can be overrided by correlated motions **(Jarymowycz & Stone, 2006)**. Correlated motions provide thermodynamic driving force in favour of ligand binding via disrruption of dynamical coupling network upon ligand binding during which some amino acid residues become "immobilised" but other amino acid residues are released from the coupling network and undergo increased motions and thus contribute favourably to entropy of binding **(Jarymowycz & Stone, 2006)**. These changes in coupling network can cancel or even outweigh entropic penalty of induced-fit binding **(Jarymowycz & Stone, 2006)**.

Role of ligand-induced changes. Induced-fit is considered to be the crucial mechanism that controls seclussion **(Koshland Jr., 1976; Jarymowycz & Stone, 2006)**, involves positive and negative cooperativity **(Koshland Jr., 1976)** and thus feedback and feedforward mechanism of signal amplification and signal sensitivity **(Koshland Jr., 1998)**.

Positive and negative cooperativity. Cooperativity, i.e. allosteric effects and signal transduction between protein subunits, is achieved by motions that propagate over substantial distance **(Demchenko, 2001; Koshland Jr. & Hamadani, 2002)**. The conformational changes induced by a ligand create subunit interactions that have either favourable (positive cooperativity) or unfavourable (negative cooperativity) effects on the binding of subsequent ligands. Big conformational change does not necessarily imply cooperativity as is the case of no cooperativity in aldolase and lactic dehydrogenase, e.g. **(Koshland Jr. & Hamadani, 2002)**. Some enzymes show positive cooperativity with one ligand and negative cooperativity with another ligand, and some enzymes show both positive and negative cooperativity with a single ligand during the sequential binding of that ligand **(Koshland Jr. & Hamadani, 2002)**.

Cooperativity and evolution. Occurrence of positive and negative cooperativity in nature is probably equal **(Koshland Jr. & Hamadani, 2002)**. Cooperativity can change by single amino acid residue substitution (i) from no cooperativity to positive cooperativity, e.g. in pyruvate kinase **(Ikeda et al., 1997)**, (ii) from positive to negative cooperativity, e.g. in aspartate receptor **(Kolodziej et al., 1996)**, and (iii) from negative to no cooperativity, e.g. in aspartate receptor **(Yu & Koshland Jr., 2001)**. These examples demonstrate delicate balance between cooperativity effects and ease of change of cooperativity during evolution **(Koshland Jr. & Hamadani, 2002)**, and link between protein dynamics and protein function in the course of evolution **(Kurakin, 2009)**.

Amplitudes of ligand-induced motions. It has long been disputed about "how big must the motions be to have functional importance?" and the question is still relevant **(Koshland Jr., 1995; Koshland Jr., 1996; Koshland Jr., 1998)**. In general, any motion that is functionally important is big enough **(Koshland Jr., 1995; Koshland Jr., 1996; Koshland Jr., 1998)**. Both big and small movement can be important **(Koshland Jr., 1995; Koshland Jr., 1996; Koshland Jr., 1998)**. The smaller the structural change required for the function or correlated with the function the better because the lower thermodynamic energy is required and therefore it is more likely to be easy kinetically **(Yu & Koshland Jr., 2001)**. Hence some proteins, e.g. aspartate receptor, exploit dynamics with amplitude as small as ~ 0.5 Å for performing the function **(Yu & Koshland Jr., 2001)**. Consequences of small conformational changes are profound because they are responsible for the enormous amplification of stimulus to response which is essential in living organisms **(Koshland Jr., 1998)**.

Role of water for protein dynamics. Water is the universal solvent medium of cells **(Helms, 2007)**. Water surrounds proteins, water is integral part of proteins and can be involved in key mechanistic steps **(Helms, 2007)**. Water can be considered as a special kind of a ligand. Protein dynamics is thus tightly connected to the dynamics of surrounding and internal water solvent with implication for protein function **(Jimenez et al., 1994; Nandi et al., 2000; Daniel et al., 2003; Pal & Zewail, 2004; Halder et al., 2007; Helms, 2007; Murugan & Agren, 2009)**. Water has the ability to promote conformational changes in α-helices and β-sheets (**Sundaralingam** & **Sekharudu, 1989)**. Solvent fluctuations dominate some part of protein dynamics and may even control function of a protein because the fluctuation of the water molecules provide the enthalpy needed by the protein, e.g. myoglobin **(Parak, 2003)**, to go from the "rigid" to the "flexible" state **(Parak, 2003)**. The protein, together with its hydration shell, determines the entropy which controls the motions in the flexible state, and is thus responsible for opening and closing of channels connecting buried binding site to protein surface **(Parak, 2003)**.

1.4.4 Role of dynamics in enzyme catalysis

Trade-off between conformational stability and conformational changes. Enzyme activity requires a precise balance between conformational stability and conformational changes because enzymes must be stable enough to retain their native three-dimensional folds, and dynamic enough to allow sufficient substrate binding, chemical reaction and product release **(Henzler-Wildman et al., 2007b; Strasser & Wittmann, 2007)**. Hence, there exists an intimate relation between overall native enzyme fold, its conformational diversity (in time-scale, amplitude and type of motion) and its enzymatic function **(Wolfenden, 1974; Karplus McCammon, 1983; Miller & Benkovic, 1998; Davis & Agard, 1998; Kitao & Go, 1999; Kohen et al., 1999; Mine et al., 1999; Berendsen & Hayward, 2000; Radkiewicz & Brooks III, 2000; Eisenmesser et al., 2002; Eisenmesser et al., 2005; Daniel et al., 2003; Garcia-Viloca et al., 2004; Teeter, 2004; Tousignant & Pelletier, 2004; Busenlehner & Armstrong, 2005; Otyepka et al., 2008)**.

Substrate-induced conformational changes. All enzymes essentially undergo conformational changes induced by substrate binding **(Koshland Jr., 1995)**, because enzymes are present in environment of many biochemical pathways involving substrate analogs and they need to prevent side reactions with the analogs **(Koshland Jr., 1995)**. Enzymes that show the least conformational changes are hydrolases (e.g. proteases and nucleases) because they do not need to exclude water **(Koshland Jr., 1995)**. Any enzymatic reaction requires motion of some sort because (i) substrates need to be admitted and bound, (ii) cofactors need to be brought to contact, (iii) active site needs to be shielded against the adverse effects of the surrounding aqueous solvent, (iv) protein needs to adjust itself to accommodate the changing stereochemistry along the reaction pathway, and (v) products need to be expelled **(Schmidt & Lamzin, 2007)**. For example, by active site loop amino acid residues repositioning, integral membrane protein PagP interconverts between highly dynamic state allowing substrate entry and more rigid state that supports catalysis **(Kay, 2005; Foster et al., 2007)**.

Promoting and dynamical motions in enzyme catalysis. Two types of motions can be distinguished according to their relevance for enzymatic function: promoting motions and dynamical motions **(Tousignant & Pelletier, 2004)**.

Promoting motions are conformational changes that occur on time-scale of overall reaction along the reaction coordinate and modify height of activation free energy barrier **(Garcia-Viloca et al., 2004; Tousignant & Pelletier, 2004)**. Dynamical motions occur on femtosecond time-scale and these specifically influence transmission coefficient **(Tousignant & Pelletier, 2004)**. Thus, motions influence both lowering free energy barrier of transition state and generalised transmission coefficient that includes tunneling, non-equilibrium effects and transition state recrossing **(Garcia-Viloca et al., 2004)**. Promoting motions should have in general higher impact on enzyme catalysis because they influence transition state theory constant which affects reaction rate exponentially whereas dynamical motions should have in general lower impact on enzyme catalysis because they influence generalised transmission coefficient which affects reaction rate only as a prefactor **(Hammes-Schiffer, 2002)**.

Preorganisation of active site. Promoting motions involve conformational changes. Random sampling of all possible folded configurations would, however, degrade catalytic efficiency, a situation analogous to protein folding **(Henzler-Wildman et al., 2007a)**. Thus there are defined conformational changes that preorganise active site amino acid residues in the configuration needed to facilitate the reaction **(Bruice, 2006; Hammes-Schiffer & Benkovic, 2006; Nagel & Klinman, 2006; Henzler-Wildman et al., 2007a)**. It has been proposed by Bruice & Benkovic **(2000)**, that in some cases, intrinsic turnover rate of enzyme, k_{cat}, is related to frequency (probability) with which enzyme populates conformations competent to catalyse reactions, the so-called near attack configurations, NACs **(Bruice & Benkovic, 2000)**. The NAC concept could be superfluous because it comprises enzyme-induced conformational changes in substrate and/or substrate-induced conformational changes in enzyme, the phenomena that can be explained by conformational selection and/or induced-fit mechanisms **(Jarymowycz & Stone, 2006)**. Effeciency of formation of active (competent) enzyme-substrate complex may be further enhanced by correlated motions **(Jarymowycz & Stone, 2006)**. If active site groups move independently then probability of active enzyme-substrate (ES) complex formation is a product of individual group probabilities, whereas if active site groups are appropriately motionally coupled then active ES complex formation probability is not product of individual functional group probabilities but higher and if active ES complex formation is the limiting event of the reaction cycle then it results in more efficient catalysis **(Jarymowycz & Stone, 2006)**.

Correlated motions and generalised transmission coefficient. Correlated motions also have possible functional role in quantum tunneling, exploited in enzymatic reactions involving electron and proton transfer **(Jarymowycz & Stone, 2006)**. Tunneling is extremely sensitive to distance between original and final positions of the tunneling particle and therefore molecular motions that modulate the distance influence tunneling rates and mechanism **(Jarymowycz & Stone, 2006)**. Correlated motions are, for example, required for completion of reaction cycle of dihydrofolate reductase **(Brooks III et al., 2003)**.

Location of important motions in enzymes. Both motions in and around the active site and transition state of enzymatic reaction, and motions distant from the active site might be important for enzyme function **(Ma et al., 2000; Gao, 2003; Tousignant & Pelletier, 2004)**. In some cases, transition state ensemble may be homogeneous around the active site, i.e. with rather a small influence on the substrate binding affinity, and heterogeneous and contributing to the reaction in terms of activation entropy, away from the active site, e.g. in 5-monophosphate decarboxylase **(Ma et al., 2000; Gao, 2003)**. Motions of certain non-catalytic amino acid residues may help defining preorganisation of enzyme active site and transition state stabilisation **(Tousignant & Pelletier, 2004)**, e.g. in dihydrofolate reductase **(Agarwal et al., 2002; Rajagopalan et al., 2002; Rod et al., 2003; Watney et al., 2003)**, triosephosphate isomerase **(Lolis & Petsko, 1990; Derreumaux & Schlick, 1998; Rozovsky & McDermott, 2001)**, horse liver alcohol dehydrogenase **(Hammes-Schiffer, 2002)**, and *Escherichia coli* TEM-1 β-lactamase **(Meroueh et al., 2002)**. Therefore, functional protein dynamics may not be always restricted to the active site and catalytic amino acid residues **(Ma et al., 2000)**.

Advantage of conformational changes in enzyme function. In summary, enzyme dynamics, not accounted for by the key-lock model **(Koshland Jr., 1976)**, is responsible for the following phenomena **(Koshland Jr., 1976)**: (i) similar structures to substrate bind but are unable to induce catalysis in reactions that are controlled not by steric exclusion but by failure to react, the so-called kinetic specificity **(Koshland Jr., 1976)**; (ii) if a highly reactive intermediate is formed during enzymatic reaction it is desirable that the intermediate exists only transiently to avoid wasteful side-reactions; the transient existence can be achieved by the so-called ordered (also known as “sequential”) binding **(Koshland Jr., 1976)**; (iii) binding of a non-competitive inhibitor does not affect substrate binding but affects enzyme action because the non-competitive inhibitor binds at second site and induces a conformation which disorganises catalytic groups of enzyme without affecting binding groups **(Koshland Jr., 1976)**; (iv) substrate analogs that are not large enough to induce proper alignment of catalytic groups of enzyme can become substrate if they are supplemented by non-reacting molecule containing the missing part of structure **(Koshland Jr., 1976)**; (v) if protein is composed of two or more subunits then conformational change of one subunit affects neighbouring subunits,

the so-called cooperativity phenomenon **(Koshland Jr., 1976)**; for enzymes following Henri-Michaelis-Menten kinetics (see 1.3.3.1), cooperativity is an advantegous mechanism for tuning enzyme activity according to ligand concentration **(Koshland Jr., 1996)**; (vi) conformational change may cause exposure of previously buried amino acid residues and thus cause freezing conformational state in active or inactive form; such a "switching" between active and inactive form plays important role in controlling the reaction cycle **(Koshland Jr., 1976)**; (vii) enzyme may use conformational energy for catalytic power – e.g. strain in lysosyme and exclusion of water from active site **(Koshland Jr., 1976)**; (viii) enzyme dynamics allows for better handling regulation of enzyme action and excluding side-reactions **(Koshland Jr., 1976)**. At least some of these phenomena are needed and exploited by every enzyme **(Koshland Jr., 1976; Koshland Jr., 1995)**.

1.4.5 Ligand exchange in proteins

Ligand binding and release. Binding of a ligand to a protein is followed not only by a specific biological response but also by release of the ligand to restore free protein for binding of another ligand **(Schmidt & Lamzin, 2007)**. Since protein-ligand interaction requires both ligand binding and release, there is and inevitable trade-off between ease of the two processes **(Xu et al., 2003; Ye et al., 2006)**. Therefore, protein conformations are selected during evolution to optimise both the unliganded and liganded state **(Koshland Jr., 1995; Yu & Koshland Jr., 2001)**. In order to bind at a protein binding site, ligand must diffuse or be transported to the protein surface, and if the binding site is buried, both ligand binding and release essentially includes an additional step – diffusion through protein **(Wade et al., 1998)**. The diffusion can occur (i) directly through protein matrix in the case of small ligand with zero net charge, e.g. O_2, CO, CO_2, water, or (ii) through a tunnel, or (iii) via large conformational change that makes the binding site transiently solvent-exposed to allow for the exchange of ligands **(Fig 22)**. The migration can be rate-limiting step of a protein function and is thus of high importance **(Schanstra & Janssen, 1996; Bell-Parikh & Guengerich, 1999; Bosma et al., 2003; Yao et al., 2007)**.

Ligand migration through protein matrix. Protein matrix is not homogeneous, but rather heterogeneous and more liquid-like due to thermal fluctuations than solid-like **(Liang & Dill, 2001; Lindorff-Larsen et al., 2005; Socolich et al., 2005)**. Different parts of protein interior thus have differently densed packing and different size of thermal fluctuations which allows small ligand to pass through low density regions of protein matrix to reach the binding site from the surface and vice versa **(Fig 22a)**, e.g. in myoglobin **(Carugo & Argos, 1998; Cohen et al., 2006)**. Additionally, a ligand can induce conformational changes to facilitate its passage through the protein matrix **(Pinakoulaki et al., 2006; Tomita et al., 2009)**. Due to rugged energy landscape associated with the conformational changes induced by a ligand, the ligand does not move "smoothly" but rather via "jerky" movements **(Váró et al., 1995; Pikkemaat et al., 1999)**, literally "hopping" between neighbouring docking sites **(Brunori et al., 1999; Bikiel et al., 2006; Lavalette et al., 2006)**, as a "migrating cavity" **(Teeter, 2004)**.

Ligand migration through a tunnel. Tunnel provides a continuous empty space whose size allows passage of ligands without entering protein matrix. Tunnel can be either permanent or transient **(Fig 22bc)**. The latter is a consequence of natural conformational changes (thermal fluctuations) in the protein that cause fluctuation of the size of the tunnel, i.e. working by conformational selection mechanism **(Karush, 1950; Zwanzig, 1992; Wlodek et al., 1997; Tara et al., 1999)**, or transient opening is a ligand-induced event, i.e. working by induced-fit mechanism **(Koshland Jr., 1976; Lüdemann et al., 1997; Lüdemann et al., 2000a; Prasad et al., 2000; Podust et al., 2001; Wade et al., 2004; Li et al., 2005; Schleinkofer et al., 2005; Carlsson et al., 2006; Hritz et al., 2006; Seifert et al., 2006; Wang & Duan, 2007; Sullivan & Holyoak, 2008)**. Transient opening of a tunnel is advantegous in providing the protein with additional mechanisms to control its biological role: (i) seclussion, e.g. in P450 enzymes **(Lüdemann et al., 1997; Lüdemann et al., 2000a; Wade et al., 2004; Schleinkofer et al., 2005)**, membrane protein rhodopsin **(Wang & Duan, 2007)**, retinoic acid receptor **(Carlsson et al., 2006)**, NADH oxidase **(Hritz et al., 2006)**]; and (ii) enzyme catalysis, e.g. in P450 enzymes **(Podust et al., 2001; Cojocaru et al., 2007)** and NADH oxidase **(Hritz et al., 2006)**] **(Koshland Jr., 1976)**. Tunnel accessibility in proteins can be controlled by various mechanisms involving protein motions, (non-)bonded interactions and role of solvent **(Table 7)**. Several or all of these mechanisms can be exploited by a protein.

Accessibility of binding site via large conformational changes. Switching between open and closed form causes transient exposure of binding site for binding and release of a ligand **(Fig 22d)**. This mechanism is exploited by lid-gated lipases, e.g. **(Jaeger & Reetz, 1998; Nardini & Dijkstra, 1999)**. The motion is rooted in loops that serve as hinges for rigid body motion of a helix **(Brzozowski et al., 1991; Derewenda, 1994; Jaeger & Reetz, 1998; Nardini & Dijkstra, 1999)**.

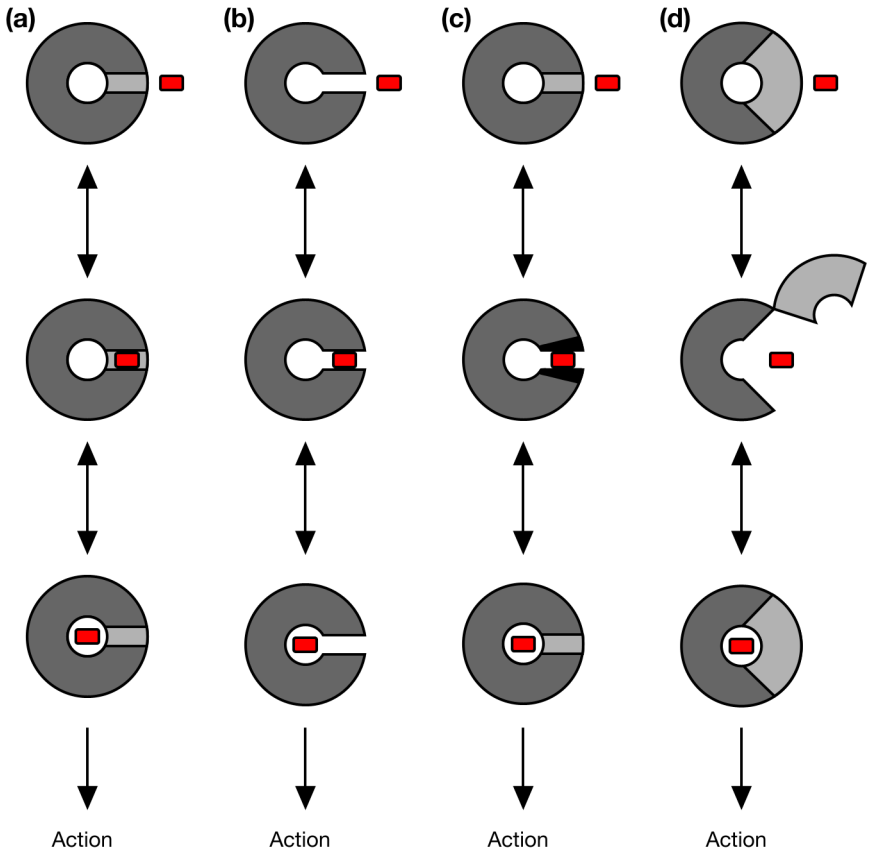

Fig 22 | Ligand migration between buried cavity and surface of a protein. **(a)** Migration through protein matrix, **(b)** migration through permanent tunnel, **(c)** migration through transient tunnel, **(d)** migration upon transient lid opening. Protein, grey/black; empty space, white; ligand, red. Portions of a protein shaded by light grey indicate lower packing density of a protein matrix and a lid in *a-c* and *d*, respectively. Redistribution of protein matrix packing densities is indicated by black in *c*.

Alternative tunnels and protein matrix pathways. The trade-off between ease of ligand binding and release is solved by some proteins by providing alternative tunnels, e.g. in P450 enzymes **(Lüdemann et al., 2000a; Lüdemann et al., 2000b; Wade et al., 2004)**, acetylcholinesterase **(Tara et al., 1999; Van Belle et al., 2000)**, or by alternative protein matrix pathways, e.g. in myoglobin **(Scott et al., 2001; Cohen et al., 2006)**. Different tunnels and pathways can be specific to different ligands due to differential interaction with tunnel or pathway amino acid residues **(Tara et al., 1999; Van Belle et al., 2000; Lüdemann et al., 2000a; Podust et al., 2001; Wade et al., 2004)** thus allowing synchronisation of ligand/substrate binding and ligand/product release **(Wombacher et al., 2006)**, e.g. in P450 enzymes **(Oprea et al., 1997; Podust et al., 2001; Wade et al., 2004; Cojocaru et al., 2007; Yao et al., 2007)**, in catalase HPII **(Sevinc et al., 1999)**, and acetylcholinesterase **(Kovach et al., 1994)**. Alternative tunnels may have direct impact on enzymatic reaction because depending on which tunnel is used by a substrate, different enantiomeric products can be generated **(Wombacher et al., 2006)**. Alternative tunnels and pathways may be also coupled with cellular localisation. For example, membrane P450 enzymes may bind a hydrophobic ligand from the membrane space via one tunnel, and expell more hydrophilic product into the cytoplasm via another tunnel **(Schleinkofer et al., 2005; Cojocaru et al., 2007)**. Since enzymatic reactions are coupled in the metabolic network, the products of one enzymatic reactions may be substrates for another enzymatic reaction. In order to shorten delay between release of the product of the first reaction into cytoplasm and diffusion and encounter and binding of the product as a substrate into another enzyme for the second reaction, some enzymes can be associated in such a way, that the product of the first reaction moves via a tunnel into the second enzyme without entering the bulk solvent, a phenomenon referred to as “substrate channeling”, observed, e.g., in P450 enzymes **(Cojocaru et al., 2007)** and dihydrofolate reductase-thymidylate synthase pair **(Elcock et al., 1997)**.

Table 7 | Mechanisms of controlling tunnel accessibility.

Mechanism	Protein
Loop (gating) motion	triosephosphate isomerase **(Wade et al., 1993)**
	P450 enzymes **(Wade et al., 2004; Schleinkofer et al., 2005; Li et al., 2005; Seifert et al., 2006; Cojocaru et al., 2007)**
	acetylcholinesterase **(Kovach et al., 1994; Xu et al., 2003)**
Rigid-body motion	P450 enzymes **(Wade et al., 2004; Yao et al., 2007)**[c]
	gpH1-receptor **(Strasser & Wittmann, 2007)**
Secondary structure element fluctuation[a]	P450 enzymes **(Lüdemann et al., 2000b; Prasad et al., 2000; Podust et al., 2001; Li et al., 2005)**
	acetylcholinesterase **(Tara et al., 1999)**
	gpH1-receptor **(Strasser & Wittmann, 2007)**
Aromatic gating[b]	P450 enzymes **(Lüdemann et al., 2000a; Lüdemann et al., 2000b; Winn et al., 2002; Li et al., 2005)**
	acetylcholinesterase **(Ripoll et al., 1993; Enyedy et al., 1998; Zhou et al., 1998; Tara et al., 1999; Van Belle et al., 2000; Xu et al., 2003)**
	NADH oxidase **(Hritz et al., 2006)**
	horseradish peroxidase **(Khajehpour et al., 2003; Zelent et al., 2004)**
Salt-bridge interaction	P450 enzymes **(Deprez et al., 1994; Di Primo et al., 1997; Lounnas & Wade, 1997; Oprea et al., 1997; Lüdemann et al., 2000a; Winn et al., 2002; Yao et al., 2007)**
	acetylcholinesterase **(Kovach et al., 1994; Enyedy et al., 1998)**
	catalase HPII **(Sevinc et al., 1999)**
Disulphide-bridge interaction	rhodopsin **(Lüdemann et al., 2000a; Wang & Duan, 2007)**
Hydrogen bonding interaction	P450 enzymes **(Li et al., 2005; Schleinkofer et al., 2005)**
	acetylcholinesterase **(Kovach et al., 1994)**
Solvation	P450 enzymes **(Dunn et al., 2001)**
	acetylcholinesterase **(Henchman et al., 2002)**

[a]Stability, extension, shortening, bending, or breakage of a secondary structure element, mostly helix.
[b]Conformational change of aromatic amino acid residue side-chain.
[c]Helix displacement.

Dynamics of internal water molecules. Water is not only the solvent that surrounds the protein but it also enters the protein via protein matrix or a tunnel. Internal water molecules may help stabilising regions of unsatisfied backbone hydrogen bonding **(Chau, 2004; Damjanović et al., 2005)**. Although buried binding sites are selected by evolution to favour binding of a hydrophobic ligand and disfavour binding of hydrophilic ligand including water, biological role of the protein often necessitates presence of some polar or even charged groups in the binding site **(Kendrew, 1962)** that can attract bulk water molecules. Thus, ligand binding into buried binding site can be hindered by tightly bound water molecules and these must be displaced to allow ligand binding **(Koshland Jr., 1976)**. On the other hand, release of the ligand might be facilitated by water and some enzymes (hydrolases) use water as a co-substrate. Hence, there must be a delicate balance between selectivity of the binding site for ligand and accessibility of the binding site for water. This balance can be controlled by the above mentioned transient opening of tunnels, switching between open and closed forms by large conformational changes, and by providing an alternative tunnel for water escape while ligand enters the protein via another tunnel **(Oprea et al., 1997; Tara et al., 1999; Xu et al., 2003)**.

1.5 Protein research

1.5.1 Basic principles of scientific research

Scientific discovery. According to Koshland Jr.'s Cha-Cha-Cha theory **(2007)**, there are three categories of scientific discoveries: (i) charge, i.e. seeing what everyone else has seen and thinking what no one else has thought before; (ii) challenge, i.e. responding to accumulation of facts or concepts and anomalies unexplained by or incongruous with scientific theories of the time; and (iii) chance, i.e. seeing what no one else has seen and being able to realise its importance. In general, scientists should be non-conformists because non-conformism is essential for progress in science **(Woese, 2001; Koshland Jr., 2004; Trevors & Abel, 2004)**. At the same time, however, the non-conformism should be restrained to prevent anarchy **(Koshland Jr., 2004)**. The restraint should be performed at two

levels: (i) by self-criticism of scientists themselves **(Popper, 1959)**; and (ii) by peer-reviewed journals and grant agencies **(Koshland Jr., 2004)**.

Knowledge. Scientific discoveries lead to progress in our understanding of the scientific problems. Up to date body of information obtained by scientific discoveries constitutes a knowledge, which can be represented by a model, a hypothesis or a theory **(Koshland Jr., 1995)**. Importantly, facts are not enriched by the model but the model is enriched, and made more complex, by the facts **(Woese, 2001)**. To be useful, scientific model should lead to predictions **(Jeffares et al., 1998)** and should suggest how to test its validity **(Jones, 2003; Trevors & Abel, 2004)**. However, the fact that an experimental result is not inconsistent with a theory does not necessarily speaks to the theory's predictivity or to its validity **(Woese, 2001)**. Thus, to be meaningful, predictions need to be specific in a way that the theory can stand or fall with the experimental result **(Woese, 2001)**. Whether the experiments prove validity of the model or prove invalidity of the model, is equally worth. When the bulk of information accummulates that refutates validity of a model, then a new model should be established, while purging past prejudices **(Koshland Jr., 1995; Woese, 2001)**.

Scientific goal. There are two possible goals of any scientific research: (i) to get primary knowledge about the studied problem, i.e. basic research, or (ii) to explore how to exploit already acquired knowledge for human benefit, i.e. applied research. Today science is being under tremendous formative pressure from the society, at large from medical-industrial complex in particular, to become a discipline of applications, to merely be society's handmaiden **(Woese, 2001)**.

1.5.2 Protein research strategy

Key steps in protein research. There are several key issues in protein research **(Jones, 2003)**: (i) choice of a problem to solve, or model to test and gathering all relevant information that pertain to the problem; (ii) choice of an organism; (iii) choice of a protein; (iv) choice of methods; (v) setup of the methods; (vi) running the methods; (vii) analysis of results; (viii) interpretation of the analysed results; (ix) confrontation of the interpretation with current knowledge about the problem; (x) sharing conclusions with scientific community and when aproved then also sharing the findings with public community. Steps *i-iii* may go in any order depending on what is the focus field – a protein, an organism, or a model.

Experiments and computations. According to methods used, two approaches can be distinguished – experiments and computations, the latter comprising the use of molecular modelling and/or bioinformatics methods. Experiments and computationss do not contradict, but rather complement each other **(Wlodawer et al., 2008)**. Moreover, these two approaches are more and more dependent on each other in protein research. Nowadays, every experiment in protein research depends at some extent on computations, and vice versa **(Halperin et al., 2002; Altieri & Byrd, 2004; Billeter et al., 2008; Wlodawer et al., 2008; Güntert, 2009)**. Experiments and computations are so much intertwinned in protein research that their seperation is somewhat artificial **(Halperin et al., 2002; Altieri & Byrd, 2004; Billeter et al., 2008; Wlodawer et al., 2008; Güntert, 2009)**. Although, at the end, it is the experiment that must test model derived by experiments and/or computations, not the other way around **(Pross, 2004)**. In some sense, even computation can be regarded as a kind of an experiment **(Kurzyński, 1998)**. Anyway, both the approaches are equally invaluable in protein research. Disappreciating any of the them means half-closing the gate on the path towards full understanding of proteins.

Protein research points of view. The full understanding of proteins requires simultaneous study of their structure, dynamics and function. Moreover, these three protein properties must be essentially considered from evolutionary point of view, because nothing in biology makes sense except in the light of evolution **(Dobzhansky, 1964; Koshland Jr., 1976; Woese, 2001)**. Various methods have been developed and established as reliable tools for probing protein structure, dynamics and function (see 1.5.3). Due to tight relationship between hierarchies of protein structure, hierarchies of protein dynamics and complexity of their effects on protein function, one method may bring information on various aspects of structure-dynamics-function relationships of a protein, and oppositely, several methods complement in providing valuable information on a specific property of a protein. Thus, the most comprehensive understanding of the studied protein can be obtained only by combination of various methods.

1.5.3 Basic tasks in protein research

1.5.3.1 Determination and prediction of protein structure

Determination of primary protein structure. Identification of amino acid residues at every position in the protein

primary structure is an indispensable step in protein research aimed at understanding structure-dynamics-function relationships from evolutionary point of view. As the relationship between gene sequence and primary protein structure is defined by the genetic code, knowing the gene sequence means knowing primary protein structure. Consequently, there are two possible approaches in determination of primary protein structure: (i) direct determination of protein primary structure, i.e. protein sequencing, that can be performed using mass spectrometry (MS) or Edman degradation **(Edman, 1949; Edman, 1950)**; and (ii) determination of primary protein structure indirectly by determination of the nucleotide sequence of the corresponding gene, i.e. gene sequencing. Protein sequencing is nowadays used for peptide sequencing and for quick assessment of protein similarities by identification of few tens of amino acid residues at N-terminus of proteins. Gene sequencing is nowadays a routine approach to determine sequence of genes. There are three approaches in gene sequencing – (i) chemical sequencing developed by Gilbert & Maxam **(1977)**, (ii) plus-minus sequencing developed by Sanger and co-workers **(Sanger et al., 1977a; Sanger, 1980)**; and (iii) dideoxynucleoside termination sequencing developed by Sanger et al. **(1977b)**. Dideoxynucleoside termination sequencing replaced plus-minus sequencing and chemical sequncing for higher precision and speed **(Sanger et al., 1978)**, and for lower consumption of chemicals and lower toxicity, respectively. Newly determined nucleotide sequences should be deposited in publicly available databases – GenBank **(Benson et al., 2005;** http://www.ncbi.nlm.nih.gov/Genbank/**)**, EMBL nucleotide sequence database **(Cochrane et al., 2009;** http://www.ebi.ac.uk/embl/**)** or DNA Ddata Bank of Japan (DDBJ; http://www.ddbj.nig.ac.jp/). Data are being shared among these three databases through International Nucleotide Sequence Database Collaboration (INSDC; http://www.insdc.org/).

Determination of secondary protein structure. Some regions of protein sequence fold into secondary structure elements, helices and β-strands, whereas others form connections between them. Since limited repertoir of secondary structure elements and their arrangement in space **(Chothia, 1992; Vitkup et al., 2001)**, knowing whether the protein contains amino acid residues in helical and/or extended conformation, how many and where, narrows the space of possible tertiary protein structure folds for the given protein sequence. Qualitative and quantitative information about secondary protein structure can be obtained by means of far-UV (180-260 nm) circular dichroism (CD) spectroscopy **(Kelly et al., 2005)**. Distinguishing different helical conformations (α-, 3_{10}- and π-) can be achieved by UV resonance RAMAN (UVRR) spectroscopy **(Mikhonin & Asher, 2006)**. The same quantitative information as provided by CD and UVRR spectroscopic approaches, further enriched by assignment of individual amino acid residues to secondary structure elements, can be obtained from protein backbone chemical shifts **(Spera & Bax, 1991; Wishart & Sykes, 1994; Kuszewski et al., 1995; Cornilescu et al., 1999; Wang & Jardetzky, 2002)** and vicinal scalar couplings **(Karplus, 1959; Karplus, 1963)** determined using nuclear magnetic resonance (NMR) spectroscopy **(Teng, 2005)**. While NMR chemical shifts and vicinal scalar coupling can be used directly to determine secondary protein structure, protein crystallography techniques need first to be applied to determine tertiary structure of an entire protein whose geometry can only then be analysed to identify secondary protein structure elements **(Wlodawer et al., 2008)**. Several methods are available for such purpose **(Martin et al., 2005)**, e.g. DSSP **(Kabsch & Sander, 1983)**, KAKSI **(Martin et al., 2005)**, STRIDE **(Frishman & Argos, 1995)**, XTLSSTR **(King & Johnson, 1999)**, PSEA **(Labesse et al., 1997)**, SECSTR **(Fodje & Karadaghi, 2002)**, DEFINE **(Richards & Kundrot, 1988)**.

Prediction of secondary protein structure. It is well established, by means of CD spectroscopy and NMR spectroscopy, that different amino acid residues show different propensities for location in helical and extended conformations, and even at different positions within an element in the case of a helix **(Penel et al., 1999)**. Therefore, it should be possible to predict secondary structure elements from primary protein sequence alone. Indeed, several bioinformatics methods are available for this purpose, e.g. PSIPRED **(Jones, 1999;** http://bioinf.cs.ucl.ac.uk/psipred/**)** and JPRED **(Cole et al., 2008;** http://www.compbio.dundee.ac.uk/www-jpred/**)**, with average prediction accuracy ~ 75% **(Montgomerie et al., 2006)**. Considering tertiary aspects of secondary structure elements **(Kumar & Bansal, 1998; Pal & Chakrabarti, 2000)**, the accuracy can be further improved (up to 90%) by including tertiary protein structure database comparisons as part of the prediction process, e.g. as implemented in PROTEUS **(Montgomerie et al., 2006;** http://wks16338.biology.ualberta.ca/proteus/**)**. Higher reliability of secondary structure prediction can be achieved by combination of various approaches, i.e. using consensus strategy which is so typical for bioinformatics field, e.g. using NPS@ **(Deléage et al., 1997;** http://npsa-pbil.ibcp.fr/cgi-bin/npsa_automat.pl?page=/NPSA/npsa_seccons.html**)**.

Determination of tertiary protein structure. Determination of tertiary protein structure is at the very heart of any attempt to understand protein structure-dynamics-function relationships. Tertiary protein structure fingerprint, useful for comparison between mutant proteins and for validation of sample prior the application of low and high resolution protein structure determination, can be obtained by near-UV CD spectroscopy **(Kelly et al., 2005)** and

Raman optical activity **(Wilson et al., 1996)**. Molecular weight can be identified by gel filtration, electrophoresis, dynamic light scattering, and by low resolution (~ 10 Å) structural techniques **(Schmidt & Lamzin, 2007)**. The latter include electron microscopy, small angle X-ray scattering (SAXS) and small angle neutron scattering (SANS), and additionally provide information about molecular shape **(Petoukhov & Svergun, 2007; Schmidt & Lamzin, 2007)**. The deepest insight into protein structure can be obtained by atomic resolution methods, crystallography **(Kendrew et al., 1958; Kendrew et al., 1960; Kendrew, 1962; Acharya & Lloyd, 2005)** and NMR spectroscopy **(Altieri & Byrd, 2004)**, that ideally identify positions of all atoms of a protein in the three-dimensional space. Crystallographic techniques can be classified according to nature of the diffraction beam into X-ray crystallography, XC **(Kendrew et al., 1958; Kendrew et al., 1960; Kendrew, 1962)**, neutron crystallography, NC **(Blakeley et al., 2008)** and electron crystallography, EC **(Unwin & Henderson, 1975; Henderson & Unwin, 1975; Henderson et al., 1990; Kimura et al., 1997)**. NMR spectroscopy can be applied to determine tertiary protein structure in solution using a variety of two-dimensional (HSQC, COSY, TOCSY, NEOSY, HSQC), three-dimensional (HNCO, HN(CA)CO, HNCA, NOESY/HSQC, TOCSY/HSQC) experiments **(Altieri & Byrd, 2004; Foster et al., 2007; Güntert, 2009)** and even four-dimensional experiments **(Kay, 2005; Foster et al., 2007)**, or via chemical shifts only **(Cornilescu et al., 1999; Neal et al., 2003; Cavalli et al., 2007; Shen et al., 2008; Wishart et al., 2008)**. Chemical shifts can also be used in solid state NMR structure determination **(Baldus, 2007; Robustelli et al., 2008; Shen et al., 2009)**. Despite rapid development in NMR **(Altieri & Byrd, 2004; Billeter et al., 2008)** and ever increasing size limitation, nowadays > 82 kDa **(Tugarinov et al., 2005b)**, XC is the only technique routinely used to determine structures of large proteins > 20 kDa **(Foster et al., 2007; Billeter et al., 2008)**. XC will likely remain the primary technique for determining structures of large proteins for the forseeable future **(DeLucas et al., 2003; McPherson, 2004)**. Other approaches will find applications when XC fails **(Bard et al., 2004; McPherson, 2004; Acharya & Lloyd, 2005; DeLucas et al., 2005; Pusey et al., 2005; Manjasetty et al., 2008)** and/or when NC-specific information, i.e. position of hydrogen atoms **(Blakeley et al., 2008)**, EC-specific information, i.e. determination of tertiary structure of membrane proteins and determination of charge state of individual amino acid residues **(Kimura et al., 1997; Mitsuoka et al., 1999; Hite et al., 2007)**, is needed; solution and solid state NMR will find application especially for characterisation of "unstructured" functional proteins **(Billeter et al., 2008)** and membrane proteins **(Robustelli et al., 2008; Shen et al., 2009)**, respectively. Determined protein structures should be deposited in publicly available Protein Data Bank (PDB; **Berman et al., 2003**). Additionally, there exists also specialised NMR structure database, DRESS **(Nabuurs et al., 2004)**, Hydrogen and Hydration in proteins Data Base (HHDB) storing positions of hydrogen atoms determined by NC **(Blakeley et al., 2008)**, and protein fold classification databases, CATH **(Orengo et al., 1997; Orengo et al., 1998; Orengo et al., 2002; Reeves et al., 2006; Cuff et al., 2009)** and SCOP **(Murzin et al., 1995; Hubbard et al., 1998)**. It should be emphasised that both NMR protein structures and protein crystal structures are models, i.e. interpretations of NMR and crystallographic experiments, respectively **(Lupas, 2008)**. Atomic-detail determination of tertiary protein structure is thus an examplary example of interdependence of experiment and molecular modelling **(Lupas, 2008)**.

Prediction of tertiary protein structure. Sometimes, the protein resists XC/NC/EC determination or is too large to be tackled by NMR spectroscopy. In such cases, atomic-detail structure can still be obtained – using bioinformatics and molecular modelling techniques. Based on the assumption, that similar protein sequences fold into similar native tertiary structures **(Chothia & Lesk, 1986; Dalal et al., 1997; Baldwin & Rose, 1999b; Orengo et al., 2002)**, the so-called homology model can be build using sufficiently similar **(Vitkup et al., 2001)**, i.e. likely evolutionary homologeous **(Aloy et al., 2005)**, NMR, XC, NC or EC high or atomic resolution tertiary protein structures, e.g. by means of MODELLER **(Sali & Blundell, 1993;** http://www.salilab.org/modeller/**)**, SWISSMODEL **(Schwede et al., 2003;** http://swissmodel.expasy.org//SWISS-MODEL.html**)** and Genesilico MetaServer **(Kurowski & Bujnicki, 2003;** https://www.genesilico.pl/meta2/**)**. Quality of a homology model depends on number of available template structures, sequence identity, distribution of non-similar regions, presence of long insertions and deletions, methods applied, and whether the case belongs to majority of similar sequence-similar fold "rule" or is an exception **(Vitkup et al., 2001)**. At target-template sequence identity > 30-35%, the homology model quality often allows to correlate structural variations with differences in function **(Vitkup et al., 2001)**. For sequence identity > 40%, homology model quality increases linearly with increasing sequence identity **(Vitkup et al., 2001)**. Since limited number of folds in nature, carefully chosen proteins for NMR or crystallographic tertiary structure determination may identify all 95% of all 10^4 natural folds **(Chothia, 1992; Vitkup et al., 2001)** in ten years, according to estimation of growing speed of structure determination in subsequent years **(Vitkup et al., 2001)**. Then, almost all protein sequences would have sufficiently similar sequence with one or more experimental model that would allow high-quality homology models to be built **(Vitkup et al., 2001)**. Higher number of template structures is convenient as it allows building higher quality

fragments of the target protein and subsequent recombining the fragments into final model, a strategy used by Frankenstein3D approach **(Kosinski et al., 2003; Kosinski et al., 2005;** https://genesilico.pl/toolkit/unimod?method=FrankensteinWebOptimizeAlignment**)**. If no template protein structure is available, the tertiary protein structure can be predicted by de novo building using information from secondary structure prediction, turn prediction, atomic interactions, fragment insertion and numerical simulations, e.g. ROSETTA **(Bradley et al., 2003)**. Alternatively, fold can be identified via the so-called threading approaches, e.g. SUPERFAMILY **(Gough et al., 2001)**, PHYRE **(Kelley & Sternberg, 2009)**, pGenTHREADER **(Bryson et al., 2005)** and pDomTHREADER **(Bryson et al., 2005)**, i.e. by secondary structure prediction and advanced sequence comparison followed by testing compatibility of the sequence with the selected known folds **(Bowie et al., 1991; Bryant & Lawrence, 1993; Moult et al., 1997)**. Despite the heavy effort to predict tertiary protein structures, eight rounds of Critical Assessment of Structure Prediction (CASP) competitions **(Moult et al., 1995;** http://predictioncenter.org/**)**, initiated by Moult in response to periodic, poorly substantiated claims of decisive progress in solving the protein folding problem reveal that so far, no methods has produced results suggesting that the problem of predicting protein structure has been reached at a fundamental level **(Kryshtafovych et al., 2005; Lupas, 2008)**.

Determination of quarternary protein structure. Oligomeric state of a protein can be identified by gel filtration, electrophoresis, dynamic light scattering, electron microscopy, SAXS and SANS **(Petoukhov & Svergun, 2007; Schmidt & Lamzin, 2007)**. Atomic resolution quarternary protein structure can be obtained by NMR, XC, NC and EC, as in the case of tertiary protein structure. NMR spectral perturbation **(Huang et al., 1998; Fiaux et al., 2002)**, cross-relaxation **(Garrett et al., 1999)** and cross-saturation experiments **(Nishida et al., 2003)** can be used to determine quarternary interaction interface quickly without the need to solve three-dimensional structure of an entire complex and without "intrinsic" size limitation. Therefore, the NMR techniques are conveniently applicable to large complexes > 300 kDa **(Huang et al., 1998; Fiaux et al., 2002; Nishida et al., 2003; Foster et al., 2007)**, whereas XC/NC/EC must be first applied to solve the three-dimensional structure that only then can be used to predict, and analyse quarternary contacts and to distinguish them from packing interactions in the crystal lattice **(Bahadur et al., 2004; Janin et al., 2007; Kobe et al., 2008)**. Biologically relevant quarternary interface is usually more hydrophobic, contains more fully buried atoms, and shows more compact atomic packing compared to crystal packing **(Bahadur et al., 2004; Janin et al., 2007)**. Nevertheless, distinguishing biologically relevant interface from crystal contacts is often not straightforward because physical basis is the same. Moreover, biologically relevant interface may not be always present in the crystal. Thus absence of these interactions cannot be granted as the proof of absence of quarternary structure **(Kobe et al., 2008)**. These limitations necessitate complementing the crystallographic analysis with computational predictions and multiple complementary experimental techniques, including the above mentioned NMR spectroscopy, electron microscopy, CD spectroscopy, SAXS, SANS, atomic force microscopy (ATF), MS, fluorescence resonance energy transfer (FRET), electron paramagnetic resonance (EPR) spectroscopy, and mutagenesis of putative interface amino acid residues **(Kobe et al., 2008)**.

Prediction of quarternary protein structure. Based on physico-chemical models of macromolecular interactions and chemical thermodynamics, quarternary protein structure can be detected in XC structures with the use of Protein Interfaces, Surface and Assemblies (PISA) with 80-90% success rate **(Krissinel & Henrick, 2007;** http://www.ebi.ac.uk/msd-srv/prot_int/pistart.html**)**. Using PISA, biological role of the macromolecular interface can be assessed and the predicted interface can be further compared with previously identified interfaces **(Krissinel & Henrick, 2007)**. Similar success rate was reported for another computational approach that is based on interface area, fraction of surface involved, numbers and properties of atomic pair contacts, and amino acid residue propensities **(Bahadur et al., 2004)**. Although biological quarternary contacts are usually conserved, combination of size information and conservation criteria in quarternary contacts predictions showed only little predictive benefit added by the latter **(Valdar & Thornton, 2001)** because of presence of two extremes: (i) two protein complexes can show similar quarternary interactions despite very weak sequence similarity, e.g. fibroblast growth factors and their receptors vs interleukins-1 and its receptor; and (ii) two protein complexes can show different quarternary interactions despite high sequence similarity, e.g. interaction between CheY and CheA-P2 differs by a rotation of 180° in different bacterial species **(Aloy et al., 2005)**. Nevertheless, on average, there is low, medium and high correlation between sequence identity of < 30%, 30-60% and > 60%, respectively, and interaction similarity **(Aloy et al., 2005)**. Since limited number of interfaces used by nature, estimated ~ 10^4 **(Aloy et al., 2005)**, as new interfaces are being detected, the coverage of the quarternary interaction space increases which will yield ever more secure predictions in future **(Vitkup et al., 2001)**.

1.5.3.2 Determination and prediction of protein dynamics

Experimental approaches. Protein structure determines protein dynamics and they jointly determine protein function **(Karush, 1950; Wolfenden, 1974; Parak, 2003; Busenlehner & Armstrong, 2005; Igumenova et al., 2006; Jarymowycz & Stone, 2006)**. Information about conformational changes of native individual protein molecules can be obtained by SAXS and SANS **(Petoukhov & Svergun, 2007)**. Atomic resolution of protein motions including ligand-induced motions can be obtained by high-resolution techniques, XC **(Smith et al., 1994; Wilson & Brunger, 2000; Acharya & Lloyd, 2005; Bourgeois & Royant, 2005)**, NC, EC and NMR **(Palmer, 2004; Mittermaier & Kay, 2006)**. Exceptional information on protein dynamics is also provided by combination of Hydrogen/Deuterium (H/D) exchange with NC **(Blakeley et al., 2008)**, NMR **(Englander & Kallenbach, 1983)** or MS **(Busenlehner & Armstrong, 2005)**. Ligand-induced conformational changes can be also detected by differential scanning calorimetry **(Gohlke & Klebe, 2002)**, far-UV CD spectroscopy **(Kelly et al., 2005)**, and by wide-angle X-ray scattering with 2-3 Å resolution if high resolution XC structure of the protein is available **(Fischetti et al., 2004)**. Far-UV CD spectroscopy can be also applied to study protein folding by study of refolding of denaturated proteins and can be used to measure rate of tertiary protein structure acquisition **(Kelly et al., 2005)**. Protein folding can be also studied by real-time NMR spectroscopy **(Zeeb & Balbach, 2004)** allowing detection of folding equilibrium intermediates that can be silent to far-UV CD spectroscopy or fluorescence spectroscopy **(Zeeb & Balbach, 2004)**.

Determination of protein dynamics by XC. Proteins in crystal can perform function **(Bourgeois & Royant, 2005)** which is a proof of presence of biologically important motions in proteins in crystals **(Smith et al., 1994; Wilson & Brunger, 2000; Acharya & Lloyd, 2005)**, although some large-scale motions can be impeded by the crystal lattice **(Wilson & Brunger, 2000)**. XC can provide information about the protein motions through (i) atomic displacement parameter or its mathematical transformation into temperature factor (also known as "*B*-factor"), which is part of the final crystal structure model, (ii) translation-libration-screw (TLS) parameters for XC structures with resolution higher than 2 Å **(Winn et al., 2001; Chaudhry et al., 2004)**, and (iii) when a series of static structures are assigned to various states along a reaction pathway morphed into movies **(Echols et al., 2003)**. *B*-factors provide information about mobility of each atom around its mean position: the higher the *B*-factor the higher the atomic mobility **(Acharya & Lloyd, 2005)**. While XC structures solved at resolution < 1.2 Å should be always provided with isotropically refined *B*-factors, i.e. showing spherical shape of mobility, *B*-factors for XC structures solved to high resolution, i.e. > 1.2 Å, can be refined anisotropically, i.e. showing different mobility of atoms in different directions via three-dimensional ellipsoid defined by length and three-principal axes and thus providing information about directional motion **(Acharya & Lloyd, 2005; Schmidt & Lamzin, 2007)**. Secondary structure elements, especially β-sheets, are among the regions with the lowest *B*-factors, whereas loops, especially those located at protein surface, and N- and C-termini often belong to high *B*-factor regions. Derivative *B*-factors, i.e. differences between average *B*-factors for two consecutive amino acid residue main-chain groups, reveal regions of flexibility, i.e. hinge regions responsible for rigid body motion **(Carugo, 2001)**. Different protein molecules often possess different conformations even in the crystal lattice, although some may be consequence of protein molecules being in the crystalline state **(Acharya & Lloyd, 2005)**. If these conformations are highly populated, they give rise to smear in electron density map or alternative electron density for the group that differs in conformation among the ensemble of protein molecules in the crystal lattice. High mobility of some region of a protein and solvent content surrounding the protein molecule may cause missing electron density and therefore the final XC structure may have some regions missing, which is an indication of mobility or solvent effects **(Acharya & Lloyd, 2005)**. If some groups populate two or more different conformations, these can be identified by the alternative electron density for the group and these are included in the final model with occupancy information, from 0 for no occupancy to 1 for 100% occupancy **(Acharya & Lloyd, 2005)**. Although dynamics of protein in crystal lattice is not severely ceased because protein molecules are surrounded by solvent and contacts between protein molecules in crystal lattice are rather loose **(Wilson & Brunger, 2000)** XC provides only limited information about protein dynamics, because the final protein crystal structure is a time and space average of a large ensemble of protein molecules **(Acharya & Lloyd, 2005)**. Deeper insight into mobility and flexibility in protein molecule, i.e. beyond static, time and space averaged image of XC, that might be important for function can be obtained: (i) by time-resolved XC which can provide a reaction kinetics of conformational changes at the atomic level, but the pathway from one conformation to the other is different for each individual protein molecule in the crystal thus the time-resolved experiments cannot visualise the atomic trajectories by which one molecule passes from one state to the next **(Parak, 2003)**; or (ii) by multi-wavelength technique, e.g. picosecond time-resolved Laue diffraction using unfiltered polychromatic X-ray pulses, for fast data collection allowing catching transient chemical states in the crystal and identification of direction of motions **(Schotte et al., 2004; Schmidt & Lamzin, 2007)**.

Determination of protein dynamics by NMR spectroscopy. One of the greatest strengths of NMR spectroscopy is the possibility to measure molecular motion at near-atomic resolution **(Palmer, 2004; Mittermaier & Kay, 2006)**, and to identify (i) motions on various time-scales (~ 10^{-13} to ~ 10^{5} s), i.e. involving local, rigid-body, and global motions, and (ii) correlations between motions **(Tousignant & Pelletier, 2004; Zeeb & Balbach, 2004; Kay, 2005)**. TROSY NMR experiments and advance in labeling allows molecular motions to be studied in large proteins and their complexes, e.g. macromolecular assembly involving 300 kDa cylindrical protease ClpP, a 14-subunit oligomer consisting of two symmetrical heptameric rings **(Sprangers et al., 2005)**. Thus motions can be studied by NMR directly in a biological functional context **(Zhu et al., 2000; Tugarinov et al., 2005a)**. NMR measurements of residual dipolar coupling (^{1}HN-^{15}N) resulting from the weak alignment of solute proteins in dilute solution of ordering media provides information about protein backbone dynamics **(Tolman & Ruan, 2006)**. If these measurements are supplemented by ^{15}N spin relaxation experiments then information about protein internal dynamics change upon ligand binding can be obtained **(Kay, 2005)**. ^{2}H spin relaxation NMR experiments provide information about: (i) molecular recognition **(Kay et al., 1998)**; (ii) protein folding **(Choy et al., 2003)**; (iii) protein stability **(Lee & Wand, 2001)**; and (iv) response of protein dynamics to hydrophobic core amino acid residue mutations **(Mittermaier & Kay, 2004)**. These examples of NMR techniques demonstrate why NMR spectroscopy is currently at the centre of efforts to illuminate the nature of protein dynamics and their role in biological function **(Igumenova et al., 2006)**.

Computational approaches. Molecular modelling, normal mode analysis (NMA) and molecular dynamics (MD) simulations, provide finer time and space resolution of protein dynamics compared to experimental techniques **(Skjaerven et al., 2009)**. However, it should be emphasised that both NMA and MD simulations rely on high resolution protein models that can be obtained only by experimental techniques.

Prediction of protein dynamics by NMA. Correlated, shear and hinge, motions can be predicted by analysis of vibrational normal modes **(Table 8)**. Compared to MD simulations, NMA is better suited to study the slow dynamics involving large structural rearrangements because NMA is less computationally demanding. NMA proved to reproduce vibrational spectra **(Wilson et al., 1955)** which demonstrated predictive power of the computational approach **(Skjaerven et al., 2009)**. NMA includes: (i) characterising and visualising displacements associated with the modes, directly comparable with *B*-factors; (ii) identifying correlated motions; (iii) measuring degree of collectivity of displacement for assessment of degree of flexibility of domains; (iv) identifying number of NM needed to describe transconformation; and (v) simulating transition pathways between two conformations **(Skaerjven et al., 2009)**.

Table 8 | Normal mode analysis programs.

Program	Link
AD-ENM	http://enm.lobos.nih.gov/start.html
DC-ENM	http://enm.lobos.nih.gov/start_dc.html
DFProt	http://sbg.cib.csic.es/Software/DFprot/
ElNémo	http://igs-server.cnrs-mrs.fr/elnemo/index.html
iGNM	http://ignm.ccbb.pitt.edu/Index.htm
MinActionPath	http://lorentz.immstr.pasteur.fr/maxL_traj.php
MolMovDB	http://molmovdb.org/
NOMAD-Ref	http://lorentz.immstr.pasteur.fr/nomad-ref.php
NORMA	http://www.igs.cnrs-mrs.fr/elnemo/NORMA/
oGNM	http://ignm.ccbb.pitt.edu/GNM_Online_Calculation.htm
Path-ENM	http://enm.lobos.nih.gov/start_path.html
ProMode Database	http://promode.socs.waseda.ac.jp/pages/jsp/index.jsp
TMM	http://services.cbu.uib.no/tools/tmma
WEBnm	http://services.cbu.uib.no/tools/normalmodes

Prediction of protein dynamics by MD simulations. MD simulation is the most powerful theoretical method for description of protein dynamics **(Karplus & Kuriyan, 2005; Rueda et al., 2007)** because it provides atomic-detail resolution of all types of protein motions and their time-scales, if only not limited by short simulation time. Nevertheless, suppossing reasonable approximations are applied **(Carloni et al., 2002)**, MD simulation is the only technique, and well established, that can provide dynamical behaviour of a protein in "real time" movie; some such movies are being shared via publicly available MolMovDB database **(Gerstein & Krebs, 1998; Echols et al., 2003; Flores et al., 2006)**. The limitation of simulated time can be handled by enhanced conformational sampling by using implicit solvent model or by enhanced sampling MD simulation methods **(Roitberg & Simmerling, 2004)**, e.g. replica exchange MD **(Sugita & Okamoto, 1999)** which is one of the most effective sampling method **(Liwo et al., 2008)**, locally enhanced sampling MD, LES **(Elber & Karplus, 1990)**, targeted MD, TMD **(Schlitter et al., 1993)**, steered MD, SMD **(Phillips et al., 2005)**, random acceleration MD, RAMD **(Lüdemann et al., 2000a)**, and umbrella

sampling MD, USMD **(Kumar et al., 1992; Kumar et al., 1995)**. Most MD simulations in the future are expected to be of the steered type **(Phillips et al., 2005)**. In general, each MD method relies on a force field, i.e. parameters that describe atomic properties and interatomic bonded and non-bonded interactions (forces), and a potential energy function that uses the parameters for description of the relationship between structure and energy of the system **(Mackerell, 2004)**. Interatomic forces are derived empirically and electronic degrees of freedom are integrated out **(Carloni et al., 2002)**. Several MD packages have emerged within last three decades; the most widely used are AMBER **(Weiner & Kollman, 1981; Case et al., 2005)**, CHARMM **(Brooks et al., 1983)**, GROMOS **(Christen et al., 2005)**, GROMACS **(Van Der Spoel et al., 2005)**, NAMD **(Humphrey et al., 1996; Phillips et al., 2005)**, OPLS **(Jorgensen & Tirado-Rives, 1988)**, and OPLS-AA **(Jorgensen et al., 1996)**. Modern protein force fields, e.g. CHARMM, AMBER and OPLS-AA, behave comparably in MD simulations **(Price & Brooks III, 2002)**. The progress in MD simulations is almost entirely dependent on advances in computing power **(Borrell, 2008)**. either through the growth of supercomputing centres (e.g. MetaCentrum; http://meta.cesnet.cz/cms/opencms/en) or through imaginative distributive computing, e.g. folding@home **(Shirts & Pande, 2000)**. For illustration, the first successful MD simulation of a protein, 9.2 ps of 58-amino acid residue bovine pancreatic trypsin inhibitor was reported in 1977 **(McCammon & Karplus, 1977)**. 39 years later, > 50 ns long all-atom MD simulation of entire living system, satellite tobbacco mosaic virus composed of ~ 10^6 atoms, was reported **(Freddolino et al., 2006)**. MD simulation length progressed rapidly: 10 ps for years 1970-1979, 10-100 ps for years 1980-1995, 100 ps to 1 ns for years 1995-1999, and 1-100 ns for years 2000-2007 **(Sanbonmatsu & Tung, 2007)**. Despite the progress, however, the desired depth of understanding of protein action in time by using MD is not particularly close **(Lupas, 2008)**.

1.5.3.3 Determination and prediction of protein function

Determination and prediction of protein function by sequence and structure comparison. There are two possible scenarios how to match a protein with a function, both starting by creating a genome library. In the first approach, the genome library is searched for known function. The genome fragment of the clone that acquired the function is sequenced and gene that encodes for the protein responsible for the function can thus be identified. In the second approach, entire genome library is sequenced to determine nucleotide sequence of the whole genome. The genome sequence is then searched for all possible non-stop frames (also known as “open reading frames”), which represent set of putative genes. Comparison of the sequences of open reading frames with protein sequences stored in publicly available nucleotide sequence databases, GenBank, EMBL nucleotide sequence database and DDBJ, and protein sequence database, UniProt **(Apweiler et al., 2004a; Apweiler et al., 2004b; Bairoch et al., 2005; UniProt Consortium, 2009)**, can reveal similarity with a gene whose protein product and its function is known **(McLachlan, 1971; Gaboriaud et al., 1987; Altschul et al., 1990; Altschul & Lipman, 1990; Altschul et al., 1997; Callebaut et al., 2000)**. The higher is the sequence similarity, the higher is the confidence about functional similarity, although exceptions may exist. There are numerous approaches for sequence-based function prediction **(Table 9; Watson et al., 2005)**. These tools play important role in proposing function of newly identified putative genes, that nowadays emerge in large number from genome and metagenome sequencing projects. Once prediction of function suggests some possible functions, these must be tested experimentally by biochemical characterisation and, if possible, structural characterisation, including solving atomic-detail resolution protein structure by XC, NC, EC or NMR. The experimental protein structure can be then used for structure-based function prediction **(Table 9)**. Determination/prediction of protein function is thus a classic example of tight cooperation between experiment, bioinformatics and molecular modelling.

Table 9 | Function prediction. (pp. 59-60)

Approach	Methods
Sequence-based function prediction	BLAST/PSI-BLAST (http://blast.ncbi.nlm.nih.gov/Blast.cgi)
	SSEARCH/FASTA (http://fasta.bioch.virginia.edu/fasta_www2/fasta_list2.shtml)
	PROSITE (http://www.expasy.org/prosite/)
	PRINTS (http://www.bioinf.manchester.ac.uk/dbbrowser/PRINTS/index.php)
	Pfam (http://pfam.sanger.ac.uk/)
	ProDom (http://prodom.prabi.fr/prodom/current/html/home.php)
	TIGRFAMs (http://www.jcvi.org/cms/research/projects/tigrfams/overview/)
	SMART (http://smart.embl-heidelberg.de/)
	SUPERFAMILY (http://supfam.cs.bris.ac.uk/SUPERFAMILY/)
	InterProScan (http://www.ebi.ac.uk/Tools/InterProScan/)
	Hhpred/HHsearch (http://toolkit.tuebingen.mpg.de/hhpred)
	COACH (http://drive5.com/lobster/)

Approach	Methods
Sequence-based function prediction	QuasiMotiFinder (http://quasimotifinder.tau.ac.il/)
Fold similarity-based function prediction	DALI (http://ekhidna.biocenter.helsinki.fi/dali_server/) SSM (http://www.ebi.ac.uk/msd-srv/ssm/) CATHEDRAL (http://www.cathdb.info/cgi-bin/Grath.pl) VAST (http://structure.ncbi.nlm.nih.gov/Structure/VAST/vast.shtml) CE (http://cl.sdsc.edu/ce.html) FAST (http://biowulf.bu.edu/FAST/)
Pockets and clefts-based function prediction	CASTp **(Dundas et al., 2006;** http://sts-fw.bioengr.uic.edu/castp/index.php**)** VOIDOO **(Kleywegt & Jones, 1994)** SURFNET (http://cbm.bio.uniroma2.it/surface/[http://www.biochem.ucl.ac.uk/~roman/surfnet/surfnet.html) SURFACE (http://cbm.bio.uniroma2.it/surface/)
Active sites-based function prediction	MSDsite (http://www.ebi.ac.uk/pdbe-site/PDBeSite/) CSA **(Porter et al., 2004;** http://www.ebi.ac.uk/thornton-srv/databases/CSA/**)** PINTS (http://www.russell.embl-heidelberg.de/pints/) SPASM/RIGOR (http://xray.bmc.uu.se/usf/spasm.html) SuMo (http://sumo-pbil.ibcp.fr/cgi-bin/sumo-welcome) PDBSiteScan (http://wwwmgs.bionet.nsc.ru/mgs/gnw/pdbsitescan/) DRESPAT (http://www.it.iitb.ac.in/~ashish/research/drespat.html) SARIG (http://bioinfo2.weizmann.ac.il/%7Epietro/SARIG/V3/index.html)
Phylogenetic analysis-based function prediction	ConSurf (http://consurf.tau.ac.il/) FunShift (http://funshift.sbc.su.se/) ET (http://www-cryst.bioc.cam.ac.uk/~jiye/evoltrace/evoltrace.html)
Prediction of protein-DNA interaction	PDNA-pred (http://www.ebi.ac.uk/thornton-srv/databases/PDNA-pred/) PreDS (http://pre-s.protein.osaka-u.ac.jp/preds/) Protein-Nucleic Acid Interaction Server (http://www.biochem.ucl.ac.uk/bsm/DNA/server/)
Prediction of networks and protein-protein interactions	STRING (http://string.embl.de/) IntAct (http://www.ebi.ac.uk/intact/site/index.jsf) MIPS (http://mips.gsf.de/proj/ppi/) ProMate (http://bioinfo.weizmann.ac.il/promate/)
Function definition	KEGG (http://www.genome.jp/kegg/) Enzyme nomenclature (http://www.chem.qmul.ac.uk/iubmb/enzyme/) GO (http://geneontology.org/) GOA (http://www.ebi.ac.uk/GOA/)
Function prediction servers	ProFunc (http://www.ebi.ac.uk/thornton-srv/databases/ProFunc/) ProKnow (http://proknow.mbi.ucla.edu/) SiteEngine (http://bioinfo3d.cs.tau.ac.il/SiteEngine/SiteEngine.html) AnaGram (http://mango.ac.uma.es/anagram/) Gene3D (http://gene3d.biochem.ucl.ac.uk/Gene3D/)

Determination of protein-ligand binding. Since many proteins function by binding ligands, determination of protein-ligand complexes at high/atomic resolution is important step towards deeper understanding of protein function. Both NMR **(Huang et al., 1998; Garrett et al., 1999; Fiaux et al., 2002; Nishida et al., 2003; Foster et al., 2007)** and with greater certainty crystallography **(Blundell & Patel, 2004)** can suggest both region where the protein function is being executed and ligands that are capable of binding. NMR allows mapping of binding interfaces of interacting partners without the need for de novo tertiary protein structure determination, i.e. without any intrinsic size limitation, which makes determination of protein-ligand binding interaction the most common application of protein NMR **(Huang et al., 1998; Garrett et al., 1999; Fiaux et al., 2002; Nishida et al., 2003; Foster et al., 2007)**. H/D-exchange coupled with MS can be used for mapping unknown ligand binding sites and for correlating the observed changes in protein dynamics to function **(Busenlehner & Armstrong, 2005)**. Since protein function can be greatly influenced by solvent, solving XC in various solvents, the so-called experimental solvent mapping, can reveal solvent and potential ligand binding sites **(Ringe & Mattos, 1999)**. This approach has also its NMR counterpart **(Liepinsh & Otting, 1997)**. Binding affinity can be determined by two approaches: (i) indirect methods, e.g. fluorescence quenching; and (ii) direct measurement of thermodynamic parameters by means of microcalorimetric measurements using isothermal titration calorimetry and diffferential scanning calorimetry **(Gohlke & Klebe, 2002)**.

Prediction of protein-ligand binding. Discrimination between ligand and non-ligand in complexes determined to high-resolution by XC, NC, EC, or NMR spectroscopy can be done computationally by various tools, e.g. LIGPLOT **(Wallace et al., 1995)**, TESS **(Wallace et al., 1997)**, ASSAM **(Artymiuk et al., 1994)** and Relibase **(Kleywegt,**

1999). Rapid assessment of possible ligand binding sites can be performed by computational solvent mapping, the counterpart of XC and NMR solvent mappings **(Silberstein et al., 2003)**. An alternative to the computational solvent mapping is represented by molecular docking, pioneered during early 1980s **(Kuntz et al., 1982)**, This approach plays an important complementary and supportive role in determination of protein-ligand association from several perspectives – protein binding site, ligand affinity and ligand specificity **(Halperin et al., 2002)**. The most widely used docking programs include ADAM **(Mizutani et al., 1994)**, AutoDock **(Goodsell & Olson, 1990; Morris et al., 1996; Morris et al., 1998)**, DARWIN **(Taylor & Burnett, 2000)**, DIVALI **(Clark & Ajay, 1995)**, DOCK 4.0 **(Ewing et al., 2001)**, DockVision **(Hart & Read, 1992)**, EUDOC **(Perola et al., 2000)**, FlexE **(Claussen et al., 2001)**, FlexX **(Rarey et al., 1996)**, FLOG **(Miller et al., 1994)**, FTDOCK **(Gabb et al., 1997)**, GOLD **(Jones et al., 1997)**, Hammerhead **(Welch et al., 1996)**, ICM **(Abagyan et al., 1994)**, LIGIN **(Sobolev et al., 1996)**, LUDI **(Böhm, 1992)**, MCDOCK **(Liu & Wang, 1999)**, Prodock **(Trosset & Scheraga, 1999)**, PRO_LEADS **(Baxter et al., 1998)**, QXP **(McMartin & Bohacek, 1997)**, SANDOCK **(Burkhard et al., 1998)**, SFDock **(Hou et al., 1999)**, and Soft docking **(Jiang & Kim, 1991)**. As of year 2006, the most cited program was AUTODOCK with 27% share **(Sousa et al., 2006)**. However, performance of most docking tools is highly dependent on the specific characteristics of both the binding site and the ligand. Therefore, establishing which method would be most suitable in a precise context is almost impossible **(Sousa et al., 2006)**. As tertiary protein structure prediction has its CASP, so has molecular docking its CAPRI, Critical Assessment of Predicted Interactions **(Janin et al., 2007)**. CAPRI revealed that docking algorithms work efficiently and accurately when predicting the mode of assembly of proteins that do not "significantly" change conformation upon association and perform less well in the presence of large conformational changes **(Janin et al., 2007)**. Thus, the most challenging problem of molecular docking is treatment of ligand and especially protein dynamics as both may be important for formation of the protein-ligand complex in both conformational selection and induced-fit binding scenarios **(May & Zacharias, 2005)**. Although every docking approach contains scoring function for discriminating between ligand binding modes and between various ligands, reliable estimation of free energy of binding must be obtained by other approaches. Currently, one of the best ways to calculate binding energy is to use the linear response approximation (LRA) treatment which provides good estimate for the free energy associated with change between potential surfaces and possibility of decomposition of free energies to their individual additive contributions, in contrast to free energy perturbation, FEP **(Lee et al., 1992; Olsson et al., 2004)**.

Determination of ligand migration through protein. Ligand migration through protein may play crucial role for function of proteins with buried binding sites. Ligand migration through protein can be inferred experimentally by capturing protein-ligand complexes by XC **(Verschueren et al., 1993a; Pikkemaat et al., 1999; Dunn et al., 2001; Podust et al., 2001; Teeter, 2004)** or by NMR **(Berlow et al., 2007; Yao et al., 2007)**, by identification of cavities in high-resolution experimental protein structures **(Williams et al., 1994; Oprea et al., 1997; Takano et al., 1997; Brunori et al., 1999)**, by various physico-chemical methods, e.g. flash (laser) photolysis **(Austin et al., 1975; Brunori et al., 1999; Scott et al., 2001; Lavalette et al., 2006)**, time-resolved photoacustic calorimetry **(Di Primo et al., 1997)**, fluorescence spectroscopy **(Verschueren et al., 1993a; Brunori et al., 1999; Pikkemaat et al., 1999; Prasad et al., 2000; Prasad & Mitra, 2002)**, phosphorescence spectroscopy **(Khajehpour et al., 2003)**, UV-VIS and resonance Raman spectroscopy **(Jakopitsch et al., 2005)** and charge-transfer absorption spectroscopy **(Zelent et al., 2004)**, and in case of an enzyme by appropriate methods for enantioselectivity measurements **(Wombacher et al., 2006)**, and for steady-state kinetics **(Scott et al., 2002; Jakopitsch et al., 2005)** and pre-steady state kinetics measurements **(Jakopitsch et al., 2005)**.

Prediction of ligand migration through protein. Possible ligand pathway through protein can be identified by searching for continuous region of high *B*-factor amino acid residues or atoms in the so-called thermal motion pathway approach **(Lüdemann et al., 1997; Carugo & Argos, 1998)**. High-resolution XC, NC, EC and NMR structures can be also explored for presence of internal cavities, e.g. by CASTP **(Dundas et al., 2006)** and VOIDOO **(Kleywegt & Jones, 1994)**, and tunnels, e.g. by CAVER 1.0 **(Banáš et al., 2006; Petřek et al., 2006; Cojocaru et al., 2007; Negri et al., 2007; Silberstein et al., 2007;** http://www.loschmidt.chemi.muni.cz/caver-1.0/), MOLE **(Petřek et al., 2007;** http://mole.chemi.muni.cz/index.php), MOLAXIS **(Yaffe et al., 2008;** http://bioinfo3d.cs.tau.ac.il/MolAxis/molaxis.html), CHUNNEL **(Coleman & Sharp, 2009;** http://crystal.med.upenn.edu/software.html), and SLITHER **(Lee et al., 2009;** http://slither.rcas.sinica.edu.tw/index.php). However, ligand migration is a dynamic process characteristic by motions in both protein and ligand, and by protein-ligand interactions. MD is currently the only approach that can provide atomic-detail movie of ligand migration in proteins. Both classical MD **(Kottalam & Case, 1988; Wlodek et al., 1997; Enyedy et al., 1998; Brunori et al., 1999; Tara et al., 1999; Wriggers & Schulten, 1999; Henchman et**

al., 2002; Khajehpour et al., 2003; Xu et al., 2003; Chau, 2004; Damjanović et al., 2005; Wen et al., 2005; Schleinkofer et al., 2005; Banáš et al., 2006; Hritz et al., 2006; Zhou et al., 2006; Negri et al., 2007; Wang & Duan, 2007) and enhanced sampling MD simulations **(Kottalam & Case, 1988; Lüdemann et al., 1997; Enyedy et al., 1998; Wriggers & Schulten, 1999; Lüdemann et al., 2000a; Van Belle et al., 2000; Isralewitz et al., 2001; Scott et al., 2001; Bui et al., 2003; Xu et al., 2003; Wade et al., 2004; Li et al., 2005; Schleinkofer et al., 2005; Bikiel et al., 2006; Carlsson et al., 2006; Cohen et al., 2006; Wang & Duan, 2007)** were employed in numerous studies and proved useful in identification of pathways and dynamical behaviour associated with ligand diffusion through protein, and protein-ligand interactions during the process. The enhanced sampling MD simulations include RAMD **(Lüdemann et al., 1997; Lüdemann et al., 2000a; Wade et al., 2004; Schleinkofer et al., 2005; Carlsson et al., 2006; Wang & Duan, 2007)**, SMD **(Wriggers & Schulten, 1999; Isralewitz et al., 2001; Xu et al., 2003; Li et al., 2005; Bikiel et al., 2006)**, LES **(Scott et al., 2001)**, multiple copy sampling **(Van Belle et al., 2000)**, activated MD **(Bikiel et al., 2006)**, USMD **(Kottalam & Case, 1988; Enyedy et al., 1998; Bui et al., 2003)**, extended MD **(Bikiel et al., 2006)**, and implicit ligand sampling **(Cohen et al., 2006)**. Both classical and especially enhanced sampling MD simulations provide such a level of information that cannot be achieved by contemporary experimental methods. This apparent advantage of computations over experiments is at the same time the major drawback of the simulations as they do not have corresponding experimental validation. Thus, interpretation of the simulations requires a special caution.

Determination of enzyme reaction mechanism. The task of determination of reaction mechanism can be tackled using variety of techniques and its scenario largely depends on particular case. From chemical point of view, there are various possibilities, how a substrate can be chemically modified by an enzyme into particular product; and the reaction can include more than one distinct chemical step, and thus one or more intermediates. It is therefore of high importance to get understanding of the underlying chemistry of the enzymatic reaction. This problem needs to be tackled from three points of view – structural (see 1.5.3.1), dynamical (see 1.5.3.2) and chemical. Identification of catalytic amino acid residues, substrate binding residues, co-substrate/co-factor/co-enzyme requirement and their binding sites, is crucial structural information for determination of reaction mechanism. This structural information can be obtained from both NMR and crystallography determination of protein structure in presence of substrates, products, co-substrates and co-factors/co-enzymes. Even in the protein crystal, an enzyme can perform its function. It is therefore possible to observe intermediates formed during complex enzymatic reaction by means of the so-called kinetic XC, by employing catching inermediate structures by freeze trapping methods or "real-time-resolved" Laue diffraction to "film proteins in action", complemented by UV/visible single-crystal spectroscopy **(Bourgeois & Royant, 2005)** or by single-crystal microspectrophotometry **(Pearson et al., 2004)**. Trapping intermediate states in a reaction pathway of membrane proteins is possible using time-resolved EC **(Hite et al., 2007)**. Many enzymatic reactions involve hydrogen transfer **(Howard et al., 2004; Stranzl et al., 2004)**, therefore ultra-high resolution XC structure **(Schmidt & Lamzin, 2007)** or NC structure can be valuable source of structural information. Simultaneously, biochemical characterisation of the reaction with selected substrate should be performed aimed at determining steady-state kinetic constants, K_m and k_{cat}. Both chemical nature of the product and its quantification can be done by MS **(Liesener & Karst, 2005)**. Finer degree of product identification can be achieved by combining gas chromatography, GC **(James & Martin, 1952)** with MS **(Holmes & Morrell, 1957; Gohlke & McLafferty, 1993; Honour, 2006)** and NMR spectroscopy. The deepest understanding of the reaction mechanism means identification of all intermediates, reversibility of individual reaction steps and their rate constants, thus determining the rate-limiting step of the reaction. This requires to measure enzyme kinetics before reaching steady-state. Two complementary approaches are available – rapid quench-flow **(Ferguson & Roughton, 1934; Barman et al., 2006)** and stopped-flow **(Roughton, 1963; Copeland, 2000c)**. These biochemical experiments should be complemented with substrate and product inhibition experiments, and determination of cooperativity in oligomeric proteins, especially if there is indication of deviation from Henri-Michaelis-Menten kinetics. Valuable information can be also provided by specific isotopic exchange experiments, in which certain atom of substrate, co-substrate, solvent or enzyme is exchanged for heavier isotope. If the isotope exchange affects enzymatic reaction, i.e. increases or decreases its rate, the particular species plays important role **(Paneth, 2003)**.

Prediction of enzyme reaction mechanism. Proposed reaction mechanism can be further explored by molecular modelling techniques – hybrid QM/MM methods **(Warshel & Levitt, 1976; Senn & Thiel, 2009)**, empirical valence bond (EVB) methods **(Senn & Thiel, 2009)**, or by their combination **(Olsson & Warshel, 2004; Rosta et al., 2006)**. The reaction must be modelled in both protein and water to get further structural and dynamical insight into the reaction and to identify source of catalytic power. This requires direct observation of transition states which is accessible by the molecular modelling techniques while it is beyond reach of contemporary experimental methods because of extremely short life-time of transition state species **(Lightstone et al., 1997)**.

Generating protein variants by rational design. One of the key logical elements of scientific research is comparison. In the case of a protein, its full understanding requires determination of a structural, dynamical and functional role for all amino acid residues in the protein. Role of each amino acid residue can be best determined by comparison of the original protein with the one with the given position replaced by another amino acid residue. These changes in protein structure can be obtained via two possible ways: isolation of mutant protein from in vivo mutant, or performing specific mutagenesis of the gene in vitro. However, it is not possible to test all positions within protein for all 20 possible amino acid residue substitutions, and all their combinations because of limited number of atoms in Universe, estimated to ~ 9×10^{78} **(Voet, 1999)**. Therefore, mutagenesis need to be performed at specific selected positions or regions, via the so-called site-directed mutagenesis. This type of mutagenesis involves specific substitutions, deletions and insertions that are selected prior to mutagenesis based on structural **(Chica et al., 2005)** and, if available, dynamical and functional information available, and is thereby called "rational design" **(Craik et al., 1985)**. The resulting mutant protein is structurally, dynamically, and functionally characterised and compared with original variant and role of the given amino acid residue for protein structure, dynamics and function can be assessed. Since not only the small number of amino acid residues in protein binding site, but also much larger number amino acid residues distant from the active site can be important for protein folding (e.g. folding gate-keepers) and protein dynamics linked to function (e.g. coupled motions, rigid-body motions, spider-web motions, tunnel gating amino acid residues and binding site loop gate), the rational design might fail to identify all important amino acid residues and regions **(Tousignant & Pelletier, 2004)**.

Generating protein variants by directed evolution. If the rational design fails to identify all important amino acid residues and coupling between them, or prior knowledge of structure, dynamics and function, and relationships between them is missing or limited due to complexity of the relationships, which is often the case **(Cedrone et al., 2000; Tao & Cornish, 2002)**, then such a situation favours the use of an alternative mutagenesis approach – random mutagenesis **(Chica et al., 2005)**. There is a number of random mutagenesis techniques that can generate the so-called naïve mutant libraries **(Dalby, 2003; Sen et al., 2007)**, e.g.: error-prone PCR (epPCR); DNA shuffling **(Stemmer, 1994a; Stemmer, 1994b)**; staggered extension process (StEP); random chimeragenesis on transient templates, RACHITT **(Pelletier, 2001)**; increamental truncation for the creation of hybrid enzymes, ITCHY **(Lutz et al., 2001)**; combination of ITCHY with DNA shuffling, SCRATCHY **(Zhao et al., 2002)**; recombined extension on truncated templates, RETT; random-priming recombination, RPR; heteroduplex recombination; degenerate oligonucleotide gene shuffling, DOGS **(Gibbs et al., 2001)**; random drift mutagenesis, RNDM **(Bergquist et al., 2005)**; sequence saturation mutagenesis, SeSaM **(Wong et al., 2004);** and nucleotide exchange and excision technology, NexT **(Müller et al., 2005)**. Due to randomness of the mutations, it is likely, that the mutant proteins are not capable to reach native fold **(Chica et al., 2005)**. While site-directed mutagenesis makes specific change which is subsequently explored for its effect on function, random mutagenesis must be followed by rapid and sensitive screen or selection method for the properties of interest **(Chica et al., 2005)**, which is the major obstacle in this approach **(Tao & Cornish, 2002)**. The combination of low-frequency introduction of randomly distributed mutations in a gene, or genome **(Patnaik et al., 2002; Zhang et al., 2002)**, of interest with selection/screening of naïve mutant library and sequencing of selected candidates, is referred to as "directed evolution", a concept introduced already in 1967 by Spiegelman and co-workers **(Mills et al., 1967; Tao & Cornish, 2002; Henry & Romesberg, 2005; Sen et al., 2007)**. Although, the use of this denomation has been disputed by Trevors & Abel **(2004)** who argue that experiment that is directed cannot be evolutionary, because evolution has no goal. Directed evolution differs from natural evolution in two key aspects: (i) natural evolution occurs under multiple and variable selection pressures, whereas directed evolution is accomplished under controlled selection pressure for predetermined function **(Sen et al., 2007)**; and (ii) natural evolution favours functions advantageous to the survival of the organism **(Schmidt-Dannert, 2001; Williams et al., 2004)**, whereas in directed evolution, "non-natural" functions can be obtained **(Sen et al., 2007)**.

Generating protein variants by semi-rational approach. Since both rational design and directed evolution have different advantages and disadvantages, they can be combined beneficially into the so-called semi-rational approach **(Chica et al., 2005)**, e.g. saturation mutagenesis **(Chica et al., 2005)**. The semi-rational approach exploits structure/dynamics-based design to target random mutagenesis into specific regions or even individual amino acid residue positions, to generate the so-called smart mutant libraries that are supposed to more likely yield mutant with desired properties compared to naïve mutant libraries generated by random mutagenesis alone **(Santoro & Schultz, 2002; Dalby, 2003; Mildvan, 2004; Chica et al., 2005)**. Improved search in sequence space can be also achieved by incorporating a strategy for analysis of protein sequence activity relationships, ProSAR **(Fox et al., 2007)**, or by the use of non-natural amino acids with novel functions **(Wang et al., 2001)**. The semi-rational approach can be further aided by semi-rational combinatorial design, e.g. using protein design automation method, to eliminate protein sequences incompatible with protein fold **(Hayes et al., 2002)**, by exploiting Indel PDB database of insertions and

deletions derived from sequence alignment of closely related proteins **(Hsing & Cherkasov, 2008)**, and by considering organism-specific codon usage **(Angov et al., 2008; Welch et al., 2009)**. It can be also beneficial to introduce some mutations via random mutagenesis to identify "leads" and then fine-tune the leads by saturation mutagenesis of the identified amino acid residues **(Chica et al., 2005)**, or to perform several rounds of saturation mutagenesis in the so-called iterative saturation mutagenesis (ISM) approaches. Examples of ISM include combinatiorial active site saturation test (CAST) approach for evolving substrate acceptance and/or enantioselectivity **(Reetz et al., 2005; Reetz et al., 2006a; Reetz et al., 2009)**, and *B*-factor saturation test (*B*-FIT) approach for isolation of mutant proteins with improved stability **(Reetz et al., 2006b; Reetz & Carballeira, 2007; Reetz et al., 2009)**. Semi-rational approach, compared to rational design and directed evolution, can more likely yield proteins with improved (fine-tuned) an already existing function, e.g. change in ligand binding affinity, ligand specificity, and/or rate of enzymatic reaction **(Sen et al., 2007)**, and is thus exploited when aimed (i) at understanding possible evolutionary pathways towards modification or change in function **(Valuev et al., 2002)** or (ii) to obtain protein with improved properties for use in industrial applications. It should be noted that the successes in redesigning or "evolving" proteins, while occasionally very impressive, are precisely impressive because they are so hard to reproduce **(Lupas, 2008)** because of complexity of protein structure-dynamics-function relationships that are not yet understood to the fundamental level.

1.6 Model system

1.6.1 Selecting a protein

Scientific criteria. Every protein is worth to study because every protein may reveal important information on structure-dynamics-function relationships in evolutionary perspective that might fill a gap in our understanding of the role of proteins in living organisms **(Kendrew, 1962)**. Particular choice of a protein depends on many criteria that can be divided into two broad aspects, living organism (bacteria, archaea, eucarya) and biological role of a protein. Bacteria are often the choice because of the following properties: (i) bacteria are ubiquitous; (ii) life on Earth depends on bacteria; (iii) some bacteria cause diseases; (iv) some bacteria can be exploited for human benefit; (v) bacteria are unicellular, haploid (although they might contain more than just one copy of genome at a time) and rapidly reproducing; and (vi) laboratory manipulation (e.g. mutagenesis and killing) is apparently considered by the general public as ethically acceptable. Enzymes are then often the choice because of all the protein functions, fundamentally the most important for life is the catalytic function **(Koshland Jr., 2002b)**.

Non-scientific criteria. Besides the scientific criteria, there are also some non-scientific criteria, e.g. funding and established laboratory. Ease of obtaining funding for the research is influenced by the apparent "attractivity" of the selected living organism and/or protein. For me, as a student, the choice was also influenced by focus of the laboratory that offered me the possibility to perform doctoral research.

Choice for a bacterial haloalkane dehalogenase enzyme. All the above mentioned aspects contributed to the choice for a bacterial haloalkane dehalogenase enzyme for study of structure-dynamics-function relationships within the scope of my doctoral research.

1.6.2 Haloalkane dehalogenases

1.6.2.1 Source of haloalkane dehalogenases

Bacteria *and* Eucarya. Haloalkane dehalogenase genes have been so far identified only in bacteria primarily isolated from environment contaminated by halogenated compounds **(Keuning et al., 1985; Scholtz et al., 1987; Yokota et al., 1987; Janssen et al., 1988; Sallis et al., 1990; Kulakova et al., 1995; Kulakova et al., 1997; Nagata et al., 1997; Poelarends et al., 1998; Poelarends et al., 1999; Kulakov et al., 1999)** or identified from genome sequences **(Jesenská et al., 2002; Sato et al., 2005)**. More than 48 bacterial species are known to possess a gene encoding for haloalkane dehalogenase, or putative haloalkane degalogenase gene **(Table 10; van den Wijngaard et al., 1992; Chovancová et al., 2007)**. Phylogenetic diversity of the bacterial species harbouring haloalkane dehalogenase genes suggests widespread occurrence of these genes in bacteria **(Chovancová et al., 2007)**. Additionally, three putative haloalkane dehalogenase genes have been identified in three eucaryotic organisms **(Table 10; Chovancová et al., 2007)**. It can be expected that many more bacterial and eucaryotic species will be identified to bear putative haloalkane dehalogenase genes as more and more genome and metagenome sequences will

be determined **(Janssen et al., 2005)**.

Table 10 | Source of (putative) haloalkane dehalogenases.[a,b]

Bacteria[c]		**Eucarya**
Agrobacterium tumefaciens (DatA)	*Pseudomonas pavonaceae*	*Renilla muelleri*[d]
Ancylobacter aquaticus (DhlA)	*Psychrobacter cryohalolentis*	*Renilla reniformis*[d]
Bradyrhizobium japonicum (DbjA)	*Rhodococcus sp.* (DhaA)	*Strongylocentrotus purpuratus*[e]
Burkholderia sp.	*Rhodococcus rhodochrous* (DhaA)	
Burkholderia cenocepacia	*Rhodopirellula baltica* (DrbA)	
Caulobacter crescentus	*Shewanella sp.*	
Chloroflexus aurantiacus	*Shewanella amazonensis*	
Colwellia psychrerythraea	*Shewanella baltica*	
Desulfotalea psychrophila	*Shewanella denitrificans*	
Desulfuromonas acetoxidans	*Shewanella frigidimarina*	
Erythrobacter litoralis	*Shewanella oneidensis*	
Jannaschia sp.	*Shewanella putrefaciens*	
Lyngbya majuscula	*Sphingobium francense* (LinB)	
Mesorhizobium loti (DmlA)	*Sphingobium japonicum* (LinB)	
Mycobacterium sp. (DhaA)	*Sphingobium indicum* (LinB)	
Mycobacterium avium (DhmA)	*Streptomyces avermitilis*	
Mycobacterium bovis (DmbA, DmbB, DmbC)	*Xanthobacter autotrophicus* {DhlA)	
Mycobacterium smegmatis (DmsA)	*Xanthobacter flavus* {DhlA)	
Mycobacterium tuberculosis (DmbA, DmbB, DmbC)	*Xanthomonas axonopodis*	
Nocardia farcinica	*Xanthomonas oryzae*	
Pelobacter propionicus	*Xanthomonas campestris*	
Photobacterium profundum	*Xylella fastidiosa*	
Polaromonas sp.		
Pseudoalteromonas atlantica		

[a]Obtained by PSI-BLAST search.
[b]According to Chovancová et al. **(2007)**.
[c]Experimentally characterised haloalkane dehalogenases are given in parentheses.
[d]Also known as sea pansy.
[e]Also known as purple sea urchin.

Evolution of haloalkane dehalogenase genes. Some bacteria have already revealed to bear two or more same or different genes encoding haloalkane dehalogenases **(Jesenská et al., 2005; Ito et al., 2007)** or putative haloalkane dehalogenase genes **(Table 11; Chovancová et al., 2007)** and different strains of same or even different bacterial species isolated from different sites around the World have been identified to contain identical or nearly identical haloalkane dehalogenase genes encoding identical enzymes **(Table 12; Janssen et al., 1995; Poelarends et al., 1998; Poelarends et al., 1999; Poelarends et al., 2000a; Poelarends et al., 2000b; Chovancová et al., 2007)**. These observations suggest recent distribution and divergence of haloalkane dehalogenase genes from ancestral genes **(Poelarends et al., 2000a; Ito et al., 2007)** by gene duplication **(Jesenská et al., 2000; Jesenská et al., 2005; Chovancová et al., 2007; Pavlová et al., 2007)** and horizontal gene transfer **(van den Wijngaard et al., 1992; Janssen et al., 1995; Poelarends et al., 1998; Poelarends et al., 1999; Poelarends et al., 2000a; Poelarends et al., 2000b; Ito et al., 2007; Wu et al., 2007; Mazumdar et al., 2008)**. Although, the recent distribution has been recently disputed by Janssen **(2004)**.

Table 11 | Bacteria with two or more (putative) haloalkane dehalogenase genes.[a,b]

Bacteria	**Number of genes**
Jannaschia sp. CCS1	2
Mycobacterium avium K-10	2
Mycobacterium bovis AF2122/97	3
Mycobacterium tuberculosis H37Rv	3
Shewanella frigidimarina NCIMB 400	3

[a]Obtained by PSI-BLAST search.
[b]According to Chovancová et al. **(2007)**.

Table 12 | Different species of bacteria with identical or nearly identical (putative) haloalkane dehalogenases.[a,b,c]

Protein	Bacteria
DhlA	*Xanthobacter autotrophicus*
	Xanthobacter flavus
	Ancylobacter aquaticus
DhaA	*Rhodococcus rhodochrous*
	Pseudomonas pavonaceae
	Mycobacterium sp. GP1
LinB	*Sphingobium francense*
	Sphingobium indicum
	Sphingobium japonicum
DmbA	*Mycobacterium bovis*
	Mycobacterium tuberculosis
DmbB	*Mycobacterium bovis*
	Mycobacterium tuberculosis
DmbC	*Mycobacterium bovis*
	Mycobacterium tuberculosis
Putative	*Xanthomonas axonopodis*
	Xanthomonas campestris
	Xanthomonas oryzae
Putative	*Shewanella baltica*
	Shewanella oneidensis
	Shewanella putrefaciens

[a]Obtained by PSI-BLAST search.
[b]According to Chovancová et al. **(2007)**.
[c]Amino acid sequence identity > 90%.

1.6.2.2 Biological role of haloalkane dehalogenases

Detoxification. Haloalkane dehalogenases have been so far determined to perform only hydrolytic dehalogenation of some halogenated aliphatic hydrocarbons into corresponding alcohols and halides, EC 3.8.1.5 **(Janssen et al., 1985; Nagata et al., 1993; Kulakova et al., 1995; Jesenská et al., 2000; Jesenská et al., 2002; Sato et al., 2005; Jesenská et al., 2009)**. Some of the substrates of haloalkane dehalogenases are known to be produced naturally as secondary metabolites by living organisms, e.g. by marine algae presumably for chemical defense **(Gribble, 2003)**, and by abiogenic processes **(Table 13; Gribble, 2003; Gribble, 2004)**. However, wast majority of the substrates of haloalkane dehalogenases have been introduced into the environment also or exclusively by human during last century, as the so-called xenobiotics **(Table 14)**. Since many of these xenobiotics are highly toxic and genotoxic **(Chroust et al., 2007)**, haloalkane dehalogenases could have evolved to convert the highly toxic halogenated aliphatic hydrocarbons into less toxic alcohols. Haloalkane dehalogenase could have been derived for such purpose from enzymes converting natural halogenated substrates, or evolved from enzymes catalysing the same reaction type on non-halogenated compounds **(Janssen et al., 1995)**.

Table 13 | Natural source of substrates of haloalkane dehalogenases.[a]

Marine algae	Volcano	Rock, minerals and shales	Biomass burning	Humification processes in peat	Rice paddies
Chloromethane	Chloromethane	Chloromethane	Chloromethane	Chloromethane	Chloromethane
Bromomethane	Bromomethane	Bromoethane	Bromomethane	Bromomethane	Bromomethane
Iodomethane	Iodomethane			Iodomethane	Iodomethane
Bromochloromethane					
Bromoethane					
Iodoethane					
Bromoiodoethane					
1,2-Dibromoethane					
1-Bromopropane					
1-Iodopropane					
1-Iodobutane					
1-Bromopentane					
1-Iodopentane					

[a]According to Gribble **(2003; 2004)**.

Table 14 | Anthropogenic source of substrates of haloalkane dehalogenases.[a]

Compound	Use
Bromomethane	Pesticide
	Solvent
Chloroethane	Solvent
	Refrigerant
	Production of cellulose
	Production of dyes
	Production of medicinal drugs
1,2-Dichloroethane	Production of vinyl chloride
	Solvent
	Lead remover from gasoline
1,2-Dibromoethane	Industrial fumigant
1,2-Dichloropropane[b]	Soil fumigant
	Industrial solvent
1,2,3-Trichloropropane[c]	Industrial solvent
	Paint remover
	Varnish remover
	Cleaning agent
	Degreasing agent
1,2-Dibromo-3-chloropropane	Nematocide
1,2,3-Tribromopropane	Nematocide
1,3-Dichloropropene	Pesticide
Hexachlorocyclohexane	Insecticide

[a]According to Agency for Toxic Substances & Disease Registry (http://www.atsdr.cdc.gov/).
[b]Also produced as by-product of epichlorohydrine and propylene oxid manufacture.
[c]Also produced as by-product of epichlorohydrine and 1,2-dichloropropene manufacture.

Metabolism. Additionally, the alcohols could be further metabolised and used as carbon and energy source, if approriate metabolic pathways are established within the bacterium. Indeed, some bacteria are capable of growing on halogenated aliphatic hydrocarbons as a sole carbon and energy source with haloalkane dehalogenase being the initial enzyme of the catabolic metabolic pathway **(Table 15 and Fig 23; Janssen et al., 1984; Janssen et al., 1985; Janssen et al., 1987; Yokota et al., 1987; van den Wijngaard et al., 1992; Janssen et al., 1995; Kulakova et al., 1997; Nagata et al., 1993; Poelarends et al., 1998; Poelarends et al., 1999; Poelarends et al., 2000b)**. These bacteria can thus manage both: (i) protection against deleterious effects of the toxic halogenated aliphatic hydrocarbons; and (ii) use of these compounds as carbon and energy source. Presence of the whole metabolic pathway thus provides selective advantage for these bacteria in highly poluted environments. On the other hand, other bacteria possess haloalkane dehalogenase genes but not the other components for the use of these compounds as carbon and energy source. This may suggest that (i) haloalkane dehalogenase genes evolved and/or have been acquired only recently by the bacteria and full metabolic pathway could have not yet been established in the bacterium **(Bosma et al., 1999)**, and (ii) that the primary biological role of haloalkane dehalogenases is protection against adverse effects of the toxic compounds, whereas providing alcohols for their use as carbon and energy source represents a secondary advantage.

Another function. Another possibility is that haloalkane dehalogenases may execute an additional function which, however, remains to be identified. In this context, presence of haloalkane dehalogenases in mycobacteria isolated from animal tissues is especially intruiging **(Jesenská et al., 2000; Jesenská et al., 2002)**. Attempts to understand role of haloalkane dehalogenases in mycobacteria has so far been sparse and rather speculative **(Janssen, 2004)**: Haloalkane dehalogenases in mycobacteria could had been acquired before they evolved from soil bacteria to animal parasites **(Jesenská et al., 2000)** or could be involved in the detoxification of halogenated compounds produced in animal tissues by peroxidases **(Janssen, 2004)**. Recently, haloalkane dehalogenase DmbA have been identified to be overexpressed after phagocytosis of *Mycobacterium tuberculosis* K-strain by human monocytic cell line U-937 but it is not clear whether the protein expression profile change is truly due to phagocytosis **(Ryoo et al., 2007)** and what would be the function of the protein. Hence the biological role of haloalkane dehalogenases in mycobacteria still remains to be solved.

Table 15 | Bacteria growing on haloalkanes as sole carbon and energy source and responsible haloalkane dehalogenase for initial dehalogenation.

Bacteria	Haloalkane dehalogenase	Sole carbon and energy source
Xanthobacter autothrophicus GJ10	DhlA	Bromochloromethane **(Torz et al., 2007)** Dibromomethane **(Torz et al., 2007)** 1,2-Dichloroethane **(Janssen et al., 1984; Janssen et al., 1985; Janssen et al., 1987)** 1-Bromo-2-chloroethane **(Torz et al., 2007)**
Ancylobacter aquaticus AD20, AD25, AD27	DhlA	1,2-Dichloroethane **(van den Wijngaard et al., 1992)**
Pseudomonas pavonaceae 170	DhaA	1,3-Dichloropropene **(Poelarends et al., 1998)**
Mycobacterium sp. GP1	DhaA	1,2-Dibromoethane **(Poelarends et al., 1999)** 1-Chloropropane **(Poelarends et al., 1999)** 1-Bromopropane **(Poelarends et al., 1999)**
Rhodococcus rhodochrous NCIMB 13064	DhaA	1-Chlorooalkanes (C3-C8) **(Kulakova et al., 1997; Poelarends et al., 2000b)**
Rhodococcus sp. m15-3	DhaA	1-Chlorobutane **(Yokota et al., 1987)**
Shingobium japonicum UT26	LinB	γ-Hexachlorocyclohexane **(Nagata et al., 1993)**

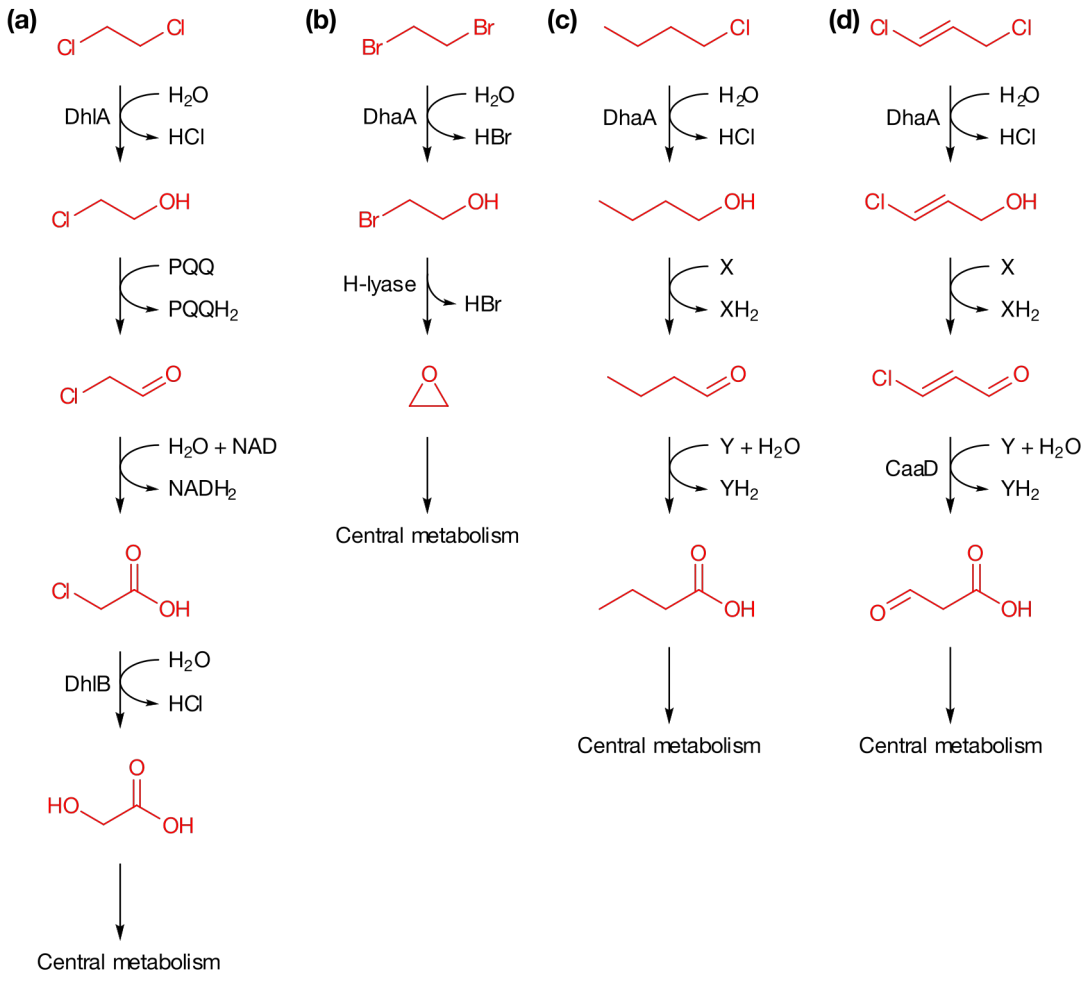

Fig 23 (pp. 68-69) | Examples of halogenated aliphatic hydrocarbon utilisation metabolic pathways in bacteria. **(a)** Utilisation of 1,2-dichloroethane by *Xanthobacter autothrophicus* GJ10 and *Ancylobacter aquaticus* by the action of haloalkane dehalogenase, DhlA, alcohol dehydrogenase with PQQ cofactor, aldehyde dehydrogenase with NAD cofactor and haloacetate dehydrogenase, DhlB **(Janssen et al., 1995; Poelarends et al., 1999)**; **(b)** utilisation of 1,2-dibromoethane by *Mycobacterium* sp. GP1 by the action of haloalkane dehalogenase, DhaA, and halohydrin halogen-halide lyase, H-lyase **(Poelarends et al., 1999; Poelarends et al., 2000b)**; **(c)** utilisation of 1-chlorobutane by *Rhodococcus rhodococcus* NCIMB 13064 by the action of haloalkane dehalogenase, DhaA, cofactor-dependent (X) alcohol dehydrogenase and cofactor-

dependent (Y) aldehyde dehydrogenase **(Poelarends et al., 2000b)**; **(d)** utilisation of 1,3-dichloropropene by *Pseudomonas pavonaceae* 170 by the action of haloalkane dehalogenase, DhaA, cofactor-dependent (X) alcohol dehydrogenase, and cofactor-dependent (Y) 3-chloroacrylic acid dehydrogenase, CaaD **(Poelarends et al., 1998; Poelarends et al., 2000b)**.

1.6.2.3 Structure of haloalkane dehalogenases

Size and shape. Haloalkane dehalogenase genes are ~ 900 nucleotide in length. Hence the corresponding haloalkane dehalogenase proteins are composed of ~ 300 amino acid residues that corresponds to ~ 35 kDa **(Chovancová et al., 2007)**, which is an average size among proteins **(Kent, 2009)**. By November 3, 2009, 36 XC structures of four haloalkane dehalogenases, DhlA **(Franken et al., 1991; Verschueren et al., 1993a; Verschueren et al., 1993b)**, DhaA **(Newman et al., 1999)**, LinB **(Marek et al., 2000; Oakley et al., 2004)**, and Rv2579 **(Mazumdar et al., 2008)** further referred to as DmbA **(Chovancová et al., 2007)**, have been deposited into PDB **(Table 16)**, and determination of DbjA **(Sato et al., 2007)** and DbeA **(Prudnikova et al., 2009)** is in progress. XC structures revealed that haloalkane dehalogenases possess globular shape **(Fig 24a)** with large cavity inside the globule **(Fig 24b; Marek et al., 2000)**. The cavity is closed in all 17 XC structures of DhlA and in two XC structures of LinB, open to a surface at two alternative sites, the so-called "upper tunnel" in one XC structure of LinB and the so-called "lower tunnel" in eight XC structures of LinB, or open to a surface at one site, the so-called "main tunnel" in two XC structures of DhaA and in all three XC structures of DmbA, or two sites, "main tunnel" and the so-called "slot tunnel" in one XC structure of DhaA. When the XC structures of LinB with the two alternative openings are superimposed to each other and to XC structures of DhaA, the alternative openings can be seen as a bifurcated main tunnel.

Table 16 | XC structures of haloalkane dehalogenases. (pp. 69-70)

Protein	PDB-ID	Cavity	Special features	Ligands	Resolution (Å)	Year
DhlA[a]	2HAD	Closed	–	–	1.90	1993
	2EDA	Closed	–	Iodide ion	2.19	1993
	1EDB	Closed	–	Chloride ion	2.01	1993
	1EDD	Closed	–	Chloride ion	2.19	1993
	1EDE	Closed	pH 8.2	–	1.90	1993
	2EDC	Closed	–	Iodide ion	2.30	1994
	2DHC	Closed	Complexed with substrate	1,2-Dichloroethane	2.30	1994
	2DHD	Closed	Reaction intermediate	Ethylene dichloride Chloroethyl group[e] Chloride ion	2.13	1994
	2DHE	Closed	–	Chloride ion	2.13	1994
	1HDE	Closed	F172W	–	2.70	1997
	1BEE	Closed	W175Y	–	2.60	1998
	1BEZ	Closed	W175Y at pH 5	Acetic acid	2.10	1998
	1BE0	Closed	–	Acetate ion	1.96	1998
	1B6G	Closed	Near-atomic resolution	Acetic acid Sulfate ion Chloride ion Glycerol	1.15	1999
	1CIJ	Closed	Solved at high bromide concentration	Bromide ion	2.30	1999
	2YXP	Closed	Perdeuterated	–	1.53	2007
	2PKY	Closed	–	–	1.55	2007
DhaA[b]	1CQW	Main tunnel	–	Iodide ion	1.50	1999
	1BN6	Main tunnel Slot tunnel	Unidentified ligand in the cavity	–	1.50	2000
	1BN7	Main tunnel	–	Acetate ion	1.50	2000
DhaA[c]	2V9Z	Main tunnel	Mutant	–	3.00	2008
LinB	1D07	Lower tunnel	Complexed with alcohol product	Bromide ion 1,3-Propanediol	2.00	2000
	1CV2		–	–	1.58	2000
	1G42	Closed	Unproductive substrate binding	Acetate ion Calcium ion Chloride ion 1,2-Dichloropropane	1.80	2001

Protein	PDB-ID	Cavity	Special features	Ligands	Resolution (Å)	Year
LinB	1G4H	Closed	Complexed with alcohol product	Calcium ion Chloride ion 1-Butanol	1.80	2001
	1G5F	Upper tunnel	Unproductive substrate binding	1,2-Dichloroethane	1.80	2001
	1IZ7	Lower tunnel		Chloride ion Calcium ion	1.58	2002
	1IZ8	Lower tunnel	Complexed with alcohol product	Bromide ion Calcium ion 1,3-Propanediol	2.00	2002
	1K5P	Lower tunnel	–	Chloride ion Magnesium ion	1.80	2003
	1K6E	Lower tunnel	Complexed with alcohol product	Bromide ion Chloride ion Magnesium ion 1,2-Propanediol 1-Bromopropane-2-ol	1.85	2003
	1K63	Lower tunnel	Complexed with alcohol product	Bromide ion Chloride ion Magnesium ion 2-Bromo-2-propene-1-ol	1.80	2003
	1MJ5	Lower tunnel	Atomic resolution	Magnesium ion Chloride ion	0.95	2003
	2BFN	Lower tunnel	Complexed with alcohol product	Calcium ion Chloride ion 2,3-Dichloropropane-1-ol	1.60	2006
DmbA[d]	2O2H	Main tunnel	Unproductive substrate binding	Chloride ion Acetate ion 1,2-Dichloroethane Ethylene dichloride	1.60	2007
	2O2I	Main tunnel	Complexed with alcohol product	Bromide ion 1,3-Propandiol	1.50	2007
	2QVB	Main tunnel	–	Chloride ion 1,2-Ethanediol	1.19	2008

[a]Source – *Xanthobacter autotrophicus* GJ10.
[b]Source – *Rhodococcus* sp.
[c]Source – *Rhodococcus rhodochrous* NCIMB 13064.
[d]Source – *Mycobacterium tuberculosis* H37Rv.
[e]Covalently attached to Asp124.

Fold. The XC structures also revealed that haloalkane dehalogenases contain an eight-stranded central β-sheet and eleven α-helices located in the excursions from the β-sheet **(Figs 24c and 25; Franken et al., 1991; Verschueren et al., 1993a; Verschueren et al., 1993b; Newman et al., 1999; Marek et al., 2000; Oakley et al., 2004; Mazumdar et al., 2008)**. Six of the eleven α-helices (A-F) are located between consecutive β-strands and they are packed against the β-sheet faces in αβα arrangement **(Figs 24c and 25)** that was also identified in some other hydrolases, e.g. acetylcholinesterase from *Torpedo californica*, carboxypeptidase II from wheat, dienelactone hydrolase from *Pseudomonas* sp. B13 and lipase from *Geotrichum candidum* **(Ollis et al., 1992)**. Sequence and structure comparison revelead that all these hydrolases are related by extreme divergent evolution from a common ancestor and the α/β-fold was called according to the structure and function, α/β-hydrolase fold **(Ollis et al., 1992)**. The extreme divergence of α/β-hydrolase superfamily is manifested by extensive secondary structure embellishments with β-strands 3 to 7 and α-helix C being the only fully conserved secondary structure elements **(Ollis et al., 1992; Heikinheimo et al., 1999; Nardini & Dijkstra, 1999; Holmquist, 2000)**. The largest variability among α/β-hydrolases is situated between the β-strand 6 and the α-helix D that may be few amino acid residues or large enough to be considered as a separate domain **(Ollis et al., 1992; Heikinheimo et al., 1999; Nardini & Dijkstra, 1999)**; the latter is the case of haloalkane dehalogenases which contain about 80 amino acid residue long excursion between the β-strand 6 and the α-helix D. The excursion is composed of five α-helices collocated in space and packed one to each other and to the β-sheet edge **(Fig 25)**. In haloalkane dehalogenases, the α/β-hydrolase fold and the helical excursion are called main domain and cap domain, respectively **(Fig 24d)**.

Functional role of the main domain. The main domain provides three catalytic amino acid residues, the so-called catalytic triad, in the sequence order conserved among all α/β-hydrolases as follows: nucleophile, Asp; acid, Asp or

Glu; and base, His **(Fig 25; Ollis et al., 1992; Heikinheimo et al., 1999; Nardini & Dijkstra, 1999; Holmquist, 2000)**. The topological arrangement of the catalytic triad is conserved among α/β-hydrolases which explains why the β-strands 3 to 7 are always present and signifies the importance of the arrangement for performing the hydrolytic function **(Ollis et al., 1992; Heikinheimo et al., 1999; Nardini & Dijkstra, 1999; Holmquist, 2000)**. The nucleophile is located in a highly conserved sharp γ-like turn, the so-called nucleophile elbow, located between β-strand 5 and the only conserved α-helix C **(Ollis et al., 1992; Arand et al., 1994; Cousin et al., 1998; Nardini & Dijkstra, 1999; Holmquist, 2000; Orengo et al., 2002)**. The sequence around the nucleophile has the canonical form of Sm-X-Nu-X-Sm-Sm, where Sm is a small amino acid residue important to allow sharp protein backbone direction reversal, usually Gly, X is a variable amino acid residue and Nu is the nucleophile, Asp in haloalkane dehalogenases and Asp/Ser/Cys in other α/β-hydrolases **(Ollis et al., 1992; Heikinheimo et al., 1999; Nardini & Dijkstra, 1999; Holmquist, 2000)**. The φ and ψ dihedral angles of the nucleophile take unfavourable values suggesting importance of the strained geometry for function **(Ollis et al., 1992)**. The base is always His located at the first position of a reverse turn in the so-called His loop between the β-strand 8 and α-helix F **(Ollis et al., 1992)**. In contrast to the nucleophile and the base, the acid shows variability in both nature and position even among haloalkane dehalogenases which is yet another evidence for extreme robustness of the α/β-hydrolase fold **(Heikinheimo et al., 1999; Nardini & Dijkstra, 1999; Holmquist, 2000; Skjøt et al., 2009)**. Asp as the acid is situated in the loop between the β-strand 8 and α-helix F in DhlA **(Fig 25a)** whereas Glu as the acid is situated in the loop between the β-strand 6 and the cap domain in DhaA, LinB and DmbA **(Fig 25b)**. It has been proposed that repositioning of the catalytic acid occurred for optimising the substrate specificity of DhlA **(Krooshof et al., 1997)** although this proposal has been recently disputed by phylogenetic analysis **(Chovancová et al., 2007)**.

Functional role of the cap domain. The internal, predominantly hydrophobic cavity is formed due to the cap domain that buries the catalytic triad and other amino acid residues at the edge of the β-sheet. The cavity is contributed both by the main and especially by the cap domain amino acid residues. While the main domain contribution to the cavity is largely conserved among haloalkane dehalogenases as it includes catalytic triad and their neighbouring, often conserved, amino acid residues and only few others, the cap domain contributions differ due to differences in arrangement of α-helices and their amino acid residue composition **(Chovancová et al., 2007)**. The cap domain also provides the openings to the surface observed in DhaA, LinB and DmbA **(Fig 24b)**. The differences in size and shape of the cavity and its openings imposed by different cap domains are therefore considered to be the major determinants of substrate specificity that varies among haloalkane dehalogenases **(Pries et al., 1994b; Callebaut et al., 2000; Marek et al., 2000; Jesenská et al., 2002; Chaloupková et al., 2003)**. The ancestor cap domain has been proposed to be composed of α-helices 4, 5', 5, 6 and 7 based on phylogenetic analysis **(Chovancová et al., 2007)**. Loss of the α-helix 5' and insertion of the α-helix 4' at the N-terminus of the cap domain has been proposed as an evolutionary event towards DhlA cap domain composed of α-helixes 4', 4, 5, 6 and 7 **(Chovancová et al., 2007)**. Interestingly, the α-helices 4, 5, 6 and 7 of the cap domain of DhlA as well as the corresponding excursion in some other α/β-hydrolases, e.g. carbon-carbon bond hydrolase and haloperoxidase families **(Callebaut et al., 2000)** resembles uteroglobin fold **(Russell & Sternberg, 1997)**. It is, however, not clear whether the similarity represents a remote homology, implying horizontal gene transfer, or a convergence to a common four-α-helix binding motif devoted to hydrophobic ligand binding **(Callebaut et al., 2000)**. Considering the proposed origin of the DhlA cap domain, the latter is more parsimonious and thus more likely **(Chovancová et al., 2007)**. Although, evolutionary changes do not always follow the most parsimonious solution **(Albert, 2005)**.

Substrate binding site. Even though haloalkane dehalogenases are functionally active in the crystal making capturing the enzyme-substrate complex an extremely difficult task, by specifc crystalisation conditions (low temperature and pH), a complex of DhlA with 1,2-dichloroethane (PDB-ID 2DHC) was captured by Verschueren et al. **(1993d)**. The 2DHC structure revealed binding of the substrate into the cavity with one halogen positioned in-between two indol ring nitrogens of two Trp amino acid residues: one Trp immediately follows the catalytic nucleophile and the other Trp is situated in the cap domain α-helix 4 **(Fig 25a)**. DhaA, LinB and DhaA are conserved with DhlA in the position and the nature of the main domain Trp. In the position of the other halogen/halide Trp, DhaA, LinB and DmbA contain Asn provided by the loop between the β-strand 3 and the α-helix A **(Fig 25b)**. The catalytic triad and the two halide-stabilising amino acid residues have been denoted collectively as the catalytic pentad **(Janssen, 2004)**.

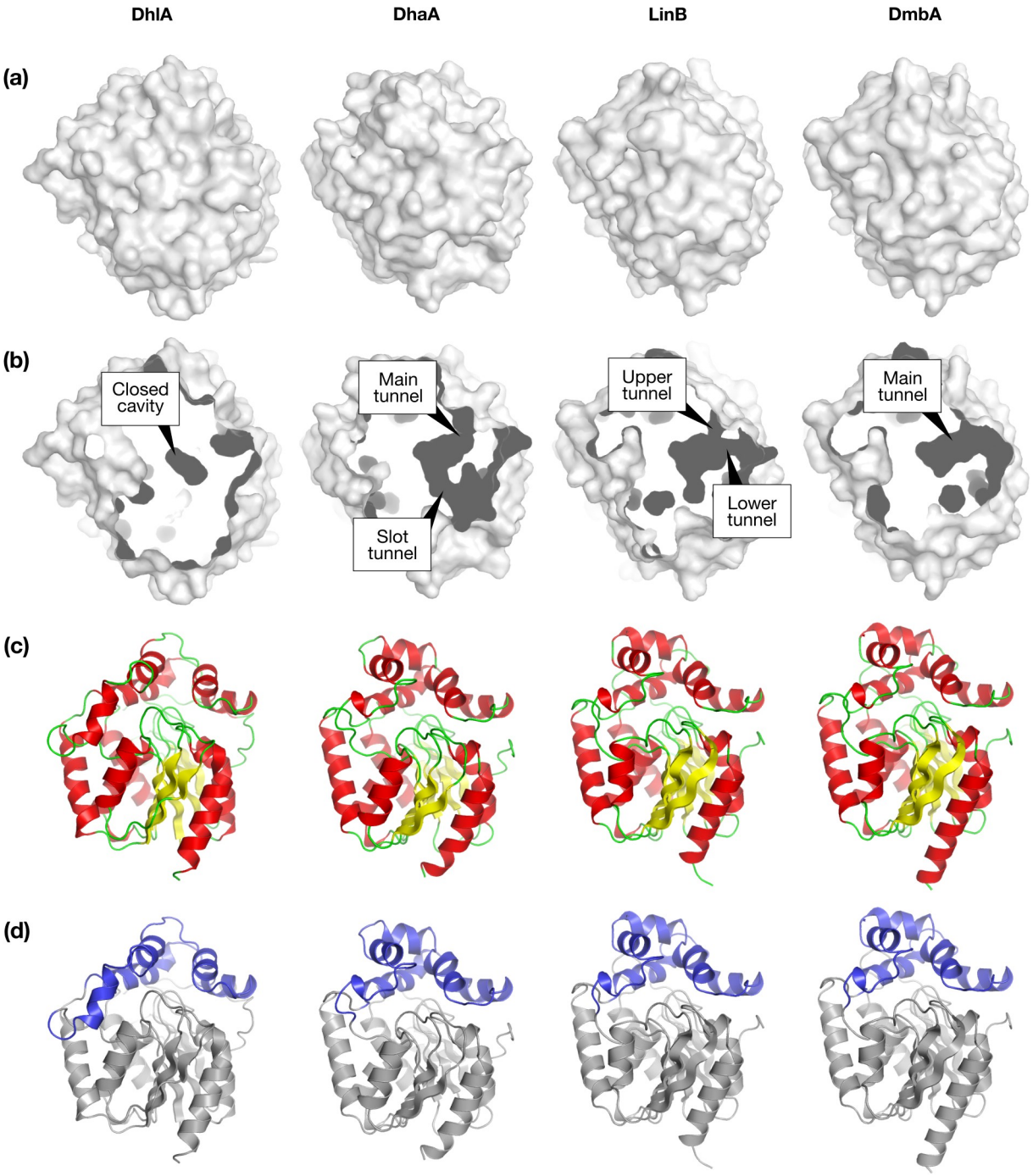

Fig 24 | XC structures of haloalkane dehalogenases. **(a)** Surface representation of the XC structures of DhlA (PDB-ID 2HAD), DhaA (PDB-ID 1BN6), LinB (PDB-ID 1CV2) and DmbA (PDB-ID 2QVB); **(b)** cross-section of the surface representation of the XC structures of DhlA (PDB-ID 2HAD), DhaA (PDB-ID 1BN6), LinB (PDB-IDs 1G5F + 1CV2) and DmbA (PDB-ID 2QVB), showing the cavity and its openings to the surface; **(c)** cartoon representation of the XC structures of DhlA (PDB-ID 2HAD), DhaA (PDB-ID 1CQW), LinB (PDB-ID 1CV2) and DmbA (PDB-ID 2QVB), coloured by secondary structure elements: α-helices, red; β-strands, yellow; turns and loops, green; **(d)** cartoon representation of the XC structures of DhlA (PDB-ID 2HAD), DhaA (PDB-ID 1CQW), LinB (PDB-ID 1CV2) and DmbA (PDB-ID 2QVB), coloured by domains: the main domain, grey; the cap domain, blue. The surface representations are modelled by 1.4 Å probe corresponding to the approximate size of a water molecule. The β-sheet has an obligatory right-handed twist: the β-strands 1 and 8 cross each other at an angle ~ 90°. The domain boundaries are approximate. The view in *a-b* is different from *c-d*.

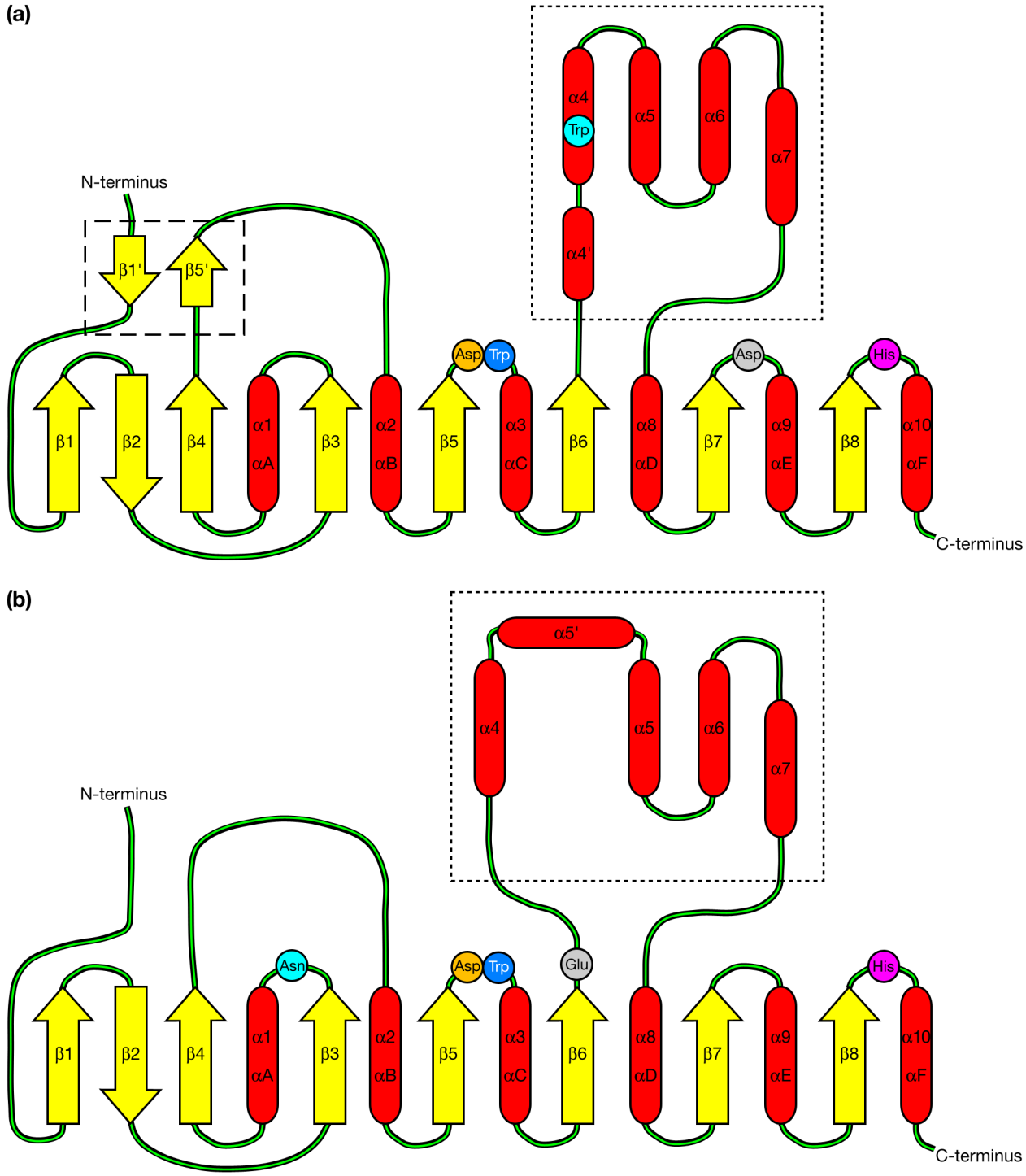

Fig 25 | Topological arrangement of secondary structure elements in haloalkane dehalogenases. **(a)** DhlA, **(b)** DhaA, LinB and DmbA. The central β-sheet has the β-strand order 12435678, of which all β-strands run in parallel except for an antiparallel β-strand 2. α-helix A is located between β-strands 3 and 4, α-helix B is located between β-strands 4 and 5, α-helix C is located between β-strands 5 and 6, α-helix D is located between β-strands 6 and 7, α-helix E is located between β-strands 7 and 8, and α-helix F is located after β-strand 8. Four of the six α-helices are packed against one face (B, C, D and E) and two are packed against the other face of the β-sheet (A and F). The largest excursion, the cap domain (highlight by dotted box) is located between the β-strand 6 and the α-helix D, and contains five α-helices. DhlA contains an aditional two-stranded β-sheet embellishment close to the N-terminus (highlighted by dashed box). The catalytic amino acid residues are coloured as follows: the nucleophile, orange; the acid, grey; the base, magenta; halide-stabilising amino acid residues, blue and cyan. Both conventional α/β-hydrolase-specific (letters) and haloalkane-dehalogenase-specific annotation (numbers) of the main domain α-helices is given. Redrawn according to Chovancová et al. **(2007)**.

Classification of the haloalkane dehalogenase family. Recently, a phylogenetic tree of haloalkane dehalogenase family has been reported that classified 12 experimentally characterised and 32 putative haloalkane dehalogenases **(Table 10)** into three subfamilies denoted by Roman numerals, I, II and III **(Table 17; Chovancová et al., 2007)**. The major determinants of the classification are (i) variability in the cap domains, (ii) variability in the position and nature of the catalytic acid and (iii) variability in the second halide-stabilising amino acid residue **(Chovancová et al., 2007)**. Although no XC structure is available for haloalkane dehalogenases from subfamily III, the phylogenetic analysis allowed identification of the catalytic triad amino acid residues to be analogous to the subfamily I, identification of halide-stabilising amino acid residues to be analogous to the subfamily II, and identification of the arrangement of the cap domain α-helices to be analogous to the subfamily II **(Chovancová et al., 2007)**.

Table 17 | Haloalkane dehalogenase subfamilies and their experimentally characterised representatives.[a]

Subfamily	Catalytic nucleophile	Catalytic acid	Catalytic base	Halide-stabilising	Protein	Source
I	Asp123	Asp250	His279	Trp124 and Trp164	DhmA	*Mycobacterium avium* N85
	Asp123	Asp250	His279	Trp124 and Trp164	DmbB	*Mycobacterium tuberculosis* H37Rv
	Asp124	Asp260	His289	Trp125 and Trp175	DhlA	*Xanthobacter autotrophicus* GJ10
II	Asp114	Glu138	His280	Asn49 and Tyr115	DatA	*Agrobacterium tumefaciens* C58
	Asp103	Glu127	His280	Asn38 and Trp104	DbjA	*Bradyrhizobium japonicum* USDA110
	Asp110	Glu134	His278	Asn45 and Trp111	DmlA	*Mesorhizobium loti* MAFF303099
	Asp107	Glu131	His272	Asn37 and Trp108	DmsA	*Mycobacterium smegmatis* ATCC700084
	Asp109	Glu133	His273	Asn39 and Trp110	DmbA	*Mycobacterium tuberculosis* H37Rv
	Asp106	Glu130	His272	Asn38 and Trp107	DhaA	*Rhodococcus rhodochrous* NCIMB 13064
	Asp108	Glu132	His272	Asn41 and Trp109	LinB	Sphingobium japonicum UT26
III	Asp109	Asp238	His267	Asn43 and Trp110	DmbC	*Mycobacterium tuberculosis* H37Rv
	Asp139	Asp272	His300	Asn71 and Trp140	DrbA	*Rhodopirellula baltica* SH1

[a]According to Chovancová et al. **(2007)**.

1.6.2.4 Function of haloalkane dehalogenases

Substrate specificity. So far, haloalkane dehalogenases have been found to be active with a wide range of halogenated aliphatic alkanes, alcohols, ethers, esters, alkylbenzenes and cyanides with the cleaving halogen being bound to sp^3-hybridised carbon atom **(Tables 18 and 19)**. The broad substrate specificities of DhlA **(Keuning et al., 1985; Janssen et al., 1988; Pries et al., 1994b; Schanstra et al., 1996b; Schanstra et al., 1996a; Schindler et al., 1999)**, DhaA **(Yokota et al., 1987; Kulakova et al., 1997; Poelarends et al., 1998; Schindler et al., 1999; Bosma et al., 1999; Bosma et al., 2002; Bosma et al., 2003; Prokop et al., 2006)**, LinB **(Nagata et al., 1993; Nagata et al., 1997; Nagata et al., 1999; Marvanová et al., 2001; Nagata et al., 2003; Chaloupková et al., 2003; Nagata et al., 2005; Kmuníček et al., 2005; Prokop et al., 2006; Raina et al., 2007; Monincová et al., 2007; Raina et al., 2008)**, DhmA **(Jesenská et al., 2002)**, DbjA **(Sato et al., 2005)** and DmlA **(Sato et al., 2005)** that have been reported so far are in agreement with the detoxifying and metabolic biological roles of haloalkane dehalogenases because bacteria bearing haloalkane dehalogenases are being exposed to rapidly changing environment manifested by fluctuating concentrations of various haloalkanes from natural and/or anthropogenic sources. Since the inevitable trade-off between the substrate specificity and rate of conversion, haloalkane dehalogenases have apparently evolved towards plasticity while sacrificing secclusion, and hence the rate of conversion, and they are in a local evolutionary optimum because enhancement of one step of the reaction cycle (vide infra) often results in reduced rate for another step, as demonstrated for DhlA **(Schanstra et al., 1996a; Krooshof et al., 1997; Krooshof et al., 1998)** and LinB **(Chaloupková et al., 2003; Nagata et al., 2003)**. Haloalkane dehalogenases differ one to each other by the substrate range and their rate of conversions showing different preferential dehalogenating activities, the so-called substrate specificity profiles **(Kmuníček et al., 2001; Kmuníček et al., 2003; Kmuníček et al., 2005; Sato et al., 2005)**. Even chemically similar substrates can differ greatly in rate of conversion by a haloalkane dehalogenase **(Chaloupková et al., 2003)**. For example, 1,2-dibromoethane is one of the best known substrate for DhaA with $k_{cat}/K_m \approx 3.7 \times 10^3$ s^{-1} M^{-1}, whereas its chlorinated analog is not converted by DhaA at all **(Bosma et al., 1999; Schindler et al., 1999)**.

Table 18 | Substrate range of haloalkane dehalogenases DhlA, DhaA and LinB.[a] (pp. 75-76)

Group	DhlA	DhaA	LinB
Halomethanes	Chloromethane	*NR*	*NR*
	Bromomethane		
	Iodomethane		
	Dichloromethane		
	Dibromomethane		
	Bromochloromethane		
	Bromocyanomethane		
1-Haloalkanes	Chloroethane	Bromoethane	Bromoethane
	Bromoethane	1-Chloropropane	1-Chloropropane
	Iodoethane	1-Bromopropane	1-Bromopropane
	1-Chloropropane	1-Chlorobutane	1-Chlorobutane
	1-Bromopropane	1-Bromobutane	1-Bromobutane
	1-Iodopropane	1-Chloropentane	1-Iodobutane
	1-Chlorobutane	1-Chlorohexane	1-Chloropentane
	1-Bromobutane	1-Chloroheptane	1-Chlorohexane
	1-Chloropentane	1-Chlorooctane	1-Chloroheptane
	1-Bromopentane	1-Chlorononane	1-Chlorooctane
	1-Chlorohexane	1-Chlorodecane	1-Chlorononane
	1-Bromohexane	1-Chlorododecane	1-Chlorodecane
	1-Chlorooctane		
	1-Bromooctane		
2-Haloalkanes	2-Bromopropane	2-Chlorobutane	2-Chlorobutane
	2-Bromobutane	2-Bromobutane	2-Chlorooctane
	2-Bromopentane	2-Chlorooctane	
3-Haloalkanes	*NR*	*NR*	3-Chlorohexane
1,2-Haloalkanes	1,2-Dichloroethane	1,2-Dibromoethane	1,2-Dibromoethane
	1,2-Dibromoethane	1,2-Dibromopropane	1,2-Dibromopropane
	1-Bromo-2-chloroethane	1,2-Dichlorobutane	2-Bromo-1-chloropropane
	1,2-Dichloropropane	1,2-Dibromobutane	
	1,2-Dibromopropane	2-Bromo-1-chloropropane	
1,3-Haloalkanes	*NR*	1,3-Dichlorobutane	*NR*
2,3-Haloalkanes	*NR*	2,3-Dichlorobutane	*NR*
2-Substituted 1-haloalkanes	1-Bromo-2-methylpropane	1-Chloro-2-methylpropane	1-Bromo-2-methylpropane
		1-Chloro-3-methylbutane	
α,ω-Haloalkanes	1,2-Dichloroethane	1,2-Dibromoethane	1,2-Dibromoethane
	1,2-Dibromoethane	1,3-Dichloropropane	1,3-Dichloropropane
	1-Bromo-2-chloroethane	1,3-Dibromopropane	1,3-Dibromopropane
	1,3-Dichloropropane	1,4-Dichlorobutane	1,3-Diiodopropane
	1,3-Dibromopropane	1,5-Dichloropentane	1,4-Dichlorobutane
	1,4-Dichlorobutane	1,6-Dichlorohexane	1,6-Dichlorohexane
	1,6-Dichlorohexane	1,7-Dichloroheptane	1,9-Dichlorononane
	1,9-Dichlorononane	1,8-Dichlorooctane	
		1,9-Dichlorononane	
Multihalogenated alkanes	*NR*	1,2,3-Trichloropropane	1,2,3-Trichloropropane
		1,2,3-Tribromopropane	α-Hexachlorocyclohexane
		1,2-Dibromo-3-chloropropane	β-Hexachlorocyclohexane
			δ-Hexachlorocyclohexane
			2,3,5,6-Tetrachlorocyclohexane-1,4-diol
			3,4,5,6-Tetrachloro-2-cyclohexene-1-ol
			δ-Pentachlorocyclohexane
Cyclic haloalkanes	Bromocyclohexane	Chlorocyclobutane	Chlorocyclohexane
		Bromocyclobutane	Bromocyclohexane
		Bromomethylcyclobutane	α-Hexachlorocyclohexane
		Chlorocyclopentane	β-Hexachlorocyclohexane
		Bromocyclopentane	δ-Hexachlorocyclohexane
			2,3,5,6-Tetrachlorocyclohexane-1,4-diol
			3,4,5,6-Tetrachloro-2-cyclohexene-1-ol
			δ-Pentachlorocyclohexane
Haloalkenes	3-Chloropropene	1,3-Dichloropropene	3-Chloro-2-methylpropene
	1,3-Dichloropropene		
Haloalkylbenzenes	1-Phenyl-2-bromopropane	*NR*	*NR*

Group	DhlA	DhaA	LinB
Halogenated alcohols	2-Bromoethanol	2-Bromoethanol	2-Chloroethanol
	3-Bromopropanol	3-Chloro-1-propanol	4-Chlorobutanol
	1,3-Dibromo-2-propanol	3-Bromo-1-propanol	6-Chlorohexanol
	1-Chloro-6-hexanol	1.3-Dibromo-2-propanol	2,3,4,5,6-Pentachlorocyclohexanol
	1-Bromo-6-hexanol	4-Chloro-1-butanol	
Halogenated ethers	Bis(2-chloroethyl) ether	*NR*	*NR*
	2-Chloroethylvinylether		
	2-Chloroethylmethylether		
Haloepoxides	Epichlorohydrine	*NR*	*NR*
	Epibromohydrine		
Halonitriles	2-Bromoacetonitrile	*NR*	*NR*
Haloacetamides	2-Bromoacetamide	*NR*	*NR*
Alkyl-thio-alkyl halides	*NR*	Bis-(2-chloroethyl) sulphide[b]	Bis-(2-chloroethyl) sulphide[b]

[a]*NR* – not reported.
[b]Also known as "mustard gas" and "Yperite".

Table 19 | Substrate range of haloalkane dehalogenases DhmA, DbjA amd DmlA.[a]

Group	DhmA	DbjA	DmlA
Halomethanes	*NR*	*NR*	*NR*
1-Haloalkanes	Bromoethane	1-Chloropropane	1-Chloropropane
	1-Iodopropane	1-Chlorobutane	1-Chlorobutane
	1-Chlorobutane	1-Bromobutane	1-Bromobutane
	1-Bromobutane	1-Chloropentane	1-Chloropentane
	1-Iodobutane	1-Chlorohexane	1-Chlorohexane
	1-Chloropentane	1-Chlorodecane	1-Chlorodecane
2-Haloalkanes	2-Chloropropane	2-Chloropropane	2-Chloropropane
	2-Iodobutane	2-Chlorobutane	2-Chlorobutane
3-Haloalkanes	*NR*	*NR*	*NR*
1,2-Haloalkanes	1,2-Dichloroethane	1,2-Dichloroethane	1,2-Dichloroethane
	1,2-Dibromoethane	1,2-Dibromoethane	1,2-Dibromoethane
	1-Bromo-2-chloroethane	1,2-Dichloropropane	1,2-Dichloropropane
	1,2-Dichloropropane	1,2-Dibromopropane	1,2-Dibromopropane
	1,2-Dibromopropane		
	2-Bromo-1-chloropropane		
	1,2-Dichlorobutane		
1,3-Haloalkanes	*NR*	*NR*	*NR*
2,3-Haloalkanes	*NR*	*NR*	*NR*
2-Substituted 1-haloalkanes	1-Chloro-2-methylpropane	1-Chloro-2-methylpropane	1-Chloro-2-methylpropane
	1-Bromo-2-methylpropane		
α,ω-haloalkanes	1,2-Dichloroethane	1,2-Dichloroethane	1,2-Dichloroethane
	1,2-Dibromoethane	1,2-Dibromoethane	1,2-Dibromoethane
	1-Bromo-2-chloroethane	1,3-Dibromopropane	1,3-Dibromopropane
	1,3-Dichloropropane		
	1,3-Dibromopropane		
	1,3-Diiodopropane		
Multihalogenated alkanes	1,2,3-Trichloropropane	1,2,3-Trichloropropane	1,2,3-Trichloropropane
	1,2,3-Tribromopropane		
	1,2-Dibromo-3-Chloropropane		
Cyclic haloalkanes	Chlorocyclopentane	Chlorocyclohexane	Chlorocyclohexane
	Chlorocyclohexane	Bromocyclohexane	Bromocyclohexane
	Bromocyclohexane		
	1-Bromomethylcyclohexane		
Haloalkenes	3-Chloro-2-methylpropene	3-Chloro-2-methylpropene	3-Chloro-2-methylpropene
	2,3-Dichloropropene		
Haloalkylbenzenes	*NR*	*NR*	*NR*
Halogenated alcohols	*NR*	*NR*	*NR*
Halogenated ethers	Bis(2-chloroethyl) ether	*NR*	*NR*
Haloepoxides	*NR*	*NR*	*NR*
Halonitriles	4-Chlorobutyronitrile	*NR*	*NR*
	4-Bromobutyronitrile		
Haloacetamides	*NR*	*NR*	*NR*

[a]NR – not reported.

Rate enhancement. The highest catalytic performance of isolated haloalkane dehalogenases, expressed as k_{cat}/K_m ratio, differs by both value and substrate among haloalkane dehalogenases **(Table 20)**. For example, it has been estimated by QM/MM calculations that DhlA provides rate enhancement by 10^8 to 10^9 for conversion of 1,2-dichloroethane to 2-chloroethanol **(Soriano et al., 2005)**. The low effeciency can be due to the above mentioned sacrificing the rate of conversion towards plasticity, or can be due to recent origin of haloalkane dehalogenases that have not had sufficient time to evolve into high-catalytic rate enzymes **(Lau et al., 2000)**. The former is supported by the fact that even the moderate catalytic performance of haloalkane dehalogenases DhlA, DhaA and LinB can provide sufficient amount of the alcohol product as the sole carbon and energy source and thus to sustain life **(Janssen et al., 1984; Janssen et al., 1985; Janssen et al., 1987; Yokota et al., 1987; van den Wijngaard et al., 1992; Janssen et al., 1995; Kulakova et al., 1997; Poelarends et al., 1998; Poelarends et al., 1999; Poelarends et al., 2000b) (Table 15 and Fig 23)** suggesting that the judging of the catalytic performance as being low, moderate or high should be considered in the context of the living organism rather than by comparing it with the most efficient enzymes working at the diffusion limit because most enzymes do not need to achieve the kinetic perfection in order to execute its biological role.

Table 20 | The highest catalytic performances of haloalkane dehalogenases.

Enzyme	Substrate	k_{cat} [s^{-1}]	K_m [M]	k_{cat}/K_m [s^{-1} M^{-1}]
DhlA	1,2-Dibromoethane **(Schanstra et al., 1996b)**	3.0	1 x 10^{-5}	3.0 x 10^5
DhaA	1,3-Dibromopropane **(Bosma et al., 2003)**	2.7	5 x 10^{-6}	5.4 x 10^5
LinB	1-Iodohexane **(Kmuníček et al., 2005)**	2.3	1 x 10^{-5}	2.3 x 10^5
DbjA	1-Chlorohexane **(Sato et al., 2005)**	1.4	5 x 10^{-5}	2.8 x 10^4

Reaction cycle. Pre-steady state kinetics has been so far reported for conversion of 1,2-dichloroethane and 1,2-dibromoethane by DhlA **(Schanstra et al., 1996b)**, 1,3-dibromopropane by DhaA **(Bosma et al., 2003)**, and 1-chlorohexane, bromocyclohexane and chlorocyclohexane by LinB **(Prokop et al., 2003)** that together with XC structures **(Verschueren et al., 1993d; Newman et al., 1999; Marek et al., 2000; Oakley et al., 2004)** revealed multiple step reaction cycle comprising the following steps: (i) substrate binding; (ii) three distinct chemical steps; and (iii) product release **(Figs 26 and 27)**.

Substrate binding. Substrate binds into the buried active site cavity with its halogen bound between the two halide-stabilising amino acid residues and the halogen-bound electrophilic sp^3-hybridised carbon atom positioned towards the nucleophilic carboxyl oxygen of the Asp nucleophile, PDB-ID 2DHC **(Verschueren et al., 1993d)**. XC also identified unproductive binding of poor substrates of LinB, 1,2-dichloroethane (PDB-ID 1G42) and 1,2-dichloropropane (PDB-ID 1G5F), and non-substrate of DmbA, 1,2-dichloroethane (PDB-ID 2O2H), adjacent to the face of the imidazole ring of His base **(Fig 28; Oakley et al., 2002; Mazumdar et al., 2008)**. The presence of the secondary binding site has been explained as to be due to favourable interaction of the molecules with the His base and their inability to displace active site water molecules **(Oakley et al., 2002)**.

Bimolecular nucleophilic substitution (S_N2). The nucleophilic oxygen attacks the halogen-bound carbon atom yielding covalently bound intermediate (sometimes referred to as "alkyl-enzyme intermediate") and halide ion that remains to be bound between the two halide-stabilising amino acid residues, PDB-ID 2DHD **(Verschueren et al., 1993d)**. The negative charge that evolves on the other (free) carboxyl oxygen of the Asp nucleophile is stabilised by the so-called oxyanion hole **(Henderson, 1970)**, a structural feature characteristic to α/β-hydrolases **(Ollis et al., 1992; Cousin et al., 1998; Nardini & Dijkstra, 1999; Holmquist, 2000; Orengo et al., 2002)** and other enzymes related to α/β-hydrolases by convergent evolution, e.g. serine proteases **(Ollis et al., 1992)**. The oxyanion hole interaction in haloalkane dehalogenases involves hydrogen bonding interaction of the free carboxyl oxygen of the Asp nucleophile with main-chain amide group of the downstream neighbour of the nucleophile, i.e. halide-stabilising Trp, and an amino acid residue in a turn between the β-strand 3 and α-helix A, i.e. Glu in DhlA **(Verschueren et al., 1993d)** or the halide-stabilising Asn in DhaA **(Newman et al., 1999)**, LinB **(Marek et al., 2000; Oakley et al., 2004)** and DmbA **(Mazumdar et al., 2008)**.

Nucleophilic addition (Ad_N). The formation of the covalent intermediate is followed by nucleophilic addition (Ad_N) of a hydroxyl anion to the carboxyl carbon atom of the Asp nucleophile side-chain, yielding the so-called tetrahedral intermediate, also known as "alcoxy-hydroxy-olate intermediate" **(Pries et al., 1994a)**. Thus, haloalkane dehalogenases are evolved to optimise two different nucleophilic substitutions at two nucleophilic centres **(Pries et al., 1995a)**. The hydroxyl anion is formed by substraction of a proton from a catalytic water molecule by the His base **(Pries et al., 1995b)**. The catalytic water is situated near the nucleophile and the base, and interacts via three hydrogen bonds with: (i) the imidazole ring nitrogen of the His base; (ii) the main-chain carbonyl group of the halide-

stabilising Asn in DhaA **(Newman et al., 1999)**, LinB **(Marek et al., 2000; Oakley et al., 2004)** and DmbA **(Mazumdar et al., 2008)**, or Glu in DhlA **(Verschueren et al., 1993d)**; and (iii) one structural water molecule bound to the side-chain of the amino acid residue just upstream of the Asp nucleophile, i.e. Gln in DhlA **(Verschueren et al., 1993d)** or His in DhaA **(Newman et al., 1999)**, LinB **(Marek et al., 2000; Oakley et al., 2004)** and DmbA **(Mazumdar et al., 2008)**. The role of the His base as the water activator was proven by His to Gln site-directed mutagenesis in DhlA and by observation of no incorporation of ^{18}O into the Asp nucleophile upon mixing enzyme with substrate in ^{18}O-labelled water **(Pries et al., 1995b)**. Interestingly, the role of the His base is different in some α/β-hydrolases: (i) His base functions to maintain nucleophilicity of Cys nucleophile in dienelactone hydrolase of *Pseudomonas* B13; (ii) His base is involved in both formation and hydrolysis of covalent acyl-intermediate in lipase from *Geotrichum candidum* and acetylcholinesterase from *Torpedo californica*; and (iii) His was suggested to accept proton from Ser nucleophile in wheat carboxypeptidase A **(Pries et al., 1995b)**. In haloalkane dehalogenases, the functional His tautomer and the positive charge that evolves on the His base upon accepting the proton from the catalytic water is stabilised by hydrogen bonding interaction of the His+ base with the catalytic acid, i.e. Asp in DhlA or Glu in DhaA, LinB and DmbA via the other imidazole amide group **(Krooshof et al., 1997)**. The catalytic acid also functions as to increase basicity of the His thus making it stronger base, a prerequisite for efficient proton abstraction from water **(Oakley et al., 2004; Negri et al., 2007; Otyepka et al., 2008)**. However, since the base-acid interaction have been observed in various forms of enzyme along the reaction cycle **(Verschueren et al., 1993d)**, this interaction does not explain triggering the Ad_N at proper time, i.e. after formation of the ester intermediate. The triggering can be caused by change in His pK_a due to change in micro-environment caused by halide anion formation during the preceding S_N2 step which could explain different rates of hydrolysis of the identical ester intermediate, cyclohexyl-enzyme, formed during dehalogenation reaction of chlorocyclohexane and bromocyclohexane by LinB **(Prokop et al., 2003)**.

Decomposition of tetrahedral intermediate. Although the tetrahedral intermediate is being stabilised by the oxyanion hole, it is a metastable state **(Otyepka et al., 2008)** that has not been captured by XC unlike the ester intermediate. The tetrahedral intermediate decomposes into alcohol and free Asp nucleophile. As a consequence of the nucleophilic addition of the hydroxyl anion from the catalytic water to the carboxyl carbon atom of the Asp nucleophile side-chain, the catalytic water provides oxygen for the alcohol product on a long run **(Prince, 1994)**, i.e. the water virtually functions as to regenerate the Asp carboxyl group. The proton of the alcohol group can be obtained either from the His+ base or from the hydroxyl group attached to the carboxyl carbon of the Asp nucleophile, i.e. from the catalytic water. QM/MM calculations of the Ad_N step of dehalogenation of 1,2-dichloroethane by LinB suggest the former, i.e. the His base functions not only as the water activator but also as the proton carrier **(Otyepka et al., 2008)**. One or more XC structures were determined for each of DhlA, DhaA, LinB and DmbA that contain halide anion bound between the two halide-stabilising amino acid residues **(Table 16 and Fig 29; Verschueren et al., 1993d; Newman et al., 1999; Marek et al., 2000; Oakley et al., 2002; Streltsov et al., 2003; Mazumdar et al., 2008)**. Six XC structures of LinB (PDB-IDs 1D07, 1G4H, 1IZ8, 1K6E, 1K63 and 2BFN) and one XC structure of DmbA (PDB-ID 2O2I) also captured bound alcohol product of the dehalogenation reaction in the cavity **(Table 16 and Fig 29)**. In four of the XC structures (PDB-IDs 1G4H, 1IZ8, 2BFN and 2O2I), the alcohol molecule is located adjacent to the face of the imidazole ring of the His base, i.e. in the region that corresponds to the unproductive substrate binding site **(Streltsov et al., 2003; Monincová et al., 2007; Mazumdar et al., 2008)**. In other XC structures (PDB-IDs 1D07, 1K6E and 1K63), the alcohol product is shifted towards the Asp nucleophile and halide anion, and shows smaller interaction interface with the His base **(Streltsov et al., 2003)**.

Product release. Last step of the reaction cycle is regeneration of the active site, i.e. the release of all the three products, i.e. halide ion, alcohol and proton. The halide is released from the interaction with the halide-stabilising amino acid residues and the alcohol from the interaction with the halide anion, the Asp nucleophile and the His base by water molecules **(Schanstra & Janssen, 1996)** that enter the cavity to compete for the interactions and to solvate the halide ion and the hydroxyl group of the alcohol **(Negri et al., 2007)**. The two products then leave the active site through a tunnel **(Negri et al., 2007)**. All three possible sequences of product release have been already observed in haloalkane dehalogenases: (i) alcohol first (chloride ion vs 2-chloroethanol and bromide ion vs 2-bromoethanol) in DhlA **(Schanstra et al., 1996b)**; (ii) halide first (bromide ion vs 3-bromo-1-propanol) in DhaA **(Bosma et al., 2003)**; and (iii) random sequential (chloride ion vs 1-hexanol, chloride ion vs cyclohexanol and bromide ion vs cyclohexanol) in LinB **(Prokop et al., 2003)**. The fate of the proton from the Asp nucleophile remains unknown; the proton can be accepted by a water molecule and leave the active site through hydrogen bonding network connecting the active site to bulk solvent **(Otyepka et al., 2008)**.

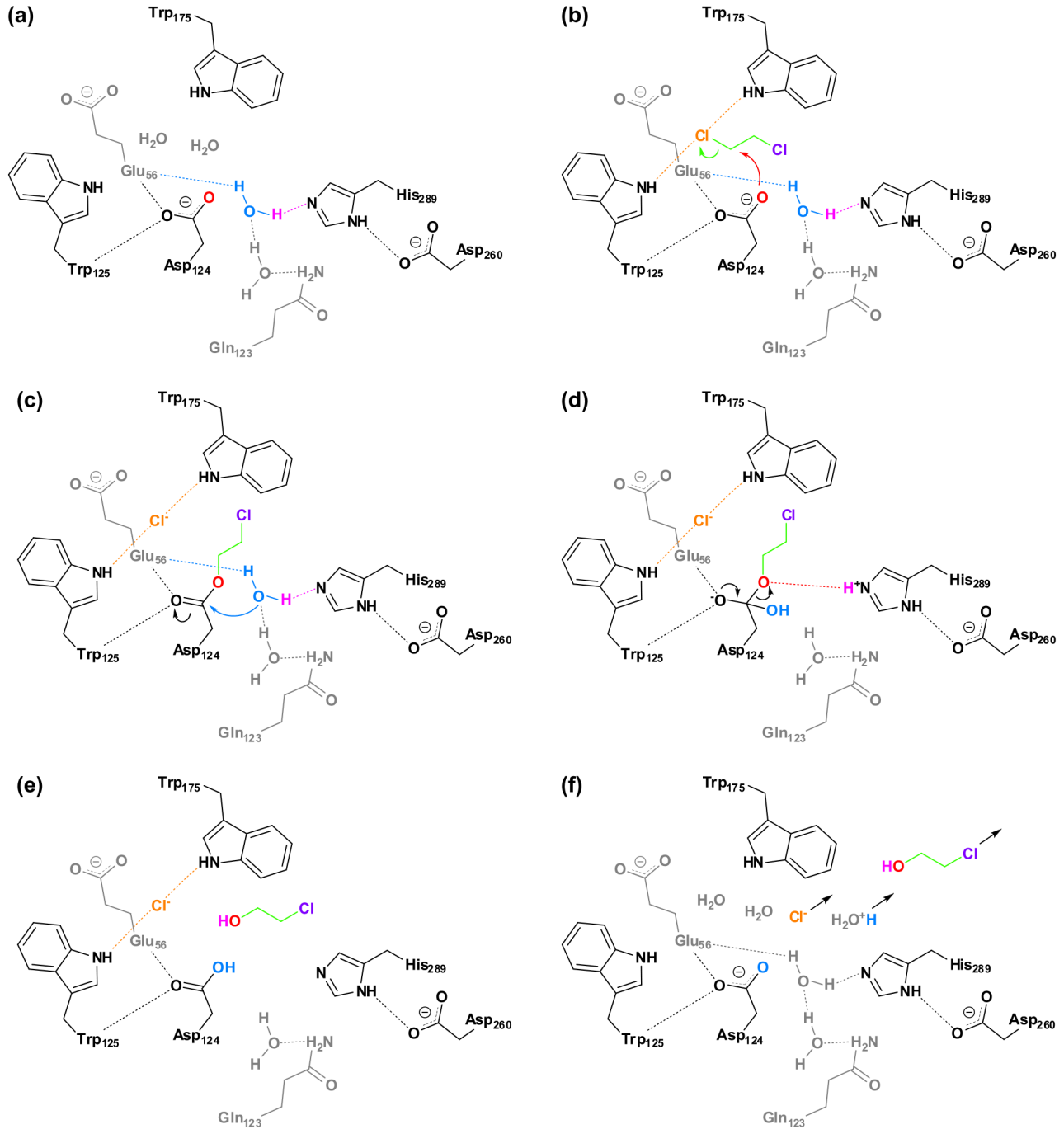

Fig 26 | Reaction cycle of haloalkane dehalogenase DhlA with 1,2-dichloroethane. **(a)** Binding of a substrate to a free enzyme and displacing of active site water molecules; **(b)** bimolecular nucleophilic substitution of a chlorine atom by carboxyl oxygen atom of the Asp124 nucleophile yielding a covalent ester intermediate and chloride anion; **(c)** nucleophilic addition of a hydroxyl anion from the catalytic water molecule to the carboxyl carbon of the Asp124 nucleophile in the ester intermediate yielding a tetrahedral intermediate; **(d)** decomposition of the metastable tetrahedral intermediate into 2-chloroethanol and free carboxyl group of the Asp124 nucleophile; **(e)** complex of DhlA with the three products of the reaction; **(f)** release of the products and binding of a new catalytic water molecule. Main-chain groups of the amino acid residues are indicated by amino acid residue annotations for clarity. Hydrogen bonding interactions are indicated by dotted lines: black, oxyanion hole; orange, halide-stabilisation; light blue, violet and grey, binding and polarisation of the catalytic water molecule. Schemes *a*, *b*, *c* and *e* are evidenced from XC structures of DhlA (see **Fig 27**). The reaction mechanism of DhaA/LinB/DmbA is analogous, except for Asn38/41/39 functioning instead of Trp175 and Glu56 as halide-stabilising amino acid residue and oxyanion hole amino acid residue, His105/107/108 functioning as the structural water binding amino acid residue instead of Gln123, and Glu130/132/133 functioning as the catalytic acid instead of Asp260. Redrawn according to Verschueren et al. **(1993d)**; the fate of the hydrogens from catalytic water molecule remains unclear; added according to the proposal by Otyepka et al. **(2008)** for LinB.

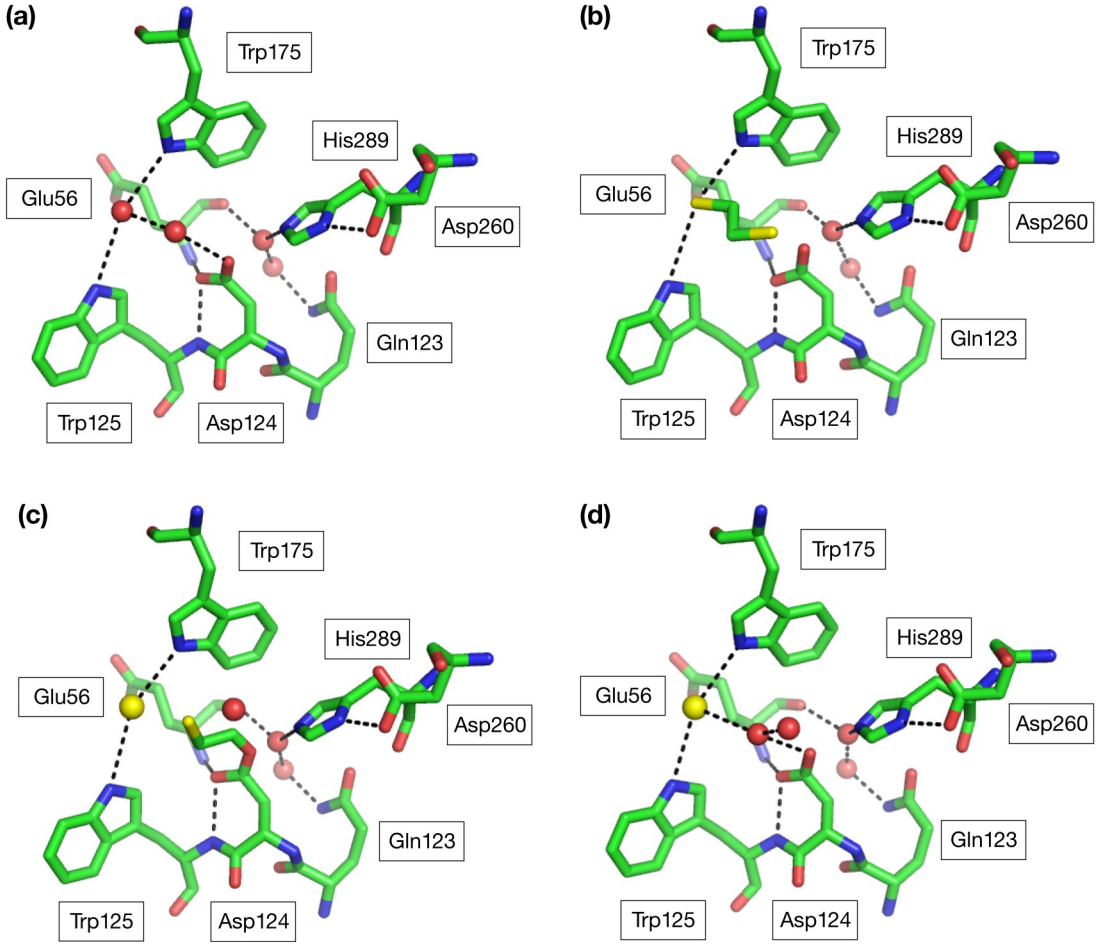

Fig 27 | XC structures along the reaction cycle of haloalkane dehalgoenase DhlA with 1,2-dichloroethane. **(a)** Free DhlA enzyme with solvated active site (PDB-ID 2HAD); **(b)** DhlA-1,2-dichloroethane complex (PDB-ID 2DHC); **(c)** DhlA-chloroethyl ester intermediate and chloride anion (PDB-ID 2DHD); **(d)** DhlA-chloride anion complex (2-chloroethanol has already left; PDB-ID 2DHE). Yellow sphere, chloride anion; red spheres, oxygen atoms of water molecules. The spheres are visualised in 30% of their actual size for clarity. The structures correspond to the schemes *a*, *b*, *c* and partially *e*, respectively, in **Fig 26**.

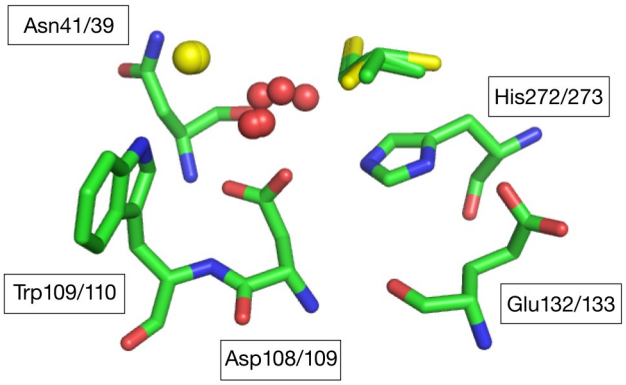

Fig 28 | Unproductive substrate binding in haloalkane dehalogenases LinB (PDB-IDs 1G42 and 1G5F) and DmbA (PDB-ID 2O2H). The substrate molecules (green sticks with chlorine atoms in yellow) are superimposed to the 1G42 structure. The substrate molecules bind adjacent to the face of the His base. The productive binding site is occupied by halide anion (yellow spheres) and water molecules (oxygen atoms shown in red spheres). The amino acid residue identifiers are in the order LinB/DmbA.

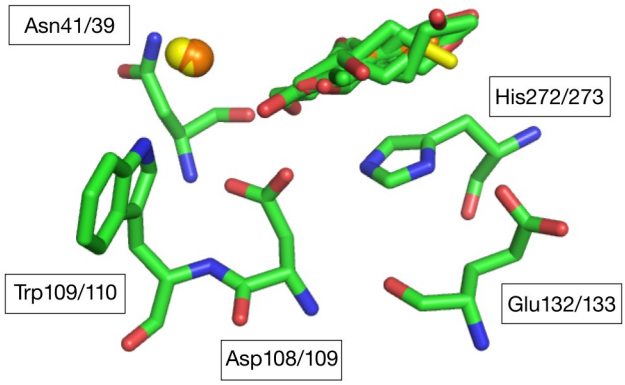

Fig 29 | Product binding sites in haloalkane dehalogenases LinB (PDB-IDs 1D07, 1G4H, 1IZ8, 1K6E, 1K63 and 2BFN) and DmbA (PDB-ID 2O2I). The products are superimposed to the 2BFN structure. Halide anions bind between the two halide-stabilising amino acid residues. Alcohol molecules (sticks) bind adjacent to the face of the His base, and close to the halide anion (sphere) and the Asp nucleophile. The spheres are visualised in 30% of their actual size for clarity. Yellow, chlorine/chloride anion; orange, bromine/bromide anion. The amino acid residue identifiers are in the order LinB/DmbA. The orientation of the protein molecule is the same as in **Fig 28**.

Rate limitation. The overall rate of the dehalogenation reaction is determined by the slowest step along the reaction cycle **(Table 21)**. Interestingly, four different rate-limiting steps have been already observed in dehalogenating reactions catalysed by haloalkane dehalogenases DhlA **(Schanstra et al., 1996b)**, DhaA **(Bosma et al., 2003)** and LinB **(Prokop et al., 2003)**. The differences in rate-limiting steps have been attributed to combination of three effects **(Prokop et al., 2003)**: (i) DhaA and LinB have larger size and better accessibility of the active site cavity compared to DhlA **(Fig 24b; Marek et al., 2000)**; (ii) two Trp halide-stabilising amino acid residues in DhlA are stronger compared to corresponding Trp and Asn in DhaA and LinB **(Krooshof et al., 1998; Boháč et al., 2002)**; and (iii) Asp catalytic acid interacts more repulsively with halide anion during its release than Glu catalytic acid due to different spatial location **(Krooshof et al., 1997; Bosma et al., 2003)**. Additionally, there are substrate-specific effects because dehalogenation reactions catalysed by a particular haloalkane dehalogenase can be limited at different steps for different substrates **(Schanstra et al., 1996b; Bosma et al., 2003)**. Interestingly, one or two amino acid residues substitution can already shift the rate-limiting step **(Krooshof et al., 1997; Krooshof et al., 1998)** which is an indication of delicately balanced rates of individual steps **(Schanstra et al., 1996a; Krooshof et al., 1997; Krooshof et al., 1998)**. Despite all these observations, current level of knowledge about haloalkane dehalogenases does not allow extrapolating rate limitation among different haloalkane dehalogenases **(Prokop et al., 2003)**, their mutants **(Krooshof et al., 1997; Krooshof et al., 1998)** and different substrates **(Schanstra et al., 1996b; Bosma et al., 2003)**.

Table 21 | Rate-limiting steps in dehalogenating reactions catalysed by haloalkane dehalogenases. (pp. 81-82)

Enzyme	Variant	Substrate	Products	Rate-limiting step
DhlA[a]	Wild-type	1,2-Dichloroethane	2-Chloroethanol Cloride anion	Release of the halide anion **(Schanstra et al., 1996b)**
		1,2-Dibromoethane	2-Bromoethanol Bromide anion	Release of the halide anion **(Schanstra et al., 1996b)**
		1-Chlorohexane	1-Hexanol Chloride anion	Substrate binding or S_N2 step **(Schanstra et al., 1996b)**
DhlA[a]	Asp260Asn +Asn148Glu[d]	1,2-Dibromoethane	2-Bromoethanol Bromide anion	Substrate binding or S_N2 step **(Krooshof et al., 1997)**
DhlA[a]	Trp175Tyr[e]	1,2-Dibromoethane	2-Chloroethanol Chloride anion	Substrate binding or S_N2 step **(Krooshof et al., 1998)**
DhaA[b]	Wild-type	1,3-Dibromopropane	3-Bromo-1-propanol Bromide anion	Release of the alcohol **(Bosma et al., 2003)**
		1,2,3-Trichloropropane	2,3-Dichloropropane-1-ol	Substrate binding or S_N2 step **(Bosma et al., 2003)**

Enzyme	Variant	Substrate	Products	Rate-limiting step
LinB[c]	Wild-type	1-Chlorohexane	1-Hexanol Chloride anion	Hydrolysis of the ester intermediate **(Prokop et al., 2003)**
		Chlorocyclohexane	Cyclohexanol Chloride anion	Hydrolysis of the ester intermediate **(Prokop et al., 2003)**
		Bromocyclohexane	Cyclohexanol Bromide anion	Hydrolysis of the ester intermediate **(Prokop et al., 2003)**

[a]Source – *Xanthobacter autotrophicus* GJ10.
[b]Source – *Rhodococcus rhodochrous* NCIMB 13064.
[c]Source – *Sphingobium japonicum* UT26.
[d]In vitro site-directed mutagenesis; repositioning of the catalytic acid.
[e]In vitro site-directed mutagenesis; substitution in the halide-stabilising amino acid residue.

Catalytic effect. Haloalkane dehalgoenases exploit mechanisms from all the five categories (see 1.3.3.2) to achieve overall rate enhancement: (i) approximation by sequestering a substrate molecule from bulk solvent into a cavity buried in the protein core **(Franken et al., 1991; Verschueren et al., 1993b; Verschueren et al., 1993a; Verschueren et al., 1993c; Newman et al., 1999; Marek et al., 2000; Oakley et al., 2004; Mazumdar et al., 2008)**; (ii) breaking the reaction into multiple steps composed of formation and breakdown of two covalent intermediates via nucleophilic catalyses **(Verschueren et al., 1993d; Pries et al., 1994a; Pries et al., 1995a; Schanstra et al., 1996b; Bosma et al., 2003; Prokop et al., 2003)**, (iii) hydrolysis of the ester intermediate involving proton transfer by His acting as the general base catalyst **(Verschueren et al., 1993d; Pries et al., 1995b; Otyepka et al., 2008)**; (iv) preorganisation of the active site for transition state complementarity, i.e. substituting water solvent by protein and solvating the transition state more than water does **(Warshel & Levitt, 1976; Warshel, 1978; Warshel & Florián, 1998; Warshel & Papazyan, 1998; Shurki et al., 2002; Warshel, 2003; Olsson & Warshel, 2004; Warshel et al., 2006; Murugan & Agren, 2009)**, achieved by a network of hydrogen bonding interactions in the active site including stabilisation of halide anion by halide-stabilising amino acid residues, stabilisation of tetrahedral intermediate by oxyanion hole interactions, stabilisation of His+ by ionic interaction with catalytic base, and binding and polarisation of catalytic water by interaction with one oxyanion hole amino acid residue and the His base **(see Fig 26)**; and (v) involving enzyme and substrate conformational changes of induced-fit and/or conformational selection type to drive the complex towards the transition state, see 1.6.2.5 **(Pries et al., 1994b; Schanstra & Janssen, 1996; Lightstone & Bruice, 1996; Lightstone et al., 1997; Krooshof et al., 1998; Lightstone et al., 1998; Bruice & Lightstone, 1999; Krooshof et al., 1999; Newman et al., 1999; Bruice & Benkovic, 2000; Marek et al., 2000; Gray et al., 2001; Lewandowicz et al., 2001; Bruice, 2002; Oakley et al., 2002; Otyepka & Damborský, 2002; Chaloupková et al., 2003; Devi-Kesavan & Gao, 2003; Paneth, 2003; Streltsov et al., 2003; Oakley et al., 2004; Negri et al., 2007)**.

1.6.2.5 Dynamics of haloalkane dehalogenases

Role of dynamics in chemical steps of the reaction. According to QM/MM calculations, the S_N2 step for the conversion of 1,2-dichloroethane by DhlA **(Warshel et al., 2000; Villa & Warshel, 2001; Shurki et al., 2002; Olssson & Warshel, 2004)** and the Ad_N step for the conversion of 1,2-dichloroethane by LinB **(Otyepka et al., 2008)** are supposed to be largely due to electrostatic preorganisation with only minor effect of dynamics in the reaction complex **(Warshel et al., 2000; Villa & Warshel, 2001; Shurki et al., 2002; Olsson & Warshel, 2004; Otyepka et al., 2008)**. According to Warshel and co-workers, ~ 90% of the catalytic effect of the S_N2 step of 1,2-dichloroethane conversion by DhlA is due to electrostatic preorganisation **(Warshel et al., 2000; Villa & Warshel, 2001; Shurki et al., 2002; Olsson & Warshel, 2004)**. Contrary, Bruice and co-workers proposed more significant role of both DhlA and 1,2-dichloroethane dynamics in restricting configurational space of the substrate in reactant state as to yield complexes close to the transition state of the S_N2 step, the so-called near attack configurations (NAC), more frequently compared to poor substrates **(Lightstone & Bruice, 1996; Lightstone et al., 1997; Lightstone et al., 1998; Bruice & Lightstone, 1999; Bruice & Benkovic, 2000; Lau et al., 2000; Bruice, 2002)**, thus reducing the activation barrier for the S_N2 step by ~ 25% compared to the corresponding reaction in aqueous solution **(Hur et al., 2003)**. The NAC for the S_N2 step of 1,2-dichloroethane conversion by DhlA was calculated to be defined by two geometrical parameters: (i) contact distance between the Asp nucleophilic oxygen atom and attacked carbon atom of the substrate molecule ≤ 3.41 Å; and (ii) angle between the Asp nucleophilic oxygen atom, attacked carbon atom of the substrate molecule and leaving chlorine atom 157-180° **(Scheme 5; Hur et al., 2003)**:

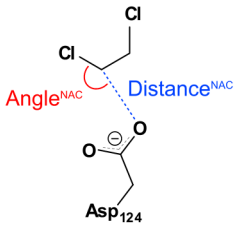

Scheme 5 | Near attack configuration for S_N2 step of 1,2-dichloroethane conversion by DhlA.

According to this definition, the XC structure of the DhlA-1,2-dichloroethane complex (PDB-ID 2DHC), in which the substrate is in a trans conformation, is not in the NAC. In fact, the 2DHC structure **(see Fig 27b)** presents an "inactive complex" because it is known from QM calculations that for the S_N2 step, 1,2-dichloroethane should be in a gauche conformation **(Lightstone et al., 1997)**. QM/MM calculations and MD simulations revealed that 1,2-dichloroethane in the gauche conformation is much more stable than trans in DhlA, and gauche in water because the gauche conformation of 1,2-dichloroethane in DhlA is stabilised by charge-dipole interaction with the Asp nucleophile **(Murugan & Agren, 2009)**. The gauche conformation then facilitates approaching of the two reacting atoms by decreased repulsion between the adjacent chlorine atom and carboxyl group of the Asp nucleophile **(Lightstone et al., 1997)**. The preference of the gauche conformation of 1,2-dichloroethane in DhlA is thus caused by strongly polarised environment of the enzyme active site compared to water solvent **(Murugan & Agren, 2009)** and hence the proposed NAC effect could be actually apparent steric effect contributed by smaller steric and larger electrostatic components **(Warshel et al., 2000; Villa & Warshel, 2001; Shurki et al., 2002; Olsson & Warshel, 2004)**.

Dynamics of catalytic amino acid residues. Even in the highly preorganised active site of haloalkane dehalogenases, some potentially functionally important motions have been observed for the Asp nucleophile **(Oakley et al., 2004)** and predicted for halide-stabilising amino acid residues **(Lewandowicz et al., 2001; Devi-Kesavan & Gao, 2003; Paneth, 2003)**. In the former case, the Asp nucleophile was determined in the ultra-high resolution XC structure of LinB (PDB-ID 1MJ5) to occur in two conformations **(Fig 30)** depending on the protonation state of the His base; during the catalytic cycle, the Asp nucleophile is supposed to switch the conformation to effectively perform its function **(Oakley et al., 2004)**. In the latter case, side-chains of the halide-stabilising Trp in DhlA were predicted by QM/MM calculations and MD simulations to be rotated out of their optimal positions like "drawing a bow"; the high-energy cost of the strain is compensated by increased hydrogen-bonding of the chlorine atom; finally, hydrolysis of the intermediate releases the strain causing return of the Trp side-chains into optimal position **(Devi-Kesavan & Gao, 2003)**. Estimation of the quantitative contribution of these motions to the total catalysis effect has not yet been reported.

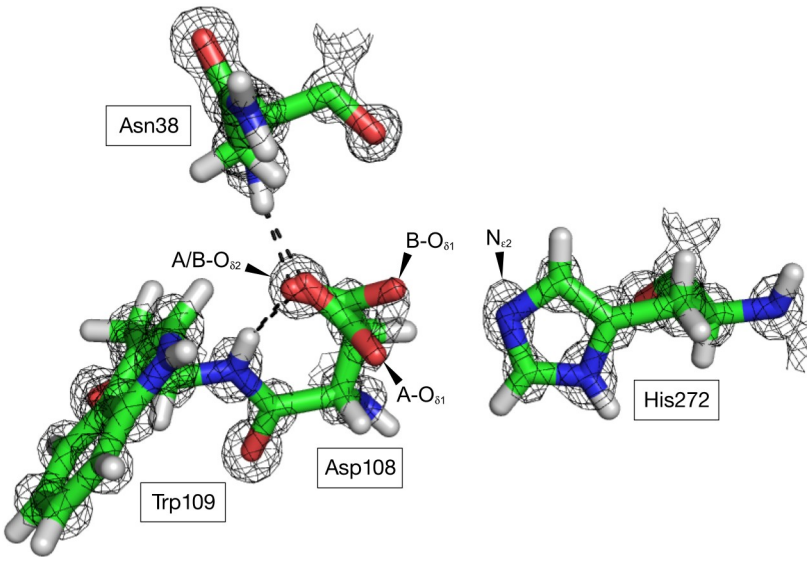

Fig 30 | Two conformations of Asp108 nucleophile (A and B) in haloalkane dehalogenase LinB. The distance between $O_{\delta1}$ and $N_{\varepsilon2}$ is 3.05 Å in the A conformation and 2.53 Å in the B conformation. The distance between $O_{\delta1}$ atoms of the two conformations is 1.49 Å. The distance between $O_{\delta2}$ atoms of the two conformations is only 0.29 Å; thus in both the conformations, $O_{\delta2}$ atom exists in favourable position for oxyanion hole interactions (dashed lines) with Trp109 and Asn38. The electron density map (2mFo-DFc) is contoured at 2.0 σ.

Role of conformational change for halide release in DhlA. Diffusion steps, substrate binding and product release, can be also rate-limiting and thus main determinants of the reaction rate **(see Table 21)**. The exchange of substrates,

products and water between bulk solvent and buried active site occurs via tunnels; XC structures revealed two tunnels in DhaA **(Newman et al., 1999)**, two tunnels in LinB **(Marek et al., 2000)**, but no tunnel in DhlA **(see Fig 24)**. The absence of a tunnel in DhlA suggests a conformational change that must accompany substrate binding and product release **(Pries et al., 1994b)**. Indeed, stopped-flow fluorescence measurements of halide binding and release **(Schanstra & Janssen, 1996)**, and thermodynamic analysis of halide binding **(Krooshof et al., 1998)** showed two-step and three-step routes for halide binding via formation of an encounter (also known as "collision") complex later proven by XC, PDB-ID 1BE0 **(Pikkemaat et al., 1999)**. The presence of the encounter complex and buried active site means that halide release in DhlA is accomplished by induced-fit mechanism **(Sullivan & Holyoak, 2008)**. Site-directed mutagenesis confirmed that the enzyme isomerisation involving conformational change is located in the cap domain **(Schanstra et al., 1996a; Schanstra et al., 1997; Krooshof et al., 1998)**. The conformational change of the cap domain is the cause of halide release being the rate-limiting step; in other words, the conformational change of the cap domain for halide release is the rate-limiting event in the reaction cycle of DhlA **(Schanstra & Janssen, 1996)**. The conformational change could involve: (i) concerted movement of aromatic amino acid residue side-chains in the cap domain **(Krooshof et al., 1998)**; (ii) movement in the region comprising first two α-helices, 4' and 4, of the cap domain **(see Fig 25a)** and the loop between them, α4'/α4-loop **(Schanstra & Janssen, 1996; Krooshof et al., 1998)**; and/or (iii) cis-trans isomerisation of the cap domain Pro168 amino acid residue located in the α4'/α4-loop **(Krooshof et al., 1999)**.

Role of dynamics in tunnels for substrate binding and/or product release. Possible sites for encounter complex formation in DhlA were determined by XC, PDB-ID 1BE0 **(Pikkemaat et al., 1999)** and further supported by computational solvent mapping **(Silberstein et al., 2007)**. Two pathways that could potentially form open tunnels due to protein motions, and that are in accordance with the proposed surface halide-binding sites **(Silberstein et al., 2007)**, were found by CAVER 1.0 tunnel calculation program **(Fig 31a; Petřek et al., 2006)**. Although, direct experimental observation of (presumably short-living) open tunnels in DhlA has not yet been reported. Even when tunnels are present in the XC structure, which is the case of LinB, DhaA and DmbA, substrate binding or product release cannot be a priori excluded as possible rate-limiting steps of the overall reaction, as shown by DhaA case: release of 3-bromopropane-1-ol is the rate-limiting step of 1,3-dibromopropane conversion by DhaA **(Bosma et al., 2003)**. The reason for the release of the alcohol being the rate-limiting step could be: (i) strong attractive interaction between product and amino acid residues of the tunnel, especially the Asp nucleophile and the His base, as suggested by the XC structures of LinB **(see Fig 29; Oakley et al., 2002; Streltsov et al., 2003)** and DmbA **(see Fig 29; Mazumdar et al., 2008)**, and MD simulations of LinB with 2-chloroethanol **(Negri et al., 2007)**; and/or (ii) dynamical fluctuations of the tunnel size at a time-scale that interfers with product release rate. In agreement with alternative conformations present for amino acid residues in XC structures **(Fig 32)** and with XC *B*-factors **(Fig 33; Streltsov et al., 2003)**, comparative analysis of protein motions in DhlA, DhaA and LinB by using classical MD simulations showed that the largest amplitudes of protein motions occur in N-terminal cap domain loop, NC loop (DhlA, DhaA and LinB), α-helix 4' (DhlA), α-helix 4 (DhlA, DhaA and LinB) and C-terminal cap domain loop, CC loop **(Otyepka & Damborský, 2002)**, i.e. in the region of tunnels observed by XC and MD simulations **(Otyepka & Damborský, 2002)** and predicted by CAVER 1.0 **(Fig 31; Petřek et al., 2006)**. Together with kinetic data, presence of the largest motions and all known tunnels in the same regions of the cap domain of haloalkane dehalogenases suggests that the cap domain provides not only the active site cavity and tunnels, but also plasticity to these structural features via motions **(Otyepka & Damborský, 2002; Streltsov et al., 2003; Oakley et al., 2004; Negri et al., 2007)** and that these motions are important for enzyme kinetics **(Schanstra & Janssen, 1996; Krooshof et al., 1998; Krooshof et al., 1999; Gray et al., 2001; Oakley et al., 2002)**. As the cap domain also contributes to the formation of the active site, the mobility of the cap domain needs to be compromised. This is achieved by stabilising β-bridge interaction between the NC- and CC-loops in DhaA and LinB **(Otyepka & Damborský, 2002)**, packing of α-helix 4' against α-helix E in DhlA **(Otyepka & Damborský, 2002)**, and by stabilising interaction of the cap domain with highly conserved main domain loop located between β-strand 4 and α-helix B, that comprises Gly-X-Gly-X-Ser-motif common to haloalkane dehalogenases **(Chovancová et al., 2007)** and their close relatives, epoxide hydrolases **(Barth et al., 2004)**.

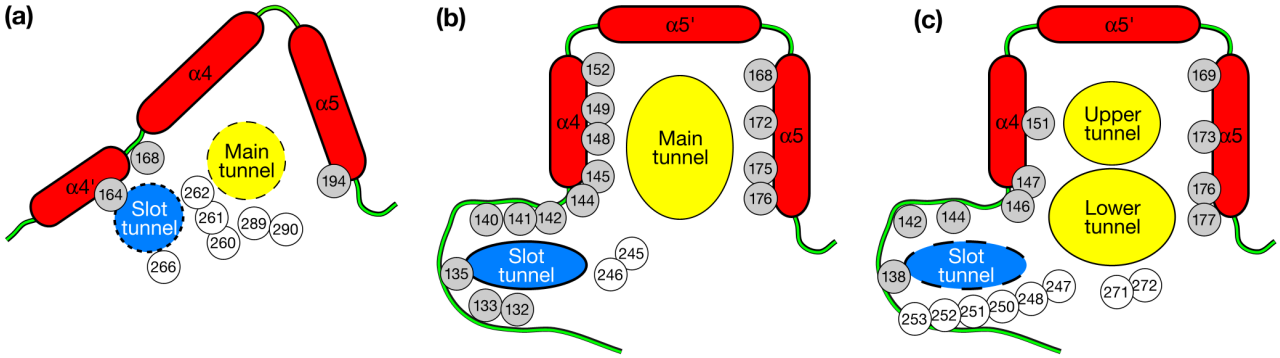

Fig 31 | Tunnels in XC structure of haloalkane dehalogenases identified by CAVER 1.0. **(a)** DhlA; **(b)** DhaA; **(c)** LinB. CAVER identifies three types of pathways: (i) tunnels (solid lines) observed in XC structures; (ii) pathways that form open tunnels via protein motions in MD simulations (dashed lines) reported by Otyepka & Damborský **(2002)**; and (iii) "uncertain" pathways highlighted by dotted lines that either open on longer time scale not sampled by the MD simulations, or do not form open tunnel but allow passage of water molecules through the low density region of protein matrix, or they are not relevant. Identifiers for amino acid residues lining the tunnels are given in grey and white circles for cap and main domain, respectively. Schematic representation of the protein is given only for N-terminal part of the cap domain. Redrawn according to Petřek et al. **(2006)**.

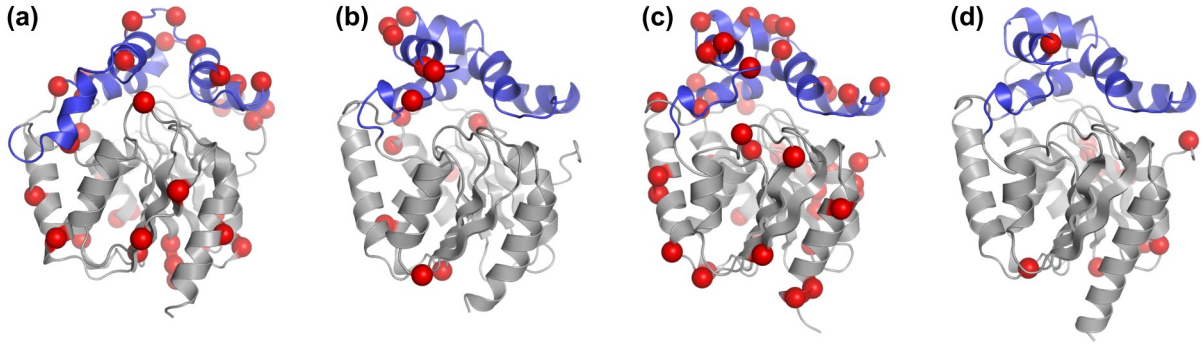

Fig 32 | Alternative conformations in haloalkane dehalogenases. **(a)** DhlA (PDB-IDs 1B6G and 2PKY mapped onto 2HAD); **(b)** DhaA (PDB-IDs 1BN6 and 1BN7 mapped onto 1CQW); **(c)** LinB (PDB-IDs 1MJ5, 1G42, 1G4H, 1G5F and 2BFN mapped onto 1CV2); **(d)** DmbA (PDB-IDs 2O2H and 2QVB mapped onto the latter). C_α atoms of amino acid residues determined in alternative conformations are highlighted by red balls. The larger number of the alternative conformations observed for DhlA and LinB can be due to near-atomic (PDB-ID 1B6G) and atomic resolution (PDB-ID 1MJ5) XC structures, respectively. Protein cartoon models are coloured by domain: grey, the main domain; blue, the cap domain.

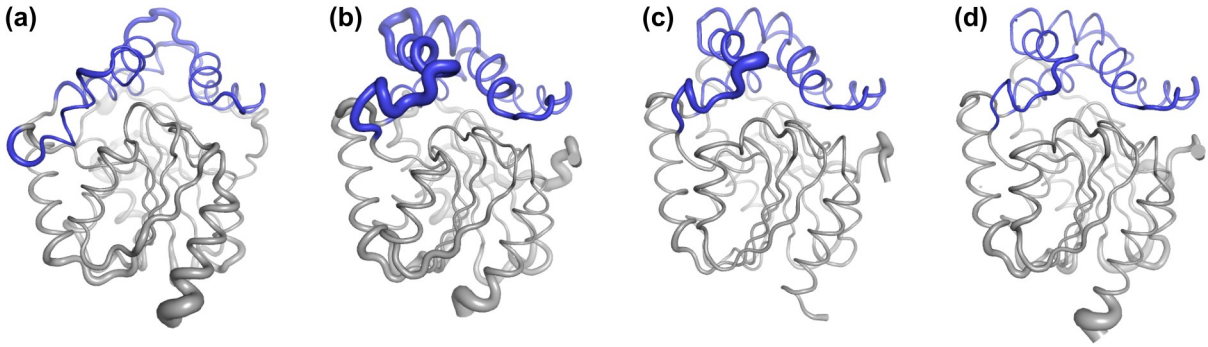

Fig 33 | High mobility regions of haloalkane dehalogenases identified by XC *B*-factors. **(a)** DhlA (PDB-ID 2HAD); **(b)** DhaA (PDB-ID 1CQW); **(c)** LinB (PDB-ID 1MJ5); **(d)** DmbA (PDB-ID 2QVB). *B*-factors for different amino acid residues are visualised by varying thickness of a cartoon tube: the thicker the tube, the higher the *B*-factor; main domain, grey; cap domain, blue. When omitting termini, the highest mobility in DhaA and LinB is situated in N-terminal part of the cap domain.

1.6.2.6 Application of haloalkane dehalogenases

Bioremediation. Bacteria bearing and expressing haloalkane dehalogenase genes were long time ago recognised to be possibly applicable for bioremediation **(Janssen et al., 1985)**, i.e. human-assisted removal of xenobiotics from polluted environment by living organisms. Bacteria expressing haloalkane dehalogenases can be used for removal of halogenated aliphatic hydrocarbons from polluted soil **(Wada et al., 1989)**, water **(Stucki & Thueer, 1995; Erable et al., 2004; Torz et al., 2007)** and gas **(van den Wijngaard et al., 1993; Dravis et al., 2000; Erable et al., 2004; Erable et al., 2005)**. Removal of 1,2-dichloroethane by *Xanthobacter autotrophicus* GJ10 with key initial action by haloalkane dehalogenase DhlA **(Fig 23)** was demonstrated to occur in a continuous stirred tank bioreactor **(Fig 34; van den Wijngaard et al., 1993; Ferreira Jorge & Livingston, 1999)**, a membrane reactor **(Freitas dos Santos & Livingston, 1994)** and at full scale in a rotating disk biological contactor **(Stucki & Thueer, 1995)**. Recently, it has been suggested that more efficient clean-up of a polluted water or gas sample could have been achieved by a combination of various bacterial strains expressing different haloalkane dehalogenases with different substrate specificities in a successive batch reactor to allow for optimising temperature and pH to various strains **(Erable et al., 2006)**. Haloalkane dehalogenase gene *dhlA* of *Xanthobacter autotrophicus* GJ10 was also successfully engineered into *Arabidopsis thaliana* **(Naested et al., 1999)** and, together with haloacid dehalogenase gene *dhlB* of *Xanthobacter autotrophicus* GJ10, into *Nicotiana tabacum* **(Mena-Benitez et al., 2008)** via *Agrobacterium* sp. PGV3101, and the possibility of phytoremediation was demonstrated **(Naested et al., 1999; Mena-Benitez et al., 2008)**. Alternatively, haloalkane dehalogenases could be isolated from the bacteria and applied directly in a cell-free form. For example, it has been proposed, that if mixed with proper additives, haloalkane dehalogenases DhaA, LinB and DmbA could be used for decontamination of Yperite-contaminated objects and perhaps even human skin stained with this horrific blistering agent **(Prokop et al., 2006)**.

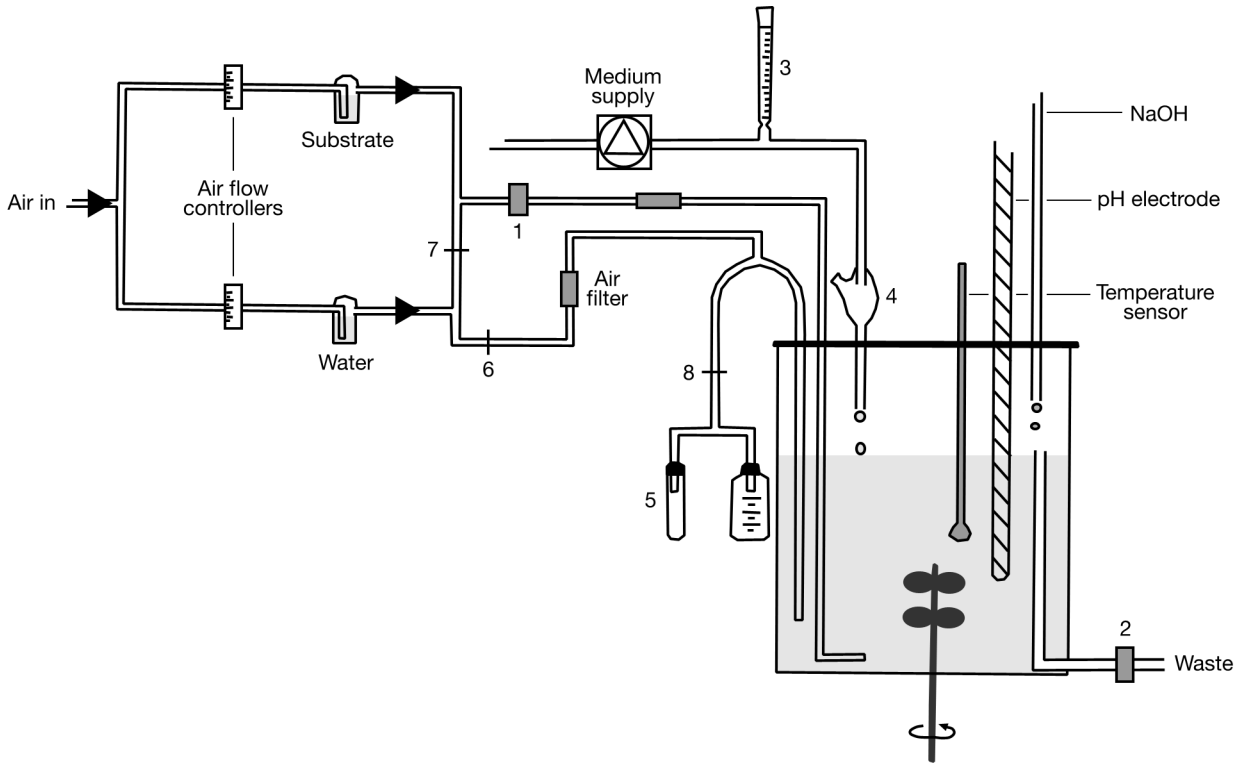

Fig 34 | Degradation of 1,2-dichloroethane by *Xanthobacter autotrophicus* GJ10 in a continuous stirred tank bioreactor. Gas samples are taken at point 1 (gas inlet) and 2 (gas outlet). The dilution rate is measured with a sterile pipet connected at point 3 with the system. At point 4, the medium enters the culture vessel. Before the aqueous sample is taken at point 5, the pipes are cleaned with air that contains no volatile substrate. For this, clamps 6 and 8 are opened for several seconds, while clamp 7 is closed. Redrawn according to van den Wijngaard et al. **(1993)**.

Biosensing. Prior to any bioremediation effort, the polluted sites must be identified first. Detection of halogenated aliphatic hydrocarbons (in mg L^{-1}) in the environment can be achieved by a biosensor with haloalkane dehalogenases

expressed by bacteria functioning as the biological element and by detecting products of the hydrolytic dehalogenation, i.e. halide ions **(Peter et al., 1996)** or protons **(Campbell et al., 2006)**. The usefulness of this approach was successfully demonstrated by a biosensor with *Rhodococcus* sp. DSM 6344 cells immobilised in alginate on a chloride or bromide ion-selective electrode and expressing haloalkane dehalogenase DhaA **(Peter et al., 1996)** and by a fiber optic biosensor for 1,2-dichloroethane detection in aqueous solution with haloalkane dehalogenase DhlA in whole cells of *Xanthobacter autotrophicus* GJ10 immobilised in calcium alginate on the tip of a fiber optic fluoresceinamine-based pH optode **(Fig 35; Campbell et al., 2006)**. The advantage of the optical biosensor is possibility of the use in situ, small size of the sensor and low cost. The in situ measurements can be, however, complicated by affected response of the biosensor by pH and buffer capacity of the environment, thus further research is needed in order to develop biosensors for practical use **(Campbell et al., 2006)**.

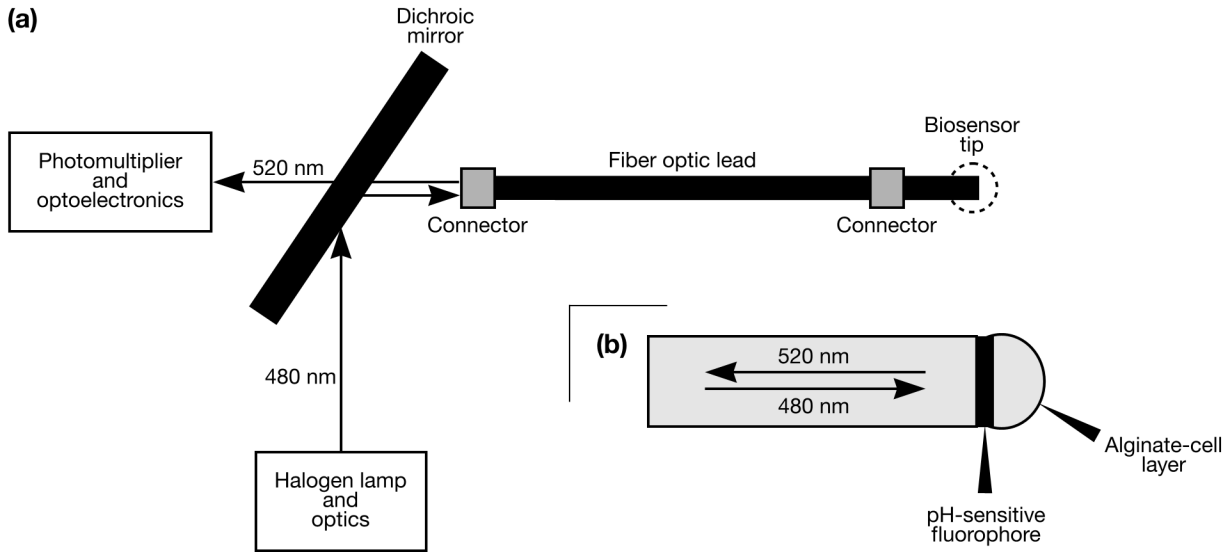

Fig 35 | Fiber optic biosensor for 1,2-dichloroethane detection in aqueous solution with haloalkane dehalogenase DhlA in whole cells of *Xanthobacter autotrophicus* GJ10 as the biocomponent. **(a)** Scheme of the biosensor; **(b)** detail of the biosensor tip. Redrawn according to Campbell et al. **(2006)**.

Production of fine chemicals. Only recently, it has been discovered that haloalkane dehalogenases are enantioselective to some substrates **(Prokop et al., 2005)**, yielding alcohol products with high enantiomeric purity. For example, DbjA converts (*R*)-2-bromopentane into (*S*)-2-pentanol with enantiomeric ratio, i.e. catalytic performance ratio between preferred and non-preferred substrate, > 200 **(Prokop et al., 2005)**. The fact, that *S*-2-pentanol is used as a key intermediate required in the synthesis of several anti-Alzheimer drugs that inhibit β-amyloid peptide release and/or its synthesis **(international patent publication No. WO 98/22494)**, suggests that new doors may open for possible exploitation of haloalkane dehalogenases for yet another human benefit **(Prokop et al., 2005)**.

Cell imaging. Another, already well established, use of haloalkane dehalogenases in the field of biomedicine and human health is in cell imaging technologies. Reaction catalysed by haloalkane dehalogenases involves essential role of His base for hydrolysis of the covalent ester intermediate **(Fig 26)**. Mutating the His base causes termination of the reaction cycle before Ad_N step, yielding accumulating ester intermediate. This is the principle of the so-called HaloTag technology developed at Promega, originally using DhaA His272Phe mutant as the HaloTag (http://www.promega.com/applications/prtn_exp/halotag.htm). A substrate, the so-called HaloTag ligand, is composed of three parts: (i) a terminally halogenated alkyl chain that binds covalently to the Asp nucleophile in the S_N2 step; (ii) a spacer of variable length and chemical nature, running through a tunnel to the protein surface in the ester intermediate; and (iii) a solvent exposed application-specific functional group, e.g. fluorescent dye, affinity handles or solid surfaces **(Los et al., 2008)**. Fusion of the HaloTag gene with a gene encoding protein of interest allows investigating the role and behaviour of the protein in live cells. Using the HaloTag technology, subcellular localisation, translocation, translocation dynamics and degradation of NF-κB proteins (p65 and IκB) was monitored by fusing genes for the proteins with the DhaA HaloTag **(Los et al., 2008)**. Fusion of the DhaA HaloTag with X-linked inhibitor of apoptosis associated factor 1 (XIAP-associated factor 1, XAF1) allowed deciphering the role of XAF1 in regulation of trophoblast cell apoptosis **(Straszewski-Chavez et al., 2007)**. The HaloTag technology was also used to study

expression, trafficking, spatial separation and real-time translocation of an β1-integrin-HaloTag fusion, thus demonstrating that this technology can be a powerful tool to investigate also membrane protein biology in live cells **(Svendsen et al., 2008)**. An extension of the HaloTag technology, the so-called covalin, was developed by Johnson and co-workers **(Chidley et al., 2008)**. Covalin is a protein chimera of two self-labeling proteins, HaloTag and O^6-alkylguanine-DNA alkyltransferease, the so-called SNAPtag **(Chidley et al., 2008)**. The advantage of the HaloTag-SNAPtag fusion is non-overlapping substrate specificity (i.e. haloalkane derivatives vs benzylguanine derivatives) that allows specific conjugation of large variety of different molecules or objects displaying appropriate functional groups **(Fig 36; Chidley et al., 2008)**.

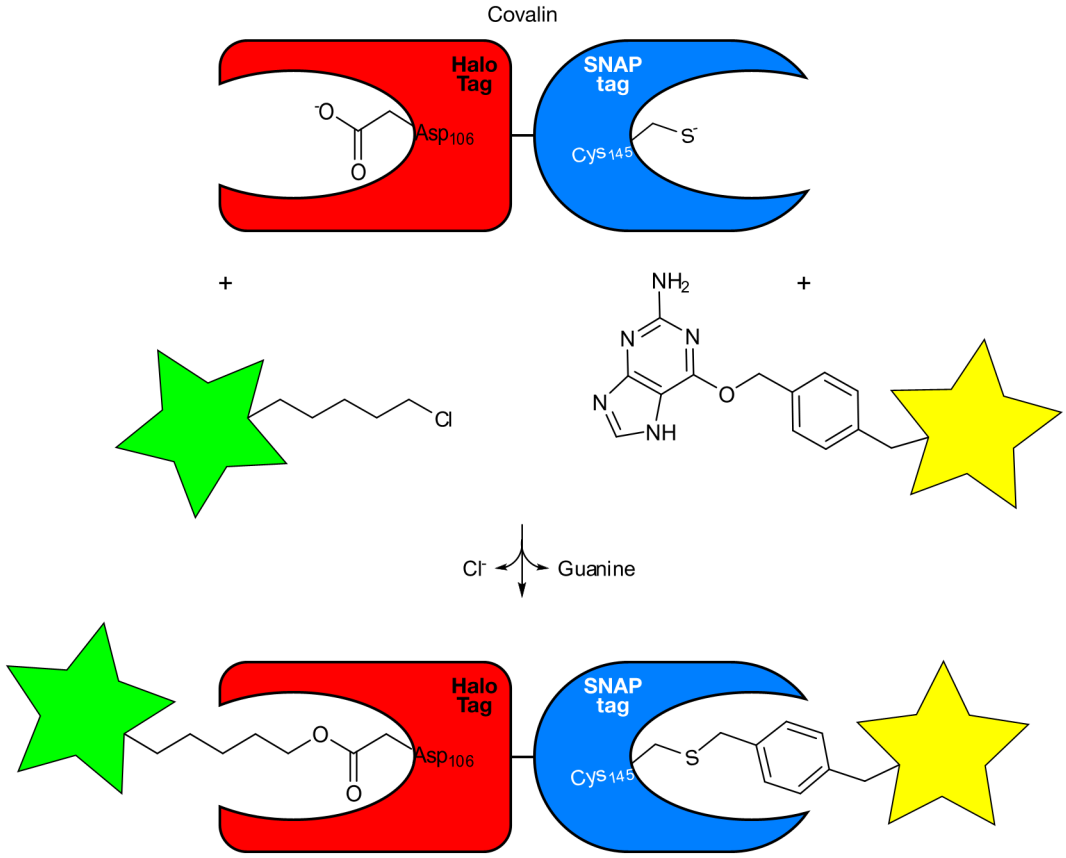

Fig 36 | General scheme of covalin-dependent bioconjugations. Objects, in green and yellow, represent synthetic probes, biomolecules, beads, or cells. Redrawn according to Chidley et al. **(2008)**.

Engineering of proteins and metabolic networks. Naturally occurring enzymes may not be efficient or stable enough for practical applications **(Chang et al., 1999)**. The above outlined potential for applications of haloalkane dehalogenases, that has attracted scientists over two decades, makes these enzyme family a good model system for better understanding of protein structure-dynamics-function relationships that in reward allows design and construction of haloalkane dehalogenase mutants with enhanced stabilities **(Gray et al., 2001; Pikkemaat et al., 2002)**, modified substrate specificities **(Pries et al., 1994b; Kmuníček et al., 2001; Chaloupková et al., 2003; Kmuníček et al., 2003; Kmuníček et al., 2005)**, enantioselectivities **(Chrobáková et al., 2006a; Chrobáková et al., 2006b; Brezovský et al., 2008)** and enhanced activities **(Pries et al., 1994b; Schanstra et al., 1996a; Schanstra et al., 1997; Holloway et al., 1998; Gray et al., 2001; Bosma et al., 2002; Chaloupková et al., 2003)**. However, when steady-state kinetic data reported, increase in k_{cat} is almost always accompanied by increase in K_m; the highest improvement of catalytic performance by engineering of haloalkane dehalogenases that has been reported so far is "only" 10.6-fold for conversion of 1-chlorohexane by DhlA Phe172Trp mutant **(Schanstra et al., 1996a)**, and 7.8-fold for conversion of 1,2,3-trichloropropane by DhaA C176Tyr+Tyr273Phe double mutant, DhaA-M2 **(Bosma et al., 2002)**. However, even such a modest improvement allowed turning the non-growth 1,2,.3-trichloropropane compound into growth substrate for *Agrobacterium radiobacter* AD1 expressing the mutant *dhaA-M2* gene **(Fig 37; Bosma et al., 2002)**. Complementary to the protein engineering, there is also an effort towards discovery of more efficient

natural catalysts: three more haloalkane dehalogenases, DbjA **(Sato et al., 2005)**, DmlA **(Sato et al., 2005)** and LinB **(Monincová et al., 2007)**, have been recently found to be active with TCP; none of these enzymes are, however, vast superior over the mutant DhaA **(Table 22)**.

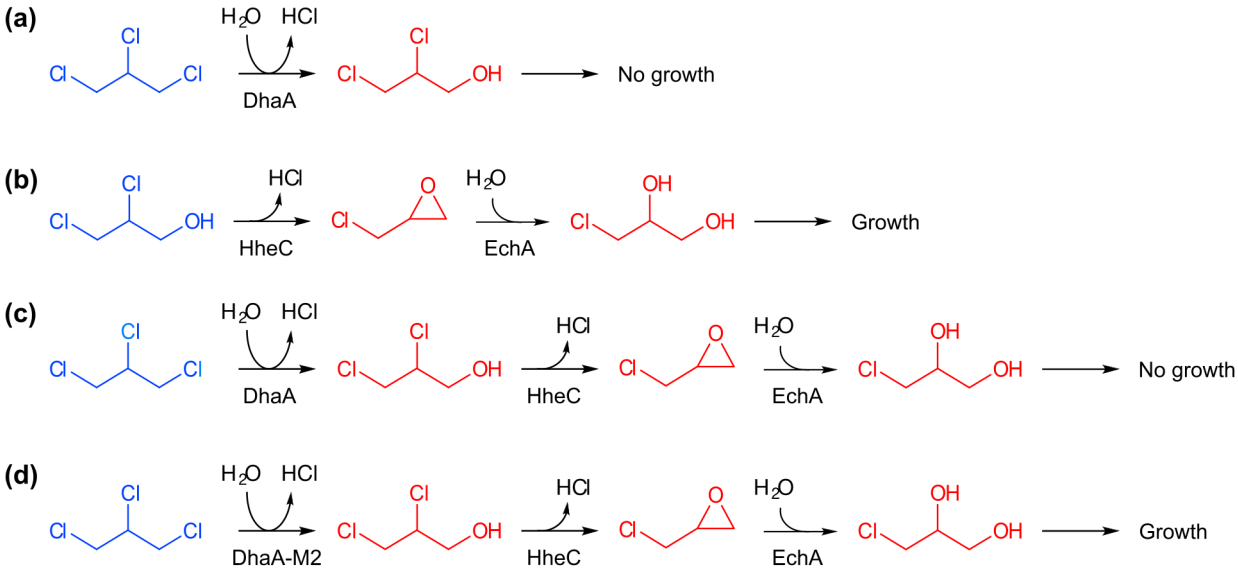

Fig 37 | Engineered TCP utilisation pathway in *Agrobacterium radiobacter* AD1. **(a)** *Rhodococcus* sp. M15-3 TCP degradation pathway; **(b)** *Agrobacterium radiobacter* AD1 2,3-dichloropropane-1-ol utilisation pathway; **(c)** *Agrobacterium radiobacter* AD1(TB3) TCP degradation pathway; **(d)** *Agrobacterium radiobacter* AD1(TB3) TCP utilisation pathway. DhaA, haloalkane dehalogenase from *Rhodococcus* sp. m15-3; DhaA-M2, Cys176Tyr+Tyr273Phe mutant of DhaA; HheC, haloalcohol dehydrogenase from *Agrobacterium radiobacter* AD1; EchA, epoxide hydrolase from *Agrobacterium radiobacter* AD1. Blue, substrate; red, metabolic intermediate. Redrawn according to Bosma et al. **(2002)**.

Table 22 | Haloalkane dehalogenases active with TCP.

Enzyme	Source	Variant	k_{cat} [s^{-1}]	K_m [M]	k_{cat}/K_m [$s^{-1}\,M^{-1}$]	Year of discovery
DhaA	*Rhodococcus* sp. m15-3	WT[a]	0.08	2.2×10^{-3}	36	1999
DhaA	*Rhodococcus* sp. m15-3	M2[b]	0.28	1.0×10^{-3}	280	2002
DbjA	*Bradyrhizobium japonicum* USDA110	WT	0.24	2.8×10^{-4}	857	2005
DmlA	*Mesorhizobium loti* MAFF303099	WT	*NR*[c]	*NR*	*NR*	2005
LinB	*Shingobium japonicum* UT26	WT	0.005	7.3×10^{-5}	68	2007

[a]WT, Wild-Type; identical to DhaA from *Rhodococcus rhodochrous* NCIMB 13064.
[b]Cys176Tyr+Tyr273Phe mutant; obtained by DNA shuffling and error-prone PCR.
[c]*NR* – Not reported.

2 Objectives

What is a digital camera? You open it and there is no film tape inside.

By means of molecular docking calculations, molecular dynamics simulations and visualisation of protein structure and dynamics, and in the view of available experimental data, my doctoral research was aimed at designing mutations in haloalkane dehalogenase DhaA from *Rhodococcus rhodochrous* NCIMB 13064 (the wild-type DhaA) for enhanced catalytic performance with toxic and recalcitrant xenobiotic compound, 1,2,3-trichloropropane, TCP **(Task 1)**, and while attempting that, bringing better understanding of structure-dynamics-function relationships of this enzyme **(Tasks 2 to 6)**.

Below follows a list of the six specific tasks that emerged in the course of conducting the research:

Task 1 | In silico design of mutants of the wild-type DhaA for enhanced conversion of TCP. The goal was to provide experimentalists with a list of amino acid residues for substitution, and if possible, to suggest suitable substitutes.

Task 2 | In silico analysis and interpretation of the effects of mutations on the enhanced conversion of TCP by DhaA mutants. The goal was to suggest what part of the reaction cycle is improved by the substitutions in the mutants, and to propose what is the basis of the improvement.

Task 3 | In silico identification of pathways and mechanisms for release of two products of TCP hydrolytic dehalogenation, i.e. 2,3-dichloropropane-1-ol (DCL) and chloride anion (CL), from the buried active site of the wild-type DhaA and the mutants. The goal was to identify all potentially functional product release pathways for the two products and to describe the release process in terms of product-enzyme and product-water interactions and dynamics.

Task 4 | In silico identification of pathways and mechanisms for water exchange between the buried active site and the surface of the wild-type DhaA and the mutants. The goal was to identify all potentially functional water exchange pathways and to describe the exchange process in terms of water-enzyme and water-product interactions and dynamics.

Task 5 | Comparison of XC structures of DhaA variants. The goal was to explore open and closed tunnels in the structures and describe the effect of mutations on the accessibility of the tunnels.

Task 6 | Testing temporary versions of CAVER 2.0 algorithm and CAVER Viewer application for calculation of pathways leading from buried cavities to surface in protein structures. The goal was to provide developers of the algorithm and the application with feedback response on the reliability of pathways identified by the CAVER 2.0 algorithm and on the user-friendliness of the graphical user interface of the CAVER Viewer.

3 Methods

There are always at least two solutions for one problem. One naturally attempts to decide for the best solution. Later on, one often realises that the best solution was actually not the best one, which is, in fact, the best proof that the realised solution was indeed the best one.

The research on the haloalkane dehalogenase DhaA outlined in the previous chapter (see 2 Objectives) was multidisciplinary, requiring tight collaboration of specialists from various fields of protein science: DNA manipulation, protein expression, protein purification, circular dichroism (CD) spectroscopy, enzyme kinetics, X-ray crystallography (XC), molecular docking calculation and molecular dynamics (MD) simulation. All experimental methods were employed by collaborators under the supervision of Jiří Damobrský, Yuji Nagata, Michal Kutý and Ivana Kutá-Smatanová (see 3.1), whereas all molecular modelling methods were employed by myself under the supervision of Jiří Damborský and Rebecca C. Wade (see 3.2). CAVER 2.0 program was developed in the collaboration of molecular modelling and bioinformatics specialists led by Jiří Damborský with specialists in the field of computer graphics and interaction of humans with computer led by Jiří Sochor (see 3.3).

3.1 Experiments

Materials and basic DNA manipulation. All used chemicals were purchased from Sigma-Aldrich (St. Louis, MO, USA). The enzymes used for DNA manipulations were obtained from Takara Bio (Kyoto, Japan), Toyobo (Osaka, Japan) and New England Biolabs (Beverly, MA USA). Modification and mutagenesis oligonucleotide primers were obtained from Hokkaido System Science (Hokkaido, Japan). Plasmids pUC18 and pAQN were obtained from (Takara Bio, Kyoto, Japan) and from Nagata et al. **(1999)**, respectively. The bacterial strains *Escherichia coli* DH5α, BL21 and XJb were obtained from Zymo Research (Orange, CA, USA) and cultivated on Lysogeny Broth (LB) medium obtained from Sigma-Aldrich (St. Louis, MO, USA). Established methods were employed for the following procedures: preparation of plasmid DNA, digestion of plasmids and PCR-amplified DNA fragments with restriction endonucleases, ligation, agarose gel electrophoresis, and transformation of *Escherichia coli* cells **(Maniatis, 1982)**.

Preparation of recombinant dhaAHis *gene.* Nucleotide sequence of pRTL1 plasmid-located *dhaA* gene (GenBank accession number AF060871; **Supplementary file genbank_AF060871**) from *Rhodoccocus rhodochrous* NCIMB 13064 **(Kulakova et al., 1997)** was modified at its termini by addition of *Bam*HI and *Hin*DIII restriction sites, Shine-Dalgarno sequence **(Shine & Dalgarno, 1975)** and six codons for His in PCR using synthetic oligonucleotide primers designed accordingly **(Fig 38)**. The PCR-amplified modified *dhaA* gene (*dhaAHis*) was inserted into high copy number pUC18 plasmid to yield recombinant plasmid pUC18::*dhaAHis* that was subsequently transformed into *Escherichia coli* DH5α **(Fig 39)**. The transformants were selected by ampicilin resistance conferred by pUC18-located *bla* gene encoding β-lactamase. Among the transformants, recombinant pUC18::*dhaAHis* were distinguished from intact plasmid by blue/white screening on LB agar with 5-bromo-chloro-indolyl-galactopyranoside, X-gal **(Fig 40)**.

Site-directed mutagenesis I. The amplified pUC18::*dhaAHis* plasmid was isolated from the recombinant *Escherichia coli* DH5α and served as the template for site-directed mutagenesis **(Table 23)** by inverted (also known as "inside out" or "inverse") PCR **(Ochman et al., 1988; Triglia et al., 1988)** using synthetic oligonucleotide primers to yield pUC18::*dhaA04His*. The mutant recombinant *dhaA04* gene was afterwards re-cloned into pAQN yielding pAQN::*dhaA04His*. The recombinant plasmids pUC18::*dhaAHis* and pAQN::*dhaA04His* served as the templates for site-directed mutagenesis using the QuikChange Site-Directed Mutagenesis Kit (Stratagene, La Jolla, CA, USA) to yield pUC18::*dhaA14His* and pAQN::*dhaA15His*, respectively **(Stsiapanava et al., 2008)**. The mutant recombinant *dhaA14* gene was afterwards re-cloned into pAQN yielding pAQN::*dhaA14His*. pAQN::*dhaA04His* also served as the template for two rounds of site-directed mutagenesis by inverted PCR with KOD Plus polymerase (Toyobo) to yield pAQN::*dhaA*M2 and pAQN::*dhaA*M3, respectively. The recombinant plasmids were transformed into *Escherichia coli* BL21 and the respective DhaA proteins were overexpressed and purified (vide infra).

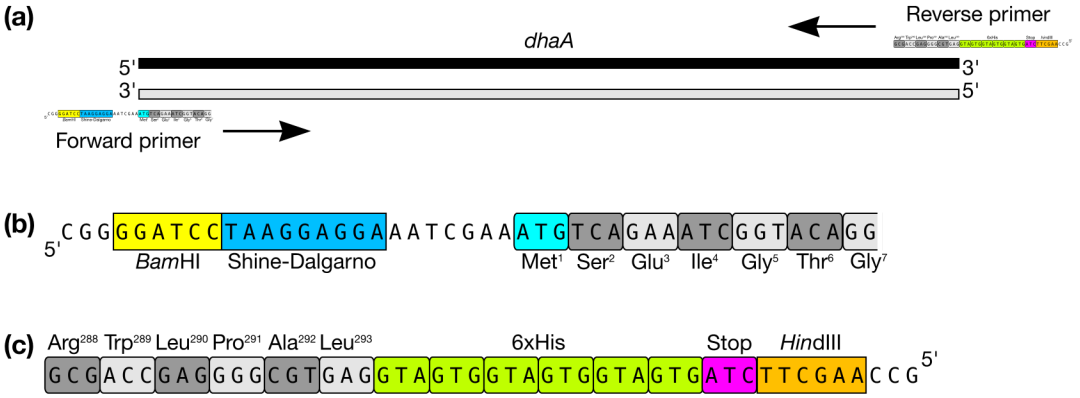

Fig 38 | Preparation of *dhaAHis* gene. **(a)** Oligonucleotide primers for PCR amplification of dhaA gene; **(b)** detail of forward primer; **(c)** detail of reverse primer. The forward oligonucleotide primer for PCR gene amplification was designed to introduce *Bam*HI restriction site for DNA manipulation purpose and Shine-Dalgarno sequence of *Escherichia coli* canonical form (TAAGGAGG) **(Makrides, 1996)** for overexpression of DhaA protein. The reverse oligonucleotide primer for PCR gene amplification was designed to introduce six codons for His (alternating two His codons, GTG and ATG) between last coding codon for Leu293 (CTC) and the amber stop codon (TAG) to aid purification of DhaA protein, and *Hin*dIII restriction site for DNA manipulation.

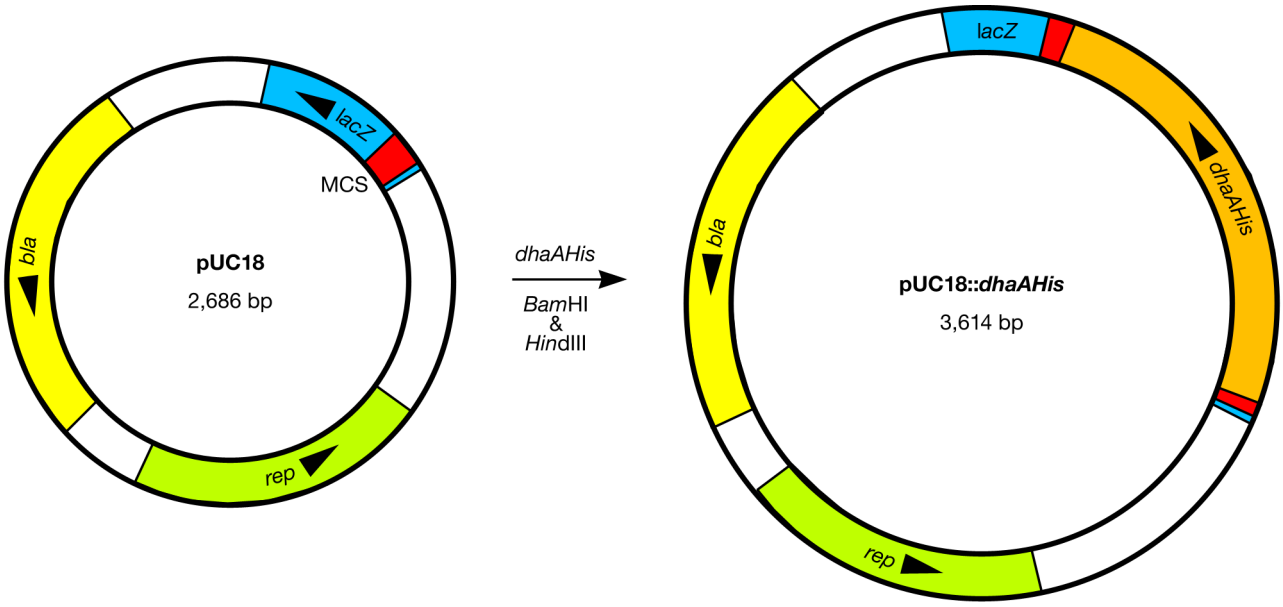

Fig 39 | Preparation of recombinant pUC18::*dhaAHis* plasmid. **(a)** pUC18 plasmid and *dhaAHis* are digested with *Bam*HI and *Hin*dIII restriction endonucleases and joined into recombinant plasmid pUC18::*dhaAHis* with *dhaAHis* inserted within multiple copy site (MCS). *bla* – gene encoding β-lactamase; *rep* – pMB1 replicon; *lacZ* – gene encoding N-terminal part of β-galactosidase.

Saturation mutagenesis and seeding. Both pAQN::*dhaAM2His* and pAQN::*dhaAM3His* served as the templates for two saturation mutagenesis experiments **(Table 24)** by inverted PCR targeting one (diversity 32) and two codons (diversity 1024), respectively, using specific oligonucleotide primers. The coding strand primers contained NNK at the position to be mutagenised, where N was an equal mixture of all four nucleotides and K was an equal mixture of G and T. The mutated amplified plasmids were treated with *Dpn*I to digest the parental DNA template, leaving the mutation-containing in vitro synthesised nicked plasmids that were transformed into *Escherichia coli* DH5α, yielding two sub-libraries for each template. All transformants were used for the stock bulk sub-library and for five-fold inoculation of 3 mL LB media with 100 μg mL^{-1} ampicilin. Plasmids from the two pAQN::*dhaAM2His*-based sub-libraries and the two pAQN::*dhaAM3His*-based sub-libraries were isolated and purified using Quantum Prep Plasmid Miniprep kit (Bio-Rad Laboratories). The isolated plasmids from respective sub-libraries were mixed in equal amounts, digested simultaneously with *Hin*dIII and *Nru*I restriction endonucleases at 37°C for 2 h. A small fragment of DNA (330 bp) from the two codon sub-library was cloned into the respective one codon sub-library (4,600 bp),

resulting in the final libraries *A* and *B*, each saturated at the three codons of interest. The libraries *A* and *B* were electroporated **(Neumann et al., 1982; Lurquin, 1997)** into *Escherichia coli* XJb cells (1 mm cuvette, 1.8 kV, 200 Ω, 25 μF).

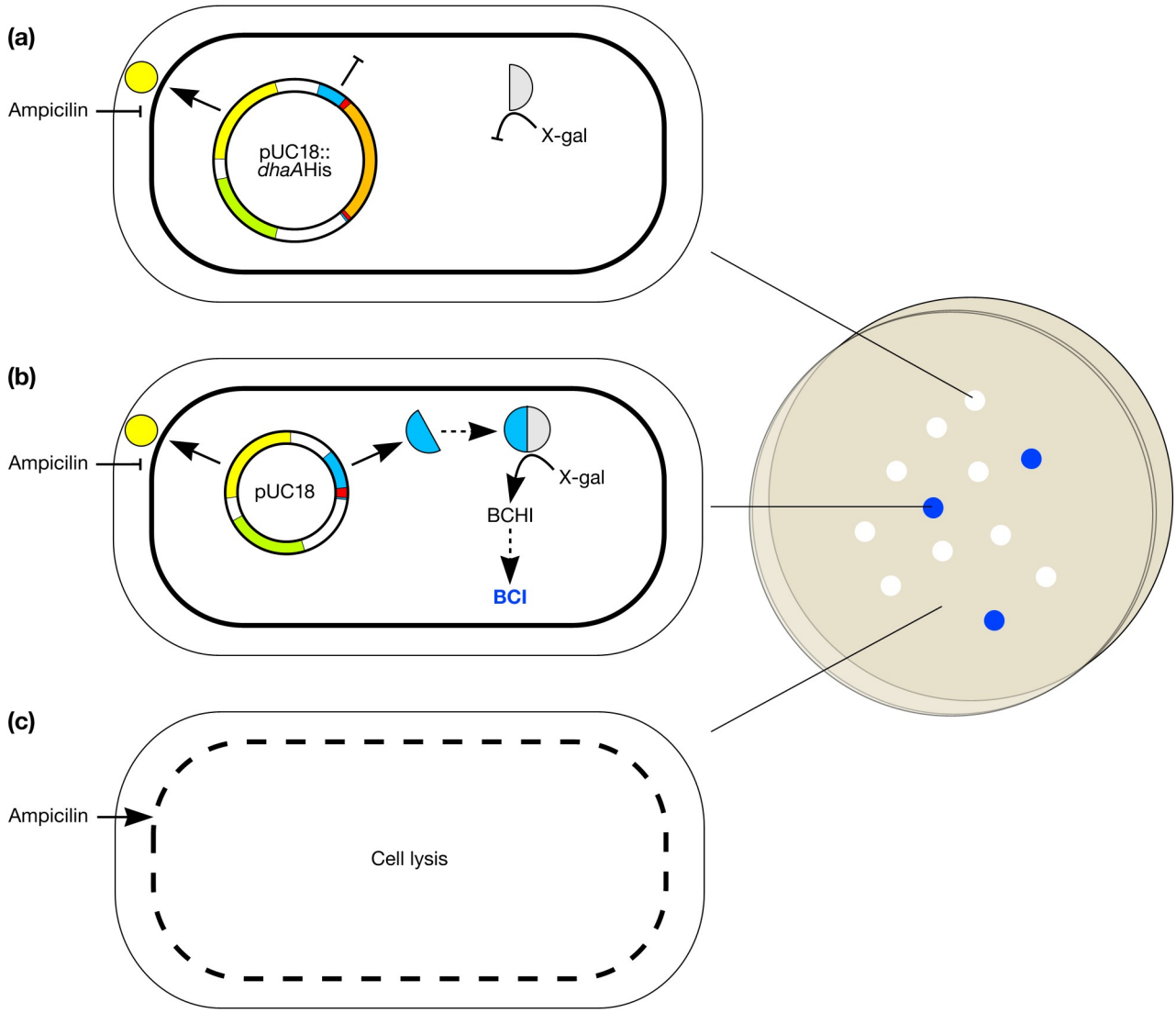

Fig 40 | Selection of *Escherichia coli* DH5α with pUC18::*dhaAHis*. **(a)** *Escherichia coli* DH5α cell with recombinant plasmid pUC18::*dhaAHis* does not produce functional β-galactosidase to convert X-gal into blue 5,5'-dibromo-4,4'-dichloro-indigo, and produces white colonies on LB agar plate with X-gal and ampicilin (right); cell lysis is protected by pUC18-encoded periplasmic-space-located β-lactamase (yellow); **(b)** *Escherichia coli* DH5α cell with intact pUC18 plasmid produces functional β-galactosidase by complementation of pUC18-encoded N-terminal part the enzyme (blue sickle) with host-encoded C-terminal part (grey sickle), to convert X-gal into blue 5,5'-dibromo-4,4'-dichloro-indigo (BCI) via 5-bromo-4-chloro-3-hydroxyindole (BCHI), and produces blue colonies on LB agar plate with X-gal (right); cell lysis is protected by β-lactamase (yellow); **(c)** *Escherichia coli* DH5α without pUC18 plasmid lyses on LB agar plate with ampicilin (right) due to absence of pUC18-encoded periplasmic-space-located β-lactamase **(Minsky et al., 1986)**.

Propagation of libraries. The recovered transformed *Escherichia coli* XJb cells were plated onto LB agar plates supplemented with 100 μg mL^{-1} ampicillin and incubated overnight at 37°C. The individual colonies were picked with sterile toothpicks and resuspended in separate wells of a 96-well plate containing LB medium and 100 μg mL^{-1} ampicillin. Each 96-well plate contained eight positive controls of M2, four negative controls with the intact pAQN plasmid and four wild-type controls. The plates were shaken at 120 r.p.m. at 37 °C for at least 16 h, and a replica of the 96 wells was made on LB agar plates. Expression of the mutant *dhaaHis* gemes from lac promoter was induced by isopropyl-b-D-thiogalactopyranoside (IPTG), that inactivates pAQN-encoded LacI repressor, at a final concentration 0.5 mM and cultivated for a further 5 h at 30 °C, pelleted at 4 °C by centrifugation at 1,800 r.p.m. for 35 min and

stored at –80 °C.

Table 23 | Site-directed mutagenesis.

Template	Primers (5' -→ 3')[a, b]	Result	Introduced mutation[d]
pUC18::*dhaAHis*	T**A**CGTCGTCCGT CCGCTTAC[fw]	pUC18::*dhaA04His*	Cys176Tyr
	TTTCGGGAGCGCACCCTC[rev]		
pAQN::*dhaAHis*	GGAATTCATCCGGCCT**T**TCCCGACGTGG[fw]	pUC18::*dhaA14His*	Ile135Phe
	CCACGTCGGGA**A**AGGCCGGATGAATTCC[rev]		
pAQN::*dhaA04His*	GGAATTCATCCGGCCT**T**TCCCGACGTGG[fw]	pAQN::*dhaA15His*	Ile135Phe
	CCACGTCGGGA**A**AGGCCGGATGAATTCC[rev]		
pAQN::*dhaA04His*	T**T**CCTCCAGGAAGACAACCC[fw]	pAQN::*dhaAM2His*	Tyr273Phe
	GTGCAATCCCGGGGC[rev]		
pAQN::*dhaAM2His*	GGACGAAT**TT**CCGGAATTCG[fw]	pAQN::*dhaAM3His*	Trp141Phe
	CACGTCGGGATAGGCC[rev]		
pAQN::*dhaA31His*	T**TC**CTCCCGAAATACGTCGTCC[fw]	pAQN::*dhaA51His*	Ala172Phe
	ACCCTCGATGAAAGCGTTCTG[fw]		
pAQN::*dhaA51His*	**TT**CCGTGAGACCTTCCAGGC[fw]	pAQN::*dhaA52His*	Ala145Phe
	GAATTCCGGCCATTCGTCCC[rev]		

[a]The introduced mutations are bold-faced and underlined.
[b]fw, forward primer; rev, reverse primer.

Table 24 | Saturation mutagenesis.

Template	Primers (5' -→ 3')[a, b, c]	Result	Introduced mutation[d]
pAQN::*dhaAM2His*	GGCCT**NNK**CCGACGTG[fw]	pAQN::*dhaAsub-libraryA1His*	Ile135X
	GGATGAATTCCATACATGCAATAC[rev]		
pAQN::*dhaAM2His*	**NNK**ATCCCCCCGGCCGAAG[fw]	pAQN::*dhaAsub-libraryA2His*	Val245X
	MNNGCCGGGTGTGCCCCAG[rev]		Leu246X
pAQN::*dhaAM3His*	GGCCT**NNK**CCGACGTG[fw]	pAQN::*dhaAsub-libraryB1His*	Ile135X
	GGATGAATTCCATACATGCAATAC[rev]		
pAQN::*dhaAM3His*	**NNK**ATCCCCCCGGCCGAAG[fw]	pAQN::*dhaAsub-libraryB2His*	Val245X
	MNNGCCGGGTGTGCCCCAG[rev]		Leu246X

[a]The introduced mutations are bold-faced and underlined.
[b]N = A, G, C or T; K = G or T; M = A or C.
[c]fw, forward primer; rev, reverse primer.
[d]X – any of the 20 standard amino acid residues.

High-throughput screening of the libraries for dehalogenating activity with TCP. The microplates with the propagated mutant *A* and *B* libraries were defrosted, and cell pellets were lysed in 1 mM HEPES buffer (pH 8.2). 10 µL of cell free extract was transferred into 140 µL of phenol red assay buffer (pH 8.2) composed of 1 mM HEPES buffer, 20 mM Na2SO4, 1 mM EDTA and phenol red at final concentration 25 µg mL^{-1}. TCP substrate was added to an apparent concentration of 10 mM, the microplates were sealed with parafilm and incubated at 25 °C for 16 h. Hydrolytic dehalogenation of TCP is accompanied by production of protons that decreased pH of the weakly buffered medium causing change in colour of the phenol red dye from red to yellow: the most active variants produced a bright yellow colour, less active in hues of orange, while inactive variants and negative controls formed a deep purple colour **(Fig 41)**. Replica colonies corresponding to the most active variants (wells) were used to inoculate 3 mL LB media and their plasmids were subsequently isolated. The nucleotide sequences of the mutant *dhaA* genes of 51 most active variants were determined by the dideoxy chain termination method using an automated DNA sequencer, ABI PRISM 310 genetic analyzer with BigDye, Terminator version 3.1 Cycle Sequencing kit (Applied Biosystems, Foster City, CA, USA; **Fig 42)**. Selected plasmids encoding 25 unique DhaA mutant proteins were transformed into *Escherichia coli* BL21.

Overexpression of selected DhaA variants. Escherichia coli BL21 cells with the selected plasmids were cultured in 10 mL (for determination of specific activity – see below) and in 2 L (for purification – see below) of LB with 100 µg mL^{-1} ampicilin at 37 °C and cultivated at 37 °C to an optical density of 0.5 at 600 nm. The induction of DhaA variant expression at 30 °C was initiated by the addition of IPTG to a final concentration of 0.5 mM. The cells were harvested by centrifugation at 8000g for 10 min after 4 h of cultivation at 30 °C. During harvesting, cells were washed and then resuspended in 20 mM KH_2PO_4 buffer (pH 7.5). The harvested cells were kept at –65 °C. Defrosted cell suspensions were disrupted by sonication using a Soniprep 150 (Sanyo Gallenkamp PLC, Loughborough, UK) or ultrasonic processor Hielscher UP200S (Hielscher Ultrasonics, Teltow, Germany). The cell-free extracts (lysates) were centrifuged at 21,000 g for 1 h to provide DhaA-containing supernatant.

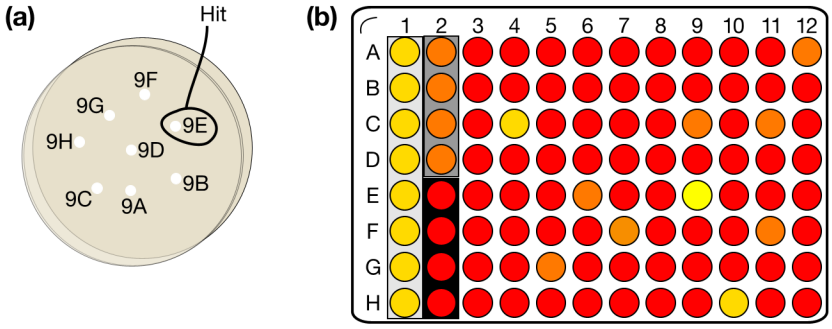

Fig 41 | Screening a saturation mutagenesis library for dehalogenation of TCP. **(a)** *Escherichia coli* Xjb replica colonies from a saturation mutagenesis library; **(b)** 96-wells microplate containing eight positive M2 mutant controls (light grey), four wild-type controls (dark grey), four negative controls (black), and 80 variants picked from the saturation mutagenesis library. In this example, variant 9E shows enhanced activity compared to the M2 mutant positive controls as the 9E contains the highest concentration of proton product of dehalogenating reaction, indicated by decrease in pH and colour-change response of phenol red pH indicator.

Comparison of substrate specificities of selected DhaA variants. Substrate specificity of wild-type DhaA and the most active mutant 31 towards a set of 31 substrates **(Table 25)** was assayed in the crude extracts by monitoring released halide anions (X^-) by addition of mercuric thiocyanate and ferric ammonium sulfate, and determining the orange colour of ferric thiocyanate product spectrophotometrically at 460 nm, the so-called Iwasaki method **(Scheme 6; Iwasaki et al., 1952)**:

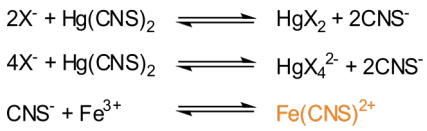

Scheme 6 | Iwasaki method.

One unit of enzymatic activity was defined as the release of 1 μmol of halide anion per minute.

Purification of selected DhaA variants. The collected cell-free extracts were purified using using FPLC Akta (Amersham Pharmacia Biotech, USA) and HiTrap affinity column packed with high performance chelating sepharose (GE Healthcare Life Sciences, NJ, USA formerly Amersham Pharmacia Biotech) or with affinity resin (Amersham Biosciences, Freiburg, Germany) charged with Ni^{2+} and equilibrated with purification buffer (pH 7.5) composed of 16.4 mM K_2HPO_4, 3.6 mM KH_2PO_4, and 0.5 M NaCl containing 10 mM imidazole. The His-tagged DhaA proteins were bound to the resin in the equilibrating buffer composed of 50 mM phosphate buffer (pH 7.5) containing 500 mM sodium chloride and 10 mM imidazole. Unbound and weakly bound proteins were washed out with buffer containing 50 mM imidazole. His-tagged DhaA proteins were eluted with the purification buffer containing 300 mM imidazole. Purified proteins were dialysed overnight against 50 mM phosphate buffer (pH 7.5) composed of 41 mM K_2HPO_4 and 9 mM KH_2PO_4. The enzymes were sterilised and stored in the same buffer. The entire purification process and storage was performed at 4 °C. DhaA protein concentrations were determined by the method of Bradford (Sigma-Aldrich, St. Louis, MO, USA).

Site-directed mutagenesis II. The plasmid with mutant *dhaA* gene encoding the most active DhaA variant, pAQN::*dhaA31His*, served as the template for two rounds of site-directed mutagenesis **(Table 23)** by inverted PCR with Phusion polymerase (Finnzymes, Espoo, Finland) and using specific oligonucleotide primers yielding pAQN::*dhaA51His* and pAQN::*dhaA52His*, respectively. The recombinant plasmids were transformed into *Escherichia coli* BL21 and the respective DhaA proteins were overexpressed and purified (see above).

Determination of steady-state kinetic constants for selected DhaA variants with TCP. Steady-state kinetic constants, k_{cat} and K_m, for the conversion of TCP by wild-type DhaA and mutants M2, M3, 04, 14, 15, 21, 27, 31, 51, and 52 were assayed with TCP by the initial velocity measurements as described previously **(Chaloupková et al., 2003)**: the substrate concentration was determined by a gas chromatography (Trace GC 2000) equipped with a flame ionization detector (Thermo Finnigan, San Jose, CA, USA) and a DB-FFAP capillary column 30 m × 0.25 mm × 0.25 mm (J&W Scientific, Folsom, CA, USA). Dehalogenation reaction was performed at 37 °C in 25-mL Reacti-Flasks closed by Mininert Valves in a shaking water bath. 10 mL reaction mixture consisted of 0.2 to 1.0 mg mL^{-1} DhaA

variant in glycine buffer (pH 8.6) and varied concentrations of substrate (0.5 to 15.0 mM). The reaction was stopped by the addition of methanol at 10 and 20 min or 15 and 30 min time points. All the data points were measured in duplicates or triplicates. Halide product concentration was determined by the Iwasaki method. The K_m and k_{cat} constants were calculated using the program Origin 6.1 (OriginLab, Northampton, MA, USA). The kinetic data were fitted using the Origin 6.1 to linear or exponential (burst) models described by equation $c = A \times (1\text{-}\exp(\text{-}k_B \times t)) + k_L \times t$, where A is the amplitude of burst, k_B is the burst phase rate and k_L is the steady-state phase rate.

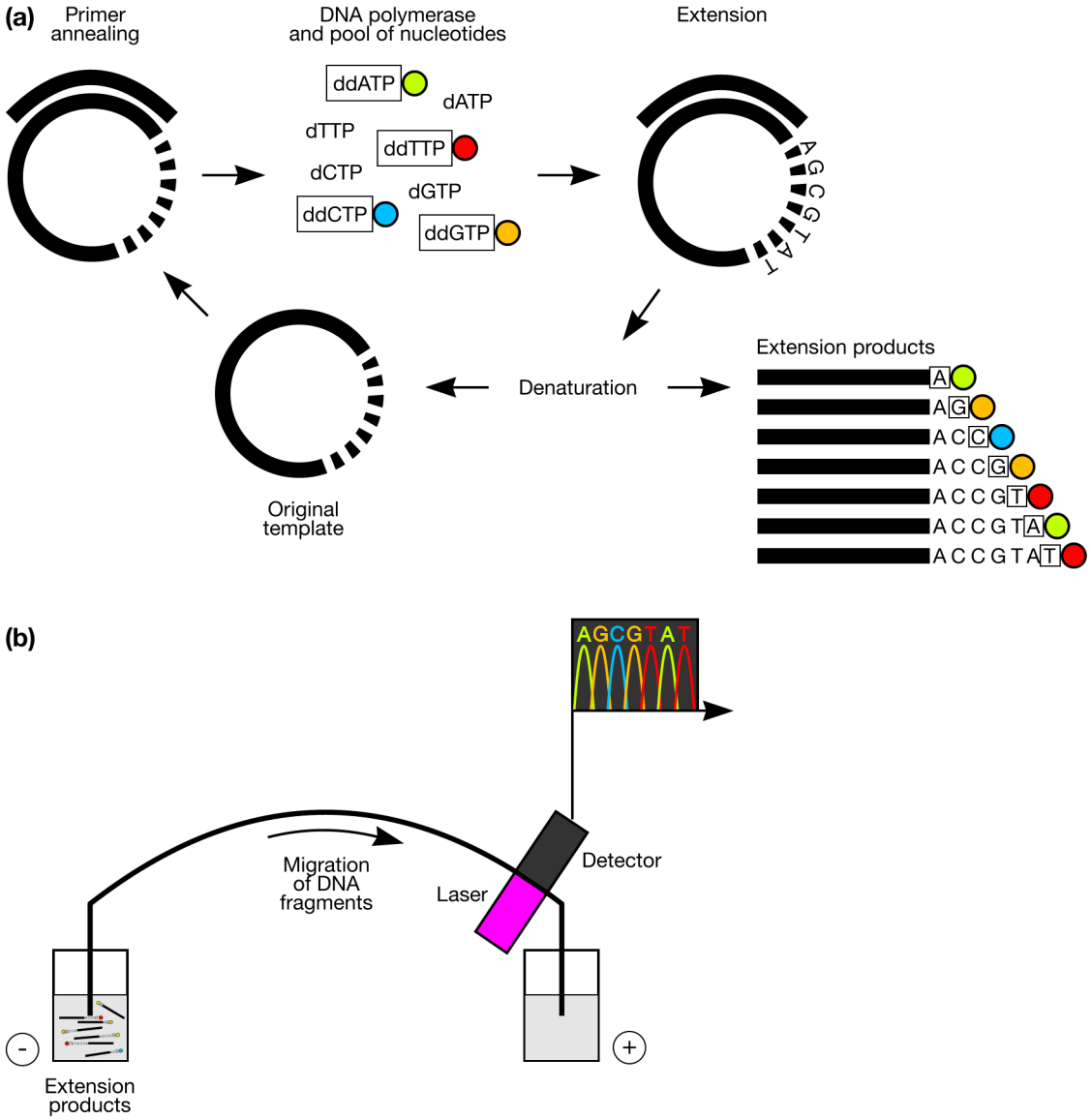

Fig 42 | Determination of nucleotide sequence of mutant *dhaA* genes. **(a)** Cycle sequencing by dideoxynucleotide termination method using differently fluorescently-labelled dideoxynucleotide terminators (BigDye, Terminator v. 3.1, Applied Biosystems, Foster city, CA, USA); **(b)** fractionating products of the sequencing reaction by capillary electrophoresis according to size, and detection of the fluorescent-dye-labelled DNA fragments by fluorescent detector yielding emission spectrum that provides the order of nucleotides in the nucleotide sequence. Redrawn according to Applied Biosystems (Foster city, CA, USA).

Determination of product inhibition for selected DhaA variants. Steady-state inhibition constants, K_i, for 2,3-dichloropropane-1-ol (DCL) were calculated using the program ORIGIN 6.1 (OriginLab, Northampton, MA, USA) for wild-type DhaA and mutants 21, 27, and 31 based on the initial rates of TCP conversion determied by the Iwasaki method at various DCL concentrations. The TCP substrate concentration was constant (1.4 mM), and the DCL inhibitor concentrations varied between 1.4 and 35.0 mM. The velocity of the reaction without the DCL inhibitor was measured as a negative control. Reactions were performed in duplicates. Halide concentrations were determined at

several times (10, 20, 30, and 40 min) in order to obtain at least three data points in the initial phase of conversion. Initial substrate and inhibitor concentrations were determined before reaction initiation by Trace GC 2000 equipped with a flame ionization detector (Thermo Finnigan, San Jose, CA, USA) and a DB-FFAP capillary column 30 m × 0.25 mm × 0.25 mm (J&W Scientific, Folsom, CA, USA).

Table 25 | Set of substrates for determination of substrate specificity.

Group	Compounds
1-Haloalkanes	1-Chloropropane
	1-Iodopropane
	1-Chlorobutane
	1-Bromobutane
	1-Iodobutane
	1-Chloropentane
	1-Chlorohexane
	1-Bromohexane
	1-Chlorodecane
	1-Iodohexane
2-Haloalkanes	2-Chloropropane
	2-Iodobutane
1,2-Haloalkanes	1,2-Dibromoethane
	1-Bromo-2-chloroethane
	1,2-Dibromopropane
	2-Bromo-1-chloropropane
α,ω-Haloalkanes	1,2-Dibromoethane
	1-Bromo-2-chloroethane
	1,3-Dichloropropane
	1,3-Dibromopropane
	1,3-Diiodopropane
	1-Bromo-3-chloropropane
	1,5-Dichloropentane
Multihalogenated alkanes	1,2-Dibromo-3-chloropropane
	1,2,3-Trichloropropane
	1,2,3-Tribromopropane
2-Substituted 1-Haloalkanes	1-Bromo-2-methylpropane
Cyclic haloalkanes	Chlorocyclopentane
	(Bromomethyl)cyclohexane
Haloalkenes	2,3-Dichloropropene
	3-Chloro-2-methylpropene
Halonitriles	4-Bromobutyronitrile
Haloethers	Bis(2-chloroethyl) ether

Determination of secondary structure fingerprint for selected DhaA variants. Secondary structure fingerprint of the purified wild-type DhaA, mutants 04, M2, M3, and six most active DhaA variants obtained by screening the saturation mutagenesis libraries *A* and *B* (mutants 17, 19, 21, 27, 31 and 33), and mutants 51 and 52, was determined by measuring far-UV CD spectra **(Fig 43)** using Jasco J-810 spectropolarimeter (Jasco, Tokyo, Japan). CD data were collected at 22°C, from 185 to 260 nm at 100 nm/min rate, 1 s response time and 2 nm bandwidth using a 0.1 cm quartz cuvette. The concentration of tested proteins was in the range of 0.26 to 0.30 mg mL^{-1}. For each DhaA variant, ten individual scans were averaged, corrected for absorbance caused by the buffer and expressed in terms of the mean residue ellipticity, θ_{MRE} in deg cm^2 $dmol^{-1}$, at wavelength λ **(Eq 11)**:

$$\Theta_{\mathrm{MRE}}(\lambda) = \frac{\Theta_{\lambda} M(N-1)}{10dc}$$

Eq 11 | Mean residue ellipticity.

where θ_{λ} is the observed ellipticity (degrees) at wavelength λ, M is the molecular mass of the protein (Da), N is the number of amino acid residue in the protein (299 in DhaAHis variants), d is the pathlength (cm) and c is the concentration (g mL^{-1}). Secondary structure content of wild-type DhaA and mutants 04, 14, 15, 21, 27, 31, 51 and 52 was calculated from the CD spectra using K2D and Self-Consistent methods **(Andrade et al., 1993; Sreerama & Woody, 1993)** implemented in the program DICROPROT **(Deléage et al., 1993)**.

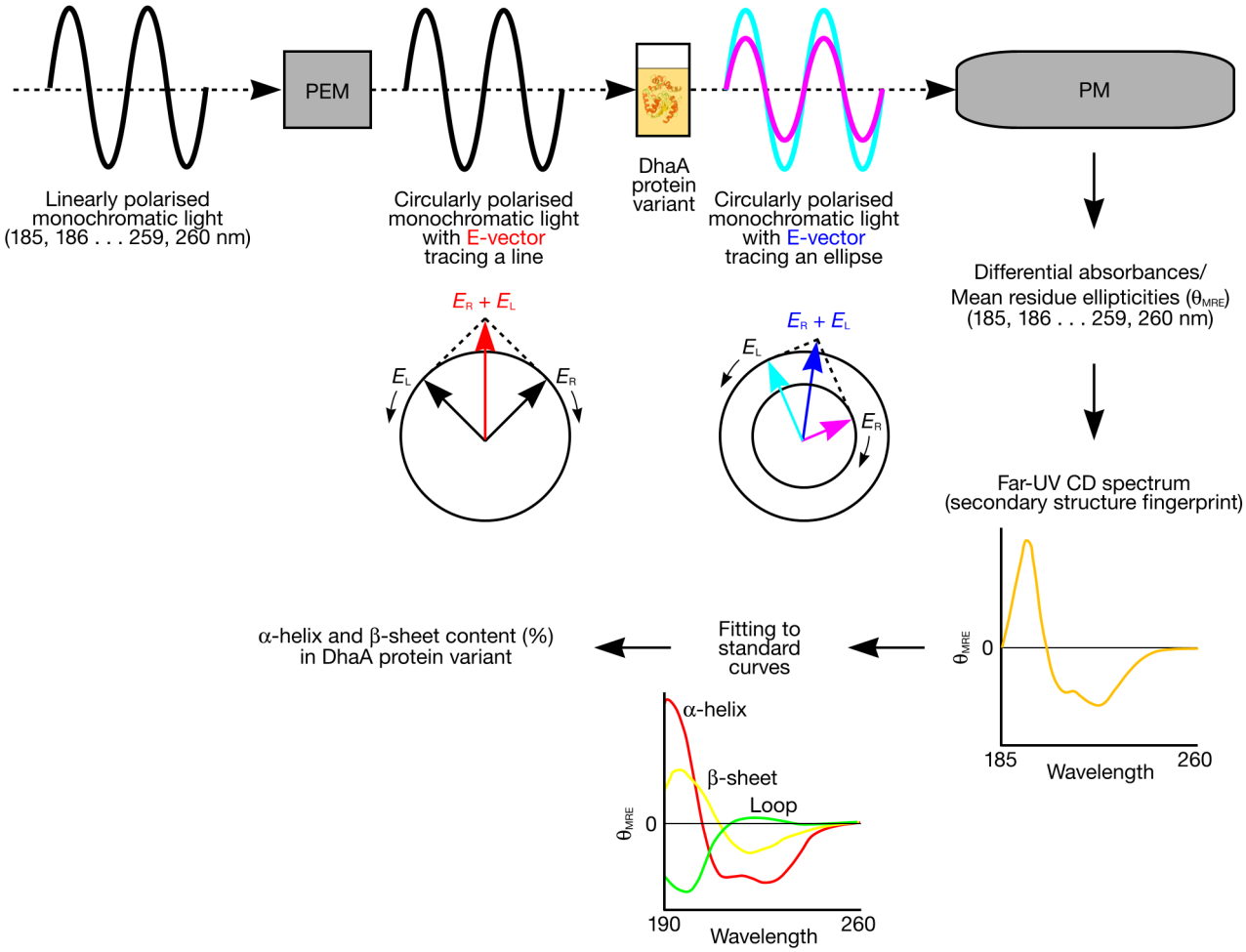

Fig 43 | Determination of secondary structure fingerprint of DhaA variants by CD spectroscopy. Circular dichroism is a phenomenon observed when optically active matter, e.g. protein, absorbs left (E_L) and right (E_R) circularly polarised light **(Supplementary files circularly_polarised_light_left.gif and circularly_polarised_light_right.gif)** slightly differently, causing the projection of the resulting amplitude to yield an ellipse instead of a line **(Kelly et al., 2005)**. Circularly polarised light is created from linearly polarised light **(Supplementary file linearly_polarised_light.gif)** by piezoelectric crystal modulator (PEM), and detected by photomultiplier (PM) after going through the protein sample. In proteins, the chromophores are peptide bonds **(Kelly et al., 2005)**. Amino acid residues in different conformational states, e.g. α-helix and β-sheet, show characteristic differential absorbance at various wavelength of far-UV region of light spectrum **(Kelly et al., 2005)**. Plotting differential absorbances or mean residue ellipticities against wavelengths in far-UV region provides far-UV CD spectrum characteristic for a given protein **(Kelly et al., 2005)**, here DhaA variant. Knowing mean residue ellipticity at 208 and 222 nm, and protein concentration, relative number of amino acid residues of the protein in α-helical and β-stranded conformations can be determined by fitting the far-UV CD spectrum to standard curves for pure α-helical and β-sheet conformations.

Determination of high-resolution structure of selected DhaA variants. High-resolution XC structure was determined for the purified DhaA variants 04 (PDB-ID 3FBW; **Supplementary file 3fbw.pdb**), 14 (PDB-ID 3G9X; **Supplementary file 3g9x.pdb**) and 15 (PDB-ID 3FWH; **Supplementary file 3fwh.pdb**) using XC structure of DhaA from *Rhodococcus* sp. (PDB-ID 1BN6) and XC structure of the mutant 15 as starting models for molecular replacement **(Fig 44 and Table 26; Stsiapanava et al., 2008)**.

Determination of rate-limiting step of selected DhaA variants. Rate-limiting step in reaction cycle of TCP dehalogenation by wild-type DhaA and the mutant 31 was determined by combinating two approaches: (i) solvent kinetic isotope effects determined by performing activity assays at 37 °C in glycine buffer (pH 8.6) containing TCP and increasing concentrations of ^2H_2O from 0 to 100%, and (ii) rapid quench-flow experiments performed at 37 °C in a glycine buffer (pH 8.6) using a QFM 400 rapid quench-flow instrument (BioLogic, Claix, France; **Fig 45**). In the latter technique, the reaction was started rapidly by mixing 70 µL enzyme and 70 µL substrate solutions, then quenched with 100 µL 0.8 M H_2SO_4 after time intervals ranging from 2 ms to 8 s. The quenched mixture was directly injected into 0.5 mL of ice-cold diethyl ether with 1,2-dichloroethane as an internal standard. After extraction, the diethyl

ether layer containing non-covalently bound TCP substrate and DCL alcohol product was collected, dried on a short column containing anhydrous Na_2SO_4 and analysed using Trace GC 2000 equipped with an MS detector (Thermo Finnigan, San Jose, CA, USA) and a DB-FFAP capillary column (J&W Scientific, Folsom, CA, USA). The amount of chloride anion (CL) product in the water phase was measured using an 861 Advanced Compact ion chromatograph equipped with a METROSEP A Supp 5 column (Metrohm, Herisau, Switzerland).

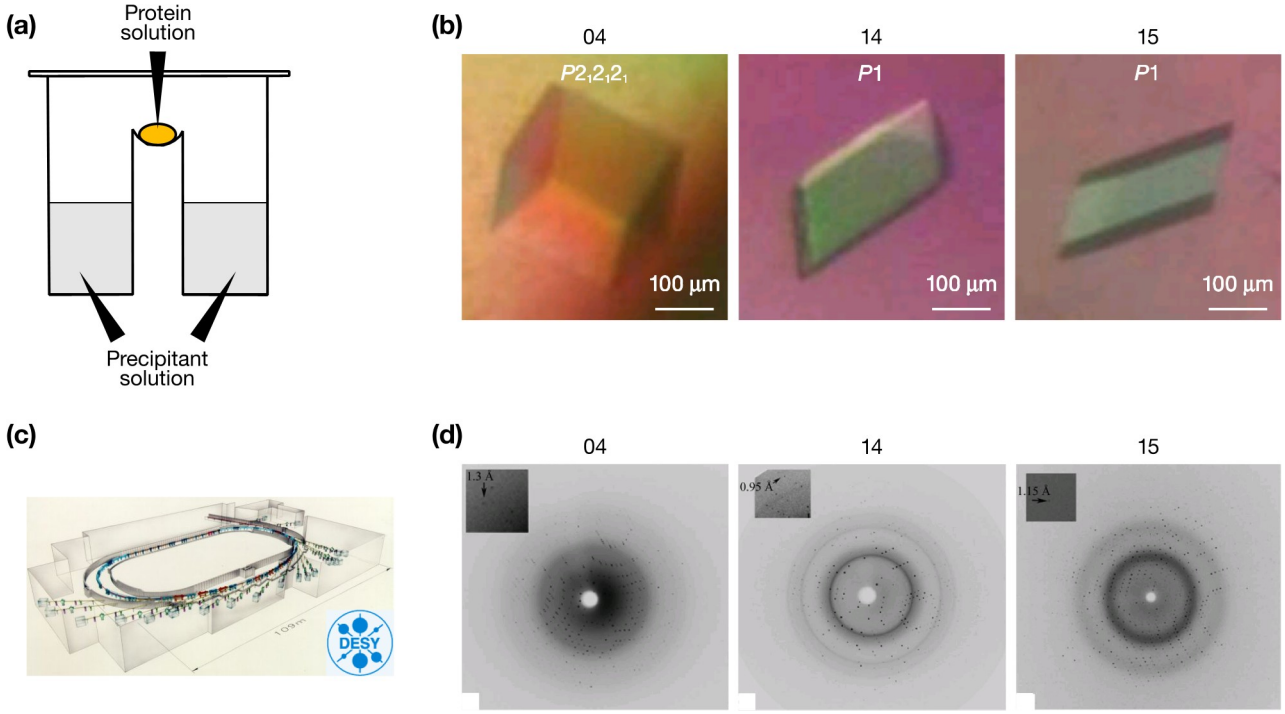

Fig 44 | Crystallisation and X-ray diffraction data collection for determination of XC structure for selected DhaA variants. **(a)** Crystallisation of DhaA mutants 04, 14, and 15 by sitting drop vapor diffusion method; **(b)** crystals of the mutant proteins; **(c)** DORIS storage ring facility (circumference of 289 m, bending radius of 12.2 m, energy of 4.45 GeV) of EMBL/DESY synchrotron used for diffraction data collection for the DhaA mutant proteins; **(d)** diffraction images of the DhaA mutant proteins. The crystals of the mutants 04, 14 and 15 diffracted to resolution of 1.30, 0.95 and 1.15 Å, respectively.

Table 26 | Summary of XC data and refinement. (pp. 99-102)

Parameters	**DhaA variant**		
	04	14	15
Crystallisation			
Conditions	0.08 M bicine 8% PEG 8000 0.08 M MgCl2 pH 9.0 Temperature 294 K	25% PEG 4000 8% 2-propanol 0.1 M sodium acetate pH 7.5 Temperature 277 K	25% PEG 4000 8% 2-propanol 0.1 M sodium acetate pH 7.5 Temperature 277 K
Technique	Sitting drop vapor diffusion[b]	Sitting drop vapor diffusion	Sitting drop vapor diffusion
Space group[b, c]	$P2_12_12_1$	$P1$	$P1$
Diffraction data collection			
Synchrotron[d]	Yes	Yes	Yes
Radiation source	EMBL/DESY, Hamburg	EMBL/DESY, Hamburg	EMBL/DESY, Hamburg
Beamline	X11	X11	X11
Wavelength (Å)[e]	0.82	0.82	1.15
Detector	CCD	CCD	Image plate
Temperature (K)	100	100	100
pH	9.0	7.5	7.5
Number of crystals used	1	1	1
Number of unique reflections[f, g]	88,814	163,495	77,114
Resolution[h] range high (Å)[i]	1.23	0.95	1.20
Resolution range low (Å)[j]	100		20.00

Parameters	DhaA variant		
	04	14	15
Completeness (%)[k]	100.0	94.2	90.7
Data redundancy[l]	7.400	5.8	3.4
R_{merge}[m]	0.05600	0.05900	0.05000
In the highest resolution shell			
Resolution range high (Å)	1.23	0.95	1.20
Resolution range low (Å)	1.25	0.97	1.24
Completeness (%)	99.9	90.6	45.0
Data redundancy	5.70	4.00	2.1
R_{merge}	0.581	0.418	0.179
Model building			
Method	Molecular replacement[n]	Molecular replacement	Molecular replacement
Software	MOLREP	MOLREP	MOLREP
Starting model (PDB-ID)	1BN6	3FWH	1BN6
Refinement			
Program	SHELXL-97	REFMAC 5.2.0019	REFMAC 5.2.0019
Data used in refinement			
Resolution range high (Å)	1.23	0.95	1.22
Resolution range low (Å)	100.00	19.86	20.00
Completeness (%)	99.9	94.17	94.4
Number of reflections	88,731	162,574	77,113
Fit to data used in refinement			
Cross-validation method	Free R	Throughout	Throughout
R-factor (working + test set)[o]	0.137	0.114	0.162
R-factor (working set)[o]	0.137	0.113	0.161
R_{free}[p]	0.167	0.125	0.186
Number of non-hydrogen atoms used in refinement			
Protein atoms	2,692	2,679	2,656
Heterogen atoms	17	8	5
Solvent atoms	454	756	645
RMS deviations from restraint target values			
Bond lengths (Å)[q]	0.011	0.012	0.013
Bond angles (degrees)	*NR*	1.498	1.467
Final model			
PDB-ID	3FBW	3G9X	3FWH
Resolution (Å)	1.23	0.95	1.22
Missing amino acid residues	Met1	Met1	Met1
	Ser2	His298	His298
	His296	His299	His299
	His297		
	His298		
	His299		
Missing atoms	His295-C_α	–	Ser2-O_γ
	His295-C		
	His295-O		
	His295-C_β		
	His295-C_γ		
	His295-$N_{\delta1}$		
	His295-$C_{\delta2}$		
	His295-$C_{\varepsilon1}$		
	His295-$N_{\varepsilon2}$		
Torsion angles outside the expected Ramachandran regions[r]	Pro29	–	Pro42
	Pro42		Thr43
	Thr43		Glu98
	Glu98		Asp106
	Asp106		Asp153
	Asp156		Asp156
	Val245		Val245
	Leu271		Leu271
	His294		

Parameters	DhaA variant		
	04	14	15
Cis-conformation of peptide bond	Asn41-Pro42 Glu214-Pro215 Thr242-Pro243	Asn41-Pro42 Glu214-Pro215 Thr242-Pro243	Asn41-Pro42 Glu214-Pro215 Thr242-Pro243
Number of discretely disordered amino acid residues	61	41	35
Mean *B*-factor (Å^2)[s]	11.57	8.76	13.46
Ligands	Benzoic acid Chloride anion (6 ×) Magnesium cation (2 ×)	2-Propanol Acetate anion Chloride anion	2-Propanol Acetate anion Chloride anion
Solvent[t]	Water (454 ×)	Water (651 ×)	Water (614 ×)

[a]Sitting drop vapor diffusion – a methods for creating supersaturation and promoting a solubility minimum **(McPherson, 2004)**.

[b]Protein crystal – a solid composed of repeated structural motifs (protein molecules) in a three-dimensional lattice **(Acharya & Lloyd, 2005)**.

[c]Space group – symmetrical arrangement of molecules in the crystal lattice where one or more protein molecules are related to others by mathematical transformations **(Acharya & Lloyd, 2005)**; the space group symmetry dictates amount of data required to solve the XC structure **(Acharya & Lloyd, 2005)**.

[d]Synchrotron – an intense X-ray source used for high-resolution data collection **(Acharya & Lloyd, 2005)**.

[e]Wavelength – wavelength of the X-ray radiation; about atomic bond length **(Acharya & Lloyd, 2005)**.

[f]Reflection (diffraction spot) – a result of the scattering of X-rays by the electrons of atoms in the crystal lattice; a series of reflections creates a diffraction pattern; rotation of the crystal through a defined angle (determined by its symmetry) is needed for obtaining diffraction spots for all the ordered atoms in the molecule **(Acharya & Lloyd, 2005)**; each reflection has three properties – wavelength of the difracted beam, amplitude (obtained from measured intensities) and phase **(Wlodawer et al., 2008)**; the intensity of each individual reflection depends on the positions of all atoms in the unit cell, therefore it is not possible to solve only a selected, small part of the crystal structure without modelling the rest of it **(Wlodawer et al., 2008)**.

[g]Number of unique reflections – minimum number of unique reflections per atom (including all hydrogen atoms and water molecules) = 4 **(Acharya & Lloyd, 2005)**.

[h]Resolution of diffraction data – minimum spacing of crystal lattice planes that still provides measurable diffraction of X-rays which defines minimum distance between structural features that can be distinguished in the electron density maps; among four customary categories distinguised today, low > 2.7 Å, medium ~ 2.7 Å, high ~ 1.5 Å, and atomic < 1.2 Å, **(Wlodawer et al., 2008)**, the resolution of the diffraction data for the DhaA variant is high/atomic.

[i]Resolution range high – high resolution is needed for obtaining accurate atomic positions in XC structure **(Acharya & Lloyd, 2005)**.

[j]Resolution range low – no data cut-off is applied when refining a protein structure; all observed reflections at low resolution are used otherwise *B*-factors would become underestimated **(Acharya & Lloyd, 2005)**.

[k]Completeness – the number of observed reflections divided by theoretical maximum; completeness approaches 100% in good-quality structures **(Acharya & Lloyd, 2005)**; if some reflections are not measured at all then data are not 100% complete; the lack of completeness negatively influences the quality and interpretability of the electron density maps computed from such data because each value of the electron density map can be correctly calculated only with the contribution of all reflections **(Wlodawer et al., 2008)**.

[l]Data redundancy – the average number of times each unique reflection is recorded **(Acharya & Lloyd, 2005)**; the higher the redundancy the more accurate the final estimation of the averaged reflection intensity which is important for good-quality model **(Wlodawer et al., 2008)**.

[m]R_{merge} – diffraction data reliability factor for judging spread of individual intensities of all symmetry-equivalent reflections, contributing to the same unique reflection; important because every reflection is measured with a certain degree of error **(Wlodawer et al., 2008)**; a good set of diffraction data is characterised by R_{merge} < 4-5%; at the highest resolution shell, R_{merge} can be allowed to reach values up to 30-40% for low symmetry crystals and up to 60% for high symmetry crystals, since in the latter case the redundancy is usually higher **(Wlodawer et al., 2008)**.

[n]Molecular replacement (MR) – a method for solving phase problem for structure determination by using a suitable existing macromolecular model **(Pusey et al., 2005; Chruszcz et al., 2008; Manjasetty et al., 2008)**.

[o]*R*-factor – global reliability factor for judging the agreement (discrepancy) between the observed reflection amplitudes, F_{obs}, and those calculated from the model, F_{calc} **(Wlodawer et al., 2008)**; *R*-factor combines the error inherent in the experimental data and the deviation of the model from reality; with increasingly better diffraction data (characterised by $R_{merge} \leq 4\%$ or less) crystallographic *R*-factor is an effective measure of model errors; *R*-factor for well-refined protein structures is expected < 20%; when *R*-factor approaches 30%, structure should be regarded with a high degree of reservation because at least some parts of the model may be incorrect; the best refined macromolecular structures have *R*-factors < 10% **(Wlodawer et al., 2008)**; inclusion of low-resolution data is essential for reliability of *R*-factor **(Acharya & Lloyd, 2005)**.

[p]R_{free} – reliability factor calculated analogously to *R* factor, but for only ~ 1000 randomly selected reflections which have never entered into model refinement, although they might have influenced model definition; if the mathematical model of the structure becomes unreasonably complex, i.e. when it includes parameters for which there is no justification in the experimental data, then R_{free} will not improve even though the *R* factor may decrease, which is an indication of over-interpretation of the data; R_{free} should

not exceed *R* factor by more than ~ 7% **(Wlodawer et al., 2008)**.
[q]RMS for bond lengths – an indicator of how much the model departs from typical or common-sense-representing bond lengths based on previous experience; good-quality medium/high resolution structures are expected RMS for bond length ~ 0.02 Å **(Wlodawer et al., 2008)**.
[r]Expected regions of Ramachandran plot – three broad regions (E, αL, αR) of φ and ψ dihedral angles sterically allowed for the L-amino acids in Ramachandran plot **(Ramachandran et al., 1963; Acharya & Lloyd, 2005)**; mapping pairs of φ amd ψ dihedral angles has strong validation power because their values are usually not restrained in the refinement, unlike bond lengths and bond angles **(Brown & Ramaswamy, 2007; Wlodawer et al., 2008)**.
[s]*B*-factor – thermal vibration factor, a measure of thermal mobility of any particular atom in the crystal structure model; there are two types of *B*-factors – isotropic (equal in all directions) and anisotropic (not equal in all directions); anisotropic refinement is possible only for atomic resolution structures **(Acharya & Lloyd, 2005)**.
[t]Solvent (ordered water molecules) – number increases with increasing resolution **(Acharya & Lloyd, 2005)**; rough estimate of the expected ratio of the number of water molecules per amino acid residue can be obtained by substracting resolution (in Å) from 3 **(Wlodawer et al., 2008)**.

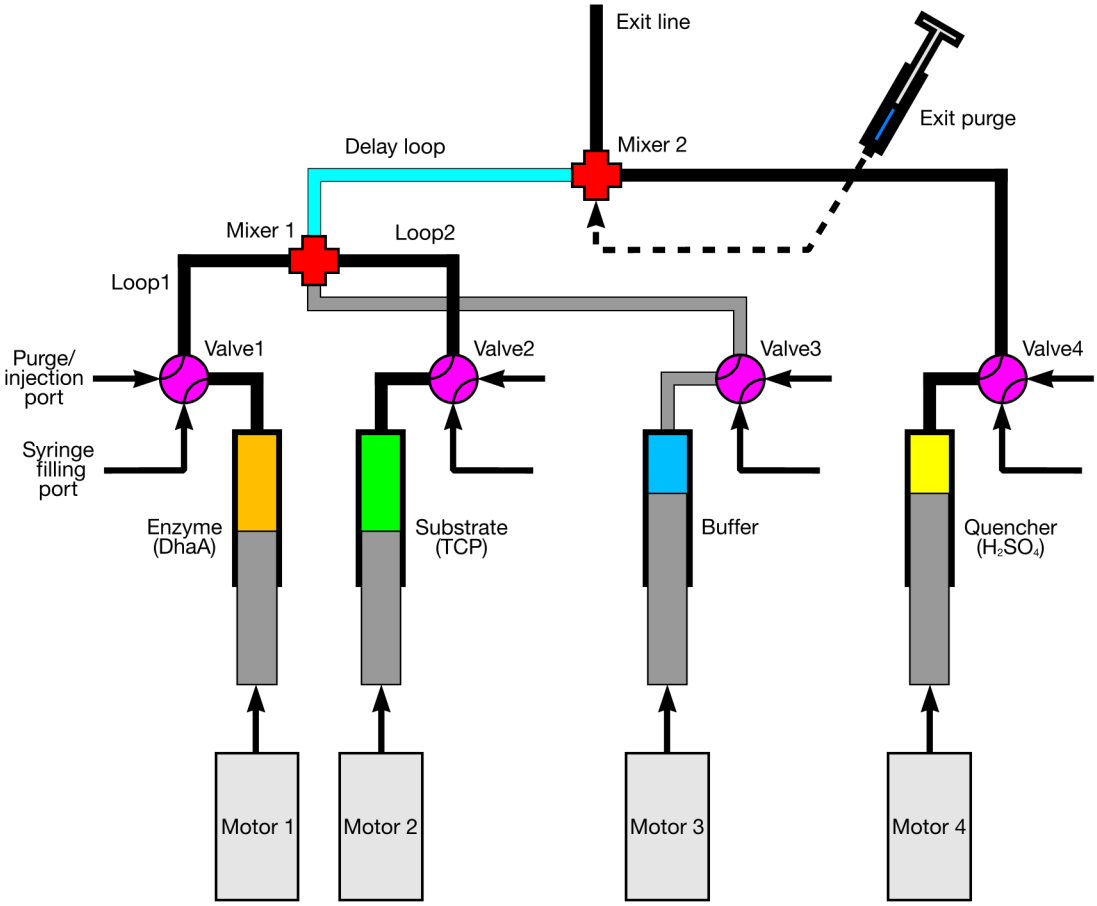

Fig 45 | Rapid quench flow experiment for determination of pre-steady state kinetics of dehalogenation of TCP by DhaA variants. Each syringe is driven by an independent stepping motor. Solutions are loaded into the instrument using four position valves. Reaction was initiated upon mixing DhaA wild-type or 31 mutant with TCP in the mixer 1. The reaction mixture moved via delay loop into mixer 2 where the reaction was stopped by quencher, and the aged solution was flushed through an exit line to a collect device. The quenched sample was subsequently analysed for concentration of TCP substrate, and DCL and CL products. Redrawn according to BioLogic (Claix, France).

3.2 Molecular Modelling

Preparation of protein structures. The XC structure of DhaA from *Rhodococcus* sp. (PDB-ID 1CQW) was truncated by five amino acid residues at the C-terminus, renumbered according to *dhaA* gene **(Supplementary file genbank_AF060871)** and modified with three amino acid residue substitutions, Val172Ala, Ile209Leu, and

Ala292Gly, using PYMOL 0.97 or 0.99 **(DeLano, 2002)** to reconstruct the structure of DhaA from *Rhodococcus rhodochrous* NCIMB 13064 (wild-type DhaA) used in experiments. The wild-type structure of DhaA served as the template for amino acid residue substitutions using PYMOL, yielding structures of mutant proteins 04, 14, 15, 21', 27', 31', 51', and 52'. The most frequently occurring rotamer that had little or no steric overlap with the neighbouring protein atoms was selected from backbone-dependent rotamer library **(Dunbrack & Cohen, 1997)** for each substitution **(Fig 46)**. The in silico mutants correspond to the mutants obtained by site-directed and saturation mutagenesis by the identifiers, except for absence of Tyr273Phe in the in silico mutants marked with the prime symbol.

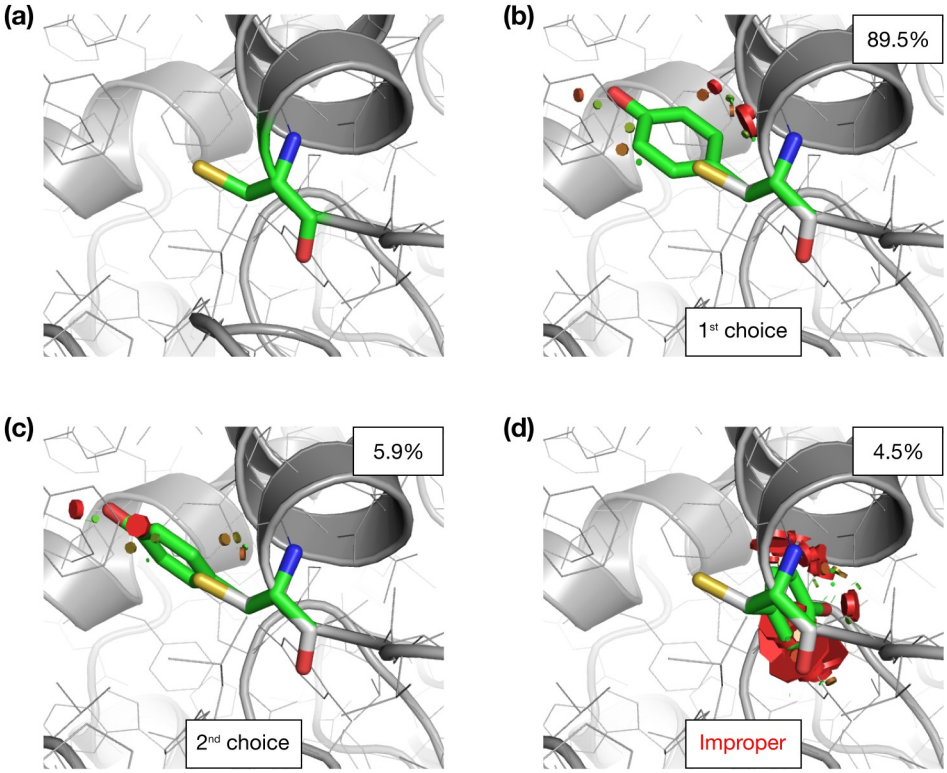

Fig 46 | In silico mutagenesis of DhaA using PYMOL mutagenesis wizard; procedure is demonstrated on Cys176Tyr substitution. **(a)** wild-type Cys176; **(b)** Cys176Tyr rotamer *1*; **(c)** Cys176Tyr rotamer *2*; **(d)** Cys176Tyr rotamer *3*. The backbone-dependent rotamers are ordered according to their frequencies of occurrence in experimental protein structures stored in PDB, the value is given at the top-right corner of each rotamer. The visible disks and their colours indicate pairwise overlap of atomic van der Waals radii. Small green disks are shown when atoms are almost in contact or slightly overlapping; large red disks indicate signficant van der Waals overlap; everything else lies between those extremes. The rotamer *1* shows high preference in proteins over the rotamer *2* and *3*; rotamer *2* shows the least steric clashes. Thus, both rotamer *2* and *3* could be used. The rotamer *1* was applied in the expectation that the steric overlaps will be removed in subsequent MD simulations. The rotamer *2* was kept as second choice in case the structure with the rotamer *1* will be unstable in MD simulations. The rotamer *3* was discarded because it shows too large van der Waals overlaps with neighbouring atoms.

Preparation of ligand structures. The three-dimensional models of (*R*)-2,3-dichloropropane-1-ol (R-DCL), (*S*)-2,3-dichloropropane-1-ol (S-DCL) and TCP **(Fig 47)** were built using PYMOL 0.97, and geometry optimised by the Austin Model 1 (AM1) method **(Dewar et al., 1985)** of MOPAC 2000 **(Stewart, 1990)** using the following keywords: SCFCRT = 1D-12, EF, POINTS = 12, LET, and PRECISE. The optimised structures were refined by energy minimisation using GAUSSIAN 94 **(Frisch et al., 1994)** employing the Hartree-Fock method **(Leach, 1996; Jensen, 2006)** and 6-31G* basis set **(Leach, 1996; Jensen, 2006)** for compatibility with AMBER force field **(Cornell et al., 1995; Cornell et al., 1996)**. Partial atomic charges were fitted to reproduce the electrostatic potential calculated with GAUSSIAN using the Restrained Electrostatic Potential fit, RESP **(Bayly et al., 1993; Cornell et al., 1993)**, module of AMBER 8 **(Case et al., 2004)**.

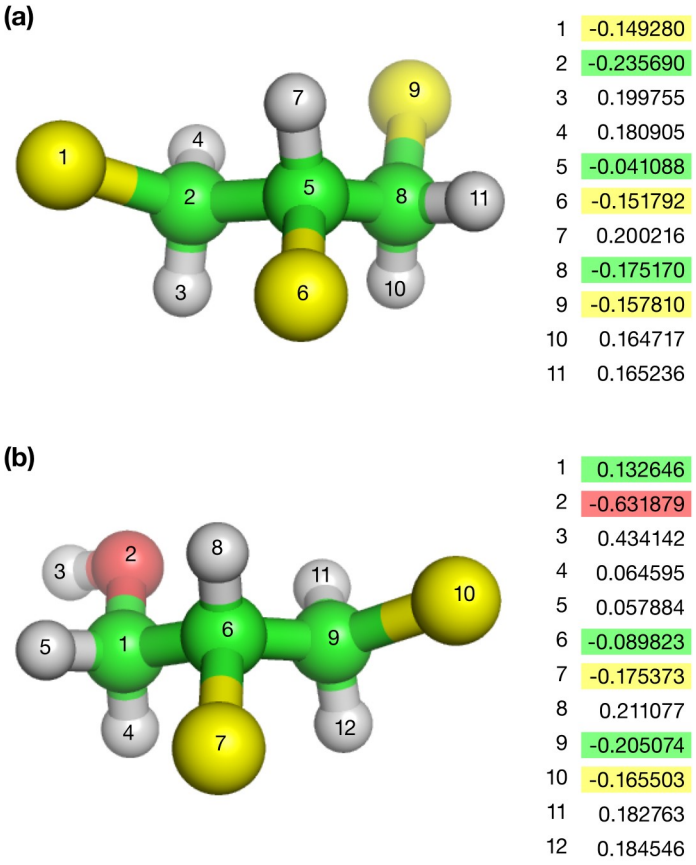

Fig 47 | Structures of ligands. **(a)** TCP; **(b)** *R*-DCL. All atoms were assigned to unique RESP partial charges (given in e, $+1.60219 \times 10^{-19}$ C). Atoms are coloured by type: carbon, green; oxygen, red; chlorine, yellow; hydrogen, white.

Modelling of enzyme-substrate and enzyme-product complexes. The initial orientation of the TCP substrate in the active site of wild-type DhaA and the initial orientation of the R- and S-DCL product in the active site of DhaA wild-type complexed with CL were modelled using AUTODOCK 3.0.5 **(Morris et al., 1998)**. Rotatable bonds were assigned to DCL and TCP using the Autotors module of AUTODOCK. All crystallographic water molecules were removed, the main tunnel iodide was removed, and the active-site iodide anion was replaced by a CL for docking of DCL, or removed, for docking of TCP. Polar hydrogens were added to wild-type DhaA using WHATIF 5 **(Vriend, 1990)**, and partial charges and solvation parameters by the *q.kollua* and *addsol* scripts of AUTODOCK, respectively. The atomic interaction maps for all atom types of DCL and TCP, using carbon, oxygen, chlorine, and hydrogen atoms as the probes, as well as electrostatic potential map using a point charge of $+1e$, $+1.60219 \times 10^{-19}$ C , as the probe, were pre-calculated for the wild-type DhaA using Autogrid module of AUTODOCK. A grid box of $81 \times 81 \times 81$ points in x, y, and z dimensions was used with a grid spacing of 0.25 Å. The grid was centred on the C_γ atom of His272 to ensure that the entire active site, the open main tunnel, and the closed slot tunnel were encompassed by the box **(Fig 48)**. The van der Waals interactions and hydrogen bonds were modelled using the 12-6 **(Eq 12 and Fig 49)** and 12-10 Lennard-Jones potential **(Eq 13)**, respectively:

$$V_{12\text{-}6}(r) = 4\varepsilon_{ij}\left[\left(\frac{\sigma}{r}\right)^{12} - \left(\frac{\sigma}{r}\right)^{6}\right]$$

Eq 12 | The Lennard-Jones 12-6 potential.

$$V_{12\text{-}10}(r) = 4\varepsilon_{ij}\left[\left(\frac{\sigma}{r}\right)^{12} - \left(\frac{\sigma}{r}\right)^{10}\right]$$

Eq 13 | The Lennard-Jones 12-10 potential.

where: r is the distance; ε_{ij} is the well-depth for two atoms, i and j; and σ = the collision diameter = the seperation of the two atoms for which the energy is zero = $r_{eqm,ij}/2^{1/6}$, where $r_{eqm,ij}$ is the equilibrium distance between the two atomic nuclei. The region of maximum affinity at ε was widened using the smoothing parameter of 0.5. Electrostatic interactions were modelled based on Coulomb's law **(Eq 14)** with no distance cutoff:

$$V_{ij}(r_{ij}) = \frac{q_i q_j}{4\pi\varepsilon_r\varepsilon_0 r_{ij}}$$

Eq 14 | Coulomb's law.

where: q_i and q_j are the partial charges of the atoms i and j; ε_0 is the permitivity of free space; ε_r is the relative dielectric coefficient of the medium between the charges; r_{ij} is the distance seperating the centres of the atoms. A sigmoidal distance-dependent dielectric function was used to model solvent screening **(Mehler & Solmajer, 1991) (Eq 15)**:

$$\varepsilon_r(r) = A + \frac{B}{1 + ke^{-\lambda Br}}$$

Eq 15 | Dielectric function.

where: r is the distance; A = -8.5525; $B = \varepsilon_0 - A$; ε_0 = the dielectric constant of bulk water at 25°C = 78.4; λ = 0.003627 and k = 7.7839 parameters **(Morris et al., 1998)**. Using the pre-calculated maps, fifty independent docking calculations were performed for R- and S-DCL, and TCP using the Autodock module of AUTODOCK, employing a Lamarckian genetic algorithm (LGA) consisted of global search using genetic algorithm (GA) and local search using pseudo-Solis&Wets algorithm, pSW **(Fig 50)**, and using the same setting as in the case docking study by Morris et al. **(1998)** and docking to haloalkane dehalogenase DhlA **(Kmuníček et al., 2003)** and LinB **(Kmuníček et al., 2005)**. The GA was used with an initial population of 50 random individuals; an ellitism value of 1, which was the number of top individuals that automatically survived into the next generation; mutation rate of 0.02, which was the probability that a gene would undergo a random change; and a cross-over rate of 0.8, which was the probability that two individuals would undergo cross-over. The pSW was used with a maximum of 300 iterations per local search; the probability of performing local search on an individual in the population was 0.06. The energetics of a particular ligand configuration was found by tri-linear interpolation of affinity values of the eight grid points surrounding each of the atoms in the substrate. The electrostatic interaction was evaluated similarly, by interpolating the values of the electrostatic potential and multiplying by the charge on the atom. Docked energy was expressed as a sum of intermolecular interaction energy between DhaA and DCL or TCP, and internal interaction energy of DCL or TCP. A maximum of 1,500,000 energy evaluations were performed. The resulting 50 conformations were clustered with a tolerance of 0.5 Å. The lowest-energy representatives of the highest-populated clusters of R- and S-DCL, and TCP in the wild-type DhaA were selected as starting conformations for subsequent MD simulations. The conformations of R- and S-DCL obtained for the wild-type DhaA were applied to mutants for subsequent MD simulations.

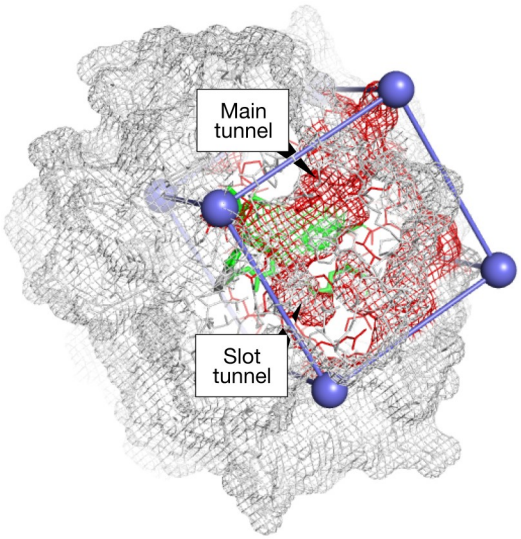

Fig 48 | Search space in the wild-type DhaA for docking of DCL and TCP using AUTODOCK. Dimensions of the searching grid box are highlighted in blue. Atoms of the protein (lines and mesh representation) that fall inside the box are coloured in red. Catalytic pentad of the active site is coloured in green. Both the main tunnel and the closed slot tunnel are encompassed by the box.

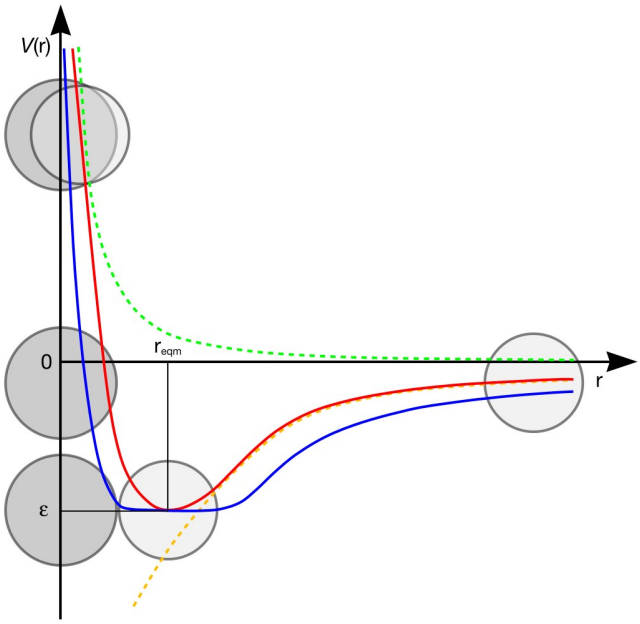

Fig 49 | van der Waals potential energy approximated by the 12-6 Lennard-Jones potential. The van der Waals interaction (–) between two atoms (balls) has two contributions: repulsive (--) and attractive (--). The repulsive contribution is due to exchange (often referred to as "overlap") forces and varies as $1/r^{12}$. The attractive contribution is due to dispersive forces and varies as $1/r^{6}$ (see **Eq 12**). The lowest value of the 12-6 Lennard-Jones potential for the pair of interacting atoms is reached at the distance r_{eqm}., which is the sum of the so-called van der Waals radii of the two atoms. At shorter distances, the two atoms overlap and the 12-6 Lennard-Jones potential increases. At longer distances, the interaction between the two atoms decreases. In AUTODOCK, the smoothed 12-6 Lennard-Jones potential (–) is used to widen the range of well depth, ε, with the lowest van der Waals potential.

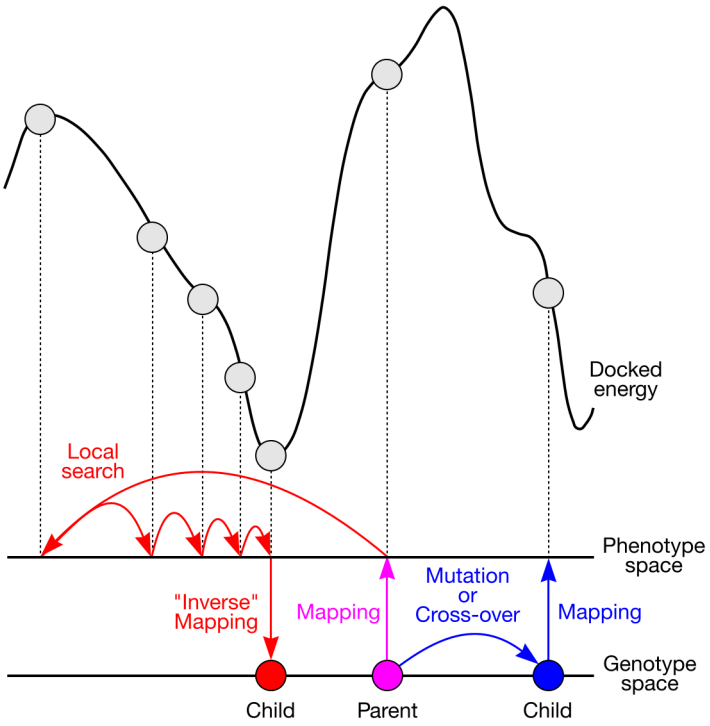

Fig 50 | Lamarckian genetic algorithm (LGA) search stage in docking using AUTODOCK. The LGA is an allusion to Jean Baptiste Lamarck's (discredited) assertion that phenotypic characteristics acquired during an individual's lifetime can become heritable traits **(Lamarck, 1809)**. The particular arrangement of a ligand and a protein is defined by a set of values (genes): x, y and z Cartesian coordinates for the ligand translation; four variables defining a quaternion (consisting of a random unit vector and a random rotation angle between -180° and +180° and specifying the ligand orientation; and one real-value for each ligand torsion, in that order. The ligand's state corresponds to the genotype, whereas its atomic coordinates correspond to the phenotype. A generation consists of five stages: mapping of the genotype into phenotype, fitness evaluation (the sum of protein-ligand intermolecular interaction energy and intramolecular interaction energy of the ligand), proportional selection of individuals that will reproduce, two-point cross-over between genes, mutation by adding random real number to the genes, and elitist selection defining how many of the top individuals automatically survive into the next generation, in that order. Each generation is followed by local search for a proportion of the population. The local search is performed by continuously converting from the genotype to the phenotype; sufficient iterations of the local search arrive at a local minimum and the genotype of the parent is replaced by the resulting genotype, in accordance with Lamarckian principles. Redrawn according to Morris et al. **(1998)**.

Classical MD simulations of enzyme-substrate and enzyme-product complexes. Classical MD simulations were performed for wild-type DhaA and mutant 31' complexed with TCP, and for all DhaA variants with R- and S-DCL and with/without CL in AMBER 8 using the 1994 Cornell force field, ff94 **(Fig 51 and Supplementary file parm94.dat; Cornell et al., 1995; Cornell et al., 1996)**. Carbon, oxygen, oxygen-bound hydrogen and carbon-bound hydrogen atoms were approximated by the CT, OH, HO and H1 atom types, respectively, of the ff94. Missing parameters for bond lengths, bond angles and dihedral angles involving chlorine atoms (the CL atom type of the ff94) were obtained from Kmuníček et al. **(2001)**; CL (chloride anion) was approximated by the IM atom type **(Smith & Dang, 1994)** of the ff94 and was assigned a charge of $-1e$ **(Supplementary file parm94_kmunicek_etal_2001.dat)**. All crystallographic water molecules not overlapping with the docked TCP and DCL, respectively, were added to the

complexes. One additional water molecule was added with oxygen centred at the position of CL for MD simulations without CL. Non-polar hydrogens were added to the protein using the Leap module of AMBER 8. Seventeen sodium cations were added with Leap to ensure a neutral net charge of the system. Finally, the complexes were immersed in a rectangular box of TIP3P **(Jorgensen et al., 1983)** water molecules with a minimum wall thickness of 10 Å using Leap and subjected to an equilibration protocol using the Sander module of AMBER 8 **(Fig 53)**. The equilibrations consisted of the following steps: (i) 300 steps of steepest descent energy minimisation of all non-crystallographic atoms, i.e. all hydrogens on protein, water, and the ligand (DCL or TCP) atoms; (ii) 20 ps periodic boundary condition MD **(Fig 52)** of water, sodium cations, and the ligand at constant temperature of 300 K using the weak coupling algorithm **(Berendsen et al., 1984)** and constant pressure of 1 atm with isotropic position scaling, with the rest of the system harmonically restrained with a 500 kcal mol^{-1} $Å^{-2}$ force constant; (iii) four consecutive steepest descent energy minimisations of 300 steps each with a decreasing restraint on the protein backbone with a force constant of 500, 125, 5, and 0 kcal mol^{-1} $Å^{-2}$, respectively; (iv) unrestrained MD using the same parameters as those for the 20 ps of MD but raising the temperature from 0 to 300 K during the initial 200 ps **(Table 27)**. The trajectories were propagated for 2.0 to 2.8 ns to ensure acquisition of well-equilibrated and stable systems. A time step of 2 fs was used with application of SHAKE algorithm **(Ryckaert et al., 1977)** to bonds involving hydrogens and a particle mesh Ewald treatment of Coulombic interactions. The cutoff distance for the nonbonded interactions was 10 Å. MD snapshots were gathered every 0.5 ps. The equilibration MD simulations of the enzyme-substrate complexes were followed by 2 ns of production classical MD simulations at 300 K using the same parameters as for the equilibration MD simulations; the equilibration MD simulations of the enzyme-product complexes were followed by production RAMD simulations.

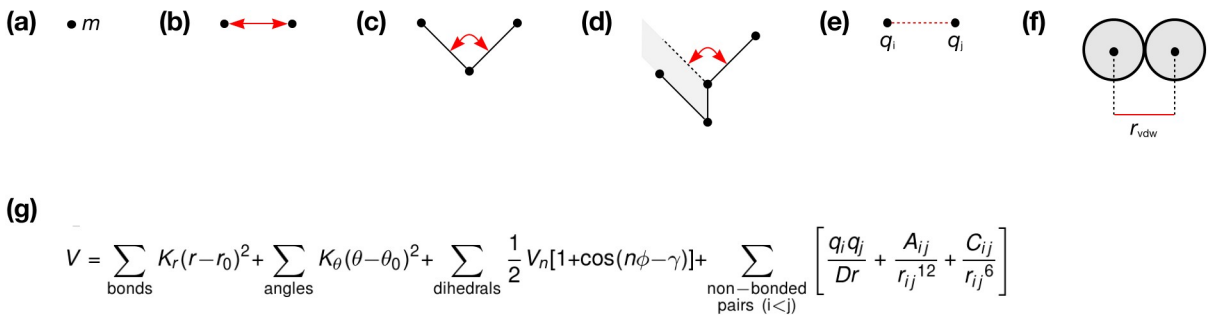

Fig 51 | The 1994 Cornell force field. **(a)** Atoms are defined by atomic mass (m) placed at atomic centres (black point); bonding atoms are further distinguished into atom types according to bonding partners. **(b)** Bonds between atoms are defined by equilibrium length, r_0, and by harmonic force constant, K_r (in kcal mol^{-1} A^{-2}). **(c)** Angles between bonded atoms are defined by equilibrium angle, θ_0, and by harmonic force constant, K_θ (in kcal mol^{-1} rad^{-2}). **(d)** Dihedral angles are defined by torsional barrier height, V_n, periodicity of the torsional barrier, n, and by phase shift, γ. **(e)** Electrostatic interactions between partial atomic charges, q_i and q_j, are treated according to Coulomb's law; the point partial atomic charges are placed at atomic centres; the charges are fitted to the atoms using the RESP method **(Bayly et al., 1993; Cornell et al., 1993; Cieplak et al., 1995)** to reproduce the electrostatic potential calculated using the Hartree-Fock method with 6-31G* basis set for molecular fragments, dipeptides. **(f)** van der Waals interactions are described by the 12-6 Lennard-Jones potential defined by atomic van der Waals radii, r_{vdw}, and potential well depth, ε **(see Fig 49)**. **(g)** The core of the 1994 force field is then an aditive potential energy function that sums all the energy contributions $b + c + d + e + f$, and thus describes the relationship between molecular structural model and energy; r, θ and Φ is the actual bond length, bond angle and dihedral angle, respectively; $D = 4\pi\varepsilon_r\varepsilon_0$; $A_{ij} = \varepsilon r_{vdw}^{12}$; $C_{ij} = \varepsilon r_{vdw}^{6}$.

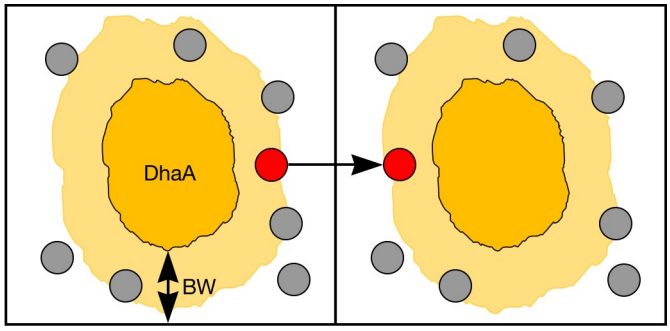

Fig 52 | Periodic boundary condition (PBC). PBC was applied in the MD simulations to model virtually infinite bulk solvent. The consequence of using PBC was that when any part of the system, e.g. a water molecule (red ball) in bulk solvent (dark grey balls) escapes from the box at one side, then it enters the box (its exact image) on the other side with same velocity. Thickness of the box wall (BW) was set to 10 Å in order that it is sufficiently larger than reach of non-bonded interactions (light orange), to avoid artificial interactions of amino acid residues located at opposite sides of the DhaA protein molecule (dark orange) in neighbouring images.

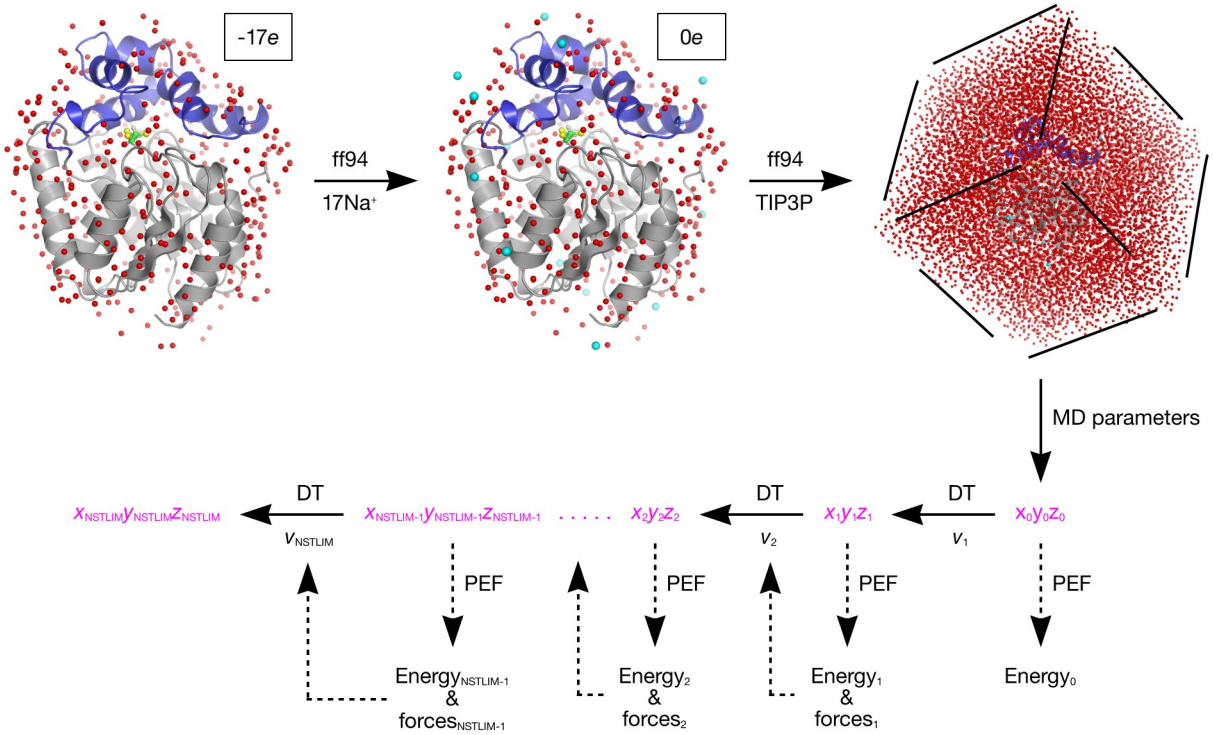

Fig 53 | Overview of a classical MD simulation of enzyme-substrate and enzyme-product complexes of the reaction cycle of DhaA with TCP using Sander module of AMBER. A docked complex with XC water molecules was neutralised to avoid summing to an infinite charge when applying PBC in the subsequent MD simulation, and immersed in a box of TIP3P water molecules; atom types, partial atomic charges, bonds, angles and dihedrals were assigned according to the ff94. MD parameters describing the MD calculation itself **(Table 27)** were supplied allowing potential energy function (PEF) to determine starting energy of the system. Initial velocity (size and direction) was assigned to each atom and the system was allowed to develop for DT time by solving the differential equations embodied in Newton's second law of motion, i.e. $F_i = m_i \times a_i$. Forces were evaluated and energy of the developed system was calculated. New velocities were assigned according to the forces and the system was allowed to propagate for another DT time. The simulation was halted when NSTLIM time step (from 1,000,000 to 1,900,000) was reached. The result was a trajectory (magenta) that specified how the positions and velocities of the particles in the system varied with time. DhaA is shown in cartoon model and coloured by domain: the main domain, grey; the cap domain, blue. In this example, TCP is shown and coloured by atom type: carbon, green; chlorine, yellow; hydrogen, white. Sodium cations and oxygen atoms of water molecules are shown as cyan and red spheres of 30% of their actual size, respectively. The structure with the box of water molecules is zoomed out by 10 Å with respect to the both left side images; the edges of the box are outlined.

Table 27 | Parameters for MD simulations of enzyme-substrate and enzyme-product complexes of the reaction cycle of DhaA with TCP using Sander module of AMBER. (pp. 108-110)

Parameter[a]	Description
Section I: MD parameters	
General flags describing the calculation	
IMIN = 0*	MD simulation will be performed.
NMROPT = 1	Weight changes will be read (see Section II).
Nature and format of input	
NTX = 1*	Initial coordinates and box size is read formatted with no initial velocity information.
IREST = 0*	
Nature and format of output	
NTXO = 1*	The final coordinates, velocities and box size is written to *restart* file in formatted form.
NTPR = 250	The most recent energy and temperature information will be printed to *mdout* and *mdinfo* files every 250 MD steps.
NTWR = 500*	The *restart* file is written every 500 MD steps.
IWRAP = 0*	The coordinates are written to the *restart* and *trajectory* files without “wrapping” into a primary box.[b]
NTWPRT = 0*	The coordinates of all atoms will be written to *coordinate* file every 250 ps.
NTWX = 250	

Parameter[a]	Description
NTWV = 0*	The velocities will not be written to *velocity* file.
NTWE = 0*	The energies and temperatures will not be written to *energy* file.
Potential function	
NTF = 1*	Complete interaction (force evaluation) is calculated.
NTB = 2	Constant pressure periodic boundary condition is applied.
DIELC = 1.0*	Dielectric multiplicative constant for the electrostatic interactions.
CUT = 10	Cutoff of 10 Å for the nonbonded interactions is used.
SCNB = 2.0*	1-4 van der Waals interactions are divided by 2.0.
SCEE = 1.2*	1-4 electrostatic interactions are divided by 1.2.
NSNB = 10	The non-bonded list is updated every 10 MD steps.
IPOL = 0*	Polarisabilities are not included in the force field.
Generalised Born	
IGB = 0*	No generalised Born term is used.
Frozen or restrained atoms	
IBELLY = 0*	No atoms are frozen.
NTR = 0*	No position restraints are applied.
Molecular dynamics	
NSTLIM = 1000000	1,000,000 MD steps will be performed.[c]
NSCM = 0*	Translational and rotational centre-of-mass motion removal at regular intervals is not applied.
T = 0.0*	The time (ps) at the start of MD simulation.
DT = 0.002	The MD time step of 0.002 ps is used.
Temperature regulation	
NTT = 1	Constant temperature scaling is performed using the weak-coupling algorithm, ensuring that the total kinetic energy is appropriate for the desired temperature.
TEMP0 = 300*	The system is to be kept at reference temperature of 300 K.
TEMPI = 0*	Initial temperature of 0 K is used.
IG = 555333	The seed of 555,333 is used for random number generator for determination of the initial velocities.
TAUTP = 1*	Heat bath coupling for the system is performed using time constant of 1 ps.
VLIMIT = 20*	Any component of the velocity that is greater than 20 will be reduced to 20.
Pressure regulation	
NTP = 1	Constant pressure MD with isotropic positon scaling is performed.
PRES0 = 1*	The system is maintained at reference pressure of 1 bar.
COMP = 44.6	Compressibility of 44.6×10^{-6} bar is used.
TAUP = 1*	Pressure relaxation time of 1 ps is used.
SHAKE bond length constraints	
NTC = 2	Bonds involving hydrogen are cosntrained.
TOL = 0.00001	Relative geometrical tolerance of 0.00001 Å is used for coordinate resetting in SHAKE.
Particle Mesh Ewald (PME) method[e]	
ORDER = 4*	A cubic spline approximation is used.
VERBOSE = 0*	Minimum output size of information about the PME run.
EW_TYPE = 0*	PME method is turned on.
DSUM_TOL = 10^{-5}	Cutoff value of the direct sum at CUT is less than 10^{-5}.
EW_COEFF = 0.27511*	Ewald coefficient is 0.27511 Å; this is determined by DSUM_TOL and CUT.
NBFLAG = 1*	NSNB is ingored, and the list is updated whenever any atom has moved more than half of SKINNB since the last list update.
SKINNB = 2*	Width of the nonbonded "skin" is 2 Å; the direct sum nonbonded list is extended to CUT + SKINNB, and the van der Waals and direct electrostatic interactions are truncated at CUT.
NETFRC = 1*	The total force on the system is artificially removed at every step
USE_PME = 1*	Reciprocal part of the sum will be computed.
VDWMETH = 1*	Continuum model is used for correction for energy and pressure for van der Waals interactions beyond those included in the direct sum.
EEDMETH = 1*	A cubic spline is used for evalutation of the switching function for the direct sum Coulombic interaction.
Section II: Weight change information	
TYPE = TEMP0	Reference temperature will be varied.
ISTEP1 = 0*	The weight will be applied over MD steps 0 through 100,000.
ISTEP2 = 100,000	
VALUE1 = 0	Temperature will change from 0 to 300 K from ISTEP1 to ISTEP2.
VALUE2 = 300	

[a]Default values are marked with asterisk.
[b]Wrapping performed using PTRAJ as a trajectory post-processing program.
[c]Some MD simulations were extended up to 1,900,000 MD steps.
[d]Method for calculation of electrostatic interactions.

RAMD simulations. RAMD simulation **(Lüdemann et al., 2000a)** is an enhanced sampling MD technique that makes the egress of a ligand from a buried enzyme active site observable in computationally accessible simulation times **(Lüdemann et al., 2000a; Winn et al., 2002; Wade et al., 2004; Schleinkofer et al., 2005; Wang & Duan, 2007)**. RAMD simulation resembles classical MD simulation except that an additional force (ACCELERATION) is applied to the centre of mass of the ligand in a randomly chosen direction. After a user-defined number of time steps (REXPUPDATE), the distance traveled by the ligand is compared to a threshold parameter (THRESHOLD). If the ligand does not reach the threshold distance, a new, randomly chosen direction is given to the force on its centre of mass; otherwise, the force direction is maintained. The process is iterated until the ligand has been released into the bulk solvent or a specified maximum simulation time is reached **(Fig 54)**. RAMD simulations were carried out using Sander module of AMBER 8 with RAMD patch **(Supplementary files ramd.patch and ramd.in;** http://projects.villa-bosch.de/mcm/software/amber**)**. RAMD simulations were performed on DCL in the CL-free complexes for wild-type DhaA and its mutants, at 300 K, and using the same MD parameters as in the preceeding classical MD simulations. First, the proper setting of the RAMD parameters (random acceleration, number of time steps and threshold distance) was tested on the wild-type DhaA complexed with R- and S-DCL, respectively. A random acceleration of 0.25, 0.20, 0.15, 0.1, 0.09, 0.08, 0.07, 0.06, 0.05, 0.04, 0.03, 0.02, and 0.01 kcal $Å^{-1}$ g^{-1} applied to the centre of mass of DCL; a number of time steps of 10, 20, 40, and 80; and a threshold distance of 0.001, 0.002, 0.004, and 0.008 Å were tested. RAMD simulations were performed with various combinations of the values of the three parameters. Three different snapshots of the MD simulations from a well-equilibrated region were used as starting structures for RAMD simulations, resulting in six RAMD trajectories for each combination of the parameters considering R- and S-DCL together. The maximum duration of RAMD simulations was set to 1 ns. If DCL left the protein for the bulk water and the distance between centre of mass of Asp106 and DCL exceeded 30 Å, the simulations were halted. RAMD simulations were selected for detailed analysis when the parameters used resulted in the release of R- or S-DCL within 1 ns in at least 4 out of 6 simulations and lasted for at least 20 ps. The final settings were 0.04 and 0.05 kcal $Å^{-1}$ g^{-1} for the random acceleration, 10 for the number of time steps, and 0.002 and 0.004 Å for the threshold distance **(Table 28)**, resulting in a total of 24 RAMD simulations of the wild-type DhaA. The parameters derived from RAMD simulations of the wild-type DhaA were adopted for the mutants. RAMD simulations of the mutants were also performed on R- and S-DCL, but only the final MD snapshot was used. Altogether, 62 RAMD trajectories of DhaA mutants were recorded. No difference in the preferential release through different pathways or in the mechanism of the release was obvious for the R- and S- enantiomers of DCL. Therefore, R-DCL and S-DCL were further considered to provide variability in the MD trajectories only. RAMD simulations were also performed on DCL for the wild-type DhaA in the presence of CL but were not extended to the mutants for highly reduced number of observed DCL release events.

Table 28 | RAMD-specific parameters for RAMD simulations of enzyme-substrate and enzyme-product complexes of the reaction cycle of DhaA with TCP using Sander module of AMBER with RAMD patch.

Paramter	Value(s)	Description
REXPMODE	1	RAMD method will be employed on the DCL specified by LSTART and LSTOP.
REXPUPDATE	10	Random acceleration will be updated every 10 MD time steps.
ACCELERATION	0.04 or 0.05	Magnitude of ligand acceleration will be 0.04 or 0.05 kcal g^{-1} A^{-1}.
THRESHOLD	0.002 or 0.004	Distance that DCL has to travel during REXPUPDATE to maintain direction of the vector; if the distance is not traveled then new direction vector is generated.
MAXTRAVEL	30	RAMD simulations will be halted if the distance between centre of mass of DhaA variant and DCL is > 30 A.
IREXPSEED	14253	Seed for random direction vector generator is 14,253.
RSTART	1	Atom identifier of the first DhaA atom is 1.
RSTOP	4596 to 4631	Atom identifier of the last DhaA atom; depending on DhaA variant.
LSTART	4597 to 4632	Atom identifier of the first DCL atom; depending on DhaA variant.
LSTOP	4608 to 4643	Atom identifier of the last DCL atom; depending on DhaA variant.

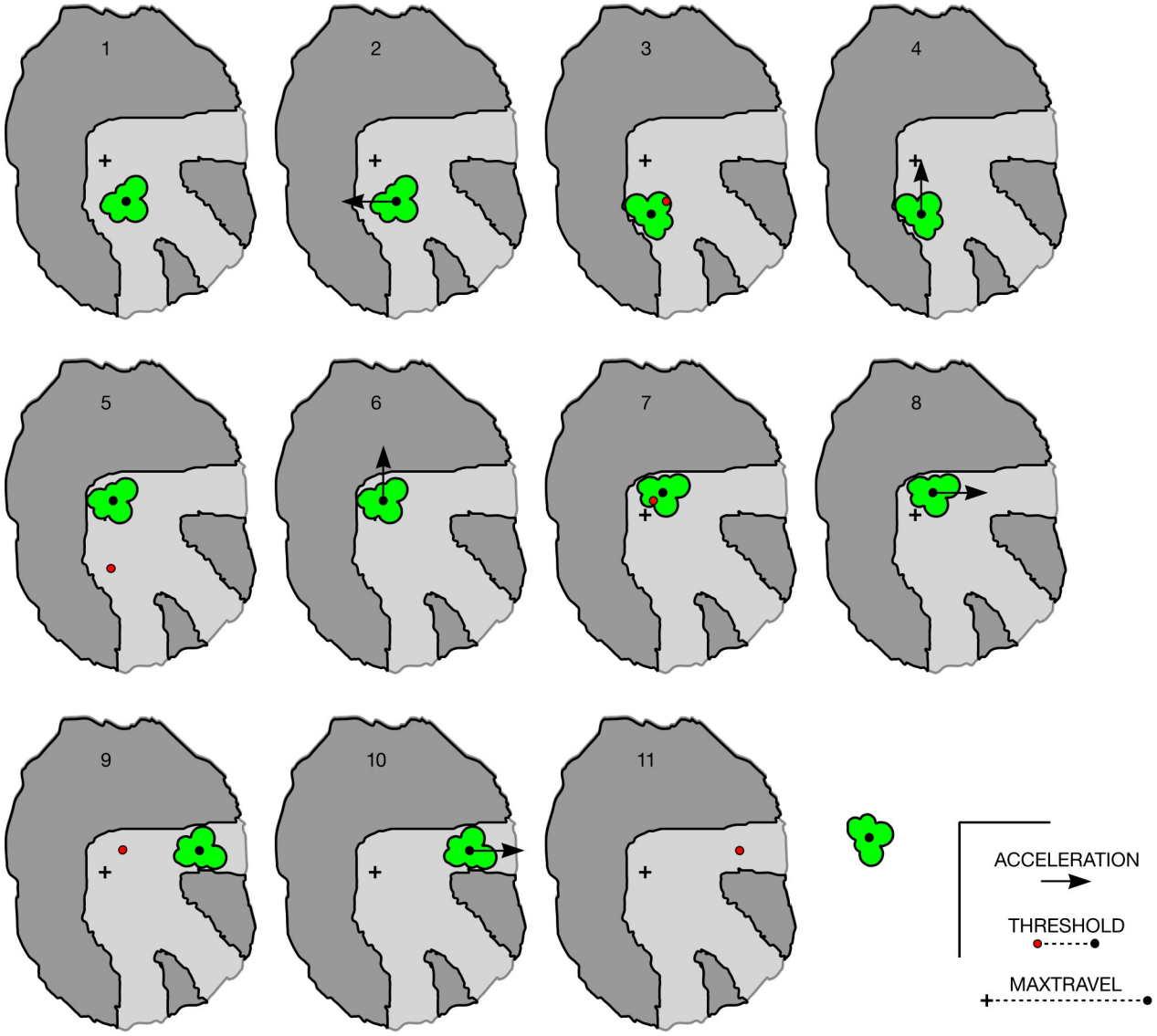

Fig 54 | Principle of RAMD simulation. The principle is demonstrated on a hypothetical release of a ligand (green) from a buried cavity in a protein (grey) in a five-REXPUDATE-step RAMD simulation. Starting protein-ligand complex was obtained from classical MD simulation (*Step 1*); centre of mass of protein and ligand are indicated by black cross and black point, respectively. The RAMD procedure is composed of alternating simulation (even numbers) and decision steps (odd numbers). ACCELERATION (arrow) is applied to the centre of mass of the ligand in a random direction for a user-defined REXPUPDATE number of MD time-steps (*Steps 2, 4, 6, 8 and 10*). After the REXPUPDATE is reached, the distance traveled by the ligand during the last REXPUPDATE (starting and ending positions are indicated by red and black point, respectively) is compared to THRESHOLD (*Steps 3, 5, 7, 9*); if the distance traveled by the ligand during the last REXPUPDATE is shorter than THRESHOLD, a new random direction for ACCELERATION is chosen (*Steps 4 and 8*); if the distance traveled by the ligand during the last REXPUPDATE is ≥ THRESHOLD, the direction for ACCELERATION is maintained for next REXPUPDATE period (*Steps 6 and 10*). At every MD time-step of each REXPUPDATE, the ligand position is compared to the centre of mass of the protein (*Steps 2-3, 4-5, 6-7, 8-9, 10-11*); if the distance traveled by the ligand is ≥ MAXTRAVEL, the simulation is halted (*Step 11*). See **Table 28** for details about the RAMD parameters. In practice, depending on a system and classical MD and RAMD parameters, the total number of REXPUPDATE steps is in the order of 10^3 and higher.

General analysis of MD simulations. The stability of the MD trajectories was assessed by all-atom RMSD and radius of gyration using the Ptraj and Carnal modules of AMBER. Stable parts of the MD simulations were decided visually by plotting RMSD versus time. The stability of the secondary elements was calculated in PYMOL for each snapshot of a trajectory using the DSSP method based on detection of hydrogen bonds by electrostatic criterion **(Kabsch & Sander, 1983)**. *B*-factors **(Supplementary file bfac.zip)** and geometrical parameters (distances, bond angles, and dihedral angles) were measured using Ptraj. Hydrogen bonds were identified using < 2.76 Å and > 120°

for the distance and angle thresholds, respectively.

Analysis of enzyme-substrate interactions in classical MD and RAMD simulations. The presence of near attack configurations for TCP in the wild-type DhaA and the mutant 31' along the production classical MD trajectories was evaluated every 0.5 ps using the two-parameter geometric conditions proposed previously for DhlA-1,2-dichloroethane complex by Hur et al. **(2003)**: (i) the distance between the nucleophilic oxygen and the attacked carbon atom ≤ 3.41 Å and (ii) the angle formed by the nucleophilic oxygen, the attacked carbon and the leaving chlorine > 157°.

Analysis of product release pathways in classical MD and RAMD simulations. Release of DCL and CL was monitored in both classical MD and RAMD simulations **(Fig 55)**. Distances between the centre of mass of the two hydrogen atoms, $H_{\varepsilon 1}$ of Trp107 and $H_{\delta 22}$ of Asn41, and CL and between the centre of mass of Asp106 and DCL were measured with Ptraj to identify regions of long residence time for CL or DCL during release from the active site to the bulk water in classical MD and RAMD simulations **(Fig 56 and Supplementary files cpr.zip and fpr.zip)**. Residues within 7 Å of the centre of mass of DCL along the trajectories were assumed to constitute the release pathways. Seven angstroms ensured that all first shell residues were included. Water molecules that resided in the protein interior or entered the protein during classical MD and RAMD simulations were identified as those located at a distance < 8 Å from any atom of Asp106 in at least one snapshot using Carnal. The selected pathway residues and the internal water molecules aided analysis of important events using VMD 1.8.5 **(Humphrey et al., 1996)** and PYMOL where especially behaviour of the pathway residues and the internal water molecules were monitored. Release pathways for CL and DCL were visualised by PYMOL as a surface representation of CL or all positions of a central carbon of DCL **(Supplementary files path.zip and bcp.zip)**. The surface representations of all release pathways for CL and DCL from all classical and RAMD simulations were superimposed onto the crystal structures of DhaA from *Rhodococcus* sp. (PDB-IDs 1CQW and 1BN6) and clustered by visual inspection according to overlap between the surface representations of the pathways and the contribution of the same secondary structure elements. Clusters were annotated by a number, and branching clusters were further distinguished by a letter. For each DhaA variant and each unique DCL release pathway, all snapshots were extracted from the selected RAMD trajectories and adjusted by 150 steps of steepest descent energy minimisation with the implicit generalised Born solvation model II **(Onufriev et al., 2004)** using Sander. The van der Waals and electrostatic interaction energies between DCL and every protein residue were calculated for each of the energy-minimised structures using the Anal module of AMBER.

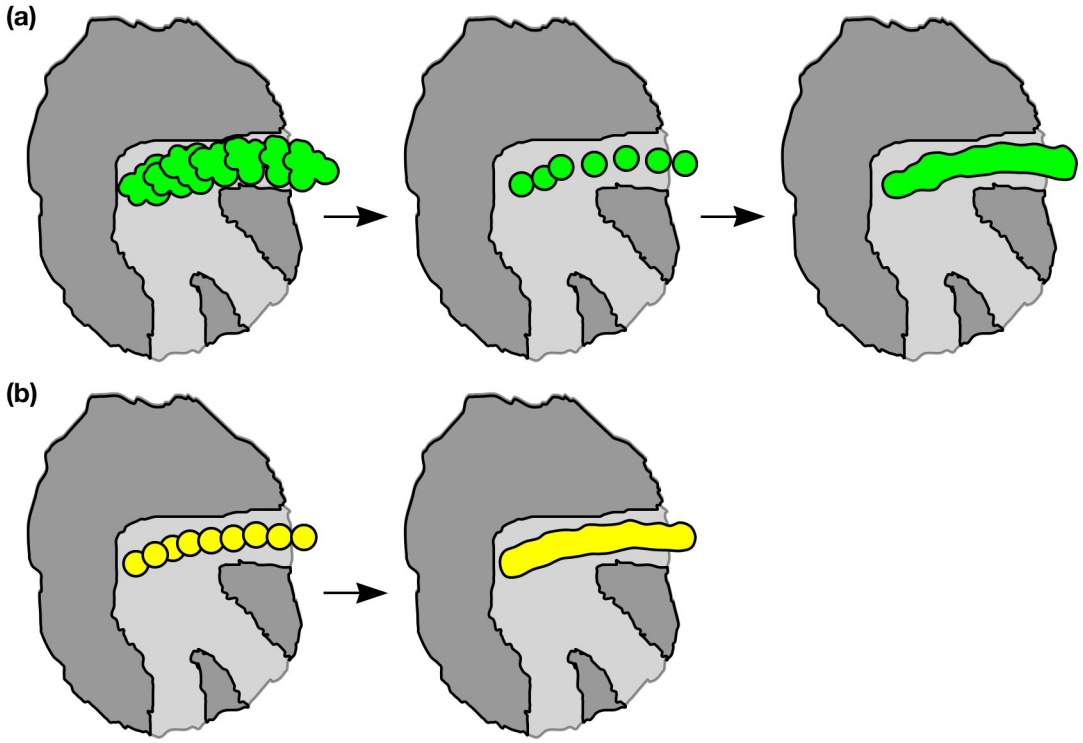

Fig 55 | Visualisation of DCL and CL release pathways observed in MD simulations. **(a)** DCL release pathway (green) in DhaA (grey) visualised as a surface representation of all positions of central carbon atom (green balls) of a single DCL molecule along MD trajectory; **(b)** CL release pathway in DhaA visualised as a surface representation of all positions of a single chloride anion (yellow balls) along MD trajectory.

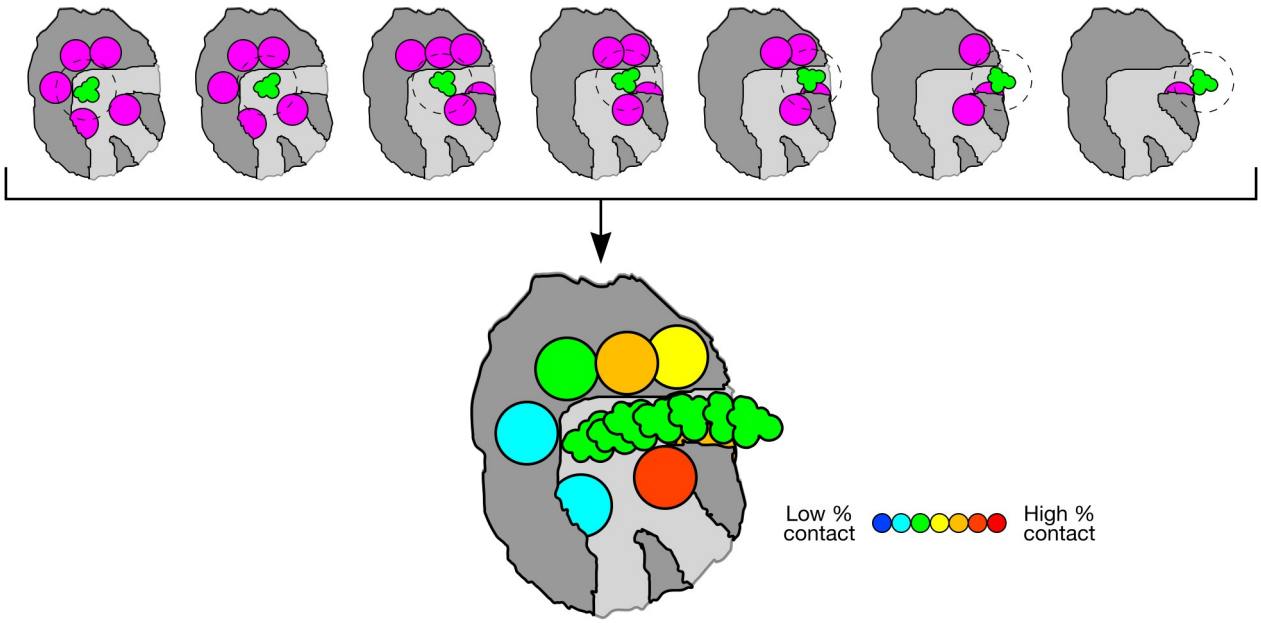

Fig 56 | Identification of amino acid residues belonging to the DCL release pathway. Amino acid residues (violet balls) in DhaA (grey) that surrounded the leaving DCL (green) were identified by the 7 Å threshold distance criterium (dashed circle) in all MD snapshots, and coloured in a red-green-blue colour scale according to frequency of occurence.

Analysis of water pathways in classical MD simulations. Water pathways were identified in classical MD simulations by superimposing all positions of oxygen atoms of all internal water molecules onto the crystal structures of DhaA in PYMOL **(Fig 57)**. Opening and closing of tunnels connecting the active site to the bulk solvent and their inducibility by CL, DCL, and water were visualised by PYMOL as a slice through the solvent-accessible surface representation (with a probe radius of 1.4 Å) of the protein with 5- and 1-ps windows for classical MD and RAMD simulations, respectively. Tunnels were classified as closed or open according to whether the solvent-accessible surface showed the active site isolated from (closed) or connected to (open) the bulk solvent.

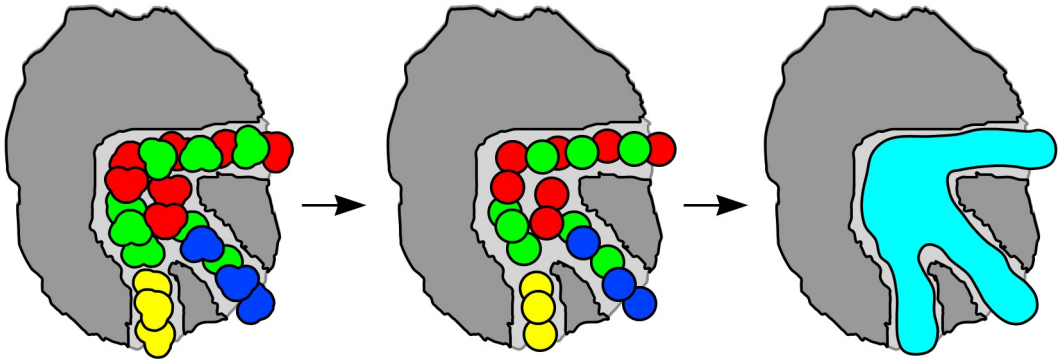

Fig 57 | Visualisation of water exchange pathways observed in classical MD simulations. Water exchange pathways (cyan) in DhaA (grey) were visualised as a surface representation of all positions of water oxygen atoms (coloured balls) along MD trajectory. In contrast to DCL and CL release pathways **(see Fig 55)**, the water exchange pathways are result of multi-molecular surface representation.

Analysis of XC structures of the DhaA mutants. XC structures of the mutant proteins 04, 14 and 15 were explored for open tunnels using PYMOL. The structures were visualised as a slice through the solvent-accessible surface representation (with a probe radius of 1.4 Å) and superimposed onto the 1CQW and 1BN6 XC structures of DhaA from *Rhodococcus* sp. with superimposed CL and DCL release pathways. Open tunnels in the XC structures of the DhaA mutants were then identified and annotated.

3.3 Software engineering

Development of CAVER 2.0 algorithm and CAVER Viewer application. Development of algorithms and their implementation is far beyond the scope of my contribution and far beyond my understanding, and is described by the software engineers elsewhere **(Kozlíková et al., 2007; Medek et al., 2007)**.

Testing temporary versions of CAVER 2.0 algorithm. Temporary versions of CAVER 2.0 algorithm were tested as a PYMOL plugin with XC structures of DhaA from *Rhodococcus* sp. (PDB-IDs 1CQW and 1BN6) and with selected snapshots of MD simulations of the wild-type DhaA and its mutants (see 3.2). Calculated tunnels were compared with visually identified open tunnels. Reliability of the calculated tunnels and proper functionality of the PYMOL plugin was assessed and reported to the algorithm developers.

Development and testing of the graphical user interface (GUI) of CAVER Viewer. The GUI of CAVER Viewer application was designed and temporary versions of the application were tested for basic functionality. Observed functionality problems and suggestions for improving userfriendliness were reported to the application developers.

4 Results

There are two players, A *and* B*, in the "Why?" game:* A *asks a question "Why?", and* B *answers the question. The game is started by an arbitrary sentence spoken by* B*.* A *asks "Why?", and* B *answers. And this goes on and on until* B *cannot find answer different from the previous one; and this happens when the last answer is about The Big Bang.*

4.1 In silico design of DhaA mutants for improved conversion of 1,2,3-trichloropropane

Klvaňa M, Pavlová M, Prokop Z, Chaloupková R, Banáš P, Otyepka M, Wade RC, Nagata Y & Damborský J (**2009**). Redesigning dehalogenase access tunnels as a strategy for degrading an anthropogenic substrate. *Nat. Chem. Biol.* 5: 727-733.

Focus of the mutagenesis effort. Bosma et al. **(2002)** isolated DhaA mutants 04 (Cys176Tyr) and M2 (M1+Tyr273Phe) that showed 2.8-fold and 7.8-fold increase in catalytic performance for conversion of 1,2,3-trichloropropane (TCP) to 2,3-dichloropropane-1-ol (DCL) and chloride anion (CL). Bosma et al. **(2002)** then proposed that the common substitution at the position 176 in the main tunnel contributes to the improvement by reducing the size of the active site cavity and thus enhancing efficiency of TCP substrate binding. In line with the proposed effect of Cys176Tyr, Bosma et al. **(2003)** proposed the S_N2 reaction to be the rate-limiting step in the conversion of TCP by wild-type DhaA based on absence of ^2H_2O kinetic isotope effect. Banáš et al. **(2006)** noted decreased size of the main tunnel by Cys176Tyr and presumed that the substitution causes shift in the rate-limiting step from the S_N2 step to DCL release due to re-direction of DCL release from the main tunnel to the slot tunnel and suggested to perform substitutive mutagenesis in the slot tunnel for further improvement of the catalytic performance of DhaA with TCP.

Identification of hot spots. Classical molecular dynamics (MD) simulations were performed for wild-type DhaA and the 04 mutant complexed with CL and docked DCL, or docked DCL only **(Fig 58)** to investigate whether DCL can escape the active site cavity through the slot tunnel **(Tables 29 and 30)**. The DCL release was, however too time-demanding to be observable within nanosecond time-scale of the classical MD simulations. Therefore, enhanced sampling random acceleration MD (RAMD) simulations were employed to facilitate the release of DCL **(Table 31)**. RAMD simulations showed (i) higher frequency of occurrence of DCL release via the main tunnel in the wild-type DhaA than in the 04 mutant **(Table 32)** and (ii) possibility of the slot tunnel to serve as an auxiliary DCL release pathway in both the wild-type DhaA and the 04 mutant, with relative higher importance in the latter due to affected main tunnel. Both these observations were thus far in accordance with the previously proposed DCL re-direction hypothesis. Considering the re-direction hypothesis as the possibility, Cys176 identified by Bosma and co-workers as a hot spot in the previous study **(Bosma et al., 2002)** and, among the slot tunnel amino acid residues identified here by the RAMD simulations **(Fig 59)**, four amino acid residues that showed close contacts to DCL via side-chains (Trp141, Leu135, Val245 and Leu246) were selected for mutagenesis **(Fig 60)**.

Design of substitutions in the hot spots. To assess the mutability of the hot spots identified by the RAMD simulations, variability of the corresponding amino acid residues among haloalkane dehalogenases belonging to subfamily II was read from the multiple sequence alignment reported by Chovancová et al. **(2007; Table 33)**. Of the two possible substitutes for Trp141, Ser and Phe, the latter was selected to be introduced by site-directed mutagenesis as it was supposed to yield stable folded mutant more likely than the former. The remaining three hot spots, Leu135, Val245 and Leu246 were proposed for randomisation using saturation mutagenesis for the following reasons: (i) 90 possible combinations were identified among members of haloalkane dehalogenase subfamily II of which no one could be discarded a priori; (ii) the three amino acid residues were located close in space where substitution at one site may require compensatory substitution at another of the two remaining sites; and (iii) our understanding of structure-dynamics-function relationships for these sites was limited. Trp141Phe was proposed to be introduced into the M2 mutant, yielding mutant M3. Both the M2 and M3 mutants served as the templates for the saturation mutagenesis, leading to libraries *A* (2,568 clones) and *B* (2,705 clones), respectively.

4.2 Analysis and interpretation of the effects of the mutations on the enhanced conversion of TCP by DhaA mutants

Klvaňa M, Pavlová M, Prokop Z, Chaloupková R, Banáš P, Otyepka M, Wade RC, Nagata Y & Damborský J (**2009**). Redesigning dehalogenase access tunnels as a strategy for degrading an anthropogenic substrate. *Nat. Chem. Biol.* 5: 727-733.

Klvaňa M, Pavlová M, Koudeláková T, Chaloupková R, Dvořák P, Prokop Z, Stsiapanava A, Kutý M, Kutá-Smatanová I, Dohnálek J, Kulhánek P, Wade RC & Damborský J (**2009**). Pathways and mechanisms for product release in the engineered haloalkane dehalogenases explored using classical and random acceleration molecular dynamics simulations. *J. Mol. Biol.* 392: 1339-1356.

DhaA mutants with enhanced activity with TCP. Most DhaA mutants in the saturation mutagenesis libraries (96%) showed little or no activity with TCP, but a small proportion appeared to have higher activity than wild-type DhaA. Sequencing of *dhaA* mutant genes of the 51 clones exhibiting up to 39-fold improvement in the activity with TCP relative to the wild-type cultures revealed 25 unique DhaA protein variants with 20 different combinations of mutations at the three randomised positions **(Table 34)**. The three most active variants from library *A* (mutants 27, 31 and 33) and library *B* (mutants 17, 19 and 21) were purified and subjected to determination of secondary structure fingerprint using far-UV CD spectroscopy to assess impact of the mutations on the relative abundance of amino acid residues in α-helices and β-sheet. The far-UV CD spectra of the selected variants were nearly identical to that of the wild-type DhaA **(Fig 61a)**. Although some minor effect of mutations on the packing of amino acid residues in α-helical conformation could be discerned, the far-UV CD spectra suggested that the mutations did not significantly alter the native folded state. Specific activities measured for the selected purified DhaA variants revealed three superior mutants, 27 and 31 from library *A* and 21 from libraby *B*, all common in Val245Phe substitution **(Fig 62)**. Steady-state kinetic experiments then showed that the enhanced activity of the three mutants with TCP was due to increased k_{cat} (up to 32-fold in the mutant 31), whereas K_m showed slight increase within experimental error **(Table 35)**. The catalytic efficiency of the mutants 21, 27 and 31, quantified by k_{cat}/K_m, was 12-, 23- and 26-fold higher, respectively, compared to the wild-type DhaA. At milimolar concentrations of DCL product of TCP conversion, the three mutants were inhibited with K_i ranging from 2.08 to 4.42 mM, similarly to the wild-type DhaA, K_i = 2.50 mM **(Fig 63)**. The effect of mutations on substrate specificity was assessed for the mutant 31 by comparing specific activities for the set of 31 substrates to the specificity profile of the wild-type DhaA **(Fig 64)**. The mutant 31 showed an increase in specific activity towards all tested 1,2-dihaloethanes, 1,2-dihalopropanes and 1,2,3-trihalopropanes, and reduced activity towards longer-chain (> C3) 1-haloalkanes and α,ω-dihaloalkanes.

Discriminating between possible sources of improvement of the conversion of TCP by DhaA mutants. RAMD simulations of DCL release were conducted with the Tyr273Phe-free variants of the mutants 21, 27 and 31, denoted 21', 27' and 31', respectively **(Tables 29, 30 and 31)**, prepared by in silico mutagenesis from the 04 mutant (approved by far-UV CD spectra), to gain better understanding on the effect of the introduced mutations on accessibility of the main tunnel and the slot tunnel and on the possible connection of the DCL release to enhanced activity of the mutants with TCP. Tyr273Phe was not included for the following reasons: (i) to allow direct comparison with the 04 mutant, and (ii) not to include mutations that will have presumably no sizeable effect on physical steps of the reaction cycle modelled by MD simulations. DCL release through the main tunnel was observed in the RAMD simulations of all the variants but with decreasing frequency from the mutant 21' through the mutant 27' to the mutant 31' **(Table 32)**, i.e. in the direction of increasing activity **(Table 35)**. The release of DCL through the slot tunnel could occur in the mutants 21' and 27', although DCL preferentially exited via branches from the slot tunnel in these mutants: pathway 2c (p2c) in mutant 21' as a result of the Trp141Phe substitution, and pathway 2b (p2b) in mutant 27' due to the Ile135Val substitution **(Table 32 and Fig 65)**. In the mutant 31', however, the release of DCL through the slot tunnel or its branches appeared to be completely prevented by the Ile135Phe substitution **(Fig 66)**. Hence, presence of three bulky substitutions, Ile135Phe, Cys176Tyr and Val245Phe together with preserved wild-type Trp141 were responsible for the mutant 31' being the least amenable to DCL release among the mutants **(Table 32)**. RAMD simulations thus indicated that DCL release could hardly be improved in the mutants. Therefore, DCL re-direction hypothesis was abandoned, and our attention ultimately focused to the substrate binding/S_N2 steps as the only remaining possible source of improvement.

Proposal on the mechanism of improvement of TCP binding or S_N2 step in the mutant 31'. The hampered DCL release in the mutants with increase in activity must be essentially supercompensated by improvement in the TCP binding or S_N2 step of the wild-type. Classical MD simulations showed, that bulky aromatic substitions in the main tunnel and the slot tunnel not only hindered DCL release but they also restricted exchange of water molecules between the bulk solvent and the buried active site, especially in the absence of chloride anion in the active site **(Fig 67)**. While water molecule is an essential co-substrate and some water molecules are required for product release,

they may unfavourably affect substrate binding or S_N2 step. The dynamics of water molecules were therefore monitored together with the stability of the substrate TCP in "reactive" near-attack configurations (NAC) in classical MD simulation of the wild-type DhaA and the mutant with most occluded active site, 31'. Two bindings modes of TCP, identified by molecular docking, and corresponding to the binding modes *2* (yielding S-DCL) and *3* (yielding R-DCL) reported previously **(Banáš et al., 2006)**, were applied. The MD simulations with the substrate revealed that the active site of the wild-type DhaA was easily accessible to water molecules from bulk solvent and that increasing numbers of water molecules in the active site competed with TCP for interaction with the nucleophile, Asp106 **(Fig 68)**. The competition led to reduced formation of the NAC since the water molecules sterically hindered access of TCP to the nucleophile. Contrary, the bulky aromatic substitutions in the access tunnels of the 31' mutant shielded the active site from the bulk solvent effeciently within the two-nanosecond MD simulation, and the complex occurred in NAC 6.7-times more frequently than in the wild-type DhaA **(Fig 68)**.

Determination of the rate-limiting step in the mutant 31. Whether the improved S_N2 step of the mutant 31 overweighed other steps of the reaction cycle was determined by ^2H_2O kinetic isotope effect and transient kinetic experiments. Increasing the fraction of ^2H_2O in the reaction mixture resulted in increased activity of the 31 mutant with TCP, indicating a shift of the rate-limiting step in the conversion of TCP in the 31 mutant, since no effect of ^2H_2O has been detected in the wild-type DhaA **(Bosma et al., 2003)**. The increase of the catalytic rate in the presence of ^2H_2O further suggested that the step determining the rate of TCP conversion by the 31 mutant is neither hydrolysis nor slow conformational change **(Bosma et al., 2003)**, leaving product, DCL or chloride anion, release as the possible rate-limiting steps **(Fig 69)**. Transient kinetic experiments conducted with the wild-type DhaA and the 31 mutant confirmed the shift in the rate-limiting step in the 31 mutant **(Fig 69)**. No sign of burst was observed for either CL or DCL formation after rapid mixing of the wild-type DhaA with excess TCP (**Fig 69a**). Instead, linear formation of both products was observed with a rate constant of 0.07 ± 0.01 s^{-1}, which corresponded well with the steady state turnover number of 0.04 ± 0.01 s^{-1}. The absence of burst for both CL and DCL formation suggested that the slowest step of TCP conversion lies at the beginning of the reaction cycle, before or in the step forming the CL product. In contrast, upon rapid mixing of the 31 mutant with excess TCP, a clear pre-steady state burst was identified for both CL and DCL, with observed rates of 5.8 ± 2.3 and 5.2 ± 1.5 s^{-1}, respectively (**Fig 69b**). The burst was followed by a linear steady-state phase, with rate constants of 1.42 ± 0.31 and 1.36 ± 0.18 s^{-1} for CL and DCL, respectively, which corresponded well with the k_{cat} value observed in steady-state kinetics (1.26 ± 0.07 s^{-1}). These findings suggested that none of the chemical steps is limiting for the 31 mutant; instead, the rate-limiting step for the reaction with TCP catalysed by this mutant is the release of a product, CL or DCL (**Fig 69c**).

Exploring the trade-off between shielding and accessibility of the active site. Based on the mutant 31, four additional mutants, denoted as mutant 14 (Ile135Phe), mutant 15 (Cys176Tyr+Ile135Phe), mutant 51 (31+Ala172Phe) and mutant 52 (51+Ala145Phe) were designed to test the robustness of the main tunnel and the slot tunnel against aromatic amino acid residue substitutions and, in the case of the mutants 51 and 52, to explore, whether the shielding of the active site could be improved further by introducing additional aromatic amino acid residues into the main tunnel wall. The mutants were constructed by site-directed mutagenesis and characterised for steady-state kinetic constants for conversion of TCP **(Table 35)** and secondary structure fingerprint using far-UV CD spectroscopy **(Fig 61b)**. The catalytic performance of the mutants 14 and 15 was similar to the wild-type DhaA and the mutant 04, respectively, indicating that Ile135Phe alone had no sizeable effect on the activity with TCP. Classical MD simulations **(Tables 29 and 30)** and RAMD simulations **(Table 31)** of the mutants 14 and 15 showed that Ile135Phe alone sealed the slot tunnel, leaving the main tunnel as the only DCL release pathway, irrespective of presence/absence of Cys176Tyr substitution **(Table 32 and Fig 66)**. The catalytic performance of the mutants 51 and 52 with TCP dropped to the wild-type level **(Table 35)**. The secondary structure fingerprint indicated that the decrease in the activity could be contributed by changes on secondary structure level **(Fig 61b)**. Classical MD simulations **(Tables 29 and 30)** and RAMD simulations **(Table 31)** of Tyr273Phe-free variants of the mutants 51 and 52, denoted as the mutants 51' and 52', respectively, showed increased ease of DCL release through the main tunnel **(Table 32 and Fig 66)**, indicating that the region of the main tunnel crowded by the aromatic amino acid residues was disturbed from the compactness of the mutant 31'.

Proposal on the order of DCL and CL release in the wild-type DhaA and its mutants. ^2H_2O kinetic isotope effect and transient kinetics experiments on the wild-type DhaA and the mutant 31 revealed product release as the rate-limiting step for conversion of TCP but did not specify which of the products, DCL or CL, is the slower on release. Classical MD simulations of the wild-type DhaA and the mutants 04, 14, 15, 21', 27', 31', 51' and 52' complexed with both DCL and CL products of TCP conversion were monitored for product release. While DCL release was not observed at all, CL release was observed in the wild-type DhaA (trajectory *c1*) and the mutant 15 (trajectory *c7*) to occur through the main tunnel with the same ease without any additional artifical force **(Table 29 and Fig 70)**.

These observations suggested that CL is faster on the release compared to DCL in the wild-type DhaA and the mutant 15. RAMD simulations of CL release were attempted for the mutant 31', but failed to provide reliable results: large acceleration had to be applied to tear off CL from the interactions with halide-stabilising amino acid residues Asn41 and Trp107 **(Fig 58)**, causing subsequent sub-picosecond release of unsolvated CL from the active site to the bulk water (data not shown).

4.3 Product release and water exchange pathways and mechanisms in DhaA and its mutants

Klvaňa M, Pavlová M, Koudeláková T, Chaloupková R, Dvořák P, Prokop Z, Stsiapanava A, Kutý M, Kutá-Smatanová I, Dohnálek J, Kulhánek P, Wade RC & Damborský J (**2009**). Pathways and mechanisms for product release in the engineered haloalkane dehalogenases explored using classical and random acceleration molecular dynamics simulations. *J. Mol. Biol.* 392: 1339-1356.

4.3.1 Identification of pathways by MD simulations

Modelling of DhaA complexed with products of TCP conversion. The structures of the enzyme-product complexes for dehalogenation of TCP were modelled by molecular docking of R- and S-DCL, respectively, into wild-type DhaA complexed with CL **(Fig 58)**. Both R- and S-DCL had similar conformations and positions in the active site with respective docked energies of -5.26 and -5.41 kcal mol^{-1} and both formed a hydrogen bond to the Asp106 side-chain and a close contact to the imidazole ring of His272 in the active site. None of the mutated residues in the eight mutants studied overlapped with the binding site of DCL. Therefore, the same initial DCL coordinates were used in all mutants (04, 14, 15, 21', 27', 31', 51' and 52'). The complexes were subjected to classical MD simulations to adjust the conformation of DCL in the active site and the conformations of the mutated residues **(Table 29)**. During these simulations, DCL preserved its docked orientation, characterised by the strong interactions with the catalytic residues Asp106 and His272. The overall stability of the complexes was supported by a flattened RMSD around 1.5 Å and a radius of gyration around 17.8 Å for all complexes.

Product release and water exchange pathways in the wild-type DhaA and its mutants. The classical MD trajectories were investigated for spontaneous release of the products (DCL and CL) and for exchange of water molecules between the buried active site and bulk solvent. In total, one release pathway for CL, p1 **(Figs 70 and 71a)**, no release pathway for DCL, and five pathways for water molecules, p1, p2a, p2b, p2c, and p3 **(Figs 67a and 71c)** were observed for the DhaA variants. Another set of MD simulations was performed with CL replaced by a water molecule to model the system after release of the halide anion from the active site **(Table 30)**. The overall stability of the complexes was supported by a flattened RMSD around 1.4 Å and a radius of gyration around 17.8 Å for all complexes. The MD trajectories were investigated for exchange of water molecules and spontaneous release of DCL. Altogether, three pathways were observed for water molecules (p1, p2a, and p2b) with the DhaA variants **(Fig 71b)**. No release of DCL was observed in any of the classical MD simulations, justifying the use of RAMD simulations to enhance DCL release. RAMD simulations of DCL release in wild-type DhaA and its mutants resulted in five pathways, p1, p2a, p2b, p2c, and p3 **(Table 31 and Figs 65, 66 and 71b)**.

4.3.2 Pathway p1

Description of p1. p1 corresponds to the main tunnel identified in the X-ray crystal (XC) structures of DhaA **(Fig 72)**. p1 is defined mainly by two helices of the cap domain α4 (Phe144, Ala/Phe145, and Phe149) and α5 (Ala/Phe172 and Cys/Tyr176) and, to a smaller extent, by the β8/α10 loop (His272) and the β8/α9 loop (Val/Phe245). The main tunnel was permanently open in wild-type DhaA and mutant 14 **(Table 36)**. The tunnel was widened during the passage of DCL, CL, and water molecules. The introduction of one or more aromatic substitutions in p1 caused a change in the opening mechanism from permanent tunnel to the transient tunnel **(Table 36 and Figs 73ab and 74)**. Decreased accessibility of the tunnel for the studied ligands was observable already after a single substitution, Cys176Tyr in mutant 04, and was further pronounced by cumulatively introduced substitutions Val245Phe, Ala172Phe, and Ala145Phe in mutants 31', 51', and 52' **(Fig 67b)**. The accessibility of p1 was controlled by the aromatic residues Phe144 and Phe149 in wild-type DhaA; by Cys176Tyr, Val245Phe, Ala172Phe, and Ala145Phe in mutants 04, 15, 21', 27', 31', 51', and 52'; by the varying length of the N-terminal part of α4 helix (143-GluPheAla/Phe-145); by a flexible residue located in the middle of the α5 helix (Gly171); and by the varying size of the C-terminal part of the α5 helix (Cys/Tyr176).

Release of CL through p1. The release of CL was observed only through p1 and only in wild-type DhaA and mutant 15 **(Figs 70, 71a, 76 and 77)**. No release of the CL was observed in the classical MD simulations of 04, 14, 21', 27', 31', 51', and 52' **(Table 29)** and RAMD simulations of CL release did not provide reliable results (data not shown). The release process in wild-type DhaA started with rapid hydration of the active site by crystallographic water molecules located in p2a, followed by water molecules from bulk water entering the active site through p1 and p2b. The position of the two crystallographic water molecules in p2a was occupied by Ile135Phe in mutant 15. Therefore, only p1 and p2b were used by bulk water molecules to access the active site of mutant 15. The water molecules entered the active site and competed with CL for hydrogen-bonding interactions with the halide-stabilising residues. Eventually, they enabled release of CL by making a hydration shell composed of three to five water molecules that accompanied the CL through the broadly widened p1. The entire release event took about 200 ps counting from the initial destabilization of the CL from the halide-stabilising residues in both wild-type DhaA and mutant 15. The vacant binding site between the halide-stabilising residues became occupied by a water molecule. Other water molecules in the active site competed with DCL for a hydrogen-bonding interaction with Asp106. DCL retained the hydrogen bond to Asp106 during the entire simulation in mutant 15, whereas in wild-type DhaA, this interaction was broken and DCL interacted with Asp106 indirectly through a water bridge.

Release of DCL through p1. p1 was the most frequently used pathway for the release of DCL in wild-type DhaA and all the mutants **(Table 32 and Fig 66)**. The release process **(Figs 78-82)** was strongly affected by the hydrogen bond between DCL and the nucleophile Asp106 **(Fig 58)**. This interaction had to be broken by water molecules to enable release of DCL from the active site and entry to the main tunnel. DCL was further attracted to the main tunnel by favourable electrostatic and van der Waals interactions with the catalytic base His272 **(Fig 75a-e)** and occasional hydrogen-bonding interactions with its $N_{\varepsilon 2}$. When the hydrogen bond to His272 was formed, DCL used exclusively pathway p1 for the release. DCL could also form occasional hydrogen bonds to the thiol group of Cys176, the hydroxy group of Cys176Tyr, and the backbone carbonyl of Ala172. During the passage, DCL induced opening of p1 by promoting conformational changes in aromatic side-chains lining p1. In wild-type DhaA, Phe144 was occasionally pushed to the bulk solvent to allow release of DCL out of the protein structure **(Fig 78)**. The introduction of bulky aromatic substitutions Cys176Tyr and Val245Phe significantly decreased the frequency of release of DCL through p1 **(Figs 79 and 80)**. The frequency was again increased by introducing additional aromatic substitutions Ala172Phe and Ala145Phe. The release of DCL from the variants carrying mutations Cys176Tyr and Val245Phe required the simultaneous flip of both the aromatic residues followed by a conformational change of Phe144 to form an open gate. The release of DCL through p1 in mutant 51' required successive conformational changes in the order Ala172Phe, Val245Phe, and Cys176Tyr **(Fig 81)**. Additionally, Ala145Phe in mutant 52' caused hindrance of DCL release through p1 **(Fig 82)**. This steric hindrance was characterised by repeated entry of DCL into the main tunnel and its return back to the active site during the simulations.

Exchange of water molecules through p1. p1 was used by water molecules in all variants, except mutant 51', in the presence of CL in the active site **(Fig 67a)**. The accessibility of p1 for water molecules was much lower in the absence of CL in the active site; aromatic residues introduced into the main tunnel of mutants 04, 15, 21', 27', 31', 51', and 52' prevented the exchange of water molecules through p1 within the 2-ns time scale of the MD simulations **(Fig 67b)**.

4.3.3 Pathway p2a

Description of p2a. p2a is equivalent to the slot tunnel observed in the XC structure 1BN6 of wild-type DhaA **(Fig 72a)**. p2a is defined by the β7/α9 loop (Leu246) and the β6/α4 loop [or N-terminal cap domain loop (NC loop); Arg133, Ile135, and Trp141]. p2a formed an open tunnel only during passage of DCL or water through p2a in the proteins with Ile135 (wild-type and mutant 04) or Val135 (mutant 27') **(Table 36; Figs 73b and 74)**. The accessibility of p2a was clearly controlled by the amino acid residue 135 and by flexibility of the NC loop, the most mobile element of the DhaA structure according to the XC and MD *B*-factors.

Release of DCL through p2a. p2a was accessible for DCL only in wild-type DhaA and mutant 04 **(Fig 66)**. The release of DCL through p2a **(Fig 83)** was initiated by the breakage of a hydrogen bond between DCL and Asp106, immediately followed by formation of a DCL-water-D106 interaction with DCL located in the entry to the slot tunnel. The breakage of the water-bridge interaction resulted in fast passage of DCL towards Arg133 located at the outer opening of p2a. Arg133 made strong electrostatic and van der Waals interactions with DCL **(Fig 75f)** and additionally formed an unstable salt link with Glu140 and a stable hydrogen bond with the carbonyl of Leu246. DCL could form a hydrogen bond with the side-chain of Arg133 when the salt link is naturally broken. Breakage of the salt link was, however, not essential for release of DCL to the bulk solvent.

Exchange of water molecules through p2a. p2a was rarely used by water molecules, and exchange of the solvent

occurred only in wild-type DhaA and mutant 04 in both the presence and absence of CL in the active site and in mutant 27' only in the presence of CL in the active site **(Fig 67)**. A single substitution, Ile135Phe, was sufficient to block exchange of water molecules through p2a.

4.3.4 Pathway p2b

Description of p2b. p2b corresponds to the deep surface depression near the slot tunnel opening in the XC structures of wild-type DhaA **(Fig 72abc)**. p2b is formed by the β7/α9 loop (Val245Phe and Leu246Ile) and the NC loop (Arg133, Ile/Leu/Val/Phe135, and Trp/Phe141). p2b formed a tunnel during the passage of DCL or water molecules through the pathway **(Table 36; Figs 73b and 74)**. p2b could be opened simultaneously with p1 and p2a. The accessibility of p2b was controlled by the aromatic residues Trp/Phe141 and Val245Phe as well as by the flexibility of the NC loop.

Release of DCL through p2b. Release of DCL through p2b was observed only in mutant 27' carrying the mutation Ile135Val **(Fig 66)**. The release process **(Fig 84)** started by breakage of the hydrogen bond between DCL and Asp106, followed by a DCL-water-D106 interaction and a transient hydrogen bond between DCL and the backbone carbonyl groups of Glu130 and Ile132. DCL entered p2b by inducing a simultaneous flip of the Val245Phe and Trp141 side-chains. DCL moved between the two aromatic side-chains and established a hydrogen bond to the Arg133 side-chain and the Val245Phe backbone **(Fig 75g)** without perturbation of the salt link between Arg133 and Glu140 and the hydrogen bond between Arg133 and Leu246Ile. This hydrogen-bonding network hindered the smooth release of DCL to the bulk water.

Exchange of water molecules through p2b. p2b was used by water molecules in all DhaA variants, except mutant 21', in the presence of CL in the active site **(Fig 67a)**. p2b was the only pathway for exchange of water molecules in mutant 51' and the preferred pathway in mutant 27'. p2b was always preferred over p2a, p2c, and p3. The accessibility of p2b for water molecules was significantly decreased in the absence of the CL in the active site. p2b was not used by water molecules in any variant except mutant 27' in MD simulations without CL **(Fig 67b)**.

4.3.5 Pathway p2c

Description of p2c. p2c was identified as a branch of p2a, which was not indicated by any of the XC structures of wild-type DhaA. p2c was formed by the NC loop (Arg133, Ile135, and Trp/Phe141) and the α7/α8 loop [or C-terminal cap domain loop (CC loop); Pro210 and P212]. p2c formed an open tunnel only in wild-type DhaA and mutant 21' and only in the presence of CL in the active site **(Table 36; Figs 73b and 74)**. The bulkier DCL promoted opening of p2c for a longer time during its release in RAMD simulations. The accessibility of p2c was controlled by the flexibility of the NC and CC loops and by a β-bridge interaction between Pro210 and Ala212 of the CC loop and Ile135 of the NC loop. The β-bridge must be disrupted to allow exchange of a ligand between bulk solvent and p2c.

Release of DCL through p2c. Release of DCL through p2c **(Fig 85)** was observed only in mutant 21' carrying the unique substitution Trp141Phe **(Fig 66)**. The release process started by obligatory breakage of the hydrogen bond between DCL and Asp106, followed by formation of the water bridge DCL-water-Asp106 positioning DCL near the entrance to p2a and p2c. After breakage of the water bridge, DCL moved along Trp141Phe, inducing a flip of its side-chain, disrupted the Ala212-Ile135Leu β-bridge interaction, and established a hydrogen bond with the backbone carbonyl group of Arg133. The arginine showed strong electrostatic and van der Waals attraction for DCL **(Fig 75h)**. While maintaining the hydrogen bond to Arg133, DCL reoriented its carbon chain towards the β-bridge. After release of DCL from Arg133, DCL moved between the NC loop and the CC loop, causing breakage of the Ala212–Ile135Leu β-bridge interaction followed by release of DCL to bulk water and the immediate reconstruction of the β-bridge. The loss of the hydrogen-bonding interactions between the NC loop and the CC loop during DCL release through p2c was partially compensated for by a hydrogen bond between the residues of the β-bridge and DCL.

Exchange of water molecules through p2c. p2c was rarely used for exchange of water molecules and occurred only in wild-type DhaA and mutant 04 and only in the presence of CL in the active site **(Fig 67b)**. The accessibility of the active site for water molecules through p2c was blocked by Ile135Phe, but the β-bridge could be disrupted by water molecules from bulk solvent as observed for the mutant in the presence of CL in the active site.

4.3.6 Pathway p3

Description of p3. p3 was not observable in any XC structure of wild-type DhaA. p3 was located between helix α4 (Phe149), the NC loop (Trp138 and Trp141), and the CC loop (Leu209 and Ile211). p3 was relatively short and straight compared to p2a, p2b, and p2c but was generally unfavourable for accommodation of water molecule or DCL due to

steric clashes with the protein structure. p3 formed an open tunnel only upon passage of DCL through the pathway, whereas water migrated through the protein matrix **(Table 36; Figs 71bc and 73bc)**. The open tunnel existed for the shortest period of time (on the order of picoseconds) among the pathways before its disappearance. Water in p3 moved solely through the protein matrix without formation of a tunnel **(Fig 73c)**.

Release of DCL through p3. The release of DCL through p3 occurred in wild-type DhaA and in mutant 27' **(Fig 66 and Fig 86).** After obligatory release of DCL from the nucleophile Asp106, a DCL-water-Asp106 interaction was established, and DCL was positioned between Trp141 and Phe149 **(Fig 75i)**, whose side-chains acted as a gate and flipped to open up the p3 pathway. The immediate release of DCL to the bulk solvent was blocked by the side-chain of Trp138 **(Fig 75i)**, and DCL was temporarily enclosed in an isolated cavity. DCL eventually pushed Trp138 into the bulk water and was released out of the protein. After DCL release, Trp138 made a fast flip to its original conformation to completely block p3.

Exchange of water molecules through p3. p3 served as the exchange pathway for one water molecule in mutant 21' carrying the mutation Trp141Phe and CL in the active site **(Fig 67a)**.

4.4 Structural characterisation of three mutants with modified tunnels

Klvaňa M, Pavlová M, Koudeláková T, Chaloupková R, Dvořák P, Prokop Z, Stsiapanava A, Kutý M, Kutá-Smatanová I, Dohnálek J, Kulhánek P, Wade RC & Damborský J (**2009**). Pathways and mechanisms for product release in the engineered haloalkane dehalogenases explored using classical and random acceleration molecular dynamics simulations. *J. Mol. Biol.* 392: 1339-1356.

Selection of the DhaA mutants for structure determination. Classical MD and RAMD simulations on DhaA wild-type and mutants 04, 14, 15, 21', 27', 31', 51' and 52' showed that single Ile135Phe of the mutants 14 and 15 was sufficient to seal the slot tunnel and that single Cys176Tyr of the mutants 04 and 15 changed the main tunnel from permanent to transient **(Fig 74 and Table 36)**. To provide experimental structural evidence to these computational findings, XC structures of the mutants 04 (PDB-ID 3FBW), 14 (PDB-ID 3G9X), and 15 (PDB-ID 3FWH) were determined to atomic resolution (Stsiapanava et al., unpublished results). The mutant structures were compared with the XC structures of DhaA from *Rhodococcus* sp. available in the PDB **(Newman et al., 1999)**. This analysis deciphered the effect of the substitutions located in the main tunnel (mutant 04), the slot tunnel (mutant 14), and both the main and slot tunnels (mutant 15) on the accessibility of the active site and the mechanisms of ligand exchange **(Fig 72)**.

Main tunnel in the XC structures of DhaA and its mutants. The main tunnel was open in all XC structures of DhaA variants carrying the wild-type Cys176 **(Fig 72a-d)**, while the single Cys176Tyr substitution blocked this tunnel **(Fig 72ef)**. This observation was in agreement with MD simulations showing the main tunnel to be mostly closed in mutants 04 and 15, unless it was temporarily opened by a passing ligand **(Fig 74)**. The side-chain of Tyr176 was resolved in two different conformations in the XC structure of mutant 04. The distance between oxygen atoms of 4-hydroxyphenyl groups of the two conformations is 4.1 Å, and there are most likely two distinct conformational states of this bulky residue at the mobile C-terminus of the α5 helix. Accommodation of the 4-hydroxyphenyl group of Tyr176 in the place formerly occupied by the thiol group of Cys176 results in one conformation pointing towards the active site and another placing the aromatic ring close to the carbonyl of Ala172. This observation is consistent with the gatekeeping function of Tyr176 and the observation of both conformations of Tyr176 in the MD simulations.

Slot tunnel in the XC structures of DhaA. The opening of the slot tunnel in the structure 1BN6 **(Fig 72a)** was due to the presence of different rotamers of Ile135 and Arg133 side-chains together with 0.8 Å displacement of the backbone of five residues of the NC loop (133-ArgProIleProThr-137), compared to structures 1CQW and 1BN7. This is in accordance with the important role of the highly mobile NC loop in controlling the accessibility of the slot tunnel in RAMD simulations of DCL release through the p2a pathway. The displacement of the NC loop in the structure 1BN6 could be due to the presence of an unknown ligand represented by an extensive electron density in the active site and five water molecules located at the mouth of the slot tunnel **(Newman et al., 1999)**. On the contrary, the active site of 1CQW contains only water molecules and 1BN7 contains an acetate ion. The slot tunnel in structures 1CQW and 1BN7 was represented only by an isolated cavity containing two water molecules **(Fig 72bc)**, while no crystallographic water molecules were identified in the region corresponding to the mouth of the slot tunnel.

Slot tunnel in the DhaA mutants. The NC loop of mutant 04 was resolved in a conformation similar to that in structures 1CQW and 1BN7, resulting in a closed slot tunnel. The introduction of a bulky Ile135Phe substitution further reduced accessibility of the slot tunnel of the XC structures of mutants 14 and 15 **(Fig 72df)**. The NC loop of mutants 14 and 15 aligned with the corresponding region of 1BN6, suggesting slight displacement of the loop upon

introduction of the bulky aromatic side-chain. This was in agreement with MD simulations that showed Ile135 to switch between four different conformations, whereas Phe135 adopted a single conformation similar to those observed in the XC structures of mutants 04 and 15.

Main tunnel versus slot tunnel. Based on available crystallographic data, it can be concluded that the slot tunnel belongs to a transient type of tunnel in all the studied proteins, while the main tunnel changes from being a permanent tunnel in the proteins with the wild-type cysteine in position 176 to being a transient tunnel in mutants 04 and 15 carrying tyrosine at position 176.

4.1 – 4.4 Tables and figures

Klvaňa M, Pavlová M, Prokop Z, Chaloupková R, Banáš P, Otyepka M, Wade RC, Nagata Y & Damborský J (**2009**). Redesigning dehalogenase access tunnels as a strategy for degrading an anthropogenic substrate. *Nat. Chem. Biol.* 5: 727-733.

Klvaňa M, Pavlová M, Koudeláková T, Chaloupková R, Dvořák P, Prokop Z, Stsiapanava A, Kutý M, Kutá-Smatanová I, Dohnálek J, Kulhánek P, Wade RC & Damborský J (**2009**). Pathways and mechanisms for product release in the engineered haloalkane dehalogenases explored using classical and random acceleration molecular dynamics simulations. *J. Mol. Biol.* 392: 1339-1356.

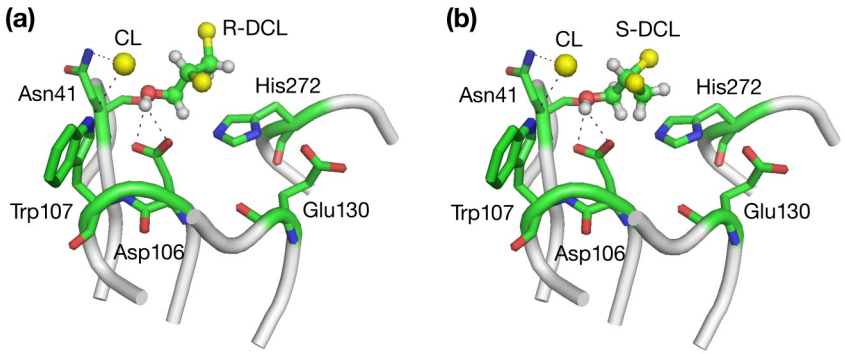

Fig 58 | Docked orientations of DCL in wild-type DhaA. **(a)** R-DCL; **(b)** S-DCL. Catalytic pentad is shown in sticks, CL is represented by a yellow sphere and DCL by balls and sticks. Dashed lines indicate hydrogen bonding interactions between DhaA and the products. All molecular graphics were created using PYMOL (**DeLano, 2002**).

Table 29 | Overview of classical MD simulations of DhaA with DCL and CL products of TCP conversion.

DhaA variant	Products	ID	Length (ns)	Average RMSD of stable part (Å)[a]	Timespan of stable RMSD (ns)	DCL release pathway	CL release pathway
wt	R-DCL and CL	c1	2.2	1.39 (±0.03)	1.60-2.20	–	p1
	S-DCL and CL	c2	2.8	1.55 (±0.03)	1.85-2.80	–	–
04	R-DCL and CL	c3	2.0	1.53 (±0.03)	1.20-2.00	–	–
	S-DCL and CL	c4	2.0	1.50 (±0.02)	1.20-2.00	–	–
14	R-DCL and CL	c5	2.0	1.33 (±0.02)	1.25-2.00	–	–
	S-DCL and CL	c6	2.0	1.43 (±0.02)	1.30-2.00	–	–
15	R-DCL and CL	c7	2.0	1.33 (±0.02)	1.45-2.00	–	p1
	S-DCL and CL	c8	2.0	1.37 (±0.03)	1.45-2.00	–	–
21'	R-DCL and CL	c9	2.0	1.29 (±0.04)	0.60-2.00	–	–
	S-DCL and CL	c10	2.0	1.57 (±0.04)	1.00-2.00	–	–
27'	R-DCL and CL	c11	2.0	1.43 (±0.02)	1.70-2.00	–	–
	S-DCL and CL	c12	2.0	1.41 (±0.03)	1.30-2.00	–	–
31'	R-DCL and CL	c13	2.0	1.44 (±0.02)	1.65-2.00	–	–
	S-DCL and CL	c14	2.0	1.47 (±0.03)	1.00-2.00	–	–
51'	R-DCL and CL	c15	2.0	1.43 (±0.03)	0.90-2.00	–	–
	S-DCL and CL	c16	2.0	1.42 (±0.03)	1.40-2.00	–	–
52'	R-DCL and CL	c17	2.0	1.58 (±0.02)	1.50-2.00	–	–
	S-DCL and CL	c18	2.0	1.67 (±0.03)	1.55-2.00	–	–

[a]Standard deviations are given in parentheses.

Table 30 | Overview of classical MD simulations of DhaA with DCL product of TCP conversion.

DhaA variant	Product	ID	Length (ns)	Average RMSD of stable part (Å)[a]	Timespan of stable RMSD (ns)	DCL release pathway
wt	R-DCL	c19	2.8	1.38 (±0.02)	1.85-2.80	–
	S-DCL	c20	2.8	1.45 (±0.02)	1.85-2.80	–
04	R-DCL	c21	2.0	1.33 (±0.03)	1.20-2.00	–
	S-DCL	c22	2.0	1.34 (±0.02)	1.20-2.00	–
14	R-DCL	c23	2.0	1.36 (±0.04)	0.90-2.00	–
	S-DCL	c24	2.0	1.31 (±0.03)	1.20-2.00	–
15	R-DCL	c25	2.0	1.34 (±0.02)	1.30-2.00	–
	S-DCL	c26	2.0	1.29 (±0.03)	1.30-2.00	–
21'	R-DCL	c27	2.0	1.29 (±0.03)	0.80-2.00	–
	S-DCL	c28	2.0	1.33 (±0.05)	0.80-2.00	–
27'	R-DCL	c29	2.0	1.34 (±0.02)	1.05-2.00	–
	S-DCL	c30	2.0	1.31 (±0.02)	1.25-2.00	–
31'	R-DCL	c31	2.0	1.35 (±0.03)	1.15-2.00	–
	S-DCL	c32	2.0	1.36 (±0.03)	1.15-2.00	–
51'	R-DCL	c33	2.0	1.59 (±0.01)	1.70-2.00	–
	S-DCL	c34	2.0	1.43 (±0.02)	1.35-2.00	–
52'	R-DCL	c35	2.0	1.37 (±0.04)	0.80-2.00	–
	S-DCL	c36	2.0	1.47 (±0.03)	0.70-2.00	–

[a]Standard deviations are given in parentheses.

Table 31 | Overview of RAMD simulations of DhaA with DCL product of TCP conversion. (pp. 123-124)

DhaA variant	Product	Starting MD snapshot (id)	ACCELERATION[a] (kcal Å^{-1} g^{-1})	THRESHOLD (Å)	ID	Length (ps)	DCL release pathway
wt	R-DCL	5178	0.04	0.002	r1	1000	–
				0.004	r2	480	p1
			0.05	0.002	r3	102	p1
				0.004	r4	60	p1
		5400	0.04	0.002	r5	1000	–
				0.004	r6	146	p1
			0.05	0.002	r7	173	p2a
				0.004	r8	143	p1
		5600	0.04	0.002	r9	572	p3
				0.004	r10	270	p1
			0.05	0.002	r11	248	p2a
				0.004	r12	99	p1
	S-DCL	5194	0.04	0.002	r13	157	p1
				0.004	r14	43	p1
			0.05	0.002	r15	185	p1
				0.004	r16	35	p1
		5398	0.04	0.002	r17	1000	–
				0.004	r18	220	p1
			0.05	0.002	r19	291	p1
				0.004	r20	135	p1
		5582	0.04	0.002	r21	141	p1
				0.004	r22	305	p1
			0.05	0.002	r23	1000	–
				0.004	r24	160	p1
04	R-DCL	4000	0.04	0.002	r25	1000	–
				0.004	r26	351	p1
			0.05	0.002	r27	69	p1
				0.004	r28	188	p1
	S-DCL	4000	0.04	0.002	r29	1000	–
				0.004	r30	1000	–
			0.05	0.002	r31	408	p2a
				0.004	r32	106	p1
14	R-DCL	4000	0.04	0.002	r33	270	p1
				0.004	r34	196	p1
			0.05	0.002	r35	252	p1
				0.004	r36	613	p1
	S-DCL	4000	0.04	0.002	r37	176	p1

DhaA variant	Product	Starting MD snapshot (id)	ACCELERATION[a] (kcal Å^{-1} g^{-1})	THRESHOLD (Å)	ID	Length (ps)	DCL release pathway
14	S-DCL	4000		0.004	r38	1000	–
			0.05	0.002	r39	1000	–
				0.004	r40	43	p1
15	R-DCL	4000	0.04	0.002	r41	1000	–
				0.004	r42	183	p1
			0.05	0.002	r43	1000	–
				0.004	r44	85	p1
	S-DCL	4000	0.04	0.002	r45	1000	–
				0.004	r46	1000	–
			0.05	0.004	r48	588	p1
21'	R-DCL	4000	0.04	0.002	r49	1000	–
				0.004	r50	356	p1
			0.05	0.002	r51	1000	–
				0.004	r52	165	p1
	S-DCL	4000	0.04	0.002	r53	140	p1
				0.004	r54	545	p2c
			0.05	0.002	r55	1000	–
				0.004	r56	232	p1
27'	R-DCL	4000	0.04	0.002	r57	230	p1
				0.004	r58	200	p2b
			0.05	0.002	r59	1000	–
				0.004	r60	155	p3
	S-DCL	4000	0.04	0.002	r61	276	p1
				0.004	r62	1000	–
			0.05	0.002	r63	1000	–
31'	R-DCL	4000	0.04	0.002	r65	1000	–
				0.004	r66	565	p1
			0.05	0.002	r67	1000	–
				0.004	r68	1000	–
	S-DCL	4000	0.04	0.002	r69	1000	–
				0.004	r70	1000	–
			0.05	0.002	r71	1000	–
				0.004	r72	1000	–
51'	R-DCL	4000	0.04	0.002	r73	148	p1
				0.004	r74	372	p1
			0.05	0.002	r75	359	p1
				0.004	r76	44	p1
	S-DCL	4000	0.04	0.002	r77	1000	–
				0.004	r78	1000	–
			0.05	0.002	r79	1000	–
				0.004	r80	485	p1
52'	R-DCL	4000	0.04	0.002	r81	1000	–
				0.004	r82	465	p1
			0.05	0.002	r83	239	p1
				0.004	r84	28	p1
	S-DCL	4000	0.04	0.002	r85	1000	–
				0.004	r86	1000	–
			0.05	0.002	r87	128	p1
				0.004	r88	273	p1

[a]REXPUDATE = 10.

Table 32 | Frequency of occurrence of DCL release in the wild-type DhaA and its mutants in RAMD simulations. (pp. 124-125)

DhaA variant	Variable amino acid residues[a]							No. of RAMD simulations	DCL release pathway					No release (%)
	176	141	135	245	246	172	146		p1[b]	p2a[c]	p2b	p2c	p3	
wt	Cys	Trp	Ile	Val	Leu	Ala	Ala	24	17	2	–	–	1	17
04	Tyr	Trp	Ile	Val	Leu	Ala	Ala	8	4	1	–	–	–	38
14	Cys	Trp	Phe	Val	Leu	Ala	Ala	8	6	–	–	–	–	25
15	Tyr	Trp	Phe	Val	Leu	Ala	Ala	7	3	–	–	–	–	57
21'	Tyr	Phe	Val	Phe	Ile	Ala	Ala	8	4	–	–	1	–	38
27'	Tyr	Trp	Leu	Phe	Ile	Ala	Ala	7	2	–	1	–	1	43

DhaA variant	Variable amino acid residues[a]							No. of RAMD simulations	DCL release pathway					No release (%)
	176	141	135	245	246	172	146		p1[b]	p2a[c]	p2b	p2c	p3	
31'	Tyr	Trp	Phe	Phe	Ile	Ala	Ala	8	1	–	–	–	–	88
51'	Tyr	Trp	Phe	Phe	Ile	Phe	Ala	8	5	–	–	–	–	38
52'	Tyr	Trp	Phe	Phe	Ile	Phe	Phe	8	5	–	–	–	–	38

[a]Mutations are highlighted in dark grey.
[b]p1 corresponds to the main tunnel.
[v]p2a corresponds to the slot tunnel.

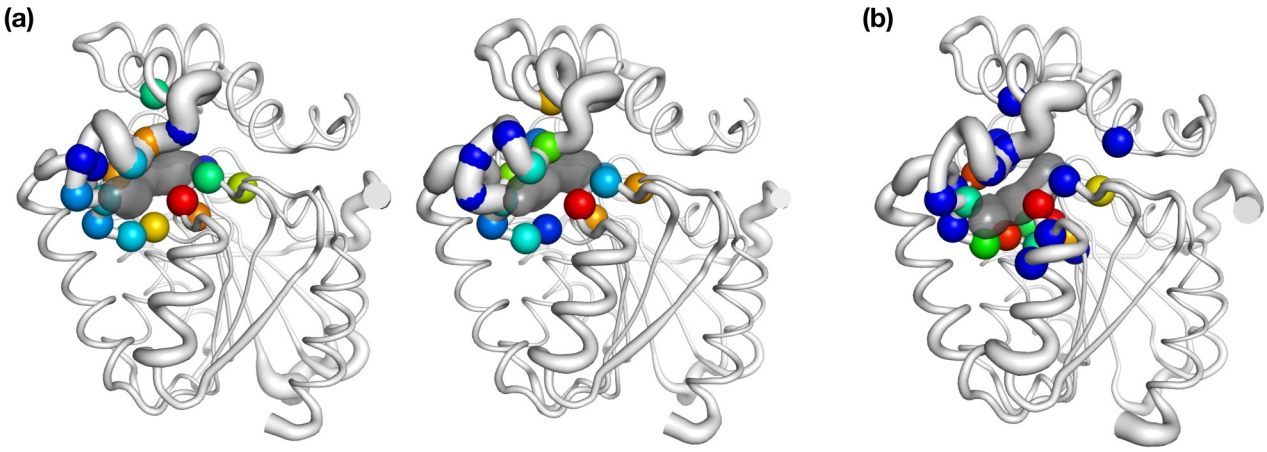

Fig 59 | Amino acid residues of the slot tunnel identified by RAMD simulations of DCL release in the wild-type DhaA and the 04 mutant. **(a)** the wild-type DhaA (trajectories *r7* and *r11*); **(b)** the mutant 04 (trajectory *r31*). DCL release pathway through the slot tunnel is shown in grey surface representation. C_α atoms of the identified amino acid residues are shown in spheres, coloured by frequency of contact with DCL during the simulations and mapped onto the starting structure of the RAMD simulations. The thickness of the ribbon corresponds to the main-chain *B*-factors for the RAMD simulations.

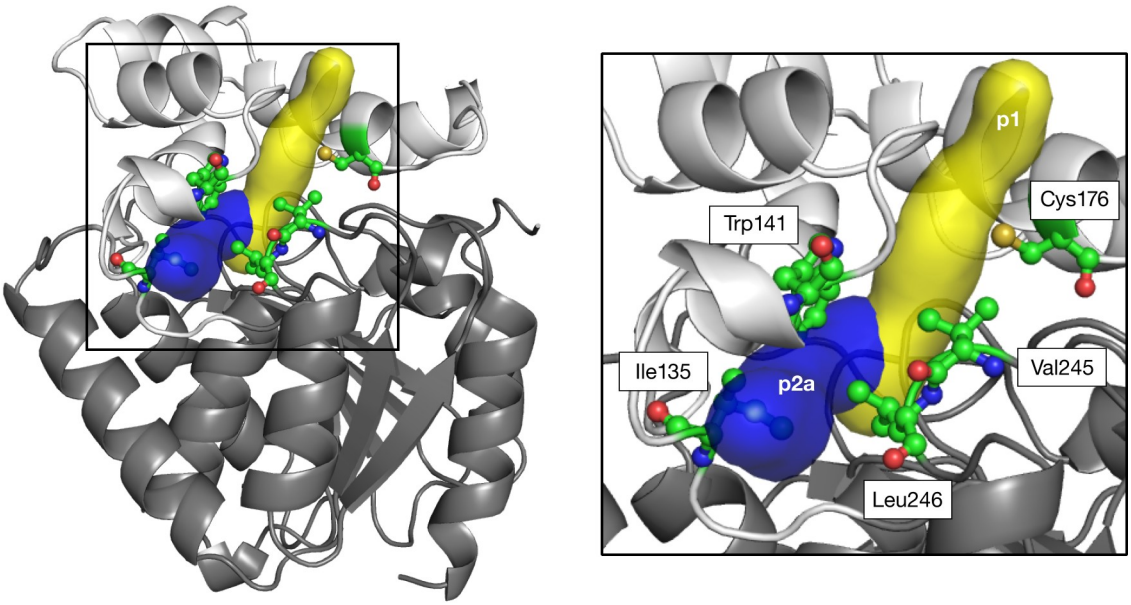

Fig 60 | Hot spot amino acid residues lining the access tunnels selected for mutagenesis by RAMD simulations of DCL release in the wild-type DhaA and the 04 mutant. The selected amino acid residues are located along DCL release pathway through the main tunnel, p1 (Cys176), the slot tunnel, p2a (Trp141, Ile135 and Leu246), or both the tunnels (Val245). DhaA wild-type is shown in cartoon model coloured by domains: grey, the main domain, white, the cap domain.

Table 33 | Variability of the hot spots among members of sub-family II haloalkane dehalogenases.

DhaA wild-type	Substitutes among subfamily II[a]
Ile135	Val, **Phe**, **Met**
Trp141	Val, **Phe**, Met, **Ser**
Val245	**Ala**, Leu, **Phe**, Ser
Leu246	**Ile**, Phe, Met

[a]bold-faced substitutes were found in experimentally characterised haloalkane dehalogenases.

Table 34 | DhaA variants obtained by screening saturation mutagenesis libraries *A* and *B* for enhanced activity towards TCP.

DhaA variant[a]	Variable amino acid residues[b]						Frequency[c]	Relative activity[e]
	176	273	141	135	245	246		
wt	Cys	Tyr	Trp	Ile	Val	Leu	-	1[f]
Templates								
M2 (Lib. A)	Tyr	Phe	Trp	Ile	Val	Leu	-	4
M3 (Lib. B)	Tyr	Phe	Phe	Ile	Val	Leu	-	5
Library *A*								
25	Tyr	Phe	Trp	Phe	Met	Leu	4	22
26	Tyr	Phe	Trp	Tyr	Phe	Ile	11	23
27[d]	Tyr	Phe	Trp	Val	Phe	Ile	1	39
28	Tyr	Phe	Trp	Tyr	Leu	Thr	1	22
29	Tyr	Phe	Trp	Phe	Ile	Leu	5	11
30	Tyr	Phe	Trp	Tyr	Met	Ile	3	13
31	Tyr	Phe	Trp	Phe	Phe	Ile	3	24
32	Tyr	Phe	Trp	Phe	Met	Ile	9	16
33	Tyr	Phe	Trp	Cys	Tyr	Leu	1	28
34	Tyr	Phe	Trp	Phe	Leu	Ile	2	17
35	Tyr	Phe	Trp	Phe	Phe	Val	2	23
36	Tyr	Phe	Trp	Phe	Cys	Leu	1	20
37	Tyr	Phe	Trp	Tyr	Ile	Leu	1	13
38	Tyr	Phe	Trp	Phe	Tyr	Ile	1	5
39	Tyr	Phe	Trp	Tyr	Met	Met	1	12
40	Tyr	Phe	Trp	Phe	Ile	Met	1	5
41	Tyr	Phe	Trp	Tyr	Met	Leu	1	16
Library *B*								
17	Tyr	Phe	Phe	Phe	Met	Ile	9	24
18	Tyr	Phe	Phe	Tyr	Phe	Ile	11	15
19	Tyr	Phe	Phe	Tyr	Met	Ile	3	26
20	Tyr	Phe	Phe	Phe	Phe	Ile	3	21
21	Tyr	Phe	Phe	Leu	Phe	Ile	1	25
22	Tyr	Phe	Phe	Ile	Phe	Ile	1	22
23	Tyr	Phe	Phe	Phe	Met	Leu	4	18
24	Tyr	Phe	Phe	Ile	Met	Leu	1	12

[a]Variants selected for detailed characterisation are underlined; wt, wild type.
[b]Mutations introduced by site-directed mutagenesis are highlighted in dark grey; mutations introduced by saturation mutagenesis are highlighted in orange.
[c]Frequency of the specific combination of mutations at positions 135, 245, and 246 among the 51 clones comprising the 25 unique variants; frequencies of the combinations found in both libraries are underlined.
[d]Variant 27 contains an additional (spontaneous) substitution Arg254Gly located at solvent exposed face of the main domain α-helix E.
[e]Specific activities of crude extracts with TCP.
[f]Specific activity of wt = 0.014 μmol s^{-1} mg^{-1} of total protein.

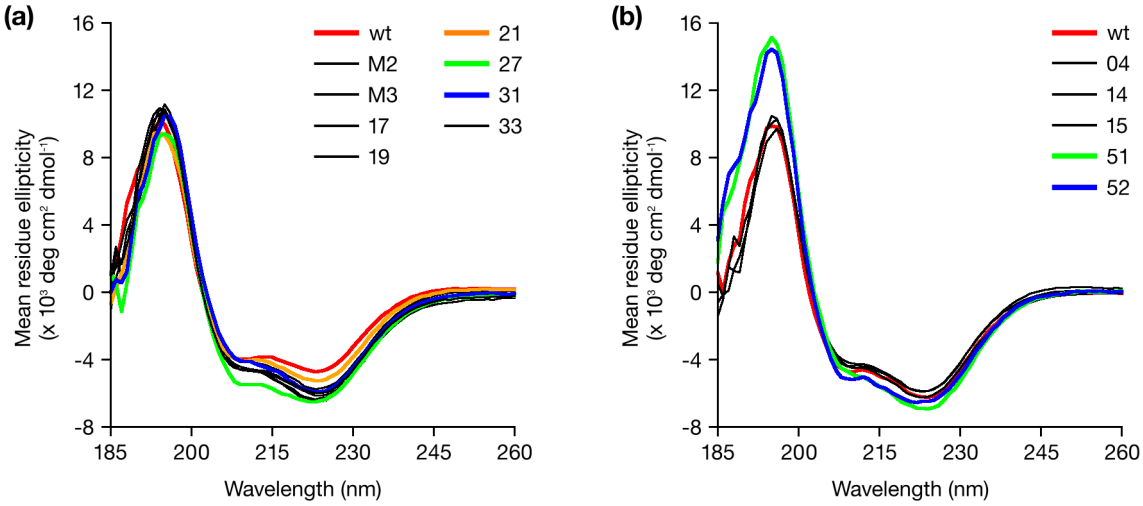

Fig 61 | Secondary structure fingerprint of DhaA variants determined by far-UV CD spectroscopy. **(a)** The far-UV CD spectra of wild-type DhaA, two templates for saturation mutagenesis, M2 and M3, and mutants obtained by saturation mutagenesis; the spectra showed two negative peaks at 208 and 222 nm, and one positive peak at 195 nm; the negative peak at 222 nm exhibited 8-35% increase in the mean residue ellipticity in the DhaA mutants compared to the wild-type DhaA. **(b)** The far-UV CD spectra of the wild-type DhaA and the mutants containing aromatic amino acid residue substitutions obtained by one or two rounds of site-directed mutagenesis of the wild-type DhaA and the mutant 31; the mutants 51 and 52 showed increased negative peak of the mean residue ellipticity at 208 and 222 nm.

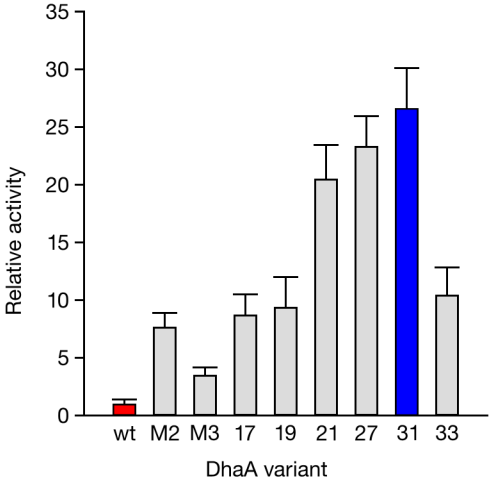

Fig 62 | Specific activities of selected DhaA variants with TCP. The specific activities were expressed as fold changes relative to the specific activity of wild-type DhaA (0.0020 ± 0.0008 μmol s^{-1} mg^{-1}).

Table 35 | Steady-state kinetic constants for TCP conversion by selected DhaA variants. (pp. 127-128)

DhaA variant	Variable amino acid residues[a]								k_{cat} (s^{-1})	K_m (mM)	k_{cat}/K_m (s^{-1} M^{-1})	Rel. k_{cat} (mt/wt)	Rel. K_m (mt/wt)	Rel. k_{cat}/K_m (mt/wt)
	176	273	141	135	245	246	172	146						
wt[a]	Cys	Tyr	Trp	Ile	Val	Leu	Ala	Ala	0.08	2.2	36	1.0	1.0	1.0
M2[a]	Tyr	Phe	Trp	Ile	Val	Leu	Ala	Ala	0.28	1.0	280	3.5	0.5	7.8
wt	Cys	Tyr	Trp	Ile	Val	Leu	Ala	Ala	0.04 ± 0.01	1.0 ± 0.2	40 ± 13	1.0	1.0	1.0
04	Tyr	Tyr	Trp	Ile	Val	Leu	Ala	Ala	0.24 ± 0.01	1.7 ± 0.1	141 ± 10	6.0	1.7	3.5
14	Cys	Tyr	Trp	Phe	Val	Leu	Ala	Ala	0.05 ± 0.02	1.5 ± 0.3	33 ± 15	1.3	1.5	0.8
15	Tyr	Tyr	Trp	Phe	Val	Leu	Ala	Ala	0.23 ± 0.01	1.8 ± 0.2	128 ± 15	5.8	1.8	3.2
M2	Tyr	Phe	Trp	Ile	Val	Leu	Ala	Ala	0.14 ± 0.04	0.9 ± 0.1	156 ± 48	3.5	0.9	3.9
M3	Tyr	Phe	Phe	Ile	Val	Leu	Ala	Ala	0.07 ± 0.01	1.0 ± 0.1	70 ± 12	1.8	1.0	1.8
21	Tyr	Phe	Phe	Val	Phe	Ile	Ala	Ala	0.55 ± 0.04	1.2 ± 0.2	458 ± 83	13.8	1.2	11.5
27	Tyr	Phe	Trp	Leu	Phe	Ile	Ala	Ala	1.02 ± 0.06	1.1 ± 0.1	927 ± 100	25.5	1.1	23.2

DhaA variant	Variable amino acid residues[a]								k_{cat} (s^{-1})	K_m (mM)	k_{cat}/K_m (s^{-1} M^{-1})	Rel. k_{cat} (mt/wt)	Rel. K_m (mt/wt)	Rel. k_{cat}/K_m (mt/wt)
	176	273	141	135	245	246	172	146						
31	Tyr	Phe	Trp	Phe	Phe	Ile	Ala	Ala	1.26 ± 0.07	1.2 ± 0.1	1,050 ± 105	31.5	1.2	26.3
51	Tyr	Phe	Trp	Phe	Phe	Ile	Phe	Ala	0.21 ± 0.02	7.1 ± 1.1	30 ± 5	5.3	7.1	0.8
52	Tyr	Phe	Trp	Phe	Phe	Ile	Phe	Phe	0.11 ± 0.01	1.7 ± 0.2	65 ± 10	2.8	1.7	1.6

Rel, relative; mt, mutant; wt, wild-type.

[a]Data reported originally by Bosma et al. **(2002)**; the s.d. for k_{cat} and K_m were ≤15% and ≤25%, respectively; kinetic constants were meausred in 50 mM $NaHCO_3$-NaOH buffer at pH 9.4 and 30 °C.

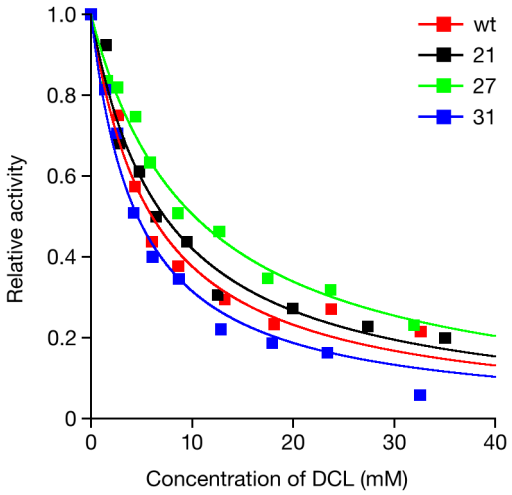

Fig 63 | Inhibition of TCP conversion by DCL product. Data were fitted to the model for competitive inhibition expressed as $a = (K_m + [S])/(K_m(1 + [I]/K_i) + [S]))$, where: a, relative activity; [S], concentration of TCP; and [I], concentration of DCL. K_i^{wt} = 2.50 ± 0.17 mM, K_i^{21} = 3.15 ± 0.20 mM, K_i^{27} = 4.42 ± 0.19 mM, K_i^{31} = 2.08 ± 0.15 mM.

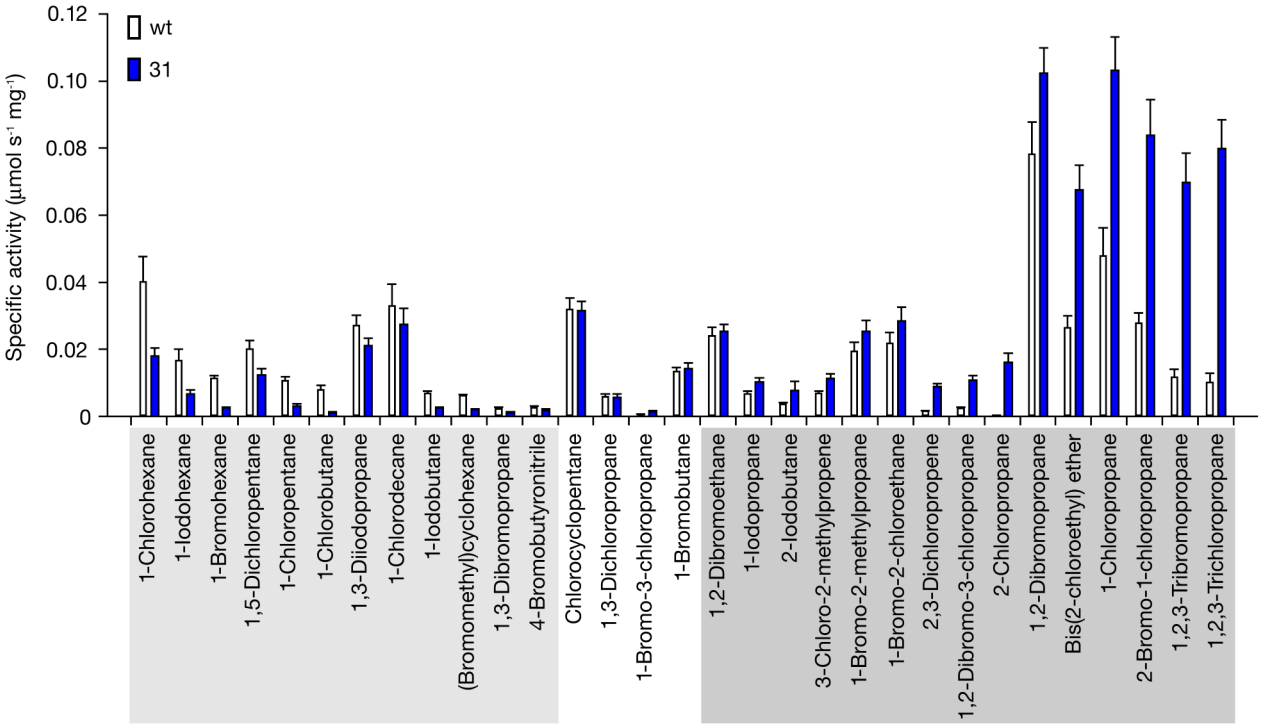

Fig 64 | Substrate specificity profiles of the wild-type (wt) DhaA and the mutant 31. The substrates are ordered by increasing 31-to-wt ratio of specific activities. Decreased and increased activities of the mutant 31 are highlighted by light and dark grey, respectively.

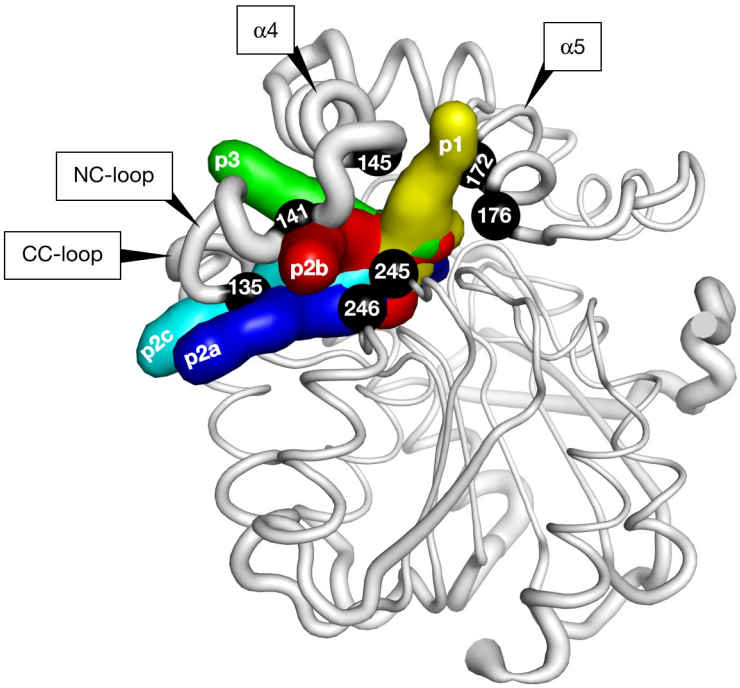

Fig 65 | DCL release pathways observed among DhaA variants. Pathways are represented by the surface and mapped on the crystal structure of DhaA from *Rhodococcus* sp. (PDB-ID 1CQW). The thickness of the ribbon corresponds to the crystallographic *B*-factors. Variable amino acid residues among the DhaA variants are represented by black balls and labeled by the residue identifier; see **Table 32** for specification of the mutations. p1 and p2a correspond to the main tunnel and the slot tunnel, respectively. NC-loop, N-terminal cap domain loop; CC-loop, C-terminal cap domain loop.

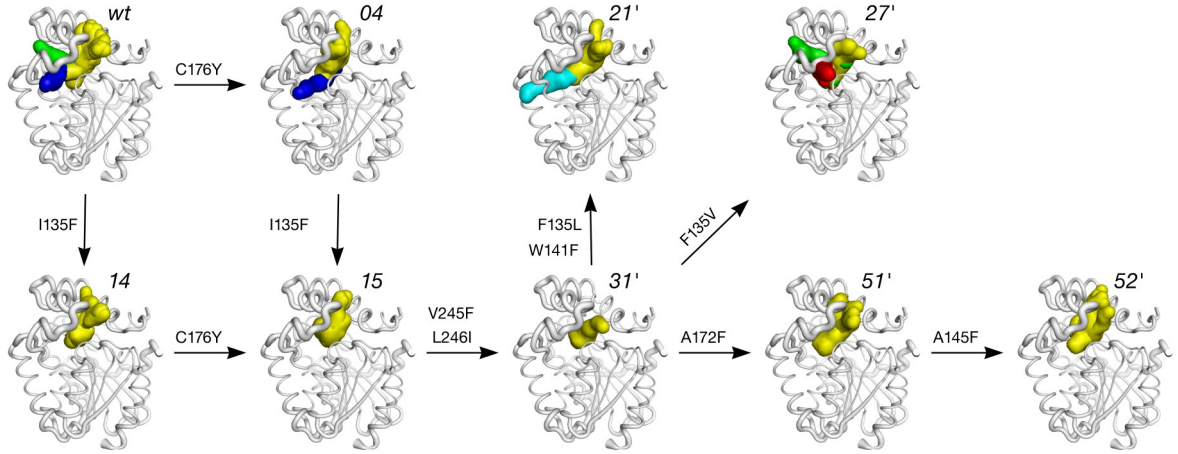

Fig 66 | Effect of mutations on the accessibility of DCL release pathways in RAMD simulations of the wild-type DhaA and its mutants. Pathways are represented by the surface and mapped on the crystal structure of DhaA from *Rhodococcus* sp. (PDB-ID 1CQW). DhaA variants are shown in ribbon; the pathways are coloured as follows: p1, yellow; p2a, blue; p2b, red; p2c, cyan; p3, green.

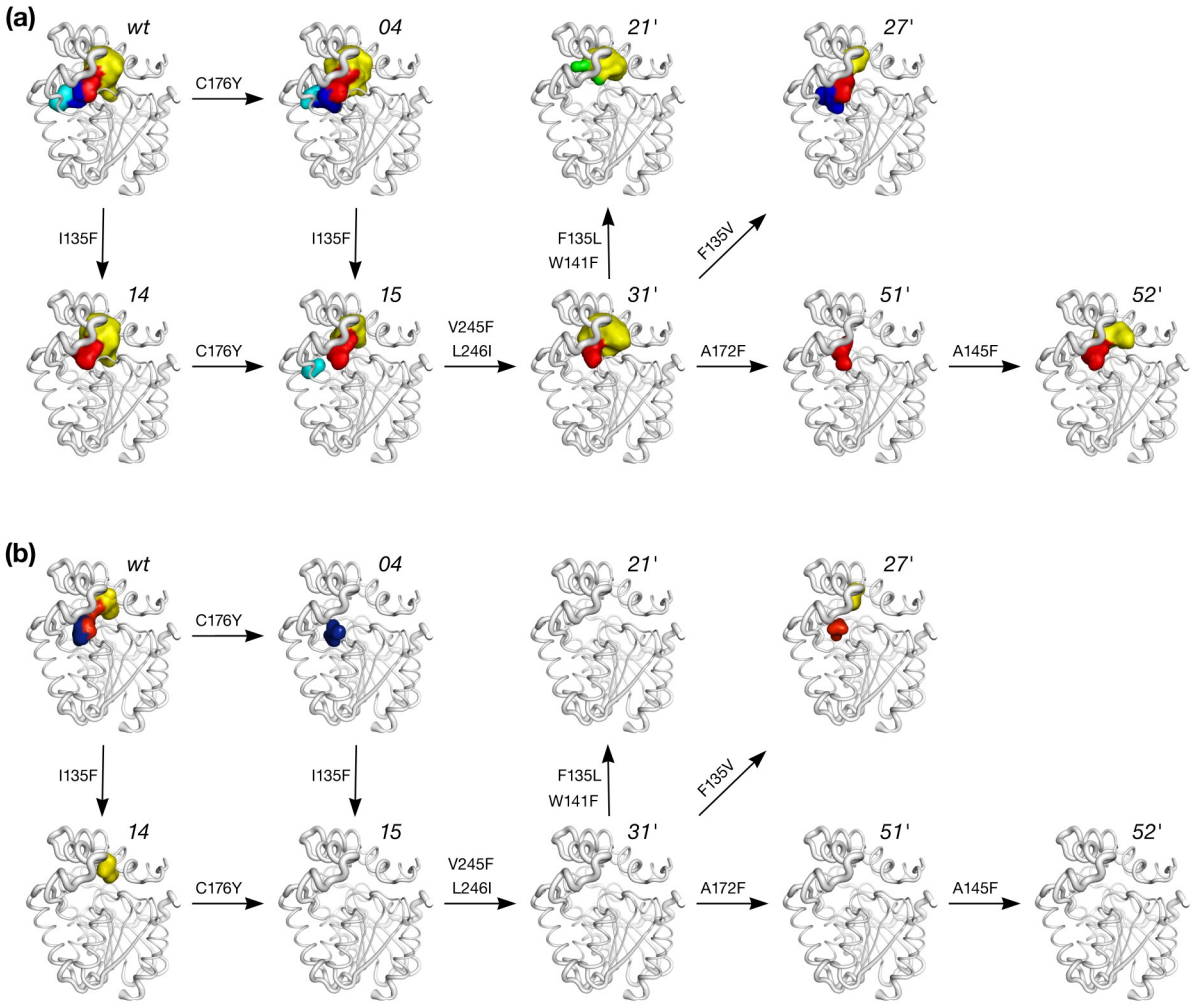

Fig 67 | Effect of mutations and CL on the accessibility of water exchange pathways in classical MD simulations of the wild-type DhaA and its mutants with products of TCP conversion. **(a)** DhaA variants with DCL and CL in the active site; **(b)** DhaA variants with DCL in the active site. Pathways are represented by the surface and mapped on the XC structure of DhaA from *Rhodococcus* sp. (PDB-ID 1CQW). DhaA variants are shown in ribbon; the water exchange pathways are coloured as follows: p1, yellow; p2a, blue; p2b, red; p2c, cyan; p3, green.

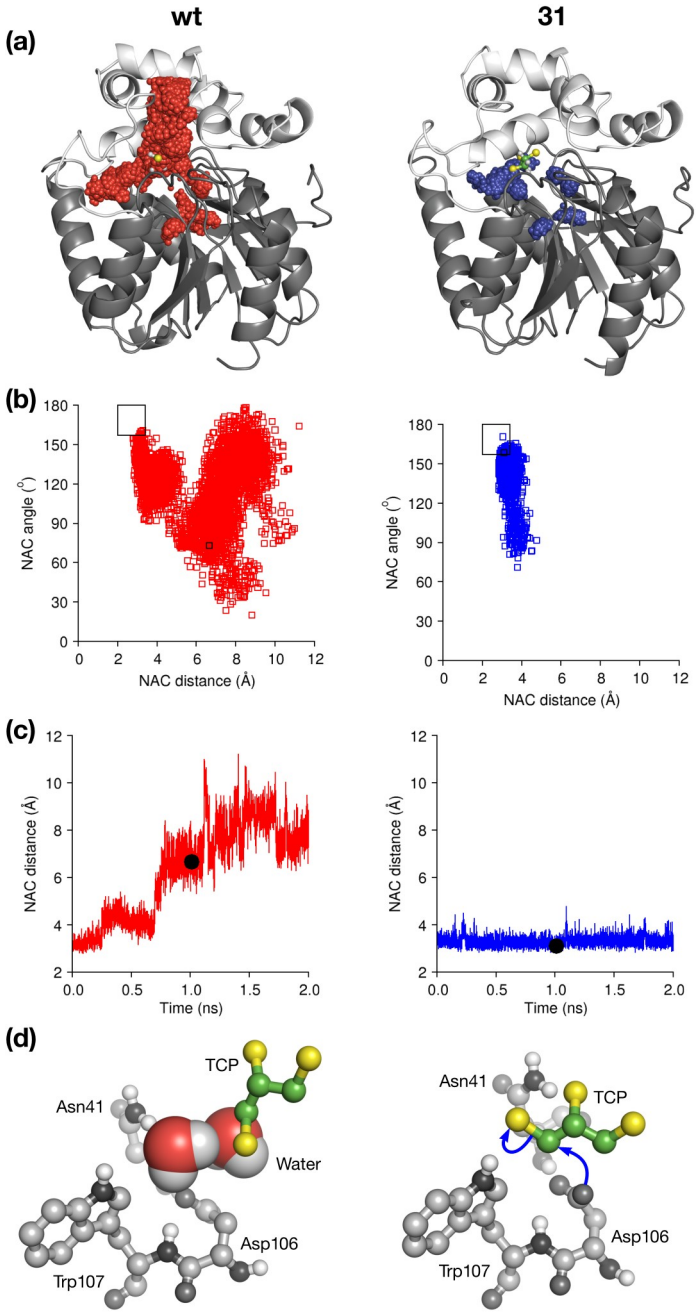

Fig 68 | Role of active site accessibility for bulk water molecules in the wild-type DhaA and the mutant 31' on formation of reactive complexes with TCP in classical MD simulations. **(a)** Active site accessibility for bulk water; the active site of the wild-type DhaA is accessible to bulk water (red); the cavity of the 31' mutant is inaccessible, and only discrete internal positions are occupied by structural water molecules (blue), also present in the wild type DhaA; spheres representing waters have a radius of 0.5 Å centred on the oxygen atoms. **(b)** The population of NAC (boxed) for TCP in the wild-type DhaA (red) and the mutant 31' (blue) in the MD simulations; snapshots shown in *d* are indicated by (□). **(c)** Evolution of the NAC distance of two reacting atoms during MD simulations; snapshots shown in *d* are indicated by (●). **(d)** Snapshots from MD simulations of the non-reactive configuration of TCP competing with water molecules for the nucleophile in the wild-type DhaA and the NAC for TCP in the 31' mutant; only polar hydrogens are shown for clarity.

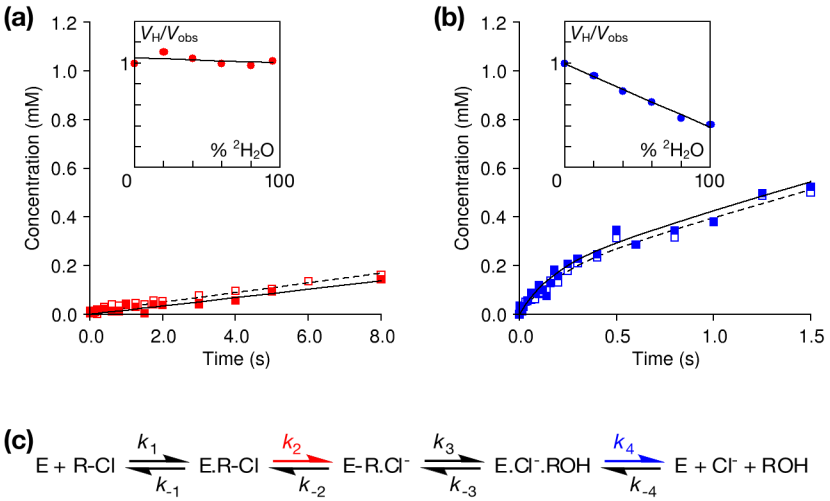

Fig 69 | The rate-limiting steps for conversion of TCP by the wild-type DhaA and mutant 31 identified by ^2H_2O kinetic isotope effect and pre-steady state kinetics. **(a)** The wild-type DhaA; **(b)** the mutant 31; **(c)** reaction scheme. Solid and dashed lines in *a* and *b* represent the best fits to the chloride ion (■) and DCL (□) kinetic data. The insets in *a* and *b* illustrate ^2H_2O kinetic isotope effect on the dehalogenase activity: the ratio between the activity in ^1H_2O (V_H) and in ^2H_2O (V_{obs}) was plotted versus various $^1H_2O/^2H_2O$ ratios; the ^2H_2O kinetic isotope effect data for the wild-type DhaA are from a previous study **(Bosma et al., 2003)**. The reaction scheme in *c* shows rate-limiting steps for the reactions catalysed by the wild-type DhaA (red) and the 31 mutant (blue); E, free enzyme; R-Cl, substrate; E.R-Cl, enzyme-substrate complex; E-R.Cl$^-$, alkyl-enzyme intermediate; E.Cl$^-$.ROH, enzyme-product complex; Cl$^-$ and ROH, products.

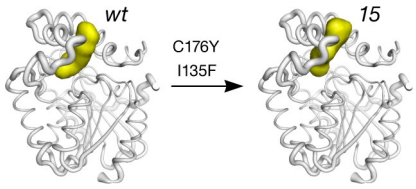

Fig 70 | No effect of single Cys176Tyr in the main tunnel on the accessibility of p1 release pathway for CL in classical MD simulations of the wild-type DhaA and its mutants. The CL release was observed only in the wild-type DhaA and the mutant 15, and only through via p1 pathway through the main tunnel. The pathways are represented by yellow surface and mapped on the XC structure of DhaA from *Rhodococcus* sp. (PDB-ID 1CQW).

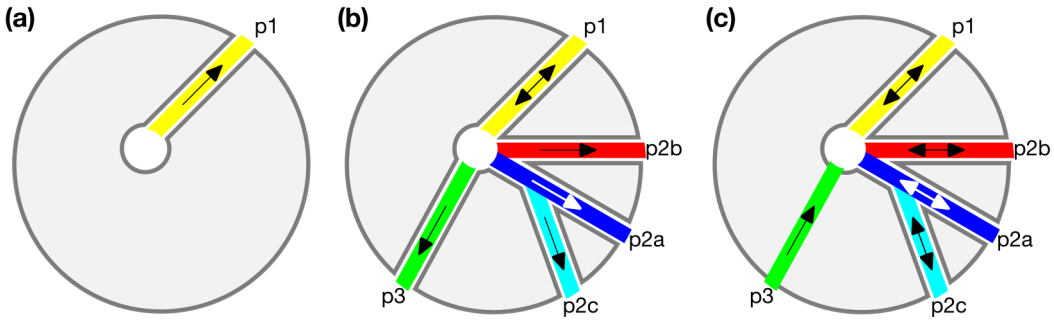

Fig 71 | Schematic representation of ligand pathways among DhaA variants. **(a)** Pathway for CL observed in classical MD simulations; **(b)** pathways for DCL observed in RAMD simulations; **(c)** pathways for water molecules observed in classical MD simulations. Arrows indicate direction of passage of ligands through a tunnel (p1, p2a, p2b and p2c for DCL and water, and p3 for DCL) or protein matrix (p3 for water); p1, the main tunnel; p2a, the slot tunnel.

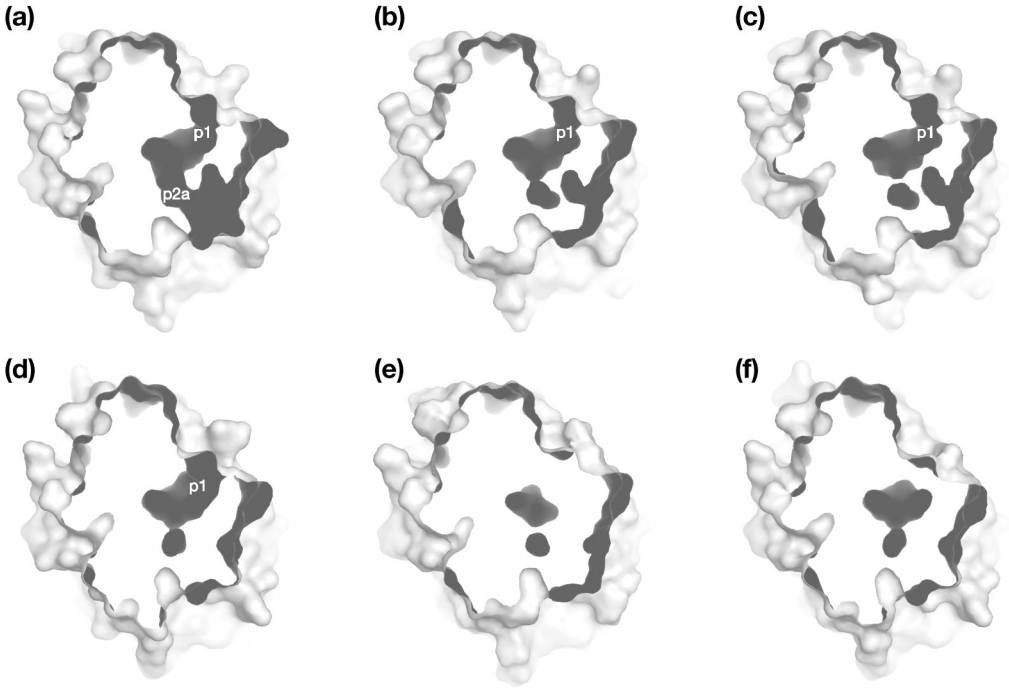

Fig 72 | The XC structures of DhaA and its mutants ordered by the accessibility of their active sites via the main tunnel and the slot tunnel. **(a)** DhaA from *Rhodococcus* sp. (PDB-ID 1BN6) with the main tunnel and the slot tunnel open; **(b-d)** DhaA from *Rhodococcus* sp. (PDB-ID 1CQW), DhaA from *Rhodococcus* sp. (PDB-ID 1BN7) and mutant 14 of the wild-type DhaA from *Rhodococcus rhodochrous* NCIMB 13064 (PDB-ID 3G9X) with the main tunnel open and the slot tunnel closed; **(e-f)** mutant 04 of the wild-type DhaA from *Rhodococcus rhodochrous* NCIMB 13064 (PDB-ID 3FBW) and mutant 15 of the wild-type DhaA from *Rhodococcus rhodochrous* NCIMB 13064 (PDB-ID 3FWH) with both the main tunnel and the slot tunnel closed. The protein structures are visualised as a slice through the surface representation with tunnels and cavities coloured in dark grey. p1, the main tunnel; p2a, the slot tunnel.

Table 36 | Occurrence of mechanisms of ligand exchange between the buried active site and bulk solvent in the wild-type (wt) DhaA and eight mutants in MD simulations.

Ligand	Pathway	Tunnel		Protein
		Permanent	Transient	matrix
Classical MD				
CL	p1	wt	15	–
	p2a	–	–	–
	p2b	–	–	–
	p2c	–	–	–
	p3	–	–	–
Water	p1	wt, 14	04, 15, 21', 27', 31', 52'	–
	p2a	–	04, 27'	–
	p2b	–	wt, 04, 14, 15, 27', 31', 51', 52'	–
	p2c	–	04	–
	p3	–	–	21'
RAMD				
DCL	p1	wt, 14	04, 15, 21', 27', 31', 51', 52'	–
	p2a	–	wt, 04	–
	p2b	–	27'	–
	p2c	–	21'	–
	p3	–	wt, 27'	–

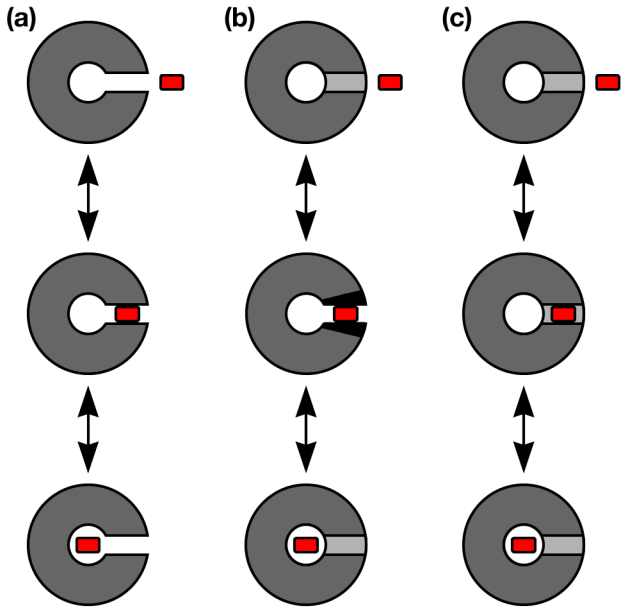

Fig 73 | Schematic representation for three mechanisms of ligand exchange between the buried active site of DhaA and bulk solvent. **(a)** Ligand passage through a permanent tunnel; **(b)** ligand passage through a transient tunnel; **(c)** ligand passage through a protein matrix. Protein and ligand are depicted in grey and red, respectively. Low-density region of the protein matrix is in light grey.

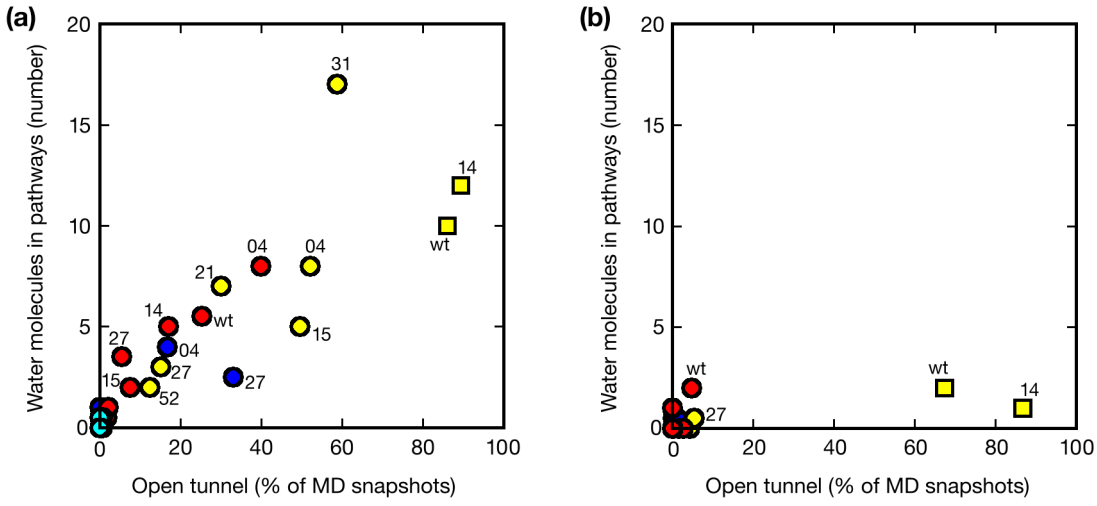

Fig 74 | The effect of mutations and CL on the opening and solvent accessibility of permanent and transient tunnels in classical MD simulations of the wild-type DhaA and its mutants. **(a)** DhaA variants complexed with DCL and CL; **(b)** DhaA variants complexed with DCL. Each value represents the average from two independent simulations. Colour coding of the pathways: p1, yellow; p2a, blue; p2b, red; p2c, cyan.

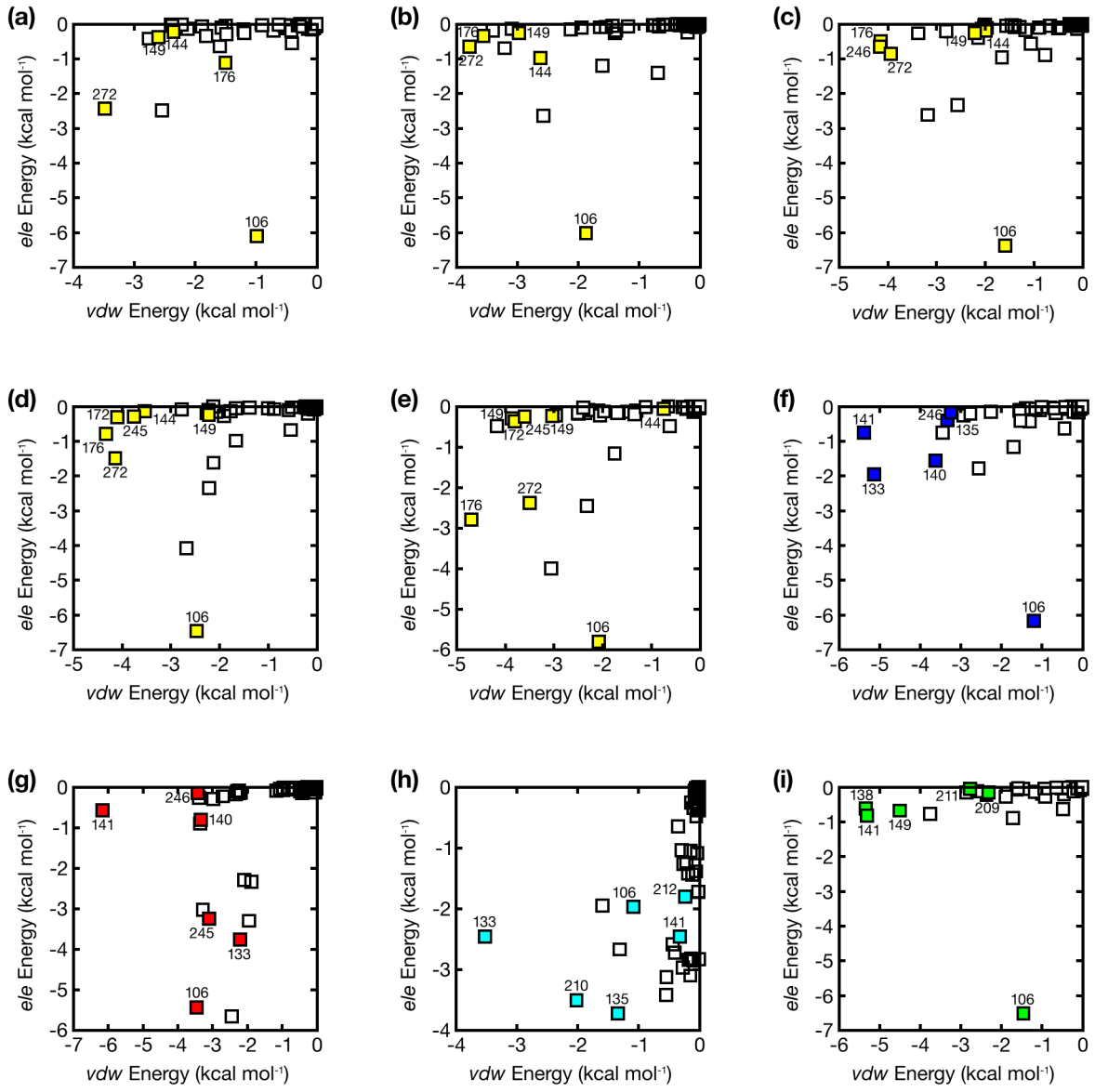

Fig 75 | Selected attractive electrostatic (*ele*) and van der Waals (*vdw*) interactions between DCL and protein residues during release of DCL through different pathways. **(a)** p1 in the wild-type DhaA (trajectory *r9*); **(b)** p1 in the 04 mutant (trajectory *r26*); **(c)** p1 in the 31' mutant (trajectory *r66*); **(d)** p1 in the 51' mutant (trajectory *r74*); **(e)** p1 in the 52' mutant (trajectory *r82*); **(f)** p2a in the wild-type DhaA (trajectory *r11*); **(g)** p2b in the 27' mutant (trajectory *r58*); **(h)** p2c in the 21' mutant (trajectory *r54*); **(i)** p3 in the wild-type DhaA (trajectory *r9*). The most important residues of the release pathways are annotated by residue identifier and colour coded: p1, yellow; p2a, blue; p2b, red; p2c, cyan; p3, green.

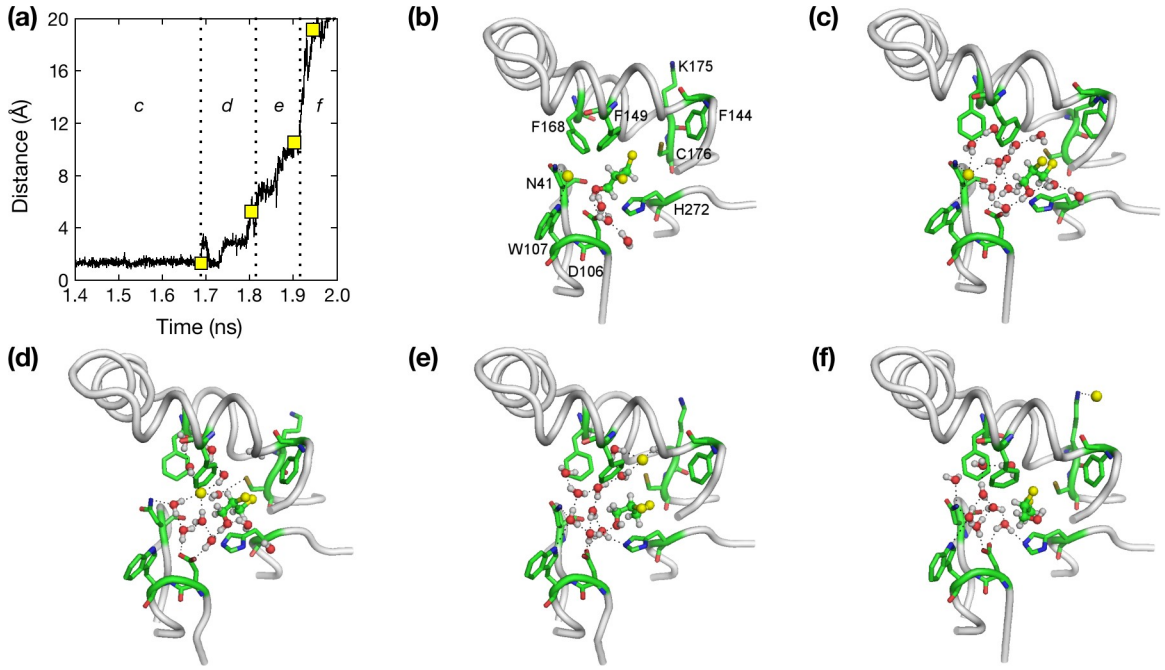

Fig 76 | Release of CL through p1 in the wild-type DhaA. **(a)** Distance of the CL from the halide-stabilising residues Asn41 and Trp107 during classical MD simulation (trajectory *c1*); representative snapshots are indicated by squares and depicted (*b-f*): **(b)** the initial state (at time = 0 ns); **(c)** solvation of the active site; (**d**) release of the CL from the halide-stabilising residues; (**e**) movement of the CL through p1 towards Cys176; (**e**) release of the CL and water molecules to the bulk solvent; **(f)** transient interaction between the CL and Lys175 during the final stage of the CL release to the bulk solvent.

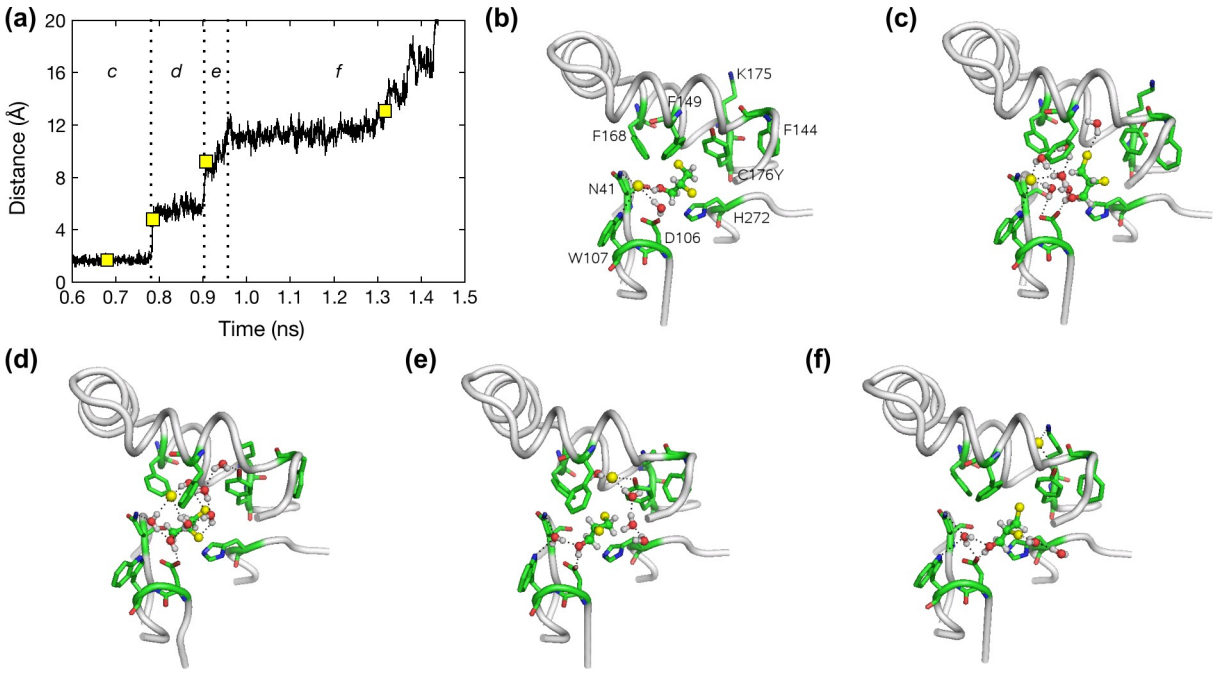

Fig 77 | Release of CL through p1 in the 15 mutant. **(a)** Distance of the CL from the halide-stabilising residues Asn41 and Trp107 during classical MD simulation (trajectory *c7*); representative snapshots are indicated by squares and depicted (*b-f*): **(b)** the initial state (at time = 0 ns); **(c)** solvation of the active site; (**d**) release of the CL from the halide-stabilising residues; (**e**) movement of the CL through p1 towards Cys176; (**e**) release of the CL and water molecules to the bulk solvent; **(f)** transient interaction between the CL, Cys176Tyr and Lys175 during the final stage of the CL release to the bulk solvent.

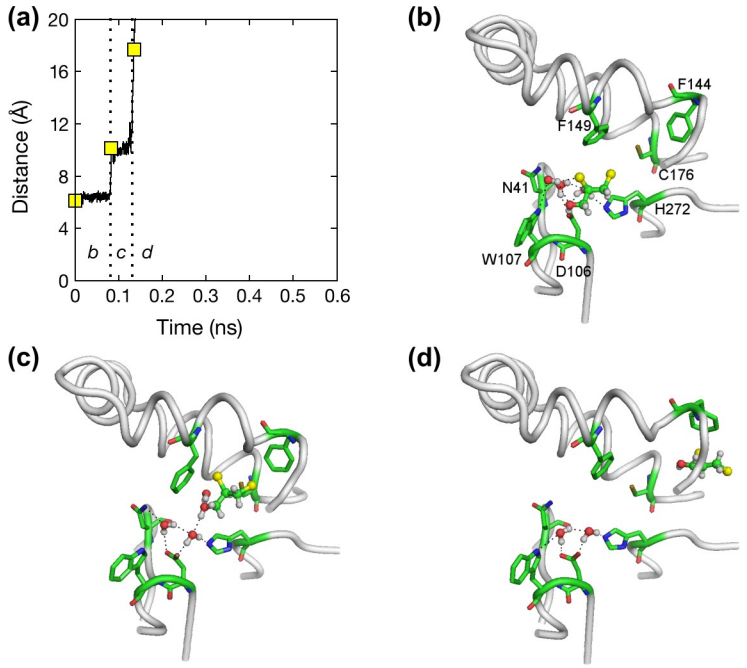

Fig 78 | Release of DCL through p1 in the wild-type DhaA. **(a)** Distance of the DCL from the the nucleophile Asp106 during RAMD simulation (trajectory *r9*); representative snapshots are indicated by squares and depicted *(b-d)*: **(b)** DCL-Asp106 hydrogen bonding interaction; **(c)** DCL-water-Asp106 interaction; **(d)** release of the DCL through p1 allowed by transient conformational change of Phe144 side-chain.

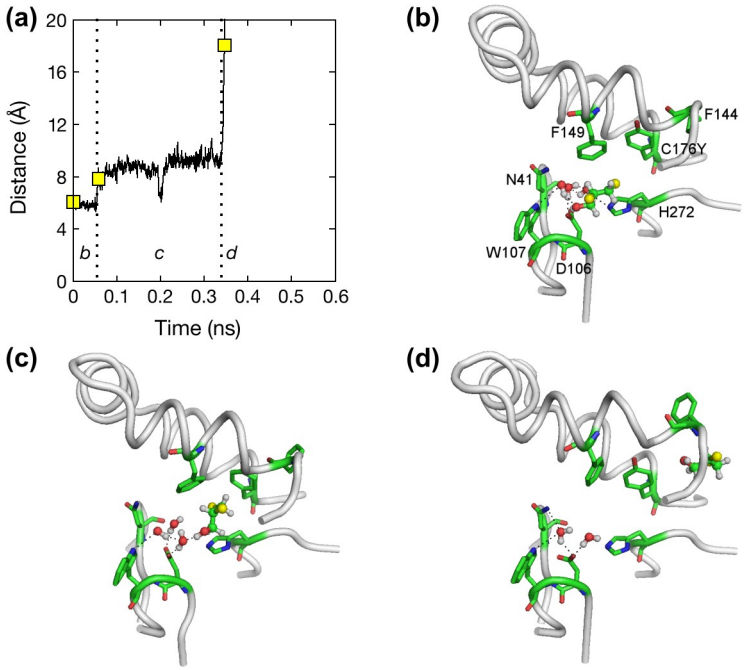

Fig 79 | Release of DCL through p1 in the 04 mutant. **(a)** Distance of the DCL from the the nucleophile Asp106 during RAMD simulation (trajectory *r26*); representative snapshots are indicated by squares and depicted (*b-d*): **(b)** DCL-Asp106 hydrogen bonding interaction; (**c**) DCL-water-Asp106 interaction; **(d)** release of the DCL through p1 allowed by transient conformational change of Cys176Tyr and Phe144 side-chains.

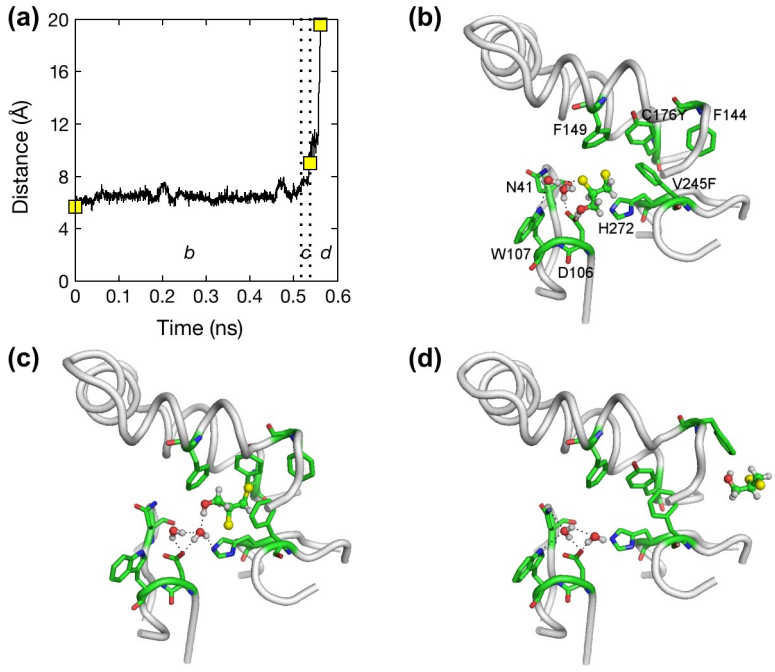

Fig 80 | Release of DCL through p1 in the 31' mutant. **(a)** Distance of the DCL from the the nucleophile Asp106 during RAMD simulation (trajectory *r66*); representative snapshots are indicated by squares and depicted (*b-d*): **(b)** DCL-Asp106 hydrogen bonding interaction; (**c**) DCL-water-Asp106 interaction; **(d)** release of the DCL through p1 allowed by transient conformational change of Val245Phe and Phe144 side-chains.

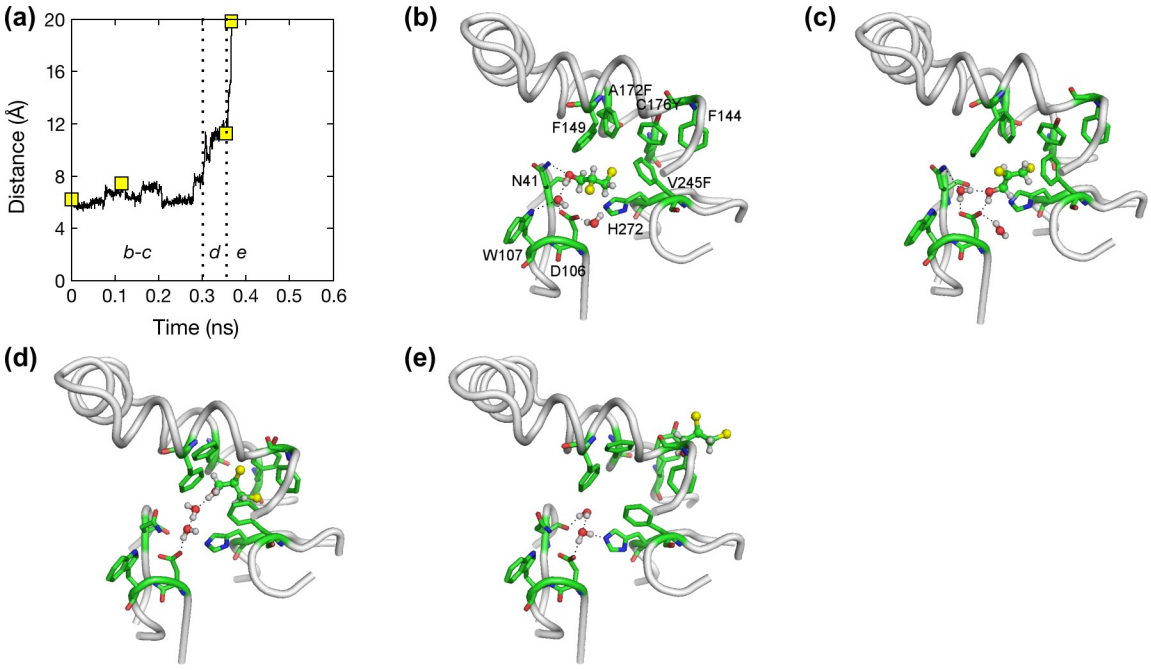

Fig 81 | Release of DCL through p1 in the 51' mutant. **(a)** Distance of the DCL from the the nucleophile Asp106 during RAMD simulation (trajectory *r74*); representative snapshots are indicated by squares and depicted (*b-d*): **(b)** DCL-Asp106 hydrogen bonding interaction; (**c**) DCL-water-Asp106 interaction; **(d)** movement of the DCL through p1 allowed by conformational change of Ala172Phe followed by conformational change of Val245Phe and Cys176Tyr; **(e)** release of the DCL to the bulk solvent allowed by transient conformational change of Phe144 side-chain.

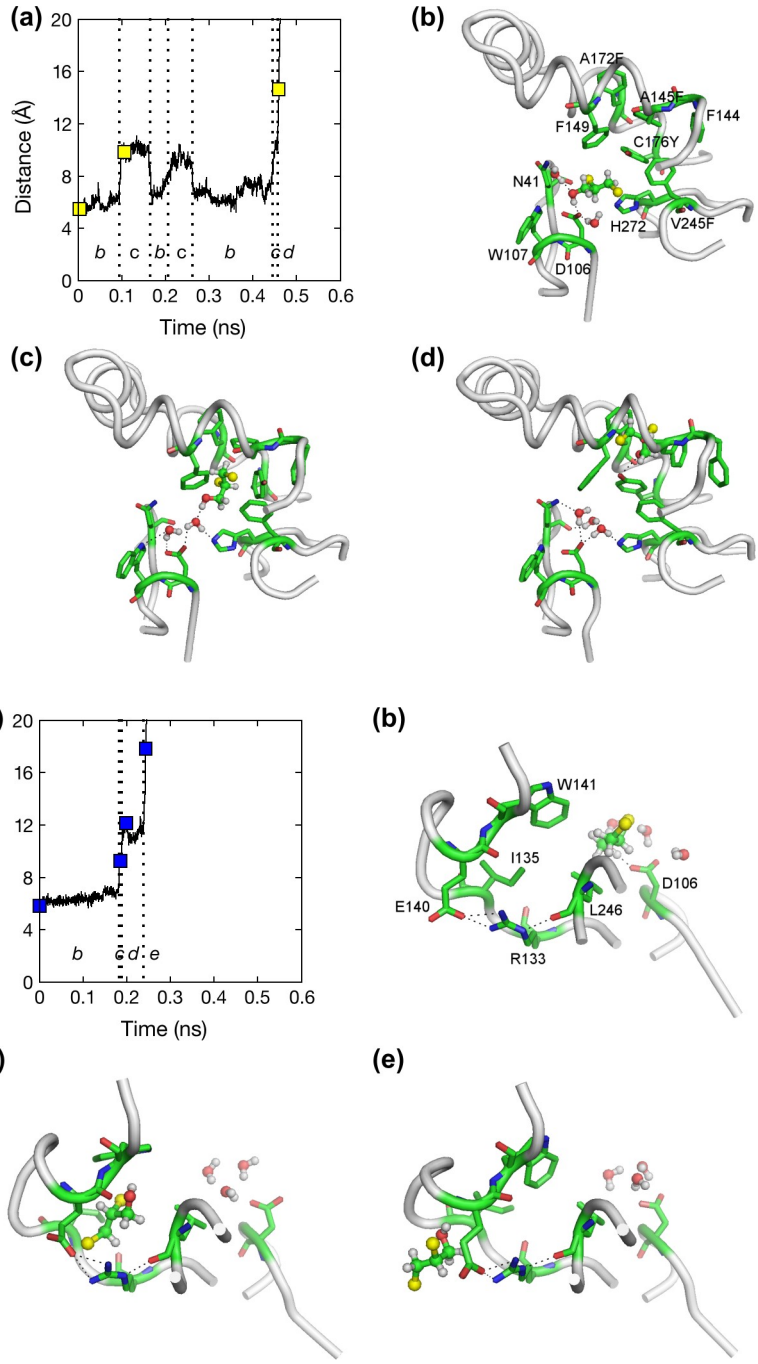

Fig 82 | Release of DCL through p1 in the 52' mutant. **(a)** Distance of the DCL from the the nucleophile Asp106 during RAMD simulation (trajectory *r82*); representative snapshots are indicated by squares and depicted (*b-d*): **(b)** DCL-Asp106 hydrogen bonding interaction; (**c**) DCL-water-Asp106 interaction and consecutive conformational change of aromatic side-chains of p1; **(d)** release of the DCL through p1 along Ala172Phe flipped to the bulk solvent due to interaction with Ala145Phe.

Fig 83 | Release of DCL through p2a in the wild-type DhaA. **(a)** Distance of the DCL from the the nucleophile Asp106 during RAMD simulation (trajectory *r11*); representative snapshots are indicated by squares and depicted (*b-e*): **(b)** DCL-Asp106 hydrogen bonding interaction; (**c**) DCL-water-Asp106 interaction; **(d)** fast movement of the DCL towards Arg133; **(e)** release of the DCL to the bulk solvent without perturbation of Arg133-Glu140 salt link.

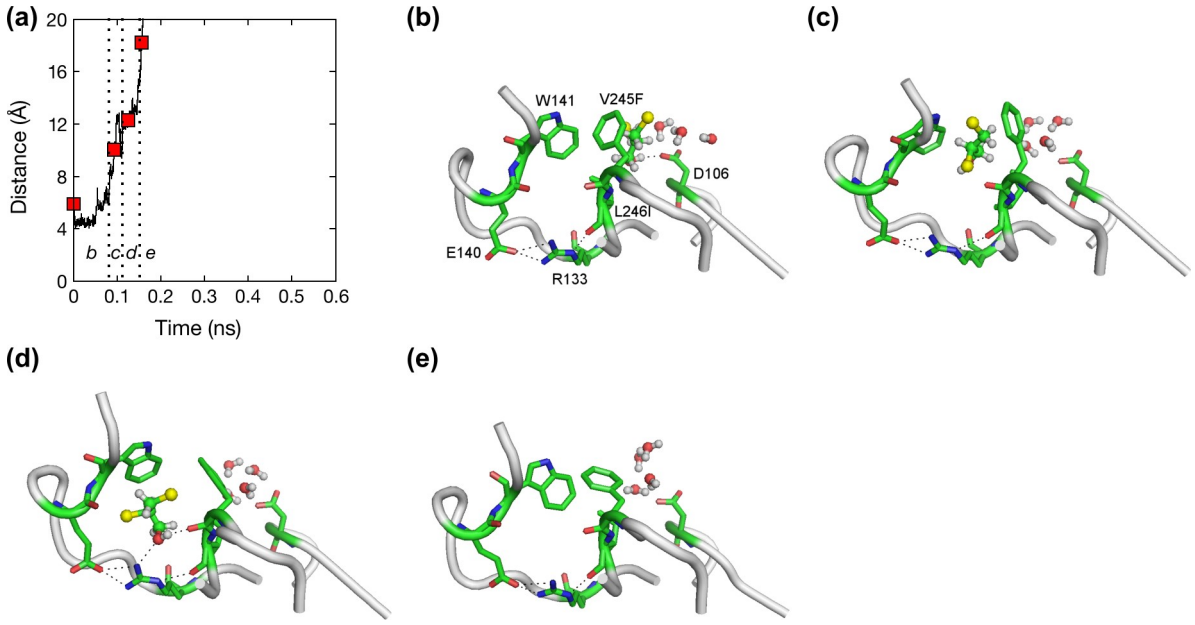

Fig 84 | Release of DCL through p2b in the 27' mutant. **(a)** Distance of the DCL from the the nucleophile Asp106 during RAMD simulation (trajectory *r58*); representative snapshots are indicated by squares and depicted (*b-e*): **(b)** DCL-Asp106 hydrogen bonding interaction; **(c)** DCL-water-Asp106 interaction and progressive conformational change of Trp141 and Val245Phe side-chains; **(d)** Arg133-DCL-Val245Phe hydrogen bonding interactions; **(e)** release of the DCL to the bulk solvent and flip of Trp141 and Val245Phe side-chains to original conformations.

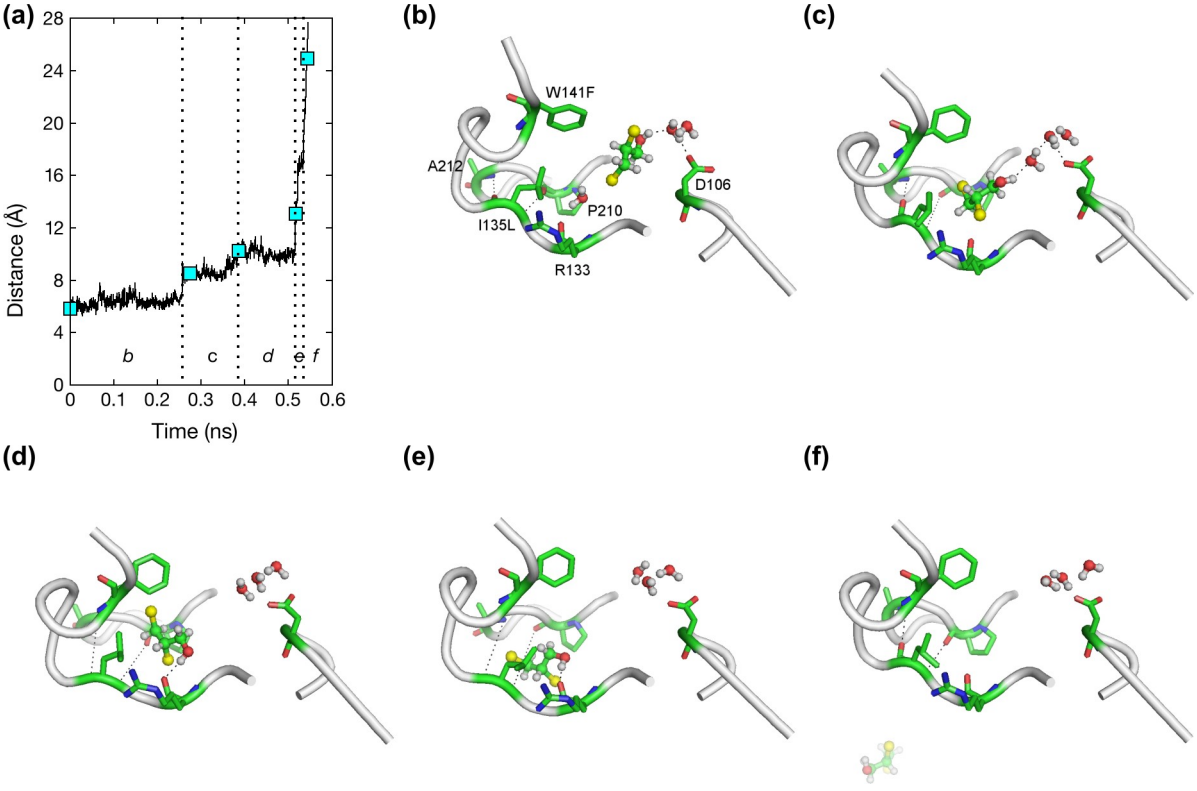

Fig 85 | Release of DCL through p2c in the 21' mutant. **(a)** Distance of the DCL from the the nucleophile Asp106 during RAMD simulation (trajectory *r54*); representative snapshots are indicated by squares and depicted (*b-f*): **(b)** DCL-Asp106 hydrogen bonding interaction; **(c)** DCL-water-Asp106 interaction and perturbation of Pro210-Ile135Leu part of a β-bridge; **(d)** DCL-Arg133 hydrogen bond and perturbation of Ala212-Ile135Leu part of the β-bridge; **(e)** release of the DCL to the bulk solvent through the region of the original β-bridge; **(f)** reconstruction of the β-bridge immediately after the release of the DCL.

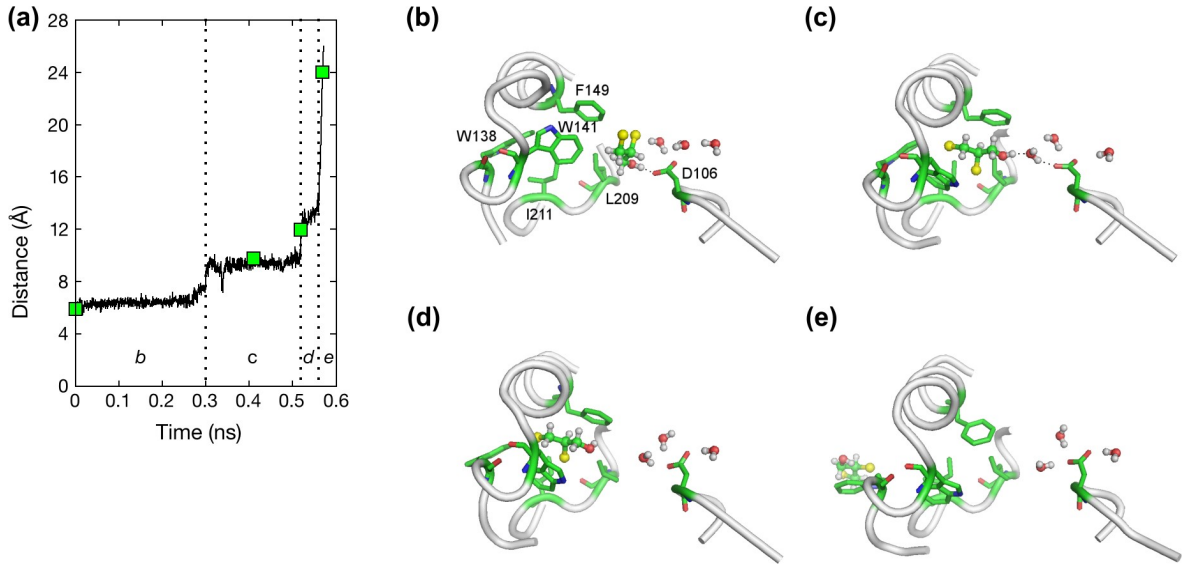

Fig 86 | Release of DCL through p3 in the wild-type DhaA. **(a)** Distance of the DCL from the the nucleophile Asp106 during RAMD simulation (trajectory *r9*); representative snapshots are indicated by squares and depicted (*b-e*): **(b)** DCL-Asp106 hydrogen bonding interaction; (**c**) DCL-water-Asp106 interaction and conformational change of Trp141 and Phe149 side-chains; (**d**) movement of the DCL between Trp141 and Phe149 side-chains, release of the DCL to the bulk solvent blocked by Trp138; **(e)** release of the DCL to the bulk solvent allowed by transient flip of Trp138 side-chain to the bulk solvent.

4.5 Development of CAVER 2.0 program for calculation of tunnels in protein structures

Andres F, Beneš P, Brezovský J, Chovancová E, Jaša P, **Klvaňa M,** Kozlíková B, Medek P, Pavelka A, Szabó T, Zamborský M, Zruban M *(in alphabetical order)*, Sochor J & Damborský J (**2009**). CAVER 2.0 tunnel calculation program. Human Computer Interaction Laboratory and Loschmidt Laboratories *(in alphabetical order)*, Masaryk University, Brno, Czech Republic. http://www.loschmidt.chemi.muni.cz/caver

CAVER 2.0 tunnel calculation program. CAVER 2.0 provides rapid, accurate, automated calculation of tunnels leading from buried cavities to the surface in the structural models of proteins, nucleic acids and inorganic materials.

Finding a tunnel using CAVER 2.0 algorithm. CAVER 2.0 treats atoms as spheres with diameter equal to the van der Waals radii according to the 1999 AMBER force field **(Wang et al., 2000)**. The Voronoi diagram for a set of atom centres is computed starting from a user-defined buried cavity. Voronoi edges and vertices are converted to a weighted graph using Delaunay triangulation. The weighted graph is processed by the modified Dijkstra's algorithm. The search starts in the graph node which is closest to the cavity specified by user. The modified Dijkstra's algorithm computes the widest tunnel with minimal length. The mouth of the tunnel is blocked and the computation is repeated if more than one tunnel needs to be identified **(Fig 87)**. Details of the computational procedure were described by Medek and co-workers **(Medek et al., 2007)**.

Implementations of CAVER 2.0 algorithm. CAVER 2.0 algorithm can be run online using CAVER Viewer GUI Java Web Start application at http://loschmidt.chemi.muni.cz/caver/index.php?page=OnlineCAVER, and as a plugin for PYMOL, available after cost free registration at http://loschmidt.chemi.muni.cz/caver/index.php?page=Download. CAVER Viewer enables visualisation of tunnel in spheres representation, and additionally provides a novel “fire spire” model that shows the actual shape of the tunnel more accurately and highlights mutual circumfluence of neighbouring tunnels **(Fig 88)**. Details of the development of the CAVER Viewer GUI application were described by Kozlíková and co-workers **(Kozlíková et al., 2007)**. The advantage of using the plugin form of CAVER 2.0 is more graphically advanced and bug-free PYMOL program; CAVER Viewer is still at the early stage of a rather bustling development.

Demonstration of CAVER 2.0 functionality. Reliability of tunnels identified by temporary versions of CAVER 2.0 tunnel calculation algorithm was tested repeatedly against the set of protein structures comprising snapshots of MD simulations of wild-type DhaA and eight mutants **(Table 29 and Fig 89)**. Although open tunnels can be easily identified by visual inspection of surface models of the protein structures e.g. in PYMOL, CAVER 2.0 brings several

benefits: (i) precision in finding tunnels differing in openings to the surface **(Fig 89a-c)**; (ii) automation; (iii) speed, enabling processing of large set of structures in short time; (iii) identification of atoms and amino acid residues lining the tunnel; (iv) determination of tunnel width at discrete points along the tunnel, useful for identification of bottlenecks in tunnels; and (v) identification of tunnels that are invisible by visual inspection yet they may open for a ligand to pass through due to dynamics of a protein in time **(Fig 89ade)**. Known limitation of the current version of CAVER is failure to find one of two tunnels possessing a common mouth **(Fig 89de)**, due to blocking the mouth after finding the first of the two tunnels, which is the current strategy used to force the algorithm to search for more than one tunnel.

User statistics. As of November 14, 2009, 2,174 users registered for CAVER 2.0; the web site of CAVER was accessed from 15,013 unique IP addresses.

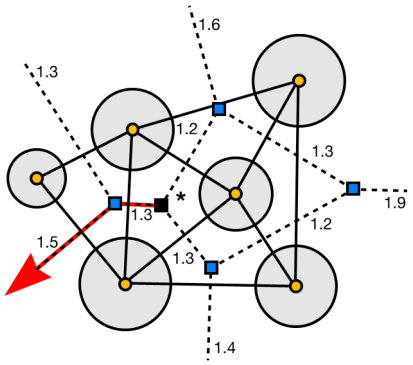

Fig 87 | Finding a tunnel using CAVER 2.0 algorithm. Weighted graph (edges, dashed lines with numbers, connected by nodes, squares) is generated from Delaunay triangulation (solid lines) for the set of protein atoms (grey spheres with centres highlighted by small orange balls). The widest tunnel with minimal length (red arrow) is computed from the weighted graph using the modified Dijkstra's algorithm, starting from the graph node (black square) closest to the user defined point in the cavity (asterisk).

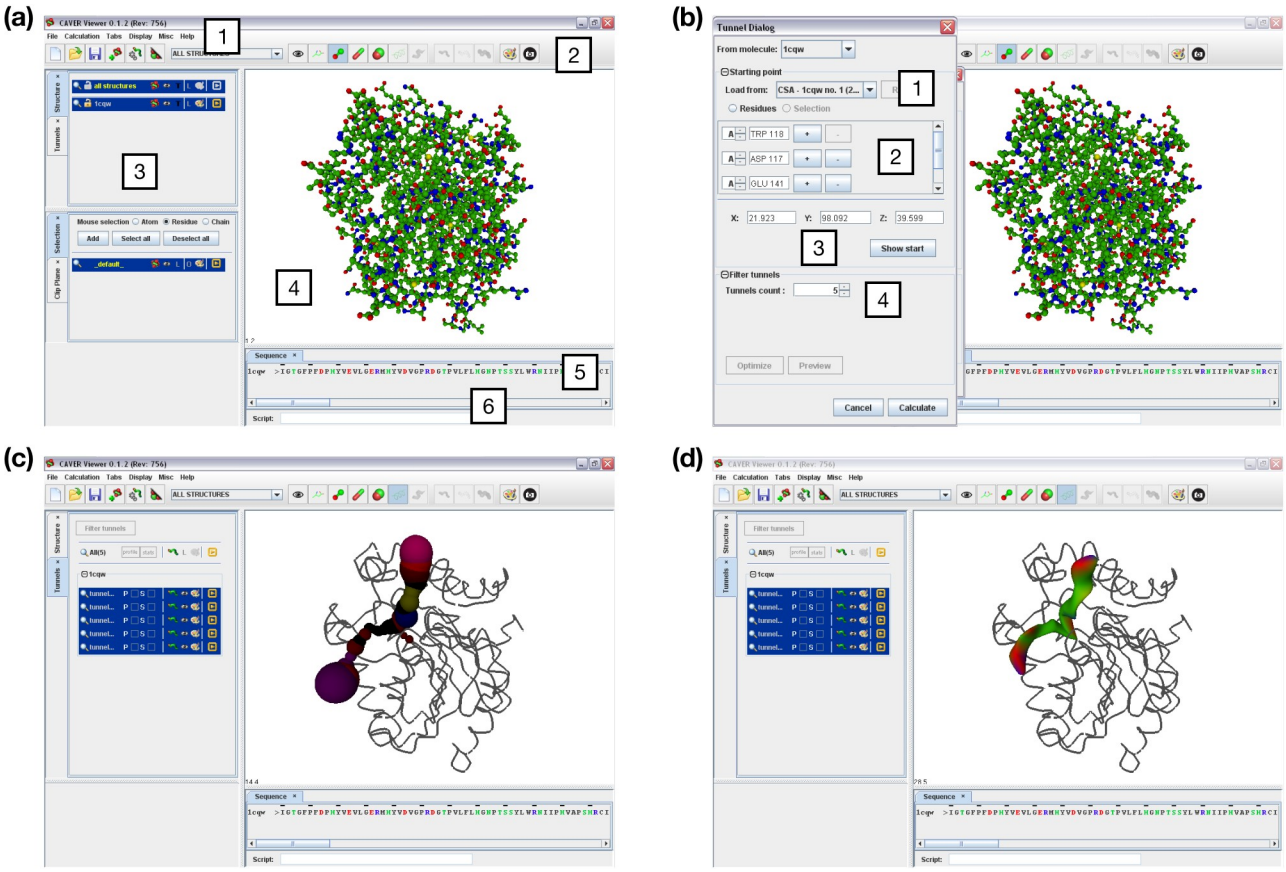

Fig 88 | Calculation and visualisation of tunnels using CAVER Viewer application. **(a)** GUI with menu bar, (*1*), shortcut icons (*2*), and structure manipulation (*3*), molecular graphics (*4*), sequence (*5*) and command line panes (*6*); **(b)** tunnel calculation dialog (left) for specifying location of the starting point using (i) catalytic amino acid residues retrieved for the protein from Catalytic Site Atlas (*1*), (ii) user-defined amino acid residues (2), or (iii) x, y an z coordinates (*3*), and specifying number of tunnels to be computed (*4*); **(c)** computed tunnels shown in spheres; **(d)** computed tunnels shown in "fire spires".

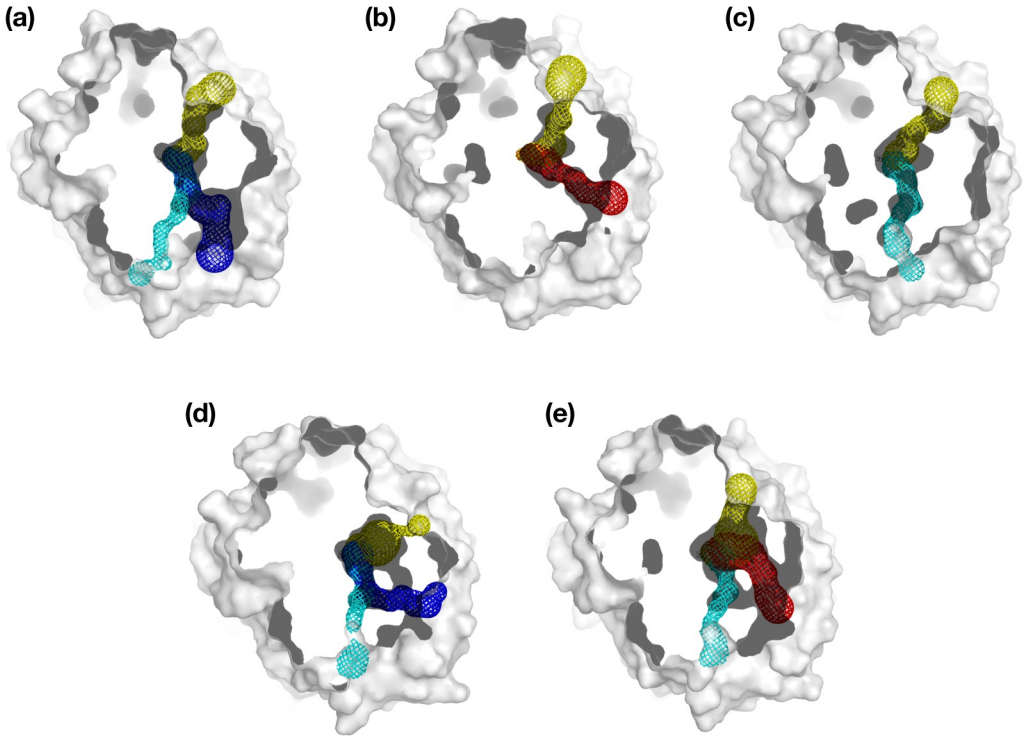

Fig 89 | Tunnels in the snapshots from MD simulations of DhaA identified manually and automatically using CAVER 2.0 plugin in PYMOL. **(a)** open p1 and p2a in the mutant 27' (trajectory *c12*; snapshot 3860); **(b)** open p1 and p2b in the mutant 27' (trajectory *c11*; snapshot 3960); **(c)** open p1 and p2c in the mutant 04 (trajectory *c4*; snapshot 3810); **(d)** open p2a and p2b in the mutant 04 (trajectory *c3*; snapshot 3550); **(e)** open p1, p2a and p2b in the mutant 04 (trajectory *c3*; snapshot 3980). Five tunnels were calculated for each structure. Starting point was defined as a centroid of three atoms: $N_{\delta 2}$ atom of Asn41, $O_{\delta 1}$ atom of Asp106 and $N_{\varepsilon 2}$ atom of Trp107. All open tunnels were identified by CAVER 2.0 in *a*, *b* and *c*. p2b tunnel in *d* and p2a tunnel in *e* was not found by CAVER 2.0 due to common mouth with p2a and p2b tunnel, respectively. In *a*, *d* and *e*, CAVER 2.0 identified additional tunnels (p2c, p1 and p2c, and p2c, respectively) that were closed in the snapshots, but that are at the same time known to open in MD simulations. Protein structures are shown in surface representation; tunnels are in dark grey. CAVER 2.0 tunnels are shown in mesh representation and coloured by tunnel as follows: p1, yellow; p2a, blue; p2b, red; p2c, cyan.

5 Discussion

Nothing is not nothing because nothing is not something, and what is not something does not exist, and what does not exist is not, and what is not cannot be defined.

5.1 Active site access tunnels in the haloalkane dehalogenase DhaA from *Rhodococcus rhodochrous* NCIMB 13064 modified using semi-rational approach yielded mutants with significantly enhanced activity towards toxic and recalcitrant xenobiotic, 1,2,3-trichloropropane

Klvaňa M, Pavlová M, Chaloupková R, Prokop Z, Banáš P, Otyepka M, Wade RC, Nagata Y & Damborský J (**2009**). Redesigning dehalogenase access tunnels as a strategy for degrading an anthropogenic substrate. *Nat. Chem. Biol.* 5: 727-733.

Three approaches to protein engineering. There are many documented cases of organisms acquiring the ability to degrade anthropogenic chemicals within a few years (or less) following contact with them **(Aharoni et al., 2005)**. It is unclear how the enzymes involved can evolve new activities so rapidly, but the ability generally depends on the introduction of new phenotypic traits by a small number of mutations. Three major approaches can be applied to mimic such rapid evolution and enhance the catalytic performance of enzymes towards non-natural substrates in the laboratory: rational protein design **(Craick et al., 1985)**, directed evolution **(Mills et al., 1967)** and their combination, the so-called semi-rational approach **(Chica et al., 2005)**. The rational design is the most promising and versatile approach for generating new activities, while the directed evolution seems to be the best way to optimise catalytic properties of existing enzymes **(Woycechowsky et al., 2007)**; the semi-rational approach then combines advantages of both these approaches **(Chica et al., 2005; Sen et al., 2007)**.

DhaA variants with enhanced activity towards 1,2,3-trichloropropane (TCP) have been obtained by the semi-rational approach. In this study, we constructed a variant of the haloalkane dehalogenase DhaA from *Rhodococcus rhodochrous* NCIMB 13064 with 32-fold higher catalytic activity and 26-fold higher catalytic performance for TCP than wild-type DhaA by the semi-rational approach employing classical molecular dynamics (MD) and random acceleration MD (RAMD) simulations with directed evolution. Identification of specific sites in the protein for combinatorial saturation mutagenesis substantially reduced the sequence space required to isolate viable mutants: A smart mutant library of ~ 5,000 clones yielded 51 positive clones and 25 unique sequences with improved TCP conversion — significantly more than in a previous study in which a random library of DhaA mutants created by DNA shuffling **(Bosma et al., 2002)** yielded 30 potentially positive variants out of 10,000 clones, and only one (04 mutant, Cys176Tyr) showing improved TCP conversion. A second-generation library created by error-prone PCR provided 14 potentially positive variants and one (M2, Cys176Tyr+Tyr273Phe) with further improved catalytic performance **(Bosma et al., 2002)**. However, neither the wild-type enzyme nor M2 have sufficient catalytic activity and catalytic efficiency with TCP (k_{cat} = 0.04 and 0.14 s^{-1}, k_{cat}/K_m = 40 s^{-1} M^{-1} and 156 s^{-1} M^{-1}, respectively) for biodegradation in a continuous-flow system, which would be essential for cost-effective, full-scale bioremediation processes. The catalytic constants of our mutant with highest activity towards TCP (k_{cat} = 1.26 s^{-1}, k_{cat}/K_m = 1,050 s^{-1} M^{-1}) are of the same order of magnitude as those of the haloalkane dehalogenase DhlA for 1,2-dichloroethane (k_{cat} = 3.3 s^{-1}, k_{cat}/K_m = 6,200 s^{-1} M^{-1}), which has proven utility in 1,2-dichloroethane–mineralising microorganisms used in a full-scale groundwater purification plant **(Stucki & Thueer, 1995)**. The haloalkane dehalogenase DhlA-producing microorganisms have survived, grown and shown potential to degrade 1,2-dichloroethane efficiently for at least five years after the startup of the plant. Construction of a TCP-degrading bacterium carrying the mutant dehalogenase identified in this work is currently in progress, thus following the work of Bosma and co-workers on the wild-type DhaA **(1999)** and the M2 mutant **(2002)**.

The enhanced activity of the mutant 31 is due to improved shielding of the active site from bulk solvent.. In the present study, focusing on the apparent importance of narrowing the main access tunnel **(Banáš et al., 2006)**, the most active mutant 31 contains the large aromatic residues in four out of five positions targeted by mutagenesis, leading to the most occluded active site. Product release was a rare event in random acceleration molecular dynamics (RAMD) simulations of variant 31', and classical molecular dynamics (MD) simulations of its enzyme-substrate

complex showed that the modification of its entrance pathways restricts access of water molecules to the occluded active site cavity. One water molecule must be present in the active site as a co-substrate for the hydrolytic step, but additional water molecules inhibit carbon-halogen bond cleavage **(Devi-Kesavan & Gao, 2003; Hur et al., 2003; Olsson & Warshel, 2004)**. Rapid quench-flow analysis confirmed indications from MD simulations that carbon-halogen bond cleavage is the rate-limiting step for TCP conversion by the wild-type DhaA — as reported previously **(Bosma et al., 2003)** — and that this step is significantly improved in the 31 mutant. The observed switch of the rate-limiting step from the chemical reaction to the product release in the 31 mutant documents the trade-off that favours catalysis in the occluded active site and disfavours product release. Substrate mapping for the 31 mutant showed that it also has increased activity towards other 1,2-dihaloethanes and 1,2-dihalopropanes, in accordance with the proposed limitation of carbon-halogen bond cleavage for these substrates. Precise formation of the activated complex and stabilisation of the transition state are important for the initial bimolecular nucleophilic substitution (S_N2) step in the conversion of 1,2-halogenated substrates by the haloalkane dehalogenases, since halogen substitutents in the 1,2-position strongly sterically hinder the nucleophilic attack.

Engineering the active site access pathways has applicability for optimising enzymes with buried active sites. Comparative analysis of X-ray crystal (XC) structures suggested that access tunnels substantially influence haloalkane dehalogenases' substrate specificity and activity **(Marek et al., 2000)** and it was verified by exhaustive site-directed mutagenesis of the tunnel amino acid residue Leu177 in the haloalkane dehalogenase LinB **(Chaloupková et al., 2003)**. Access tunnels have also been shown to affect the substrate specificity of cytochrome P450s **(Winn et al., 2002; Schleinkofer et al., 2005; Cojocaru et al., 2007)**. Numerous reports describing variants of several enzymes carrying single-point mutations in access tunnels with modified specificities, enantioselectivities or activities **(Carmichael & Wong, 2001; Lauble et al., 2002; Schmitt et al., 2002; Chaloupková et al., 2003; Fedorov et al., 2004; Fishman et al., 2004; Kotik et al., 2007; Feingersch et al., 2008)** support the general applicability of redesigning access tunnels to alter enzymes' activities. Here we have demonstrated the utility of simultaneously randomising several residues that influence ligand and water passage through access tunnels for optimising tunnel anatomy, physicochemical properties and dynamics. In summary, we provide experimental evidence that the activity of enzymes towards anthropogenic substrates can be improved by modifying access routes connecting the buried active site cavity with the surrounding solvent. The results indicate that identifying hot spot amino acid residues lining access tunnels by MD simulations combined with exhaustive mutagenesis by directed evolution may be a valuable, generally applicable methodology for engineering new biocatalysts with buried active sites. The tunnel amino acid residues remote to the active site represent good targets for mutagenesis since their replacement may not lead to loss of functionality by disruption of the active site architecture.

5.2 MD simulations identified five product release and water exchange pathways in DhaA variants

Klvaňa M, Pavlová M, Koudeláková T, Chaloupková R, Dvořák P, Prokop Z, Stsiapanava A, Kutý M, Kutá-Smatanová I, Dohnálek J, Kulhánek P, Wade RC & Damborský J (**2009**). Pathways and mechanisms for product release in the engineered haloalkane dehalogenases explored using classical and random acceleration molecular dynamics simulations. *J. Mol. Biol.* 392: 1339-1356.

Five product release and water exchange pathways were identified of which three were not evident from X-ray crystal (XC) structures. Two distinct tunnels, named the main tunnel and the slot tunnel, could be identified in the XC structures of the haloalkane dehalogenases **(Otyepka & Damborský, 2002; Petřek et al., 2006)**. The simulations conducted with wild-type DhaA confirm the relevance of the main tunnel (pathway p1) and the slot tunnel (pathway 2a) for release of products and exchange of water molecules between the buried active site and the bulk solvent. p1 is observed as the only release pathway for chloride anion (CL). The release of CL was observed only in wild-type DhaA and mutant 15, most probably due to limited time available in the classical MD simulations for the CL to become hydrated. Nevertheless, the proposed role of p1 for CL release is supported by the presence of iodide anions in the XC structure of DhaA from *Rhodococcus* sp., PDB-ID 1CQW **(Newman et al., 1999)**. The structure reveals two iodide binding sites: (i) iodide anion positioned between the halide-stabilising residues Asn41 and Trp107 and (ii) iodine covalently attached to the Sγ of Cys176 **(Newman et al., 1999)**. An imaginary line connecting the two iodide binding sites goes through the p1 pathway. p1 is also the dominant release pathway for 2,3-dichloropropane-1-ol (DCL) and for exchange of water molecules between the active site and bulk solvent. p2a functions as an auxiliary pathway for DCL and water molecules. The release of DCL through the pathway corresponding to p2a was also observed in the recent MD simulations of enzyme–product complexes of the phylogenetically closely related haloalkane dehalogenase LinB **(Negri et al., 2007)**. Besides p1 and p2a, the simulations revealed the additional p2b

and p2c for water molecules and p3 for DCL in wild-type DhaA. While p2b can be related to a deep surface depression in the three available XC structures of DhaA **(Newman et al., 1999)**, no indication for p2c or p3 can be found in these structures. DCL passing through p3 forms a transient tunnel, while water molecules pass directly through the protein matrix of the region p3. MD simulations suggest that p2b and p2c function as auxiliary pathways for water molecules, especially in the presence of charged CL in the active site. Interestingly, p2b is the preferred route for the exchange of water molecules over p2a and is observed in all but one DhaA variant.

Protein dynamics is important determinant of accessibility of ligand exchange pathways. It is noteworthy that all the pathways are located along highly mobile secondary structure elements of the DhaA cap domain comprising the N-terminal cap domain loop (NC loop), the variable N-terminal part of the α4 helix, the breakage point in the α5 helix at Gly171, the variable C-terminal part of the α5 helix, and the C-terminal cap domain loop, CC loop **(Otyepka & Damborský, 2002)**. The larger backbone fluctuations during the passage of CL, DCL, or water molecules through a pathway compared to the free, unliganded pathway also suggest that the mobility can be further enhanced by interactions with small molecules. Apparently, some of the functionally relevant pathways are not observable in the XC structures and MD simulations are necessary for their identification **(Lüdemann et al., 2000a; Winn et al., 2002; Wade et al., 2004; Schleinkofer et al., 2005; Carlsson et al., 2006; Wang & Duan, 2007)**. Previous studies on other systems have also shown that flexibility of loops and helices controls accessibility of the active site, for example, in cytochrome P450 **(Lüdemann et al., 2000b; Prasad et al., 2000; Dunn et al., 2001; Podust et al., 2001; Wade et al., 2004; Li et al., 2005; Schleinkofer et al., 2005; Seifert et al., 2006; Cojocaru et al., 2007; Yao et al., 2007)**, acetylcholinesterase **(Tara et al., 1999)**, gpH1 receptor **(Strasser & Wittmann, 2007)**, and haloalkane dehalogenase LinB **(Negri et al., 2007)**. We further demonstrate that all relevant pathways in wild-type DhaA and its mutants can be identified by monitoring of the exchange of solvent between the buried active site and the protein surface.

5.3 Solvation of products is essential for their release from buried active site of DhaA variants

Klvaňa M, Pavlová M, Koudeláková T, Chaloupková R, Dvořák P, Prokop Z, Stsiapanava A, Kutý M, Kutá-Smatanová I, Dohnálek J, Kulhánek P, Wade RC & Damborský J (**2009**). Pathways and mechanisms for product release in the engineered haloalkane dehalogenases explored using classical and random acceleration molecular dynamics simulations. *J. Mol. Biol.* 392: 1339-1356.

CL release is triggered and assisted by water molecules. Specific interactions between the two products, CL and DCL, the protein, and water solvent are essential for release of products from the buried active sites of haloalkane dehalogenases. CL formed during the dehalogenation reaction is strongly bound in between two halide-stabilising residues, which are present in all currently known haloalkane dehalogenases **(Verschueren et al., 1993d; Kennes et al., 1995; Damborský et al., 1997; Krooshof et al., 1997; Damborský & Koča, 1999; Newman et al., 1999; Schindler et al., 1999; Marek et al., 2000; Boháč et al., 2002; Janssen, 2004; Chovancová et al., 2007)**. The halide ion is positioned in between the two halide-stabilising residues in all XC structures of haloalkane dehalogenases, with the exception of enzyme-substrate complexes with the halide-binding site occupied by the substrate molecule **(Verschueren et al., 1993d; Newman et al., 1999; Marek et al., 2000)**. The stabilisation of halide ions is weaker in DhaA than in DhlA due to the different chemistry of the halide-stabilising residues. DhaA possesses tryptophan and asparagine, whereas DhlA has two tryptophans **(Schindler et al., 1999; Boháč et al., 2002)**. The stronger stabilisation of the halide product in DhlA, together with its occluded active site and different location of a catalytic acid, may explain the limitation of the reaction cycle by the halide release **(Schanstra et al., 1996b; Pikkemaat et al., 1999)**. In DhaA, halide release is a fast process, showing no effect on overall kinetics **(Bosma et al., 2002)**. The release of CL from DhaA is clearly triggered by water molecules. The CL bound in the active site induces a strong electrostatic field, which attracts water molecules from the bulk solvent to the active site not only through tunnels p1 and p2a but also through three auxiliary water pathways p2b, p2c, and p3. Water molecules compete with the halide-stabilising residues for favourable interactions with CL and facilitate the release of CL from the active site. This proposal is in very good agreement with the classical MD simulations of product release from the haloalkane dehalogenase LinB **(Negri et al., 2007)**. In DhaA, CL leaves the active site through p1 surrounded by water molecules. The polar residue Lys175 located at the mouth opening of the main tunnel of DhaA guides solvated CL out of the main tunnel to the surrounding solvent.

DCL release is triggered by water molecules and guided by interactions with aromatic amino acid residues. Both molecular docking and MD simulations suggest that the DCL, formed during the dehalogenation reaction, makes a

hydrogen bond with the nucleophile Asp106. This interaction could explain inhibition of TCP dehalogenation by DCL product. Disruption of this interaction is assisted by water molecules and represents one of the limiting events of DCL release. Several polar residues located along the release pathways make contacts with DCL during its release. Very important is van der Waals and electrostatic attraction of DCL by His272 in p1. Strong interaction of the alcohol product with the conserved catalytic histidine has been described for the enzyme-DCL complex of LinB **(Monincová et al., 2007)** as well as for other enzyme-product complexes of this enzyme **(Marek et al., 2000; Streltsov et al., 2003; Oakley et al., 2004)**. Another important interaction made by DCL, when moving away from the active site via p2a, p2b, and p2c, is with the polar Arg133. Arg133 controls p2a opening by transient formation of a salt link to Glu140. Favourable electrostatic and van der Waals interactions are provided by several aromatic side-chains in p1, p2b, and p3. Bulky aromatic side-chains function as gatekeepers and must undergo conformational change to increase the accessibility of the pathway for bulky DCL. If two or more aromatic side-chains form the gate, they change conformation in a simultaneous or consecutive way, depending on their location along the pathway. DCL moves through a pathway taking advantage of temporarily increased local space due to natural protein breathing motions, which may be further enhanced by a DCL molecule. This is in agreement with studies describing the accessibility of pathways that are being controlled locally by (i) hydrogen-bonding and salt link interactions, described for cytochrome P450 **(Deprez et al., 1994; Di Primo et al., 1997; Lounnas & Wade, 1997; Oprea et al., 1997; Lüdemann et al., 2000a; Dunn et al., 2001; Winn et al., 2002; Li et al., 2005; [Yao et al., 2007)** and acetylcholinesterase **(Kovach et al., 1994; Enyedy et al., 1998)**, and (ii) aromatic gating, described for cytochrome P450 **(Lüdemann et al., 2000a; Lüdemann et al., 2000b; Winn et al., 2002; Li et al., 2005)**, acetylcholinesterase **(Ripoll et al., 1993; Enyedy et al., 1998; Tara et al., 1999; Van Belle et al., 2000; Xu et al., 2003)**, NADH oxidase **(Hritz et al., 2006)**, horseradish peroxidase **(Khajehpour et al., 2003; Zelent et al., 2004)**, and myoglobin **(Teeter, 2004)**.

5.4 Mutations change the accessibility of the pathways in DhaA variants

Klvaňa M, Pavlová M, Koudeláková T, Chaloupková R, Dvořák P, Prokop Z, Stsiapanava A, Kutý M, Kutá-Smatanová I, Dohnálek J, Kulhánek P, Wade RC & Damborský J (**2009**). Pathways and mechanisms for product release in the engineered haloalkane dehalogenases explored using classical and random acceleration molecular dynamics simulations. *J. Mol. Biol.* 392: 1339-1356.

Effect of amino acid residue substitutions on accessibility of auxiliary exchange pathways is mutation- and ligand-dependent. The eight mutants of the DhaA haloalkane dehalogenase studied here carry various substitutions in the residues lining the main tunnel and the slot tunnel. The mutations show diverse effects on the accessibility of individual pathways for individual ligands. Four out of five possible pathways (p1, p2a, p2b, and p2c) are accessible for water molecules in wild-type DhaA, whereas one pathway (p3) becomes accessible for water molecules only after introducing the Trp141Phe substitution in mutant 21'. Residue 141, together with Phe149, forms a gate that controls accessibility of p3. The release of DCL through p3 is observed in mutant 27', but not in mutant 21', suggesting that p3 is hardly accessible for bulky alcohol regardless of the residue in position 141. On the other hand, Trp141Phe and Ile135Val are required to allow accessibility of p2b and p2c pathways for DCL. Ile135 is the key residue controlling the access to p2a, p2b, and p2c because its substitution to bulky phenylalanine effectively closes up p2a, p2b, and p2c for DCL and p2a and p2c for water molecules.

Main tunnel is the only pathway that could not be sealed against ligand exchange by amino acid residue substitutions. The only pathway that could not be completely blocked is p1. This is the main release pathway for DCL and is accessible even after the cumulative introduction of four aromatic substitutions. Introduction of aromatic substitutions in p1 (Cys176Tyr, Val245Phe, Ala172Phe, and Ala145Phe) seems to decrease its accessibility for DCL in the presence of two substitutions but surprisingly seems to restore the accessibility for DCL by the third and fourth substitutions in mutants 51' and 52'. It is noteworthy that many aromatic residues are packed close to each other in the active site (His272, Tyr273, Phe152, and Phe168) and p1 (Phe144, Ala145Phe, Phe149, Ala172Phe, Cys176Tyr, and Val245Phe) of mutant 52'. We propose that an effective gating is established because product release is not impaired in mutant 52' and the water molecules can enter the occluded active site once CL is formed during the dehalogenation reaction. Such an aromatic gating is a common way by which enzymes with buried active sites control accessibility during the reaction cycle. An interesting example of aromatic gating has been described for acetylcholinesterase **(Ripoll et al., 1993; Kovach et al., 1994; Tara et al., 1999; Bui et al., 2003)**. The gate of the main gorge of acetylcholinesterase is formed by four aromatic residues, and their pinching movement **(Tara et al., 1999; Bui et al., 2003)**, together with loop motion **(Kovach et al., 1994)** and strong dipole moment **(Ripoll et al., 1993)**, is responsible for the enzyme operating near the diffusion-limited rate.

5.5 Mutations change the mechanism of ligand exchange in DhaA variants

Klvaňa M, Pavlová M, Koudeláková T, Chaloupková R, Dvořák P, Prokop Z, Stsiapanava A, Kutý M, Kutá-Smatanová I, Dohnálek J, Kulhánek P, Wade RC & Damborský J (**2009**). Pathways and mechanisms for product release in the engineered haloalkane dehalogenases explored using classical and random acceleration molecular dynamics simulations. *J. Mol. Biol.* 392: 1339-1356.

Three common mechanisms for exchange of products and water are exploited by DhaA. Passage through a permanent tunnel, passage through a transient tunnel, and passage through a protein matrix were observed in classical MD and RAMD simulations of in the wild-type DhaA and its mutants. These mechanisms have analogies in other proteins. The exchange of ligands through permanent tunnels has been described for numerous proteins possessing a crystallographically observable tunnel in their structure **(Sevinc et al., 1999; Tara et al., 1999; Podust et al., 2001; Henchman et al., 2002; Otyepka & Damborský, 2002; Chelikani et al., 2003; Wade et al., 2004; Jakopitsch et al., 2005; Wen et al., 2005; Ye et al., 2006; Cojocaru et al., 2007; Negri et al., 2007)**. The exchange through the transient tunnels corresponds to exchange through a so-called naturally fluctuating bottleneck **(Zwanzig, 1992)**, which is a common mechanism to transiently enable access and egress of ligands in and out of the active site in the regions of lower density of protein atoms. This mechanism was previously reported for cytochrome P450 **(Deprez et al., 1994; Lüdemann et al., 2000b; Dunn et al., 2001; Seifert et al., 2006)**, acetylcholinesterase **(Van Belle et al., 2000; Bui et al., 2003)**, NADH oxidase **(Hritz et al., 2006)**, T4 lysosyme **(Carugo & Argos, 1998)**, and horseradish peroxidase **(Zelent et al., 2004)**. Passage of the ligands through the protein matrix is a well-documented phenomenon for gas migration in haem proteins **(Di Primo et al., 1997; Teeter, 2004; Cohen et al., 2006; Lavalette et al., 2006; Ye et al., 2006)**.

Single amino acid residue substitution causes change of the main tunnel from permanently to transiently open. To study the effect of mutations on the mechanism of ligand exchange, we attempted to assign one of three mechanisms to every ligand exchange observed in our molecular dynamic simulations. By comparing the mechanisms of the wild-type enzyme with its mutants, we demonstrated that substitutions introduced into the tunnels changed not only the accessibility of the individual pathways (see 5.4) but also the mechanism of ligand exchange in the case of the p1 pathway. This pathway follows the permanent tunnel in the wild-type DhaA. The XC structures of the mutants show that a single aromatic substitution in the tunnel results in its closure. However, MD reveals that ligands can pass through the p1 pathway even in the mutants with four aromatic substitutions. This is possible due to ligand-induced changes in the protein structure that cause the pathway to open up transiently to allow release of products. The opening of p1 can also be induced by water molecules entering the active site through p1 due to strong electrostatic attraction by CL. This solvation of the active site through the transiently opened tunnel is observed even in mutant 52' with the most occluded active site. The substitutions for aromatic residues in p1 changed the mechanism for ligand exchange from the passage through a permanent tunnel to the passage through a transient tunnel.

6 Conclusions

Problems often arise from incorrect interpretation of incomplete data.

Conclusion 1 | Using classical MD and RAMD simulations, three amino acid residues, Ile135, Val245 and Leu246, were proposed for saturation mutagenesis of the Cys176Tyr+Tyr273Phe mutant of the haloalkane dehalogenase DhaA. The saturation mutagenesis then yielded mutants with catalytic performance of 1,2,3-trichloropropane (TCP) conversion increased up to 26-fold (mutant 31).

Conclusion 2 | The enhanced activity of the DhaA mutants with TCP is due to improved shielding of the buried active site from bulk solvent at substrate binding and/or bimolecular nucleophilic substitution step of the reaction cycle. The shielding is best achieved by Cys176Tyr+Val245Phe+Ile135Phe substitutions of the mutant 31.

Conclusion 3 | Two active site access pathways, p1 and p2a, corresponding to crystallographically observable main tunnel and slot tunnel, respectively, and three additional pathways, p2b, p2c and p3, were identified among wild-type DhaA and eight mutants using classical MD and RAMD simulations.

Conclusion 4 | Release of chloride anion product of TCP conversion is triggered and assisted by water; release of 2,3-dichloropropane-1-ol (DCL) product is also triggered by water and guided by aromatic amino acid residues and by hydrogen bonding interactions.

Conclusion 5 | p1 is the major product release and water exchange pathway, robust against sealing attempted by four aromatic amino acid residue substitutions (Cys176Tyr+Val245Phe+Ala172Phe+Ala145Phe). Other pathways are auxiliary (p2a, p2b and p2c) or rare (p3). Accessibility of the auxiliary pathways is DCL- and/or water-specific and shows high sensitivity to substitution at position of the wild-type Ile135.

Conclusion 6 | Three mechanisms of ligand exchange are exploited among DhaA variants: passage through a permanent tunnel, passage through a transient tunnel and migration through a protein matrix. Main tunnel changes from permanently open to transiently open tunnel by single Cys176Tyr substitution.

Conclusion 7 | CAVER 2.0, a program for calculation of tunnels in protein structures, is available at: http://www.loschmidt.chemi.muni.cz/caver. The program can be used as a PYMOL plugin, or as a Java Web Start application, CAVER Viewer.

References

Seek simplicity, and distrust it.
— Alfred North Whitehead

Abagyan R, Totrov M and Kuznetsov D (**1994**). ICM – A new method for protein modeling and design: applications to docking and structure prediction from the distorted native conformation. *J. Comput. Chem.* 15: 488-506.

Acharya KR & **Lloyd** MD (**2005**). The advantages and limitations of protein crystal structures. *Trends Pharmacol. Sci.* 26: 10-14.

Agarwal PK, Billeter SR, Rajagopalan PTR, Benkovic SJ & Hammes-Schiffer S (**2002**). Network of coupled promoting motions in enzyme catalysis. *Proc. Natl. Acad. Sci. U.S.A.* 99: 2794-2799.

Aharoni A, Gaidukov L, Khersonsky O, Gould SM, Roodveldt C & Tawfik DS (**2005**). The 'evolvability' of promiscuous protein functions. *Nat. Genet.* 37: 73-76.

Albert VA (**2005**). 3. Parsimony and its presuppositions. *In* Parsimony, phylogeny, and genomics (pp. 43-53). *Oxford University Press*, New York, NY, USA.

Aloy P, Pichaud M & Russell RB (**2005**). Protein complexes: structure prediction challenges for the 21st century. *Curr. Opin. Struct. Biol.* 15: 15-22.

Altieri AS & **Byrd** RA (**2004**). Automation of NMR structure determination of proteins. *Curr. Opin. Struct. Biol.* 14: 547-553.

Altschul SF, Gish W, Miller W, Myers EW & Lipman DJ (**1990**). Basic local alignment search tool. *J. Mol. Biol.* 215: 403-410.

Altschul SF & **Lipman** DJ (**1990**). Protein database searches for multiple alignments. *Proc. Natl. Acad. Sci. U.S.A.* 87: 5509-5513.

Altschul SF, Madden TL, Schäffer AA, Zhang J, Zhang Z, Miller W & Lipman DJ (**1997**). Gapped BLAST and PSI-BLAST: a new generation of protein database search programs. *Nucleic Acids Res.* 25: 3389-3402.

Anastasi C, Buchet FF, Crowe MA, Parkes AL, Powner MW, Smith JM & Sutherland JD (**2007**). RNA: prebiotic product, or biotic invention? *Chem. Biodivers* 4: 721-739.

Anderson CM, Zucker FH & Steitz TA (**1979**). Space-filling models of kinase clefts and conformation changes. *Science*, 204: 375-380.

Anderson DE, Hurley JH, Nicholson H, Baase WA & Matthews BW (**1993**). Hydrophobic core repacking and aromatic-aromatic interaction in the thermostable mutant of T4 lysozyme Ser 117-->Phe. *Protein Sci.* 2: 1285-1290.

Andrade MA, Chacón P, Merelo JJ & Morán F (1**993**). Evaluation of secondary structure of proteins from UV circular dichroism spectra using an unsupervised learning neural network. *Protein Eng.* 6: 383-390.

Anfinsen CB, Haber E, Sela M & White FH (**1961**). The kinetics of formation of native ribonuclease during oxidation of the reduced polypeptide chain. *Proc. Natl. Acad. Sci. U.S.A.* 47: 1309-1314.

Anfinsen CB (**1973**). Principles that govern the folding of protein chains. *Science*, 181: 223-230.

Angov E, Hillier CJ, Kincaid RL & Lyon JA (**2008**). Heterologous protein expression is enhanced by harmonizing the codon usage frequencies of the target gene with those of the expression host. *PLoS ONE*, 3: e2189 (1-10).

Apweiler R, Bairoch A & Wu CH (**2004a**). Protein sequence databases. *Curr. Opin. Chem. Biol.* 8: 76-80.

Apweiler R, Bairoch A, Wu CH, Barker WC, Boeckmann B, Ferro S, Gasteiger E, Huang H, Lopez R, Magrane M, Martin MJ, Natale DA, O'Donovan C, Redaschi N & Yeh LL (**2004b**). UniProt: the Universal Protein knowledgebase. *Nucleic Acids Res.* 32: D115-119.

Arand M, Grant DF, Beetham JK, Friedberg T, Oesch F & Hammock BD (**1994**). Sequence similarity of mammalian epoxide hydrolases to the bacterial haloalkane dehalogenase and other related proteins. Implication for the potential catalytic mechanism of enzymatic epoxide hydrolysis. *FEBS Lett.* 338: 251-256.

Armen R, Alonso DOV & Daggett V (**2003**). The role of alpha-, 3(10)-, and pi-helix in helix-->coil transitions. *Protein Sci.* 12: 1145-1157.

Artymiuk PJ, Poirrette AR, Grindley HM, Rice DW & Willett P (**1994**). A graph-theoretic approach to the identification of three-dimensional patterns of amino acid side-chains in protein structures. *J. Mol. Biol.* 243: 327-344.

Aurora R, Creamer TP, Srinivasan R & Rose GD (**1997**). Local interactions in protein folding: lessons from the alpha-helix. *J. Biol. Chem.* 272: 1413-1416.

Aurora R, & **Rose** GD (**1998**). Helix capping. *Protein Sci.* 7: 21-38.

Austin RH, Beeson KW, Eisenstein L, Frauenfelder H & Gunsalus IC (**1975**). Dynamics of ligand binding to myoglobin. *Biochemistry*, 14: 5355-5373.

Avbelj F & **Fele** L (**1998**). Role of main-chain electrostatics, hydrophobic effect and side-chain conformational entropy in determining the secondary structure of proteins. *J. Mol. Biol.* 279: 665-684.

Avbelj F (**2000**). Amino acid conformational preferences and solvation of polar backbone atoms in peptides and proteins. *J. Mol. Biol.* 300: 1335-1359.

Bahadur RP, Chakrabarti P, Rodier F & Janin J (**2004**). A dissection of specific and non-specific protein-protein interfaces. *J. Mol. Biol.* 336: 943-955.

Bairoch A, Apweiler R, Wu CH, Barker WC, Boeckmann B, Ferro S, Gasteiger E, Huang H, Lopez R, Magrane M, Martin MJ, Natale DA, O'Donovan C, Redaschi N & Yeh LL (**2005**). The Universal Protein Resource (UniProt). *Nucleic Acids Res.* 33: D154-159.

Baker EN & **Hubbard** RE (**1984**). Hydrogen bonding in globular proteins. *Prog. Biophys. Mol. Biol.* 44: 97-179.

Baldus M (**2007**). ICMRBS founder's medal 2006: biological solid-state NMR, methods and applications. *J. Biomol. NMR*, 39: 73-86.

Baldwin RL & **Rose** GD (**1999a**). Is protein folding hierarchic? I. Local structure and peptide folding. *Trends Biochem. Sci.* 24, 26-33.

Baldwin RL & **Rose** GD (**1999b**). Is protein folding hierarchic? II. Folding intermediates and transition states. *Trends Biochem. Sci.* 24, 77-83.

Baldwin RL (**2007**). Energetics of protein folding. *J. Mol. Biol.* 371: 283-301.

Banáš P, Otyepka M, Jeřábek P, Petřek M & Damborský J (**2006**). Mechanism of enhanced conversion of 1,2,3-trichloropropane by mutant haloalkane dehalogenase revealed by molecular modeling. *Journal of Comput. Aided Mol. Des.* 20, 375-383.

Bard J, Ercolani K, Svenson K, Olland A & Somers W (**2004**). Automated systems for protein crystallization. *Methods*, 34: 329-347.

Barlow DJ & **Thornton** JM (**1988**). Helix geometry in proteins. *J. Mol. Biol.* 201: 601-619.

Barman TE, Bellamy SRW, Gutfreund H, Halford SE & Lionne C (**2006**). The identification of chemical intermediates in enzyme catalysis by the rapid quench-flow technique. *Cell. Mol. Life Sci.* 63: 2571-2583.

Barron LD, Hecht L & Wilson G (**1997**). The lubricant of life: a proposal that solvent water promotes extremely fast conformational fluctuations in mobile heteropolypeptide structure. *Biochemistry*, 36: 13143-13147.

Barth S, Fischer M, Schmid RD & Pleiss J (**2004**). The database of epoxide hydrolases and haloalkane dehalogenases: one structure, many functions. *Bioinformatics*, 20: 2845-2847.

Baxter CA, Murray CW, Clark DE, Westhead DR & Eldridge MD (**1998**). Flexible docking using Tabu search and an empirical estimate of binding affinity. *Proteins*, 33: 367-382.

Bayly CI, Cieplak P, Cornell W & Kollman PA (**1993**). A well-behaved electrostatic potential based method using charge restraints for deriving atomic charges: the RESP model. *J. Phys. Chem.* 97: 10269-10280.

Bell-Parikh LC & **Guengerich** FP (**1999**). Kinetics of cytochrome P450 2E1-catalyzed oxidation of ethanol to acetic acid via acetaldehyde. *J. Biol. Chem.* 274: 23833-23840.

Benkovic SJ & **Hammes-Schiffer** S (**2003**). A perspective on enzyme catalysis. *Science*, 301: 1196-1202.

Benner SA, Ellington AD & Tauer A (**1989**). Modern metabolism as a palimpsest of the RNA world. *Proc. Natl. Acad. Sci. U.S.A.* 86: 7054-7058.

Bennett WS & **Huber** R (**1984**). Structural and functional aspects of domain motions in proteins. *CRC Crit. Rev. Biochem.* 15: 291-384.

Benson DA, Karsch-Mizrachi I, Lipman DJ, Ostell J & Wheeler DL (**2005**). GenBank. *Nucleic Acids Res.* 33: D34-38.

Berendsen HJC, Postma JPM, van Gunsteren WF, DiNola A & Haak JR (**1984**). Molecular dynamics with coupling to an external bath. *J. Chem. Phys.* 81: 3684-3690.

Berendsen HJC & **Hayward** S (**2000**). Collective protein dynamics in relation to function. *Curr. Opin. Struct. Biol.* 10: 165-169.

Bergquist PL, Reeves RA & Gibbs MD (**2005**). Degenerate oligonucleotide gene shuffling (DOGS) and random drift mutagenesis (RNDM): two complementary techniques for enzyme evolution. *Biomol. Eng.* 22, 63-72.

Berlow RB, Igumenova TI & Loria JP (**2007**). Value of a hydrogen bond in triosephosphate isomerase loop motion. *Biochemistry*, 46: 6001-6010.

Berman H, Henrick K & Nakamura H (**2003**). Announcing the worldwide Protein Data Bank. *Nat. Struct. Biol.* 10: 980.

Bikiel DE, Boechi L, Capece L, Crespo A, De Biase PM, Di Lella S, González Lebrero MC, Martí MA, Nadra AD, Perissinotti LL, Scherlis DA & Estrin DA (**2006**). Modeling heme proteins using atomistic simulations. *PCCP*, 8: 5611-5628.

Billeter M, Wagner G & Wüthrich K (**2008**). Solution NMR structure determination of proteins revisited. *J. Biomol. NMR*, 42: 155-158.

Blakeley MP, Langan P, Niimura N & Podjarny A (**2008**). Neutron crystallography: opportunities, challenges, and limitations. *Curr. Opin. Struct. Biol.* 18: 593-600.

Blanco FJ, Jiménez MA, Pineda A, Rico M, Santoro J & Nieto JL (**1994**). NMR solution structure of the isolated N-terminal fragment of protein-G B1 domain. Evidence of trifluoroethanol induced native-like beta-hairpin formation. *Biochemistry*, 33: 6004-6014.

Blundell T, Barlow D, Borkakoti N & Thornton J (**1983**). Solvent-induced distortions and the curvature of alpha-helices. *Nature*, 306: 281-283.

Blundell TL & **Patel** S (**2004**). High-throughput X-ray crystallography for drug discovery. *Curr. Opin. Pharmacol.* 4: 490-496.

Boehr DD, Dyson HJ & Wright PE (**2006**). An NMR perspective on enzyme dynamics. *Chem. Rev.* 106: 3055-3079.

Boháč M, Nagata Y, Prokop Z, Prokop M, Monincová M, Tsuda M, Koča J & Damborský J (**2002**). Halide-stabilizing residues of haloalkane dehalogenases studied by quantum mechanic calculations and site-directed mutagenesis. *Biochemistry*, 41: 14272-14280.

Böhm HJ (**1992**). The computer program LUDI: a new method for the de novo design of enzyme inhibitors. *J. Comput. Aided Mol. Des.* 6: 61-78.

Bolon DN & **Mayo** SL (**2001**). Enzyme-like proteins by computational design. *Proc. Natl. Acad. Sci. U.S.A.* 98: 14274-14279.

Borrell B (**2008**). Chemistry: power play. *Nature*, 451: 240-243.

Bosma T, Kruizinga E, de Bruin EJ, Poelarends GJ & Janssen DB (**1999**). Utilization of trihalogenated propanes by *Agrobacterium radiobacter* AD1 through heterologous expression of the haloalkane dehalogenase from *Rhodococcus* sp. strain M15-3. *Appl. Environ. Microbiol.* 65: 4575-4581.

Bosma T, Damborský J, Stucki G & Janssen DB (**2002**). Biodegradation of 1,2,3-trichloropropane through directed evolution and heterologous expression of a haloalkane dehalogenase gene. *Appl. Environ. Microbiol.* 68: 3582-3587.

Bosma T, Pikkemaat MG, Kingma J, Dijk J & Janssen DB (**2003**). Steady-state and pre-steady-state kinetic analysis of halopropane conversion by a *Rhodococcus* haloalkane dehalogenase. *Biochemistry*, 42: 8047-8053.

Bourgeois D & **Royant** A (**2005**). Advances in kinetic protein crystallography. *Curr. Opin. Struct. Biol.* 15: 538-547.

Bowie JU, Lüthy R & Eisenberg D (**1991**). A method to identify protein sequences that fold into a known three-dimensional structure. *Science*, 253: 164-170.

Bradley P, Chivian D, Meiler J, Misura KMS, Rohl CA, Schief WR, Wedemeyer WJ, Schueler-Furman O, Murphy P, Schonbrun J, Strauss CEM & Baker D (**2003**). Rosetta predictions in CASP5: successes, failures, and prospects for complete automation. *Proteins*, 53 Suppl 6, 457-468.

Brezovský J, Prokop Z, Sato Y, Florián J, Mozga T, Chaloupková R, Koudeláková T, Jeřábek P, Natsume R, Janssen DB, Nagata Y, Senda T & Damborský J. Modulation of enantioselectivity in haloalkane dehalogenase DbjA by engineering of a surface loop. *Protein Design and Evolution for Biocatalysis* (Saint Feliu de Guixols, Spain), Oct 25-30, **2008**.

Britton KL, Baker PJ, Borges KM, Engel PC, Pasquo A, Rice DW, Robb FT, Scandurra R, Stillman TJ & Yip KS (**1995**). Insights into thermal stability from a comparison of the glutamate dehydrogenases from *Pyrococcus furiosus* and *Thermococcus litoralis*. *Eur. J. Biochem.* 229: 688-695.

Brooks BR, Bruccoleri RE, Olafson BD, States DJ, Swaminathan S & Karplus M (**1983**). A program for macromolecular energy, minimization, and dynamics calculations. *J. Comput. Chem.* 4: 187-217.

Brooks III CL, Karplus M & Pettitt BM (**1988**). I. Protein structure and dynamics - an overview. *In* A theoretical perspective of dynamics, structure, and thermodynamics. *Adv. Chem. Phys.* 71: 7-21.

Brooks III CL, Thorpe IF, Rod TH & Radkiewicz JL (**2003**). Dynamics coupled to protein catalysis? Factors affecting hydride transfer rates in DHFR. *Abstr. Pap. Am. Chem. Soc.* 225: U747.

Brosius J (**2003**). Gene duplication and other evolutionary strategies: from the RNA world to the future. *J. Struct. Funct. Genomics*, 3: 1-17.

Brown AJ (**1902**). XXXVI.-Enzyme action. *J. Chem. Soc. Trans.* 81: 373-388.

Brown EN & **Ramaswamy** S (**2007**). Quality of protein crystal structures. *Acta Crystallogr., Sect. D: Biol. Crystallogr.* 63: 941-950.

Bruice TC & **Lightstone** FC (**1999**). Ground state and transition state contributions to the rates of intramolecular and enzymatic reactions. *Acc. Chem. Res.* 32: 127-136.

Bruice TC & **Benkovic** SJ (**2000**). Chemical basis for enzyme catalysis. *Biochemistry*, 39: 6267-6274.

Bruice TC (**2002**). A view at the millennium: the efficiency of enzymatic catalysis. *Acc. Chem. Res.* 35: 139-148.

Bruice TC (**2006**). Computational approaches: reaction trajectories, structures, and atomic motions. Enzyme reactions and proficiency. *Chem. Rev.* 106: 3119-3139.

Brunori M, Cutruzzolà F, Savino C, Travaglini-Allocatelli C, Vallone B & Gibson QH (**1999**). Structural dynamics of ligand diffusion in the protein matrix: a study on a new myoglobin mutant Y(B10) Q(E7) R(E10). *Biophysi. J.* 76: 1259-1269.

Bryant SH & **Lawrence** CE (**1993**). An empirical energy function for threading protein sequence through the folding motif. *Proteins*, 16: 92-112.

Bryngelson JD, Onuchic JN, Socci ND & Wolynes PG (**1995**). Funnels, pathways, and the energy landscape of protein folding: a synthesis. *Proteins*, 21: 167-195.

Bryson K, McGuffin LJ, Marsden RL, Ward JJ, Sodhi JS & Jones DT (**2005**). Protein structure prediction servers at University College London. *Nucleic Acids Res.* 33: W36-38.

Brzozowski AM, Derewenda U, Derewenda ZS, Dodson GG, Lawson DM, Turkenburg JP, Bjorkling F, Huge-Jensen B, Patkar SA & Thim L (**1991**). A model for interfacial activation in lipases from the structure of a fungal lipase-inhibitor complex. *Nature*, 351: 491-494.

Buck M, Radford SE & Dobson CM (**1993**). A partially folded state of hen egg white lysozyme in trifluoroethanol: structural characterization and implications for protein folding. *Biochemistry*, 32: 669-678.

Bui JM, Henchman RH & McCammon JA (**2003**). The dynamics of ligand barrier crossing inside the acetylcholinesterase gorge. *Biophys. J.* 85: 2267-2272.

Burkhard P, Taylor P & Walkinshaw MD (**1998**). An example of a protein ligand found by database mining: description of the docking method and its verification by a 2.3 Å X-ray structure of a thrombin-ligand complex. *J. Mol. Biol.* 277: 449-466.

Burley SK & **Petsko** GA (**1985**). Aromatic-aromatic interaction: a mechanism of protein structure stabilization. *Science*, 229: 23-28.

Busenlehner LS & **Armstrong** RN (**2005**). Insights into enzyme structure and dynamics elucidated by amide H/D exchange mass spectrometry. *Arch. Biochem. Biophys.* 433: 34-46.

Caetano-Anollés G, Yafremava LS, Gee H, Caetano-Anollés D, Kim HS & Mittenthal JE (**2009**). The origin and evolution of modern metabolism. *Int. J. Biochem. Cell Biol.* 41: 285-297.

Callebaut I, Poupon A, Bally R, Demaret JP, Housset D, Delettré J, Hossenlopp P & Mornon JP (**2000**). The uteroglobin fold. *Ann. N.Y. Acad. Sci.* 923: 90-112.

Campbell DW, Müller C & Reardon KF (**2006**). Development of a fiber optic enzymatic biosensor for 1,2-dichloroethane. *Biotechnol. Lett.* 28: 883-887.

Cannon WR & **Benkovic** SJ (**1998**). Solvation, reorganization energy, and biological catalysis. *J. Biol. Chem.* 273: 26257-26260.

Carloni P, Rothlisberger U & Parrinello M (**2002**). The role and perspective of ab initio molecular dynamics in the study of biological systems. *Acc. Chem. Res.* 35: 455-464.

Carlson HA (**2002**). Protein flexibility and drug design: how to hit a moving target. *Curr. Opin. Chem. Biol.* 6: 447-452.

Carlsson P, Burendahl S & Nilsson L (**2006**). Unbinding of retinoic acid from the retinoic acid receptor by random expulsion molecular dynamics. *Biophys. J.* 91: 3151-3161.

Carmichael AB & **Wong** LL (**2001**). Protein engineering of *Bacillus megaterium* CYP102. The oxidation of polycyclic aromatic hydrocarbons. *Eur. J. Biochem.* 268: 3117-3125.

Carnevale V, Raugei S, Micheletti C & Carloni P (**2006**). Convergent dynamics in the protease enzymatic superfamily. *J. Am. Chem. Soc.* 128: 9766-9772.

Carugo O & **Argos** P (**1998**). Accessibility to internal cavities and ligand binding sites monitored by protein crystallographic thermal factors. *Proteins*, 31: 201-213.

Carugo O (**2001**). Detection of breaking points in helices linking separate domains. *Proteins*, 42: 390-398.

Cascella M, Raugei S & Carloni P (**2004**). Formamide hydrolysis investigated by multiple-steering ab initio molecular dynamics. *J. Phys. Chem. B*, 108: 369-375.

Case DA, Darden TA, Cheatham TE, Simmerling CL, Wang J, Duke RE, Luo R, Merz KM, Wang B, Pearlman DA, Crowley M, Brozell S, Tsui V, Gohlke H, Mongan J, Hornak V, Cui G, Beroza P, Schafmeister C, Caldwell JW, Ross WS & Kollman PA (**2004**). AMBER 8. *University of California*, San Francisco, CA, USA.

Case DA, Cheatham TE, Darden T, Gohlke H, Luo R, Merz KM, Onufriev A, Simmerling C, Wang B & Woods RJ (**2005**). The AMBER biomolecular simulation programs. *J. Comput. Chem.* 26: 1668-1688.

Cavalli A, Salvatella X, Dobson CM & Vendruscolo M (**2007**). Protein structure determination from NMR chemical shifts. *Proc. Natl. Acad. Sci.* 104: 9615-9620.

Cech TR (**1993**). The efficiency and versatility of catalytic RNA: implications for an RNA world. *Gene*, 135: 33-36.

Cedrone F, Ménez A & Quéméneur E (**2000**). Tailoring new enzyme functions by rational redesign. *Curr. Opin. Struct. Biol.* 10: 405-10.

Chakrabarti P & **Pal** D (**2001**). The interrelationships of side-chain and main-chain conformations in proteins. *Prog. Biophys. Mol. Biol.* 76: 1-102.

Chaloupková R, Sýkorová J, Prokop Z, Jesenská A, Monincová M, Pavlová M, Tsuda M, Nagata Y & Damborský J (**2003**). Modification of activity and specificity of haloalkane dehalogenase from *Sphingomonas paucimobilis* UT26 by engineering of its entrance tunnel. *J. Biol. Chem.* 278: 52622-52628.

Chang CH, Schindler JF, Unkefer CJ, Vanderberg LA, Brainard JR & Terwilliger TC (**1999**). In vivo screening of haloalkane dehalogenase mutants. *Bioorg. Med. Chem.* 7: 2175-2181.

Chang I, Lee JC, Winkler JR & Gray HB (**2003**). The protein-folding speed limit: intrachain diffusion times set by electron-transfer rates in denatured $Ru(NH_3)_5$(His-33)-Zn-cytochrome c. *Proc. Natl. Acad. Sci. U.S.A.* 100: 3838-3840.

Chan HS & **Dill** KA (**1998**). Protein folding in the landscape perspective: chevron plots and non-Arrhenius kinetics. *Proteins*, 30: 2-33.

Chaudhry C, Horwich AL, Brunger AT & Adams PD (**2004**). Exploring the structural dynamics of the *E. coli* chaperonin GroEL using translation-libration-screw crystallographic refinement of intermediate states. *J. Mol. Biol.* 342: 229-245.

Chau P (**2004**). Water movement during ligand unbinding from receptor site. *Biophys. J.* 87: 121-128.

Chelikani P, Carpena X, Fita I & Loewen PC (**2003**). An electrical potential in the access channel of catalases enhances catalysis. *J. Biol. Chem.* 278: 31290-31296.

Chen X, Li N & Ellington AD (**2007**). Ribozyme catalysis of metabolism in the RNA world. *Chem. Biodivers.* 4: 633-655.

Chica RA, Doucet N & Pelletier JN (**2005**). Semi-rational approaches to engineering enzyme activity: combining the benefits of directed evolution and rational design. *Curr. Opin. Biotechnol.* 16: 378-384.

Chidley C, Mosiewicz K & Johnsson K (**2008**). A designed protein for the specific and covalent heteroconjugation of biomolecules. *Bioconjugate Chem.* 19: 1753-1756.

Chothia C, Levitt M & Richardson D (**1977**). Structure of proteins: packing of alpha-helices and pleated sheets. *Proc. Natl. Acad. Sci. U.S.A.* 74: 4130-4134.

Chothia C & **Lesk** AM (**1985**). Helix movements in proteins. *Trends Biochem. Sci.* 10: 116-118.

Chothia C & **Lesk** AM (**1986**). The relation between the divergence of sequence and structure in proteins. *EMBO J.* 5: 823-826.

Chothia C (**1992**). Proteins. One thousand families for the molecular biologist. *Nature*, 357: 543-544.

Chou KC (**2000**). Prediction of tight turns and their types in proteins. *Anal. Biochem.* 286: 1-16.

Chou PY & **Fasman** GD (**1974**). Conformational parameters for amino acids in helical, beta-sheet, and random coil regions calculated from proteins. *Biochemistry*, 13: 211-222.

Chovancová E, Kosinski J, Bujnicki JM & Damborský J (**2007**). Phylogenetic analysis of haloalkane dehalogenases. *Proteins*, 67: 305-316.

Choy W, Shortle D & Kay LE (**2003**). Side chain dynamics in unfolded protein states: an NMR based 2H spin relaxation study of delta131delta. *J. Am. Chem. Soc.* 125: 1748-1758.

Christen M, Hünenberger PH, Bakowies D, Baron R, Bürgi R, Geerke DP, Heinz TN, Kastenholz MA, Kräutler V, Oostenbrink C, Peter C, Trzesniak D & van Gunsteren WF (**2005**). The GROMOS software for biomolecular simulation: GROMOS05. *J. Comput. Chem.* 26: 1719-1751.

Chrobáková T, Sato Y, Prokop Z, Monincová M, Jesenská A, Nagata Y & Damborský J. Engineering of enantioselective haloalkane dehalogenase by cumulative mutagenesis. *5th Discussions in Structural Molecular Biology* (Nové Hrady, Czech Republic), Mar 16-18, **2006a**.

Chrobáková T, Prokop Z, Sato Y, Monincová M, Jesenská A, Grodecká L, Senda T, Nagata Y & Damborský J. Engineering of haloalkane dehalogenase DhaA from *Rhodococcus rhodochrous* NCIMB 13064 towards higher enantioselectivity. *Protein Design and Evolution for Biocatalysis* (Greifswald, Germany), Aug 30 – Sep 01, **2006b**.

Chroust K, Pavlová M, Prokop Z, Mendel J, Božková K, Kubát Z, Zajíčková V & Damborský J (**2007**). Quantitative structure-activity relationships for toxicity and genotoxicity of halogenated aliphatic compounds: wing spot test of *Drosophila melanogaster*. *Chemosphere*, 67: 152-159.

Chruszcz M, Wlodawer A & Minor W (**2008**). Determination of protein structures – a series of fortunate events. *Biophys. J.* 95: 1-9.

Cieplak P, Cornell WD, Bayly C & Kollman PA (**1995**). Application of the multimolecule and multiconformational RESP methodology to biopolymers: charge derivation for DNA, RNA, and proteins. *J. Comput. Chem.* 16: 1357-1377.

Clark KP & **Ajay** (1995). Flexible ligand docking without parameter adjustment across four ligand-receptor complexes. *J. Comput. Chem.* 16: 1210-1226.

Clarke J & **Fersht** AR (**1993**). Engineered disulfide bonds as probes of the folding pathway of barnase: increasing the stability of proteins against the rate of denaturation. *Biochemistry*, 32: 4322-4329.

Claussen H, Buning C, Rarey M & Lengauer T (**2001**). FlexE: efficient molecular docking considering protein structure variations. *J. Mol. Biol.* 308: 377-395.

Cochran DA, Penel S & Doig AJ (**2001**). Effect of the N1 residue on the stability of the alpha-helix for all 20 amino acids. *Protein Sci.* 10: 463-470.

Cochran DA & **Doig** AJ (**2001**). Effect of the N2 residue on the stability of the alpha-helix for all 20 amino acids. *Protein Sci.* 10: 1305-13011.

Cochrane G, Akhtar R, Bonfield J, Bower L, Demiralp F, Faruque N, Gibson R, Hoad G, Hubbard T, Hunter C, Jang M, Juhos S, Leinonen R, Leonard S, Lin Q, Lopez R, Lorenc D, McWilliam H, Mukherjee G, Plaister S, Radhakrishnan R, Robinson S, Sobhany S, Hoopen PT, Vaughan R, Zalunin V & Birney E (**2009**). Petabyte-scale innovations at the European Nucleotide Archive. *Nucleic Acids Res.* 37, D19-25.

Cohen FE, Richmond TJ & Richards FM (**1979**). Protein folding: evaluation of some simple rules for the assembly of helices into tertiary structures with myoglobin as an example. *J. Mol. Biol.* 132: 275-288.

Cohen J, Arkhipov A, Braun RI & Schulten K (**2006**). Imaging the migration pathways for O_2, CO, NO, and Xe inside myoglobin. *Biophys. J.* 91: 1844-1857.

Cojocaru V, Winn PJ & Wade RC (**2007**). The ins and outs of cytochrome P450s. *Biochim. Biophys. Acta*, 1770: 390-401.

Cole C, Barber JD & Barton GJ (**2008**). The Jpred 3 secondary structure prediction server. *Nucleic Acids Res.* 36: W197-201.

Coleman RG & **Sharp** KA (**2009**). Finding and characterizing tunnels in macromolecules with application to ion channels and pores. *Biophys. J.* 96: 632-645.

Cooper A (**1976**). Thermodynamic fluctuations in protein molecules. *Proc. Natl. Acad. Sci. U.S.A.* 73: 2740-2741.

Copeland RA (**2000a**). 2. Chemical bonds and reactions in biochemistry. *In* Enzymes: a practical introduction to structure, mechanism, and data analysis (pp. 11-41). *John Wiley and Sons*, New York, NY, USA.

Copeland RA (**2000b**). 4. Protein-ligand binding equilibria. *In* Enzymes: a practical introduction to structure, mechanism, and data analysis (pp. 76-108). *John Wiley and Sons*, New York, NY, USA.

Copeland RA (**2000c**). 5. Kinetics of single-substrate enzyme reactions. *In* Enzymes: a practical introduction to structure, mechanism, and data analysis (pp. 109-145). *John Wiley and Sons*, New York, NY, USA.

Copeland RA (**2000d**). 6. Chemical mechanisms in enzyme catalysis. *In* Enzymes: a practical introduction to structure, mechanism, and data analysis (pp. 146-187). *John Wiley and Sons*, New York, NY, USA.

Copeland RA (**2000e**). 8. Reversible inhibitors. *In* Enzymes: a practical introduction to structure, mechanism, and data analysis (pp. 266-304). *John Wiley and Sons*, New York, NY, USA.

Copeland RA (**2000f**). 9. Tight binding inhibitors. *In* Enzymes: a practical introduction to structure, mechanism, and data analysis (pp. 305-317). *John Wiley and Sons*, New York, NY, USA.

Copeland RA (**2000g**). 10. Time-dependent inhibition. *In* Enzymes: a practical introduction to structure, mechanism, and data analysis (pp. 318-349). *John Wiley and Sons*, New York, NY, USA.

Copeland RA (**2000h**). 12. Cooperativity in enzyme catalysis. *In* Enzymes: a practical introduction to structure, mechanism, and data analysis (pp. 367-384). *John Wiley and Sons*, New York, NY, USA.

Cornell WD, Cieplak P, Bayly CI & Kollmann PA (**1993**). Application of RESP charges to calculate conformational energies, hydrogen bond energies, and free energies of solvation. *J. Am. Chem. Soc.* 115: 9620-9631.

Cornell WD, Cieplak P, Bayly CI, Gould IR, Merz KM, Ferguson DM, Spellmeyer DC, Fox T, Caldwell JW, & Kollman PA (**1995**). A second generation force field for the simulation of proteins, nucleic acids, and organic molecules. *J. Am. Chem. Soc.* 117: 5179-5197.

Cornell WD, Cieplak P, Bayly CI, Gould IR, Merz KM, Ferguson DM, Spellmeyer DC, Fox T, Caldwell JW & Kollman PA (**1996**). A second generation force field for the simulation of proteins, nucleic acids, and organic molecules J. Am. Chem. Soc. 1995, 117, 5179–5197. *J. Am. Chem. Soc.* 118: 2309.

Cornilescu G, Delaglio F & Bax A (**1999**). Protein backbone angle restraints from searching a database for chemical shift and sequence homology. *J. Biomol. NMR*, 13: 289-302.

Cousin X, Hotelier T, Giles K, Toutant JP & Chatonnet A (**1998**). aCHEdb: the database system for ESTHER, the alpha/beta fold family of proteins and the Cholinesterase gene server. *Nucleic Acids Res.* 26: 226-228.

Craik CS, Largman C, Fletcher T, Roczniak S, Barr PJ, Fletterick R & Rutter WJ (**1985**). Redesigning trypsin: alteration of substrate specificity. *Science*, 228: 291-297.

Creamer TP & **Rose** GD (**1992**). Side-chain entropy opposes alpha-helix formation but rationalizes experimentally determined helix-forming propensities. *Proc. Natl. Acad. Sci. U.S.A.* 89: 5937-5941.

Crick FHC (**1952**). Is alpha-keratin a coiled coil? *Nature*, 170: 882-883.

Cuff AL, Sillitoe I, Lewis T, Redfern OC, Garratt R, Thornton J & Orengo CA (**2009**). The CATH classification revisited--architectures reviewed and new ways to characterize structural divergence in superfamilies. *Nucleic Acids Res.* 37, D310-314.

Cui Q & **Karplus** M (**2002**). Quantum mechanical/molecular mechanical studies of the triosephosphate isomerase-catalyzed reaction: Verification of methodology and analysis of reaction mechanisms. *J. Phys. Chem. B*, 106: 1768-1798.

Cunningham BA, Hemperly JJ, Hopp TP & Edelman GM (**1979**). Favin versus concanavalin A: circularly permuted amino acid sequences. *Proc. Natl. Acad. Sci. U.S.A.* 76: 3218-3222.

Dalal S, Balasubramanian S & Regan L (**1997**). Protein alchemy: changing beta-sheet into alpha-helix. *Nat. Struct. Biol.* 4: 548-552.

Dalby PA (**2003**). Optimising enzyme function by directed evolution. *Curr. Opin. Struct. Biol.* 13: 500-505.

Damborský J, Kutý M, Němec M & Koča J (**1997**). A molecular modelling study of the catalytic mechanism of haloalkane dehalogenase: 1. quantum chemical study of the first reaction step. *J. Chem. Inf. Comput. Sci.* 37: 562-568.

Damborský J & **Koča** J (**1999**). Analysis of the reaction mechanism and substrate specificity of haloalkane dehalogenases by sequential and structural comparisons. *Protein Eng.* 12: 989-998.

Damjanović A, García-Moreno B, Lattman EE & García AE (**2005**). Molecular dynamics study of water penetration in staphylococcal nuclease. *Proteins*, 60: 433-449.

Daniel RM, Dunn RV, Finney JL & Smith JC (**2003**). The role of dynamics in enzyme activity. *Annu. Rev. Biophys. Biomol. Struct.* 32: 69-92.

Davies P (**2001**). The origin of life I: When and where did it begin? *Sci. Prog.* 84: 1-16.

Davis JH & **Agard** DA (**1998**). Relationship between enzyme specificity and the backbone dynamics of free and inhibited alpha-lytic protease. *Biochemistry*, 37: 7696-7707.

Deechongkit S, Nguyen H, Jager M, Powers ET, Gruebele M & Kelly JW (**2006**). Beta-sheet folding mechanisms from perturbation energetics. *Curr. Opin. Struct. Biol.* 16: 94-101.

DeLano WL (**2002**) The PyMOL molecular graphics system. *DeLano Scientific*, Palo Alto, CA, USA.

Deléage G & **Geourjon** C (**1993**). An interactive graphic program for calculating the secondary structure content of proteins from circular dichroism spectrum. *Comput. Appl. Biosci.* 9: 197-199.

Deléage G, Blanchet C & Geourjon C (**1997**). Protein structure prediction. Implications for the biologist. *Biochimie*, 79: 681-686.

DeLucas LJ, Bray TL, Nagy L, McCombs D, Chernov N, Hamrick D, Cosenza L, Belgovskiy A, Stoops B & Chait A (**2003**). Efficient protein crystallization. *J. Struct. Biol.* 142: 188-206.

DeLucas LJ, Hamrick D, Cosenza L, Nagy L, McCombs D, Bray T, Chait A, Stoops B, Belgovskiy A, Wilson WW, Parham M & Chernov N (**2005**). Protein crystallization: virtual screening and optimization. *Prog. Biophys. Mol. Biol.* 88: 285-309.

Demchenko AP (**2001**). Recognition between flexible protein molecules: induced and assisted folding. *J. Mol. Recognit.* 14: 42-61.

Deprez E, Gerber NC, Di Primo C, Douzou P, Sligar SG & Hui Bon Hoa G (**1994**). Electrostatic control of the substrate access channel in cytochrome P-450cam. *Biochemistry*, 33: 14464-14468.

Derewenda ZS (**1994**). Structure and function of lipases. *Adv. Protein Chem.* 45: 1-52.

Derewenda ZS, Lee L & Derewenda U (**1995**). The occurrence of C-H...O hydrogen bonds in proteins. *J. Mol. Biol.* 252: 248-262.

Derreumaux P & **Schlick** T (**1998**). The loop opening/closing motion of the enzyme triosephosphate isomerase. *Biophys. J.* 74: 72-81.

Devi-Kesavan LS & **Gao** J (**2003**). Combined QM/MM study of the mechanism and kinetic isotope effect of the nucleophilic substitution reaction in haloalkane dehalogenase. *J. Am. Chem. Soc.* 125: 1532-1540.

Dewar MJS, Zoebisch EG, Healy EF & Stewart JJP (**1985**). Development and use of quantum mechanical molecular models. 76. AM1: a new general purpose quantum mechanical molecular model. *J. Am. Chem. Soc.* 107: 3902-3909.

Di Giulio M (**1997**). On the RNA world: evidence in favor of an early ribonucleopeptide world. *J. Mol. Evol.* 45: 571-578.

Dill KA (**1990**). Dominant forces in protein folding. *Biochemistry*, 29: 7133-7155.

Dill KA & **Chan** HS (**1997**). From Levinthal to pathways to funnels. *Nat. Struct. Biol.* 4: 10-19.

Di Primo C, Deprez E, Sligar SG & Hui Bon Hoa G (**1997**). Origin of the photoacoustic signal in cytochrome P-450cam: role of the Arg186-Asp251-Lys178 bifurcated salt bridge. *Biochemistry*, 36: 112-118.

Dobzhansky T (**1964**). Biology, molecular and organismic. *Am. Zool.* 4: 443-452.

Doig AJ, MacArthur MW, Stapley BJ & Thornton JM (**1997**). Structures of N-termini of helices in proteins. *Protein Sci.* 6: 147-155.

Doolittle WF (**1978**). Genes in pieces: were they ever together? *Nature*, 272: 581-582.

Doudna JA & **Lorsch** JR (**2005**). Ribozyme catalysis: not different, just worse. *Nat. Struct. Mol. Biol.* 12: 395-402.

Dravis BC, LeJeune KE, Hetro AD & Russell AJ (**2000**). Enzymatic dehalogenation of gas phase substrates with haloalkane dehalogenase. *Biotechnol. Bioeng.* 69: 235-241.

Dunbrack RL & **Cohen** FE (**1997**). Bayesian statistical analysis of protein side-chain rotamer preferences. *Protein Sci.* 6: 1661-1681.

Dundas J, Ouyang Z, Tseng J, Binkowski A, Turpaz Y & Liang J (**2006**). CASTp: computed atlas of surface topography of proteins with structural and topographical mapping of functionally annotated residues. *Nucleic Acids Res.* 34: W116-118.

Dunn AR, Dmochowski IJ, Bilwes AM, Gray HB & Crane BR (**2001**). Probing the open state of cytochrome P450cam with ruthenium-linker substrates. *Proc. Natl. Acad. Sci. U.S.A.* 98: 12420-12425.

Dworkin JP, Lazcano A & Miller SL (**2003**). The roads to and from the RNA world. *J. Theor. Biol.* 222: 127-134.

Echols N, Milburn D & Gerstein M (**2003**). MolMovDB: analysis and visualization of conformational change and structural flexibility. *Nucleic Acids Res.* 31: 478-482.

Edman P (**1949**). A method for the determination of amino acid sequence in peptides. *Arch. Biochem.* 22: 475.

Edman P (**1950**). Method for determination of the amino acid sequence in peptides. *Acta Chem. Scand.* 4: 283-293.

Eijsink VGH, Bjørk A, Gåseidnes S, Sirevåg R, Synstad B, van den Burg B & Vriend G (**2004**). Rational engineering of enzyme stability. *J. Biotechnol.* 113: 105-120.

Eijsink VGH, Gåseidnes S, Borchert TV & van den Burg B (**2005**). Directed evolution of enzyme stability. *Biomol. Eng.* 22: 21-30.

Eisenberg D (**2003**). The discovery of the alpha-helix and beta-sheet, the principal structural features of proteins. *Proc. Natl. Acad. Sci. U.S.A.* 100: 11207-11210.

Eisenmesser EZ, Bosco DA, Akke M & Kern D (**2002**). Enzyme dynamics during catalysis. *Science*, 295: 1520-1523.

Eisenmesser EZ, Millet O, Labeikovsky W, Korzhnev DM, Wolf-Watz M, Bosco DA, Skalicky JJ, Kay LE & Kern D (**2005**). Intrinsic dynamics of an enzyme underlies catalysis. *Nature*, 438: 117-121.

Elber R & **Karplus** M (**1990**). Enhanced sampling in molecular dynamics: use of the time-dependent Hartree approximation for a simulation of carbon monoxide diffusion through myoglobin. *J. Am. Chem. Soc.* 112, 9161-9175.

Elcock AH, Huber GA & McCammon JA (**1997**). Electrostatic channeling of substrates between enzyme active sites: comparison of simulation and experiment. *Biochemistry*, 36: 16049-16058.

Englander SW & **Kallenbach** NR (**1983**). Hydrogen exchange and structural dynamics of proteins and nucleic acids. *Q. Rev. Biophys.* 16: 521-655.

Enyedy I, Kovach I & Brooks B (**1998**). Alternate pathways for acetic acid and acetate ion release from acetylcholinesterase: a molecular dynamics study. *J. Am. Chem. Soc.* 120: 8043-8050.

Erable B, Goubet I, Lamare S, Legoy MD & Maugard T (**2004**). Haloalkane hydrolysis by *Rhodococcus erythropolis* cells: comparison of conventional aqueous phase dehalogenation and nonconventional gas phase dehalogenation. *Biotechnol. Bioeng.* 86: 47-54.

Erable B, Goubet I, Lamare S, Seltana A, Legoy MD & Maugard T (**2005**). Nonconventional hydrolytic dehalogenation of 1-chlorobutane by dehydrated bacteria in a continuous solid-gas biofilter. *Biotechnol. Bioeng.*, 91: 304-313.

Erable B, Goubet I, Lamare S, Legoy M & Maugard T (**2006**). Bioremediation of halogenated compounds: comparison of dehalogenating bacteria and improvement of catalyst stability. *Chemosphere*, 65: 1146-1152.

Ewing TJ, Makino S, Skillman AG & Kuntz ID (**2001**). DOCK 4.0: search strategies for automated molecular docking of flexible molecule databases. *J. Comput. Aided Mol. Des.* 15, 411-428.

Fabiola GF, Krishnaswamy S, Nagarajan V & Pattabhi V (**1997**). C-H...O hydrogen bonds in beta-sheets. *Acta Crystallogr., Sect. D: Biol. Crystallogr.* 53, 316-320.

Fedorov R, Vasan R, Ghosh DK & Schlichting I (**2004**). Structures of nitric oxide synthase isoforms complexed with the inhibitor AR-R17477 suggest a rational basis for specificity and inhibitor design. *Proc. Natl. Acad. Sci. U.S.A.* 101: 5892-5897.

Feingersch R, Shainsky J, Wood TK & Fishman A (**2008**). Protein engineering of toluene monooxygenases for synthesis of chiral sulfoxides. *Appl. Environ. Microbiol.* 74, 1555-1566.

Ferguson JK & **Roughton** FJ (**1934**). The direct chemical estimation of carbamino compounds of CO(2) with haemoglobin. *J. Physiol.* 83, 68-86.

Ferreira Jorge RM & **Livingston** AG (**1999**). A novel method for characterisation of microbial growth kinetics on volatile organic compounds. *Appl. Microbiol. Biotechnol.* 52, 174-178.

Fiaux J, Bertelsen EB, Horwich AL & Wüthrich K (**2002**). NMR analysis of a 900K GroEL GroES complex. *Nature*, 418: 207-211.

Fischer E (**1894**). Einfluss der Configuration auf die Wirkung der Enzyme. *Ber. Deut. Chem. Ges.* 27, 2985-2993.

Fischetti RF, Rodi DJ, Gore DB & Makowski L (**2004**). Wide-angle X-ray solution scattering as a probe of ligand-induced conformational changes in proteins. *Chem. Biol.* 11: 1431-1443.

Fishman A, Tao Y, Bentley WE & Wood TK (**2004**). Protein engineering of toluene 4-monooxygenase of *Pseudomonas mendocina* KR1 for synthesizing 4-nitrocatechol from nitrobenzene. *Biotechnol. Bioeng.* 87: 779-790.

Fitzkee NC, Fleming PJ & Rose GD (**2005a**). The Protein Coil Library: a structural database of nonhelix, nonstrand fragments derived from the PDB. *Proteins*, 58: 852-854.

Fitzkee NC, Fleming PJ, Gong H, Panasik N, Street TO & Rose GD (**2005b**). Are proteins made from a limited parts list? *Trends Biochem. Sci.* 30, 73-80.

Fleming PJ, Fitzkee NC, Mezei M, Srinivasan R & Rose GD (**2005**). A novel method reveals that solvent water favors polyproline II over beta-strand conformation in peptides and unfolded proteins: conditional hydrophobic accessible surface area (CHASA). *Protein Sci.* 14: 111-118.

Flores S, Echols N, Milburn D, Hespenheide B, Keating K, Lu J, Wells S, Yu EZ, Thorpe M & Gerstein M (**2006**). The database of macromolecular motions: new features added at the decade mark. *Nucleic Acids Res.* 34, D296-301.

Fodje MN & **Al-Karadaghi** S (**2002**). Occurrence, conformational features and amino acid propensities for the pi-helix. *Protein Eng.* 15: 353-358.

Foster MP, McElroy CA & Amero CD. (**2007**). Solution NMR of large molecules and assemblies. *Biochemistry*, 46: 331-340.

Fox RJ, Davis SC, Mundorff EC, Newman LM, Gavrilovic V, Ma SK, Chung LM, Ching C, Tam S, Muley S, Grate J, Gruber J, Whitman JC, Sheldon RA & Huisman GW (**2007**). Improving catalytic function by ProSAR-driven enzyme evolution. *Nat. Biotechnol.* 25: 338-344.

Franken SM, Rozeboom HJ, Kalk KH & Dijkstra BW (**1991**). Crystal structure of haloalkane dehalogenase: an enzyme to detoxify halogenated alkanes. *EMBO J.* 10: 1297-1302.

Frauenfelder H, McMahon BH, Austin RH, Chu K & Groves JT (**2001**). The role of structure, energy landscape, dynamics, and allostery in the enzymatic function of myoglobin. *Proc. Natl. Acad. Sci. U.S.A.* 98: 2370-2374.

Frauenfelder H, Petsko GA & Tsernoglou D (**1979**). Temperature-dependent X-ray diffraction as a probe of protein structural dynamics. *Nature*, 280: 558-563.

Frauenfelder H, Sligar SG & Wolynes PG (**1991**). The energy landscapes and motions of proteins. *Science*, 254: 1598-1603.

Freddolino PL, Arkhipov AS, Larson SB, McPherson A & Schulten K (**2006**). Molecular dynamics simulations of the complete satellite tobacco mosaic virus. *Structure*, 14, 437-449.

Freitas dos Santos LM & **Livingston** AG (**1994**). Extraction and biodegradation of a toxic volatile organic compound (1,2-dichloroethane) from waste-water in a membrane bioreactor. *Appl. Microbiol. Biotechnol.* 42: 421-431.

Friedberg I & **Margalit** H (**2002**). Persistently conserved positions in structurally similar, sequence dissimilar proteins: roles in preserving protein fold and function. *Protein Sci.* 11: 350-360.

Frisch MJ, Trucks GW, Schlegel HB, Gill PMW, Johnson BJ, Robb MA, Cheeseman JR, Keith T, Petersson GA, Montgomery JA, Raghavachari K, Al-Laham MA, Zakrzewski VG, Ortiz JV, Foresman JB, Cioslowski J, Stefanov BB, Nanayakkara A, Challacombe M, Peng CY, Ayala PY, Chen W, Wong MW, Andres JL, Replogle ES, Gomperts R, Martin RL, Fox DJ, Binkley JS, Defrees DJ, Baker J, Stewart JP, Head-Gordon M, Gonzalez C & Pople JA (**1994**) *Gaussian 94 (Revision D4)*. Gaussian, Inc., Pittsburg, PA, USA.

Frishman D & **Argos** P (**1995**). Knowledge-based protein secondary structure assignment. *Proteins*, 23: 566-579.

Fuentes EJ, Der CJ & Lee AL (**2004**). Ligand-dependent dynamics and intramolecular signaling in a PDZ domain. *J. Mol. Biol.* 335: 1105-1115.

Gabb HA, Jackson RM & Sternberg MJ (**1997**). Modelling protein docking using shape complementarity, electrostatics and biochemical information. *J. Mol. Biol.* 272: 106-120.

Gaboriaud C, Bissery V, Benchetrit T & Mornon JP (**1987**). Hydrophobic cluster analysis: an efficient new way to compare and analyse amino acid sequences. *FEBS Lett.* 224: 149-155.

Gao J (**2003**). Catalysis by enzyme conformational change as illustrated by orotidine 5'-monophosphate decarboxylase. *Curr. Opin. Struct. Biol.* 13: 184-192.

Garcia-Viloca M, Gao J, Karplus M & Truhlar DG (**2004**). How enzymes work: analysis by modern rate theory and computer simulations. *Science*, 303, 186-195.

Garrett DS, Seok YJ, Peterkofsky A, Gronenborn AM & Clore GM (**1999**). Solution structure of the 40,000 Mr phosphoryl transfer complex between the N-terminal domain of enzyme I and HPr. *Nat. Struct. Biol.* 6, 166-173.

Genberg L, Richard L, McLendon G & Miller RJ (**1991**). Direct observation of global protein motion in hemoglobin and myoglobin on picosecond time scales. *Science*, 251: 1051-1054.

Gerstein M, Lesk AM & Chothia C (**1994**). Structural mechanisms for domain movements in proteins. *Biochemistry*, 33: 6739-6749.

Gerstein M & **Krebs** W (**1998**). A database of macromolecular motions. *Nucleic Acids Res.* 26, 4280-4290.

Gibbs MD, Nevalainen KM & Bergquist PL (**2001**). Degenerate oligonucleotide gene shuffling (DOGS): a method for enhancing the frequency of recombination with family shuffling. *Gene*, 271, 13-20.

Gibrat JF, Madej T & Bryant SH (**1996**). Surprising similarities in structure comparison. *Curr. Opin. Struct. Biol.* 6, 377-385.

Gilbert W, de Souza SJ & Long M (**1997**). Origin of genes. *Proc. Natl. Acad. Sci. U.S.A.* 94: 7698-7703.

Gilbert W (**1986**). Origin of life: The RNA world. *Nature*, 319: 618.

Gohlke H & **Klebe** G (**2002**). Approaches to the description and prediction of the binding affinity of small-molecule ligands to macromolecular receptors. *Angew. Chem. Int. Ed.* 41: 2644-2676.

Gohlke RS & **McLafferty** FW (**1993**). Early gas chromatography/mass spectrometry. *J. Am. Soc. Mass Spectrom.* 4: 367-371.

Goldenberg DP (**1989**). Circularly permuted proteins. *Protein Eng.* 2: 493-495.

Gong H, Fleming PJ & Rose GD (**2005**). Building native protein conformation from highly approximate backbone torsion angles. *Proc. Natl. Acadd. Sci. U.S.A.* 102: 16227-16232.

Goodsell DS & **Olson** AJ (**1990**). Automated docking of substrates to proteins by simulated annealing. *Proteins*, 8: 195-202.

Gough J, Karplus K, Hughey R & Chothia C (**2001**). Assignment of homology to genome sequences using a library of hidden Markov models that represent all proteins of known structure. *J. Mol. Biol.* 313: 903-919.

Govindarajan S, Recabarren R & Goldstein RA (**1999**). Estimating the total number of protein folds. *Proteins*, 35: 408-414.

Gray K, Richardson T, Kretz K, Short J, Bartnek F, Knowles R, Kan L, Swanson P & Robertson D (**2001**). Rapid evolution of reversible denaturation and elevated melting temperature in a microbial haloalkane dehalogenase. *Adv. Synth. Catal.* 343: 607-617.

Green RD (**1974**). Hydrogen Bonding by C-H Groups. *Macmillan*, London, England.

Gribble GW (**2003**). The diversity of naturally produced organohalogens. *Chemosphere*, 52: 289-297.

Gribble GW (**2004**). Natural organohalogens. *Euro Chlor* (http://www.eurochlor.org/).

Grishin NV (**2001**). Fold change in evolution of protein structures. *J. Struct. Biol.* 134, 167-185.

Guerrier-Takada C, Gardiner K, Marsh T, Pace N & Altman S (**1983**). The RNA moiety of ribonuclease P is the catalytic subunit of the enzyme. *Cell*, 35: 849-857.

Gunasekaran K, Ramakrishnan C & Balaram P (**1996**). Disallowed ramachandran conformations of amino acid residues in protein structures. *J. Mol. Biol.* 264, 191-198.

Gunasekaran K, Nagarajaram HA, Ramakrishnan C & Balaram P (**1998**). Stereochemical punctuation marks in protein structures: glycine and proline containing helix stop signals. *J. Mol. Biol.* 275: 917-932.

Güntert P (**2009**). Automated structure determination from NMR spectra. *Eur. Biophys. J.* 38: 129-143.

Gupta A, Van Vlijmen HWT & Singh J (**2004**). A classification of disulfide patterns and its relationship to protein structure and function. *Protein Sci.* 13: 2045-2058.

Hagen SJ, Hofrichter J, Szabo A & Eaton WA (**1996**). Diffusion-limited contact formation in unfolded cytochrome c: estimating the maximum rate of protein folding. *Proc. Natl. Acad. Sci. U.S.A.* 93: 11615-11617.

Halder M, Mukherjee P, Bose S, Hargrove MS, Song X & Petrich JW (**2007**). Solvation dynamics in protein environments: comparison of fluorescence upconversion measurements of coumarin 153 in monomeric hemeproteins with molecular dynamics simulations. *J. Chem. Phys.* 127: 055101/1- 055101/6.

Halperin I, Ma B, Wolfson H & Nussinov R (**2002**). Principles of docking: An overview of search algorithms and a guide to scoring functions. *Proteins*, 47: 409-443.

Hammes-Schiffer S (**2002**). Impact of enzyme motion on activity. *Biochemistry*, 41: 13335-13343.

Hammes-Schiffer S & **Benkovic** SJ (**2006**). Relating protein motion to catalysis. *Annu. Rev. Biochem.* 75: 519-541.

Hart TN & **Read** RJ (**1992**). A multiple-start Monte Carlo docking method. *Proteins*, 13: 206-222.

Hayes RJ, Bentzien J, Ary ML, Hwang MY, Jacinto JM, Vielmetter J, Kundu A & Dahiyat BI (**2002**). Combining computational and experimental screening for rapid optimization of protein properties. *Proc. Natl. Acad. Sci. U.S.A.* 99: 15926-15931.

Head-Gordon T, Head-Gordon M, Frisch MJ, Brooks III CL & Pople JA (**1991**). Theoretical study of blocked glycine and alanine peptide analogs. *J. Am. Chem. Soc.* 113: 5989-5997.

Hegyi H & **Gerstein** M (**1999**). The relationship between protein structure and function: a comprehensive survey with application to the yeast genome. *J. Mol. Biol.* 288: 147-164.

Heikinheimo P, Goldman A, Jeffries C & Ollis DL (**1999**). Of barn owls and bankers: a lush variety of alpha/beta hydrolases. *Structure* 7: R141-146.

Helms V (**2007**). Protein dynamics tightly connected to the dynamics of surrounding and internal water molecules. *Chemphyschem*, 8: 23-33.

Henchman RH, Tai K, Shen T & McCammon JA (**2002**). Properties of water molecules in the active site gorge of acetylcholinesterase from computer simulation. *Biophys. J.* 82: 2671-2682.

Henderson R (**1970**). Structure of crystalline alpha-chymotrypsin. IV. The structure of indoleacryloyl-alpha-chyotrypsin and its relevance to the hydrolytic mechanism of the enzyme. *J. Mol. Biol.* 54: 341-354.

Henderson R, Baldwin JM, Ceska TA, Zemlin F, Beckmann E & Downing KH (**1990**). Model for the structure of bacteriorhodopsin based on high-resolution electron cryo-microscopy. *J. Mol. Biol.* 213: 899-929.

Henderson R & **Unwin** PN (**1975**). Three-dimensional model of purple membrane obtained by electron microscopy. *Nature*, 257: 28-32.

Henri V (**1903**). L ois Generales de l'action des diastases. *Hermann*, Paris, France.

Henry AA & **Romesberg** FE (**2005**). The evolution of DNA polymerases with novel activities. *Curr. Opin. Biotechnol.* 16, 370-377.

Henzler-Wildman KA, Thai V, Lei M, Ott M, Wolf-Watz M, Fenn T, Pozharski E, Wilson MA, Petsko GA, Karplus M, Hübner C G & Kern D (**2007a**). Intrinsic motions along an enzymatic reaction trajectory. *Nature*, 450: 838-844.

Henzler-Wildman KA, Lei M, Thai V, Kerns SJ, Karplus M & Kern D (**2007b**). A hierarchy of timescales in protein dynamics is linked to enzyme catalysis. *Nature*, 450: 913-916.

Hite RK, Raunser S & Walz T (**2007**). Revival of electron crystallography. *Curr. Opin. Struct. Biol.* 17: 389-395.

Hoang TX, Trovato A, Seno F, Banavar JR & Maritan A (**2004**). Geometry and symmetry presculpt the free-energy landscape of proteins. *Proc. Natl. Acad. Sci. U.S.A.* 101: 7960-7964.

Holloway P, Knoke KL, Trevors JT & Lee H (**1998**). Alteration of the substrate range of haloalkane dehalogenase by site-directed mutagenesis. *Biotechnol. Bioeng.* 59: 520-523.

Holmes J & **Morrell** F (**1957**). Oscillographic mass spectrometric monitoring of gas chromatography. *Appl. Spectrosc.* 11: 86-87.

Holmquist M (**2000**). Alpha/Beta-hydrolase fold enzymes: structures, functions and mechanisms. *Curr. Protein Pept. Sci.* 1: 209-35.

Hol WG, van Duijnen PT & Berendsen HJ (**1978**). The alpha-helix dipole and the properties of proteins. *Nature*, 273: 443-446.

Honour JW (**2006**). Gas chromatography-mass spectrometry. *Methods Mol. Biol.* 324: 53-74.

Hou T, Wang J, Chen L & Xu X (**1999**). Automated docking of peptides and proteins by using a genetic algorithm combined with a tabu search. *Protein Eng.* 12: 639-648.

Howard EI, Sanishvili R, Cachau RE, Mitschler A, Chevrier B, Barth P, Lamour V, Van Zandt M, Sibley E, Bon C, Moras D, Schneider TR, Joachimiak A & Podjarny A (**2004**). Ultrahigh resolution drug design I: details of interactions in human aldose reductase-inhibitor complex at 0.66 Å. *Proteins*, 55: 792-804.

Hritz J, Zoldák G & Sedlák E (**2006**). Cofactor assisted gating mechanism in the active site of NADH oxidase from Thermus thermophilus. *Proteins*, 64: 465-476.

Hsing M & **Cherkasov** A (**2008**). Indel PDB: a database of structural insertions and deletions derived from sequence alignments of closely related proteins. *BMC Bioinf.* 9: 293.

Huang X, Yang X, Luft BJ & Koide S (**1998**). NMR identification of epitopes of Lyme disease antigen OspA to monoclonal antibodies. *J. Mol. Biol.* 281: 61-67.

Hubbard TJ, Ailey B, Brenner SE, Murzin AG & Chothia C (**1998**). SCOP, Structural Classification of Proteins database: applications to evaluation of the effectiveness of sequence alignment methods and statistics of protein structural data. *Acta Crystallogr., Sect. D: Biol. Crystallogr.* 54: 1147-1154.

Humphrey W, Dalke A & Schulten K (**1996**). VMD: visual molecular dynamics. *J. Mol. Graphics*, 14: 33-38.

Hur S, Kahn K & Bruice TC (**2003**). Comparison of formation of reactive conformers for the SN2 displacements by CH3CO2- in water and by Asp124-CO2- in a haloalkane dehalogenase. *Proc. Natl. Acad. Sci. U.S.A.* 100: 2215-2219.

Igumenova TI, Frederick KK & Wand AJ (**2006**). Characterization of the fast dynamics of protein amino acid side chains using NMR relaxation in solution. *Chem. Rev.* 106: 1672-1699.

Ikeda Y, Tanaka T & Noguchi T (**1997**). Conversion of non-allosteric pyruvate kinase isozyme into an allosteric enzyme by a single amino acid substitution. *J. Biol. Chem.* 272: 20495-20501.

Ikehara K & **Okazawa** E (**1993**). Unusually biased nucleotide sequences on sense strands of *Flavobacterium* sp. genes produce nonstop frames on the corresponding antisense strands. *Nucleic Acids Res.* 21: 2193-2199.

Ikehara K, Amada F, Yoshida S, Mikata Y & Tanaka A (**1996**). A possible origin of newly-born bacterial genes: significance of GC-rich nonstop frame on antisense strand. *Nucleic Acids Res.* 24: 4249-4255.

Ikehara K (**2002**). Origins of gene, genetic code, protein and life: comprehensive view of life systems from a GNC-SNS primitive genetic code hypothesis. *J. Biosci.* 27: 165-186.

Ikehara K, Omori Y, Arai R & Hirose A (**2002**). A novel theory on the origin of the genetic code: a GNC-SNS hypothesis. *J. Mol. Evol.* 54: 530-538.

Ikehara K (**2005**). Possible steps to the emergence of life: the [GADV]-protein world hypothesis. *Chem. Rec.* 5: 107-118.

Iqbalsyah TM & **Doig** AJ (**2004**). Effect of the N3 residue on the stability of the alpha-helix. *Protein Sci.* 13: 32-39.

Ismer L, Ireta J & Neugebauer J (**2008**). First-principles free-energy analysis of helix stability: the origin of the low entropy in pi helices. *J. Phys. Chem. B*, 112, 4109-4112.

Isralewitz B, Baudry J, Gullingsrud J, Kosztin D & Schulten K (**2001**). Steered molecular dynamics investigations of protein function. *J. Mol. Graphics Modell.* 19: 13-25.

Itoh T & **Tomizawa** J (**1980**). Formation of an RNA primer for initiation of replication of ColE1 DNA by ribonuclease H. *Proc. Natl. Acad. Sci. U.S.A.* 77: 2450-2454.

Ito M, Prokop Z, Klvaňa M, Otsubo Y, Tsuda M, Damborský J & Nagata Y (**2007**). Degradation of beta-hexachlorocyclohexane by haloalkane dehalogenase LinB from gamma-hexachlorocyclohexane-utilizing bacterium *Sphingobium* sp. MI1205. *Arch. Microbiol.* 188: 313-325.

Iwasaki I, Utsumi S & Ozawa T (**1952**). New colorimetric determination of chloride using mercuric thiocyanate and ferric ion. *Bull. Chem. Soc. Jap.* 25: 226.

Jackson TA, Lim M & Anfinrud PA (**1994**). Complex nonexponential relaxation in myoglobin after photodissociation of MbCO: measurement and analysis from 2 ps to 56 [upsilon]s. *Chem. Phys.* 180: 131-140.

Jaeger KE & **Reetz** MT (**1998**). Microbial lipases form versatile tools for biotechnology. *Trends Biotechnol.* 16: 396-403.

Jager M, Deechongkit S, Koepf EK, Nguyen H, Gao J, Powers ET, Gruebele M & Kelly JW (**2008**). Understanding the mechanism of beta-sheet folding from a chemical and biological perspective. *Biopolymers*, 90: 751-758.

Jakopitsch C, Droghetti E, Schmuckenschlager F, Furtmüller PG, Smulevich G & Obinger C (**2005**). Role of the main access channel of catalase-peroxidase in catalysis. *J. Biol. Chem.* 280: 42411-42422.

James AT & **Martin** AJP (**1952**). Gas-liquid partition chromatography: the separation and micro-estimation of ammonia and the methylamines. *Biochem. J.* 52: 238-242.

Janin J & **Wodak** SJ (**1983**). Structural domains in proteins and their role in the dynamics of protein function. *Prog. Biophys. Mol. Biol.* 42: 21-78.

Janin J, Rodier F, Chakrabarti P & Bahadur RP (**2007**). Macromolecular recognition in the Protein Data Bank. *Acta Crystallogr., Sect. D: Biol. Crystallogr.* 63: 1-8.

Janssen DB, Scheper A & Witholt B (**1984**). Biodegradation of 2-chloroethanol and 1,2-dichloroethane by pure bacterial cultures. *Prog. Ind. Microbiol.* 20: 169-178.

Janssen DB, Scheper A, Dijkhuizen L & Witholt B (**1985**). Degradation of halogenated aliphatic compounds by *Xanthobacter autotrophicus* GJ10. *Appl. Environ. Microbiol.* 49: 673-677.

Janssen DB, Keuning S & Witholt B (**1987**). Involvement of a Quinoprotein Alcohol Dehydrogenase and an NAD-dependent Aldehyde Dehydrogenase in 2-Chloroethanol Metabolism in *Xanthobacter autotrophicus* GJ10. *J. Gen. Microbiol.* 133: 85-92.

Janssen DB, Gerritse J, Brackman J, Kalk C, Jager D & Witholt B (**1988**). Purification and characterization of a bacterial dehalogenase with activity toward halogenated alkanes, alcohols and ethers. *Eur. J. Biochem.* 171: 67-72.

Janssen DB, van der Ploeg JR & Pries F (**1995**). Genetic adaptation of bacteria to halogenated aliphatic compounds. *Environ. Health Perspect.* 103 Suppl 5, 29-32.

Janssen DB (**2004**). Evolving haloalkane dehalogenases. *Curr. Opin. Chem. Biol.* 8, 150-159.

Janssen DB, Dinkla IJT, Poelarends GJ & Terpstra P (**2005**). Bacterial degradation of xenobiotic compounds: evolution and distribution of novel enzyme activities. *Environ. Microbiol.* 7: 1868-1882.

Jarymowycz VA & **Stone** MJ (**2006**). Fast time scale dynamics of protein backbones: NMR relaxation methods, applications, and functional consequences. *Chem. Rev.* 106: 1624-1671.

Jasanoff A & **Fersht** AR (**1994**). Quantitative determination of helical propensities from trifluoroethanol titration curves. *Biochemistry*, 33: 2129-2135.

Jeffares DC, Poole AM & Penny D (**1998**). Relics from the RNA world. *J. Mol. Evol.* 46: 18-36.

Jeffrey GA & **Maluszynska** H (**1982**). A survey of hydrogen bond geometries in the crystal structures of amino acids. *Int. J. Biol. Macromol.* 4: 173-185.

Jensen F (**2006**). 3. Electronic structure methods: independent-particle models. *In* Introduction to computational chemistry (pp. 80-132). *John Wiley and Sons*, Chichester, England.

Jesenská A, Sedláček I & Damborský J (**2000**). Dehalogenation of haloalkanes by *Mycobacterium tuberculosis* H37Rv and other mycobacteria. *Appl. Environ. Microbiol.* 66: 219-222.

Jesenská A, Bartoš M, Czerneková V, Rychlík I, Pavlík I & Damborský J (**2002**). Cloning and expression of the haloalkane dehalogenase gene dhmA from *Mycobacterium avium* N85 and preliminary characterization of DhmA. *Appl. Environ. Microbiol.* 68: 3724-3730.

Jesenská A, Pavlová M, Strouhal M, Chaloupková R, Tešínská I, Monincová M, Prokop Z, Bartoš M, Pavlík I, Rychlík I, Möbius P, Nagata Y & Damborsky J (**2005**). Cloning, biochemical properties, and distribution of mycobacterial haloalkane dehalogenases. *Appl. Environ. Microbiol.* 71: 6736-6745.

Jesenská A, Monincová M, Koudeláková T, Hasan K, Chaloupková R, Prokop Z, Geerlof A & Damborský J (**2009**). Biochemical characterization of haloalkane dehalogenases DrbA and DmbC, representatives of a novel subfamily. *Appl. Environ. Microbiol.* 75: 5157-5160.

Jiang F & **Kim** SH (**1991**). "Soft docking": matching of molecular surface cubes. *J. Mol. Biol.* 219: 79-102.

Jimenez R, Fleming GR, Kumar PV & Maroncelli M (**1994**). Femtosecond solvation dynamics of water. *Nature*, 369: 471-473.

Jiménez-Sánchez A (**1995**). On the origin and evolution of the genetic code. *J. Mol. Evol.* 41: 712-716.

Johnston WK, Unrau PJ, Lawrence MS, Glasner ME & Bartel DP (**2001**). RNA-catalyzed RNA polymerization: accurate and general RNA-templated primer extension. *Science*, 292: 1319-1325.

Jones DT (**1999**). Protein secondary structure prediction based on position-specific scoring matrices. *J. Mol. Biol.* 292: 195-202.

Jones DT (**2003**). Structural biology. Learning to speak the language of proteins. *Science*, 302: 1347-1348.

Jones G, Willett P, Glen RC, Leach AR & Taylor R (**1997**). Development and validation of a genetic algorithm for flexible docking. *J. Mol. Biol.* 267: 727-748.

Jorgensen WL, Chandrasekhar J, Madura JD, Impey RW & Klein ML (**1983**). Comparison of simple potential functions for simulating liquid water. *J. Chem. Phys.* 79: 926-935.

Jorgensen WL & **Tirado-Rives** J (**1988**). The OPLS [optimized potentials for liquid simulations] potential functions for proteins, energy minimizations for crystals of cyclic peptides and crambin. *J. Am. Chem. Soc.* 110: 1657-1666.

Jorgensen WL, Maxwell DS & Tirado-Rives J (**1996**). Development and testing of the OPLS all-atom force field on conformational energetics and properties of organic liquids. *J. Am. Chem. Soc.* 118: 11225-11236.

Kabsch W & **Sander** C (**1983**). Dictionary of protein secondary structure: pattern recognition of hydrogen-bonded and geometrical features. *Biopolymers*, 22: 2577-2637.

Kane JF & **Hartley** DL (**1988**). Formation of recombinant protein inclusion bodies in *Escherichia coli*. *Trends Biotechnol.* 6: 95-101.

Karplus M (**1959**). Contact electron-spin coupling of nuclear magnetic moments. *J. Chem. Phys.* 30: 11-15.

Karplus M (**1963**). Vicinal proton coupling in nuclear magnetic resonance. *J. Am. Chem. Soc.* 85: 2870-2871.

Karplus M & **McCammon** JA (**1981**). The internal dynamics of globular proteins. *CRC Crit. Rev. Biochem.* 9: 293-349.

Karplus M & **McCammon** JA (**1983**). Dynamics of proteins: elements and function. *Annu. Rev. Biochem.* 52: 263-300.

Karplus M (**2000**). Aspects of protein reaction dynamics: deviations from simple behavior. *J. Phys. Chem. B*, 104: 11-27.

Karplus M & **Kuriyan** J (**2005**). Molecular dynamics and protein function. *Proc. Natl. Acad. Sci. U.S.A.* 102: 6679-6685.

Karush F (**1950**). Heterogeneity of the binding sites of bovine serum albumin. *J. Am. Chem. Soc.* 72: 2705-2713.

Kay LE, Muhandiram DR, Wolf G, Shoelson SE & Forman-Kay JD (**1998**). Correlation between binding and dynamics at SH2 domain interfaces. *Nat. Struct. Biol.* 5: 156-163.

Kay LE (**2005**). NMR studies of protein structure and dynamics. *J. Magn. Reson.* 173: 193-207.

Keefe AD & **Miller** SL (**1995**). Are polyphosphates or phosphate esters prebiotic reagents? *J. Mol. Evol.* 41: 693-702.

Kelley LA & **Sternberg** MJE (**2009**). Protein structure prediction on the Web: a case study using the Phyre server. *Nat. Protoc.* 4: 363-371.

Kelly SM, Jess TJ & Price NC (**2005**). How to study proteins by circular dichroism. *Biochim. Biophys. Acta*, 1751: 119-139.

Kendrew JC, Bodo G, Dintzis HM, Parrish RG, Wyckoff H & Phillips DC (**1958**). A three-dimensional model of the myoglobin molecule obtained by X-ray analysis. *Nature*, 181: 662-666.

Kendrew JC, Dickerson RE, Strandberg BE, Hart RG, Davies DR, Phillips DC & Shore VC (**1960**). Structure of myoglobin: a three-dimensional Fourier synthesis at 2 A. resolution. *Nature*, 185: 422-427.

Kendrew JC (**1962**). Myoglobin and the structure of proteins. *In* Nobel Lectures Chemistry 1942-1962 (pp. 676-698). *Elsevier Publishing Co. (1964)*, Amsterdam, The Netherlands.

Kennes C, Pries F, Krooshof GH, Bokma E, Kingma J & Janssen DB (**1995**). Replacement of tryptophan residues in haloalkane dehalogenase reduces halide binding and catalytic activity. *Eur. J. Biochem.* 228: 403-407.

Kent SBH (**2009**). Total chemical synthesis of proteins. *Chem. Soc. Rev.* 38: 338-351.

Keuning S, Janssen DB & Witholt B (**1985**). Purification and characterization of hydrolytic haloalkane dehalogenase from *Xanthobacter autotrophicus* GJ10. *J. Bacteriol.* 163: 635-639.

Khajehpour M, Rietveld I, Vinogradov S, Prabhu NV, Sharp KA & Vanderkooi JM (**2003**). Accessibility of oxygen with respect to the heme pocket in horseradish peroxidase. *Proteins*, 53: 656-666.

Kimura Y, Vassylyev DG, Miyazawa A, Kidera A, Matsushima M, Mitsuoka K, Murata K, Hirai T & Fujiyoshi Y (**1997**). Surface of bacteriorhodopsin revealed by high-resolution electron crystallography. *Nature*, 389: 206-211.

King SM & **Johnson** WC (**1999**). Assigning secondary structure from protein coordinate data. *Proteins*, 35: 313-320.

Kitao A & **Go** N (**1999**). Investigating protein dynamics in collective coordinate space. *Curr. Opin. Struct. Biol.* 9: 164-169.

Kleywegt GJ (**1999**). Recognition of spatial motifs in protein structures. *J. Mol. Biol.* 285: 1887-1897.

Kleywegt GJ & **Jones** TA (**1994**). Detection, delineation, measurement and display of cavities in macromolecular structures. *Acta Crystallogr., Sect. D: Biol. Crystallogr.* 50: 178-185.

Kmuníček J, Luengo S, Gago F, Ortiz AR, Wade RC & Damborský J (**2001**). Comparative binding energy analysis of the substrate specificity of haloalkane dehalogenase from *Xanthobacter autotrophicus* GJ10. *Biochemistry*, 40: 8905-8917.

Kmuníček J, Boháč M, Luengo S, Gago F, Wade RC & Damborský J (**2003**). Comparative binding energy analysis of haloalkane dehalogenase substrates: modelling of enzyme-substrate complexes by molecular docking and quantum mechanical calculations. *J. Comput. Aided Mol. Design*, 17: 299-311.

Kmuníček J, Hynková K, Jedlička T, Nagata Y, Negri A, Gago F, Wade RC & Damborský J (**2005**). Quantitative analysis of substrate specificity of haloalkane dehalogenase LinB from *Sphingomonas paucimobilis* UT26. *Biochemistry*, 44: 3390-3401.

Knight RD & **Landweber** LF (**1998**). Rhyme or reason: RNA-arginine interactions and the genetic code. *Chem. Biol.* 5: R215-220.

Kobe B, Guncar G, Buchholz R, Huber T, Maco B, Cowieson N, Martin JL, Marfori M & Forwood JK (**2008**). Crystallography and protein-protein interactions: biological interfaces and crystal contacts. *Biochem. Soc. Trans.* 36: 1438-1441.

Koehl P & **Levitt** M (**1999**). Structure-based conformational preferences of amino acids. *Proc. Natl. Acad. Sci. U.S.A.* 96: 12524-12529.

Kohen A, Cannio R, Bartolucci S & Klinman JP (**1999**). Enzyme dynamics and hydrogen tunnelling in a thermophilic alcohol dehydrogenase. *Nature*, 399: 496-499.

Kolodziej AF, Tan T & Koshland Jr. DE (**1996**). Producing positive, negative, and no cooperativity by mutations at a single residue located at the subunit interface in the aspartate receptor of Salmonella typhimurium. *Biochemistry*, 35: 14782-14792.

Koshland Jr. DE (**1958**). Application of a theory of enzyme specificity to protein synthesis. *Proc. Natl. Acad. Sci. U.S.A.* 44: 98-104.

Koshland Jr. DE, Némethy G & Filmer D (**1966**). Comparison of experimental binding data and theoretical models in proteins containing subunits. *Biochemistry*, 5: 365-385.

Koshland Jr. DE (**1976**). Role of flexibility in the specificity, control and evolutiion of enzymes. *FEBS Lett.* 62: E47-52.

Koshland Jr. DE (**1995**). The key-lock theory and the induced fit theory. *Angew. Chem. Int. Ed.* 33: 2375-2378.

Koshland Jr. DE (**1996**). The structural basis of negative cooperativity: receptors and enzymes. *Curr. Opin. Struct. Biol.* 6: 757-761.

Koshland Jr. DE (**1998**). Conformational changes: how small is big enough? *Nat. Med.* 4: 1112-1114.

Koshland Jr. DE (**2002a**). The application and usefulness of the ratio k(cat)/K(M). *Bioorg. Chem.* 30: 211-213.

Koshland Jr. DE (**2002b**). The seven pillars of life. *Science*, 295: 2215-2216.

Koshland Jr. DE & **Hamadani** K (**2002**). Proteomics and models for enzyme cooperativity. *J. Biol. Chem.* 277: 46841-46844.

Koshland Jr. DE (**2004**). Crazy, but correct. *Nature*, 432: 447.

Koshland Jr. DE (**2007**). The Cha-Cha-Cha Theory of Scientific Discovery. *Science*, 317: 761-762.

Kosinski J, Cymerman IA, Feder M, Kurowski MA, Sasin JM & Bujnicki JM (**2003**). A "FRankenstein's monster" approach to comparative modeling: merging the finest fragments of Fold-Recognition models and iterative model refinement aided by 3D structure evaluation. *Proteins*, 53 Suppl 6: 369-379.

Kosinski J, Gajda MJ, Cymerman IA, Kurowski MA, Pawlowski M, Boniecki M, Obarska A, Papaj G, Sroczynska-Obuchowicz P, Tkaczuk KL, Sniezynska P, Sasin JM, Augustyn A, Bujnicki JM & Feder M (**2005**). FRankenstein becomes a cyborg: the automatic recombination and realignment of fold recognition models in CASP6. *Proteins*, 61 Suppl 7: 106-113.

Kotik, M., Štěpánek V, Kyslík P & Marešová H (**2007**). Cloning of an epoxide hydrolase-encoding gene from *Aspergillus niger* M200, overexpression in *E. coli*, and modification of activity and enantioselectivity of the enzyme by protein engineering. *J. Biotechnol.* 132: 8-15.

Kottalam J & **Case** DA (**1988**). Dynamics of ligand escape from the heme pocket of myoglobin. *J. Am. Chem. Soc.* 110: 7690-7697.

Kovach IM, Qian N & Bencsura A (**1994**). Efficient product clearance through exit channels in substrate hydrolysis by acetylcholinesterase. *FEBS Lett.* 349: 60-64.

Kozlíková B, Andres F & Sochor J (**2007**). Visualization of tunnels in protein molecules. *In* 5th international conference on virtual reality, computer graphics, visualization and interaction, Grahamstown, South Africa (pp. 111-118). *Association for Computing Machinery*, New York, NY, USA.

Krissinel E & **Henrick** K (**2007**). Inference of macromolecular assemblies from crystalline state. *J. Mol. Biol.* 372: 774-797.

Krooshof GH, Floris R, Tepper AW & Janssen DB (**1999**). Thermodynamic analysis of halide binding to haloalkane dehalogenase suggests the occurrence of large conformational changes. *Protein Sci.* 8: 355-360.

Krooshof GH, Kwant EM, Damborský J, Koča J & Janssen DB (**1997**). Repositioning the catalytic triad aspartic acid of haloalkane dehalogenase: effects on stability, kinetics, and structure. *Biochemistry*, 36: 9571-9580.

Krooshof GH, Ridder IS, Tepper AW, Vos GJ, Rozeboom HJ, Kalk KH, Dijkstra BW & Janssen DB (**1998**). Kinetic analysis and X-ray structure of haloalkane dehalogenase with a modified halide-binding site. *Biochemistry*, 37: 15013-15023.

Kruger K, Grabowski PJ, Zaug AJ, Sands J, Gottschling DE & Cech TR (**1982**). Self-splicing RNA: autoexcision and autocyclization of the ribosomal RNA intervening sequence of *Tetrahymena*. *Cell*, 31: 147-157.

Kryshtafovych A, Venclovas C, Fidelis K & Moult J (**2005**). Progress over the first decade of CASP experiments. *Proteins*, 61 Suppl 7: 225-236.

Kuhlman B, Dantas G, Ireton GC, Varani G, Stoddard BL & Baker D (**2003**). Design of a novel globular protein fold with atomic-level accuracy. *Science*, 302: 1364-1368.

Kuhn H & **Waser** J (**1994**). On the origin of the genetic code. *FEBS Lett.* 352: 259-264.

Kulakova AN, Larkin MJ & Kulakov LA (**1997**). The plasmid-located haloalkane dehalogenase gene from *Rhodococcus rhodochrous* NCIMB 13064. *Microbiol.* 143: 109-115.

Kulakova AN, Stafford TM, Larkin MJ & Kulakov LA (**1995**). Plasmid pRTL1 controlling 1-chloroalkane degradation by *Rhodococcus rhodochrous* NCIMB 13064. *Plasmid*, 33: 208-217.

Kulakov LA, Poelarends GJ, Janssen DB & Larkin MJ (**1999**). Characterization of IS2112, a new insertion sequence from *Rhodococcus*, and its relationship with mobile elements belonging to the IS110 family. *Microbiol.* 145: 561-568.

Kumar S & **Bansal** M (**1998**). Geometrical and sequence characteristics of alpha-helices in globular proteins. *Biophys. J.* 75: 1935-1944.

Kumar S, Rosenberg JM, Bouzida D, Swendsen RH & Kollman PA (**1995**). Multidimensional free-energy calculations using the weighted histogram analysis method. *J. Comput. Chem.* 16: 1339-1350.

Kumar S, Rosenberg JM, Bouzida D, Swendsen RH & Kollman PA (**1992**). THE weighted histogram analysis method for free-energy calculations on biomolecules. I. The method. *J. Comput. Chem.* 13: 1011-1021.

Kuntz ID, Blaney JM, Oatley SJ, Langridge R & Ferrin TE (**1982**). A geometric approach to macromolecule-ligand interactions. *J. Mol. Biol.* 161: 269-288.

Kurakin A (**2009**). Scale-free flow of life: on the biology, economics, and physics of the cell. *Theor. Biol. Med. Modell.* 6: 6-33.

Kurowski MA & **Bujnicki** JM (**2003**). GeneSilico protein structure prediction meta-server. *Nucleic Acids Res.* 31: 3305-3307.

Kurzyński M (**1998**). A synthetic picture of intramolecular dynamics of proteins. Towards a contemporary statistical theory of biochemical processes. *Prog. Biophys. Mol. Biol.* 69: 23-82.

Kuszewski J, Qin J, Gronenborn AM & Clore GM (**1995**). The impact of direct refinement against 13C alpha and 13C beta chemical shifts on protein structure determination by NMR. *J. Magn. Reson., Ser. B*, 106: 92-96.

Laberge M & **Yonetani** T (**2008**). Molecular dynamics simulations of hemoglobin A in different states and bound to DPG: effector-linked perturbation of tertiary conformations and HbA concerted dynamics. *Biophys. J.* 94: 2737-2751.

Labesse G, Colloc'h N, Pothier J & Mornon JP (**1997**). P-SEA: a new efficient assignment of secondary structure from C alpha trace of proteins. *Comput. Appl. Biosci.* 13: 291-295.

Lakowicz JR & **Weber** G (**1973**). Quenching of protein fluorescence by oxygen. Detection of structural fluctuations in proteins on the nanosecond time scale. *Biochemistry*, 12: 4171-4179.

Lamarck, JB (**1809**). Philosophie zoologique, ou exposition des considérations relatives a l'histoire naturelle des animaux; a la diversité de leur organisation et des facultés qu'Ils en obtiennent. *Dentu*, Paris, France.

Lauble H, Miehlich B, Förster S, Kobler C, Wajant H & Effenberger F (**2002**). Structure determinants of substrate specificity of hydroxynitrile lyase from Manihot esculenta. *Protein Sci.* 11: 65-71.

Lau EY, Kahn K, Bash PA & Bruice TC (**2000**). The importance of reactant positioning in enzyme catalysis: a hybrid quantum mechanics/molecular mechanics study of a haloalkane dehalogenase. *Proc. Natl. Acad. Sci. U.S.A.* 97: 9937-9942.

Lavalette D, Tétreau C & Mouawad L (**2006**). Ligand migration and escape pathways in haem proteins. *Biochem. Soc. Trans.* 34: 975-978.

Lazcano A, Guerrero R, Margulis L & Oró J (**1988**). The evolutionary transition from RNA to DNA in early cells. *J. Mol. Evol.* 27: 283-290.

Lazcano A & **Miller** SL (**1996**). The origin and early evolution of life: prebiotic chemistry, the pre-RNA world, and time. *Cell*, 85: 793-798.

Leach AR (**1996**). 2. Quantum mechanical models. *In* Molecular modelling: principles and applications (pp. 25-130). *Addison Wesley Longman*, Harlow, England.

Lee AL, Kinnear SA & Wand AJ (**2000**). Redistribution and loss of side chain entropy upon formation of a calmodulin-peptide complex. *Nat. Struct. Biol.* 7: 72-77.

Lee AL & **Wand** AJ (**2001**). Microscopic origins of entropy, heat capacity and the glass transition in proteins. *Nature*, 411: 501-504.

Lee FS, Chu ZT, Bolger MB & Warshel A (**1992**). Calculations of antibody-antigen interactions: microscopic and semi-microscopic evaluation of the free energies of binding of phosphorylcholine analogs to McPC603. *Protein Eng.* 5: 215-228.

Lee P, Kuo K, Chu P, Liu EM & Lin J (**2009**). SLITHER: a web server for generating contiguous conformations of substrate molecules entering into deep active sites of proteins or migrating through channels in membrane transporters. *Nucleic Acids Res.* 37: W559-564.

Lehmann J (**2000**). Physico-chemical constraints connected with the coding properties of the genetic system. *J. Theor. Biol.* 202: 129-144.

Levinthal C (**1968**). Are there pathways for protein folding? *J. Chim. Phys.* 65: 44-45.

Levinthal C (**1969**). How to fold graciously. *In* Mossbauer spectroscopy in biological systems. Proceedings of the University of Illinois Bulletin (pp. 22-24), University of Illinois Press, Champaign, IL, USA.

Lewandowicz A, Rudziński J, Tronstad L, Widersten M, Ryberg P, Matsson O & Paneth P (**2001**). Chlorine kinetic isotope effects on the haloalkane dehalogenase reaction. *J. Am. Chem. Soc.* 123: 4550-4555.

Li C, Hassler M & Bugg TDH (**2008**). Catalytic promiscuity in the alpha/beta-hydrolase superfamily: hydroxamic acid formation, C--C bond formation, ester and thioester hydrolysis in the C--C hydrolase family. *Eur. J. Chem. Biol.* 9: 71-76.

Li M, Phylip LH, Lees WE, Winther JR, Dunn BM, Wlodawer A, Kay J & Gustchina A (**2000**). The aspartic proteinase from *Saccharomyces cerevisiae* folds its own inhibitor into a helix. *Nat. Struct. Biol.* 7: 113-117.

Li W, Liu H, Scott EE, Gräter F, Halpert JR, Luo X, Shen J & Jiang H (**2005**). Possible pathway(s) of testosterone egress from the active site of cytochrome P450 2B1: A steered molecular dynamics simulation. *Drug Metab. Dispos.* 33: 910-919.

Liang J & **Dill** KA (**2001**). Are proteins well-packed? *Biophys. J.* 81: 751-766.

Liepinsh E & **Otting** G (**1997**). Organic solvents identify specific ligand binding sites on protein surfaces. *Nat. Biotechnol.* 15: 264-268.

Liesener A & **Karst** U (**2005**). Monitoring enzymatic conversions by mass spectrometry: a critical review. *Anal. Bioanal. Chem.* 382: 1451-1464.

Lightstone FC, Zheng YJ, Maulitz AH & Bruice TC (**1997**). Non-enzymatic and enzymatic hydrolysis of alkyl halides: a haloalkane dehalogenation enzyme evolved to stabilize the gas-phase transition state of an SN2 displacement reaction. *Proc. Natl. Acad. Sci. U.S.A.* 94: 8417-8420.

Lightstone FC & **Bruice** TC (**1996**). Ground state conformations and entropic and enthalpic factors in the efficiency of intramolecular and enzymatic reactions. 1. Cyclic anhydride formation by substituted glutarates, succinate, and 3,6-endoxo-Δ4-tetrahydrophthalate monophenyl esters. *J. Am. Chem. Soc.* 118: 2595-2605.

Lightstone FC, Zheng Y & Bruice TC (**1998**). Molecular dynamics simulations of ground and transition states for the SN2 displacement of Cl- from 1,2-dichloroethane at the active site of *Xanthobacter autotrophicus* haloalkane dehalogenase. *J. Am. Chem. Soc.* 120: 5611-5621.

Lindorff-Larsen K, Best RB, Depristo MA, Dobson CM & Vendruscolo M (**2005**). Simultaneous determination of protein structure and dynamics. *Nature*, 433: 128-132.

Liu F, Du D, Fuller AA, Davoren JE, Wipf P, Kelly JW & Gruebele M (**2008**). An experimental survey of the transition between two-state and downhill protein folding scenarios. *Proc. Natl. Acad. Sci. U.S.A.* 105: 2369-2374.

Liu M & **Wang** S (**1999**). MCDOCK: a Monte Carlo simulation approach to the molecular docking problem. *J. Comput. Aided Mol. Des.* 13: 435-451.

Liu T, Whitten ST & Hilser VJ (**2007**). Functional residues serve a dominant role in mediating the cooperativity of the protein ensemble. *Proc. Natl. Acad. Sci. U.S.A.* 104: 4347-4352.

Livingstone CD & **Barton** GJ (**1993**). Protein sequence alignments: a strategy for the hierarchical analysis of residue conservation. *Comput. Appl. Biosci.* 9: 745-756.

Liwo A, Czaplewski C, Ołdziej S & Scheraga HA (**2008**). Computational techniques for efficient conformational sampling of proteins. *Curr. Opin. Struct. Biol.* 18, 134-139.

Loh AP, Pawley N, Nicholson LK & Oswald RE (**2001**). An increase in side chain entropy facilitates effector binding: NMR characterization of the side chain methyl group dynamics in Cdc42Hs. *Biochemistry*, 40: 4590-4600.

Lolis E & **Petsko** GA (**1990**). Crystallographic analysis of the complex between triosephosphate isomerase and 2-phosphoglycolate at 2.5-Å resolution: implications for catalysis. *Biochemistry*, 29: 6619-6625.

Los GV, Encell LP, McDougall MG, Hartzell DD, Karassina N, Zimprich C, Wood MG, Learish R, Ohana RF, Urh M, Simpson D, Mendez J, Zimmerman K, Otto P, Vidugiris G, Zhu J, Darzins A, Klaubert DH, Bulleit RF & Wood KV (**2008**). HaloTag: a novel protein labeling technology for cell imaging and protein analysis. *ACS Chem. Biol.* 3: 373-382.

Lounnas V & **Wade** RC (**1997**). Exceptionally stable salt bridges in cytochrome P450cam have functional roles. *Biochemistry*, 36: 5402-5417.

Low BW & **Baybutt** RB (**1952**). The π helix – a hydrogen bonded configuration of the polypeptide chain. *J. Am. Chem. Soc.* 74: 5806-5807.

Lüdemann SK, Carugo O & Wade RC (**1997**). Substrate access to cytochrome P450cam: a comparison of a thermal motion pathway analysis with molecular dynamics simulation data. *J. Mol. Model.* 3: 369-374.

Lüdemann SK, Lounnas V & Wade RC (**2000a**). How do substrates enter and products exit the buried active site of cytochrome P450cam? 1. Random expulsion molecular dynamics investigation of ligand access channels and mechanisms. *J. Mol. Biol.* 303: 797-811.

Lüdemann SK, Lounnas V & Wade RC (**2000b**). How do substrates enter and products exit the buried active site of cytochrome P450cam? 2. Steered molecular dynamics and adiabatic mapping of substrate pathways. *J. Mol. Biol.* 303: 813-830.

Luo Y & **Baldwin** RL (**1998**). Trifluoroethanol stabilizes the pH 4 folding intermediate of sperm whale apomyoglobin. *J. Mol. Biol.* 279: 49-57.

Lupas AN, Ponting CP & Russell RB (**2001**). On the evolution of protein folds: are similar motifs in different protein folds the result of convergence, insertion, or relics of an ancient peptide world? *J. Struct. Biol.* 134: 191-203.

Lupas AN (**2008**). The long coming of computational structural biology. *J. Struct. Biol.* 163: 254-257.

Lurquin PF (**1997**). Gene transfer by electroporation. *Mol. Biotechnol.* 7: 5-35.

Lutz S, Ostermeier M, Moore GL, Maranas CD & Benkovic SJ (**2001**). Creating multiple-crossover DNA libraries independent of sequence identity. *Proc. Natl. Acad. Sci. U.S.A.* 98: 11248-11253.

Ma B, Kumar S, Tsai C, Hu Z & Nussinov R (**2000**). Transition-state ensemble in enzyme catalysis: Possibility, reality, or necessity? *J. Theor. Biol.* 203: 383-397.

Ma W & **Yu** C (**2006**). Intramolecular RNA replicase: possibly the first self-replicating molecule in the RNA world. *Origins Life Evol. Biosphere*, *36*, 413-20.

MacArthur MW & **Thornton** JM (**1996**). Deviations from planarity of the peptide bond in peptides and proteins. *J. Mol. Biol.* 264: 1180-1195.

Mackerell AD (**2004**). Empirical force fields for biological macromolecules: overview and issues. *J. Comput. Chem.* 25: 1584-1604.

Maher KA & **Stevenson** DJ (**1988**). Impact frustration of the origin of life. *Nature*, 331: 612-614.

Makhatadze GI, Loladze VV, Ermolenko DN, Chen X & Thomas ST (**2003**). Contribution of surface salt bridges to protein stability: guidelines for protein engineering. *J. Mol. Biol.* 327: 1135-1148.

Makrides SC (**1996**). Strategies for achieving high-level expression of genes in *Escherichia coli*. *Microbiol. Rev.* 60: 512-538.

Maniatis T (**1982**). Molecular cloning: A laboratory manual. *Cold Spring Harbor Laboratory Press*, Cold Spring Harbor, NY, USA.

Manikandan K & **Ramakumar** S (**2004**). The occurrence of C--H...O hydrogen bonds in alpha-helices and helix termini in globular proteins. *Proteins*, 56: 768-781.

Manjasetty BA, Turnbull AP, Panjikar S, Büssow K & Chance MR (**2008**). Automated technologies and novel techniques to accelerate protein crystallography for structural genomics. *Proteomics*, 8: 612-625.

Mansfeld J, Vriend G, Dijkstra BW, Veltman OR, Van den Burg B, Venema G, Ulbrich-Hofmann R & Eijsink VG (**1997**). Extreme stabilization of a thermolysin-like protease by an engineered disulfide bond. *J. Biol. Chem.* 272: 11152-11156.

Marek J, Vévodová J, Kutá-Smatanová I, Nagata Y, Svensson LA, Newman J, Takagi M & Damborský J (**2000**). Crystal structure of the haloalkane dehalogenase from *Sphingomonas paucimobilis* UT26. *Biochemistry*, 39: 14082-14086.

Martin J, Letellier G, Marin A, Taly J, de Brevern AG & Gibrat J (**2005**). Protein secondary structure assignment revisited: a detailed analysis of different assignment methods. *BMC Struct. Biol.* 5: 17.

Martí S, Andrés J, Moliner V, Silla E, Tuñón I & Bertrán J (**2001**). Transition structure selectivity in enzyme catalysis: a QM/MM study of chorismate mutase. *Theor. Chem. Acc.* 105: 207-212.

Marvanová S, Nagata Y, Wimmerová M, Sýkorová J, Hynková K & Damborský J (**2001**). Biochemical characterization of broad-specificity enzymes using multivariate experimental design and a colorimetric microplate assay: characterization of the haloalkane dehalogenase mutants. *J. Microbiol. Methods* 44: 149-157.

Mas JM, Aloy P, Martí-Renom MA, Oliva B, Blanco-Aparicio C, Molina MA, de Llorens R, Querol E & Avilés FX (**1998**). Protein similarities beyond disulphide bridge topology. *J. Mol. Biol.* 284: 541-548.

Mas JM, Aloy P, Martí-Renom MA, Oliva B, de Llorens R, Avilés FX, & Querol E (**2001**). Classification of protein disulphide-bridge topologies. *J. Comput. Aided Mol. Des.* 15: 477-487.

Matsumura M, Signor G & Matthews BW (**1989**). Substantial increase of protein stability by multiple disulphide bonds. *Nature*, 342: 291-293.

Matthews BW, Nicholson H & Becktel WJ (**1987**). Enhanced protein thermostability from site-directed mutations that decrease the entropy of unfolding. *Proc. Natl. Acad. Sci. U.S.A.* 84: 6663-6667.

Matthews BW (**1993**). Structural and genetic analysis of protein folding and stability: Current Opinion in Sturctural Biology 1993, 3:589-593. *Curr. Opin. Struct. Biol.* 3: 589-593.

Maxam AM & **Gilbert** W (**1977**). A new method for sequencing DNA. *Proc. Natl. Acad. Sci. U.S.A.* 74: 560–564.

May A & **Zacharias** M (**2005**). Accounting for global protein deformability during protein-protein and protein-ligand docking. *Biochim. Biophys. Acta*, 1754: 225-231.

Mazumdar PA, Hulecki JC, Cherney MM, Garen CR & James MNG (**2008**). X-ray crystal structure of *Mycobacterium tuberculosis* haloalkane dehalogenase Rv2579. *Biochim. Biophys. Acta*, 1784: 351-362.

McCammon JA & **Karplus** M (**1977**). Internal motions of antibody molecules. *Nature*, 268: 765-766.

McCammon JA & **Karplus** M (**1980**). Dynamics of tyrosine ring rotations in a globular protein. *Biopolymers*, 19: 1375-1405.

McDonald IK & **Thornton** JM (**1994**). Satisfying hydrogen bonding potential in proteins. *J. Mol. Biol.* 238: 777-793.

McLachlan AD (**1971**). Tests for comparing related amino-acid sequences. Cytochrome c and cytochrome c 551. *J. Mol. Biol.* 61: 409-424.

McLachlan AD (**1972**). Repeating sequences and gene duplication in proteins. *J. Mol. Biol.* 64: 417-437.

McMartin C & **Bohacek** RS (**1997**). QXP: powerful, rapid computer algorithms for structure-based drug design. *J. Comput. Aided Mol. Des.* 11: 333-344.

McPherson A (**2004**). Introduction to protein crystallization. *Methods*, 34: 254-265.

Medek P, Beneš P & Sochor J (**2007**). Computation of tunnels in protein molecules using Delaunay triangulation. *In* 15th international conference in central Europe on computer graphics, visualization and computer vision '2007, Journal of WSCG (pp. 107-114). *University of West Bohemia*, Plzeň, Czech Republic.

Mehler EL & **Solmajer** T (**1991**). Electrostatic effects in proteins: comparison of dielectric and charge models. *Protein Eng. 4*, 903-910.

Meli M, Albert-Fournier B & Maurel MC (**2001**). Recent findings in the modern RNA world. *Int. Microbiol.* 4: 5-11.

Mena-Benitez GL, Gandia-Herrero F, Graham S, Larson TR, McQueen-Mason SJ, French CE, Rylott EL & Bruce NC (**2008**). Engineering a catabolic pathway in plants for the degradation of 1,2-dichloroethane. *Plant Physiol.* 147: 1192-1198.

Meroueh SO, Roblin P, Golemi D, Maveyraud L, Vakulenko SB, Zhang Y, Samama J & Mobashery S (**2002**). Molecular dynamics at the root of expansion of function in the M69L inhibitor-resistant TEM beta-lactamase from *Escherichia coli*. *J. Am. Chem. Soc.* 124: 9422-9430.

Merutka G & **Stellwagen** E (**1990**). Positional independence and additivity of amino acid replacements on helix stability in monomeric peptides. *Biochemistry*, 29: 894-898.

Michaelis L & **Menten** M (**1913**). Die Kinetik der Invertinwirkung. *Biochem. Zeits.* 49: 333-369.

Mikhonin AV & **Asher** SA (**2006**). Direct UV Raman monitoring of 3(10)-helix and pi-bulge premelting during alpha-helix unfolding. *J. Am. Chem. Soc.* 128: 13789-13795.

Mildvan AS (**2004**). Inverse thinking about double mutants of enzymes. *Biochemistry*, 43: 14517-14520.

Miller GP & **Benkovic** SJ (**1998**). Deletion of a highly motional residue affects formation of the Michaelis complex for *Escherichia coli* dihydrofolate reductase. *Biochemistry*, 37: 6327-6335.

Miller MD, Kearsley SK, Underwood DJ & Sheridan RP (**1994**). FLOG: a system to select 'quasi-flexible' ligands complementary to a receptor of known three-dimensional structure. *J. Comput. Aided Mol. Des.* 8: 153-174.

Miller SL (**1953**). A production of amino acids under possible primitive earth conditions. *Science*, 117: 528-529.

Miller SL & **Orgel** LE (**1974**). The origins of life on the earth. *Prentice-Hall*, New Yersey, NJ, USA.

Millhauser GL (**1995**). Views of helical peptides: A proposal for the position of 310-helix along the thermodynamic folding pathway. *Biochemistry*, 34: 10318.

Mills DR, Peterson RL & Spiegelman S (**1967**). An extracellular Darwinian experiment with a self-duplicating nucleic acid molecule. *Proc. Natl. Acad. Sci. U.S.A.* 58: 217-224.

Milstien S & **Cohen** LA (**1970**). Rate acceleration by stereopopulation control: models for enzyme action. *Proc. Natl. Acad. Sci. U.S.A.* 67: 1143-1147.

Mine S, Tate S, Ueda T, Kainosho M & Imoto T (**1999**). Analysis of the relationship between enzyme activity and its internal motion using nuclear magnetic resonance: 15N relaxation studies of wild-type and mutant lysozyme. *J. Mol. Biol.* 286: 1547-1565.

Minsky A, Summers RG & Knowles JR (**1986**). Secretion of beta-lactamase into the periplasm of *Escherichia coli*: evidence for a distinct release step associated with a conformational change. *Proc. Natl. Acad. Sci. U.S.A.* 83: 4180-4184.

Mirsky AE & **Pauling** L (**1936**). On the structure of native, denatured, and coagulated proteins. *Proc. Natl. Acad. Sci. U.S.A.* 22: 439-447.

Mitsuoka K, Hirai T, Murata K, Miyazawa A, Kidera A, Kimura Y & Fujiyoshi Y (**1999**). The structure of bacteriorhodopsin at 3.0 Å resolution based on electron crystallography: implication of the charge distribution. *J. Mol. Biol.* 286: 861-882.

Mittermaier A & **Kay** LE (**2004**). The response of internal dynamics to hydrophobic core mutations in the SH3 domain from the Fyn tyrosine kinase. *Protein Sci.* 13: 1088-1099.

Mittermaier A & **Kay** LE (**2006**). New tools provide new insights in NMR studies of protein dynamics. *Science*, 312: 224-228.

Mizutani MY, Tomioka N & Itai A (**1994**). Rational automatic search method for stable docking models of protein and ligand. *J. Mol. Biol.* 243: 310-326.

Monincová M, Prokop Z, Vévodová J, Nagata Y & Damborský J (**2007**). Weak activity of haloalkane dehalogenase LinB with 1,2,3-trichloropropane revealed by X-Ray crystallography and microcalorimetry. *Appl. Environ. Microbiol.* 73: 2005-2008.

Monod J, Wyman J & Changeux JP (**1965**). On the nature of allosteric transitions: A plaussible model. *J. Mol. Biol.* 12: 88-118.

Montgomerie S, Sundararaj S, Gallin WJ & Wishart DS (**2006**). Improving the accuracy of protein secondary structure prediction using structural alignment. *BMC Bioinf.* 7: 301.

Morowitz HJ (**1999**). A theory of biochemical organization, metabolic pathways, and evolution. *Complexity*, 4: 39-53.

Morris GM, Goodsell DS, Huey R & Olson AJ (**1996**). Distributed automated docking of flexible ligands to proteins: parallel applications of AutoDock 2.4. *J. Comput. Aided Mol. Des.* 10: 293-304.

Morris GM, Goodsell DS, Halliday RS, Huey R, Hart WE, Belew RK & Olson AJ (**1998**). Automated docking using a Lamarckian genetic algorithm and an empirical binding free energy function. *J. Comput. Chem.* 19: 1639-1662.

Moult J, Pedersen JT, Judson R & Fidelis K (**1995**). A large-scale experiment to assess protein structure prediction methods. *Proteins*, 23: ii-v.

Moult J, Hubbard T, Bryant SH, Fidelis K & Pedersen JT (**1997**). Critical assessment of methods of protein structure prediction (CASP): Round II. *Proteins*, Suppl 1: 2-6.

Mu T, Ong DST, Wang Y, Balch WE, Yates JR, Segatori L & Kelly JW (**2008**). Chemical and biological approaches synergize to ameliorate protein-folding diseases. *Cell*, 134: 769-781.

Mulkidjanian AY & **Galperin** MY (**2007**). Physico-chemical and evolutionary constraints for the formation and selection of first biopolymers: towards the consensus paradigm of the abiogenic origin of life. *Chem. Biodivers.* 4: 2003-2015.

Müller KM, Stebel SC, Knall S, Zipf G, Bernauer HS & Arndt KM (**2005**). Nucleotide exchange and excision technology (NExT) DNA shuffling: a robust method for DNA fragmentation and directed evolution. *Nucleic Acids Res.* 33: e117.

Müller UF (**2006**). Re-creating an RNA world. *Cell. Mol. Life Sci.* 63: 1278-1293.

Murugan NA & **Agren** H (**2009**). 1,2-dichloroethane in haloalkane dehalogenase protein and in water solvent: a case study of the confinement effect on structural and dynamical properties. *J. Phys. Chem. B*, 113: 3257-3263.

Murzin AG, Brenner SE, Hubbard T & Chothia C (**1995**). SCOP: a structural classification of proteins database for the investigation of sequences and structures. *J. Mol. Biol.* 247: 536-540.

Myers JK & **Oas** TG (**2002**). Mechanism of fast protein folding. *Annu. Rev. Biochem.* 71: 783-815.

Nabuurs SB, Nederveen AJ, Vranken W, Doreleijers JF, Bonvin AMJJ, Vuister GW, Vriend G & Spronk CAEM (**2004**). DRESS: a database of REfined solution NMR structures. *Proteins*, 55: 483-486.

Naested H, Fennema M, Hao L, Andersen M, Janssen DB & Mundy J (**1999**). A bacterial haloalkane dehalogenase gene as a negative selectable marker in Arabidopsis. *Plant J.* 18: 571-576.

Nagata Y, Nariya T, Ohtomo R, Fukuda M, Yano K & Takagi M (**1993**). Cloning and sequencing of a dehalogenase gene encoding an enzyme with hydrolase activity involved in the degradation of gamma-hexachlorocyclohexane in *Pseudomonas paucimobilis*. *J. Bacteriol.* 175: 6403-6410.

Nagata Y, Miyauchi K, Damborský J, Manová K, Ansorgova A & Takagi M (**1997**). Purification and characterization of a haloalkane dehalogenase of a new substrate class from a gamma-hexachlorocyclohexane-degrading bacterium, *Sphingomonas paucimobilis* UT26. *Appl. Environ. Microbiol.* 63: 3707-3710.

Nagata Y, Hynková K, Damborský J & Takagi M (**1999**). Construction and characterization of histidine-tagged haloalkane dehalogenase (LinB) of a new substrate class from a gamma-hexachlorocyclohexane-degrading bacterium, *Sphingomonas paucimobilis* UT26. *Protein Expression and Purif.* 17: 299-304.

Nagata Y, Prokop Z, Marvanová S, Sýkorová J, Monincová M, Tsuda M & Damborský J (**2003**). Reconstruction of mycobacterial dehalogenase Rv2579 by cumulative mutagenesis of haloalkane dehalogenase LinB. *Appl. Environ. Microbiol.* 69: 2349-2355.

Nagata Y, Prokop Z, Sato Y, Jeřábek P, Kumar A, Ohtsubo Y, Tsuda M & Damborský J. (**2005**). Degradation of beta-hexachlorocyclohexane by haloalkane dehalogenase LinB from *Sphingomonas paucimobilis* UT26. *Appl. Environ. Microbiol.* 71: 2183-2185.

Nagel ZD & **Klinman** JP (**2006**). Tunneling and dynamics in enzymatic hydride transfer. *Chem. Rev.* 106: 3095-3118.

Nam K, Prat-Resina X, Garcia-Viloca M, Devi-Kesavan LS & Gao J (**2004**). Dynamics of an enzymatic substitution reaction in haloalkane dehalogenase. *J. Am. Chem. Soc.* 126: 1369-1376.

Nandi N, Bhattacharyya K & Bagchi B (**2000**). Dielectric relaxation and solvation dynamics of water in complex chemical and biological systems. *Chem. Rev.* 100: 2013-2046.

Nardini M & **Dijkstra** BW (**1999**). Alpha/beta hydrolase fold enzymes: the family keeps growing. *Curr. Opin. Struct. Biol.* 9: 732-737.

Neal S, Nip AM, Zhang H & Wishart DS (**2003**). Rapid and accurate calculation of protein 1H, 13C and 15N chemical shifts. *J Biomol. NMR*, 26: 215-240.

Negri A, Marco E, Damborsky J, & Gago F (**2007**). Stepwise dissection and visualization of the catalytic mechanism of haloalkane dehalogenase LinB using molecular dynamics simulations and computer graphics. *J. Mol. Graphics Modell.* 26: 643-651.

Nelson JW & **Kallenbach** NR (**1986**). Stabilization of the ribonuclease S-peptide alpha-helix by trifluoroethanol. *Proteins*, 1: 211-217.

Némethy G & **Printz** MP (**1972**). The γ turn, a possible folded conformation of the polypeptide chain. Comparison with the β turn. *Macromolecules*, 5: 755-758.

Neumann E, Schaefer-Ridder M, Wang Y & Hofschneider PH (**1982**). Gene transfer into mouse lyoma cells by electroporation in high electric fields. *EMBO J.* 1: 841-845.

Newman J, Peat TS, Richard R, Kan L, Swanson PE, Affholter JA, Holmes IH, Schindler JF, Unkefer CJ & Terwilliger TC (**1999**). Haloalkane dehalogenases: structure of a *Rhodococcus* enzyme. *Biochemistry*, 38: 16105-16114.

Nielsen PE (**1993**). Peptide nucleic acid (PNA): a model structure for the primordial genetic material? *Origins Life Evol. Biosphere*, 23: 323-327.

Nirenberg M, Leder P, Bernfield M, Brimacombe R, Trupin J, Rottman F & O'Neal C (**1965**). RNA codewords and protein synthesis, VII. On the general nature of the RNA code. *Proc. Natl. Acad. Sci. U.S.A.* 53: 1161-1168.

Nishida N, Sumikawa H, Sakakura M, Shimba N, Takahashi H, Terasawa H, Suzuki E & Shimada I (**2003**). Collagen-binding mode of vWF-A3 domain determined by a transferred cross-saturation experiment. *Nat. Struct. Mol. Biol.* 10: 53-58.

Oakley AJ, Prokop Z, Boháč M, Kmuníček J, Jedlička T, Monincová M, Kutá-Smatanová I, Nagata Y, Damborský J & Wilce MCJ (**2002**). Exploring the structure and activity of haloalkane dehalogenase from *Sphingomonas paucimobilis* UT26: evidence for product- and water-mediated inhibition. *Biochemistry*, 41: 4847-4855.

Oakley AJ, Klvaňa M, Otyepka M, Nagata Y, Wilce MCJ & Damborský J (**2004**). Crystal structure of haloalkane dehalogenase LinB from *Sphingomonas paucimobilis* UT26 at 0.95 Å resolution: dynamics of catalytic residues. *Biochemistry*, 43: 870-878.

O'Brien PJ & **Herschlag** D (**1999**). Catalytic promiscuity and the evolution of new enzymatic activities. *Chem. Biol.* 6: R91-R105.

Ochman H, Gerber AS & Hartl DL (**1988**). Genetic applications of an inverse polymerase chain reaction. *Genetics*, 120: 621-623.

Ohmine I & **Tanaka** H (**1993**). Fluctuation, relaxations, and hydration in liquid water. Hydrogen-bond rearrangement dynamics. *Chem. Rev.* 93: 2545-2566.

Ohno S (**1970**). Evolution by gene duplication. *Springer-Verlag*, Heidelberg, Germany.

Oliveberg M (**2001**). Characterisation of the transition states for protein folding: towards a new level of mechanistic detail in protein engineering analysis. *Curr. Opin. Struct. Biol.* 11: 94-100.

Ollis DL, Cheah E, Cygler M, Dijkstra B, Frolow F, Franken SM, Harel M, Remington SJ, Silman I & Schrag J (**1992**). The alpha/beta hydrolase fold. *Protein Eng.* 5: 197-211.

Olsson MHM & **Warshel** A (**2004**). Solute solvent dynamics and energetics in enzyme catalysis: the S(N)2 reaction of dehalogenase as a general benchmark. *J. Am. Chem. Soc.* 126: 15167-15179.

Onufriev A, Bashford D & Case DA (**2004**). Exploring protein native states and large-scale conformational changes with a modified generalized born model. *Proteins*, 55 383-394.

Oprea TI, Hummer G & Garcia AE (**1997**). Identification of a functional water channel in cytochrome P450 enzymes. *Proc. Natl. Acad. Sci. U.S.A.* 94: 2133-2138.

Orengo CA, Michie AD, Jones S, Jones DT, Swindells MB & Thornton JM (**1997**). CATH – a hierarchic classification of protein domain structures. *Structure*, 5: 1093-1108.

Orengo CA, Martin AM, Hutchinson G, Jones S, Jones DT, Michie AD, Swindells MB & Thornton JM (**1998**). Classifying a protein in the CATH database of domain structures. *Acta Crystallogr., Sect. D: Biol. Crystallogr.* 54: 1155-1167.

Orengo CA, Bray JE, Buchan DWA, Harrison A, Lee D, Pearl FMG, Sillitoe I, Todd AE, & Thornton JM (**2002**). The CATH protein family database: a resource for structural and functional annotation of genomes. *Proteomics*, 2, 11-21.

Orgel LE (**1998**). The origin of life--a review of facts and speculations. *Trends Biochem.Sci.* 23: 491-495.

Osawa S (**1995**). Evolution of the genetic code. *Oxford University Press*, New York, NY, USA.

Otyepka M & **Damborský** J (**2002**). Functionally relevant motions of haloalkane dehalogenases occur in the specificity-modulating cap domains. *Protein Sci.* 11, 1206-1217.

Otyepka M, Banáš P, Magistrato A, Carloni P & Damborský J (**2008**). Second step of hydrolytic dehalogenation in haloalkane dehalogenase investigated by QM/MM methods. *Proteins*, 70: 707-717.

Otzen DE & **Fersht** AR (**1995**). Side-chain determinants of beta-sheet stability. *Biochemistry*, 34: 5718-5724.

Otzen DE & **Oliveberg** M (**1999**). Salt-induced detour through compact regions of the protein folding landscape. *Proc. Natl. Acad. Sci. U.S.A.* 96: 11746-11751.

Pace CN, Alston RW & Shaw KL (**2000**). Charge-charge interactions influence the denatured state ensemble and contribute to protein stability. *Protein Sci.* 9: 1395-1398.

Pal D & **Chakrabarti** P (**1999**). Estimates of the loss of main-chain conformational entropy of different residues on protein folding. *Proteins*, 36: 332-339.

Pal D & **Chakrabarti** P (**2000**). beta-sheet propensity and its correlation with parameters based on conformation. *Acta Crystallogr., Sect. D: Biol. Crystallogr.* 56: 589-594.

Pal SK & **Zewail** AH (**2004**). Dynamics of water in biological recognition. *Chem. Rev.* 104: 2099-2123.

Palmer AG (**2004**). NMR characterization of the dynamics of biomacromolecules. *Chem. Rev.* 104: 3623-3640.

Paneth P (**2003**). Chlorine kinetic isotope effects on enzymatic dehalogenations. *Acc. Chem. Res.* 36: 120-126.

Parak FG (**2003**). Proteins in action: the physics of structural fluctuations and conformational changes. *Curr. Opin. Struct. Biol.* 13: 552-557.

Parak FG, Achterhold K, Schmidt M, Prusakov V & Croci S (**2006**). Protein dynamics on different timescales. *J. Non-Cryst. Solids* 352: 4371-4378.

Pascarella S & **Argos** P (**1992**). Analysis of insertions/deletions in protein structures. *J. Mol. Biol.* 224: 461-471.

Patnaik R, Louie S, Gavrilovic V, Perry K, Stemmer WPC, Ryan CM & del Cardayré S (**2002**). Genome shuffling of *Lactobacillus* for improved acid tolerance. *Nat. Biotechnol.* 20: 707-712.

Pauling L (**1946**). Molecular architecture and biological reactions. *Chem. Eng. News* 24: 1375-1377.

Pauling L & **Corey** RB (**1950**). Two hydrogen-bonded spiral configurations of the polypeptide chain. *J. Am. Chem. Soc.* 72: 5349.

Pauling L, Corey RB & Branson HR (**1951**). The structure of proteins: two hydrogen-bonded helical configurations of the polypeptide chain. *Proc. Natl. Acad. Sci. U.S.A.* 37: 205–211.

Pauling L & **Corey** RB (**1951a**). Atomic coordinates and structure factors for two helical configurations of polypeptide chains. *Proc. Natl. Acad. Sci. U.S.A.* 37: 235-240.

Pauling L & **Corey** RB (**1951b**). The pleated sheet, a new layer configuration of polypeptide chains. *Proc. Natl. Acad. Sci. U.S.A.* 37: 251-256.

Pauling L & **Corey** RB (**1951c**). The structure of feather rachis keratin. *Proc. Natl. Acad. Sci. U.S.A.* 37: 256-261.

Pauling L & **Corey** RB (**1951d**). The structure of hair, muscle, and related proteins. *Proc. Natl. Acad. Sci. U.S.A.* 37: 261-271.

Pauling L & **Corey** RB (**1951e**). The structure of fibrous proteins of the collagen-gelatin group. *Proc. Natl. Acad. Sci. U.S.A.* 37: 272-281.

Pauling L & **Corey** RB (**1951f**). Configurations of polypeptide chains with favored orientations around single bonds: two new pleated sheets. *Proc. Natl. Acad. Sci. U.S.A.* 37: 729-740.

Pauling L & **Corey** RB (**1953**). Compound helical configurations of polypeptide chains: structure of proteins of the alpha-keratin type. *Nature*, 171: 59-61.

Pauling L (**1960**). The nature of the chemical bond. *Cornell University Press*, Ithaca, NY, USA.

Pavlová M, Klvaňa M, Jesenská A, Prokop Z, Konečná H, Sato T, Tsuda M, Nagata Y & Damborský J (**2007**). The identification of catalytic pentad in the haloalkane dehalogenase DhmA from *Mycobacterium avium* N85: reaction mechanism and molecular evolution. *J. Struct. Biol.* 157: 384-392.

Pearson AR, Mozzarelli A & Rossi GL (**2004**). Microspectrophotometry for structural enzymology. *Curr. Opin. Struct. Biol.* 14: 656-662.

Pelletier JN (**2001**). A RACHITT for our toolbox. *Nat. Biotechnol.* 19: 314-315.

Penel S, Hughes E & Doig AJ (**1999**). Side-chain structures in the first turn of the alpha-helix. *J. Mol. Biol.* 287: 127-143.

Penel S & **Doig** AJ (**2001**). Rotamer strain energy in protein helices - quantification of a major force opposing protein folding. *J. Mol. Biol.* 305: 961-968.

Perola E, Xu K, Kollmeyer TM, Kaufmann SH, Prendergast FG & Pang YP (**2000**). Successful virtual screening of a chemical database for farnesyltransferase inhibitor leads. *J. Med. Chem.* 43: 401-408.

Peter J, Hutter W, Stöllnberger W & Hampel W (**1996**). Detection of chlorinated and brominated hydrocarbons by an ion sensitive whole cell biosensor. *Biosens. Bioelectron.* 11: 1215-1219.

Petock JM, Torshin IY, Weber IT & Harrison RW (**2003**). Analysis of protein structures reveals regions of rare backbone conformation at functional sites. *Proteins*, 53: 872-879.

Petoukhov MV & **Svergun** DI (**2007**). Analysis of X-ray and neutron scattering from biomacromolecular solutions. *Curr. Opin. Struct. Biol.* 17: 562-571.

Petřek M, Otyepka M, Banáš P, Kosinová P, Koča J & Damborský J (**2006**). CAVER: a new tool to explore routes from protein clefts, pockets and cavities. *BMC Bioinf.* 7: 316.

Petřek M, Kosinová P, Koča J & Otyepka M (**2007**). MOLE: a Voronoi diagram-based explorer of molecular channels, pores, and tunnels. *Structure*, 15: 1357-1363.

Phillips JC, Braun R, Wang W, Gumbart J, Tajkhorshid E, Villa E, Chipot C, Skeel RD, Kalé L & Schulten K (**2005**). Scalable molecular dynamics with NAMD. *J. Comput. Chem.* 26: 1781-1802.

Piana S, Carloni P & Parrinello M (**2002**). Role of conformational fluctuations in the enzymatic reaction of HIV-1 protease. *J. Mol. Biol.* 319: 567-583.

Pikkemaat MG, Ridder IS, Rozeboom HJ, Kalk KH, Dijkstra BW & Janssen DB (**1999**). Crystallographic and kinetic evidence of a collision complex formed during halide import in haloalkane dehalogenase. *Biochemistry*, 38: 12052-12061.

Pikkemaat MG, Linssen ABM, Berendsen HJC & Janssen DB (**2002**). Molecular dynamics simulations as a tool for improving protein stability. *Protein Eng.* 15: 185-192.

Pinakoulaki E, Yoshimura H, Daskalakis V, Yoshioka S, Aono S & Varotsis C (**2006**). Two ligand-binding sites in the O2-sensing signal transducer HemAT: Implications for ligand recognition/discrimination and signaling. *Proc. Natl. Acad. Sci. U.S.A.* 103: 14796-14801.

Podust LM, Poulos TL & Waterman MR (**2001**). Crystal structure of cytochrome P450 14alpha -sterol demethylase (CYP51) from *Mycobacterium tuberculosis* in complex with azole inhibitors. *Proc. Natl. Acad. Sci. U.S.A.* 98: 3068-3073.

Poelarends GJ, Wilkens M, Larkin MJ, van Elsas JD & Janssen DB (**1998**). Degradation of 1,3-dichloropropene by *Pseudomonas cichorii* 170. *Appl. Environ. Microbiol.* 64: 2931-2936.

Poelarends GJ, van Hylckama Vlieg JE, Marchesi JR, Freitas Dos Santos LM & Janssen DB (**1999**). Degradation of 1,2-dibromoethane by *Mycobacterium* sp. strain GP1. *J. Bacteriol.* 181: 2050-2058.

Poelarends GJ, Kulakov LA, Larkin MJ, van Hylckama Vlieg JE & Janssen DB (**2000a**). Roles of horizontal gene transfer and gene integration in evolution of 1,3-dichloropropene- and 1,2-dibromoethane-degradative pathways. *J. Bacteriol.* 182: 2191-2199.

Poelarends GJ, Zandstra M, Bosma T, Kulakov LA, Larkin MJ, Marchesi JR, Weightman AJ & Janssen DB (**2000b**). Haloalkane-utilizing *Rhodococcus* strains isolated from geographically distinct locations possess a highly conserved gene cluster encoding haloalkane catabolism. *J. Bacteriol.* 182: 2725-2731.

Poole AM, Jeffares DC & Penny D (**1998**). The path from the RNA world. *J. Mol. Evol.* 46: 1-17.

Popper KR (**1959**). The Logic of Scientific Discovery. *Hutchinson education*, Hutchinson, MN, USA.

Porter CT, Bartlett GJ & Thornton JM (**2004**). The Catalytic Site Atlas: a resource of catalytic sites and residues identified in enzymes using structural data. *Nucleic Acids Res.* 32: D129-133.

Prasad S, Mazumdar S & Mitra S (**2000**). Binding of camphor to *Pseudomonas putida* cytochrome p450(cam): steady-state and picosecond time-resolved fluorescence studies. *FEBS Lett.* 477: 157-160.

Prasad S & **Mitra** S (**2002**). Role of protein and substrate dynamics in catalysis by *Pseudomonas putida* cytochrome P450cam. *Biochemistry*, 41: 14499-14508.

Presta LG & **Rose** GD (**1988**). Helix signals in proteins. *Science*, 240: 1632-1641.

Price DJ & **Brooks III** CL (**2002**). Modern protein force fields behave comparably in molecular dynamics simulations. *J. Comput. Chem.* 23: 1045-1057.

Pries F, Kingma J, Pentenga M, van Pouderoyen G, Jeronimus-Stratingh CM, Bruins AP & Janssen DB (**1994a**). Site-directed mutagenesis and oxygen isotope incorporation studies of the nucleophilic aspartate of haloalkane dehalogenase. *Biochemistry*, 33: 1242-1247.

Pries F, van den Wijngaard AJ, Bos R, Pentenga M & Janssen DB (**1994b**). The role of spontaneous cap domain mutations in haloalkane dehalogenase specificity and evolution. *J. Biol. Chem.* 269: 17490-17494.

Pries F, Kingma J & Janssen DB (**1995a**). Activation of an Asp-124-->Asn mutant of haloalkane dehalogenase by hydrolytic deamidation of asparagine. *FEBS Lett.* 358: 171-174.

Pries F, Kingma J, Krooshof GH, Jeronimus-Stratingh CM, Bruins AP & Janssen DB (**1995b**). Histidine 289 is essential for hydrolysis of the alkyl-enzyme intermediate of haloalkane dehalogenase. *J. Biol. Chem.* 270: 10405-10411.

Prince RC (**1994**). Haloalkane dehalogenase caught in the act. *Trends Biochem.Sci.* 19: 3-4.

Prokop Z, Monincová M, Chaloupková R, Klvaňa M, Nagata Y, Janssen DB & Damborský J (**2003**). Catalytic mechanism of the maloalkane dehalogenase LinB from *Sphingomonas paucimobilis* UT26. *J. Biol. Chem.* 278: 45094-45100.

Prokop Z, Janssen DB, Sato Y, Nagata Y & Damborský J (**2005**). Enantioselectivity of haloalkane dehalogenases. *Biotrans Symposium: The key to industrial biotechnology* (Jul 3-8, 2005). Delft, The Netherlands.

Prokop Z, Oplustil F, DeFrank J & Damborský J (**2006**). Enzymes fight chemical weapons. *Biotechnol. J.* 1: 1370-1380.

Pross A (**2004**). Causation and the origin of life. Metabolism or replication first? *Origins Life Evol. Biosphere*, 34: 307-321.

Prudnikova T, Mozga T, Řezáčová P, Chaloupková R, Sato Y, Nagata Y, Brynda J, Kutý M, Damborský J & Kutá-Smatanová I (**2009**). Crystallization and preliminary X-ray analysis of a novel haloalkane dehalogenase DbeA from *Bradyrhizobium elkani* USDA94. *Acta Crystallogr., Sect. F: Struct. Biol. Cryst. Commun.* 65: 353-356.

Puchkaev AV, Koo L S & Ortiz de Montellano PR (**2003**). Aromatic stacking as a determinant of the thermal stability of CYP119 from *Sulfolobus solfataricus*. *Arch. Biochem. Biophys.* 409: 52-58.

Pusey ML, Liu Z, Tempel W, Praissman J, Lin D, Wang B, Gavira JA & Ng JD (**2005**). Life in the fast lane for protein crystallization and X-ray crystallography. *Prog. Biophys. Mol. Biol.* 88: 359-386.

Radkiewicz JL & **Brooks III** CL (**2000**). Protein dynamics in enzymatic catalysis: exploration of dihydrofolate reductase. *J. Am. Chem. Soc.* 122: 225-231.

Radzicka A & **Wolfenden** R (**1995**). A proficient enzyme. *Science*, 267: 90-93.

Raina V, Hauser A, Buser HR, Rentsch D, Sharma P, Lal R, Holliger C, Poiger JT, Müller MD & Kohler HE (**2007**). Hydroxylated metabolites of beta- and delta-hexachlorocyclohexane: bacterial formation, stereochemical configuration, and occurrence in groundwater at a former production site. *Environ. Sci. Technol.* 41: 4292-4298.

Raina V, Rentsch D, Geiger T, Sharma P, Buser HR, Holliger C, Lal R & Kohler HE (**2008**). New metabolites in the degradation of alpha- and gamma-hexachlorocyclohexane (HCH): pentachlorocyclohexenes are hydroxylated to cyclohexenols and cyclohexenediols by the haloalkane dehalogenase LinB from *Sphingobium indicum* B90A. *J. Agric. Food Chem.* 56: 6594-6603.

Rajagopalan PTR, Lutz S & Benkovic SJ (**2002**). Coupling interactions of distal residues enhance dihydrofolate reductase catalysis: mutational effects on hydride transfer rates. *Biochemistry*, 41: 12618-12628.

Ramachandran GN, Ramakrishnan C & Sasisekharan V (**1963**). Stereochemistry of polypeptide chain configurations. *J. Mol. Biol.* 7: 95-99.

Ramachandran GN (**1968**). Need for nonplanar peptide units in polypeptide chains. *Biopolymers*, 6: 1494-1496.

Ramakrishnan V & **Moore** PB (**2001**). Atomic structures at last: the ribosome in 2000. *Curr. Opin. Struct. Biol.* 11: 144-154.

Rarey M, Kramer B, Lengauer T & Klebe G (**1996**). A fast flexible docking method using an incremental construction algorithm. *J. Mol. Biol.* 261: 470-489.

Reetz MT, Bocola M, Carballeira JD, Zha D & Vogel A (**2005**). Expanding the range of substrate acceptance of enzymes: combinatorial active-site saturation test. *Angew. Chem. Int. Ed.* 44: 4192-4196.

Reetz MT, Wang L & Bocola M (**2006a**). Directed evolution of enantioselective enzymes: iterative cycles of CASTing for probing protein-sequence space. *Angew. Chem. Int. Ed.* 45: 1236-1241.

Reetz MT, Carballeira JD & Vogel A (**2006b**). Iterative saturation mutagenesis on the basis of B factors as a strategy for increasing protein thermostability. *Angew. Chem. Int. Ed.* 45: 7745-7751.

Reetz MT & **Carballeira** JD (**2007**). Iterative saturation mutagenesis (ISM) for rapid directed evolution of functional enzymes. *Nat. Protoc.* 2: 891-903.

Reetz MT, Kahakeaw D & Sanchis J (**2009**). Shedding light on the efficacy of laboratory evolution based on iterative saturation mutagenesis. *Mol. Biosyst.* 5: 115-122.

Reeves GA, Dallman TJ, Redfern OC, Akpor A & Orengo CA (**2006**). Structural diversity of domain superfamilies in the CATH database. *J. Mol. Biol.* 360: 725-741.

Richards FM & **Kundrot** CE (**1988**). Identification of structural motifs from protein coordinate data: secondary structure and first-level supersecondary structure. *Proteins*, 3: 71-84.

Richardson JS (**1976**). Handedness of crossover connections in beta sheets. *Proc. Natl. Acad. Sci. U.S.A.* 73: 2619-2623.

Richardson JS, Getzoff ED & Richardson DC (**1978**). The beta bulge: a common small unit of nonrepetitive protein structure. *Proc. Natl. Acad. Sci. U.S.A.* 75: 2574-2578.

Richardson JS & **Richardson** DC (**1988**). Amino acid preferences for specific locations at the ends of alpha helices. *Science*, 240: 1648-1652.

Ringe D & **Mattos** C (**1999**). Analysis of the binding surfaces of proteins. *Med. Res. Rev.* 19: 321-331.

Ripoll DR, Faerman CH, Axelsen PH, Silman I & Sussman JL (**1993**). An electrostatic mechanism for substrate guidance down the aromatic gorge of acetylcholinesterase. *Proc. Natl. Acad. Sci. U.S.A.* 90: 5128-5132.

Robustelli P, Cavalli A & Vendruscolo M (**2008**). Determination of protein structures in the solid state from NMR chemical shifts. *Structure*, 16: 1764-1769.

Rod TH, Radkiewicz JL & Brooks III CL (**2003**). Correlated motion and the effect of distal mutations in dihydrofolate reductase. *Proc. Natl. Acad. Sci. U.S.A.* 100: 6980-6985.

Rode BM, Eder AH & Yongyai Y (**1997**). Amino acid sequence preferences of the salt-induced peptide formation reaction in comparison to archaic cell protein composition. *Inorg. Chim. Acta*, 254: 309-314.

Rodnina MV, Beringer M & Wintermeyer W (**2007**). How ribosomes make peptide bonds. *Trends Biochem.Sci.* 32: 20-26.

Rohl CA & **Doig** AJ (**1996**). Models for the 3_{10}-helix/coil, pi-helix/coil, and alpha-helix/3_{10}-helix/coil transitions in isolated peptides. *Protein Sci.* 5: 1687-1696.

Roitberg A & **Simmerling** C (**2004**). Foreword. *J. Mol. Graphics Modell.* 22: 317.

Rose GD (**1979**). Hierarchic organization of domains in globular proteins. *J. Mol. Biol.* 134: 447-470.

Rose GD, Fleming PJ, Banavar JR & Maritan A (**2006**). A backbone-based theory of protein folding. *Proc. Natl. Acad. Sci. U.S.A.* 103: 16623-16633.

Rosta E, Klähn M & Warshel A (**2006**). Towards accurate ab initio QM/MM calculations of free-energy profiles of enzymatic reactions. *J. Phys. Chem. B*, 110: 2934-2941.

Roughton FJW & **Chance** B (**1963**). 2. Investigation of rates and mechanisms of reactions. *In* Techniques of Organic Chemistry, Vol. VIII (pp. 703-792). *John Wiley and Sons*, New York, NY, USA.

Rozovsky S & **McDermott** AE (**2001**). The time scale of the catalytic loop motion in triosephosphate isomerase. *J. Mol. Biol.* 310: 259-270.

Rueda M, Ferrer-Costa C, Meyer T, Pérez A, Camps J, Hospital A, Gelpí JL & Orozco M (**2007**). A consensus view of protein dynamics. *Proc. Natl. Acad. Sci. U.S.A.* 104: 796-801.

Ruiz-Mirazo K, Peretó J & Moreno A (**2004**). A universal definition of life: autonomy and open-ended evolution. *Origins Life Evol. Biosphere*, 34: 323-346.

Russell RB & **Sternberg** MJ (**1997**). Two new examples of protein structural similarities within the structure-function twilight zone. *Protein Eng.* 10: 333-338.

Russell RB & **Ponting** CP (**1998**). Protein fold irregularities that hinder sequence analysis. *Curr. Opin. Struct. Biol.* 8: 364-371.

Russ WP, Lowery DM, Mishra P, Yaffe MB & Ranganathan R (**2005**). Natural-like function in artificial WW domains. *Nature*, 437: 579-583.

Ryckaert J, Ciccotti G & Berendsen HJC (**1977**). Numerical integration of the cartesian equations of motion of a system with constraints: molecular dynamics of n-alkanes. *J. Comput. Phys.* 23: 327-341.

Ryoo SW, Park YK, Park S, Shim YS, Liew H, Kang S & Bai G (**2007**). Comparative proteomic analysis of virulent Korean *Mycobacterium tuberculosis* K-strain with other mycobacteria strain following infection of U-937 macrophage. *J. Microbiol.* 45: 268-271.

Sali A & **Blundell** TL (**1993**). Comparative protein modelling by satisfaction of spatial restraints. *J. Mol. Biol.* 234: 779-815.

Sallis PJ, Armfield SJ, Bull AT & Hardman DJ (**1990**). Isolation and characterization of a haloalkane halidohydrolase from *Rhodococcus erythropolis* Y2. *J. Gen. Microbiol.* 136: 115-120.

Samatey FA, Imada K, Nagashima S, Vonderviszt F, Kumasaka T, Yamamoto M & Namba K (**2001**). Structure of the bacterial flagellar protofilament and implications for a switch for supercoiling. *Nature*, 410: 331-337.

Sanbonmatsu KY & **Tung** C (**2007**). High performance computing in biology: multimillion atom simulations of nanoscale systems. *J. Struct. Biol.* 157: 470-480.

Sanger F, Thompson EO & Kitai R (**1955**). The amide groups of insulin. *Biochem. J.* 59: 509-518.

Sanger F, Air GM, Barrell BG, Brown NL, Coulson AR, Fiddes CA, Hutchison CA, Slocombe PM & Smith M (**1977a**). Nucleotide sequence of bacteriophage phi X174 DNA. *Nature*, 265: 687-695.

Sanger F, Nicklen S & Coulson AR (**1977b**). DNA sequencing with chain-terminating inhibitors. *Proc. Natl. Acad. Sci. U.S.A.* 74: 5463-5467.

Sanger F, Coulson AR, Friedmann T, Air GM, Barrell BG, Brown NL, Fiddes JC, Hutchison CA, Slocombe PM & Smith M (**1978**). The nucleotide sequence of bacteriophage phiX174. *J. Mol. Biol.* 125: 225-246.

Sanger F (**1980**). Determination of nucleotide sequences in DNA. *In* Nobel Lectures Chemistry 1971-1980 (pp. 431-447). *World Scientific Publishing Co. (1993)*, Singapore, Singapore.

Santoro SW & **Schultz** PG (**2002**). Directed evolution of the site specificity of Cre recombinase. *Proc. Natl. Acad. Sci. U.S.A.* 99: 4185-4190.

Sato Y, Monincová M, Chaloupková R, Prokop Z, Ohtsubo Y, Minamisawa K, Tsuda M, Damborský J & Nagata Y (**2005**). Two rhizobial strains, *Mesorhizobium loti* MAFF303099 and *Bradyrhizobium japonicum* USDA110, encode haloalkane dehalogenases with novel structures and substrate specificities. *Appl. Environ. Microbiol.* 71: 4372-4379.

Sato Y, Natsume R, Tsuda M, Damborský J, Nagata Y & Senda T (**2007**). Crystallization and preliminary crystallographic analysis of a haloalkane dehalogenase, DbjA, from *Bradyrhizobium japonicum* USDA110. *Acta Crystallogr., Sect. F: Struct. Biol. Cryst. Commun.* 63: 294-296.

Schanstra JP & **Janssen** DB (**1996**). Kinetics of halide release of haloalkane dehalogenase: evidence for a slow conformational change. *Biochemistry*, 35: 5624-5632.

Schanstra JP, Ridder IS, Heimeriks GJ, Rink R, Poelarends GJ, Kalk KH, Dijkstra BW & Janssen DB (**1996a**). Kinetic characterization and X-ray structure of a mutant of haloalkane dehalogenase with higher catalytic activity and modified substrate range. *Biochemistry*, 35: 13186-13195.

Schanstra JP, Kingma J & Janssen DB (**1996b**). Specificity and kinetics of haloalkane dehalogenase. *J. Biol. Chem.* 271: 14747-14753.

Schanstra JP, Ridder A, Kingma J & Janssen DB (**1997**). Influence of mutations of Val226 on the catalytic rate of haloalkane dehalogenase. *Protein Eng.* 10: 53-61.

Scheiner S, Kar T & Gu Y (**2001**). Strength of the Calpha H..O hydrogen bond of amino acid residues. *J. Biol. Chem.* 276: 9832-9837.

Schiffer M & **Edmundson** AB (**1967**). Use of helical wheels to represent the structures of proteins and to identify segments with helical potential. *Biophys. J.* 7: 121-135.

Schindler JF, Naranjo PA, Honaberger DA, Chang CH, Brainard JR, Vanderberg LA & Unkefer CJ (**1999**). Haloalkane dehalogenases: steady-state kinetics and halide inhibition. *Biochemistry*, 38: 5772-5778.

Schleinkofer K, Sudarko, Winn PJ, Lüdemann SK & Wade RC (**2005**). Do mammalian cytochrome P450s show multiple ligand access pathways and ligand channelling? *EMBO Rep.* 6: 584-589.

Schlitter J, Engels M, Krüger P, Jacoby E & Wollmer A (**1993**). Targeted molecular dynamics simulation of conformational change – application to the T ↔ R transition in insulin. *Mol. Simulation*, 10: 291.

Schmidt A & **Lamzin** VS (**2007**). From atoms to proteins. *Cell. Mol. Life Sci.* 64: 1959-1969.

Schmidt-Dannert C (**2001**). Directed evolution of single proteins, metabolic pathways, and viruses. *Biochemistry*, 40: 13125-13136.

Schmitt J, Brocca S, Schmid RD & Pleiss J (**2002**). Blocking the tunnel: engineering of *Candida rugosa* lipase mutants with short chain length specificity. *Protein Eng.* 15: 595-601.

Scholtz JM, Marqusee S, Baldwin RL, York EJ, Stewart JM, Santoro M & Bolen DW (**1991**). Calorimetric determination of the enthalpy change for the alpha-helix to coil transition of an alanine peptide in water. *Proc. Natl. Acad. Sci. U.S.A.* 88: 2854-2858.

Scholtz R, Leisinger T, Suter F & Cook AM (**1987**). Characterization of 1-chlorohexane halidohydrolase, a dehalogenase of wide substrate range from an Arthrobacter sp. *J. Bacteriol.* 169: 5016-5021.

Schomburg I, Chang A, Ebeling C, Gremse M, Heldt C, Huhn G & Schomburg D (**2004**). BRENDA, the enzyme database: updates and major new developments. *Nucleic Acids Res.* 32: D431-433.

Schönbrunner N, Wey J, Engels J, Georg H & Kiefhaber T (**1996**). Native-like beta-structure in a trifluoroethanol-induced partially folded state of the all-beta-sheet protein tendamistat. *J. Mol. Biol.* 260: 432-445.

Schotte F, Lim M, Jackson TA, Smirnov AV, Soman J, Olson JS, Phillips GN, Wulff M & Anfinrud PA (**2003**). Watching a protein as it functions with 150-ps time-resolved x-ray crystallography. *Science*, 300: 1944-1947.

Schotte F, Soman J, Olson JS, Wulff M & Anfinrud PA (**2004**). Picosecond time-resolved X-ray crystallography: probing protein function in real time. *J. Struct. Biol.* 147: 235-246.

Schwede T, Kopp J, Guex N & Peitsch MC (**2003**). SWISS-MODEL: an automated protein homology-modeling server. *Nucl. Acids Res.*, 31: 3381-3385.

Schwehm JM, Fitch CA, Dang BN, García-Moreno EB & Stites WE (**2003**). Changes in stability upon charge reversal and neutralization substitution in staphylococcal nuclease are dominated by favorable electrostatic effects. *Biochemistry*, 42: 1118-1128.

Scott EE, Gibson QH & Olson JS (**2001**). Mapping the pathways for O2 entry into and exit from myoglobin. *J. Biol. Chem.* 276: 5177-5188.

Scott EE, He YQ & Halpert JR (**2002**). Substrate routes to the buried active site may vary among cytochromes P450: mutagenesis of the F-G region in P450 2B1. *Chem. Res. Toxicol.* 15: 1407-1413.

Seifert A, Tatzel S, Schmid RD & Pleiss J (**2006**). Multiple molecular dynamics simulations of human p450 monooxygenase CYP2C9: the molecular basis of substrate binding and regioselectivity toward warfarin. *Proteins*, 64: 147-155.

Senn HM & **Thiel** W (**2009**). QM/MM methods for biomolecular systems. *Angew. Chem. Int. Ed.* 48: 1198-1229.

Sen S, Venkata Dasu V & Mandal B (**2007**). Developments in directed evolution for improving enzyme functions. *Appl. Biochem. Biotechnol.* 143: 212-223.

Serrano L, Bycroft M & Fersht AR (**1991**). Aromatic-aromatic interactions and protein stability. Investigation by double-mutant cycles. *J. Mol. Biol.* 218: 465-475.

Serrano L & **Fersht** AR (**1989**). Capping and alpha-helix stability. *Nature*, 342: 296-299.

Serrano L, Horovitz A, Avron B, Bycroft M & Fersht AR (**1990**). Estimating the contribution of engineered surface electrostatic interactions to protein stability by using double-mutant cycles. *Biochemistry*, 29: 9343-9352.

Sevinc MS, Maté MJ, Switala J, Fita I & Loewen PC (**1999**). Role of the lateral channel in catalase HPII of *Escherichia coli*. *Protein Sci.* 8: 490-498.

Shen Y, Lange O, Delaglio F, Rossi P, Aramini JM, Liu G, Eletsky A, Wu Y, Singarapu KK, Lemak A, Ignatchenko A, Arrowsmith CH, Szyperski T, Montelione GT, Baker D & Bax A (**2008**). Consistent blind protein structure generation from NMR chemical shift data. *Proc. Natl. Acad. Sci. U.S.A.* 105: 4685-4690.

Shen Y, Vernon R, Baker D & Bax A (**2009**). De novo protein structure generation from incomplete chemical shift assignments. *J Biomol. NMR*, 43: 63-78.

Shepherd JC (**1981**). Periodic correlations in DNA sequences and evidence suggesting their evolutionary origin in a comma-less genetic code. *J. Mol. Evol.* 17: 94-102.

Sheridan RP, Levy RM & Salemme FR (**1982**). alpha-Helix dipole model and electrostatic stabilization of 4-alpha-helical proteins. *Proc. Natl. Acad. Sci. U.S.A.* 79: 4545-4549.

Shine J & **Dalgarno** L (**1975**). Determinant of cistron specificity in bacterial ribosomes. *Nature*, 254: 34-38.

Shirts M & **Pande** VS (**2000**). COMPUTING: Screen savers of the world unite! *Science*, 290: 1903-1904.

Shoemaker KR, Kim PS, Brems DN, Marqusee S, York EJ, Chaiken IM, Stewart JM & Baldwin RL (**1985**). Nature of the charged-group effect on the stability of the C-peptide helix. *Proc. Natl. Acad. Sci. U.S.A.* 82: 2349-2353.

Shoemaker KR, Kim PS, York EJ, Stewart JM & Baldwin RL (**1987**). Tests of the helix dipole model for stabilization of alpha-helices. *Nature*, 326: 563-567.

Shurki A, Strajbl M, Villà J & Warshel A (**2002**). How much do enzymes really gain by restraining their reacting fragments? *J. Am. Chem. Soc.* 124: 4097-4107.

Silberstein M, Dennis S, Brown L, Kortvelyesi T, Clodfelter K & Vajda S (**2003**). Identification of substrate binding sites in enzymes by computational solvent mapping. *J. Mol. Biol.* 332: 1095-1113.

Silberstein M, Damborský J & Vajda S (**2007**). Exploring the binding sites of the haloalkane dehalogenase DhlA from *Xanthobacter autotrophicus* GJ10. *Biochemistry*, 46: 9239-9249.

Skjaerven L, Hollup SM & Reuter N (**2009**). Normal mode analysis for proteins. *J. Mol. Struct.* 898: 42-48.

Skjøt M, De Maria L, Chatterjee R, Svendsen A, Patkar SA, Ostergaard PR & Brask J (**2009**). Understanding the plasticity of the alpha/beta hydrolase fold: lid swapping on the *Candida antarctica* lipase B results in chimeras with interesting biocatalytic properties. *Eur. J. Chem. Biol.* 10: 520-527.

Smith DE & **Dang** LX (**1994**). Computer simulations of NaCl association in polarizable water. *J. Chem. Phys.* 100: 3757-3766.

Smith LJ, Redfield C, Smith RA, Dobson CM, Clore GM, Gronenborn AM, Walter MR, Naganbushan TL & Wlodawer A (**1994**). Comparison of four independently determined structures of human recombinant interleukin-4. *Nat. Struct. Biol.* 1: 301-310.

Sobolev V, Wade RC, Vriend G & Edelman M (**1996**). Molecular docking using surface complementarity. *Proteins*, 25: 120-129.

Socolich M, Lockless SW, Russ WP, Lee H, Gardner KH & Ranganathan R (**2005**). Evolutionary information for specifying a protein fold. *Nature*, 437: 512-518.

Söll D, Ohtsuka E, Jones DS, Lohrmann R, Hayatsu H, Nishimura S & Khorana HG (**1965**). Studies on polynucleotides, XLIX. Stimulation of the binding of aminoacyl-sRNA's to ribosomes by ribotrinucleotides and a survey of codon assignments for 20 amino acids. *Proc. Natl. Acad. Sci. U.S.A.* 54: 1378-1385.

Soriano A, Silla E, Tuñón I & Ruiz-López MF (**2005**). Dynamic and electrostatic effects in enzymatic processes. An analysis of the nucleophilic substitution reaction in haloalkane dehalogenase. *J. Am. Chem. Soc.* 127: 1946-1957.

Sousa SF, Fernandes PA & Ramos MJ (**2006**). Protein-ligand docking: current status and future challenges. *Proteins*, 65: 15-26.

Spera S & **Bax** A (**1991**). Empirical correlation between protein backbone conformation and C.alpha. and C.beta. 13C nuclear magnetic resonance chemical shifts. *J. Am. Chem. Soc.* 113: 5490-5492.

Sprangers R, Gribun A, Hwang PM, Houry WA & Kay LE (**2005**). Quantitative NMR spectroscopy of supramolecular complexes: dynamic side pores in ClpP are important for product release. *Proc. Natl. Acad. Sci. U.S.A.* 102: 16678-16683.

Srajer V, Ren Z, Teng T, Schmidt M, Ursby T, Bourgeois D, Pradervand C, Schildkamp W, Wulff M & Moffat K (**2001**). Protein conformational relaxation and ligand migration in myoglobin: a nanosecond to millisecond molecular movie from time-resolved Laue X-ray diffraction. *Biochemistry*, 40: 13802-13815.

Sreerama N & **Woody** RW (**1993**). A self-consistent method for the analysis of protein secondary structure from circular dichroism. *Anal. Biochem.* 209: 32-44.

Steitz TA & **Moore** PB (**2003**). RNA, the first macromolecular catalyst: the ribosome is a ribozyme. *Trends Biochem.Sci.* 28: 411-418.

Stemmer WPC (**1994a**). Rapid evolution of a protein in vitro by DNA shuffling. *Nature*, 370: 389-391.

Stemmer WPC (**1994b**). DNA shuffling by random fragmentation and reassembly: in vitro recombination for molecular evolution. *Proc. Natl. Acad. Sci. U.S.A.* 91: 10747-10751.

Stewart JJ (**1990**). MOPAC: a semiempirical molecular orbital program. *J. Comput. Aided Mol. Des.* 4: 1-105.

Stickle DF, Presta LG, Dill KA & Rose GD (**1992**). Hydrogen bonding in globular proteins. *J. Mol. Biol.* 226: 1143-1159.

Stranzl GR, Gruber K, Steinkellner G, Zangger K, Schwab H & Kratky C (**2004**). Observation of a short, strong hydrogen bond in the active site of hydroxynitrile lyase from *Hevea brasiliensis* explains a large pK_a shift of the catalytic base induced by the reaction intermediate. *J. Biol. Chem.* 279: 3699-3707.

Strasser A & **Wittmann** H (**2007**). LigPath: a module for predictive calculation of a ligand's pathway into a receptor-application to the gpH1-receptor. *J. Mol. Model.* 13: 209-218.

Straszewski-Chavez SL, Visintin IP, Karassina N, Los G, Liston P, Halaban R, Fadiel A & Mor G (**2007**). XAF1 mediates tumor necrosis factor-alpha-induced apoptosis and X-linked inhibitor of apoptosis cleavage by acting through the mitochondrial pathway. *J. Biol. Chem.* 282: 13059-13072.

Streltsov VA, Prokop Z, Damborský J, Nagata Y, Oakley A & Wilce MCJ (**2003**). Haloalkane dehalogenase LinB from *Sphingomonas paucimobilis* UT26: X-ray crystallographic studies of dehalogenation of brominated substrates. *Biochemistry*, 42: 10104-10112.

Strop P & **Mayo** SL (**2000**). Contribution of surface salt bridges to protein stability. *Biochemistry*, 39: 1251-1255.

Stsiapanava A, Koudelaková T, Lapkouski M, Pavlová M, Damborský J & Kutá-Smatanová I (**2008**). Crystals of DhaA mutants from *Rhodococcus rhodochrous* NCIMB 13064 diffracted to ultrahigh resolution: crystallization and preliminary diffraction analysis. *Acta Crystallogr., Sect. F: Struct. Biol. Cryst. Commun.* 64: 137-140.

Stucki G & **Thueer** M (**1995**). Experiences of a large-scale application of 1,2-dichloroethane degrading microorganisms for groundwater treatment. *Environ. Sci. Technol.* 29: 2339-2345.

Sugita Y & **Okamoto** Y (**1999**). Replica-exchange molecular dynamics method for protein folding. *Chem. Phys. Lett.* 314: 141-151.

Sullivan SM & **Holyoak** T (**2008**). Enzymes with lid-gated active sites must operate by an induced fit mechanism instead of conformational selection. *Proc. Natl. Acad. Sci. U.S.A.* 105: 13829-13834.

Sundaralingam M & **Sekharudu** YC (**1989**). Water-inserted alpha-helical segments implicate reverse turns as folding intermediates. *Science*, 244: 1333-1337.

Svendsen S, Zimprich C, McDougall MG, Klaubert DH & Los GV (**2008**). Spatial separation and bidirectional trafficking of proteins using a multi-functional reporter. *BMC Cell Biol.* 9: 17.

Szathmáry E (**1999**). The origin of the genetic code: amino acids as cofactors in an RNA world. *Trends Genet.* 15: 223-229.

Takano K, Funahashi J, Yamagata Y, Fujii S & Yutani K (**1997**). Contribution of water molecules in the interior of a protein to the conformational stability. *J. Mol. Biol.* 274: 132-142.

Tanford C, De PK & Taggart VG (**1960**). The role of the α-helix in the structure of proteins. Optical rotatory dispersion of β-lactoglobulin. *J. Am. Chem. Soc.* 82: 6028-6034.

Tao H & **Cornish** VW (**2002**). Milestones in directed enzyme evolution. *Curr. Opin. Chem. Biol.* 6: 858-864.

Tara S, Helms V, Straatsma TP & McCammon JA (**1999**). Molecular dynamics of mouse acetylcholinesterase complexed with huperzine A. *Biopolymers*, 50: 347-359.

Taylor JS & **Burnett** RM (**2000**). DARWIN: a program for docking flexible molecules. *Proteins*, 41: 173-191.

Teague SJ (**2003**). Implications of protein flexibility for drug discovery. *Nat. Rev. Drug Discovery*, 2: 527-541.

Teeter MM (**2004**). Myoglobin cavities provide interior ligand pathway. *Protein Sci.* 13: 313-318.

Teichmann SA, Chothia C & Gerstein M (**1999**). Advances in structural genomics. *Curr. Opin. Struct. Biol.* 9: 390-399.

Teichmann SA, Rison SC, Thornton JM, Riley M, Gough J & Chothia C (**2001**). The evolution and structural anatomy of the small molecule metabolic pathways in *Escherichia coli*. *J. Mol. Biol.* 311: 693-708.

Teng Q (**2005**). Protein structure determination from NMR data. *In* Structural Biology: Practical NMR Applications (pp. 211-243). *Springer Science+Business Media*, New York, NY, USA.

Thapar R, Nicholson EM, Rajagopal P, Waygood EB, Scholtz JM & Klevit RE (**1996**). Influence of N-cap mutations on the structure and stability of *Escherichia coli* HPr. *Biochemistry*, 35: 11268-11277.

Todd AE, Orengo CA & Thornton JM (**2001**). Evolution of function in protein superfamilies, from a structural perspective. *J. Mol. Biol.* 307: 1113-1143.

Todd AE, Orengo CA & Thornton JM (**2002**). Plasticity of enzyme active sites. *Trends Biochem.Sci.* 27: 419-426.

Tolman JR & **Ruan** K (**2006**). NMR residual dipolar couplings as probes of biomolecular dynamics. *Chem. Rev.* 106: 1720-1736.

Tomita A, Sato T, Ichiyanagi K, Nozawa S, Ichikawa H, Chollet M, Kawai F, Park S, Tsuduki T, Yamato T, Koshihara S & Adachi S (**2009**). Visualizing breathing motion of internal cavities in concert with ligand migration in myoglobin. *Proc. Natl. Acad. Sci. U.S.A.* 106: 2612-2616.

Toniolo C (**1980**). Intramolecularly hydrogen-bonded peptide conformations. *CRC Crit. Rev. Biochem.* 9: 1-44.

Torz M, Wietzes P, Beschkov V & Janssen DB (**2007**). Metabolism of mono- and dihalogenated C1 and C2 compounds by *Xanthobacter autotrophicus* growing on 1,2-dichloroethane. *Biodegradation*, 18: 145-157.

Tousignant A & **Pelletier** JN (**2004**). Protein motions promote catalysis. *Chem. Biol.* 11: 1037-1042.

Trevors JT & **Abel** DL (**2004**). Chance and necessity do not explain the origin of life. *Cell Biol. Int.* 28: 729-739.

Trifonov EN (**2004**). The triplet code from first principles. *J. Biomol. Struct. Dyn.* 22: 1-11.

Triglia T, Peterson MG & Kemp DJ (**1988**). A procedure for in vitro amplification of DNA segments that lie outside the boundaries of known sequences. *Nucleic Acids Res.* 16: 8186.

Trosset J & **Scheraga** HA (**1999**). PRODOCK: Software package for protein modeling and docking. *J. Comput. Chem.* 20: 412-427.

Tugarinov V, Ollerenshaw JE & Kay LE (**2005a**). Probing side-chain dynamics in high molecular weight proteins by deuterium NMR spin relaxation: an application to an 82-kDa enzyme. *J. Am. Chem. Soc.* 127: 8214-8225.

Tugarinov V, Choy W, Orekhov VY & Kay LE (**2005b**). Solution NMR-derived global fold of a monomeric 82-kDa enzyme. *Proc. Natl. Acad. Sci. U.S.A.* 102: 622-627.

UniProt Consortium (**2009**). The Universal Protein Resource (UniProt) 2009. *Nucleic Acids Res.* 37: D169-174.

Unwin PN & **Henderson** R (**1975**). Molecular structure determination by electron microscopy of unstained crystalline specimens. *J. Mol. Biol.* 94: 425-440.

Valdar WS & **Thornton** JM (**2001**). Conservation helps to identify biologically relevant crystal contacts. *J. Mol. Biol.* 313: 399-416.

Valencia A (**2005**). Automatic annotation of protein function. *Curr. Opin. Struct. Biol.* 15: 267-274.

Valuev VP, Afonnikov DA, Ponomarenko MP, Milanesi L & Kolchanov NA (**2002**). ASPD (Artificially Selected Proteins/Peptides Database): a database of proteins and peptides evolved in vitro. *Nucleic Acids Res.* 30: 200-202.

Van Belle D, De Maria L, Iurcu G & Wodak SJ (**2000**). Pathways of ligand clearance in acetylcholinesterase by multiple copy sampling. *J. Mol. Biol.* 298: 705-726.

Van Der Spoel D, Lindahl E, Hess B, Groenhof G, Mark AE & Berendsen HJC (**2005**). GROMACS: fast, flexible, and free. *J. Comput. Chem.* 26: 1701-1718.

Vargas R, Garza J, Dixon DA & Hay BP (**2000**). How strong is the Cα–H...OC hydrogen bond? *J. Am. Chem. Soc.* 122: 4750-4755.

Váró G, Needleman R & Lanyi JK (**1995**). Light-driven chloride ion transport by halorhodopsin from *Natronobacterium pharaonis*. 2. Chloride release and uptake, protein conformation change, and thermodynamics. *Biochemistry*, 34: 14500-14507.

Venkatachalam CM (**1968**). Stereochemical criteria for polypeptides and proteins. V. Conformation of a system of three linked peptide units. *Biopolymers*, 6: 1425-1436.

Verschueren KH, Kingma J, Rozeboom HJ, Kalk KH, Janssen DB & Dijkstra BW (**1993a**). Crystallographic and fluorescence studies of the interaction of haloalkane dehalogenase with halide ions. Studies with halide compounds reveal a halide binding site in the active site. *Biochemistry*, 32: 9031-9037.

Verschueren KH, Franken SM, Rozeboom HJ, Kalk KH & Dijkstra BW (**1993b**). Non-covalent binding of the heavy atom compound $[Au(CN)_2]$- at the halide binding site of haloalkane dehalogenase from *Xanthobacter autotrophicus* GJ10. *FEBS Lett.* 323: 267-270.

Verschueren KH, Franken SM, Rozeboom HJ, Kalk KH & Dijkstra BW (**1993c**). Refined X-ray structures of haloalkane dehalogenase at pH 6.2 and pH 8.2 and implications for the reaction mechanism. *J. Mol. Biol.* 232: 856-872.

Verschueren KH, Seljée F, Rozeboom HJ, Kalk KH & Dijkstra BW (**1993d**). Crystallographic analysis of the catalytic mechanism of haloalkane dehalogenase. *Nature*, 363: 693-698.

Villa J & **Warshel** A (**2001**). Energetics and dynamics of enzymatic reactions. *J. Phys. Chem. B*, 105: 7887-7907.

Vitkup D, Melamud E, Moult J & Sander C (**2001**). Completeness in structural genomics. *Nat. Struct. Biol.* 8: 559-566.

Vlassov AV, Kazakov SA, Johnston BH & Landweber LF (**2005**). The RNA world on ice: a new scenario for the emergence of RNA information. *J. Mol. Evol.* 61: 264-273.

Voet DJ, Voet JG, & Pratt CW (**1999**). Fundamentals of biochemistry. *John Wiley and Sons*, New York, NY, USA.

Vriend G (**1990**). WHAT IF: a molecular modeling and drug design program. *J. Mol. Graphics*, 8: 52-56.

Wada A (**1976**). The alpha-helix as an electric macro-dipole. *Adv. Biophys.* 9: 1-63.

Wada H, Senoo K & Takai Y (**1989**). Rapid degradation of gamma-HCH in upland soil after multiple applications. *Soil Sci. Plant Nutr.* 35: 71-77.

Wade RC, Davis ME, Luty BA, Madura JD & McCammon JA (**1993**). Gating of the active site of triose phosphate isomerase: Brownian dynamics simulations of flexible peptide loops in the enzyme. *Biophys. J.* 64: 9-15.

Wade RC, Gabdoulline RR, Lüdemann SK & Lounnas V (**1998**). Electrostatic steering and ionic tethering in enzyme-ligand binding: insights from simulations. *Proc. Natl. Acad. Sci. U.S.A.* 95: 5942-5949.

Wade RC, Winn PJ, Schlichting I & Sudarko (**2004**). A survey of active site access channels in cytochromes P450. *J. Inorg. Biochem.* 98: 1175-1182.

Waldburger CD, Schildbach JF & Sauer RT (**1995**). Are buried salt bridges important for protein stability and conformational specificity? *Nat. Struct. Biol.* 2: 122-128.

Wallace AC, Laskowski RA & Thornton JM (**1995**). LIGPLOT: a program to generate schematic diagrams of protein-ligand interactions. *Protein Eng.* 8: 127-134.

Wallace AC, Borkakoti N & Thornton JM (**1997**). TESS: a geometric hashing algorithm for deriving 3D coordinate templates for searching structural databases. Application to enzyme active sites. *Protein Sci.* 6: 2308-2323.

Wang J, Cieplak P & Kollman PA (**2000**). How well does a restrained electrostatic potential (RESP) model perform in calculating conformational energies of organic and biological molecules? *J. Comput. Chem.* 21: 1049-1074.

Wang L, Brock A, Herberich B & Schultz PG (**2001**). Expanding the genetic code of *Escherichia coli*. *Science*, 292: 498-500.

Wang T & **Duan** Y (**2007**). Chromophore channeling in the G-protein coupled receptor rhodopsin. *J. Am. Chem. Soc.* 129: 6970-6971.

Wang Y & **Jardetzky** O (**2002**). Probability-based protein secondary structure identification using combined NMR chemical-shift data. *Protein Sci.* 11: 852-861.

Warshel A & **Levitt** M (**1976**). Theoretical studies of enzymic reactions: dielectric, electrostatic and steric stabilization of the carbonium ion in the reaction of lysozyme. *J. Mol. Biol.* 103: 227-249.

Warshel A (**1978**). Energetics of enzyme catalysis. *Proc. Natl. Acad. Sci. U.S.A.* 75: 5250-5254.

Warshel A (**1991**). Computer modeling of chemical reactions in enzymes and solutions. *John Wiley and Sons*, New York, NY, USA.

Warshel A & **Papazyan** A (**1998**). Electrostatic effects in macromolecules: fundamental concepts and practical modeling. *Curr. Opin. Struct. Biol.* 8: 211-217.

Warshel A & **Florián** J (**1998**). Computer simulations of enzyme catalysis: finding out what has been optimized by evolution. *Proc. Natl. Acad. Sci. U.S.A.* 95: 5950-5955.

Warshel A, Strajbl M, Villa J & Florián J (**2000**). Remarkable rate enhancement of orotidine 5‘-monophosphate decarboxylase is due to transition-state stabilization rather than to ground-state destabilization. *Biochemistry*, 39: 14728-14738.

Warshel A (**2003**). Computer simulations of enzyme catalysis: methods, progress, and insights. *Annu. Rev. Biophys. Biomol. Struct.* 32: 425-443.

Warshel A, Sharma PK, Kato M, Xiang Y, Liu H & Olsson MHM (**2006**). Electrostatic basis for enzyme catalysis. *Chem. Rev.* 106: 3210-3235.

Waterhous DV & **Johnson** WC (**1994**). Importance of environment in determining secondary structure in proteins. *Biochemistry*, 33: 2121-2128.

Watney JB, Agarwal PK & Hammes-Schiffer S (**2003**). Effect of mutation on enzyme motion in dihydrofolate reductase. *J. Am. Chem. Soc.* 125: 3745-3750.

Watson JD, Laskowski RA & Thornton JM (**2005**). Predicting protein function from sequence and structural data. *Curr. Opin. Struct. Biol.* 15: 275-284.

Weaver TM (**2000**). The pi-helix translates structure into function. *Protein Sci.* 9: 201-206.

Weber AL & **Miller** SL (**1981**). Reasons for the occurrence of the twenty coded protein amino acids. *J. Mol. Evol.* 17: 273-284.

Weiner PK & **Kollman** PA (**1981**). AMBER: Assisted model building with energy refinement. A general program for modeling molecules and their interactions. *J. Comput. Chem.* 2: 287-303.

Welch M, Villalobos A, Gustafsson C & Minshull J (**2009**). You're one in a googol: optimizing genes for protein expression. *J. R. Soc. Interface*, 6 Suppl 4: S467-476.

Welch W, Ruppert J & Jain AN (**1996**). Hammerhead: fast, fully automated docking of flexible ligands to protein binding sites. *Chem. Biol.* 3: 449-462.

Wen Z, Baudry J, Berenbaum MR & Schuler MA (**2005**). Ile115Leu mutation in the SRS1 region of an insect cytochrome P450 (CYP6B1) compromises substrate turnover via changes in a predicted product release channel. *Protein Eng. Des. Sel.* 18: 191-199.

Whisstock JC & **Lesk** AM (**2003**). Prediction of protein function from protein sequence and structure. *Q. Rev. Biophys.* 36: 307-340.

White HB (**1976**). Coenzymes as fossils of an earlier metabolic state. *J. Mol. Evol.* 7: 101-104.

van den Wijngaard AJ, van der Kamp KW, van der Ploeg J, Pries F, Kazemier B & Janssen DB (**1992**). Degradation of 1,2-dichloroethane by *Ancylobacter aquaticus* and other facultative methylotrophs. *Appl. Environ. Microbiol.* 58: 976-983.

van den Wijngaard AJ, Wind RD & Janssen DB (**1993**). Kinetics of bacterial growth on chlorinated aliphatic compounds. *Appl. Environ. Microbiol.* 59: 2041-2048.

Williams GJ, Nelson AS & Berry A (**2004**). Directed evolution of enzymes for biocatalysis and the life sciences. *Cell. Mol. Life Sci. 61*, 3034-3046.

Williams MA, Goodfellow JM & Thornton JM (**1994**). Buried waters and internal cavities in monomeric proteins. *Protein Sci.* 3: 1224-1235.

Wilson G, Hecht L & Barron LD (**1996**). Residual structure in unfolded proteins revealed by Raman optical activity. *Biochemistry*, 35: 12518-12525.

Wilson J, Decius JG, Cross PG & Lagemann RT (**1955**). Molecular vibrations. *Am. J. Phys.* 23: 550.

Wilson MA & **Brunger** AT (**2000**). The 1.0 Å crystal structure of Ca(2+)-bound calmodulin: an analysis of disorder and implications for functionally relevant plasticity. *J. Mol. Biol.* 301: 1237-1256.

Winn MD, Isupov MN, & Murshudov GN (**2001**). Use of TLS parameters to model anisotropic displacements in macromolecular refinement. *Acta Crystallogr., Sect. D: Biol. Crystallogr.* 57: 122-133.

Winn PJ, Lüdemann SK, Gauges R, Lounnas V & Wade RC (**2002**). Comparison of the dynamics of substrate access channels in three cytochrome P450s reveals different opening mechanisms and a novel functional role for a buried arginine. *Proc. Natl. Acad. Sci. U.S.A.* 99: 5361-5366.

Wishart DS, Arndt D, Berjanskii M, Tang P, Zhou J & Lin G (**2008**). CS23D: a web server for rapid protein structure generation using NMR chemical shifts and sequence data. *Nucleic Acids Res.* 36: W496-502.

Wishart DS & **Sykes** BD (**1994**). The 13C chemical-shift index: a simple method for the identification of protein secondary structure using 13C chemical-shift data. *J Biomol. NMR*, 4: 171-180.

Wlodawer A, Minor W, Dauter Z & Jaskolski M (**2008**). Protein crystallography for non-crystallographers, or how to get the best (but not more) from published macromolecular structures. *FEBS J.* 275: 1-21.

Wlodek ST, Clark TW, Scott LR & McCammon JA (**1997**). Molecular dynamics of acetylcholinesterase dimer complexed with tacrine. *J. Am. Chem. Soc.* 119: 9513-9522.

Woese CR (**2001**). Translation: in retrospect and prospect. *RNA*, 7: 1055-1067.

Wolfenden R (**1969**). Transition state analogues for enzyme catalysis. *Nature*, 223: 704-705.

Wolfenden R (**1974**). Enzyme catalysis: conflicting requirements of substrate access and transition state affinity. *Mol. Cell. Biochem.* 3: 207-211.

Wolfenden R & **Snider** MJ (**2001**). The depth of chemical time and the power of enzymes as catalysts. *Acc. Chem. Res.* 34: 938-945.

Wolf-Watz M, Thai V, Henzler-Wildman K, Hadjipavlou G, Eisenmesser EZ & Kern D (**2004**). Linkage between dynamics and catalysis in a thermophilic-mesophilic enzyme pair. *Nat. Struct. Mol. Biol.* 11: 945-949.

Wombacher R, Keiper S, Suhm S, Serganov A, Patel DJ & Jäschke A (**2006**). Control of stereoselectivity in an enzymatic reaction by backdoor access. *Angew. Chem. Int. Ed.* 45: 2469-2472.

Wong TS, Tee KL, Hauer B & Schwaneberg U (**2004**). Sequence saturation mutagenesis (SeSaM): a novel method for directed evolution. *Nucleic Acids Res.* 32: e26.

Woycechowsky KJ, Vamvaca K & Hilvert D (**2007**). Novel enzymes through design and evolution. *Adv. Enzymol. Relat. Areas Mol. Biol.* 75: 241-294.

Wriggers W & **Schulten** K (**1999**). Investigating a back door mechanism of actin phosphate release by steered molecular dynamics. *Proteins*, 35: 262-273.

Wu J, Hong Q, Han P, He J & Li S (**2007**). A gene linB2 responsible for the conversion of beta-HCH and 2,3,4,5,6-pentachlorocyclohexanol in *Sphingomonas* sp. BHC-A. *Appl. Microbiol. Biotechnol.* 73: 1097-1105.

Xiong H, Buckwalter BL, Shieh HM & Hecht MH (**1995**). Periodicity of polar and nonpolar amino acids is the major determinant of secondary structure in self-assembling oligomeric peptides. *Proc. Natl. Acad. Sci. U.S.A.* 92: 6349-6353.

Xu Y, Shen J, Luo X, Silman I, Sussman JL, Chen K & Jiang H (**2003**). How does huperzine A enter and leave the binding gorge of acetylcholinesterase? Steered molecular dynamics simulations. *J. Am. Chem. Soc.* 125: 11340-11349.

Yaffe E, Fishelovitch D, Wolfson HJ, Halperin D & Nussinov R (**2008**). MolAxis: efficient and accurate identification of channels in macromolecules. *Proteins*, 73: 72-86.

Yang AS, Hitz B & Honig B (**1996**). Free energy determinants of secondary structure formation: III. beta-turns and their role in protein folding. *J. Mol. Biol.* 259: 873-882.

Yang AS & **Honig** B (**1995a**). Free energy determinants of secondary structure formation: I. alpha-Helices. *J. Mol. Biol.* 252: 351-365.

Yang AS & **Honig** B (**1995b**). Free energy determinants of secondary structure formation: II. Antiparallel beta-sheets. *J. Mol. Biol.* 252: 366-376.

Yao H, McCullough CR, Costache AD, Pullela PK & Sem DS (**2007**). Structural evidence for a functionally relevant second camphor binding site in P450cam: model for substrate entry into a P450 active site. *Proteins*, 69: 125-138.

Yarus M (**1988**). A specific amino acid binding site composed of RNA. *Science*, 240: 1751-1758.

Yarus M & **Christian** EL (**1989**). Genetic code origins. *Nature*, 342: 349-350.

Yarus M (**1998**). Amino acids as RNA ligands: a direct-RNA-template theory for the code's origin. *J. Mol. Evol.* 47: 109-117.

Yarus M (**1999**). Boundaries for an RNA world. *Curr. Opin. Chem. Biol.* 3: 260-267.

Ye X, Yu A & Champion PM (**2006**). Dynamics of nitric oxide rebinding and escape in horseradish peroxidase. *J. Am. Chem. Soc.* 128: 1444-1445.

Yokota T, Omori T & Kodama T (**1987**). Purification and properties of haloalkane dehalogenase from *Corynebacterium* sp. strain m15-3. *J. Bacteriol.* 169: 4049-4054.

Yonetani T, Tsuneshige A, Zhou Y & Chen X (**1998**). Electron paramagnetic resonance and oxygen binding studies of alpha-nitrosyl hemoglobin. A novel oxygen carrier having no-assisted allosteric functions. *J. Biol. Chem.* 273: 20323-20333.

Yonetani T & **Laberge** M (**2008**). Protein dynamics explain the allosteric behaviors of hemoglobin. *Biochim. Biophys. Acta*, 1784: 1146-1158.

Yu EW & **Koshland Jr.** DE (**2001**). Propagating conformational changes over long (and short) distances in proteins. *Proc. Natl. Acad. Sci. U.S.A.* 98: 9517-9520.

Zeeb M & **Balbach** J (**2004**). Protein folding studied by real-time NMR spectroscopy. *Methods*, 34: 65-74.

Zelent B, Kaposi A, Nucci N, Sharp K, Dalosto S, Wright W & Vanderkooi J (**2004**). Water channel of horseradish peroxidase studied by the charge-transfer absorption band of ferric heme. *J. Phys. Chem. B*, 108: 10317-10324.

Zhang Y, Perry K, Vinci VA, Powell K, Stemmer WPC & del Cardayré SB (**2002**). Genome shuffling leads to rapid phenotypic improvement in bacteria. *Nature*, 415: 644-646.

Zhao H, Chockalingam K & Chen Z (**2002**). Directed evolution of enzymes and pathways for industrial biocatalysis. *Curr. Opin. Biotechnol.* 13: 104-110.

Zhou HX, Wlodek ST & McCammon JA (**1998**). Conformation gating as a mechanism for enzyme specificity. *Proc. Natl. Acad. Sci. U.S.A.* 95: 9280-9283.

Zhou Y, Zheng Q, Li Z, Zhang Y, Sun M, Sun C, Si D, Cai L, Guo Y & Zhou H (**2006**). On the human CYP2C9*13 variant activity reduction: a molecular dynamics simulation and docking study. *Biochimie*, 88: 1457-1465.

Zhu G, Xia Y, Nicholson L K & Sze KH (**2000**). Protein dynamics measurements by TROSY-based NMR experiments. *J. Magn. Reson.* 143: 423-426.

Zwanzig R (**1992**). Dynamical disorder: Passage through a fluctuating bottleneck. *J. Chem. Phys.* 97: 3587-3589.

List of tables and figures

It's only natural, actual facts are thrown at you; the impact'll blow trees back and crack statues.
— Jason Hunter

Abbreviations

OK, now where was I? Prepared, was I. Your man broke his jaw tryin' to say what I.

— Clifford Smith

A **a**denine
alanine
Ala **ala**nine
Arg **arg**inine
Asn **as**paragi**n**e
Asp **asp**artic acid
asparate
ATF **a**tomic **f**orce microscopy
Å **Å**ngström

B*-FIT** ***B-**f**actor saturat**i**on **t**est
BCI 5,5'-di**b**romo-4,4'-di**c**hloro-**i**ndigo
BCHI 5-**b**romo-4-**c**hloro-3-**h**ydroxy**i**ndole

C **c**ytosine
cysteine
carbon
CAPRI **C**ritical **A**ssessment of **P**redicted **I**nteractions
CASP **C**ritical **A**ssessment of **S**tructure **P**rediction
CAST **c**ombinatorial **a**ctive site **s**aturation **t**est
CATH **C**lass-**A**rchitecture-**T**opology-**H**omologous superfamily
CC loop **C**-terminal **c**ap domain **loop**
CD **c**ircular **d**ichroism
CL **c**h**l**oride anion
CO carbon monooxide
CO_2 carbon dioxide
COSY **co**rrelation **s**pectroscop**y**
Cys **cys**teine

D aspartic acid
aspartate
DCL 2,3-**d**i**c**hloropropane-1-o**l**
DDBJ **D**NA **D**ata**b**ank of **J**apan
DNA **d**eoxyribo**n**ucleic **a**cid
DOGS **d**egenerate **o**ligonucleotide **g**ene **s**huffling
dATP **d**eoxy**a**denosine **t**ri**p**hosphate
dCTP **d**eoxy**c**ytidine **t**ri**p**hosphate
dGTP **d**eoxy**g**uanosine **t**ri**p**hosphate
dTTP **d**eoxy**t**hymidine **t**ri**p**hosphate
ddATP **d**i**d**eoxy**a**denosine **t**ri**p**hosphate
ddCTP **d**i**d**eoxy**c**ytidine **t**ri**p**hosphate
ddGTP **d**i**d**eoxy**g**uanosine **t**ri**p**hosphate
ddTTP **d**i**d**eoxy**t**hymidine **t**ri**p**hosphate

E glutamic acid
glutamate
[E] **e**nzyme concentration
E_a **a**ctivation **e**nergy
EC **e**nzyme **c**omission; **e**lectron **c**rystallography

EMBL **E**uropean **M**olecular **B**iology **L**aboratory
EPR **e**lectron **p**aramagnetic **r**esonance
[ES] **e**nzyme-**s**ubstrate complex concentration
EVB **e**mpirical **v**alence **b**ond
epPCR **e**rror-**p**rone **p**olymerase **c**hain **r**eaction
ε_0 permitivity of free space
ε_r dielectric constant of medium

F phenylalanine
FEP **f**ree **e**nergy **p**erturbation
FRET **f**luorescence **r**esonance **e**nergy **t**ransfer
ff94 19**94** Cornell **f**orce **f**ield

G **g**uanine
glycine
GC **g**as **c**hromatography
Gly **gly**cine
Gln **gl**utami**n**e
Glu **glu**tamic acid
glutamate
GNA **g**lycol **n**ucleic **a**cid

H **h**istidine
hydrogen
H/D **h**ydrogen/**d**euterium
HHDB **H**ydrogen and **H**ydration in proteins **D**atabase
His **his**tidine
HSQC **h**eteronuclear **s**ingle **q**uantum **c**oherence
h Planck's constant

I **i**soleucine
[I] **i**nhibitor concentration
Ile **i**so**le**ucine
IM AMBER atom type for chloride anion
INSDC **I**nternational **N**ucleotide **S**equence **D**atabase **C**ollaboration
IPTG **i**so**p**ropyl-β-D-**t**hio**g**alactopyranoside
ISM **i**terative **s**aturation **m**utagenesis
ITCHY **i**ncreamental **t**runcation for **c**reation of **h**ybrid enz**y**mes

K lysine
K_d **d**issociation constant
K_i equilibrium **i**nhibition constant
K_m apparent dissociation (**M**ichaelis) constant
KNF **K**oshland-**N**émethy-**F**ilmer
k_b **B**oltzmann constant
kcal **k**ilo**cal**ory
k_{cat} **cat**alytic constant
k_{cat}/K_m performance constant

L **l**eucine
[L] **l**igand concentration
LB **l**ysogeny **b**roth
LES **l**ocally **e**nhanced **s**ampling
Leu **leu**cine
LRA **l**inear **r**esponse **a**pproximation
LUCA the **l**ast **u**niversal **c**ommon **a**ncestor
Lys **lys**ine

M **m**ethionine
molar concentration

MCS **m**ultiple **c**opy **s**ite
MD **m**olecular **d**ynamics
Met **met**hionine
MM **m**olecular **m**echanics
MR **m**olecular **r**eplacement
MS **m**ass **s**pectrometry
MWC **M**onod-**W**yman-**C**hangeux
mM **m**illi**m**olar concentration
ms **m**illi**s**econd

N asparagi**n**e
nitrogen
NAC **n**ear **a**ttack **c**onfiguration
Na_2SO_4 sodium sulphate
NC **n**eutron **c**rystallography
NC loop **N**-terminal **c**ap domain **loop**
NexT **n**ucleotide **ex**change and **e**xcision **t**echnology
NM **n**ormal **m**ode
NMA **n**ormal **m**ode **a**nalysis
NMR **n**uclear **m**agnetic **r**esonance
NOESY **n**uclear **O**verhauser **e**ffect **s**pectroscop**y**

O_2 molecular **o**xygen

P **p**roline
[P] **p**rotein concentration; **p**roduct concentration
PCR **p**olymerase **c**hain **r**eaction
PDB **P**rotein **D**ata **B**ank
Phe **phe**nylalanine
PISA **P**rotein **I**nterfaces, **S**urface and **A**ssemblies
[PL] concentration of **p**rotein-**l**igand complex
Pro **pro**line

Q glutamine
QM **q**uantum **m**echanics

R a**r**ginine
universal gas constant
RACHITT **ra**ndom **chi**meragenesis on **t**ransient **t**emplates
RAMD **r**andom **a**cceleration **m**olecular **d**ynamics
R-DCL ***(R)*-2,3-di*c*hloropropane-1-o*l***
RESP **r**estrained **e**lectrostatic **p**otential fit
RETT **r**ecombined **e**xtension on **t**runcated **t**emplates
***R*-factor** global **r**eliability **factor**
R_{merge} diffraction data **r**eliability factor
RMS **r**oot-**m**ean-**s**quare
RMSD **r**oot-**m**ean-**s**quare deviation
RNA **r**ibo**n**ucleic **a**cid
RNDM **r**a**n**dom **d**rift **m**utagenesis
RPR **r**andom **p**riming **r**ecombination

S **s**erine
[S] **s**ubstrate concentration
SANS **s**mall **a**ngle **n**eutron **s**cattering
SAXS **s**mall **a**ngle **X**-ray **s**cattering
SCOP **S**tructural **C**lassification **O**f **P**roteins
S-DCL ***(S)*-2,3-di*c*hlororopane-1-o*l***
Sec **se**leno**c**ysteine
Ser **ser**ine
SeSaM **se**quence **sa**turation **m**utagenesis

SMD **s**teered **m**olecular **d**ynamics
S_N2 **bi**molecular **n**ucleophilic **s**ubstitution
StEP **st**aggered **e**xtension **p**rocess
s **s**econd

T **t**hyime
threonine
temperature
TCP 1,2,3-**t**ri**c**hloro**p**ropane
T_{dt} **d**ynamic **t**ransition **t**emperature
Thr **thr**eonine
TLS **t**ranslation-**l**ibration-**s**crew

TMD **t**argeted **m**olecular **d**ynamics
TNA **t**hreose **n**ucleic **a**cid
TOCSY **t**otal **c**orrelation **s**pectroscop**y**
TROSY **t**ransverse **r**elaxation **o**ptimised **s**pectroscop**y**
Trp **tr**y**p**tophane
Tyr **ty**r**r**osine

U **u**racil
selenocysteine
USMD **u**mbrella **s**ampling **m**olecular **d**ynamics
UV **u**ltra-**v**iolet
UVRR **UV** **r**esonance **R**AMAN

V **v**aline
Val **val**ine
VIS **vi**sible **s**pectrum
V_{max} **max**imum reaction **v**elocity

W tryptophane

Y t**y**rosine

XC **X**-ray **c**rystallography

Original research articles

You scream as it enters your bloodstream; erupts your brain from the pain these thoughts contain.
— Elgin Turner

Klvaňa M,[1,5] **Pavlová M,[1,5] Prokop Z,[1] Chaloupková R,[1] Banáš P,[2] Otyepka M,[2] Wade RC,[3] Nagata Y[4] & Damborský J[1*] (2009). Redesigning dehalogenase access tunnels as a strategy for degrading an anthropogenic substrate. *Nat. Chem. Biol.* 5: 727-733.**

[1]Loschmidt Laboratories, Department of Experimental Biology and National Centre for Biomolecular Research, Faculty of Science, Masaryk University, Brno, Czech Republic. [2]Department of Physical Chemistry and Center for Biomolecules and Complex Molecular Systems, Palacký University, Olomouc, Czech Republic. [3]Molecular and Cellular Modeling Group, EML Research gGmbH, Heidelberg, Germany. [4]Department of Environmental Life Sciences, Graduate School of Life Sciences, Tohoku University, Sendai, Japan.

[5]These authors contributed equally to this work.
[*]Corresponding author. E-mail address: jiri@chemi.muni.cz.

Submission process | Received 20 January 2009; accepted 28 May 2009; published online 23 August 2009. Edited by Catherine Goodman.

Abstract | Engineering enzymes to degrade anthropogenic compounds efficiently is challenging. We obtained *Rhodococcus rhodochrous* haloalkane dehalogenase mutants with up to 32-fold higher activity than wild-type toward the toxic, recalcitrant anthropogenic compound 1,2,3-trichloropropane (TCP) using a new strategy. We identified key residues in access tunnels connecting the buried active site with bulk solvent by rational design and randomized them by directed evolution. The most active mutant has large aromatic residues at two out of three randomized positions and two positions modified by site-directed mutagenesis. These changes apparently enhance activity with TCP by decreasing accessibility of the active site for water molecules, thereby promoting activated complex formation. Kinetic analyses confirmed that the mutations improved carbon-halogen bond cleavage and shifted the rate-limiting step to the release of products. Engineering access tunnels by combining computer-assisted protein design with directed evolution may be a valuable strategy for refining catalytic properties of enzymes with buried active sites.

Keywords | haloalkane dehalogenase; 1,2,3-trichloropropane; tunnel; semi-rational design; molecular dynamics; saturation mutagenesis; enhanced activity; reaction mechanism; substrate specificity.

Author contributions | *Pavlová* performed mutagenesis and activity measurements; *Klvaňa* performed molecular modelling and designed mutants; *Prokop* performed pre-steady state kinetics measurements; *Chaloupková* performed CD spectroscopy measurements and solvent kinetic isotopic effect measurements; *Banáš* and *Otyepka* designed mutants; *Wade* contributed the RAMD modelling tool; *Tsuda* and *Nagata* contributed molecular biology tools; *Damborský* interpreted data and designed mutants. All authors contributed to the writing of the paper.

Klvaňa M,[1] **Pavlová M,[1] Koudeláková T,[1] Chaloupková R,[1] Dvořák P,[1] Prokop Z,[1] Stsiapanava A,[2] Kutý M,[2,3] Kutá-Smatanová I,[2,3] Dohnálek J,[4] Kulhánek P,[5] Wade RC[6] & Damborský J[1*] (2009). Pathways and mechanisms for product release in the engineered haloalkane dehalogenases explored using classical and random acceleration molecular dynamics simulations. *J. Mol. Biol.* 392: 1339-1356.**

[1]Loschmidt Laboratories, Department of Experimental Biology and National Centre for Biomolecular Research, Faculty of Science, Masaryk University, Kamenice 5/A4, 625 00 Brno, Czech Republic. [2]Institute of Physical Biology, University of South Bohemia, Zámek 136, 373 33 Nové Hrady, Czech Republic. [3]Institute of Systems Biology and Ecology, Academy of Sciences of the Czech Republic, Zámek 136, 373 33 Nové Hrady, Czech Republic. [4]Institute of Macromolecular Chemistry, Academy of Sciences of the Czech Republic, Heyrovského náměstí 2, 162 06 Praha 6, Czech Republic. [5]Laboratory of Computational Chemistry, National Centre for Biomolecular Research, Faculty of Science, Masaryk University, Kamenice 5/A4, 625 00 Brno, Czech Republic. [6]Molecular and Cellular Modeling Group, EML Research, Schloss-Wolfsbrunnenweg 33, D-69118 Heidelberg, Germany.

*Corresponding author. E-mail address: jiri@chemi.muni.cz.

Submission process | Received 11 March 2009; received in revised form 25 June 2009; accepted 29 June 2009; available online 3 July 2009. Edited by David A. Case.

Abstract | Eight mutants of the DhaA haloalkane dehalogenase carrying mutations at the residues lining two tunnels, previously observed by protein X-ray crystallography, were constructed and biochemically characterized. The mutants showed distinct catalytic efficiencies with the halogenated substrate 1,2,3-trichloropropane. Release pathways for the two dehalogenation products, 2,3-dichloropropane-1-ol and the chloride ion, and exchange pathways for water molecules, were studied using classical and random acceleration molecular dynamics simulations. Five different pathways, denoted p1, p2a, p2b, p2c, and p3, were identified. The individual pathways showed differing selectivity for the products: the chloride ion releases solely through p1, whereas the alcohol releases through all five pathways. Water molecules play a crucial role for release of both products by breakage of their hydrogen-bonding interactions with the active-site residues and shielding the charged chloride ion during its passage through a hydrophobic tunnel. Exchange of the chloride ions, the alcohol product, and the waters between the buried active site and the bulk solvent can be realized by three different mechanisms: (i) passage through a permanent tunnel, (ii) passage through a transient tunnel, and (iii) migration through a protein matrix. We demonstrate that the accessibility of the pathways and the mechanisms of ligand exchange were modified by mutations. Insertion of bulky aromatic residues in the tunnel corresponding to pathway p1 leads to reduced accessibility to the ligands and a change in mechanism of opening from permanent to transient. We propose that engineering the accessibility of tunnels and the mechanisms of ligand exchange is a powerful strategy for modification of the functional properties of enzymes with buried active sites.

Keywords | haloalkane dehalogenase; product release; random acceleration molecular dynamics; tunnel; water exchange.

Author contributions | *Klvaňa* performed molecular modelling, designed mutants and interpreted data; *Pavlová* performed mutagenesis, activity measurements and inhibition kinetics; *Koudeláková* performed mutagenesis; *Chaloupková* performed CD spectroscopy measurements; *Dvorak* performed activity measurements; *Prokop* performed inhibition kinetics; *Stsiapanava*, *Kutý*, *Kutá-Smatanová* and *Dohnálek* determined X-ray crystal structures of mutant proteins; *Kulhánek* and *Wade* contributed the RAMD modelling tool; Damborský designed mutants and interpreted data. All authors contributed to the writing of the paper.

Supplementary material

That's what ya get when ya misuse what I invent; your empire falls and ya lose every cent.
— Gary Grice

The electronic version of the dissertation thesis and the summary of the dissertation thesis in PDF format (klvana_phdthesis_2009.pdf and klvana_phdthesis_2009_sum.pdf) and all figures in PNG format as well as supplementary material is available on a DVD attached to the inside front cover. All files can be accessed by launching the "klvana_phdthesis_2009.html" file in a web browser; description of each file is provided in the HTML file. The DVD content is listed below:

/	klvana_phdthesis_2009.pdf	klvana_phdthesis_2009_sm.html	klvana_phdthesis_2009_sum.pdf
/Introduction	md.avi	fig01.png *to* fig37.png	
/Methods	1cqw.pdb	circularly_polarised_light_right.gif	linearly_polarised_light.gif
	3fbw.pdb	cpr.zip	parm94.dat
	3fwh.pdb	dhaawt.pdb	parm94_kmunicek_etal_2001.dat
	3g9x.pdb	fig38.png *to* fig57.png	path.zip
	bfac.zip	fpr.zip	ramd.in
	circularly_polarised_light_left.gif	genbank_AF060871	ramd.patch
/Publications	klvana_etal_2009.pdf	klvana_pavlova_etal_2009.pdf	
/References	*PDF files of selected articles*		
/Results	c01a.avi	c18.avi	fig58.png *to* fig89.png
	c01b.avi	c19.avi	r06a.avi
	c02.avi	c20.avi	r06b.avi
	c03.avi	c21.avi	r09a.avi
	c04.avi	c22.avi	r09b.avi
	c05.avi	c23.avi	r11a.avi
	c06.avi	c24.avi	r11b.avi
	c07a.avi	c25.avi	r26a.avi
	c07b.avi	c26.avi	r26b.avi
	c08.avi	c27.avi	r54a.avi
	c09.avi	c28.avi	r54b.avi
	c10.avi	c29.avi	r58a.avi
	c11.avi	c30.avi	r58b.avi
	c12.avi	c31.avi	r66a.avi
	c13.avi	c32.avi	r66b.avi
	c14.avi	c33.avi	r74a.avi
	c15.avi	c34.avi	r74b.avi
	c16.avi	c35.avi	r82a.avi
	c17.avi	c36.avi	r82b.avi

The DVD content is also available at http://phdthesis.martinklvana.com/.

Never make your home in a place. Make a home for yourself inside your own head. You`ll find what you need to furnish it – memory, friends you can trust, love of learning, and other such things. That way it will go with you wherever you journey.

— Tad Williams

Curriculum vitae

If you do not know how to divide a word at the end of a line then do not divide it; simply put the whole word at the beginning of next line. I am the master of dividing words: I do not divide any.

First name: Martin
Last name: Klvaňa
Nationality: Czech
Languages: Czech (native), English (advanced)
Residence: Brno, Czech Republic
E-mail address: martin.mk.klvana@gmail.com
Cell phone: +420 737 319 948
Web site: http://www.martinklvana.com/

Education

M.S. General Biology/Microbiology (2004): Faculty of Science, Masaryk University, Brno, Czech Republic.

Affiliation

None: Mar 13, 2009 to present.
Loschmidt Laboratories (formerly Protein Engineering Group): May 06, 2002 to Mar 12, 2009, National Centre for Biomolecular Research (2002-2008) and Department of Experimental Biology (2009), Faculty of Science, Masaryk University, Brno, Czech Republic.

Research visits

Computational Chemistry Group of Prof. Shigenori Tanaka: Sep 01 to Nov 29, 2005, Graduate School of Science and Technology, Kobe University, Kobe, Japan.
Molecular and Cellular Modelling group of Dr. Rebecca C. Wade: Sep 24 to Dec 18, 2004, EML Research, Heidelberg, Germany.
Laboratory of Bioinformatics and Protein Engineering of Dr. Janusz M. Bujnicki: Jun 30 to Jul 11, 2003, International Institute of Molecular and Cell Biology Warsaw, Poland.

Awards

Award of the Rector of the Masaryk University (2004): Brno, Czech Republic.
2nd prize at Student Scientific Conference (2003): Komensky University, Bratislava, Slovakia.

Research interests

Keywords: (Micro)biology; general principles of life; relationships between structure, dynamics, function and evolution of proteins; molecular docking; molecular dynamics; collaboration with experimentalists.
Primary goal: Knowledge.

Theses

Diploma thesis (2004): Computer modelling of bacterial enzymes involved in degradation of halogenated hydrocarbons (research supervisor: Jiří Damborský; methodological advisors: Michal Boháč and Jan Kmuníček). Department of Microbiology, Faculty of Science, Masaryk University, Brno, Czech Republic.

Research articles

6. Klvaňa M, Pavlová M, Koudeláková T, Chaloupková R, Dvořák P, Prokop Z, Stsiapanava A, Kutý M, Kutá-Smatanová I, Dohnálek J, Kulhánek P, Wade RC & Damborský J (**2009**). Pathways and mechanisms for product release in the engineered haloalkane dehalogenases explored using classical and random acceleration molecular dynamics simulations. *J. Mol. Biol.* 392: 1339-1356. PMID: 19577578.
5. Klvaňa M, Pavlová M, Prokop Z, Chaloupková R, Banáš P, Otyepka M, Wade R, Nagata Y & Damborský J (**2009**). Redesigning dehalogenase access tunnels as a strategy for degrading an anthropogenic substrate. *Nat. Chem. Biol.* 5: 727-733. PMID: 19701186.
4. Ito M, Prokop Z, **Klvaňa M,** Otsubo Y, Tsuda M, Damborský J & Nagata Y (**2007**). Degradation of β-hexachlorocyclohexane by haloalkane dehalogenase LinB from hexachlorocyclohexane-utilizing bacterium *Sphingobium* sp. MI1205. *Arch. Microbiol.* 188: 313-325. PMID: 17516046.
3. Pavlová M, **Klvaňa M,** Jesenská A, Prokop Z, Konečná H, Sato T, Tsuda M, Nagata Y & Damborský J (**2007**). The identification of catalytic pentad in the haloalkane dehalogenase DhmA from *Mycobacterium avium* N85: Reaction mechanism and molecular evolution. *J. Struct. Biol.* 157: 384-392. PMID: 17084094.
2. Oakley A, **Klvaňa M,** Otyepka M, Nagata Y, Wilce MCJ & Damborský J (**2004**). Crystal structure of haloalkane dehalogenase LinB from *Sphingomonas paucimobilis* UT26 at 0.95 Å resolution: Dynamics of catalytic residues. *Biochemistry* 43: 870-878. PMID: 14744129.
1. Prokop Z, Monincová M, Chaloupková R, **Klvaňa M,** Nagata Y, Janssen DB & Damborský J (**2003**). Catalytic Mechanism of the Haloalkane Dehalogenase LinB from *Sphingomonas paucimobilis* UT26. *J. Biol. Chem.* 278: 45094-45100. PMID: 12952988.

Software

Andres F, Beneš P, Brezovský J, Chovancová E, Jaša P, **Klvaňa M,** Kozlíková B, Medek P, Pavelka A, Szabó T, Zamborský M, Zruban M *(in alphabetical order)*, Sochor J & Damborský J (**2009**). CAVER 2.0 tunnel calculation program. Human Computer Interaction Laboratory and Loschmidt Laboratories *(in alphabetical order)*, Masaryk University, Brno, Czech Republic. http://www.loschmidt.chemi.muni.cz/caver

Lectures

6. Klvaňa M & Damborský J: Cavities and tunnels in enzymes *(Czech)*. *Bioinformatics III – Structural bioinformatics and molecular modelling.* October 12, **2006**; Brno, Czech Republic.
5. Klvaňa M, Kulhánek P, Wade RC & Damborský J: Modelling of product release and identification of export routes in the haloalkane dehalogenase DhaA *(English)*. *5th Discussions in Structural Biology and Bioinformatics.* March 16-18, **2006**; Nové Hrady, Czech Republic.
4. Klvaňa M, Kulhánek P, Wade RC & Damborský J: Modelling of export routes in haloalkane dehalogenase DhaA *(English)*. September 6, **2005**; Kobe University, Japan.
3. Klvaňa M, Pavlová M, Jesenská A, Konečná H, Nagata Y & Damborský J: Homology modelling of haloalkane dehalogenase DhmA *(Czech)*. *Czech and Slovak Student Scientific Conference.* May 1, **2004**; Brno, Czech Republic.
2. Klvaňa M, Oakley A & Damborský J: Dynamics of catalytic residues of haloalkane dehalogenase LinB: Insight from X-ray crystallography and quantum mechanical calculations *(English)*. July 9, **2003**, International Institute of Molecular and Cell Biology, Warsaw, Poland.
1. Klvaňa M, Boháč M & Damborský J: Computer modelling of bacterial hydrolytic dehalogenation reaction *(Czech)*. *Student Scientific Conference.* April 9-10, **2003**, Bratislava, Slovakia.

Posters

2. Klvaňa M, Pavlová M, Koudeláková T, Chaloupková R, Dvořák P, Stsiapanava A, Kutý M, Kutá Smatanová I, Dohnálek J, Kulhánek P, Wade RC & Damborský J: Pathways and mechanisms of product exit and water exchange pathways in engineered haloalkane dehalogenase DhaA explored using classical and random acceleration molecular dynamics simulations *(English)*. *ESF Conference: Protein Design and Evolution for Biocatalysis*, October 25-30, **2008**, Saint-Feliu de Guixols, Spain.
1. Klvaňa M, Pavlová M, Konečná H, Nagata Y & Damborský J: Homology modelling of haloalkane dehalogenase DhmA *(English)*. *EMBO Course on Biomolecular Simulation*, July 18-25, **2004**, Paris, France.

Thirty-six more chambers to take you through.

— Clifford Smith